

# **Investigations into intracellular mechanisms of chemokine signalling in cancer**

---

**Wing Yee Lai**

**A thesis presented for the degree of Doctor of Philosophy at the University  
of East Anglia, Norwich, UK**

**April 2023**

© This copy of the thesis has been supplied on condition that anyone who consults it is understood to recognise that its copyright rests with the author and that use of any information derived therefrom must be in accordance with current UK Copyright Law. In addition, any quotation or extract must include full attribution.

# Abstract

---

**Aim:** Chemokine signalling plays a critical regulatory role in cancer, which was found to be either tumour-promoting or tumour-suppressive. Although chemokine signalling is a potential target for anti-cancer drugs, the success in drug design is hindered by the complexity of biased signalling and signalling redundancy in the signalling system. Our aim is to understand cell-specific mechanisms and isoform-specific roles of signalling proteins underlying context-dependent chemokine signalling system in cancer cells.

**Methodology:** Experimentation was undertaken in breast cancer MCF-7 and MDA-MB-231 cells, leukaemic T-lymphocyte Jurkat cell and monocytic leukaemic THP-1 cells, to investigate cellular responses from the activation of endogenously expressed chemokine receptors. Small molecule inhibitors and RNA interventions were employed to determine the involvement of target proteins in cellular responses using intracellular  $\text{Ca}^{2+}$  mobilisation, chemotaxis and receptor internalisation assays. Immunocytochemistry was applied to reveal the change in localisation and quantities of cell surface chemokine receptors and intracellular proteins following chemokine stimulation.

**Results:** CXCL12-induced CXCR4 internalisation in Jurkat cells is caveolae-dependent, while CCL3-induced CCR5 internalisation in MCF-7 cells is independent of clathrin. Arrestin-2 (Arr-2) responds to CCL3 stimulation, whereas Arrestin-3 (Arr-3) responds to CXCL12 stimulation in MCF-7 cells. Inhibition of protein kinase D (PrKD) blocks  $\text{Ca}^{2+}$  mobilisation induced by CXCL12 in MCF-7 cells but not for THP-1 cells. Basal PrKD potentially negatively regulate actin cytoskeletal rearrangement in cell migration in MCF-7 cells.

**Conclusion:** Our study shows that chemokine signalling pattern vary between cancer cell types due to the activation of different receptor-chemokine partners and involvement of diverse combinations of signalling proteins in isoform-specific manner. Overall, the research in this thesis has highlighted the necessity of verifying specific signalling mechanisms in different cell lines in chemokine research.

## **Access Condition and Agreement**

Each deposit in UEA Digital Repository is protected by copyright and other intellectual property rights, and duplication or sale of all or part of any of the Data Collections is not permitted, except that material may be duplicated by you for your research use or for educational purposes in electronic or print form. You must obtain permission from the copyright holder, usually the author, for any other use. Exceptions only apply where a deposit may be explicitly provided under a stated licence, such as a Creative Commons licence or Open Government licence.

Electronic or print copies may not be offered, whether for sale or otherwise to anyone, unless explicitly stated under a Creative Commons or Open Government license. Unauthorised reproduction, editing or reformatting for resale purposes is explicitly prohibited (except where approved by the copyright holder themselves) and UEA reserves the right to take immediate 'take down' action on behalf of the copyright and/or rights holder if this Access condition of the UEA Digital Repository is breached. Any material in this database has been supplied on the understanding that it is copyright material and that no quotation from the material may be published without proper acknowledgement.

# Abbreviations

---

|                   |   |
|-------------------|---|
| AML               | Acute myeloid leukaemia                       |
| AMPA              | AMPA type glutamate receptors                 |
| AR                | $\alpha_{1A/B}$ -adrenergic receptors         |
| Arp2/3            | Actin Related Protein 2/3 complex             |
| ATCC              | American Type Culture Collection              |
| AT <sub>1</sub> R | Angiotensin II Type I Receptor                |
| BRET              | Bioluminescence Resonance Energy Transfer     |
| Cav-1             | Caveolin-1                                    |
| CCP               | Clathrin-coated pit                           |
| CCV               | Clathrin-coated vesicle                       |
| Cdc42             | Cell division control protein 42 homolog      |
| CHO               | Chinese hamster ovary                         |
| CRC               | Colorectal cancer                             |
| CRS               | Chemokine recognition site                    |
| CAFs              | Cancer-associated fibroblasts                 |
| CTLs              | Cytotoxic T lymphocytes                       |
| DAG               | Diacylglycerol                                |
| DAPI              | 4',6-Diamidino-2-phenylindole dihydrochloride |
| Dyn-2             | Dynamin-2                                     |
| ECL               | Extracellular loop                            |
| ECM               | Extracellular matrix                          |
| EEA-1             | Early endosomal antigen-1                     |
| EMT               | Epithelial-to-mesenchymal transition          |
| ER                | Oestrogen receptor                            |
| ERK1/2            | Extracellular signal-regulated kinases 1/2    |
| F-actin           | Filamentous actin                             |
| FAK               | Focal Adhesion Kinase                         |
| FC                | Flow cytometry                                |
| FDA               | Food and Drug Administration                  |
| FITC              | Fluorescein isothiocyanate                    |

|                          |  |
|--------------------------|--|
| FRET                     | Förster resonance energy transfer  |
| FSC                      | Forward scatter  |
| GAG                      | Glycosaminoglycan  |
| GED                      | GTPase effector domain   |
| GPCR                     | G protein-coupled receptor   |
| GRK                      | G protein-coupled receptor kinases   |
| HIV                      | Human immunodeficiency virus   |
| HTRF                     | Homogenous time-resolved fluorescence  |
| ICLs                     | Intracellular loops  |
| IF                       | Immunofluorescence   |
| IFN                      | Interferon   |
| Ins(1,4,5)P <sub>3</sub> | Inositol trisphosphate<br>(aka IP <sub>3</sub> )   |
| JNK                      | c-Jun N-terminal kinase  |
| LIMK                     | LIM kinase   |
| MAPK                     | Multiple mitogen activated protein kinase  |
| MDSCs                    | Myeloid-derived suppressor cells   |
| MIG                      | Monokine induced by gamma interferon   |
| MLC                      | Myosin Light Chain   |
| MMPs                     | Matrix metalloproteases  |
| MTS                      | 3-(4,5-dimethylthiazol-2-yl)-5-(3-carboxymethoxyphenyl)-2-(4-sulfophenyl)-2H-tetrazolium |
| NHERF-1                  | Sodium Hydrogen Exchanger Regulatory Factor-1  |
| NHL                      | Non-Hodgkin's lymphoma   |
| NMDAR                    | N-methyl-D-aspartate receptor  |
| N-WASP                   | Neuronal Wiskott-Aldrich Syndrome Protein  |
| OS                       | Osteosarcoma   |
| PAK4                     | p21-activated kinase 4   |
| PB                       | PDZ binding motif  |
| PH                       | Plekstrin homology   |
| PI3K                     | Phosphatidylinositol 3-kinase  |
| PI(4,5)P <sub>2</sub>    | Phosphatidylinositol 4,5-bisphosphate  |

|                         |  |
|-------------------------|--|
| PI(3,4,5)P <sub>3</sub> | Phosphatidylinositol(3,4,5) trisphosphate            |
| PKA                     | Protein kinase A                                     |
| PKC                     | Protein kinase C                                     |
| PKG                     | cGMP-dependent kinase                                |
| PLC                     | Phospholipase C                                      |
| PMN-MDSCs               | Polymorphonuclear Myeloid-Derived Suppressor Cells   |
| PR                      | Progesterone receptor                                |
| PRD                     | Prolinerich domain                                   |
| PrKD                    | Protein kinase D                                     |
| PTEN                    | Phosphatase and TENsin homolog                       |
| PTM                     | Post-translational modification                      |
| RANTES                  | CCL5   |
| RCC                     | Renal cell carcinoma                                 |
| ROCK                    | Rho-associated protein kinase                        |
| ROI                     | Region of interest                                   |
| SERCA                   | Sarco/endoplasmic reticulum Ca <sup>2+</sup> -ATPase |
| shRNA                   | short hairpin RNA                                    |
| siRNA                   | small interfering RNA                                |
| SIM                     | Structured-illumination Microscopy                   |
| SSC                     | Side scatter   |
| SSH1L                   | Slingshot-1L   |
| STED                    | Stimulated Emission Depletion                        |
| STORM                   | Stochastic Optical Reconstruction microscopy         |
| TGF                     | Transforming growth factor                           |
| TLR                     | Toll-like receptor                                   |
| TMD                     | Transmembrane domain                                 |
| TME                     | Tumour microenvironment                              |
| TNBC                    | Triple-negative breast cancer                        |
| TNF                     | Tumour necrosis factor                               |
| TRP                     | Transient receptor potential                         |
| ULD                     | Ubiquitin-like domain                                |
| WASP                    | Wiskott-Aldrich Syndrome Protein                     |

WHIM      Warts, Hypogammaglobulinemia, Infections, and  
Myelokathexis

# Contents

---

|  |    |
|--|----|
| Abstract .....   | 2  |
| Abbreviations .....  | 3  |
| Contents .....   | 7  |
| List of Tables .....   | 13 |
| List of Figures .....  | 15 |
| Statement of Special Circumstances .....   | 24 |
| Publications .....   | 25 |
| Acknowledgements .....   | 26 |
| Chapter 1: Introduction .....  | 28 |
| 1.1 Cancer and chemokine signalling system .....                                       | 28 |
| 1.1.1 Cancer invasion and metastasis .....   | 29 |
| 1.1.2 Immune evasion in cancer .....   | 35 |
| 1.2 Chemokine classification and structure .....                                       | 35 |
| 1.2.1 Chemokine homodimers .....   | 41 |
| 1.2.2 Chemokine heterodimers .....   | 43 |
| 1.2.3 Interaction of chemokines with glycosaminoglycans (GAGs) .....                   | 45 |
| 1.3 Chemokine receptor structure and classification .....                              | 46 |
| 1.3.1 Chemokine receptor activation .....  | 49 |
| 1.3.2 Chemokine receptor dimerisation .....  | 52 |
| 1.4 Chemokine signalling .....   | 54 |
| 1.4.1 G protein-dependent chemokine signalling .....                                   | 54 |
| 1.4.2 G protein-independent chemokine signalling .....                                 | 57 |
| 1.4.3 Biased signalling .....  | 59 |
| 1.4.4 Downstream effector: $\beta$ -arrestins .....                                    | 61 |
| 1.4.5 Downstream effector: Protein kinase D (PrKD) (previously named PKC $\mu$ ) ..... | 69 |

|  |   |     |
|--|---|-----|
| 1.5                                    | Chemokine receptor internalisation and trafficking -----          | 78  |
| 1.5.1                                  | Receptor internalisation through clathrin-dependent pathway ----- | 78  |
| 1.5.2                                  | Receptor internalisation through caveolae-dependent pathway ----- | 81  |
| 1.5.3                                  | Receptor degradation and recycling -----                          | 84  |
| 1.6                                    | Roles of CCR5 in cancer -----                                     | 85  |
| 1.6.1                                  | Structure of CCR5 -----   | 86  |
| 1.6.2                                  | CCR5-targeting small molecules-----                               | 90  |
| 1.7                                    | Roles of CXCR4 in cancer -----                                    | 90  |
| 1.7.1                                  | Structure of CXCR4 -----  | 91  |
| 1.7.2                                  | CXCR4-targeting small molecules-----                              | 94  |
| 1.8                                    | Concluding remarks -----  | 98  |
| 1.9                                    | Research objectives -----   | 99  |
| Chapter 2: Materials and methods ----- |   | 102 |
| 2.1                                    | Cell lines and tissue culture-----                                | 102 |
| 2.1.1                                  | Cell culture medium and cell lines -----                          | 102 |
| 2.1.2                                  | Routine tissue culture procedures -----                           | 104 |
| 2.1.3                                  | Cyopreservation of cells-----                                     | 104 |
| 2.2                                    | Small molecule inhibitors-----                                    | 105 |
| 2.3                                    | Chemokine ligands-----  | 108 |
| 2.4                                    | Antibodies -----  | 109 |
| 2.5                                    | Intracellular protein stains -----                                | 110 |
| 2.6                                    | Plasmid DNA -----   | 110 |
| 2.7.1                                  | Plasmid transformation into bacterial culture -----               | 113 |
| 2.7.2                                  | Amplification of plasmid DNA from bacterial broth -----           | 114 |
| 2.7.3                                  | Chemical transfection of plasmid DNA -----                        | 115 |
| 2.7.4                                  | Electroporation transfection of plasmid DNA -----                 | 115 |
| 2.8                                    | Calcium (Ca <sup>2+</sup> ) flux-----                             | 116 |
| 2.9                                    | Migration assays-----   | 116 |

|   |     |
|---|-----|
| 2.9.1 ChemoTX chemotaxis assay -----  | 116 |
| 2.9.2 ORIS™ Cell migration assay-----   | 117 |
| 2.10 Imaging techniques -----   | 118 |
| 2.10.1 Intracellular protein staining -----   | 118 |
| 2.10.2 Cell surface receptor staining -----   | 119 |
| 2.10.3 Image acquisition-----   | 120 |
| 2.10.4 Analysis of cell area and cell circularity-----  | 120 |
| 2.11 Internalisation assay and flow cytometry analysis-----   | 121 |
| 2.12 Cell viability tests -----   | 122 |
| 2.12.1 CellTitre 96® Aqueous One Solution Cell Proliferation Assay -----  | 122 |
| 2.12.2 Trypan blue staining -----   | 122 |
| Chapter 3: Characterisation of chemokine-induced responses in different cancer cell lines-----  | 123 |
| 3.1 Introduction -----  | 123 |
| 3.2 Chapter aims -----  | 124 |
| 3.3 Results -----   | 124 |
| 3.3.1. Localisation and quantification of endogenously expressed chemokine receptor in cancer cells -----                                       | 124 |
| 3.3.2 Measurement of intracellular calcium (Ca <sup>2+</sup> ) mobilisation in response to chemokine stimulation in MCF-7 and THP-1 cells ----- | 137 |
| 3.3.3 Actin cytoskeletal rearrangement in response to chemokine stimulation -----   | 141 |
| 3.3.4 Chemotaxis in response to chemokine stimulation-----  | 147 |
| 3.3.5 Receptor internalisation in response to chemokine stimulation -----   | 150 |
| 3.4 Discussion-----   | 158 |
| 3.5 Chapter conclusions -----   | 165 |
| Chapter 4: Investigations into the mechanisms underlying chemokine-induced receptor internalisation-----  | 170 |
| 4.1 Introduction -----  | 170 |

|  |     |
|--|-----|
| 4.2 Chapter aims .....   | 174 |
| 4.3 Results .....  | 174 |
| 4.3.1 Caveolin-1 (Cav-1) is expressed intracellularly in MCF-7 cells. Following CCL3 or CXCL12 stimulation, Cav-1 translocate towards the leading edge of MCF-7 cells but no significant change in Cav-1 expression is observed in MCF-7 cells. .... | 174 |
| 4.3.2 Cav-1 express intracellularly in Jurkat cells. CXCL12 stimulation does not induce a significant change in Cav-1 expression in Jurkat cells. ....   | 178 |
| 4.3.3 Protein synthesis inhibitor, cycloheximide, has no effect on Cav-1 expression following chemokine stimulation in MCF-7 and Jurkat cells. -   | 180 |
| 4.3.4. Caveolae-blocking agents, filipin and nystatin, disrupt intracellular localisation of Cav-1 in MCF-7 cells. ....  | 182 |
| 4.3.5 Caveolae-blocking agents significantly block CXCL12-induced CXCR4 internalisation in Jurkat cells but mediate less significant effect on CCL3-induced CCR5 internalisation in MCF-7 cells. ....  | 184 |
| 4.3.6 Caveolae-blocking agents induces increased CXCR4 internalisation in MCF-7 cells potentially due to non-specific effects. ....  | 188 |
| 4.3.7 Negative control for clathrin inhibitor, Pitstop 2, causes non-specific effects on CXCR4 receptor endocytosis with increased CXCR4 internalisation seen following CXCL12 stimulation in MCF-7 and Jurkat cells. ....                           | 190 |
| 4.3.8. Pitstop 2 has no inhibitory effect on CCL3-induced CCR5 internalisation in MCF-7 cells. ....  | 196 |
| 4.3.9. Dynamin-2 (Dyn-2) translocate towards the cytosol with increased expression level following CCL3 or CXCL12 stimulation in MCF-7 cells-  | 200 |
| 4.3.10. Arrestin-2 (Arr-2) constructs translocate out of the nucleus in response to CCL3 stimulation, whereas arrestin-3 constructs translocate towards the nucleus in response to CXCL12 stimulation in MCF-7 cells.                                | 202 |
| 4.3.11. Dynamin inhibitors, Dynasore and Dyngo-4a, have no effect on CCL3-induced Arr-2 translocation but abolish CXCL12-induced Arr-3 translocation in MCF-7 cells. ....  | 206 |
| 4.4 Discussion.....  | 213 |

|   |     |
|---|-----|
| 4.5 Chapter conclusions   | 221 |
| Chapter 5: The roles of protein kinase D (PrKD) in regulating chemokine-induced cellular responses  | 225 |
| 5.1 Introduction  | 225 |
| 5.2 Chapter aims  | 226 |
| 5.3 Results   | 227 |
| 5.3.1 Protein kinase D (PrKD) inhibitors reduce intracellular Ca <sup>2+</sup> release induced by CCL3 and CXCL12 in MCF-7 cells, while PrKD inhibitors reduce intracellular Ca <sup>2+</sup> release mediated by CCL3 but not CXCL12 in THP-1 cells. | 227 |
| 5.3.2 PrKD inhibitors significantly block chemotaxis driven by CXCL12 stimulation in both Jurkat and THP-1 cells.   | 232 |
| 5.3.3 Protein kinase D (PrKD) inhibitors cause elongated morphology with increased cell surface area in MCF-7 cells alone in the absence of chemokine stimulation.  | 234 |
| 5.3.4 ROCK inhibitor, Y27632, disrupts the organisation of actin cytoskeleton, while Arp2/3 inhibitor, CK666, prevents the formation of lamellipodia and filopodia in MCF-7 cells stimulated with CCL3 or CXCL12.                                     | 237 |
| 5.3.5. Disruption of F-actin arrangement and elongated cell morphology with increased cell surface is resulted by the combined treatment of Y27632 and PrKD inhibitor.  | 242 |
| 5.3.6. CK666 overrides the basal effect of PrKD inhibitor as a result of inhibition of actin polymerisation observed in MCF-7 cells.  | 245 |
| 5.3.7 PrKD inhibitors, CID755673 and CID2011756, have no blocking effect on chemokine receptor internalisation following CCL3 or CXCL12 stimulation in MCF-7 and Jurkat cells.  | 248 |
| 5.3.8 PrKD2 knockout has no effect on the change in endosomal sorting following CXCL12 stimulation.   | 255 |
| 5.4 Discussion  | 259 |
| 5.5 Chapter conclusions   | 269 |

|   |     |
|---|-----|
| Chapter 6: Final discussion and thesis conclusion ----- | 272 |
| References -----  | 283 |
| Appendix 1 -----  | 322 |
| Appendix 2 -----  | 323 |
| Appendix 3 -----  | 325 |
| Appendix 4 -----  | 326 |
| Appendix 5 -----  | 327 |
| Appendix 6 -----  | 328 |
| Appendix 7 -----  | 329 |
| Appendix 8 -----  | 330 |
| Appendix 9 -----  | 331 |
| Appendix 10 -----                                       | 332 |
| Appendix 11 -----                                       | 333 |
| Appendix 12 -----                                       | 334 |

# List of Tables

---

## Chapter 1:

|  |    |
|--|----|
| Table 1.1. List of chemokine receptors and their cognate ligands -----   | 40 |
| Table 1.2. Differential functional roles and mechanisms of the three PrKD isoforms in cell migration and their association with different cancer types ----- | 77 |
| Table 1.3. List of CCR5 and CXCR4 antagonists currently on clinical trial for the application of cancer therapy-----   | 97 |

## Chapter 2:

|  |     |
|--|-----|
| Table 2.1. Cell culture medium -----                       | 102 |
| Table 2.2. Cell lines-----                                 | 103 |
| Table 2.3. Small molecule inhibitors-----                  | 105 |
| Table 2.4. Chemokine ligands used for experiments-----     | 108 |
| Table 2.5. Primary antibodies used for experiments -----   | 109 |
| Table 2.6. Secondary antibodies used for experiments ----- | 110 |
| Table 2.7. Intracellular stains-----                       | 110 |

## Chapter 3:

|   |     |
|---|-----|
| Table 3.1. Comparison of relative quantities of chemokine receptors localised on the cell surface among different cell lines -----  | 135 |
| Table 3.2. Percentage of receptor expression on cell surface following chemokine stimulation in MCF-7 and Jurkat cells -----        | 158 |
| Table 3.3. Summary of characterisation of chemokine receptor expression and cellular responses in different cancer cell lines ----- | 167 |

## Chapter 4:

|  |     |
|--|-----|
| Table 4.1. Summary of the extent of receptor internalisation from studies investigating CCR5 and CXCR4 internalisation in different cell lines ----- | 172 |
| Table 4.2. Effect of caveolae-depleting agents and clathrin inhibitor on chemokine-induced receptor internalisation -----                            | 199 |

Table 4.3. Summary of the experimental approaches used and extent of receptor internalisation in MCF-7 and Jurkat cells----- 223

Table 4.4. Summary of the involvement of intracellular proteins in receptor internalisation in MCF-7 and Jurkat cells----- 224

**Chapter 5:**

Table 5.1. Effect of PrKD inhibitors, CID755673 and CID0211756, on chemokine-induced receptor internalisation ----- 254

Table 5.2. IC50 values of protein kinase D inhibitor ----- 260

Table 5.3. Summary of the involvement of protein kinase D (PrKD) in cellular responses in different cancer cell lines ----- 270

# List of Figures

---

## Chapter 1:

|  |    |
|--|----|
| Figure 1.1. Modes of cell migration adopted by cancer cells-----   | 30 |
| Figure 1.2. Sequential events of cell migration in the regulation of cytoskeleton dynamics -----   | 31 |
| Figure 1.3. Schematic diagram of the structure of chemokine -----  | 37 |
| Figure 1.4. Simplified representation of sequential patterns of the four chemokine subfamilies: C-, CC-, CXC- and CX3C- chemokines-----                                  | 38 |
| Figure 1.5. Three-dimensional diagrams representing structures of chemokine dimers -----   | 42 |
| Figure 1.6. Three-dimensional diagrams representing structures of CXCL4/CCL5 heterodimers-----   | 44 |
| Figure 1.7. Schematic two-dimensional diagrams of the structures of chemokine receptor -----   | 48 |
| Figure 1.8. Hypothetical three-dimensional model of chemokine docking on a chemokine receptor in the activation state-----   | 51 |
| Figure 1.9. Overall chemokine binding mode of receptor-chemokine (CCR5-CCL3) complex -----   | 52 |
| Figure 1.10. G protein-dependent chemokine signalling pathways-----  | 57 |
| Figure 1.11. G protein-independent signalling -----  | 59 |
| Figure 1.12. Structural representation of $\beta$ -arrestin-----   | 62 |
| Figure 1.13. Schematical diagrams indicating the three distinct conformations of active arrestin in the interaction with GPCR -----                                      | 63 |
| Figure 1.14. Schematical diagram showing the flute model for elaborating the model on the phosphorylation barcoding of arrestin-dependent signalling -----               | 65 |
| Figure 1.15. Schematical diagram showing the QR code model for elucidating differential signalling transduction from specific receptor phosphorylation recognition ----- | 66 |
| Figure 1.16. Schematical diagram showing two major cancer-associated downstream signalling pathway regulated by arrestins-----   | 68 |

|  |     |
|--|-----|
| Figure 1.17. Localisation of PrKD .....  | 70  |
| Figure 1.18. Structural differences in the three PrKD isoforms (PrKD1, PrKD2 and PrKD3) .....  | 72  |
| Figure 1.19. Schematical diagram showing PrKD activation and downstream signalling transduction associated with cell migration through interactions with multiple protein kinases..... | 74  |
| Figure 1.20. Schematical diagram summarising the two major pathways in chemokine receptor internalisation .....  | 79  |
| Figure 1.21. Schematical diagram showing the molecular dynamics of clathrin-dependent endocytosis .....  | 80  |
| Figure 1.22. Structure of caveolae (also known as lipid rafts) in the plasma membrane.....   | 82  |
| Figure 1.23. Structure of caveolae-coated membrane invaginations .....   | 83  |
| Figure 1.24. Two-dimensional structure of CCR5.....  | 87  |
| Figure 1.25. Molecular models of receptor-chemokine (CCR5-CCL3) complex. ....  | 89  |
| Figure 1.26. Two-dimensional structure of CXCR4.....   | 92  |
| Figure 1.27. Molecular models of receptor-chemokine (CXCR4-CXCL12) complex. ....   | 93  |
| <b>Chapter 2:</b>  |     |
| Figure 2.1. MISSION Prkd2 shRNA pLKO.1-puro lentiviral plasmid vector containing a verified mammalian Prkd2 shRNA sequence insert. ....  | 111 |
| Figure 2.2. MISSION Non-target pLKO.1-puro lentiviral plasmid vector containing a non-target shRNA sequence insert.....  | 112 |
| Figure 2.3. Mammalian HindIII/ApaI digested pEGFP-N1 plasmid vector containing PCR-amplified arrestin 2 (Clontech) .....   | 113 |
| Figure 2.4 ChemoTX 5 $\mu$ m pore plate (Neuroprobe Inc, USA) .....  | 117 |
| Figure 2.5 Illustration of the steps from cell seeding, creating a cell-free detection zone to cell imaging for the detection of cell migration in a 96-well ORIS™ plate .....         | 118 |

### Chapter 3:

|   |     |
|---|-----|
| Figure 3.1. CXCR4 and CCR5 receptors are abundantly localised on the cell surface of MCF-7 cells -----  | 127 |
| Figure 3.2. Flow cytometry of MCF-7 showing the relative quantities of chemokine receptor localised on the cell surface -----   | 128 |
| Figure 3.3. MDA-MB-231 cells express IL-8RA and IL-8RB more abundantly compared to other chemokine receptors -----  | 130 |
| Figure 3.4. CXCR4 receptors are abundantly localised on the cell surface of Jurkat cells -----  | 131 |
| Figure 3.5. Flow cytometry of Jurkat showing the relative quantities of chemokine receptor localised on the cell surface.-----  | 132 |
| Figure 3.6. IL-8RB receptors are abundantly localised on the cell surface of THP-1 cells-----   | 133 |
| Figure 3.7. Flow cytometry of THP-1 showing the relative quantities of chemokine receptor localised on the cell surface -----   | 134 |
| Figure 3.8. Comparisons of relative quantities of chemokine receptors localised on the cell surface among different cancer cell lines. -----  | 136 |
| Figure 3.9. More increase in intracellular Ca <sup>2+</sup> release was observed in CCL3 stimulation compared to CXCL12 stimulation in MCF-7 and THP-1 cells-----   | 139 |
| Figure 3.10. Representative traces of real-time change in intracellular Ca <sup>2+</sup> level in response to CCL3 or CXCL12 stimulation -----  | 140 |
| Figure 3.11. Increase in the formation of filopodia and lamellipodia at the leading edge and formation of stress fibres at the contractile tail was observed in MCF-7 cells stimulated with CCL3 or CXCL12 -----  | 143 |
| Figure 3.12. No significant change in actin rearrangement was observed in MCF-7 cells stimulated with CCL4, CCL5, CCL23, IL-8 and CXCL9 respectively, but some individual cells appeared to be more elongated morphology -----                                      | 144 |
| Figure 3.13. CCL3 and CXCL12 stimulation induces a significant increase in cell area and significant reduction in cell circularity, while CCL23 induces a significant reduction in cell circularity but no significant difference in cell area in MCF-7 cells ----- | 145 |

|  |     |
|--|-----|
| Figure 3.14. Distinct formation of pseudopodia with membrane blebbing and amoeboid-like cell morphology was observed in MDA-MB-231 cells stimulated with all chemokine ligands tested -----  | 146 |
| Figure 3.15. Stimulation of CCL3, CCL4, CXCL9 and CXCL12 induces a significant increase in cell area, while cell circularity is significantly reduced following the stimulation of CCL3, CCL4, CCL5, CCL23 and CXCL9 in MDA-MB-231 cells ----- | 147 |
| Figure 3.16. Jurkat migrate towards CXCL12 more significantly than THP-1 in the chemotaxis assay -----   | 149 |
| Figure 3.17. No significant cell migration towards the detection zone following incubation with CXCL12 was observed for MDA-MB-231 cells-----  | 150 |
| Figure 3.18. Reduced cell surface expression of CXCR4 was observed following the stimulation with CXCL12 in MCF-7 and Jurkat cells compared to unstimulated basal controls-----  | 153 |
| Figure 3.19. A significant reduction in relative CXCR4 expression on cell surface following CXCL12 stimulation was observed in both MCF-7 and Jurkat cells   | 154 |
| Figure 3.20. Cell surface CCR5 expression was reduced following CCL3 stimulation in MCF-7 cells-----   | 155 |
| Figure 3.21. A significant reduction in relative CCR5 expression on cell surface following CCL3 stimulation was observed in MCF-7 cells -----  | 156 |

**Chapter 4:**

|  |     |
|--|-----|
| Figure 4.1. Translocation of caveolin-1 (Cav-1) towards the leading edge of the cells following CCL3 or CXCL12 stimulation in MCF-7 cells. Immunofluorescence staining of intracellular Cav-1 in MCF-7 cells ----- | 176 |
| Figure 4.2. There was a trend of increased Cav-1 expression following CCL3 or CXCL12 stimulation in MCF-7 cells, but it was not significant -----  | 177 |
| Figure 4.3. A trend of increased Cav-1 expression following CXCL12 stimulation was observed in Jurkat cells, but it was not significant -----  | 179 |
| Figure 4.4. Cycloheximide has no effect on Cav-1 expression change in MCF-7 cells stimulated with CCL3 or CXCL12 -----   | 181 |

|  |     |
|--|-----|
| Figure 4.5. Cycloheximide has no effect on Cav-1 expression change in Jurkat cells stimulated with CXCL12 -----  | 182 |
| Figure 4.6. Caveolae-blocking agents, filipin and nystatin, reduce Cav-1 localised on the plasma membrane in MCF-7 cells -----   | 184 |
| Figure 4.7. Caveolae-blocking agents significantly block CXCL12-induced CXCR4 internalisation in Jurkat cells-----   | 185 |
| Figure 4.8. A trend of reduced CCL3-induced CCR5 internalisation in MCF-7 cells after the treatment of caveolae-blocking agents was observed, but it was not significant-----  | 187 |
| Figure 4.9. Increased CXCL12-induced CXCR4 internalisation in MCF-7 cells treated with caveolae-blocking agents was observed-----  | 189 |
| Figure 4.10. Mode of action of clathrin inhibitor, Pitstop 2 -----   | 191 |
| Figure 4.11. Chemical structure of pitstop 2 and negative control for pitstop 2 (pitstop 2 neg) -----  | 192 |
| Figure 4.12. Increased CXCR4 internalisation following CXCL12 stimulation was observed in MCF-7 cells treated with negative control for pitstop 2 (pitstop 2 neg) -----  | 193 |
| Figure 4.13. A trend of Increased CXCR4 internalisation following CXCL12 stimulation was observed in Jurkat cells treated with negative control for pitstop 2 (pitstop 2 neg) -----  | 195 |
| Figure 4.14. No significant change in the level of CCL3-induced CCR5 internalisation by the treatment of pitstop 2 or pitstop 2 neg was observed in MCF-7 cells-----   | 197 |
| Figure 4.15. Effects of chemokine stimulation on dynamin-2 (Dyn-2) expression in MCF-7 cells -----   | 201 |
| Figure 4.16. Arrestin 2 (Arr-2) constructs translocate out of the nucleus and accumulate on the plasma membrane in CCL3-stimulated MCF-7 cells, whereas no observable change was observed following CXCL12 stimulation ----- | 204 |
| Figure 4.17. Arrestin 3 (Arr-3) constructs translocate towards the nucleus following CXCL12 stimulation in MCF-7 cells, but no observable change was observed in CCL3 stimulation -----                                      | 205 |

|  |     |
|--|-----|
| Figure 4.18. Mutant for Arr-2 (Arr Mut) constructs mainly accumulate within the nucleus and no observable change in localisation in the stimulation of CCL3 or CXCL12-----                                     | 206 |
| Figure 4.19. Chemical structures of dynamin inhibitors, Dynasore and Dyngo 4a, used in our study -----   | 207 |
| Figure 4.20. Dynamin inhibitors, Dyngo-4a and Dynasore, had no effect on Arr-2 distribution in MCF-7 cells, particularly no inhibition was seen on CCL3-induced Arr-2 translocation-----                       | 209 |
| Figure 4.21. CXCL12-induced Arr-3 translocation was abolished by the treatment of Dyngo-4a or Dynasore in MCF-7 cells, while no effect was observed under basal condition and in the stimulation of CCL3 ----- | 211 |
| Figure 4.22. Dyngo-4a or Dynasore had no effect on the distribution of Arr Mut under basal conditions and in the stimulation of CCL3 or CXCL12 -----   | 212 |
| Figure 4.23. Structure of dynamin. -----   | 217 |

## **Chapter 5:**

|   |     |
|---|-----|
| Figure 5.1. CCL3-induced Ca <sup>2+</sup> response was reduced when treated with PrKD inhibitors in both THP-1 and MCF-7 cells -----  | 229 |
| Figure 5.2. CXCL12-induced Ca <sup>2+</sup> response was reduced by the treatment of PrKD inhibitors in MCF-7 cells, but an opposing effect was seen in THP-1 cells -----   | 231 |
| Figure 5.3. A significant reduction in the number of cells migrating towards CXCL12 was observed in Jurkat and THP-1 cells treated with PrKD inhibitors, CID755673 and CID2011756, in the chemotaxis assay-----                       | 233 |
| Figure 5.4. MCF-7 cells appear to be more elongated and spreading in the treatment of PrKD inhibitor, CID755673 or CID2011756, in the absence of chemokine stimulation -----  | 235 |
| Figure 5.5. PrKD inhibitors, CID755673 and CID2011756, induce a significant increase in cell surface area and a significant reduction in cell circularity, similar to the effects of CCL3 and CXCL12 stimulation in MCF-7 cells ----- | 236 |
| Figure 5.6. Signalling mechanisms in the regulation of actin cytoskeleton network -----   | 238 |

|   |     |
|---|-----|
| Figure 5.7. ROCK inhibitor, Y27632, induces ruffling and clustering of F-actin, while Arp2/3 inhibitor, CK666, abolishes the elongated morphology seen in both CCL3-stimulated and CXCL12-stimulated MCF-7 cells -----          | 240 |
| Figure 5.8. The effects of increased cell surface area and decreased circularity mediated by chemokine stimulation are abolished by the treatment of ROCK inhibitor, Y27632, and Arp2/3 inhibitor, CK666 in MCF-7 cells -----   | 241 |
| Figure 5.9. Ruffling and clustering of F-actin is still seen in MCF-7 cells treated with Y27632 in addition of PrKD inhibitor -----   | 243 |
| Figure 5.10. Combined treatment of Y27632 and PrKD inhibitor, CID755673 or CID2011756, induces increase in cell area and reduction in cell circularity with or without CCL3 or CXCL12 stimulation in MCF-7 cells -----          | 244 |
| Figure 5.11. A combination of Arp2/3 inhibitor, CK666, and PrKD inhibitor, CID755673 or CID2011756, induces elongated morphology but no observable change in cell surface area following chemokine stimulation in MCF-7 cells - | 246 |
| Figure 5.12. Combined treatment of CK666 and PrKD inhibitor, CID755673 or CID2011756, induces reduction in cell circularity but no change in cell surface area with or without chemokine stimulation in MCF-7 cells-----        | 247 |
| Figure 5.13. PrKD inhibitors had no significant effect on CCL3-induced CCR5 internalisation in MCF-7 cells-----   | 249 |
| Figure 5.14. PrKD inhibitors had no significant effect on CXCL12-induced CXCR4 internalisation in MCF-7 cells-----  | 250 |
| Figure 5.15. PrKD inhibitors had no significant effect on CXCL12-induced CXCR4 internalisation in Jurkat cells-----   | 252 |
| Figure 5.16. Chemically transfected MCF-7 cells for PrKD2 knockout (PrKD2 KO) experiments-----  | 255 |
| Figure 5.17. Reduction in endosomal acidity following CXCL12 stimulation is not affected by PrKD2 knockdown in MCF-7 cells -----  | 258 |
| Figure 5.18. Chemical structure and biochemical activity of PrKD inhibitors used in our study-----  | 260 |
| Figure 5.19. Signalling mechanisms in the regulation of cytoskeleton dynamics in migrating cells-----   | 265 |

|   |     |
|---|-----|
| Figure 5.20. Signalling pathway of cortactin/WASP/ARP2/3 in the regulation of actin cytoskeletal rearrangement----- | 267 |
|---|-----|

## Chapter 6:

|  |     |
|--|-----|
| Figure 6.1. Key downstream signalling transducers involved in the stimulation of $G\alpha_s$ , $G\alpha_i$ , $G\alpha_q$ and $G\beta\gamma$ proteins ----- | 276 |
| Figure 6.2. Revised version of bridge chemotaxis chamber (Insall)-----   | 281 |

## Appendices:

|  |     |
|--|-----|
| Figure A1. Protein synthesis inhibitor, cycloheximide, is toxic in MCF-7 and Jurkat cells following 72 hours incubation while the trend of toxicity following 24 hours incubation is less significant -----                            | 322 |
| Figure A2. Caveolae-blocking agents, filipin and nystatin, have no toxicity in MCF-7 and Jurkat cell -----   | 323 |
| Figure A3. Clathrin inhibitor, pitstop 2, and negative control for pitstop 2 (pitstop 2 negative) have no toxicity in MCF-7 and Jurkat cell -----  | 325 |
| Figure A4. Dyn-2 inhibitors, Dyngo-4a and Dynasore have no toxicity in MCF-7 and Jurkat cell-----  | 326 |
| Figure A5. PrKD inhibitor, CID755673, is toxic in MCF-7 cells at 20 $\mu$ M with a trend of toxicity at lower concentrations, while no toxicity was observed in MDA-MB-231 cells across all tested concentrations -----                | 327 |
| Figure A6. PrKD inhibitor, CID755673, is not toxic at 10 $\mu$ M in THP-1 and Jurkat cells -----   | 328 |
| Figure A7. PrKD inhibitor, CID2011756, is toxic in MCF-7 and MDA-MB-231 cells at 20 $\mu$ M with a trend of toxicity at lower concentrations, while no toxicity was observed in MDA-MB-231 cells across all tested concentrations----- | 329 |
| Figure A8. PrKD inhibitor, CID2011756, is toxic in MCF-7 cells at high concentrations, while the toxicity at 1 $\mu$ M is minimal -----  | 330 |
| Figure A9. PrKD inhibitor, CID2011756, is toxic in MDA-MB-231 cells at high concentrations, while the toxicity at 1 $\mu$ M is minimal -----   | 331 |
| Figure A10. ROCK inhibitor, Y27632, is not toxic in MCF-7 cells-----   | 332 |

Figure A11. Arp2/3 inhibitor, CK666, is not toxic in MCF-7 cells ----- 333

Figure A12. Two sets of combinations of inhibitors, CK666 and PrKD inhibitor (CID755673 or CID2011756), and Y27632 and PrKD inhibitor are not toxic in MCF-7 cells ----- 334

# Statement of Special Circumstances

---

This PhD research was conducted during a period affected by the COVID-19 Pandemic. Some of the studies and collaboration work might have been disrupted due to travel restrictions and limited access to facilities.

# Publications

---

Lai, W.Y., Mueller, A., 2021. Latest update on chemokine receptors as therapeutic targets. *Biochemical Society Transactions* 49, 1385–1395. <https://doi.org/10.1042/BST20201114>

# Acknowledgements

---

I would like to thank my Ph.D. supervisor, Prof Anja Mueller, for her continuous support, encouragement and guidance during my research. Additionally, I would like to thank my secondary supervisor, Prof Maria O'Connell for her knowledge and advice. I would also like to thank Dr Leanne Stokes for her technical support by kindly providing me training on flow cytometry during my research. Likewise thanks to UEA for providing me a scholarship to support my progress to Ph.D. after the completion of MPharm.

I would like to thank all my colleagues who have helped and supported me throughout these years of research: Dr Isabel Hamshaw, Dr Enana Alassaf, Dr Gerald Keil, Dr Nursabah Atli and Emily Hobson. Special thanks to Dr Isabel Hamshaw for her time and effort to proofread my thesis and provide me lots of helpful feedback, as well as her assistance with experiments. Another sincere thanks to Dr Enana Alassaf for kindly training me in all the techniques and helping me settle into the lab when I first started my Ph.D.

I would particularly like to acknowledge Dr Rosemary Davidson and Dr Orla Jupp for providing me a valuable opportunity to work as part of Norwich Testing Initiative during the SARS-CoV-2 pandemic. I would like to express my gratitude to all my colleagues: Dr Janine Wilkinson, Dr Matthew Felgate, Sarah Gardner and other colleagues in the Microbiology Department at NNUH for all their support, training and assistance. Additionally, I would like to acknowledge Prof Andrew Page for offering me a three-month internship on SARS-CoV-2 sequencing at QIB. My sincere thanks go to my colleagues: Dr Alex Trotter, Darcie Burgess, Rebecca Sutcliffe, Ana Martinez Gascuena, Dr Nabil-Fareed Alikhan, Michaela Matthews and David Baker, for teaching me advanced techniques and knowledge on bioinformatics during the time in my internship. I would also like to acknowledge Dr James Smith and Terri Holmes for kindly providing me lab shadowing and giving me an overview of stem cell research.

Finally, I would like to say a special thank you to my family, not only for their financial support but also for their unconditional love, companionship and care.

To my grandmother in heaven, thank you for your selfless love, thank you for being my life model and mentor, teaching me how resilience is like. Now I have taken a step forward to my promise I made with you. Although it is still a long way to go, I will strive to continue my contribution of cancer research.

# Chapter 1: Introduction

---

## 1.1 Cancer and chemokine signalling system

Cancer metastasis refers to the spread of cancer cells from a primary site to distal secondary sites, contributing to the major cause of death in most cancer patients. Over the last decade, cancer has been well defined in terms of the typical biological capabilities acquired in the development of human tumours, known as hallmarks of cancer (Hanahan and Weinberg, 2011). In addition to cancer cells themselves, within the tumour microenvironment, a repertoire of normal cells also takes part in contributing to foster the hallmark functions (Hanahan and Weinberg, 2011). The addition of complexity implies that cell-cell communication between normal and cancer cells is the key to study the development of cancer from benign stage to metastatic stage. (Hanahan and Weinberg, 2011).

In the past decades, emerging studies revealed that chemokine signalling plays important roles in modulating immune surveillance and cell migration in tumour development, representing as a potential therapeutic target for cancer (Balkwill, 2004). Within tumour microenvironment, crosstalk between stromal cells and cancer cells in the form of an array of different chemokines dictates the process of tumorigenesis and metastasis (Balkwill, 2004; Mollica Poeta et al., 2019). The altered expression of chemokines and their cognate receptors in cancer contributes to a diversity of pathophysiological responses, including cancer cell proliferation, angiogenesis and leukocyte recruitment (Mollica Poeta et al., 2019). Yet, the complex mechanisms underlying the chemokine signalling in cancer remains to be elucidated in depth. The aspects to be further investigated include biased signalling, signalling redundancy, receptor desensitisation and co-expression of atypical chemokine receptors (ACKRs) (Drouillard et al., 2023).

In the approach of conventional anti-cancer therapies, the mechanism of action generally works on interfering with cell cycle, leading to cell death involving normal cells (Bates and Eastman, 2017). This implicates that a vast majority of patients on conventional chemotherapy experience numerous unwanted adverse effects. By understanding the distinct complexity in chemokine signalling pathways employed by different cancer cells, cancer-specific signalling proteins

or signalling axes in chemokine pathway can be targeted in the design of new anti-cancer drug. Novel strategies can potentially be implemented in combination with chemotherapy or immune checkpoint inhibitors (ICIs) to potentiate the therapeutic efficacy whilst minimise adverse effects.

### **1.1.1 Cancer invasion and metastasis**

Cancer invasion is a cell-driven process initiated by signalling pathways that regulates cytoskeleton dynamics driving cell migration into the adjacent tissue in cancer (Friedl and Alexander, 2011). There are two modes of cancer cell migration proposed by previous studies: amoeboid migration and mesenchymal migration (**Figure 1.1**). Amoeboid migration is referred to cells adopting morphologically spherical shapes with weak adhesion force (Friedl et al., 2001). Amoeboid movement primarily adopts Rho-dominated actin rearrangement mechanism, generating propulsion by membrane blebbing. Cells utilising amoeboid movement tend to squeeze through tissue gaps without extracellular matrix (ECM) proteolysis involved during migration (Lorentzen et al., 2011; Wolf et al., 2003). Amoeboid cells are common to be seen in hematopoietic and neuroectodermal cancer, such as leukaemia and small cell lung carcinoma (Madsen and Sahai, 2010; Poincloux et al., 2011). On the other hand, mesenchymal migration is defined by cells adopting elongated or spindle-shaped morphology with strong focal adhesions and ECM proteolysis involved (Wolf et al., 2007). Several microtracks are usually generated by focalised proteases on the cell surface for cells to follow during migration (Wolf et al., 2007). The origin of mesenchymal migration is tumours of connective tissues. Yet, both movements are also observed in other tumour types as well (Brabletz et al., 2001; Wolf et al., 2007).

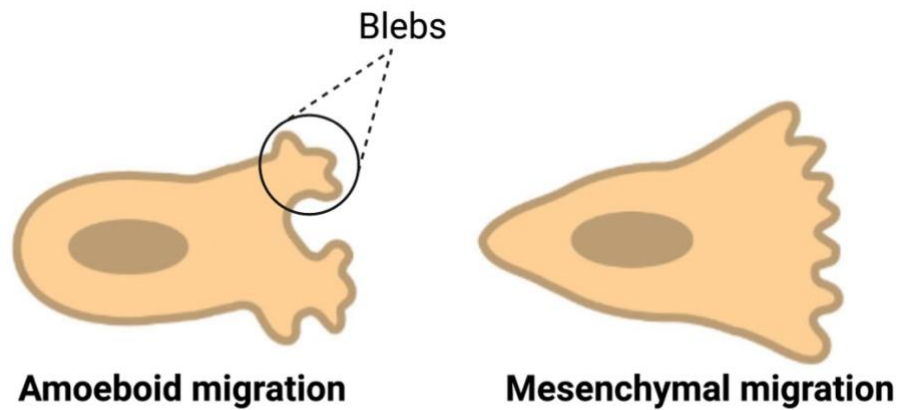


**Figure 1.1. Modes of cell migration adopted by cancer cells.** During cancer invasion and metastasis, cancer cells can migrate individually or collectively by adopting either amoeboid or mesenchymal morphology depending on the microenvironment at the tumour site. Amoeboid migration is featured with spherical cell morphology with the formation of membrane blebs. No extracellular matrix (ECM) degradation is occurred during the process. Mesenchymal migration is characterised as elongated cell morphology with strong focal adhesions. ECM proteolysis is involved (Image created with BioRender.com).

Cytoskeleton dynamics in migrating cells is primarily regulated by an actin-binding protein, cofilin, and a group of the Rho family GTPases involving RhoA, Rac1 and Cell division control protein 42 homolog (Cdc42) (**Figure 1.2**). During the process of cell migration, cofilin modulates actin filaments (F-actin) rearrangement by actin severing and nucleation, while Rho GTPases are involved in the organisation of F-actin in order to generate protrusions at the leading edge and retractions at the contractile tail (Hall, 1992). The three Rho GTPases have distinct roles and effects in cytoskeleton dynamics (Hall, 1992). Rac1 is involved in membrane ruffling associated with lamellipodia protrusions at the leading edge of migrating cells (Ridley et al., 1992). On the other hand, RhoA contributes to cytoskeletal contractility by the formation of stress fibres, driving the tail retraction in migrating cells (Chrzanowska-Wodnicka and Burridge, 1996). The dynamic pattern of Rac1/RhoA coordination is spatially and temporally regulated and plays an important role in cancer cell migration (Pertz et al., 2006).

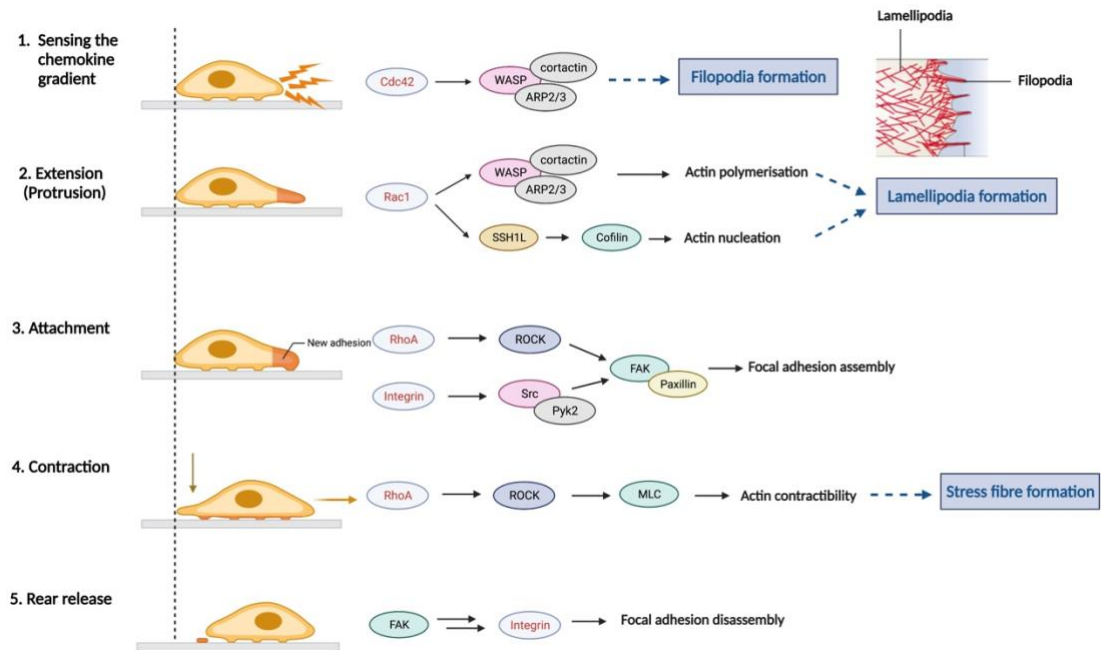


**Figure 1.2. Sequential events of cell migration in the regulation of cytoskeleton dynamics.** 1. Sensing of the chemokine gradient is dependent of Cdc42, which in turn activates the WASP/cortactin/Arp2/3 complex, to form filopodia at the leading edge (Mattila and Lappalainen, 2008). 2. Rac1 is the key player in mediating lamellipodia protrusions by activating an actin severing protein, cofilin, through dephosphorylation by SSH1L (Kligys et al., 2007). In the meanwhile, Rac1 also activates the WASP/cortactin/Arp2/3 complex, contributing to actin polymerisation (Mattila and Lappalainen, 2008). 3. Cell attachment at focal adhesions involves the activation of Focal Adhesion Kinase (FAK)/paxillin by RhoA/ROCK and integrin/Src/Pyk2 (Narumiya et al., 2009). 4. Contraction at the rear of the cell body generates forward progression. RhoA/ROCK plays a critical role in actin contractibility and stress fibre formation through the activation of MLC (Narumiya et al., 2009). 5. The rear of the cell body is released by traction forces through focal adhesion disassembly (Narumiya et al., 2009) (Image created with BioRender.com).

(Abbreviations definitions: Arp2/3- Actin Related Protein 2/3 complex; Cdc42- Cell division control protein 42 homolog; FAK- Focal Adhesion Kinase; MLC- Myosin Light Chain; ROCK- Rho-associated protein kinase; SSH1L- Slingshot-1L; WASP- Wiskott-Aldrich Syndrome Protein)

With regards to the mechanisms underlying the Rho GTPases regulate cytoskeleton dynamics, they generally function as molecular switches and

interact with downstream effectors to propagate signalling transduction. The downstream target of RhoA is Rho-associated kinase (ROCK) (Narumiya et al., 2009). ROCK is a kinase that directly phosphorylates actin cytoskeleton regulators, including myosin light chain (MLC) (Narumiya et al., 2009) and LIM kinase (LIMK) (Maekawa et al., 1999). Phosphorylation of MLC contributes to the contractility. The antiparallel contractile structures at the tail of migrating cells are implicated by RhoA-activated MLC on actin filaments (F-actin) (Riento and Ridley, 2003).

In the meantime, phosphorylation of LIMK is associated with the phosphorylation of ADF/cofilin (Lin et al., 2003). Phosphorylation of cofilin by LIMK prevents cofilin from actin binding by the formation of an intramolecular ionic bridge blocking the actin binding interface (Bernstein and Bamburg, 2010). Consequently, phosphorylated inactive cofilin is unable to mediate actin severing and nucleation at the tail of migrating cells, favouring membrane contractility.

Cofilin-mediated severing of pre-existing F-actin is one of the important regulatory mechanisms in the protrusive dynamics at the leading edge of migrating cells (Bernstein and Bamburg, 2010; DesMarais et al., 2005). On the other hand, unphosphorylated active cofilin binds to Phosphatidylinositol 4,5-bisphosphate (PIP<sub>2</sub>) and cortactin, which sequester the activated cofilin together to interact with F-actin (Bernstein and Bamburg, 2010). Furthermore, LIMK is also a downstream target of Rac1 and Cdc42 through the activation of p21 activated kinase 1 (PAK1) (Edwards et al., 1999). However, in the meantime, Rac1 activates the slingshot-1L phosphatases (SSH1L), which dephosphorylate cofilin as a result of accumulation of unphosphorylated active cofilin (Kligys et al., 2007). Subsequently, active cofilin interacts with F-actin and mediates actin nucleation and severing (Huang et al., 2006). The effects of SSH1L override deactivation of cofilin by LIMK, which induces membrane protrusions at the leading edge of migrating cells. Furthermore, Rac1 and Cdc42 are also involved in activating Wiskott-Aldrich Syndrome family of proteins including Wiskott-Aldrich Syndrome Protein (WASP), neuronal Wiskott-Aldrich Syndrome Protein (N-WASP) and WAVE. WASP and N-WASP are directly activated by Rac1 and Cdc42 (Derivery and Gautreau, 2010; Symons et al., 1996), while WAVE is activated by Rac1 through an adaptor protein, IRSp53 (Ishiguro et al., 2004; Miki et al., 2000, 1998).

WASP, N-WASP and WAVE then form a complex with cortactin and Actin Related Protein 2/3 complex (Arp2/3), which contributes to actin polymerisation (Carlier et al., 2000). Overall, the combination of cofilin-mediated actin nucleation and actin polymerisation leads to branching and crosslinking of F-actin, contributing to membrane protrusions at the leading edge, also known as lamellipodia formation (Nakagawa et al., 2001; Oser and Condeelis, 2009).

Apart from lamellipodia formation, filopodia is also found protruding from the lamellipodial actin network (Svitkina et al., 2003). The formation of filopodia is regulated by Cdc42 through WASP/N-WASP, in which F-actin are protected from capping by multiple tip-complex proteins, including ENA/VASPs, Dia2 formin and myosin-X, and nucleated at filopodial tips by formins (Mattila and Lappalainen, 2008). Filopodia is thought to be important in cell migration towards the guidance of chemoattractants and adhesion on extracellular matrix (ECM) (Gupton and Gertler, 2007).

In the involvement of chemokine signalling, actin cytoskeleton dynamics is typically triggered by G $\alpha$ i-dependent signalling following chemokine stimulation. At the leading edge of migrating cells, G $\alpha$ i activates Cdc42, which in turn activates Arp2/3 complex, leading to filopodia formation (Gérard et al., 2007). Recent studies revealed that an alternative pathway independent of G $\alpha$ i is also involved in actin cytoskeleton reorganisation (Ambriz-Peña et al., 2014; Pérez-Rivero et al., 2013). It was found that Jak3 plays a major regulatory role in actin polymerisation in response to CCL21 or CXCL12 stimulation in T lymphocytes. Two main roles of Jak3 in actin polymerisation and lamellipodia formation were identified: (1) Jak3 directly activate Rac1 associated with the Arp2/3 complex contributing to actin polymerisation; (2) Jak3 activates SSH1L while inactivates LIMK1, which favours cofilin activation, driving actin severing and the formation of branched F-actin in the assembly of the actin network (Ambriz-Peña et al., 2014). At the opposite end of migrating cells, Jak3 and G $\alpha$ i are also involved in RhoA activation, resulting in actin contractility and the formation of stress fibres (Ambriz-Peña et al., 2014; Nimnual et al., 2003).

Numerous studies have been done to elucidate the effects of chemokines on actin rearrangement. Particularly in CXCL12/CXCR4 signalling, CXCL12 was

shown to have a dual action to promoting the formation of stress fibre for actin contractibility at contractile tail (Moyer et al., 2007). (1) CXCL12 mediates F-actin accumulation by activating cofilin through LIMK pathway (Maekawa et al., 1999; Nishita et al., 2002). (2) CXCL12 stimulates MLC phosphorylation via ROCK (Moyer et al., 2007). In addition, accumulating evidence revealed that heterotrimeric G protein and Janus kinases (JAKs) play an important role in regulating cofilin and Rac/Rho GTPases activation independently (Ambriz-Peña et al., 2014; Mueller and Strange, 2004). In response to chemokine stimulation,  $G_{\alpha i}$  is activated and JAK (JAK2 for CCL3 and JAK3 for CXCL12) is activated through G protein-independent pathway (Ambriz-Peña et al., 2014; Mueller and Strange, 2004). A combination of the effects of  $G_{\alpha i}$  and JAK results in a complementary activation of the Rac GTPase, which in turn leads to actin polymerisation at the leading edge for sensing the chemokine gradient (Ambriz-Peña et al., 2014). At the early stage, actin polymerisation involves  $G_{\alpha i}$  only, which activates Cdc42, associating with the WASP/Arp2/3 complex, resulting in the formation of filopodia. Later both  $G_{\alpha i}$  and Jak3 activate Rac, which mediates the formation of lamellipodia. In parallel, JAK is involved in cofilin inactivation through LIMK pathway, whereas  $G_{\alpha i}$  activate SSH1L, which inactivates LIMK, leading to cofilin activation. This process is crucial to maintain a balance of active and inactive forms of cofilin for cell migration (Ambriz-Peña et al., 2014).

In migrating cells, chemokine receptors were found to localise at the leading edge in response to the chemokine gradient formed by the interactions of glycosaminoglycan (GAG) and chemokines (Hoogewerf et al., 1997). Particularly for CXCL12/CXCR4 signalling, a recent structural study reported that CXCL12 binding and actin cytoskeleton is critical for CXCR4 nanoclustering at the leading edge. Chemokine receptor nanoclusters tend to adhere to the lipid bilayer of the plasma membrane where ICAM1/CXCL12 is embedded, triggering integrin activation (Martínez-Muñoz et al., 2018). Not only does chemokine stimulation directly affects actin rearrangement, but also it could enhance receptor nanoclustering that facilitates integrin activation for mesenchymal cell migration (Martínez-Muñoz et al., 2018).

### 1.1.2 Immune evasion in cancer

Immune evasion is defined by cancer cells hijacking the host immune system to suppress the activation and infiltration of immune cells into the tumour sites (Vinay et al., 2015). In recent years, immunotherapy, for example, anti-PD1, has been emerging as a frontline treatment in multiple cancers (Alsaab et al., 2017). In general, the mechanism of action of immunotherapy depends on T-cell activation and interactions with cancer cells within tumour microenvironment (TME) (Alsaab et al., 2017). Despite the huge success in therapeutic efficacy of immunotherapy, the interference of T cell-tumour immune response is a major causation to treatment resistance. Chemokine signalling is the key regulator in innate and adaptive immune responses. In respect of CXCR4 widely expressed in monocytes, macrophages, neutrophils, T- and B-lymphocytes, CXCL12/CXCR4 signalling possesses inducible effect hindering normal T-cell immune response to tumour, contributing to immunotherapy resistance (García-Cuesta et al., 2019). There are two ways that cause immunosuppression induced by CXCL12/CXCR4 signalling: (1) Cancer-associated fibroblasts (CAFs) sequester cytotoxic T lymphocytes (CTLs) through CXCL12 secretion, which in turn excludes the exposure of CTLs at tumour site (Öhlund et al., 2014) (Ene-Obong et al., 2013); (2) Upregulation of CXCL12 in TME triggers the recruitment of myeloid-derived suppressor cells (MDSCs), regulatory T cells ( $T_{reg}$ ) and M2 cells differentiated from monocytes towards tumour site (García-Cuesta et al., 2019; Gok Yavuz et al., 2019). The infiltration of immunocytes override and prohibit the normal T cell-tumour immune response. The process of immune evasion in cancer elicited by chemokine signalling has been discovered in multiple cancer types including metastatic breast cancer (J. Zhang et al., 2019) and gastric cancer (Lv et al., 2019) and colorectal cancer (Yu et al., 2019).

### 1.2 Chemokine classification and structure

Chemokines are defined as chemotactic cytokines that stimulate the directed migration of cells along a concentration gradient in a spatial and temporal manner (Griffith et al., 2014). Chemokines are low molecular weight proteins (8-30 kDa) featured with 1-3 disulfide bridges. A highly conserved tertiary structure of chemokine is comprised of a disordered N-terminus and N-loop, a triple-stranded anti-parallel  $\beta$  sheet and a folded  $\alpha$ -helix at the C-terminus (**Figure 1.3**) (Clöre

and Gronenborn, 1995). Together with the disulphide bridges, the overall topology is stabilised. In particular, the residues in the N-loop are important in receptor binding and the disordered N-terminus is the critical component in receptor activation (Miller and Mayo, 2017).

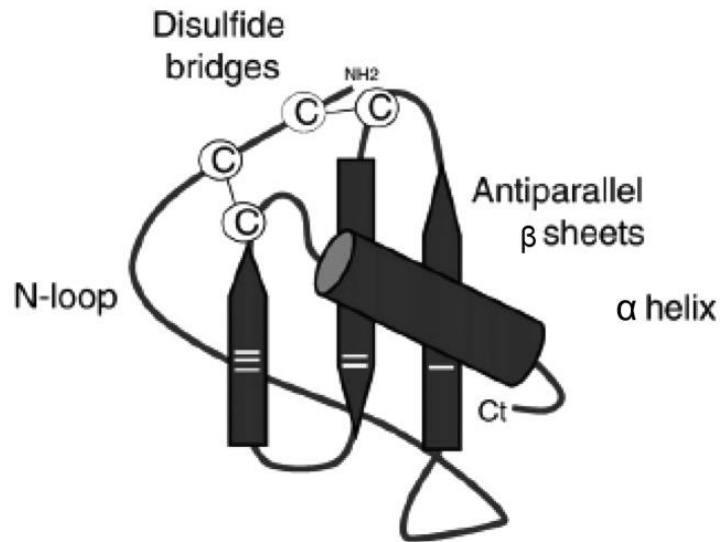


**Figure 1.3. Schematic diagram of the structure of chemokine.** Representation of a N-loop, a triple-stranded antiparallel  $\beta$  sheet and a folded  $\alpha$ -helix at the C-terminus. The structure is stabilised by multiple disulfide bridges between Cys residues (Image taken from Chew et al., 2013).

Despite the highly conserved structural fold, the quaternary structures are distinctive among subfamilies, contributing to functional interactions between chemokines, known as chemokine interactome (Miller and Mayo, 2017). Within the chemokine interactome, the formation of specific heterodimers differentially dictates functional activity involved in immunity potentially to be exploited for therapeutic targeting of pathogenic disorders (von Hundelshausen et al., 2017; D’Agostino et al., 2018).

To date, approximately 50 chemokines have been identified. Originally, chemokines are named by their structure and specific conditions where they express. For example, CXCL9 was named as “monokine induced by gamma interferon (MIG)” (Farber, 1990; Murphy et al., 2000). Through the advances in the discovery of chemokines, a system of nomenclature has been introduced to classify and name chemokine ligands and receptors. In general, they are subdivided into four subfamilies defined by the pattern of the sequentially conserved cysteine residues (C) and non-cysteine residues represented by X in the N-terminus: C, CC, CXC and CX<sub>3</sub>C (**Figure 1.4**) (Zlotnik and Yoshie, 2000). In addition to the classification of these subfamilies, the CXC chemokines are

divided by the presence or absence of an N-terminal tripeptide Glu-Leu-Arg (ELR) motif. In humans, there are seven ELR<sup>+</sup>CXC chemokines (CXCL1, CXCL2, CXCL3, CXCL5, CXCL6, CXCL7, and CXCL8). All of these are the ligands of CXCR2, yet only CXCL6 and CXCL8 are the ligands of CXCR1. ELR<sup>+</sup>CXC chemokines possess the ability to recruit neutrophils specifically, whereas ELR<sup>-</sup>CXC chemokines induces the migration of lymphocytes (Hébert et al., 1991).

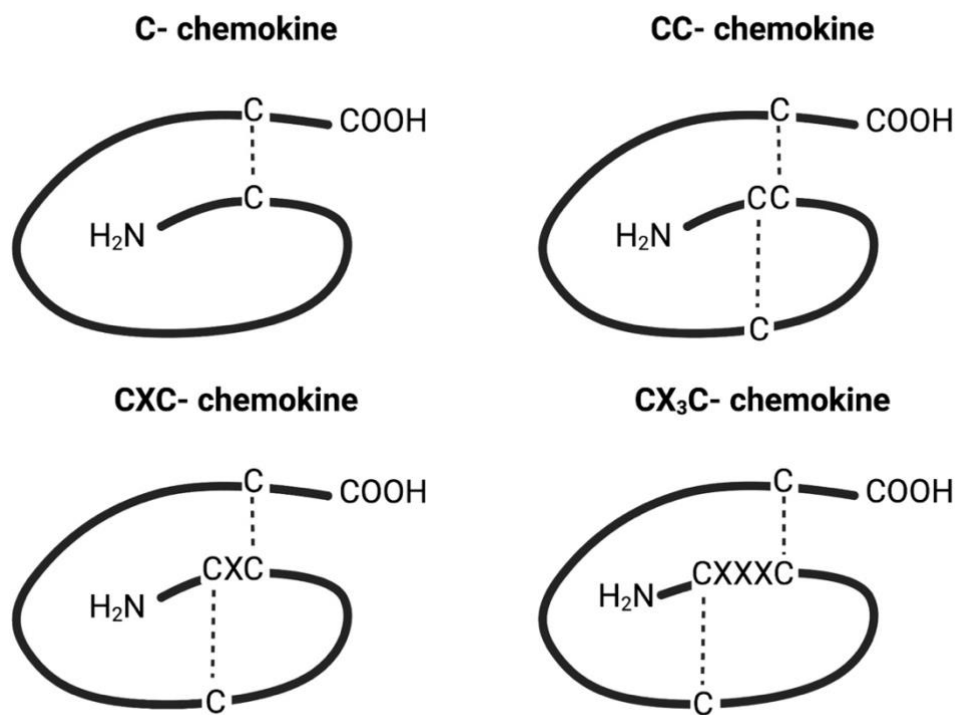


**Figure 1.4. Simplified representation of sequential patterns of the four chemokine subfamilies: C-, CC-, CXC- and CX<sub>3</sub>C- chemokines.** A nomenclatural system based on the pattern of the conserved Cys residues annotated by “C” and non-Cys residues annotated by “X” in the N-terminus. The disulfide bonds between Cys residues are represented by dash lines (Adapted from de Munnik et al., 2015) (Image created with BioRender.com).

In the field of chemokine study, chemokines are typically classified into two main groups based on their functions: homeostatic and inflammatory chemokines. In normal conditions, constitutively expressed homeostatic chemokines, such as CCL19, CCL20 and CCL21, are involved in regulating lymphocyte and dendritic cell trafficking in immune surveillance. In pathological conditions, inflammatory chemokines, such as CCL3, CCL4 and CXCL8, are typically induced by pro-

inflammatory stimuli and promote innate and adaptive immune responses in inflammation (Murphy et al., 2000; Le et al., 2004).

As listed in **Table 1.1**, multiple chemokines can activate the same chemokine receptor and majority of chemokines can bind multiple chemokine receptors (Balkwill, 2004; Allen et al., 2007). As supported by numerous evidence, chemokine signalling is associated with a range of cancer types (Balkwill, 2004; Allen et al., 2007). Understanding the mechanisms and functional consequences of the redundancy could possibly be useful for modulating and fine-tuning the chemokine signalling in cancer as a novel therapeutic strategy.

**Table 1.1. List of chemokine receptors and their cognate ligands.** Chemokine receptors are classified into two categories: inflammatory and homeostasis, based on their functional roles. Each chemokine/chemokine receptor pair is associated with a range of cancer types (Adapted from Allen et al., 2007)

| Chemokine receptors | Cognate ligands  | Chemokine receptor types     | Associated sites of cancer  |
|---------------------|--|------------------------------|---|
| CCR1                | CCL3 (MIP-1 $\alpha$ ), CCL5 (RANTES), CCL7 (MCP-3), CCL13 (MCP-4), CCL14 (HCC-1), CCL15 (Lkn-1/HCC-2), CCL16 (HCC-4), CCL23 (MPIF-1)                            | Inflammatory                 | Breast, blood, colon/ stomach   |
| CCR2                | CCL2 (MCP-1), CCL7 (MCP-3), CCL8 (MCP-2), CCL13 (MCP-4), CCL16 (HCC-4)   | Inflammatory                 | Breast, pancreas, ovary/prostate, liver                                 |
| CCR3                | CCL5 (RANTES), CCL7 (MCP-3), CCL8 (MCP-2), CCL11 (eotaxin), CCL13 (MCP-4), CCL15 (Lkn-1/HCC-2), CCL16 (HCC-4), CCL24 (eotaxin-2), CCL26 (eotaxin-3), CCL28 (MEC) | Inflammatory                 | Breast, prostate, liver, skin, blood                                    |
| CCR4                | CCL17 (TARC), CCL22 (MDC)  | Inflammatory                 | Kidney, skin, blood, colon/ stomach, lungs                              |
| CCR5                | CCL3(MIP-1 $\alpha$ ), CCL4 (MIP-1 $\beta$ ), CCL5(RANTES), CCL8 (MCP-2), CCL11 (eotaxin), CCL14 (HCC-1), CCL16 (HCC-4)  | Inflammatory                 | colon/ stomach  |
| CCR6                | CCL20 (LARC)   | Inflammatory                 | Breast, colon/stomach, ovaries/prostate, lungs                          |
| CCR7                | CCL19 (ELC), CCL21 (SLC)   | Homeostatic                  | ovary/prostate, blood, colon/ stomach                                   |
| CCR8                | CCL1 (I309)  | Inflammatory                 | Breast, colon, lungs  |
| CCR9                | CCL25 (TECK)   | Inflammatory and homeostatic | Breast, colon, skin, blood, ovaries, lungs, liver                       |
| CCR10               | CCL27 (eskine/CTACK), CCL28 (MEC)  | Homeostatic                  | Breast, lungs, skin   |
| CXCR1               | CXCL6(GCP-2), CXCL7 (NAP-2), CXCL8 (IL-8)  | Inflammatory                 | Breast, lungs, skin   |
| CXCR2               | CXCL1 (GRO $\alpha$ ), CXCL2 (GRO $\beta$ ), CXCL3 (GRO $\gamma$ ), CXCL5(ENA78), CXCL6 (GCP-2), CXCL7 (NAP-2), CXCL8 (IL-8)                                     | Inflammatory                 | Breast, pancreas, ovaries/prostate, skin, colon/ stomach                |
| CXCR3-A             | CXCL9 (MIG), CXCL10 (IP10), CXCL11(I-TAC)  | Inflammatory                 | Breast, prostate, skin blood  |
| CXCR3-B             | CXCL4 (platelet factor 4), CXCL9 (MIG), CXCL10 (IP10), CXCL11(I-TAC)   | Inflammatory                 |   |
| CXCR4               | CXCL12 (SDF-1)   | Inflammatory and homeostatic | Breast, brain, pancreas, ovaries/prostate, blood, colon/ stomach, lungs |
| CXCR5               | CXCL13 (BLC)   | Homeostatic                  | Ovaries/prostate, skin, blood   |
| ACKR3 (CXCR7)       | CXCL12 (SDF-1)   | Inflammatory and homeostatic | Brain   |

### 1.2.1 Chemokine homodimers

Most chemokines primarily appear to be dimers, but some are observed to form tetramers, like CXCL4 (Mayo et al., 1995), or even high-order structures, such as CCL5 (Wang et al., 2011) and CCL27 (Jansma et al., 2010). The dimer structures of chemokines vary among different subfamilies but are in common within each sub-family (**Figure 1.5**). For the CC-motif chemokines, dimers are formed by the contact between the N-terminal  $\beta$ -strands from each monomer with the two C-terminal helices in different orientations on the opposite side. On the other hand, CXC-motif dimer is formed by the contact between  $\beta$ 1 strands from each monomer. By combining, the triple-stranded anti-parallel  $\beta$ -sheet from one monomer is extended to six-stranded with the two antiparallel C-terminal  $\alpha$ -helices on top of each side (Miller and Mayo, 2017). Exclusively for CXCL4, which associates to form a tetramer instead, the  $\beta$ -sheets are interacted laterally on top of each other as the centre of the tetramer structure (Mayo et al., 1995).

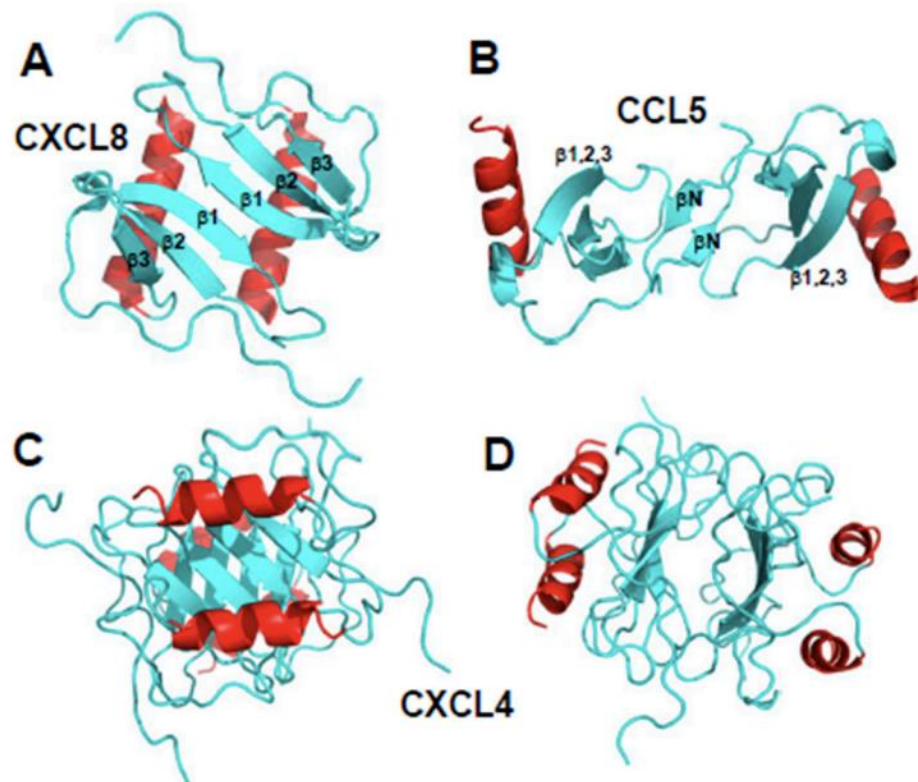


**Figure 1.5. Three-dimensional diagrams representing structures of chemokine dimers.** A: CXCL8, an example of CXC- chemokines. CXC- motif dimer is featured with the interactions between  $\beta 1$  strands from each monomer. B: CCL5, an example of CC- chemokines. CC- motif dimer is featured with the interactions between N-terminal  $\beta$ -strands from each monomer. C, D: CXCL4 tetramer. CXCL4 exclusively forms tetramer that could exist in either of the two orientations as shown (Image taken from Miller and Mayo, 2017).

With respect to the functional aspects of signalling induced by chemokine homodimers, different cellular responses from homodimers were observed compared to monomers. Using CXCL12/CXCR4 pair as an example, monomeric CXCL12 promotes cell migration and stimulates filamentous actin (F-actin) accumulation through the recruitment of  $\beta$ -arrestin-2, whereas dimeric CXCL12 exerts the opposite effects. The study demonstrates that dimerisation causes the loss of specific contacts of CXCL12 monomers with CXCR4 illustrated by NMR analyses (Drury et al., 2011). The finding implies that dimeric CXCL12 could potentially inhibit CXCR4-mediated metastasis. Understanding the functional

roles and precise signalling of chemokine monomers/dimers opens a new avenue for targeted anti-cancer therapeutic strategies.

### **1.2.2 Chemokine heterodimers**

Relative to homodimers, emerging studies demonstrate that the formation of heterodimers is energetically favourable, which could alter intracellular responses in chemokine signalling. CCL3/CCL4 (also known as MIP-1 $\alpha$ /MIP-1  $\beta$ ) was the first discovered heterodimer naturally produced by activated monocytes and peripheral blood lymphocytes (PBLs). With regards to the functionality of heterodimers, heterodimers typically stabilise the activity of chemokines, subsequently, inducing downregulation of their cognate receptor, CCR5 (Guan et al., 2001). By further investigations into the formation of possible heterodimers in cells, a structural study demonstrate the existence of a range of combinations of chemokine heterodimers: CXC-chemokine pairs (CXCL4/ CXCL1, CXCL4/CXCL7, and CXCL4/CXCL8), CC-chemokine pairs (CCL2/CCL5 and CCL2/CCL8), and mixed chemokine pairs (CXCL4/CCL5, CCL2/CXCL4 and CCL2/CXCL8) (Nesmelova et al., 2008). With regards to the mixed chemokine pairs (**Figure 1.6**), CC-type could be energetically favoured than CXC-type, or vice versa, based on the molecular mechanics and the Poisson-Boltzmann surface area analysis. For example, in the case of CCL5/CXCL4, CC-type is greatly favoured over CXC-type.

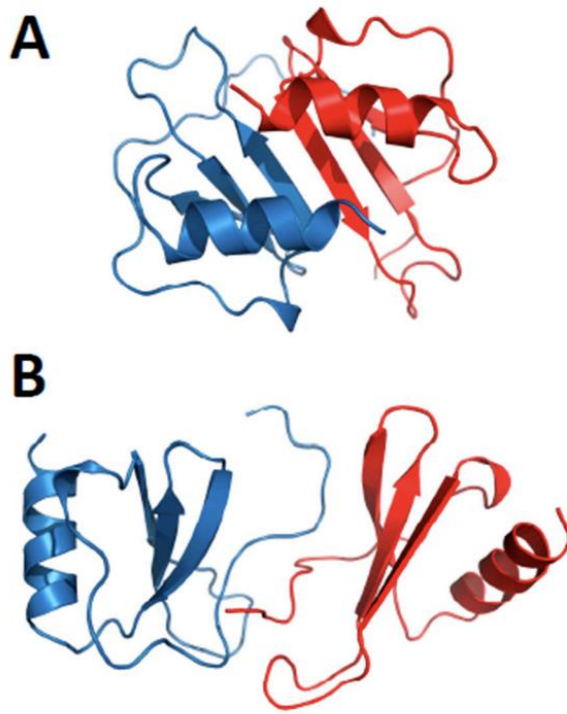


**Figure 1.6. Three-dimensional diagrams representing structures of CXCL4/CCL5 heterodimers.** As an example of mixed chemokine heterodimers (CXC- and CC-), there are two distinct orientations existing, known as CXC-type and CC-type. One orientation is energetically favoured than the other. A: Docking of CXC-type orientation; B: Docking of CC-type orientation, which is highly energetically favoured over the CXC-type (Image taken from Miller and Mayo, 2017).

Following the discovery of chemokine in dimeric forms as described above, chemokine synergism has been proposed by pioneering studies. Chemokine synergism is defined as potentiating chemokine signalling by the formation of heterocomplex from multiple chemokines interacting with a selective chemokine receptor (Proudfoot and Ugucioni, 2016).

The formation of heterocomplex could enhance leukocyte migration, exemplified by the complexes of CXCL13/CCL19 and CXCL13/CCL21 triggering CCR7 signalling (Paoletti et al., 2005). Another example demonstrates that CCL19 or CCL21 could prevent the degradation of CCL2 and CCL7 to enhance the migratory activity from CCR2 signalling in monocyte trafficking (Kuscher et al., 2009).

### **1.2.3 Interaction of chemokines with glycosaminoglycans (GAGs)**

Glycosaminoglycans (GAGs) are carbohydrate structures composed of repeating disaccharide units that are heterogenous in composition and length. They are usually found on cell surface and possess unique sulfation patterns which are cell-type specific and tightly regulated spatially and temporally (Handel et al., 2005; Raman et al., 2005).

In the interactions with chemokines, binding specificity and selectivity between chemokines and GAGs are observed, where the binding affinity of chemokines for GAGs is dependent on the classes of GAG and their sulfation patterns (Witt and Lander, 1994; Proudfoot et al., 2001; Rek et al., 2009). Typically, the highly negative-charged GAGs bind positive-charged residues in highly basic chemokines through non-specific electrostatic interactions, as demonstrated in chemokines, such as CCL2 (Seo et al., 2013), CCL5 (Shaw et al., 2004) and CCL11 (Ellyard et al., 2007). However, other interactions of GAGs, such as van der Waals' forces and hydrogen bonds, are also exemplified by binding of some acidic chemokines, including CCL3 and CCL4 (Johnson et al., 2005; Proudfoot et al., 2003).

In addition, it has been demonstrated that chemokine oligomerisation enhances the binding affinity for GAGs. For example, CXCL12 dimer with a disulfide bridge has a higher binding affinity compared to wild-type CXCL12, which exists as a mixture of monomers and dimers in equilibrium (Dyer et al., 2016). Furthermore, GAG-chemokine interactions also contribute to chemokine function. GAG binding of CXCL12 was found to be necessary to prevent the fusion of human immunodeficiency virus (HIV) in leukocytes (Valenzuela-Fernández et al., 2001).

In terms of the roles of GAGs in chemotaxis, it was demonstrated that GAG-chemokine interactions are necessary to establish and maintain cell surface chemokine concentration gradient for directional cell migration, instead of random movements (Proudfoot et al., 2003). However, some controversial findings showed that GAGs binding could reduce chemotactic activity. The contrary can be explained by alternative roles of GAGs in modulating intracellular signalling. A recent study revealed that GAG-bound CXCL12 interacts with sulfotyrosines in the N-terminal region of CXCR4 in high affinity. GAGs prevent the interaction

between CXCL12 and CXCR4, resulting in “non-productive” binding and subsequently reducing intracellular signalling necessary for chemotaxis (Connell et al., 2016). Similar effects were seen in other chemokines, including CCL21 (Hjortø et al., 2016), CXCL1 (Sawant et al., 2016), CXCL5 (Sepuru et al., 2016) and CXCL8 (Webb et al., 1993).

### **1.3 Chemokine receptor structure and classification**

Chemokine receptors are classified in the rhodopsin-like family (Family A) of G-protein coupled receptors (GPCR), identified as seven transmembrane receptors coupled to a trimeric GTP-binding protein (G-protein). In humans, 20 chemokine receptors and 50 chemokines have been identified (Balkwill, 2004). Most chemokine receptors bind multiple chemokines, or vice versa as mentioned previously (**Table 1.1**). The promiscuity of interactions among chemokines and their cognate receptors generates a diversity of signalling pathways and cellular responses (Balkwill, 2004; Richmond and Fan, 2004).

The structure of chemokine receptor is composed of an extracellular acidic N-terminus, seven transmembrane  $\alpha$ -helices connected by three extracellular loops (ECLs) and three intracellular loops (ICLs), and a C-terminus in the cytoplasm (**Figure 1.7**). In the aspect of their functional roles, the N-terminal domain and second binding site in the ECLs are essential for the speciality of chemokine binding. The intracellular C-terminal domain with other motifs, for example, the DRYLAIV motif located between the second and third ICLs are important for G protein coupling in intracellular receptor signalling (Schwartz et al., 2006).

The superfamily is subdivided into four classes based on the binding motif of chemokine ligands: CC, CXC, CX3C and XC (Murphy et al., 2000). Apart from the conventional chemokine receptors, emerging studies have been investigating into a subfamily, named atypical chemokine receptors (ACKRs). The family of ACKRs consists of DARC (ACKR1), D6 (ACKR2), CXCR7 (ACKR3) and CCX-CKR (ACKR4). The major structural difference of ACKRs is the lack of the DRYLAIVVH motif constitutively present within the ICLs in the canonical chemokine receptors (Nibbs and Graham, 2013). Owing to this unique feature, ACKRs typically do not initiate G-protein dependent signalling in response to

chemokine stimulation, yet ACKRs bind chemokines with high affinity. Instead, ACKRs internalise with chemokines to direct their ligands for lysosomal degradation. This implies that ACKRs are the critical regulators of chemokine bioavailability and known as scavenger or decoy receptors working with the canonical chemokine receptors (Nibbs and Graham, 2013). As characterised by chemokine scavengers, ACKRs possess an immunosuppressive role in various inflammatory diseases and cancer (Nibbs and Graham, 2013; Gowhari Shabgah et al., 2022).

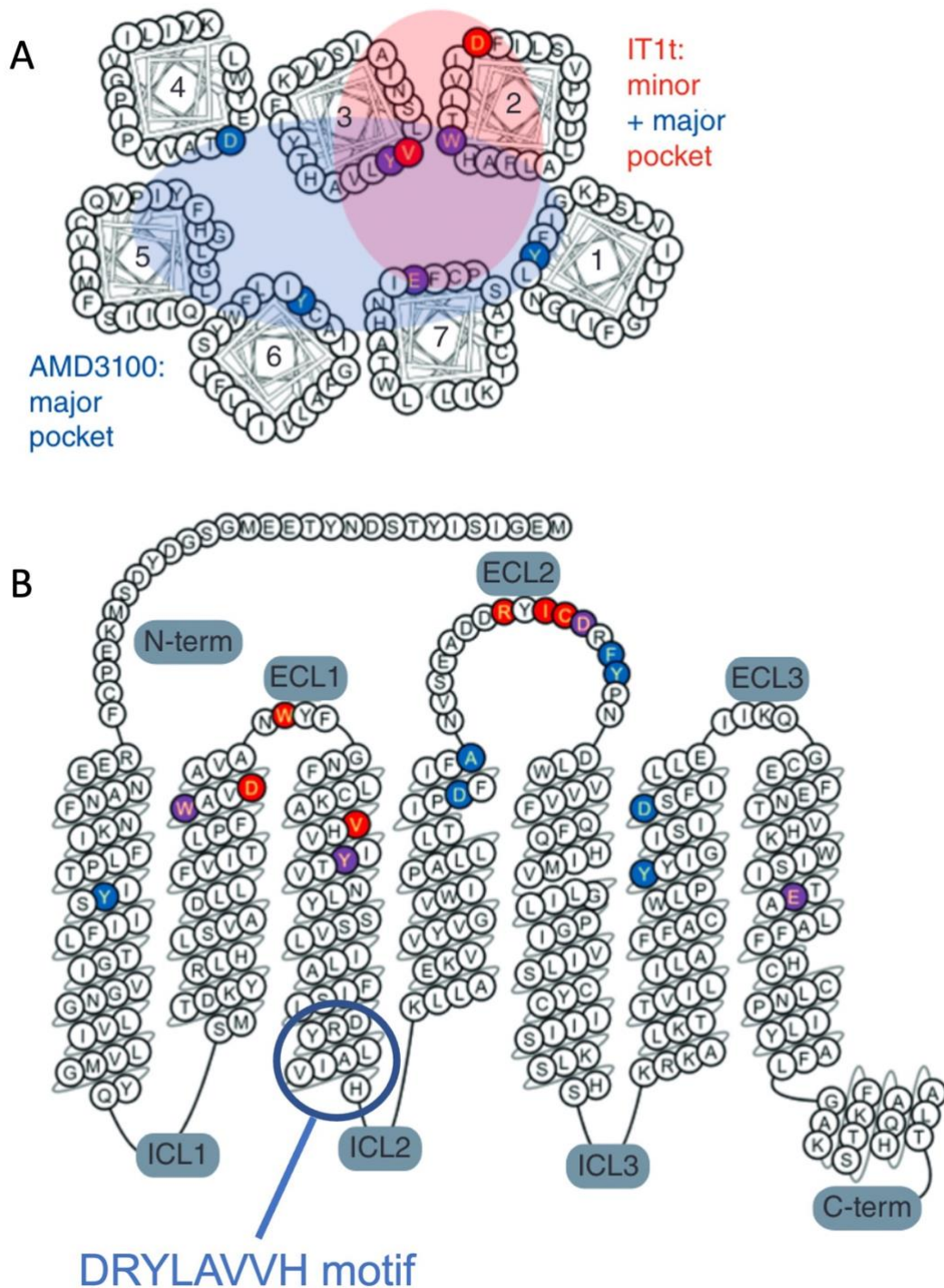


**Figure 1.7. Schematic two-dimensional diagrams of the structures of chemokine receptor.** A: from the top view on the extracellular side showing the upper halves of the 7TMDs with annotated key residues interacting with AMD3100 (highlighted in blue), IT1t (highlighted in red) and both inhibitors (highlighted in purple, major binding pocket (circled in shaded blue) and minor binding pocket (circled in shaded red)); B: from the side view showing the N-terminus, three ECLs, three ICLs and C-terminus with annotated key residues interacting with AMD3100 (highlighted in blue), IT1t (highlighted in

red) and both inhibitors (highlighted in purple, major binding pocket (circled in shaded blue) and minor binding pocket (circled in shaded red). The DRYLAIV motif located between the second and third ICLs is indicated (circled). Note that the DRYLAIV motif is absent in atypical chemokine receptors. (Image taken from Caspar et al., 2022).

### 1.3.1 Chemokine receptor activation

In the process of chemokine receptor activation, the interactions of chemokine and chemokine receptor was originally described by a two-step model (**Figure 1.8**), in which the N-terminus of chemokine receptor recognises the N-loop core of chemokine (Site 1), followed by the insertion of the disordered chemokine N-terminus into the transmembrane domain (TMD) of the chemokine receptor (Site 2) to activate the receptor (Rajagopalan and Rajarathnam, 2006). More details on receptor-chemokine interaction epitopes have been revealed by the crystal structures of chemokine receptors in complex with their associated ligands from recent studies. These new paradigms on chemokine receptor conformational selection model are emerging to replace the oversimplified two-step model. In general, three major receptor-chemokine interaction epitopes have been classified into chemokine recognition site 1 (CRS1), CRS1.5 and CRS2 (Figure 1.9). CRS1 is located at the N terminus of the receptor (residues P8-E18 for CCR5 as an example) where the N-loop, 40s-loop and  $\beta$ 2-strand of the chemokine is accommodated. CRS1.5 is where an anti-parallel  $\beta$ -sheet is formed between the receptors (residues P19-K22 for CCR5) and chemokines (residues T8-C11). CRS2 is where the N terminus,  $\beta$ 1-strand and 30s-loop of the chemokines penetrate into the ligand-binding pocket within the transmembrane helical bundle, in the contacts with the second extracellular loop (ECL2), third extracellular loop (ECL3) and helices I, II, III, V, VI and VII (Zhang et al., 2021). The binding modes are distinct in other receptor-chemokine complexes (Burg et al., 2015; Qin et al., 2015; Wasilko et al., 2020). The differences revealed from the crystal structures reflect the diversity of the binding of different chemokines, greatly expanding our knowledge on the complexity of chemokine recognition and receptor activation leading to distinct signalling transduction. In addition, It was demonstrated that post-translational modification (PTM) of chemokine receptors can enhance the binding affinity and specificity in chemokine recognition and binding (Kleist et al., 2016). For example, polysialylation of CCR7 is specifically

crucial for CCL21-mediated activation, which is shown to release CCL21 from an auto-inhibition conformation (Kiermaier et al., 2016). Evidence suggests that the two independent ligand-receptor binding sites from previous model are supposed to link each other. Specific motifs of the chemokine N-terminus have been shown to potentially modulate the crosstalk between sites 1 and 2 in receptor activation (Kleist et al., 2016). For example, in CXCL8, the GP motif of the ELR residues is an important regulator for the diversity of signalling pathways (Joseph et al., 2013).

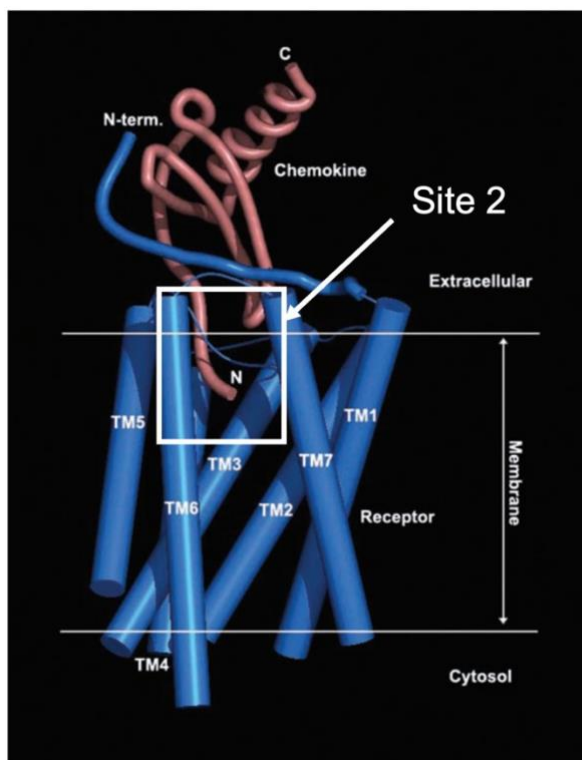


**Figure 1.8. Hypothetical three-dimensional model of chemokine docking on a chemokine receptor in the activation state.** Chemokine (coloured in pink) interacts with a chemokine receptor (coloured in blue) and activates the receptor through Site 2 (stated). In the process of receptor activation, two major interaction sites between chemokine and chemokine receptor are involved as proposed by the two-step model: Site 1 (not shown), between the N-terminus of chemokine receptor and the N-loop core of chemokine; Site 2 (as shown), between the N-terminus of chemokine and the TMD of the chemokine receptor (Image taken from Rajagopalan and Rajarathnam, 2006).

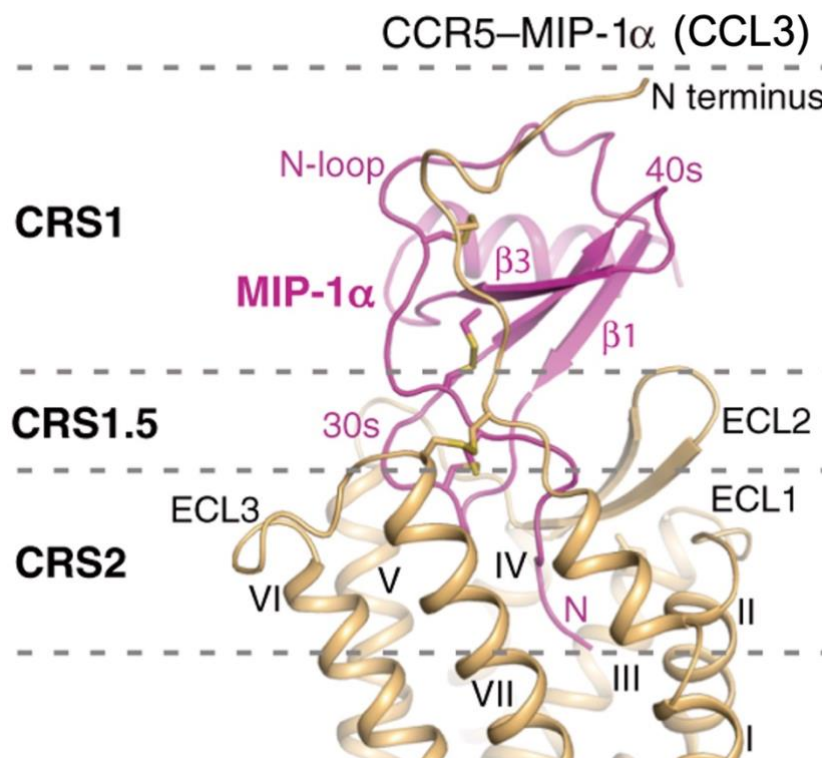


**Figure 1.9. Overall chemokine binding mode of receptor-chemokine (CCR5-CCL3) complex.** The chemokine (CCL3) is coloured magenta and the receptor (CCR5) is coloured in gold. The regions of CRS1, CRS1.5 and CRS2 are indicated by grey dashed lines. The key interacting components of the receptor and chemokine are annotated. (Image taken from Zhang et al., 2021).

### 1.3.2 Chemokine receptor dimerisation

Increasing evidence largely supports that Family A GPCRs exist as homodimers or heterodimers that modulate a variety of physiological and pathological functions linked to biased signalling (Cai et al., 2023). The binding interface between two GPCRs is found to be the transmembrane domain mainly, which is also known as the binding minor pocket (see **Figure 1.7**). The transmembrane domain is the key player in the formation and stability of GPCR dimers, as well as their functionality (Baltoumas et al., 2016). Owing to the ligand and functional selectivity observed in GPCR dimers exhibiting allosteric properties, compounds targeting the transmembrane domain at GPCR interface have emerging developed potentially to be highly selective therapeutic drugs.

Particularly in chemokine receptors, CXCR4 dimerisation have widely been investigated in the past decade, alongside with the development of several

compounds targeting the minor pocket of CXCR4, including LY251092, IT1t, and FC131 (Mona et al., 2016). It is revealed that CXCR4 dimerisation is dynamic dependent of receptor expression level. CXCR4 exists as a monomeric form at low expression and can form homodimers transiently as increasing expression level. CXCL12 stimulation induces CXCR4 dimerisation required for full G protein activation. Inverse agonists that bind minor pockets of CXCR4 were demonstrated to disrupt CXCR4 dimerisation and basal activity of G proteins (Işbilir et al., 2020). The effects of CXCR4 inverse agonists functioning as dimer-destabilising agents have been found clinically useful to reverse inflammation (Zirafi et al., 2015). More investigations can be done on the binding motifs of CXCR4 minor pocket in the development of efficacious CXCR4-targeting compounds for clinical uses. In relation to downstream signalling, CXCR4 homodimerisation was found to lead to G protein-independent signalling through JAK/STAT3 pathway that promotes chemotaxis (Ahr et al., 2005).

Apart from the formation of CXCR4 homodimers, it was unveiled that CXCR4 can form heterometric dimer with  $\alpha_{1A/B}$ -adrenergic receptors (AR), which plays an important regulatory role for vascular function and is a potential clinical target for blood pressure therapeutics. AR was shown to interact with the TM helix 2 of CXCR4 and subsequently potentiate  $Ca^{2+}$  mobilisation, myosin light chain (MLC) 2 phosphorylation, and contraction of vascular smooth cells (VMSCs) (Tripathi et al., 2015). In the aspect of clinical uses, a study demonstrated that co-treatment of CXCR4 agonists and the  $\alpha_1$ -AR agonist, phenylephrine, could enhance the potency of monotherapy of phenylephrine for increase in blood pressure (Tripathi et al., 2015). This provides an example of GPCR heteromerization for optimising pharmacological outcomes of existing therapeutics.

Another well-studied receptor, CCR5, was also revealed to form homodimers and heterodimers. Within a CCR5 homodimer, TM helices 1 and 4 are the critical binding interfaces between CCR5 receptors (Hernanz-Falcón et al., 2004). With respect to CCR5 heterodimers, a study demonstrated a negative binding cooperativity between CCR2 and CCR5, where CCR5 ligands block signalling through CCR2 while CCR2 ligands inhibit signalling through CCR5 (El-Asmar et al., 2005). This implies heterodimerisation of chemokine receptors could modulate competing signalling through both receptors, resulting in distinct

functional responses. Further work should be done on the functional roles of CCR5 dimerisation in clinical uses.

## **1.4 Chemokine signalling**

Without chemokine activation, chemokine receptors are constitutively coupled to a heterotrimeric GTP-binding protein (G protein) comprising of  $\alpha$ ,  $\beta$  and  $\gamma$  subunits (Rosenbaum et al., 2009). Upon chemokine ligand binding and activation, conformation change of chemokine receptor is induced, involving the exchange of GDP for a GTP in the  $\alpha$  subunit and dissociation of the GTP-bound  $\alpha$  subunit from  $\beta$  and  $\gamma$  G protein subunits. Subsequently  $G\alpha$  and  $G\beta\gamma$  separate from the receptor and transduce a diversity of downstream signalling accordingly (**Figure 1.10**) (Pierce et al., 2002; Rosenbaum et al., 2009).

### **1.4.1 G protein-dependent chemokine signalling**

Four different isoforms of  $G\alpha$  subunit ( $G\alpha_s$ ,  $G\alpha_i$ ,  $G\alpha_{q/11}$  and  $G_{12/13}$ ) are involved in activating different effector proteins, which may account for the divergent downstream signalling pathways and cellular responses (**Figure 1.10**) (Rosenbaum et al., 2009). Typically, the  $G\beta\gamma$  subunits activate phospholipase C  $\beta_2$  (PLC $\beta_2$ ), an enzyme which hydrolyses phosphatidylinositol 4,5-bisphosphate (PI(4,5)P $_2$ ) to produce inositol trisphosphate (Ins(1,4,5)P $_3$ , aka IP $_3$ ) and diacylglycerol (DAG). IP $_3$  translocates from the plasma membrane to mediate intracellular Ca $^{2+}$  release in the cytoplasm. DAG activates protein kinase C (PKC), which in turn phosphorylates various effector kinases in downstream signalling. It is noteworthy that the isotypes of PLC involved vary in different cell types, resulting in the activation of distinct signalling pathways (Stephens et al., 1994). This implies that differential cellular responses could be mediated even from the same chemokine receptor-ligand pair.

In parallel, like the  $G\beta\gamma$  subunits,  $G\alpha$  subunits are also involved in regulating multiple downstream signalling transducers that target a range of effector kinases, such as cAMP-dependent kinase (PKA) (Howe, 2011), protein kinase C (PKC) (Griner and Kazanietz, 2007), cGMP-dependent kinase (PKG), and calcium-calmodulin regulated kinases (CAMKs) (Prevarskaya et al., 2011).  $G\alpha_s$  stimulates adenylyl cyclase, inducing cyclic adenosine monophosphate (cAMP)

synthesis in the cytoplasm. cAMP in turn activates protein kinase A (PKA), which is an important regulator for multiple transcription factors in the nucleus. On the contrary,  $G\alpha_i$  inhibits adenylyl cyclase, reducing the cytosolic level of cAMP (Taussig et al., 1993).  $G\alpha_{q/11}$  subunit activates  $PLC\beta_2$ , inducing intracellular calcium ( $Ca^{2+}$ ) release and activation of PKC, like  $G\beta\gamma$  subunits (Hubbard and Hepler, 2006) (**Figure 1.10**).

Apart from the involvement in regulating second messengers in downstream signalling, G protein subunits also activate multiple mitogen activated protein kinase (MAPK) cascades involving a group of serine-threonine kinases, such as Extracellular signal-regulated kinases 1/2 (ERK1/2), p38MAPKs and c-Jun N-terminal kinase 1-3 (JNK1-3) (Gutkind, 1998). These kinases are critical regulators for several nuclear transcription factors, contributing to cell growth, proliferation and migration. The MAPK cascades are distinctively regulated by multiple GTPases from different subfamilies. ERK1/2 is regulated by Ras GTPase, whereas JNKs and p38MAPKs are regulated by GTPases of the Rho family, including Rho, Rac and Cdc42 (Coso et al., 1995) (**Figure 1.10**).

Specifically, receptor coupled to  $G\alpha_i$  subunit, in parallel with the interaction of  $G\beta\gamma$  subunits with Rac guanine exchange factors (GEFs), preferentially activates Rac GTPases, which in turn activates JNK (Rosenfeldt et al., 2004).  $G\alpha_q$ ,  $G\alpha_{12}$  and  $G\alpha_{13}$  also mediate the activation of Rac and Cdc42 GTPases to induce the JNK signalling cascade to regulate the activity of nuclear transcription factors (Coso et al., 1995). On the other hand,  $G\alpha_q$  subunit activates Rho GTPases through the interaction with p63-Rho GEF and Trio (Lutz et al., 2007), whereas  $G\alpha_{12}$  and  $G\alpha_{13}$  subunits interacts with a family of Rho GEFs (p115, PDZ-RhoGEF and LARG) in the activation of Rho GTPases (Mikelis et al., 2013) (**Figure 1.10**). Except their regulatory roles in nuclear events, Rho GTPases play an additional part in cell migration through the downstream signalling of P21 activated kinase (PAK), WASP and Arp2/3 that mediate the actin cytoskeletal changes, as detailed in the section above (**Figure 1.2**) (Spiering and Hodgson, 2011).

In addition,  $G\beta\gamma$  subunits are also involved in the PI3K-AKT-mTOR cascade, which is crucial for cell growth, proliferation and cell migration (Hemmings and Restuccia, 2012).  $G\beta\gamma$  subunits interacts with phosphoinositide 3-kinases (PI3K),

which convert the membrane-bound lipid, PI(4,5)P<sub>2</sub>, to phosphatidylinositol-3,4,5-trisphosphate (PI(3,4,5)P), resulting in the activation of the serine-threonine kinase AKT (Welch et al., 2002). AKT promotes cell proliferation and protein synthesis by inactivating pro-apoptotic proteins (Hemmings and Restuccia, 2012) whilst activating mTOR (Laplante and Sabatini, 2012) (**Figure 1.10**). Specifically, for PI3K $\gamma$ , this specific isoform of PI3K elicits leukocyte migration, playing a central role in innate immunity. Evidence reveals that cells lack of PI3K $\gamma$  expression utilises PI3K $\beta$  instead for cell proliferation and metabolism (Ciraolo et al., 2008).

Overall, the whole signalling network plays a central role to regulate cell growth, proliferation and migration in normal conditions (**Figure 1.10**). Uncontrolled activation of chemokine receptors and their downstream signalling pathways could potentially result in cancer development and metastasis.

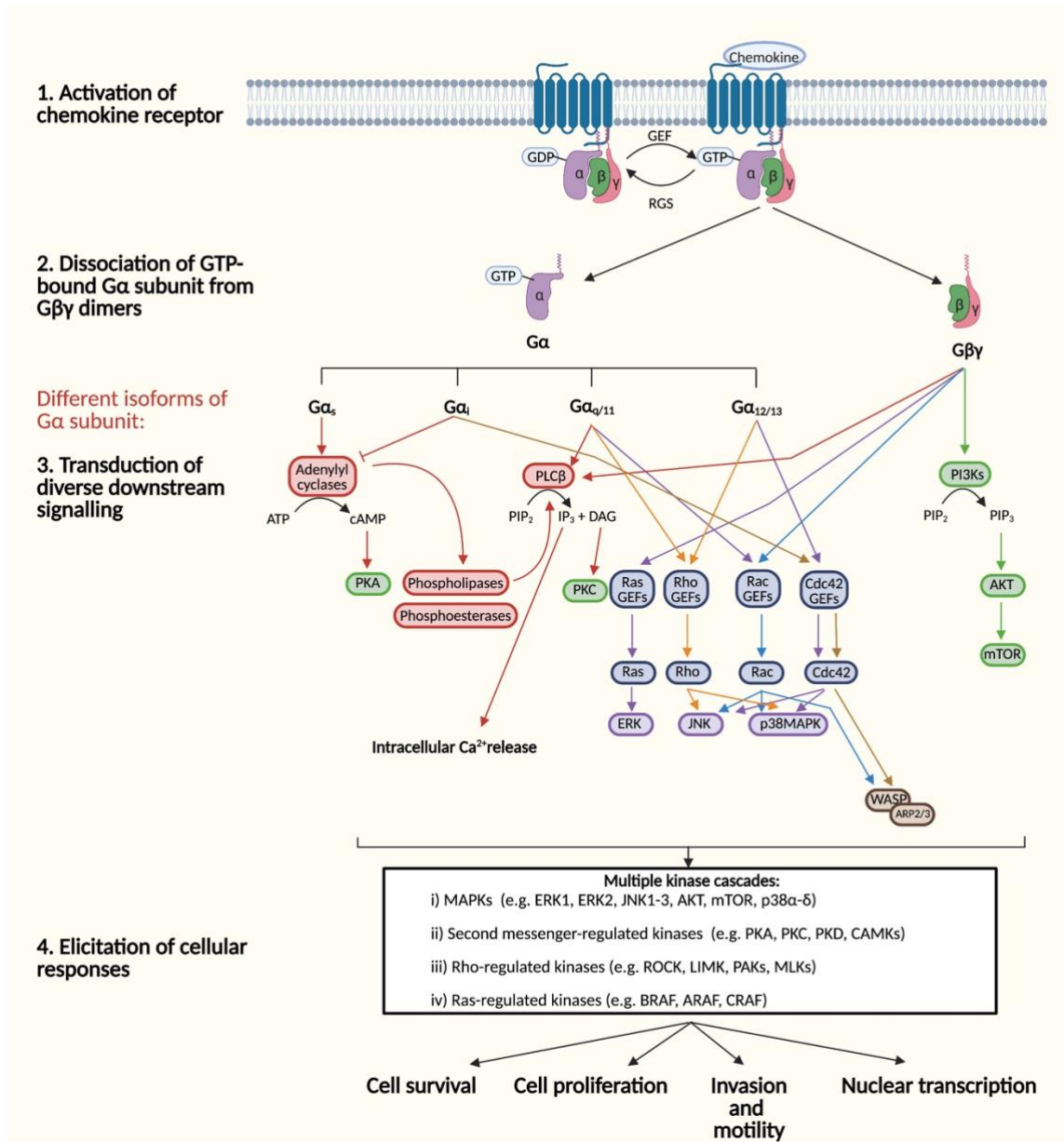


**Figure 1.10. G protein-dependent chemokine signalling pathways.**

Following the activation of chemokine receptor, the Gα subunit dissociates from the Gβγ subunits and leave the receptor to transduce a variety of downstream signalling accordingly and mediate multiple kinase cascades (Rosenbaum et al., 2009). Overall, the signalling network contributes to multiple cellular processes, including cell survival, proliferation, invasion and nuclear transcription (Original image taken from Lai and Mueller, 2021 and modified with BioRender.com).

### 1.4.2 G protein-independent chemokine signalling

Alternatively, chemokine receptors could initiate downstream signalling in G protein-independent manner. With regards to chemokine signalling independent

of G proteins, recent studies have uncovered multiple roles of a critical mediator,  $\beta$ -arrestin, in more detailed.  $\beta$ -arrestin is not only involved in receptor desensitisation and internalisation, but also in intracellular signal propagation and amplification acting as a multifunctional scaffolding protein for the downstream signalling proteins mentioned above (**Figure 1.11**) (Peterson and Luttrell, 2017; Bagnato and Rosanò, 2019).

Following chemokine stimulation, chemokine receptor is phosphorylated by G protein-coupled receptor kinases (GRKs), which in turn promote  $\beta$ -arrestin recruitment to the phosphorylated receptor at the cytosolic face (**Figure 1.11**). Emerging studies were attempting to unveil an in-depth insight into the mechanisms underlying  $\beta$ -arrestin-dependent intracellular signalling by proposing a hypothesis named “phosphorylation barcoding” (Nobles et al., 2011). Evidence demonstrates that different GRKs isoforms or subtypes might possess preferential phosphorylation patterns, triggering specific conformational changes in chemokine receptors. Distinct conformational states of the receptor- $\beta$ -arrestin complex dictate specific functional outcomes by permitting the interactions with specific intracellular signalling proteins through a selected downstream pathway, known as signalling selectivity (Marshall, 2016; Thomsen et al., 2016; Nobles et al., 2011).

Acting as a scaffolding protein,  $\beta$ -arrestin forms multiprotein complexes with multiple signalling proteins, such as MAPK (McDonald et al., 2000), PI3K, AKT (Zhang et al., 2014), NF- $\kappa$ B (Gao et al., 2004), Phosphatase and TENsin homolog (PTEN) (Lima-Fernandes et al., 2011) and E3 ubiquitin ligases (Jean-Charles et al., 2016). These  $\beta$ -arrestin-dependent complexes are then localised to various intracellular compartments, such as endosomes, cytoskeleton and nucleus, for protein ubiquitination (Jean-Charles et al., 2016), cytoskeletal rearrangement (McGovern and DeFea, 2014) and gene transcription (Dasgupta et al., 2011), contributing to cancer proliferation and metastasis.

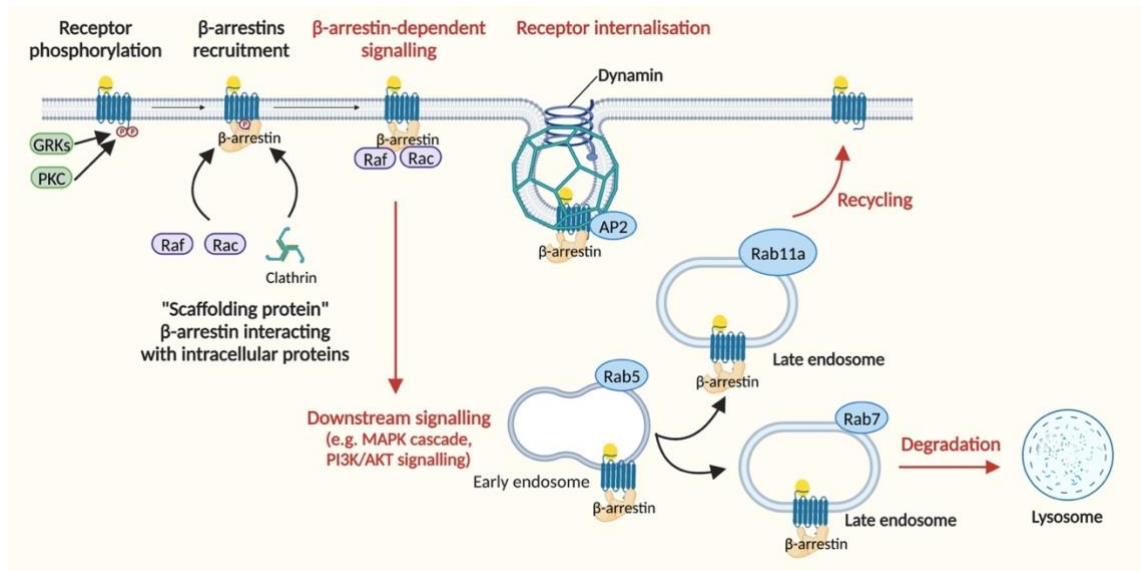


**Figure 1.11. G protein-independent signalling.** Following ligand binding,  $\beta$ -arrestins are recruited from the cytosol to the plasma membrane by phosphorylated receptor.  $\beta$ -arrestins can act as multifunctional scaffolding proteins by associating with multiple intracellular signalling proteins to transduce downstream signalling pathways. On the other hand,  $\beta$ -arrestins are involved in receptor internalisation. By engaging with the adaptor proteins, AP2 and clathrin, receptor- $\beta$ -arrestin complex is endocytosed into endosomes for either lysosomal degradation or recycling back to the plasma membrane (Original image taken from Lai and Mueller, 2021 and modified with BioRender.com).

### 1.4.3 Biased signalling

With the complexity of the redundancy in the chemokine signalling system and the discovery of distinct G protein-dependent and -independent pathways as described above, it could be possible that a preferential signalling pathway is induced by a specific chemokine receptor-ligand pairs, which is known as biased signalling, as supported by evidence from recent studies including CCL19/CCR7, CCL21/CCR7 (Hauser and Legler, 2016) and CXCL12/CXCR4-ACKR3 (Décaillot et al., 2011a). It is notable that one of the preferentially activated signalling pathways is considered to be cancer-promoting, while another could be anti-cancer (Roy et al., 2017). Therefore, specifically targeting its selectivity towards the cancer-promoting pathway can potentially be a therapeutic strategy for the design of drugs targeting chemokine signalling in cancer, instead of inhibiting the

whole chemokine system that possibly affects its normal physiological functions (Roy et al., 2017).

In CCR7 signalling, CCL19 and CCL21 are the well-known associated ligands of CCR7. It was shown that CCL19 and CCL21 exert differential functional outcomes even binding to the same receptor, which is implicated by biased signalling (Raju et al., 2015). For example, CCL19 promotes chemotaxis through  $\beta$ -arrestin-dependent pathway, whereas CCL21 impairs chemotaxis through G protein-dependent pathway (Hauser and Legler, 2016; Raju et al., 2015). One of the factors influencing their signalling preference is the structural difference between CCL19 and CCL21. The unique 37-amino acid long, positive-charged C-terminal tail of CCL21 increases the likelihood of CCL21 binding glycosaminoglycans (GAGs), which obscures its interaction with CCR7 for CCR7 activation. Attenuation of CCL21-induced CCR7 implies that chemotaxis is potentially impaired (Hjortø et al., 2016). As opposed to the structural feature of CCL21, the long, positive-charged C-terminal tail is absent in CCL19, which is less likely to be GAG-bound. Thus, chemotaxis could be induced without obscure of CCR7 activation from GAGs (Hjortø et al., 2016). In addition, the signalling bias towards  $\beta$ -arrestin-dependent pathway for CCL19 is implicated by the unique phosphorylation patterns from CCL19 at the C-terminus of CCR7 (Zidar et al., 2009). Emerging studies demonstrate that receptor phosphorylation patterns by different isoforms of GRKs dictate distinct functions of chemokine, known as phosphorylation barcode (Nobles et al., 2011). Notably, CCL21 activates GRK6, whereas CCL19 activates GRK6 and also GRK3 (Zidar et al., 2009; Hjortø et al., 2016). The additional phosphorylation sites from GRK3 from CCL19/CCR7 signalling favour the functionality of  $\beta$ -arrestin, which in turn elicits  $\beta$ -arrestin-dependent signalling (Hjortø et al., 2016).

CXCL12/CXCR4-ACKR3 is an example of receptor bias where two different receptors bind the same ligand. As supported by numerous evidence, ACKR3 is primarily biased towards  $\beta$ -arrestin dependent signalling, unlike a balance of G protein-dependent and  $\beta$ -arrestin dependent signalling pathways seen in CXCL12/CXCR4 (Szpakowska et al., 2018; Nguyen et al., 2020; Fumagalli et al., 2019). It is noteworthy that high plasticity of the binding pocket was observed in ACKR3, which could diverse signalling stimulated by a variety of chemokine

ligands towards  $\beta$ -arrestin dependent signalling. For example, alterations on the key residues of CXCL12 essential for receptor binding do not affect ACKR3 activation and signalling activity. Even CXCR4 antagonists were found to act as agonist for ACKR3, leading to  $\beta$ -arrestin recruitment and downstream signalling (Szpakowska et al., 2018). As described as a “decoy” receptor, ACKR3 functions as a co-receptor with CXCR4 to activate  $\beta$ -arrestin dependent signalling pathway but not G protein-mediated pathway (Fumagalli et al., 2019). Recent studies have been attempting to characterise the interaction between CXCR4 and ACKR3 to explain the “decoy” function of ACKR3 in signalling modulation (Rajagopal et al., 2010; Fumagalli et al., 2019). It was revealed that ACKR3 interacts with the C-terminal tail of CXCR4 in the formation of CXCR4-ACKR3 heterodimer, which contributes to constitutive  $\beta$ -arrestin recruitment and attenuates Gai-dependent signalling. Following phosphorylation of GRK2 in a site-specific manner on the CXCR4-ACKR3 heterodimer,  $\beta$ -arrestin-mediated signalling is induced and subsequently activate MAPK cascades, such as ERK1/2 activation and p38MAPK activation (Fumagalli et al., 2019). Overall, CXCL12/CXCR4-ACKR3 signalling largely contributes to proliferation and cell migration by activating pro-tumour  $\beta$ -arrestin-mediated signalling while inactivating anti-tumour Gai-dependent signalling. By targeting the signalling bias of CXCL12/CXCR4-ACKR3, emerging studies have developed ACKR3-targeting molecules, including an allosteric modulator, ITAC (Fumagalli et al., 2019), and a competitive antagonist, ACT-1004-1239 (Richard-Bildstein et al., 2020). Both specifically block CXCL12-induced  $\beta$ -arrestin recruitment without affecting G protein-mediated signalling from CXCR4. One study has proven the effect of ITAC that cell migration was reduced as a result of the resumption of Gai-dependent signalling from CXCR4 activation (Rajagopal et al., 2010; Fumagalli et al., 2019).

#### **1.4.4 Downstream effector: $\beta$ -arrestins**

Arrestins are a small family of proteins comprised of arrestins 1, 2, 3 and 4. Arrestin 1 and 4 are visual arrestins, while arrestins 2 (also known as  $\beta$ -arrestin 1) and 3 (also known as  $\beta$ -arrestin 2) are non-visual. Arrestin 1 is expressed in rod and cones, whereas arrestin 4 is present in cones exclusively. Both arrestins play a significant role in regulating rhodopsin signalling in photoreceptor cells (Gurevich et al., 2011). For arrestins 2 and 3 (generally named  $\beta$ -arrestins), both are ubiquitously present in various cells. Specifically, arrestin 2 is typically

localised in the nucleus and cytoplasm, while arrestin 3 is localised in the cytoplasm only (Ferguson, 2001). Within the structure of arrestin family, it comprises of a N-domain and C-domain, which consist of anti-parallel  $\beta$ -sheets connected with small loop regions (**Figure 1.12**) (Kang et al., 2015).

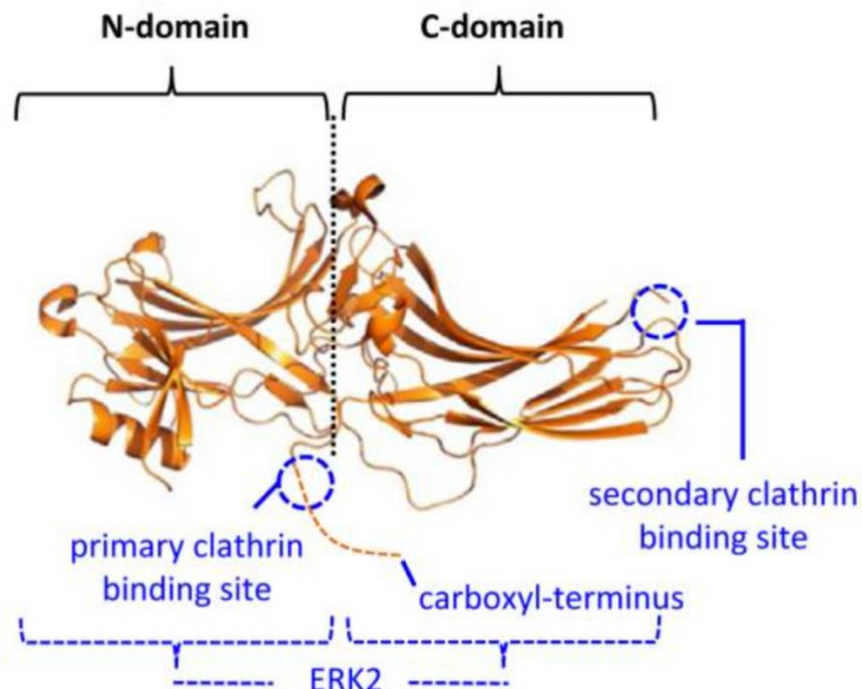


**Figure 1.12. Structural representation of  $\beta$ -arrestin.**  $\beta$ -arrestins contain two major domains: N- and C- domains. In each domain, it consists of anti-parallel  $\beta$ -sheets linked by small loops. In terms of functionality,  $\beta$ -arrestins interact with multiple downstream signalling proteins at the major interaction interfaces as indicated, playing a multifunctional regulatory role in GPCR signalling (Image taken from Shukla and Dwivedi-Agnihotri, 2020).

As previously mentioned, arrestins act as multifunctional regulators for signalling transduction at GPCRs. They are involved in multiple processes, such as receptor desensitisation and internalisation, endoplasmic vesicle trafficking and G protein-independent signalling, potentially leading to cancer development and invasion (Song et al., 2018).

On the mechanistic aspect,  $\beta$ -arrestins can be activated by the receptor in three distinct conformations: “tail”, “core” and GRK-independent “core” conformations (**Figure 1.13**). Within the “tail” conformation, the twisted long C tail of arrestin interacts with the phosphorylated C-terminus of the receptor, leading to

prolongation in active state (Latorraca et al., 2018). Whereas interactions between the back loop of the C-domain of arrestin and the ICLs of the receptor are observed in “core” conformation (Kang et al., 2015). The GRK-independent “core” conformation is proposed to be a transient engagement of arrestin with the TM core of the receptor without the activation of the receptor. Subsequently, arrestin dissociates from the receptor and interacts with membrane-bound PIP<sub>2</sub>, leading to  $\beta$ -arrestin-dependent ERK1/2 signalling from clathrin-coated structures (Eichel et al., 2016). A recent study demonstrated that sustained activation of arrestin and downstream signalling transduction only require interactions in the “core” conformation, not necessarily “tail” conformation (Eichel et al., 2018). According to the proposed phosphorylation barcoding, the distinct patterns of phosphorylation on the receptor C-terminus induces specific conformation changes in arrestin, either “tail” or “core” conformation, leading to distinct regulatory functions (Tobin et al., 2008).

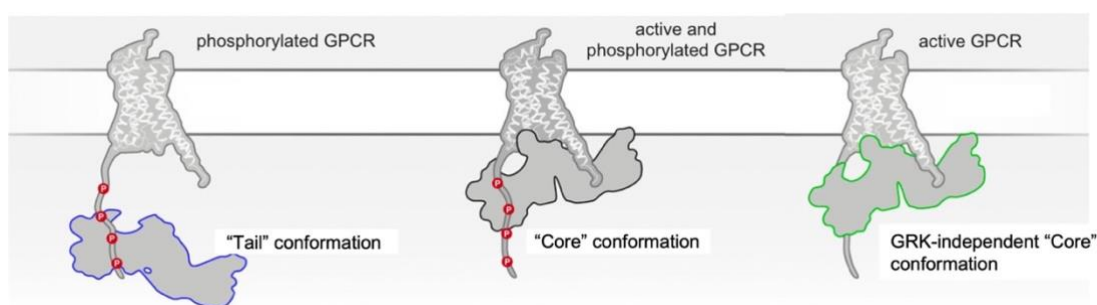


**Figure 1.13. Schematical diagrams indicating the three distinct conformations of active arrestin in the interaction with GPCR.** “Tail” conformation is defined by interaction of the phosphorylated C-terminal tail of GPCR with the C-domain of arrestin. “Core” conformation is referred to the interaction between TM core of GPCR and the C-domain of arrestin. “Core” conformation is also adopted by arrestin in the absence of receptor activation and phosphorylation, in order to transduce  $\beta$ -arrestin-dependent signalling (Image taken from Haider et al., 2022).

The phosphorylation barcode model was originally proposed where different protein kinases phosphorylate the receptor C-terminus in different patterns, resulting in the activation of different signalling pathways following binding and activation of arrestins (Tobin et al., 2008; Tobin, 2008). More recently, the model has been elaborated into more details in three-dimensional structural basis

(Latorraca et al., 2020). So far there have been three new insights revealed: (1) The spatial arrangement of phosphorylated residues at the receptor C-terminus is the critical determinant in arrestin binding, not only dependent of the number of phosphorylated residues. (2) The phosphorylation patterns favouring arrestin binding could be different from those favouring arrestin activation. (3) Different phosphorylation patterns could lead to different arrestin binding conformations determining whether arrestins are in active or inactive state (Latorraca et al., 2020). Yet, more investigations into the implications of the relationship between phosphorylation patterns and arrestin spatial structures onto signalling selectivity need to be done.

Another study proposed a novel model, named “phosphorylation flute” model (**Figure 1.14**) to explain further how a few isoforms of arrestins and protein kinases induce a diversity of downstream signalling (Yang et al., 2015). Different GRKs were found to phosphorylate the receptor in distinct phosphorylation patterns (Yang et al., 2015). Arrestin subsequently recognises the phosphorylation patterns in different conformations, leading to specific signalling pathways (Yang et al., 2015). For example, within the seven phosphorylation sites (p1-7) in the V<sub>2</sub>R/ $\beta$ -arrestin1 complex, GRK6 catalyses phosphorylation sites p1 and p5, triggering the interaction of Src with arrestin 2. Whereas GRK2 catalyses p1, p4, p6 and p7 phosphorylation, which mediates clathrin recruitment to arrestin 2 (Yang et al., 2015).

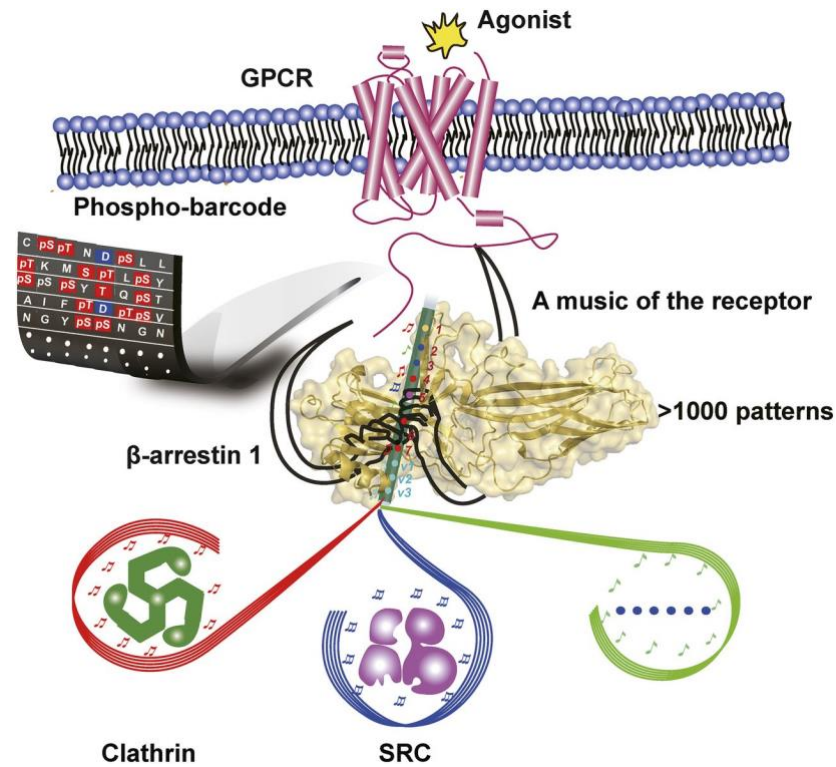


**Figure 1.14. Schematic diagram showing the flute model for elaborating the model on the phosphorylation barcoding of arrestin-dependent signalling.** Different GRKs phosphorylates the receptor in distinct phosphorylation patterns, which are subsequently recognised by arrestins in different conformations and consequently a diversity of signalling pathways is resulted (Image taken from Yang et al., 2015).

Most recently, studies have revealed that phosphorylation patterns of  $\beta$ -arrestin by a combination of factors dictates specific downstream signalling. The factors include ligand, receptor type, GRK isoform, arrestin isoform and the phosphorylation sites. It is known as “phosphorylation QR code” model (**Figure 1.15**) (Chen et al., 2022). For example, following the stimulation of  $AT_{1A}$  receptor ( $AT_{1A}R$ ) with angiotensin II (Ang II), arrestin 3 recruited by GRK5/6 mediates ERK activation, whereas  $AT_{1A}R$  endocytosis is induced by arrestin 3 activated by GRK2/3 (Kim et al., 2005). Another pathophysiological ligand,  $AT_{1R}$  autoantibody ( $AT_{1-AA}$ ) was recently revealed to activate  $AT_{1R}$  in a sustained manner, blocking  $AT_{1A}R$  endocytosis dependent of arrestin 3, contributing to sustained vasoconstriction in preclampsia (Bian et al., 2019).

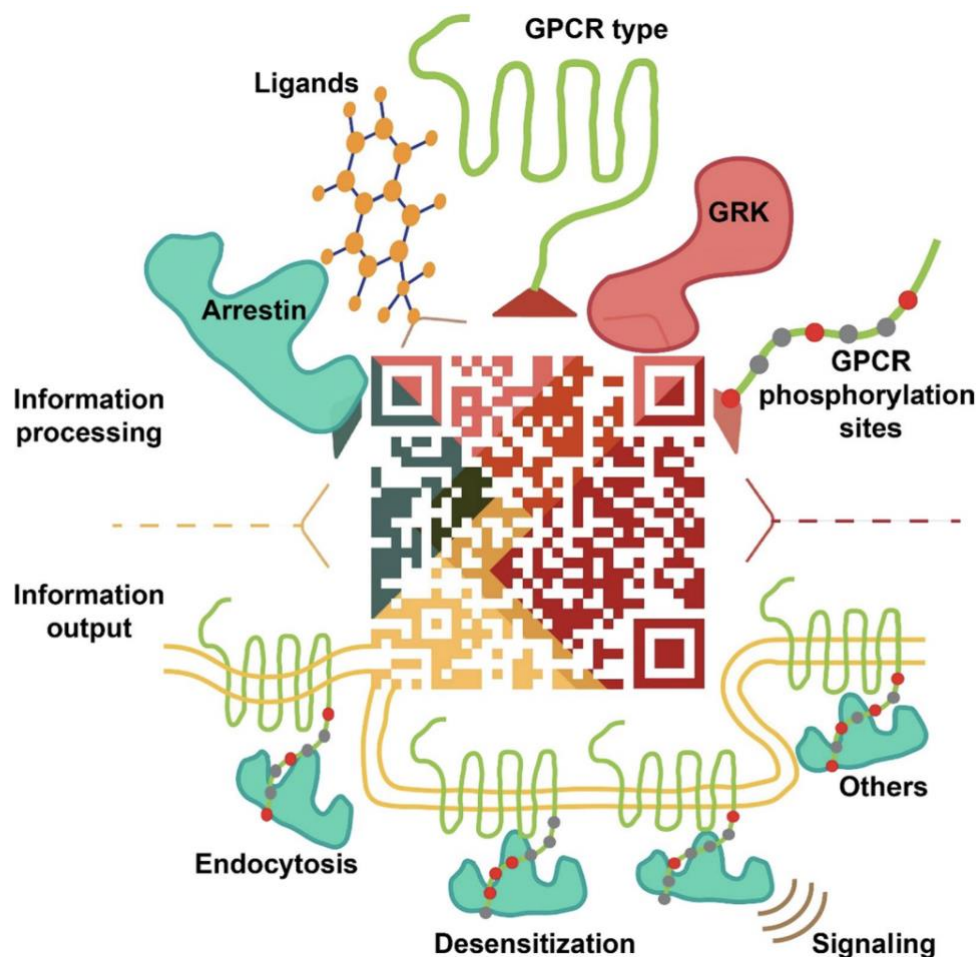


**Figure 1.15. Schematic diagram showing the QR code model for elucidating differential signalling transduction from specific receptor phosphorylation recognition.** A combination of factors including ligand types, receptor types, GRK isoforms, arrestin isoforms and receptor phosphorylation sites determine specific signalling outcomes, such as receptor endocytosis, desensitisation and transduction of specific signalling pathways (Image taken from Chen et al., 2022).

In the example of CCL5/CCR5 signalling, CCL5-activated CCR5 has been shown to be phosphorylated on four major serine residues, Ser336, Ser337, Ser342, and Ser349, at the C-terminus through arrestins 2 and 3 recruitment (Oppermann et al., 1999). The phosphorylation process is strongly dependent of the “tail” conformation of arrestins, and more biased towards arrestin 2 versus arrestin 3. Furthermore, a study using N-terminally engineered analogues of CCL5 demonstrated that the different CCL5 analogues elicit CCR5 phosphorylation in a distinct manner dependent of arrestin conformation (“core” or “tail”) adopted and the interaction with specific arrestin isoform (Martins et al., 2020). For

example, PSC-CCL5 was found to hyperphosphorylate CCR5, leading to increase in arrestin recruitment with lower dependence on the arrestin “tail” conformation than that seen by wild-type CCL5 (WT-CCL5). On the other hand, 5P14-RANTE induces CCR5 phosphorylation in a comparable level to WT-CCL5 with dependence on arrestin “tail” conformation but the arrestin recruitment is biased towards arrestin 3 instead (Martins et al., 2020).

With regards to another chemokine receptor common in cancer, CXCR4, receptor phosphorylation mediated by CXCL12 stimulation takes place on multiple specific serine residues, including Ser321, Ser324, Ser325, Ser330, Ser339, and two sites between Ser346 and Ser352. Evidence has been shown that site-specific phosphorylation regulated by specific kinases and isoform-specific arrestins results in differential CXCR4 signalling modulation. In the aspect of site-specific phosphorylation by kinases, for example, GRK6 was shown to phosphorylate Ser324, Ser325, 330 and 339 (Busillo et al., 2010), whereas GRK3 is responsible for Ser346 and 347 phosphorylation only (Luo et al., 2017). In terms of differential signalling modulation, GRK2 was found to be a negative modulator in Ca<sup>2+</sup> mobilisation and ERK1/2 activation through arrestin 3 recruitment, whereas GRK3 was revealed to positively regulate ERK1/2 activation through arrestin 2 recruitment (Busillo et al., 2010). However, specific structural conformations of receptor-arrestin complex following site-specific receptor phosphorylation are yet to be elucidated.

In terms of the intracellular regulatory roles of arrestins following arrestin recruitment to chemokine receptor, it has been revealed that arrestins are associated with multiple intracellular signalling pathways, such as MAPK cascade and PI3K/AKT pathway, contributing to cancer metastasis (**Figure 1.16**).

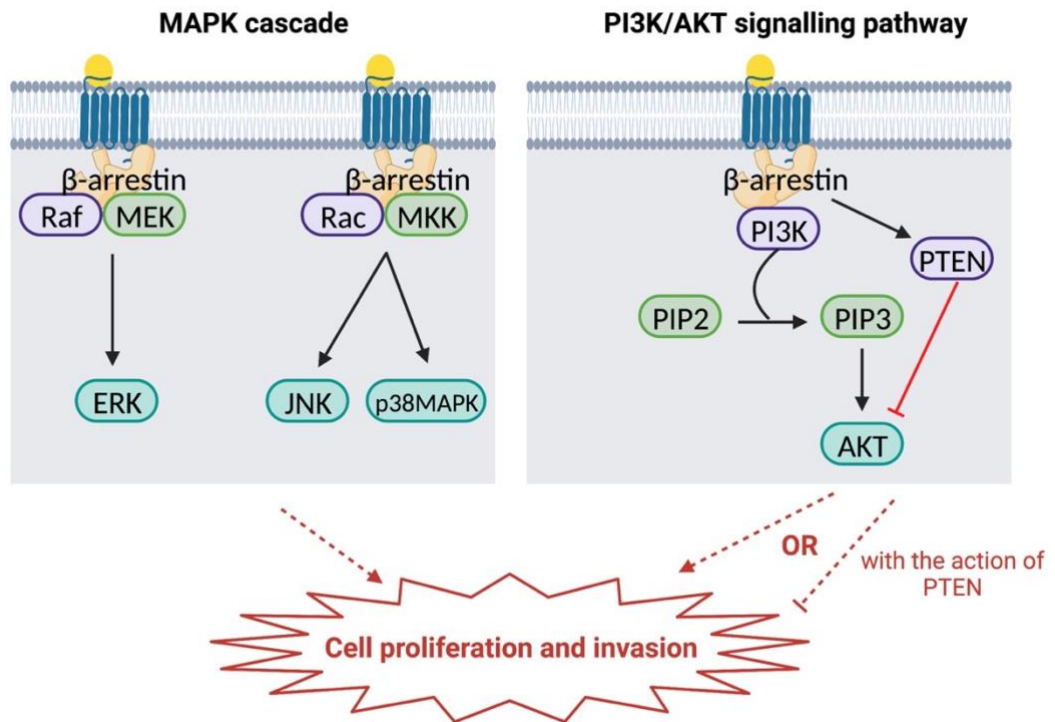


**Figure 1.16. Schematical diagram showing two major cancer-associated downstream signalling pathway regulated by arrestins.** Arrestins serves as scaffolding protein associated with the constituents of the MAPK cascade and are involved in the activation of downstream effectors, including ERK, JNK, p38MAPK, which induces cell migration. Arrestins could also activate PI3K and elicit PI3K/AKT signalling, which promotes cell proliferation and migration. On the other hand, arrestins could activate PTEN, which inhibit AKT, as a result of inhibition of cell proliferation. This implies that arrestins serve as positive or negative regulators in cancer in context-dependent manner (Modified from Lai and Mueller, 2021 with BioRender.com).

In the association of  $\beta$ -arrestins with the constituents of the MAPK cascade, the process activates downstream effectors including ERK, JNK and p38 (Luttrell et al., 2001). Subsequently, this leads to epithelial-mesenchymal transition (EMT) and increased expression of matrix metalloproteases (MMPs), which promotes cancer metastasis (Cepeda et al., 2017). Several studies demonstrated that phosphorylation of ACKR3/CXCR4 receptor heterodimer by GRK6 promotes the recruitment of arrestin 3 exclusively to activate ERK1/2, p38 MAPK and SAPK through a preferential  $\beta$ -arrestin-dependent signalling pathway, leading to

increase in cell migration (Fong et al., 2002; Décaillot et al., 2011b; Coggins et al., 2014). In addition, a study by Liu et al., 2016 uncovered a new prognostic marker, USP33, which is a deubiquitinating enzyme involved in regulating the expression of  $\beta$ -arrestins, for advanced colorectal cancer (CRC). Low expression of USP33 in CRC tissue was found to indicate poor prognosis. It was demonstrated that USP33 is responsible for deubiquitinating  $\beta$ -arrestins, and subsequently block  $\beta$ -arrestin-dependent ERK activation, negatively regulating cell migration (Liu et al., 2016). This implies that USP33 possesses tumour-inhibitory effects, playing a significant role in regulating  $\beta$ -arrestin-dependent signalling.

For the link of  $\beta$ -arrestins to the PI3K/AKT signalling pathway, a study on human osteosarcoma (OS) demonstrated that ACKR3 associated with arrestin 2 induces PI3K activation, and in turn increases membrane PI (3-5)P3 accumulation to activate AKT, proliferating cell nuclear antigen and MMP9 (Zhang et al., 2014). This implies that  $\beta$ -arrestin-dependent PI3K signalling pathway is associated with cancer proliferation and invasion in human OS. On the contrary, a study showed that  $\beta$ -arrestins increase the activity of PTEN, leading to the suppression of PI3K pathway, as a result of inhibition of cell proliferation (Lima-Fernandes et al., 2011). Thus,  $\beta$ -arrestins serve as positive and negative regulators in cancer proliferation and invasion via PI3K signalling pathway in context-dependent manner.

#### **1.4.5 Downstream effector: Protein kinase D (PrKD) (previously named PKC $\mu$ )**

Protein kinase D (PrKD) is classified into the Ca<sup>2+</sup>/Calmodulin-dependent protein kinases (CaMKs) superfamily within the family of serine/threonine kinases (Rozenfurt et al., 2005). PrKD is not only activated by diacylglycerol (DAG), but also activated by protein kinase C (PKC) through direct phosphorylation. Functionally, PrKD is a critical mediator in regulating multiple cellular processes, including cell survival (Storz and Toker, 2003), motility (Döppler et al., 2014), intracellular vesicle transport (Bossard et al., 2007) and gene transcription (Dequiedt et al., 2005). Emerging studies revealed that dysregulation of PrKD associates with the pathophysiology in a variety of human diseases, such as

cancer (Roy et al., 2017), inflammatory diseases (Yuan and Pandol, 2016) and cardiovascular diseases (Wood and Bossuyt, 2017; Simsek Papur et al., 2018). To date, three isoforms of the PrKD family has been identified: PrKD1, PrKD2 and PrKD3 (Manning et al., 2002; X. Zhang et al., 2021). PrKD can be localised or translocated to different subcellular locations, including the plasma membrane, Golgi, nucleus, mitochondria and cytosol, to exert differential functional outcomes (Fu and Rubin, 2011). Under the unstimulated state, all PrKD isoforms are typically localised in the cytoplasm, and PrKD3 is also expressed in the nucleus (**Figure 1.17**). Upon ligand stimulation and DAG activation, PrKD 1 can translocate to the nucleus, mitochondria, cytoplasm and Golgi, PrKD 2 can be mobilised to the Golgi and cytoplasm, while PrKD3 is exclusively found in the cytoplasm only (**Figure 1.17**) (Fu and Rubin, 2011). With regards to the association with cancer, the three isoforms of PrKD are expressed in different levels possibly acting cancer promoting or inhibitory effects in different cancer types (Zhang et al., 2021).

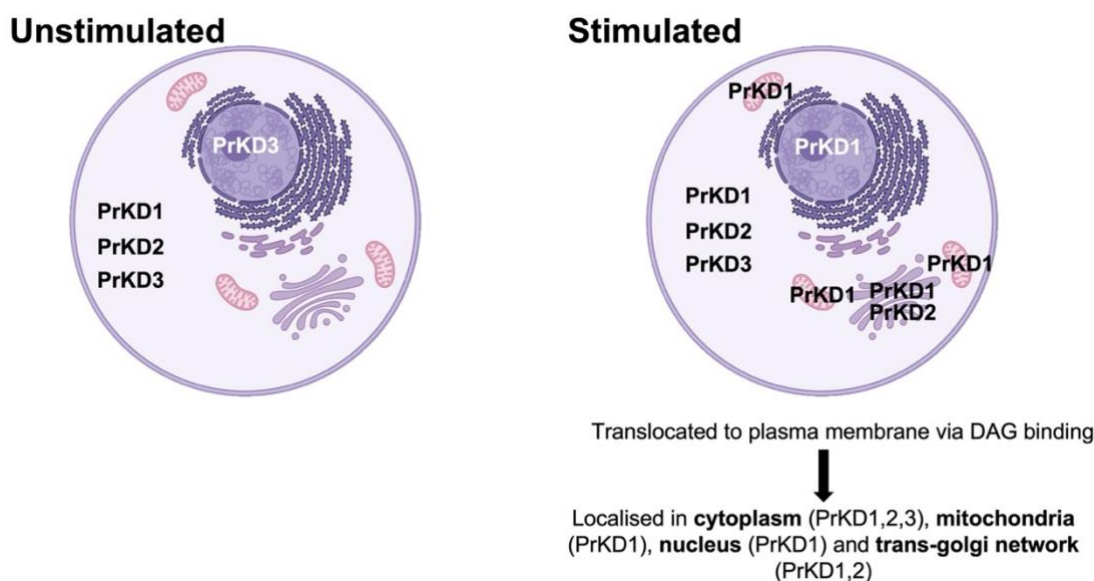


**Figure 1.17. Localisation of PrKD.** Under basal conditions, all the PrKD isoforms are constitutively present in the cytoplasm, and PrKD3 are also found in the nucleus. Following ligand stimulation and DAG activation, translocation of PrKD is occurred. PrKD 1 can be translocated to the nucleus, mitochondria, cytoplasm and Golgi, PrKD 2 can be mobilised to the Golgi and cytoplasm, while PrKD3 is exclusively found in the cytoplasm only (Fu and Rubin, 2011) (Image created with BioRender.com).

The three isoforms of PrKD contains an N-terminal regulatory domain, a plekstrin homology (PH) and followed by a C-terminal catalytic kinase domain (**Figure 1.18**) (Rykx et al., 2003). The regulatory domain comprises of a C1 domain in two different tandem cysteine-rich Zn-finger like motifs, which are C1a and C1b. The C1 domain bind membrane-bound ligands, DAG and phorbol esters, and regulate the localisation of PrKD to the plasma membrane, mitochondria, nucleus and Golgi (Spitaler et al., 2006). The major functional difference of the two C1 motifs is the binding affinity to their ligands. C1a binds DAG with a high affinity, whereas C1b binds DAG with a low affinity but with a high affinity in the binding of phorbol ester (Wang, 2006). Among the three PrKD isoforms, PrKD3 is the most sensitive to DAG/phorbol esters in terms of its activity and selectivity for substrates (Chen et al., 2008). The PH domain plays a critical auto-regulatory role to maintain PrKD in an inactivated state by auto-inhibiting the catalytic kinase domain. Thereby, mutation or deletion of corresponding residues of the PH domain contributes to constitutive activation of basal PrKD (Iglesias and Rozengurt, 1999). The catalytic kinase domain in all three PrKD isoforms comprises of an activation loop where PrKD activation takes place. Following DAG binding or direct binding of PKC, transphosphorylation between a pair of conserved serine residues (Ser<sup>738</sup> and Ser<sup>742</sup> for PrKD1, Ser<sup>706</sup> and Ser<sup>710</sup> for PrKD2, Ser<sup>731</sup> and Ser<sup>735</sup> in PrKD3) occurs (Fu and Rubin, 2011).

Additionally, the N-terminal ubiquitin-like domain (ULD) shared by all three isoforms is demonstrated to be involved in inducing PrKD dimerization for transphosphorylation at the activation loop in response to increase in DAG concentration. The ULD-mediated transphosphorylation is independent of PKC (Elsner et al., 2019). Except PrKD3, the type 1 PDZ binding motif (PB) is present at the C-terminus of PrKD1 and PrKD2 (**Figure 1.18**). It is shown to interact with protein scaffolds that control the amplitude and duration of PrKD activity, for example, Sodium Hydrogen Exchanger Regulatory Factor-1 (NHERF-1) (Kunkel et al., 2009). Within the PB, the autophosphorylation site (Ser<sup>910</sup> for PrKD1, Ser<sup>876</sup> for PrKD2) is important for late sustained PrKD activation following phosphorylation at the activation loop (Rybin et al., 2009). Particularly, the Ser<sup>916</sup> residue in PrKD1 has been utilised as a marker to study PrKD1 activity status in many studies based on the evidence demonstrating that phosphorylation of Ser<sup>916</sup> is positively correlated with PrKD catalytic activity (Iglesias et al., 1998).

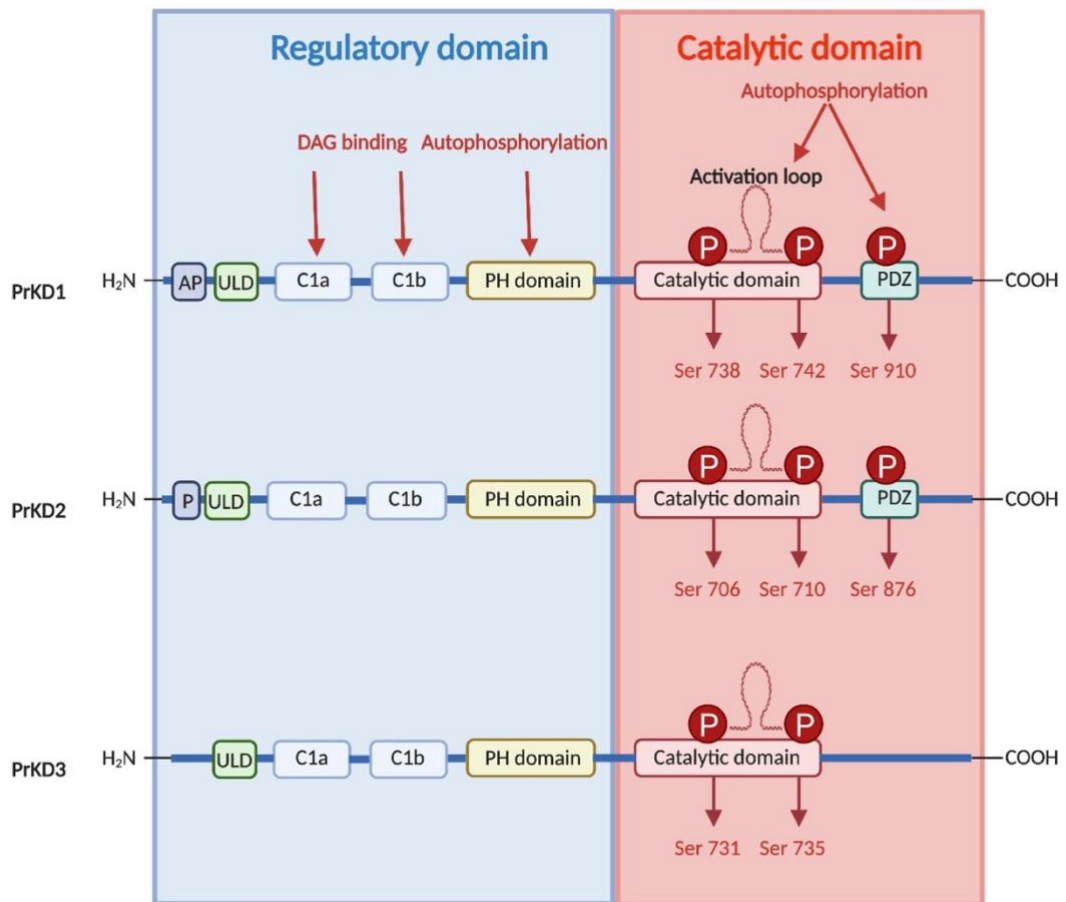


**Figure 1.18. Structural differences in the three PrKD isoforms (PrKD1, PrKD2 and PrKD3).** PrKD is generally composed of an N-terminal regulatory domain, a plekstrin homology (PH) and followed by a C-terminal catalytic kinase domain, which are in common across all three isoforms (Ryx et al., 2003). Within the catalytic domain, the PDZ binding motif is present in PrKD1 and PrKD2, but not PrKD3. PDZ binding motif is where autophosphorylation takes place for late sustained PrKD activation. The autophosphorylation sites are different between PrKD1 and PrKD2 (Rybin et al., 2009) (Image created with BioRender.com).

PrKD activation is initiated from the binding and activation of GPCRs by extracellular stimuli, such as growth factors, chemokines and tumour necrosis factor (TNF) (Roy et al., 2017). In a canonical pathway, upon receptor stimulation, phospholipase Cs (PLCs) are activated to cleave PI(4,5)P<sub>2</sub> into DAG and IP<sub>3</sub>. IP<sub>3</sub> induces intracellular Ca<sup>2+</sup> mobilisation. Along with the Ca<sup>2+</sup> influx, DAG binds classic or novel isoforms of PKC (c/n PKC) at the plasma membrane. In the

meantime, DAG binds the C1 domain of the cytosolic PrKD and recruits PrKD to the plasma membrane. At the plasma membrane, PrKD colocalised with PKC, which in turn induces transphosphorylation at a conserved serine residue in the C-terminus of PrKD. Subsequently, this process leads to the autophosphorylation of the adjacent serine residue and ease of the autoinhibition from the PH domain, as a result of a full activation of the catalytic kinase domain of PrKD (**Figure 1.19**) (Rozenfurt et al., 2005).

Alternatively, PrKD activation can occur independent of PKC supported by a number of recent studies (Bossard et al., 2007; Aicart-Ramos et al., 2016; Elsner et al., 2019). A conserved ULD domain was recently determined to initiate PrKD dimerization, leading to trans-autophosphorylation between a pair of the conserved C-terminal serine residues and consequently activation of PrKD (Reinhardt et al., 2020).

Upon activation, PrKD is involved in regulating downstream signalling proteins associated with pathophysiological conditions, particularly in cancer. A variety of key signalling targets of PrKD have been identified to be positively or negatively associated with cancer development and metastasis, such as  $\beta$ -catenin, E-cadherin, SSH1L and p21-activated kinase 4 (PAK4)/ LIM kinase (LIMK1) (**Figure 1.19**) (detailed in **Table 1.2**). The three PrKD isoforms mediate distinct functional outcomes by interacting with different downstream substrates in different cancer types. The conformational changes in the phosphorylated form of target substrate induced by PrKD phosphorylation determine the activity status of the target substrate (Olayioye et al., 2013). Phosphorylation can enhance the binding affinity of target substrate and subsequently form a functional complex with downstream proteins or enhance substrate localisation to its target site for activation. On the contrary, phosphorylation can inactivate the target substrate. The conformation of some phosphorylated substrates can favour binding to 14-3-3 adaptor proteins, leading to sequestration to the cytoplasm. The binding of 14-3-3 adaptor protein also prevents substrates from interaction with downstream proteins, as a result of inactivation of the target substrate (Roy et al., 2017).

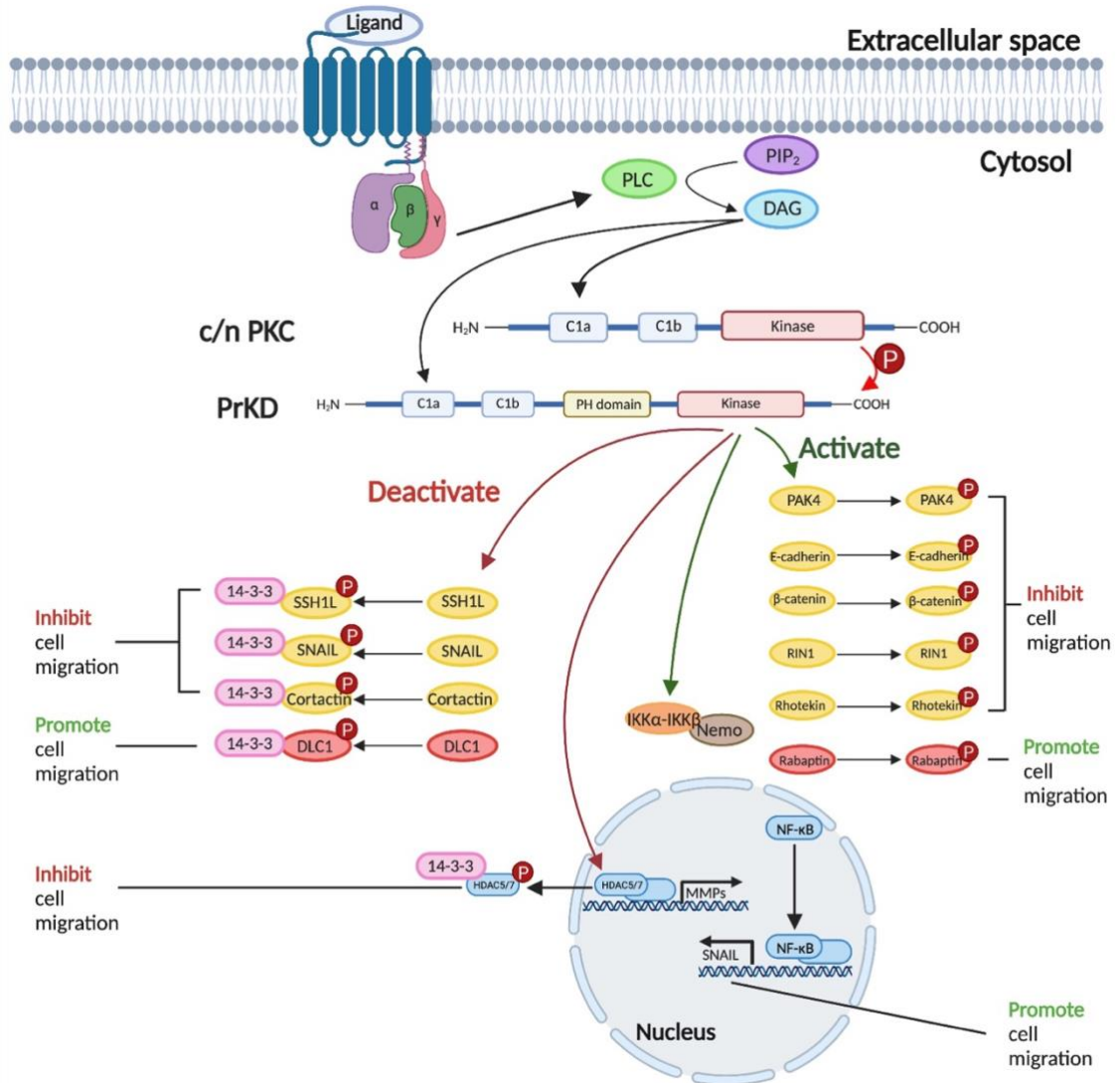


**Figure 1.19. Schematic diagram showing PrKD activation and downstream signalling transduction associated with cell migration through interactions with multiple protein kinases.** PrKD is activated by DAG directly or indirectly through PKC. Activated PrKD is then translocated to multiple cellular locations in the cytosols and interacts with a range of intracellular target substrates through phosphorylation. The process of phosphorylation can either activate or deactivate the activity states of the target substrates. Among the target substrates of PrKD, some substrates are positive regulators in cell migration while some negatively regulate cell migration. Activation of cell migration promoters or deactivation of suppressors induces cell migration, which might lead to cancer metastasis (Roy et al., 2017) (Image created with BioRender.com).

In respect of the involvement of PrKD in cell migration, PrKD is involved in maintaining the balance of kinases and phosphatases involved in cofilin activity cycle (Döppler et al., 2014). Cell migration involves extending protrusion movement at the leading edge and retracting at the rear of the cell, associated with actin cytoskeletal rearrangement. As mentioned previously, actin cytoskeletal rearrangement is regulated by a group of actin-associated proteins, such as cofilin and Arp2/3 (Stossel et al., 2006). In the mechanistic view of protrusion movement, cofilin, an actin-binding protein, severs actin filaments (F-actin) at the leading edge of migrating cells, generating free barbed ends for actin filament turnover. Together with the formation of WAVE-2–cortactin–Arp2/3 complex, the process ultimately induces F-actin turnover in the formation of a branched actin network known as lamellipodia (Bravo-Cordero et al., 2013; Tania et al., 2011). The activity of cofilin is tightly controlled, particularly dependent on the phosphorylation state of Ser<sup>3</sup> regulated by LIMK and slingshot-1L (SSH1L). Cofilin can be inactivated by LIMK through phosphorylation of Ser<sup>3</sup>, as a result of suppression of cell migration (Scott and Olson, 2007). On the other hand, cell migration can be restored by a phosphatase, SSH1L through dephosphorylation of Ser<sup>3</sup> (Niwa et al., 2002). Several studies revealed that active PrKD1 plays a significant role in inhibition of cell migration. Particularly, PrKD was demonstrated to phosphorylate p21-activated kinase 4 (PAK4), an upstream kinase for LIMK1 (Spratley et al., 2011). Activation of PAK4/LIMK1 signalling leads to the accumulation inactive phosphorylated cofilin, which in turn inhibits cell migration. A study by Niwa et al., 2002 showed that PrKD1 phosphorylates SSH1L at Ser<sup>978</sup>. This triggers the binding of SSH1L to 14-3-3 proteins and prevents SSH1L from localising to F-actin for dephosphorylating cofilin, consequently suppressing cell migration. Apart from cofilin, PrKD1 also activates adherens junctional proteins (E-cadherin and  $\beta$ -catenin) (Du et al., 2009; Jaggi et al., 2005) and RIN1 (Ziegler et al., 2011), which mediate inhibition of cell migration. On the other hand, PrKD1 represses EMT promoter (Snail) (Zheng et al., 2014) and the expression of matrix metalloproteinases (MMPs) (Eiseler et al., 2009), which induce cell migration. Thus, PrKD1 is thought to be a negative regulator in cell migration.

In contrary, PrKD2 and PrKD3 appear to be positive regulators in cell migration. With regards to their expression profile in cancer cell lines, PrKD2 and PrKD3, but not PrKD1, are overexpressed in a metastatic triple-negative breast cancer

cell line, MDA-MB-231 (Borges et al., 2013; Döppler et al., 2014). It was shown that PrKD3 is constitutively active in metastatic cancer cell lines under basal conditions (Döppler et al., 2014). Active PrKD3 at basal level specifically promotes PAK4/LIMK signalling, though SSH1L is not inactivated, which consequently promotes cell migration (Döppler et al., 2014). A number of evidence further supports the involvement of PrKD2 and PrKD3 in promoting EMT and cell migration. It was demonstrated both isoforms are involved in activating multiple regulators or pathways for promoting cell migration, including SNAIL through NF- $\kappa$ B activation (Zou et al., 2012), MMP (Wille et al., 2014), PI3K/AKT/glycogen synthase kinase 3 beta (GSK-3 $\beta$ )/ $\beta$ -catenin pathway (Zhu et al., 2016), urokinase-type plasminogen activator (tPA) (Zou et al., 2012), G-protein-coupled receptor kinase-interacting protein 1 (GIT1) (Huck et al., 2012).

To summarise, PrKD1, as a negative regulator of cell migration, is typically expressed in non-invasive cancer cell lines and downregulated in invasive cancer, whereas PrKD2 and PrKD3 are found to be overexpressed in invasive cancer cell lines as a role of promoting cell migration and EMT (X. Zhang et al., 2021). As summarised in **Table 1.2**, PrKD regulates cell migration through distinct downstream signalling pathways in different cancer types. Thus, the functional roles of PrKD is not only isoform-specific in cancer, the mechanism of signalling transduction by the same PrKD isoform can also be context-dependent, differing in cancer types, such as prostate (Du et al., 2010; Jaggi et al., 2005; Zou et al., 2012; Zhu et al., 2016), breast (Eiseler et al., 2009; Christoforides et al., 2012; Zheng et al., 2014; Zou et al., 2012; LaValle et al., 2012; Döppler et al., 2014; Huck et al., 2012), liver (Wille et al., 2014; Bernhart et al., 2013) and melanoma cancer (Peterburs et al., 2009; Merzoug-Larabi et al., 2017).

**Table 1.2. Differential functional roles and mechanisms of the three PrKD isoforms in cell migration and their association with different cancer types** (adopted from Zhang et al., 2021)

| PrKD isoforms | Functional roles   | Mechanisms  | Cancer types | Ref                         |
|---------------|--------------------|---|--------------|-----------------------------|
| PrKD1         | Negative regulator | Inactivate SNAIL  | Prostate     | Du et al., 2010             |
|               |                    |   | Breast       | Zheng et al., 2014          |
|               |                    | Phosphorylate junctional proteins (E-cadherin and $\beta$ -catenin)               | Prostate     | Jaggi et al., 2005          |
|               |                    | Phosphorylate Rabaptin-5  | Breast       | Christoforides et al., 2012 |
|               |                    | Repress the expression of MMPs  |              | Eiseler et al., 2009        |
|               |                    | Phosphorylate SSH1L and inhibit cofilin dephosphorylation                         | Melanoma     | Peterburs et al., 2009      |
|               |                    | Upregulate E-cadherin expression and $\beta$ -catenin localisation                |              | Merzoug-Larabi et al., 2017 |
| PrKD2         | Positive regulator | Phosphorylate IKK $\beta$ , nuclear translocation and activation of NF $\kappa$ B | Prostate     | Zou et al., 2012            |
|               |                    | Promotes PI3K/Akt/GSK-3 $\beta$ signalling  |              | Zhu et al., 2016            |
|               |                    | Stimulate expression and secretion of MMP-7 and MMP-9                             | Liver        | Wille et al., 2014          |
|               |                    | Regulate MMP-1 and integrin expression  |              | Bernhart et al., 2013       |
| PrKD3         | Positive regulator | Activate NF $\kappa$ B and deactivate HDAC1                                       | Breast       | Zou et al., 2012            |
|               |                    | Stimulate secretion of MMP-9  |              | LaValle et al., 2012        |
|               |                    | Activate PAK4/LIMK signalling   |              | Döppler, 2014               |
|               |                    | Phosphorylate GIT1 to regulate cytoskeletal remodelling                           |              | Huck et al., 2012           |

## 1.5 Chemokine receptor internalisation and trafficking

Chemokine receptors can undergo constitutive receptor internalisation and trafficking in the absence of chemokine ligands (Meiser et al., 2008). Although the biological significance is not evident for conventional chemokine receptors, ligand-independent internalisation has been considered as a mechanism for the properties of chemokine scavenger receptors, such as US28 (Fraile-Ramos et al., 2003) and D6 (Bonecchi et al., 2004). Though the dynamics of receptor sensitisation and desensitisation is highly dependent of ligand stimulation, and the receptor trafficking pathways may vary with different receptor-ligand combinations involved.

To date, two distinct pathways of receptor endocytosis have been proposed: clathrin-dependent pathway and caveolae-dependent pathway (**Figure 1.20**) (Borrioni et al., 2010). Some receptors may favour one pathway over the other (Signoret et al., 2005), while some may utilise both (Mueller et al., 2002). This could be implicated by the constitutive expression of specific adaptor proteins, the lipid composition of the plasma membrane in proximity to the receptor domain or post-translational modifications of the receptor.

### 1.5.1 Receptor internalisation through clathrin-dependent pathway

Clathrin-dependent pathway is the best understood pathway in GPCR endocytosis (Ferguson et al., 1996). Particularly for chemokine receptor internalisation, clathrin-mediated pathway is demonstrated an important role for a variety of chemokine receptors, including CXCR1 (Barlic et al., 1999), CXCR2 (Yang et al., 1999), CXCR4 (Signoret et al., 1997), CCR5 (Signoret et al., 2005) and CCR7 (Otero et al., 2006). Following the binding of chemokine ligand, intracellular kinases, such as G-protein coupled receptor kinases (GRKs) and protein kinase C (PKC), phosphorylate serine and threonine residues in the intracellular loops and carboxyl-terminus of chemokine receptors (Borrioni et al., 2010). Together with the di-leucin motifs in the carboxyl-terminal domain, the phosphorylated receptor facilitates the recruitment of adaptor proteins associated with clathrin. The main adaptor proteins are adaptin 2 (AP-2) (Laporte et al., 1999) and  $\beta$ -arrestins (Goodman et al., 1996; Robinson, 2015). Evidence revealed that phosphorylated residues in the carboxyl terminus and intracellular

loops are necessary for  $\beta$ -arrestin binding (Cheng et al., 2000; Hüttenrauch et al., 2002). AP-2 binding involves highly conserved Leu-Leu, Ile-Leu, Leu-Ile motifs in the carboxyl terminus (Heilker et al., 1996). After the assembly of clathrin-coated pits, the plasma membrane is then invaginated by the action of the GTPase dynamin, inducing the budding of clathrin-coated pits and severing from the plasma membrane. The receptor-ligand complex are eventually translocated to the early endosomal compartment (**Figure 1.20**) (Hanyaloglu and Zastrow, 2008; van der Blik et al., 1993).

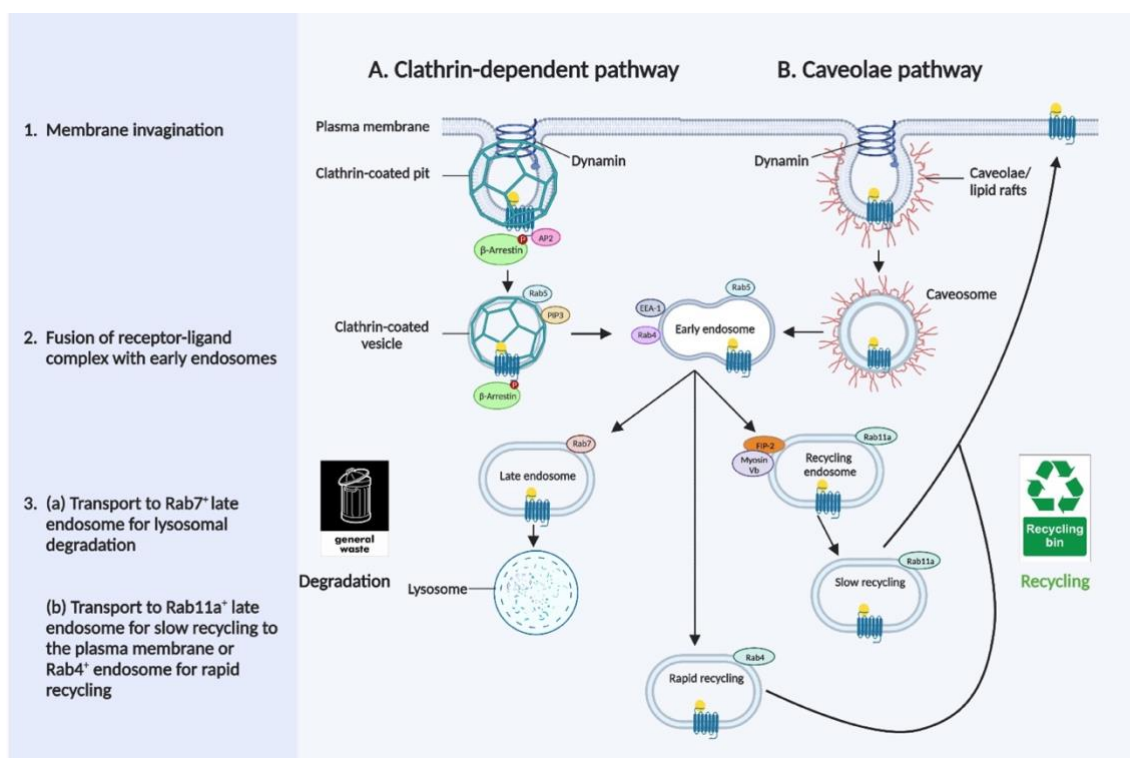


**Figure 1.20. Schematic diagram summarising the two major pathways in chemokine receptor internalisation.** A: Clathrin-dependent pathway; B: Caveolae-dependent pathway. In clathrin-dependent pathway, following the activation of chemokine receptor, receptor is phosphorylated by intracellular kinases, which facilitates the recruitment of  $\beta$ -arrestins.  $\beta$ -arrestins serve as scaffold proteins and associate with clathrin and other adaptor proteins, e.g. AP2, in the assembly of a clathrin-coated pit on the plasma membrane. By the action of dynamin, the plasma membrane is subsequently invaginated, inducing the budding of clathrin-coated pit and endocytosis of the receptor complex into the early endosomes (Signoret et al., 1997). In caveolae-dependent pathway, the process is primarily dependent of lipid rafts, named caveolae, localised in the plasma

membrane. Without the requirement of receptor phosphorylation, upon the stimulation of chemokine ligands, chemokine receptor is internalised together with caveolae to form a caveosome compartment by the action of dynamin. The caveosome then fuses with early endosomes independent of clathrin (Nichols and Lippincott-Schwartz, 2001). In both pathways, consequently, the fate of receptor is dependent of its localisation either in the late endosomal compartment for lysosomal degradation or the perinuclear compartment for recycling (Ferguson, 2001) (Image created with BioRender.com).

In the aspect of molecular dynamics of clathrin-dependent receptor endocytosis, the process begins with nucleation of a group of plasma membrane adaptor proteins, such as F-BAR domain proteins and clathrin (Ehrlich et al., 2004). By the acquisition of cargo and interaction with receptor, the plasma membrane proteins are stabilised to form a clathrin-coated pit (CCP), followed by CCP invagination via clathrin polymerisation (Gaidarov et al., 1999) together with the addition of adaptor proteins and actin (Ferguson et al., 2009). The deeply invaginated CCP is then formed with an invaginated neck that is pinched off by the action of the GTPase dynamin and phosphoinositide (PI) phosphatase (Bashkirov et al., 2008; Liu et al., 2010). The clathrin-coated vesicle (CCV) is uncoated in the recruitment of GAK/auxilin proteins, and subsequently processed by endosomal machinery (Lee et al., 2006) (**Figure 1.21**).

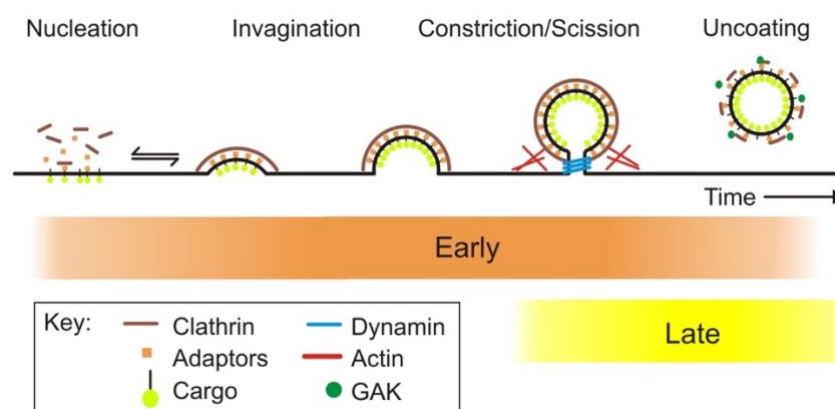


**Figure 1.21. Schematic diagram showing the molecular dynamics of clathrin-dependent endocytosis.** The process begins with nucleation of adaptor proteins on the plasma membrane, which are in turn stabilised by the interactions with cargos to form a CCP. CCP is invaginated via clathrin

polymerisation, followed by scission by the action of the GTPase dynamin. Through the recruitment of GAK/auxilin, CCV is formed and uncoated, which is subsequently processed by endosomal machinery (Image taken from Taylor et al., 2011).

### **1.5.2 Receptor internalisation through caveolae-dependent pathway**

Alternative pathway of receptor endocytosis, independent of clathrin, is regulated by caveolae (also known as lipid rafts). The lipid rafts are cholesterol and glycosphingolipid-rich, detergent-resistant structures localised in the plasma membrane (Anderson, 1998). The lipid rafts are formed by a set of caveolin proteins (caveolin-1, -2, and -3) in oligomer held by the hydrophobic interactions between sphingomyelin and glycosphingolipids (Anderson, 1998). The microdomain is stabilised by the intercalation of cholesterol molecules (**Figure 1.22**) (Anderson, 1998; Williams and Lisanti, 2004). In the formation of membrane invaginations, the key proteins involved are caveolin, cavins, the BAR protein domain-containing syndapin/Pacsin2, and the dynamin-related ATPase EHD2 (Parton et al., 2020b) (**Figure 1.23**). Current studies proposed that the incorporation of caveolin proteins and cholesterol molecules is crucial in the formation of the bulb-shaped membrane invaginations (Hayer et al., 2010; Ariotti et al., 2015). Cavins oligomerise into trimers, which surround the membrane invagination in the formation of caveolar coating (Gambin et al., 2014). Pacsin2 and EHD2 are localised at the neck of the membrane invaginations and involved in bending and stabilising caveolae (Hansen et al., 2011; Morén et al., 2012).

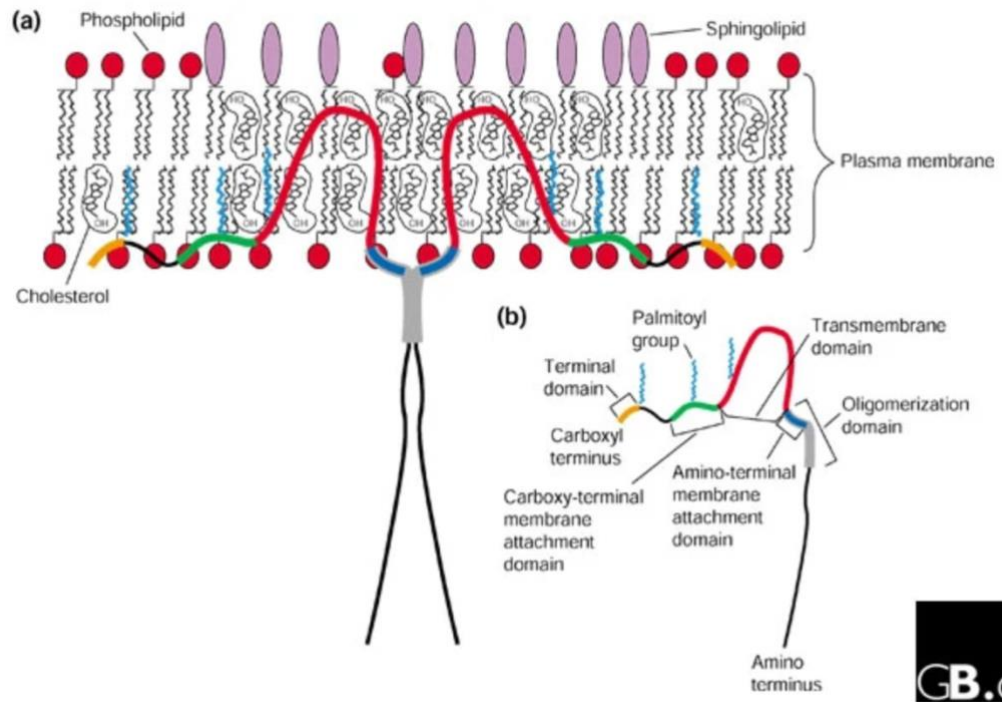


**Figure 1.22. Structure of caveolae (also known as lipid rafts) in the plasma membrane.** The lipid rafts are comprised of cholesterol and glycosphingolipids localised in the plasma membrane. A unit of lipid rafts are formed by a set of caveolin proteins in oligomer held by hydrophobic interactions between sphingomyelin and glycosphingolipids and stabilised by cholesterol (Image taken from Williams and Lisanti, 2004).

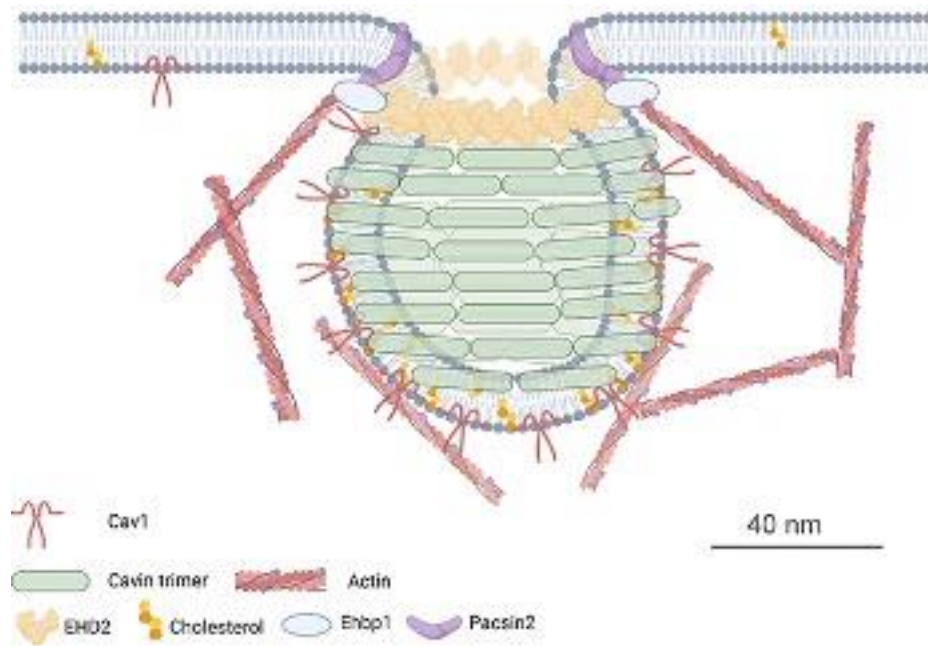


**Figure 1.23. Structure of caveolae-coated membrane invaginations.**

The assembly of membrane proteins, including actin, caveolin, caveins, the BAR protein domain-containing syndapin/Pacsin2, and the dynamin-related ATPase EHD2 triggers the formation of membrane invaginations for caveolae-dependent endocytosis (Parton et al., 2020b) (Image taken from Matthaeus and Taraska, 2021).

In general, four steps are involved in the process of caveolae-dependent receptor internalisation: (1) caveolae dynamics at the plasma membrane, (2) caveolae detachment from plasma membrane, (3) intracellular trafficking either through endosomes or other intracellular organelles, (4) recycling of caveolae. Receptors on the plasma membrane are constitutively localised with the cytoplasmic coat on caveolae (Parton and Howes, 2010; Cheng and Nichols, 2016). Caveolae-dependent endocytosis begins with the assembly of caveolae proteins to form membrane invaginations associated with the receptor as mentioned above. How the receptor activation by the ligand triggers the process of caveolae dynamics is yet to be elucidated. In caveolae detachment, it was revealed that the removal of EHD2 from the neck of caveolae promotes detachment from plasma membrane followed by intracellular trafficking (Morén et al., 2012). Apart from EHD2, dynamin has also been proposed to be involved in this process (Nichols and Lippincott-Schwartz, 2001). Yet, whether dynamin interacts directly with caveolae or in combination with other intracellular proteins needs to be further investigated.

Following caveolae detachment from plasma membrane, the receptor-caveolae complex is internalised and traffic to intracellular organelles (Pelkmans et al., 2004; Bravo-Sagua et al., 2019; Foster et al., 2020). In the conventional endocytic pathway, the receptor-caveolae complex transport to endosomes, followed by being directed either into lysosome for degradation or back to plasma membrane for recycling (Pelkmans et al., 2004). This will be detailed in the next section. Other trafficking pathways involving endoplasmic reticulum (ER) and mitochondria has recently been uncovered by the advances in proteomics and imaging. Caveolae has been found to form specific contact sites with ER or mitochondria following translocation from the plasma membrane to ER or mitochondria in the regulation of energy and metabolism (Bravo-Sagua et al., 2019; Foster et al., 2020). However, further downstream mechanisms involved is yet to be investigated.

Relating to chemokine receptors, CCR2 (García Lopez et al., 2009), CCR4 (Mariani et al., 2004), CCR5 (Mueller et al., 2002; Fraile-Ramos et al., 2003) and CXCR4 (Mañes et al., 2000) have been demonstrated to use caveolae-dependent pathway, in addition to clathrin-dependent pathway. Post-translational modification of chemokine receptors is a key factor for association with the lipid rafts. More specifically, the palmitoylation of cysteine residues in C-terminal tail in CCR5 is prone to insertion in cholesterol-enriched raft microdomains, which structurally favours the caveolae-dependent pathway (Venkatesan et al., 2003).

### **1.5.3 Receptor degradation and recycling**

In both pathways of receptor internalisation, following endocytosis of receptor, the receptor-ligand complex then localises to Rab5-positive early endosome. PI3K is recruited by Rab5, promoting PI(4,5)P<sub>2</sub> accumulation (Miaczynska and Zerial, 2002). In the recruitment of early endosomal antigen-1 (EEA-1), the process stimulates fusion of the receptor-ligand complex with early endosomes, particularly for CXCR4 and CCR5 (Bucci et al., 1992; Venkatesan et al., 2003). Subsequently, the fate of receptor is dependent of its localisation either in the late endosomal compartment for lysosomal degradation or the perinuclear compartment for recycling back to the plasma membrane (**Figure 1.20**) (Ferguson, 2001).

For receptor degradation, the receptor complex transports to Rab7-positive late endosome. Rab7, in association with microtubule motor proteins, mediates translocation of late endosome to lysosome for lysosomal degradation (Jordens et al., 2001). Studies demonstrate that prolonged treatment of chemokine ligand results in translocation of receptor to lysosomal-associated membrane protein-1 (LAMP-1)-positive lysosomal compartment regulated by Rab7 (Marchese and Benovic, 2001; Fan et al., 2003).

For receptor recycling, there are two pathways: slow and rapid. Rab11a is responsible for the slow recycling process, whereas Rab4 contributes to the rapid process. The receptor complex can localise in Rab11a-positive perinuclear recycling compartment and trafficking back to the membrane (Ullrich et al., 1996). Alternatively, rapid recycling, which bypasses Rab11a-positive endosomes, can occur in a PI3K-dependent manner through the Rab4-positive endosomes. Instead of localising in Rab11a-positive compartment, receptor complex is recycled via Rab4-positive endosomes (Hunyady et al., 2002).

### **1.6 Roles of CCR5 in cancer**

CCR5, a chemokine receptor for the chemokine ligands: CCL3 (MIP1 $\alpha$ ), CCL4 (MIP1 $\beta$ ) and CCL5 (RANTES), was first discovered in 1996 and known to be a HIV-1 co-receptor. Studies later revealed the immune-associated roles of CCR5 in clearance of viral infections, allograft rejection and autoimmunity. Emerging evidence demonstrates the controversial pro- and anti-tumour roles of CCR5 in cancer.

The anti-tumour role of CCR5 is implicated by the expression of CCR5 in CD4<sup>+</sup>, CD8<sup>+</sup> T cells and antigen-presenting cell acting as a coordinator to potentiate CD8<sup>+</sup> T cell priming. Subsequently, CD8<sup>+</sup> T cell infiltrates from the lymph node to the tumour environment as a result of tumour clearance (González-Martín et al., 2012). On the other hand, evidence shows that CCR5 in myeloid cells contributes the pro-tumour role in cancer metastasis. The secretion of CCL3, 4 and 5 from tumour cells initiates proliferation of CCR5<sup>+</sup> polymorphonuclear myeloid-derived suppressor cells (PMN-MDSCs) at the bone marrow, which in turn triggers PMN-MDSCs to mobilise from the bone marrow to the tumour site through the blood

circulation. The colonisation of PMN-MDSCs within the tumour environment inhibits the anti-tumour function of T cells. Along with inducing arginase-1 (Arg-1), PMN-MDSCs potentiate the immune-suppressive effect in tumour and promote tumour growth (Hawila et al., 2017).

By translating the immunosurveillance roles of CCR5 into a clinical trial, it was demonstrated that inhibition of CCL5/CCR5 axis using a CCR5 antagonist, maraviroc, leads to repolarisation of tumour-associated macrophages in colorectal cancer (CRC), resulting in mitigating pro-tumour inflammatory microenvironment (Halama et al., 2016). This finding has proven CCR5 antagonist has potential to be an adjuvant therapy for metastatic cancers. Yet, the activity of CCR5 on T cells in other cancer types remain to be elucidated as it could be context dependent.

### **1.6.1 Structure of CCR5**

The human CCR5 receptor is made up of 352 amino acids with a molecular weight of 40.6kDa (Samson et al., 1996). As mentioned previously, chemokine receptors typically contain an extracellular N-terminus, seven transmembrane domains (7TMDs) including two antiparallel  $\beta$ -sheets, three disulfide bonds, an amino-terminal  $\alpha$ -helix linked by three extracellular loops (ECLs) and three intracellular loops (ICLs), and a cytoplasmic C-terminus (**Figure 1.24**). Within the conserved structure, CCR5 additionally possesses specific motifs of ionic or hydrophobic regions with post-translational modifications that dictates chemokine ligand binding and functional responses of the receptor (**Figure 1.24**).

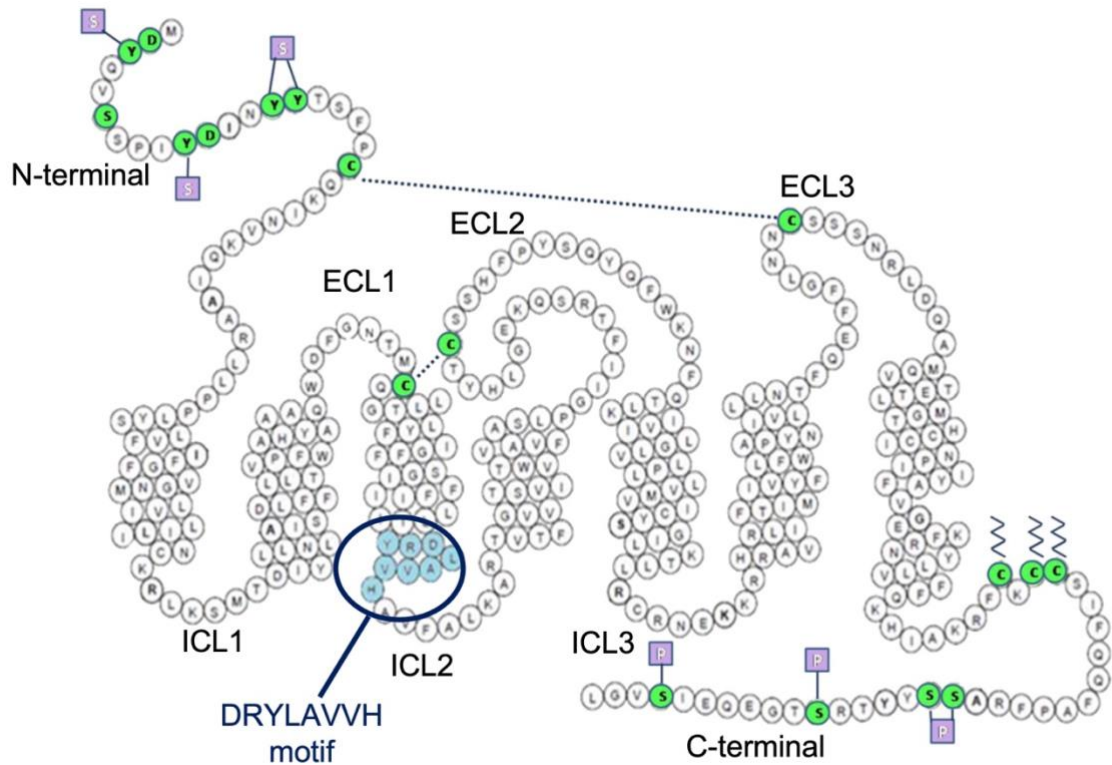


**Figure 1.24. Two-dimensional structure of CCR5.** Protein structure of CCR5 indicating important regions, including disulfide linkages (represented by the dotted lines), DRYLAVVH motif (highlighted in blue), palmitoylation C-terminal site (represented by the zig-zag lines), sulfate and phosphate moieties (boxed “S” and “P”) (Image taken from Barmania and Pepper, 2013).

Tyrosine and acidic amino acid-rich N-terminus is critical in chemokine binding and HIV co-receptor activity (Dragic et al., 1998; Blanpain et al., 1999a). By post-translationally sulfation of the N-terminal tyrosine residues in CCR5, it facilitates the receptor interaction with ligands and gp120 of HIV due to the increase in the net negative charge (Farzan et al., 1999). In addition, O-linked glycosylation modification of N-terminal Ser<sup>6</sup> was also found to affect chemokine binding affinity of CCR5 (Bannert et al., 2001). Like other chemokine receptors, the three ECLs and N-terminus is featured with cysteine residues which are critical in cell surface receptor expression. It was demonstrated that the cysteine mutants in CCR5 diminishes their response to CCR5 agonists due to reduced cell surface expression (Blanpain et al., 1999b). Within the ICLs, there is a conserved sequence motif (DRYLAVVA) in the second ICL and the short third ICL contains charged amino acids (Oppermann, 2004). It is notable that there is a conserved

disulfide bridge between the first and second ECLs, and an additional disulfide bond is found between the N-terminus and third ECL (Tan et al., 2013). The disulfide bonds play an important role in stabilising receptor conformation in a form of constraint in ECL, which is essential for specific ligand binding (Perlman et al., 1995; Dohlman et al., 1990; Wheatley et al., 2012). In the second TMD, a specific TxP motif, consisting of threonine and proline residues with any amino acids in-between annotated by “x”, creates a structural constraint for receptor functionality (Govaerts et al., 2001). At the C-terminus, the region is enriched in serine and threonine residues, which are the phosphorylation sites for G-protein coupled receptor kinases (Oppermann et al., 1999). Apart from N-terminus, other PTMs also take place at the C-terminus that affect CCR5 cell surface expression and functionality (Blanpain et al., 2001; Percherancier et al., 2001). A study showed that palmitoylation at Cys<sup>321</sup>, Cys<sup>323</sup> and Cys<sup>324</sup> of the C-terminus is involved in receptor-mediated endocytosis via caveolae, facilitating transport of CCR5 from the cell surface (Blanpain et al., 2001; Venkatesan et al., 2003).

In respect to the binding modes of CCR5-CCL3 complex, the N terminus of CCR5 interacts with a groove between the N-loop, 40s-loop and  $\beta_3$ -strand in CCL3. The three potentially sulphated tyrosine residues (Y10, Y14 and Y15) in the N terminus of CCR5 are known to be essential for binding to positively charged residues of CCL3 (R17, K44, R45 and R47) (**Figure 1.25**) (Zhang et al., 2021). Apart from the tyrosine-based interactions, other interactions have been identified: a hydrophobic interaction between the residues (I9, Y10 and I12) in CCR5 and residue (F23) in CCL3, and a hydrophilic interaction between residues (D11 and N13) in CCR5 and residue (R47) in CCL3 (Zhang et al., 2021) (**Figure 1.25**).

At the CRS2 region, the N terminus of CCL3 adopt a ‘hook’-like conformation stabilised by a salt bridge formed between the negatively charged residue (D5) in CCL3 and the positively charged nitrogen of residue (S1) (**Figure 1.25**). In the formation of hydrophobic interactions with W86<sup>2.60</sup>, T105<sup>3.29</sup>, Y108<sup>3.32</sup> and F109<sup>3.33</sup> [superscript indicates Ballesteros-Weinstein nomenclature for GPCRs] (Ballesteros and Weinstein, 1995) in helices II and III of CCR5, the first three residues of CCL3 accommodate at the bottom of the binding pocket (**Figure 1.25**) (Zhang et al., 2021).

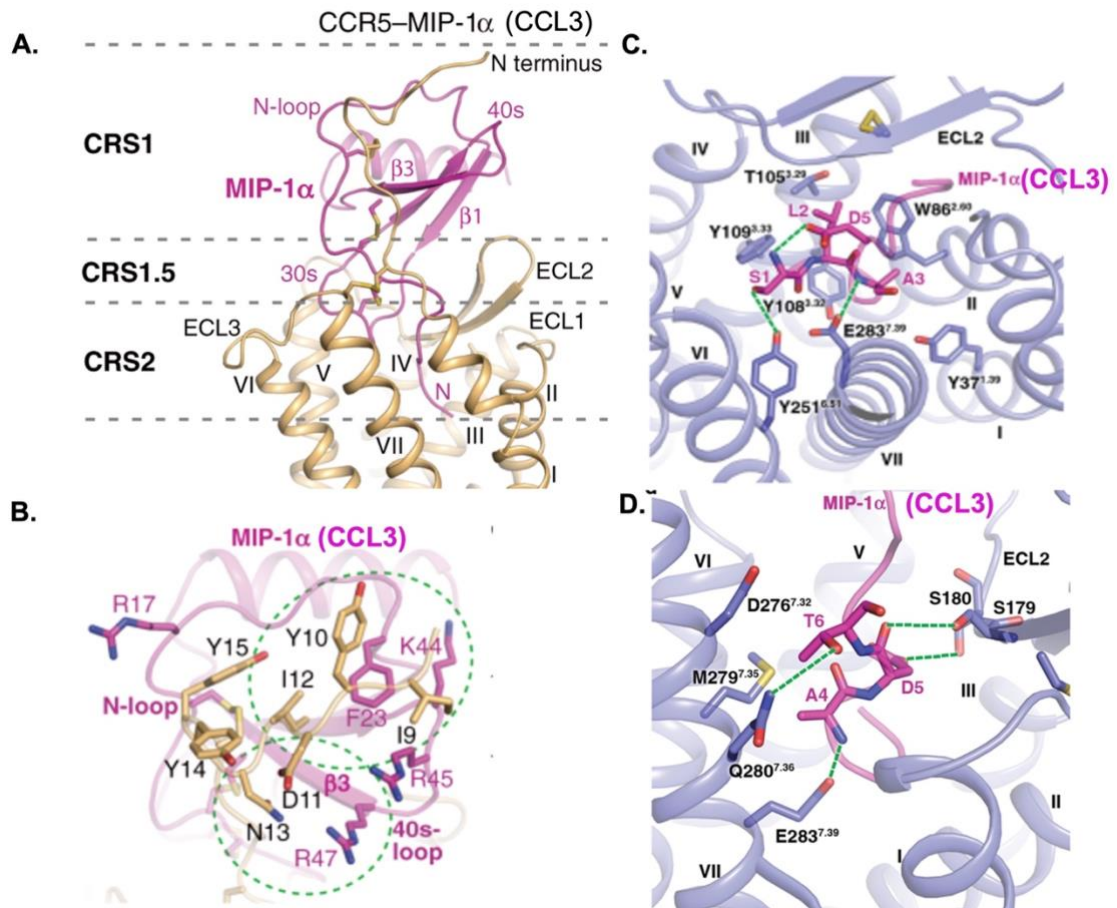


**Figure 1.25. Molecular models of receptor-chemokine (CCR5-CCL3) complex.** (a) Overall chemokine CCL3 binding mode in CCR5 including regions of CRS1, CRS1.5 and CRS2. CCR5 is coloured in gold and CCL3 is coloured in magenta. The regions of CRS1, CRS1.5 and CRS2 are indicated by grey dashed lines; (b) The closer illustration of the CRS1 of the CCR5-CCL3 structure. The key residues involved in interactions between CCR5 and CCL3 are shown as structural skeletons coloured in gold and magenta respectively. The two interaction cores apart from the tyrosine-based interactions are indicated by green dashed circles; (c) Illustration of the CRS2 of the CCR5-CCL3 structure showing the binding mode of the CCL3 residues (S1-A3); (d) Illustration of the CRS2 of the CCR5-CCL3 structure showing the binding mode of the CCL3 residues (A4-T6). The residues involved in interactions between CCL3 and CCR5 are shown as structural skeleton coloured in magenta and blue respectively. The polar interactions are indicated as green dashed lines (Image taken from Zhang et al., 2021).

## 1.6.2 CCR5-targeting small molecules

Maraviroc, is the only CCR5-targeting drug clinically approved for AIDS treatment (**Table 1.3**) (Dorr et al., 2005). In the clinical application of anti-cancer therapy, maraviroc has been progressed to a phase II clinical trial for liver metastases of advanced refractory colorectal cancer (CRC) as a combination therapy (clinicaltrials.gov identifier: NCT01736813) (Halama et al., 2016). Maraviroc is characterised as an inverse agonist of CCR5, which was demonstrated to stabilise CCR5 in an inactive conformation (Garcia-Perez et al., 2011b). With regards to the structure of CCR5, the highly conserved residues, Trp248<sup>6.48</sup> and Tyr244<sup>6.44</sup> [superscript indicates Ballesteros-Weinstein nomenclature for GPCRs] (Ballesteros and Weinstein, 1995), are involved in relaying the conformational changes in the binding pocket into the cytoplasmic domain following ligand binding (Katritch et al., 2013). Within the conformation of both residue in inactive state of CCR5, the phenyl group of Maraviroc interacts with Trp248<sup>6.48</sup> [superscript indicates Ballesteros-Weinstein nomenclature for GPCRs] (Ballesteros and Weinstein, 1995) through hydrophobic interactions, preventing from the activation of CCR5. The inactive conformation of CCR5/Maraviroc complex triggers a locking effect of helix VI with other helices of the 7TM domains by ionic interactions between residues at the intracellular side of CCR5, which prevent from G-protein binding (Garcia-Perez et al., 2011b). It was also shown that Maraviroc is an allosteric modulator that inhibits the interaction of chemokine with CCR5 at an allosteric site of the receptor (Garcia-Perez et al., 2011a). Relating to the mechanisms of HIV-1 infection, the N-terminus and ECL2 of CCR5 are the major counterparts in gp120 binding on HIV-1 (Huang et al., 2007). The mode of action of Maraviroc is thought to be by interfering with the binding of gp120 in an allosteric inhibition manner by stabilising CCR5 in inactive conformation, leading to inactivation of CCR5 (Garcia-Perez et al., 2011a).

## 1.7 Roles of CXCR4 in cancer

CXCL12/CXCR4 signalling is well-known to play a critical role in homeostasis and pathogenesis in malignant diseases including cancer supported by numerous studies (García-Cuesta et al., 2019; Mortezaee, 2020). CXCR4 is shown to be highly expressed in various types of cancer: breast cancer (Chen et al., 2013), colorectal cancer (CRC) (D'Alterio et al., 2016), renal cell carcinoma (RCC) (Pan et al., 2006), pancreatic cancer (Zhang et al., 2018), adrenocortical

cancer (Bluemel et al., 2017) and prostate cancer (Akashi et al., 2008). However, the functional significance in tumorigenesis and metastasis might not be implicated by high expression of CXCR4. No correlation between CXCR4 expression and the extent of metastasis and tumour growth was observed in some types or subtypes of cancer (Akashi et al., 2008; Chen et al., 2013).

There is emerging evidence that the CXCL12/CXCR4 axis is involved in modulating immune surveillance contributing to cancer growth and invasion. Studies demonstrate that CXCL12/CXCR4 signalling leads to transforming growth factor (TGF)-mediated metastasis through the infiltration of myeloid-derived suppressor cells (MDSCs) into tumours (Yang et al., 2008), and also suppresses NK cell-mediated immune surveillance in tumours to enhance tumour growth (Yang et al., 2018). Moreover, a recent study shows that CXCR4 inhibition has synergistic effect of anti-PD1 therapy by activating and enhancing T-cell infiltration to tumours (Zboralski et al., 2017). Taken together, these findings support CXCR4 targeting could potentially be a therapeutic target to improve immune surveillance in cancer for positive prognosis.

### **1.7.1 Structure of CXCR4**

The overall structure of CXCR4 (**Figure 1.26**) is similar to CCR5 as described above, however, CXCR4 also displays some structural differences that differentiate CXCR4 binding to its cognate chemokine ligands and functional responses from other chemokine receptors. With regards to the differences in the disposition of the TM domains in CXCR4, a tighter helical turn of helix II on the extracellular side was observed in CXCR4, which redefines a ligand-binding pocket differential from other chemokine receptor models. Also, CXCR4 possesses longer helices V and VII reaching further into the extracellular space (Wu et al., 2010). On the intracellular side, an extended conformation of the C-terminus is adopted by CXCR4, which forms a number of contacts with symmetry-related molecules, for example, IT1t. Unlike CCR5, the palmitoylation sites at the C-terminus are absent in CXCR4 (Wu et al., 2010).

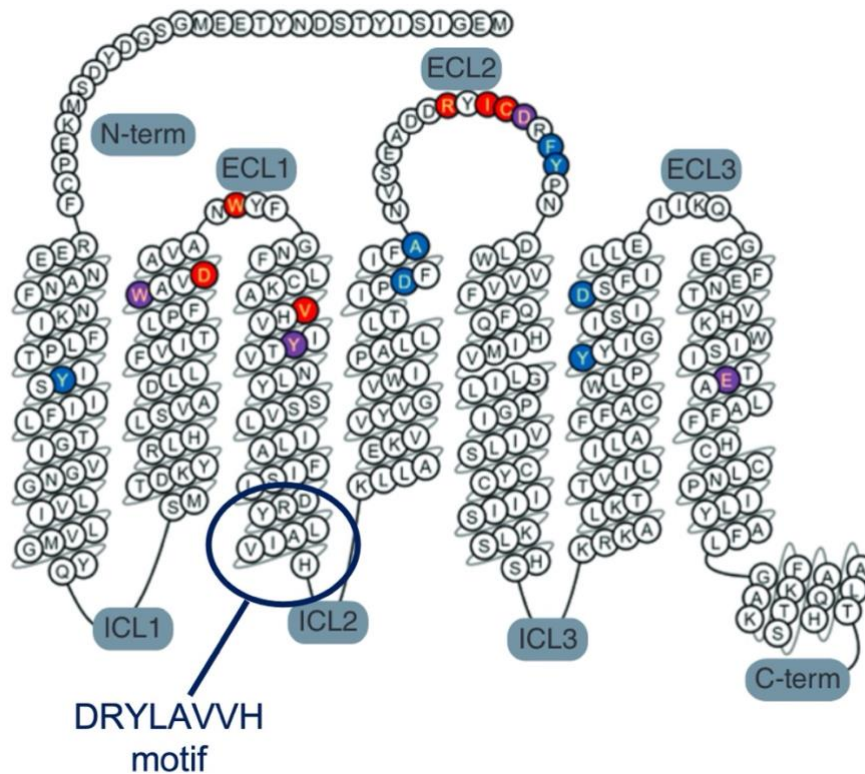


**Figure 1.26. Two-dimensional structure of CXCR4.** Protein structure of CXCR4 indicating the DRYLAVVH motif (circled in blue) and key residues interacting with AMD3100 (highlighted in blue), IT1t (highlighted in red) and both (highlighted in purple) (Image taken from Caspar et al., 2022).

With respect to distinct binding modes of CXCR4-CXCL12 complex, the basic N-loop and  $\beta_2$ - $\beta_3$  loops of CXCL12 interact with a sulfotyrosine specifically present in the proximal N terminus of CXCR4. This interaction is further enhanced by an epitope in the  $\beta_3$  strand of CXCL12 that interacts with residues (D22 and E26) in CXCR4 (**Figure 1.27**) (Qin et al., 2015). Moreover, particularly for CRS1.5, the binding region of CXCL12 is bend without formation of protein-protein interface contacts (**Figure 1.27**), unlike CCL3 with a straight binding region through  $\beta$ -sheet interactions within chemokine dimers (Zhang et al., 2021). The bend region directs the N terminus of CXCL12 towards helices V and VI of CXCR4 in the formation of hydrogen bonding between CXCL12 (R8) and CXCR4 (D262<sup>6.58</sup>) [superscript indicates Ballesteros-Weinstein nomenclature for GPCRs] (Ballesteros and Weinstein, 1995) (**Figure 1.27**). These residues are highly conserved in CXC- chemokines and receptors, but not in CC- chemokines and receptors (Qin et al., 2015)..

As illustrated previously that CXC- chemokines can dimerise by  $\beta_1$  strands (Figure 1.5) (Miller and Mayo, 2017), the conformation of the CXCL12 dimers favours the binding to single receptor subunits in a CXCR4 dimer, instead of binding to both subunits in a receptor dimer (Figure 1.27) (Qin et al., 2015).

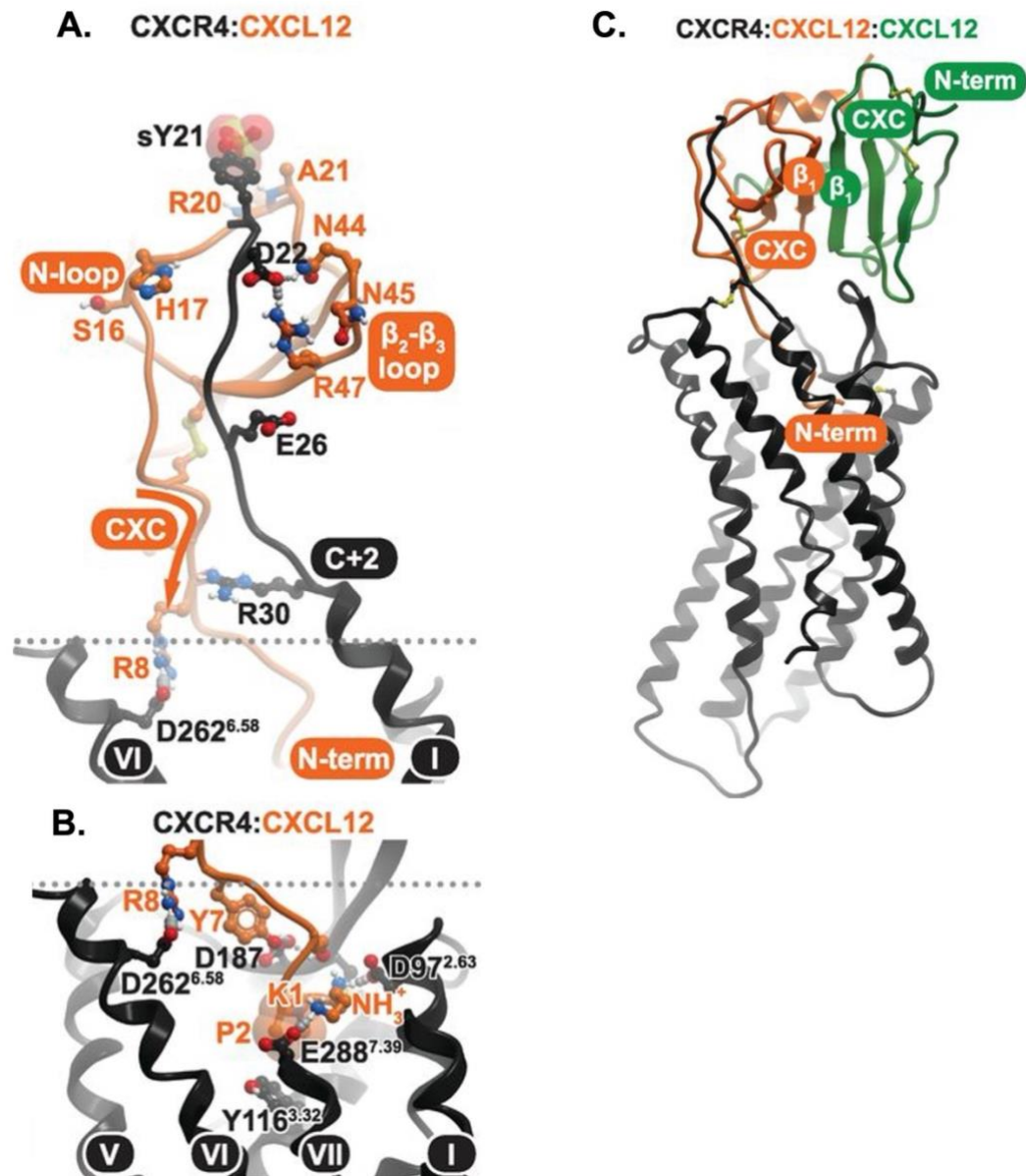


**Figure 1.27. Molecular models of receptor-chemokine (CXCR4-CXCL12) complex.** (a) CRS1 and CRS1.5 interactions in CXCR4-CXCL12 complex annotated with key binding components. CXCR4 is coloured in grey and CXCL12 is coloured in orange; (b) CRS2 interactions in CXCR4-CXCL12 complex annotated with key residues involved; (c) Superposition of the CXCL12 dimer onto the CXCR4 dimer. Two subunits of the CXCL12 dimer are coloured in orange and green respectively. Two subunits of the

CXCR4 dimer are coloured in grey and black (Image taken from Qin et al., 2015).

### 1.7.2 CXCR4-targeting small molecules

In the past decade, multiple small molecule CXCR4 antagonists have been developed based on established knowledge and evidence on CXCR4 structure and its functional importance in cancer (**Table 1.3**) and other immune disorders. The most well-known CXCR4 antagonist is Plerixafor (also known as Mozobil®, AMD3100), which was initially approved by the US Food and Drug Administration (FDA) for autologous transplantation in patients with Non-Hodgkin's lymphoma (NHL) or multiple myeloma (MM) (De Clercq, 2005). Currently, clinical trials for anti-cancer application are in progress from safety assessment of drug administration in Phase I to effectiveness testing for various types of cancer in Phase II (De Clercq, 2019). AMD3100 is a reversible antagonist for CXCR4. Through reversibly blocking of CXCL12/CXCR4 interaction, the mechanism of action by AMD3100 is to mobilise CXCR4-expressing hematopoietic stem cells from their reservoir in the bone marrow containing high concentration of CXCL12 (Liles et al., 2003). In the structural aspects of AMD3100, AMD3100 is composed of two cyclam moieties with a heteroaromatic phenylenebis(-methylene) linker in-between, known as bicyclam. It mainly binds into the major binding pocket of CXCR4, where one cyclam ring interacts with Asp171 in helix IV, whereas another is intercalated between the carboxylic acid groups of Asp262 and Glu288 in helices VI and VII respectively (Rosenkilde et al., 2007).

Apart from AMD3100, other CXCR4 antagonists intended for application in cancer, HIV and Warts, Hypogammaglobulinemia, Infections, and Myelokathexis (WHIM) syndrome have been developed, including mavorixafor (X4P-001) (Dale et al., 2021), LY2510924 (Peng et al., 2015), balixafortide (POL6326) (Pernas et al., 2018) and BKT140 (BL-804) (Peled et al., 2014). They are currently in clinical trials, and unfortunately some failed to be clinically approved due to high toxicity, low efficacy or poor pharmacokinetic properties.

Particularly for cancer, CXCR4 antagonists is generally thought to be synergistic to chemotherapy as an adjuvant therapy in metastatic cancers. Cancers under investigations include relapsed acute myeloid leukaemia (AML) (NCT00512252)

(Uy et al., 2012), advanced pancreatic, ovarian and colorectal cancers (NCT02179970) (Theme, 2019) (NCT03277209) (Weill Medical College of Cornell University, 2020).

Recently, emerging studies proposed a new mode of action of CXCR4-targeted ligands using a small molecule inverse agonist, IT1t. IT1t is characterised as an immunomodulator for CXCR4 through the activation of a non-canonical pathway (Thoma et al., 2008). Unlike AMD3100 targeting the major pocket, IT1t targets the minor pocket of CXCR4 defined by the side chains from helices I, II, III and VII. IT1t consists of two cyclohexane rings connected by a short flexible linker with an imidazothiazole ring. Both cyclohexane rings dock into the binding pockets of CXCR4 through hydrophobic interactions, while the imidazothiazole ring forms ionic interactions with Glu288 in helix VII of CXCR4 (Wu et al., 2010). Signalling of CXCR4 minor pocket targeted by IT1t has been thought to be distinct from the signalling of CXCL12 or AMD3100 interacting with the major pocket of CXCR4 (Caspar et al., 2022). In canonical pathway, CXCL12 primarily activates G-protein dependent pathways for downstream signalling, or recruits  $\beta$ -arrestin-2 following C-terminal phosphorylation by GRKs leading to clathrin-dependent receptor internalisation (Heuninck et al., 2019). Recent findings revealed that signalling of CXCR4 minor pocket mediates non-canonical signalling pathway, which directly interacts with the downstream signalling of Toll-like receptor (TLR) activation regulating type-I interferon (IFN) levels (Gomariz et al., 2010). This implies that IT1t potentially blocks TLR activation and reduces IFN level, exerting anti-inflammatory effect. Moreover, IT1t was demonstrated to completely block CXCL12-induced CXCR4 internalisation (White et al., 2020). Whether IT1t is directly involved in G-protein independent signalling through  $\beta$ -arrestin recruitment is yet to be investigated. On the other hand, CXCL12 also promotes dimerisation of CXCR4, which is shown to be correlated with the basal activity of  $G_i$  protein coupled to CXCR4 (Işbilir et al., 2020). IT1t was demonstrated to inhibit CXCR4 dimerisation, which in turn block the basal activity of  $G_i$  (Işbilir et al., 2020; Mona et al., 2016). This could lead to an increase in cAMP concentration and a reduction in G-protein dependent signalling including  $Ca^{2+}$  mobilisation, activation of MAPK cascade and PI3K/AKT pathway. These decremental outcomes are linked to anti-inflammatory effects with a reduction in pro-inflammatory mediators and an increase in anti-inflammatory mediators. Accumulating the findings on

IT1t, IT1t could be a potential CXCR4-targeting molecule for cancer immunotherapy.

**Table 1.3. List of CCR5 and CXCR4 antagonists currently on clinical trial for the application of cancer therapy**

| Receptor targets | Antagonists                            | Cancer types   | Study purposes   | Phases      | clinicaltrials.gov identifier               | References  |
|------------------|--|--|--|-------------|---|---|
| CCR5             | Maraviroc                              | Colorectal cancer (CRC)  | Impact on the immune microenvironment  | II          | NCT01736813                                 | Halama et al., 2016                               |
| CXCR4            | Plerixafor (AMD3100)                   | Refractory AML   | Use in combination with mitoxantrone, etoposide and cytarabine (MEC) chemotherapy    | I/II        | NCT00512252                                 | Washington University School of Medicine, 2016    |
|                  |  | Advanced pancreatic, ovarian and colorectal cancers  | Safety assessment of continuous IV administration                                    | I           | NCT02179970                                 | Cancer Theme, 2019                                |
|                  |  |  | Impact on the immune microenvironment  | I           | NCT03277209                                 | Weill Medical College of Cornell University, 2020 |
|                  | Refractory haematologic malignancies   | Use in combination with fludarabine, thiotepa and melphalan for a second allogeneic stem cell transplantation for paediatric haematologic malignancies | I  | NCT01068301 | St. Jude Children's Research Hospital, 2014 |   |
|                  | BL-8040                                | AML  | Evaluation on safety, tolerability and efficacy in the combination with Atezolizumab | IB/II       | NCT03154827                                 | BioLineRx, Ltd., 2020                             |
| Aplastic anaemia |  | Evaluation on safety and efficacy on top of standard immunotherapy regime  | IIA  | NCT02462252 | BioLineRx, Ltd., 2020                       |   |
| Balixafortide    | HER2-negative metastatic breast cancer | Use in combination with eribulin chemotherapy  | I  | NCT01837095 | Pernas et al., 2018                         |   |

## 1.8 Concluding remarks

Chemokine signalling is a complicated, multidimensional system that involves redundancy of chemokine receptor-ligand binding, biased signalling and highly context-dependent signalling properties. As described above, chemokine signalling plays a critical regulatory role in a diversity of cancer types in either tumour-promoting or tumour-suppressive manner. Therefore, accurately understanding the mechanisms underlying the complexity of chemokine signalling system is necessary for the design and development of chemokine-targeted therapies. By applying novel chemokine-targeted drugs in combination with conventional chemotherapy or immune therapy, it is aimed to better improve therapeutic outcomes and reduce toxicity and side effects. In summary:

- Chemokine ligands can form dimers or interact with GAGs that adopt different conformations and binding interfaces with chemokine receptors, which could lead to selectivity in receptor binding and signalling bias.
- Formation of chemokine receptor homodimers and heterodimers contributes to ligand and functional selectivity, exhibiting allosteric properties in receptor pharmacology.
- Protein kinases exhibits isoform-specific roles in receptor phosphorylation (known as phosphorylation barcode) and phosphorylation of specific downstream signalling proteins that divert signalling transduction towards a selective pathway.
- Activated chemokine receptors not only could signal from cell surface through G proteins, but also could signal after internalisation independent of G proteins from subcellular sites and activate distinct signalling pathways.
- The signalling pattern of chemokine system strongly vary between cell types as different cellular contexts exhibit different receptor expression profiles and different sets of proteins in different isoforms directly or indirectly interacting with the receptors. In this respect, distinct interactions

between different signalling partners could contribute to a variety of cellular outcomes in different cell types.

### **1.9 Research objectives**

The introduction has detailed more thorough understanding on the structural aspects of chemokines and chemokine receptors to elucidate biased signalling in relation to favourable conformational changes revealed by numerous latest studies. In the past decade, emerging research focussed on G protein-independent signalling with the involvement of  $\beta$ -arrestins as it was found to be adopted by atypical chemokine receptors particularly and even conventional chemokine receptors in signalling modulation. In the process of G protein-independent signalling, it involves receptor phosphorylation by protein kinases, receptor internalisation and interactions with intracellular proteins for downstream signalling. In order to assess ligand-receptor interactions and interactions between intracellular proteins, studies were performed mainly using bioluminescence resonance energy transfer (BRET)-based and Förster resonance energy transfer (FRET) -based techniques in transfected cells. However, the cell lines compatible for these techniques are very limited in current technology. As mentioned previously, chemokine signalling system is highly context dependent. The observations from the effects of chemokine signalling can be cell-specific. Also, the techniques depend on cell transfection, which could generate artifacts as a result of overexpression of proteins of interest. The results might not accurately reflect the signalling mechanisms happening in cancer cell lines. By addressing these issues, there is a need to use cell lines derived from different types of cancer and endogenously expressing chemokine receptors as study models to support and confirm the accuracy of the latest findings.

Although many studies have been done on investigating the roles of critical downstream signalling proteins, such as  $\beta$ -arrestins and protein kinases, there are still some gaps in understanding on their roles particularly in CCL3-CCR5 and CXCL12-CXCR4 signalling axes. Also, there is lacking evidence on the possibility of isoform-specific and cell-specific differences in signalling outcomes.

To achieve these, the experimentation that was undertaken is as follow:

**Chapter 3:** Characterise chemokine-induced responses in different cancer cell lines. We hypothesised that different cancer cell lines express different receptor profiles and signalling proteins, resulting in different signalling patterns and resultant cellular responses mediated by chemokine stimulation. By using different cancer cell lines representing different cancer types (adherent breast cancer MCF-7 cells, T-cell leukaemia Jurkat cells and monocytic leukemia THP-1 cells), cell surface expression profile on a range of common chemokine receptors (CXCR1, CXCR2, CXCR3, CXCR4, ACKR3 and CCR5) was determined to identify which chemokine receptors are overexpressed. Focussing on the chemokine receptors overexpressed in the cancer cell lines, cellular responses were tested in the stimulation of chemokine ligands associated with the receptors, including intracellular calcium mobilisation, actin cytoskeletal rearrangement, chemotaxis and receptor internalisation.

**Chapter 4:** Investigate the mechanisms underlying chemokine-induced receptor internalisation. We hypothesised that cancer cells adopt either one of the pathways of receptor internalisation (clathrin-dependent and caveolae-dependent pathways) or both in context-dependent manner upon chemokine stimulation. By using two different cancer cell lines (adherent breast cancer MCF-7 cells and T-cell leukaemia Jurkat cells), the preferential pathways of chemokine-induced receptor internalisation were explored particularly on CCL3-CCR5 and CXCL12-CXCR4 signalling axes. To determine the involvement of the major signalling components, caveolin-1 (Cav-1) and  $\beta$ -arrestins, in receptor internalisation, immunofluorescence staining of caveolin-1 (Cav-1) was undertaken to reveal the effects of chemokine stimulation on expression level. For  $\beta$ -arrestins, overexpression of different isoforms of  $\beta$ -arrestins (arrestin-2, arrestin-3 and arrestin mutant) by plasmid DNA transfection was undertaken to examine the isoform-specific involvement and localisation of  $\beta$ -arrestins in chemokine-induced receptor internalisation. Furthermore, for the receptor internalisation assay, fluorescence-based flow cytometry was undertaken to quantify cell surface receptor expression in chemokine-stimulated condition comparable to basal condition. The roles of caveolae and clathrin in chemokine-induced receptor internalisation were determined by utilising small molecule

inhibitor treatments: membrane cholesterol-blocking agents and clathrin inhibitors respectively.

**Chapter 5:** Determine the roles of protein kinase D (PrKD) in regulating chemokine-induced cellular responses. We hypothesised that PrKD phosphorylation induces a variety of cellular responses contributing to cell migration in different cancer cell lines. In the application of two pan-PrKD inhibitors, the roles of PrKD in multiple cellular responses ( $\text{Ca}^{2+}$  mobilisation, chemotaxis, actin rearrangement and receptor internalisation) were determined in MCF-7 and Jurkat cells. By comparisons of the effects of the PrKD inhibitors in different cancer cell lines under CCL3 or CXCL12 stimulation, cell-specific or ligand-specific effects of PrKD can be confirmed. Furthermore, knockdown of protein kinase D 2 (PrKD2) using plasmid DNA transfection was attempted to identify isoform-specific effects in chemokine-induced cellular responses in MCF-7 cells.

# Chapter 2: Materials and methods

---

## 2.1 Cell lines and tissue culture

### 2.1.1 Cell culture medium and cell lines

A list of cell culture medium is detailed below:

**Table 2.1. Cell culture medium**

| Medium          | Contents   |
|-----------------|--|
| RPMI complete   | 500 mL Roswell Park Memorial Institute 1640 Medium (Corning, Biosera)<br>50 mL Heat-inactivated FCS (Invitrogen)<br>5 mL L-glutamine 200mM (Invitrogen)<br>5 mL MEM Non-essential Amino Acid Solution (100X) (Gibco)     |
| DMEM complete   | 500 mL Dulbecco's Modified Eagle's Medium-high glucose (Corning, Biosera)<br>50 mL Heat-inactivated FCS (Invitrogen)<br>5 mL L-glutamine 200mM (Invitrogen)<br>5 mL MEM Non-essential Amino Acid Solution (100X) (Gibco) |
| Serum-free RPMI | 500 mL Roswell Park Memorial Institute 1640 Medium (Corning, Biosera)<br>5 mL L-glutamine 200mM (Invitrogen)<br>5 mL MEM Non-essential Amino Acid Solution (100X) (Gibco)  |
| Serum-free DMEM | 500 mL Dulbecco's Modified Eagle's Medium-high glucose (Corning, Biosera)<br>5 mL L-glutamine 200mM (Invitrogen)<br>5 mL MEM Non-essential Amino Acid Solution (100X) (Gibco)  |

A list of cell lines used is detailed below:

**Table 2.2. Cell lines**

| Cell line* | Growth properties | Growth medium | Source  |
|------------|-------------------|---------------|---|
| THP-1      | Suspension        | RPMI complete | <i>Homo sapiens</i> monocyte cell line from peripheral blood of a one year old male infant suffering acute monocytic leukaemia  |
| Jurkat     | Suspension        | RPMI complete | <i>Homo sapiens</i> lymphoblast cell line from peripheral blood of a male donor suffering acute T cell leukaemia  |
| MCF-7      | Adherent          | DMEM complete | <i>Homo sapiens</i> breast epithelial cell line from a female donor suffering non-invasive oestrogen receptor (ER)-positive and progesterone receptor (PR)-positive breast ductal carcinoma |
| MDA-MB-231 | Adherent          | DMEM complete | <i>Homo sapiens</i> breast epithelial cell line from female adenocarcinoma patient suffering invasive triple-negative breast cancer   |

\*All cell lines are supplied by American Type Culture Collection (ATCC).

### **2.1.2 Routine tissue culture procedures**

All cell lines were cultured in 75 cm<sup>2</sup> flasks (Corning) in a humidified incubator at 37°C with 5% CO<sub>2</sub>. Cells were split at 80-95% confluency and maintained in the relevant culture medium stated in Table 2.2.

For MCF-7, cells were washed with PBS (1.5mM potassium phosphate monobasic, 3mM potassium phosphate dibasic, 150 mM NaCl; pH 7.2), then detached by adding PBS supplemented with 5 mM EDTA and left for 5 – 10 minutes at 37°C with 5% CO<sub>2</sub>. Flask was then gently agitated and cell solution was transferred to a centrifuge tube. Cells were centrifuged at 1200 rpm for 5 minutes and cell pellet was resuspended in a relevant complete culture medium. Cells were either passaged by 80-90% reduction of cell density or used for experimentation.

For MDA-MB-231 cells, cells were gently rinsed with PBS before 2 mL Trypsin/0.05% EDTA (Gibo) was added and left for 5 minutes at 37°C with 5% CO<sub>2</sub>. Cells were harvested or passaged as described above.

For suspension cells, cells were passaged or used for experimentation by directly removing appropriate volume of cell solution based on cell density and replacing with relevant fresh complete culture medium.

### **2.1.3 Cyopreservation of cells**

To freeze cells, cells were harvested as described above and centrifuged at 1200 rpm for 5 minutes. The supernatant was discarded, and the remaining cell pellet was resuspended in 1 mL freezing medium (sterile FCS + filtered 10% v/v DMSO). Cells in freezing medium were then transferred into cryotubes and chilled to -80°C for at least 24 hours before long-term storage in liquid nitrogen at -196°C.

To thaw cells, a cryotube was rapidly warmed in water bath at 37°C. Once contents were liquified, for suspension cells, cell solution was transferred into relevant complete culture medium. For adherent cells, cell solution was transferred into 5 mL relevant serum-free culture medium and centrifuged at 1200 rpm for 5 minutes. The cell pellet was resuspended in 10 mL relevant complete culture medium.

## 2.2 Small molecule inhibitors

A list of small molecule inhibitors used is detailed below:

**Table 2.3. Small molecule inhibitors**

| Inhibitor  | Target                  | Supplier | Stock concentration/<br>vehicle | Working concentration <sup>†</sup>                         | IC50   | Reference   |
|------------|-------------------------|----------|---------------------------------|--|--|---|
| CID755673  | Protein kinase D (PrKD) | Tocris   | 1 mM in DMSO                    | 2.5 $\mu\text{M}^{\ddagger}$ , 10 $\mu\text{M}^{\ddagger}$ | PrKD1 – 0.182 $\mu\text{M}$<br>PrKD2 – 0.280 $\mu\text{M}$<br>PrKD3 – 0.227 $\mu\text{M}$<br>PKC - >10 $\mu\text{M}$ | (Sharlow et al., 2008)                            |
| CID2011756 | Protein kinase D (PrKD) | Tocris   | 1 mM in DMSO                    | 2.5 $\mu\text{M}^{\ddagger}$ , 10 $\mu\text{M}^{\ddagger}$ | PrKD1 – 3.2 $\mu\text{M}$<br>PrKD2 – 0.6 $\mu\text{M}$<br>PrKD3 – 0.7 $\mu\text{M}$                                  | IC50 values are provided by the supplier (Tocris) |
| Dynasore   | Dynamin                 | Abcam    | 10 mM in DMSO                   | 80 $\mu\text{M}$   | Dynamin 1 (Dyn1) - 15 $\mu\text{M}$<br>Dynamin 2 (Dyn2) - 15 $\mu\text{M}$   | (Macia et al., 2006)                              |

| Inhibitor                  | Target   | Supplier | Stock concentration/<br>vehicle | Working concentration <sup>†</sup> | IC50   | Reference                   |
|----------------------------|----------|----------|---------------------------------|------------------------------------|--|-----------------------------|
| Dyngo-4a                   | Dynamin  | Abcam    | 10 mM in DMSO                   | 80 $\mu$ M                         | Dyn1 – 400 nM<br>Dyn2 – 200 nM<br>Clathrin-mediated endocytosis<br>– 5.5 $\mu$ M | (McCluskey et al., 2013)    |
| Filipin                    | Caveolae | Tocris   | 10 mg/ml in EtOH                | 5 $\mu$ g/ml                       | Cholera toxin<br>– 0.5 $\mu$ M   | (Orlandi and Fishman, 1998) |
| Nystatin                   | Caveolae | Tocris   | 10 mg/ml in EtOH                | 50 $\mu$ g/ml                      | N.A.   | N.A.                        |
| Pitstop 2                  | Clathrin | Abcam    | 30 mM in DMSO                   | 30 $\mu$ M                         | Amphiphysin association of clathrin terminal domain – 12 $\mu$ M                 | (von Kleist et al., 2011)   |
| Pitstop 2 negative control | Clathrin | Abcam    | 30 mM in DMSO                   | 30 $\mu$ M                         | Amphiphysin association of clathrin terminal domain – >100 $\mu$ M               | (von Kleist et al., 2011)   |

| Inhibitor     | Target                          | Supplier | Stock concentration/<br>vehicle | Working concentration <sup>†</sup> | IC50  | Reference               |
|---------------|---------------------------------|----------|---------------------------------|------------------------------------|---|-------------------------|
| Cycloheximide | Inhibition of protein synthesis | Tocris   | 1 mg/ml in DMSO                 | 10 µg/ml                           | Protein synthesis – 532.5 nM<br>RNA synthesis – 2.88 µM<br>Anti-cancer activity – 0.12 - 1 µM | (Shi et al., 1999)      |
| Y27632        | ROCK                            | Tocris   | 2 mM in DMSO                    | 20 µM                              | ROCK1 – 0.14 - 0.22 µM*<br>ROCK2 – 0.3 µM*<br>PKA – 25 µM*<br>PKC – 26 µM*<br>MLCK – >250 µM* | (Narumiya et al., 2000) |
| CK666         | Arp2/3                          | Tocris   | 1 mM in DMSO                    | 10 µM                              | Arp2/3 – 4 µM   | (Nolen et al., 2009)    |

† All working concentrations have been tested for cytotoxicity using MTS assay (see Appendices 1-12).

‡ Depending on cell lines, MCF-7 and MDA-MB-231 cells: 2.5 µM; THP-1 and Jurkat cells: 10 µM

\* The values are expressed as inhibitory constant (Ki)

## 2.3 Chemokine ligands

A list of chemokine ligands used is detailed below:

**Table 2.4. Chemokine ligands used for experiments:** CF- calcium flux, CTX- chemotaxis assay, IF- immunofluorescence, FC- flow cytometry. All chemokine ligands were dissolved in purified water.

| Chemokine                                    | Supplier  | Working concentration  |
|--|---|--|
| CXCL8 (IL-8)                                 | A gift from Katja Schmitz<br>(University of<br>Darmstadt) | 50 nM IF<br>10 nM time lapse                                     |
| CXCL9 (MIG)                                  | PeptoTech   | 50 nM IF   |
| CXCL10 (IP-10)                               | PeptoTech   | 50 nM IF   |
| CXCL11 (I-TAC)                               | PeptoTech   | 50 nM IF<br>10 nM time lapse                                     |
| CXCL12 (SDF-1 $\alpha$ )                     | PeptoTech   | 20 nM CF<br>1 nM CTX<br>50 nM IF<br>50 nM FC<br>10 nM time lapse |
| CCL3 (MIP-1 $\alpha$ , isoform<br>2-70 D26A) | A gift from L. Czaplewski<br>(British Biotech)            | 200 nM CF<br>1 nM CTX<br>100 nM IF<br>100 nM FC                  |
| CCL4 (MIP-1 $\beta$ )                        | PeptoTech   | 50 nM IF   |
| CCL5 (RANTES)                                | PeptoTech   | 50 nM IF   |
| CCL23 (MIP-3)                                | PeptoTech   | 50 nM IF   |

## 2.4 Antibodies

A list of chemokine ligands used is detailed below:

**Table 2.5. Primary antibodies used for experiments:** IF- immunofluorescence, FC- flow cytometry.

| Primary antibody   | Supplier                            | Assay use | Dilution factor          |
|--|-------------------------------------|-----------|--------------------------|
| Caveolin-1 rabbit polyclonal: sc-894                       | Santa Cruz Biotechnology            | IF, FC    | 1:500 (IF)<br>1:200 (FC) |
| CCR5 (HEK/1/85a/7a) cell growth supernatant rat monoclonal | A gift from J.A. McKeating (Oxford) | IF, FC    | 1 to 100 (IF, FC)        |
| CXCR3 mouse monoclonal: sc-133087                          | Santa Cruz Biotechnology            | IF, FC    | 1:200 (IF)<br>1:100 (FC) |
| CXCR4 (4G10) mouse monoclonal: sc-53534                    | Santa Cruz Biotechnology            | IF, FC    | 1:500 (IF)<br>1:200 (FC) |
| ACKR3 mouse monoclonal                                     | R&D Systems                         | IF, FC    | 1:50 (FC)                |
| Dynamin-2 mouse monoclonal: ab65556                        | Abcam                               | IF        | 1:500 (IF)               |
| IL-8RA mouse monoclonal: sc-7303                           | Santa Cruz Biotechnology            | IF, FC    | 1:50 (IF, FC)            |
| IL-8RB mouse monoclonal: sc-7304                           | Santa Cruz Biotechnology            | IF, FC    | 1:50 (IF, FC)            |

**Table 2.6. Secondary antibodies used for experiments:** IF- immunofluorescence, FC- flow cytometry

| <b>Secondary antibody</b>                     | <b>Supplier</b>          | <b>Assay use</b> | <b>Dilution factor</b>     |
|---|--------------------------|------------------|----------------------------|
| Goat anti-mouse Alexa 488: ab150113           | Abcam                    | IF, FC           | 1: 500 (IF)<br>1:200 (FC)  |
| Goat anti-rat Alexa 555                       | Invitrogen               | FC               | 1: 200 (FC)                |
| Anti-rabbit fluorescein isothiocyanate (FITC) | Santa Cruz Biotechnology | IF, FC           | 1: 500 (IF)<br>1: 200 (FC) |
| Goat anti-rat Alexa 488: ab150157             | Abcam                    | IF, FC           | 1: 500 (IF)<br>1: 200 (FC) |
| Goat anti-rat Alexa 555                       | Invitrogen               | FC               | 1: 200 (FC)                |

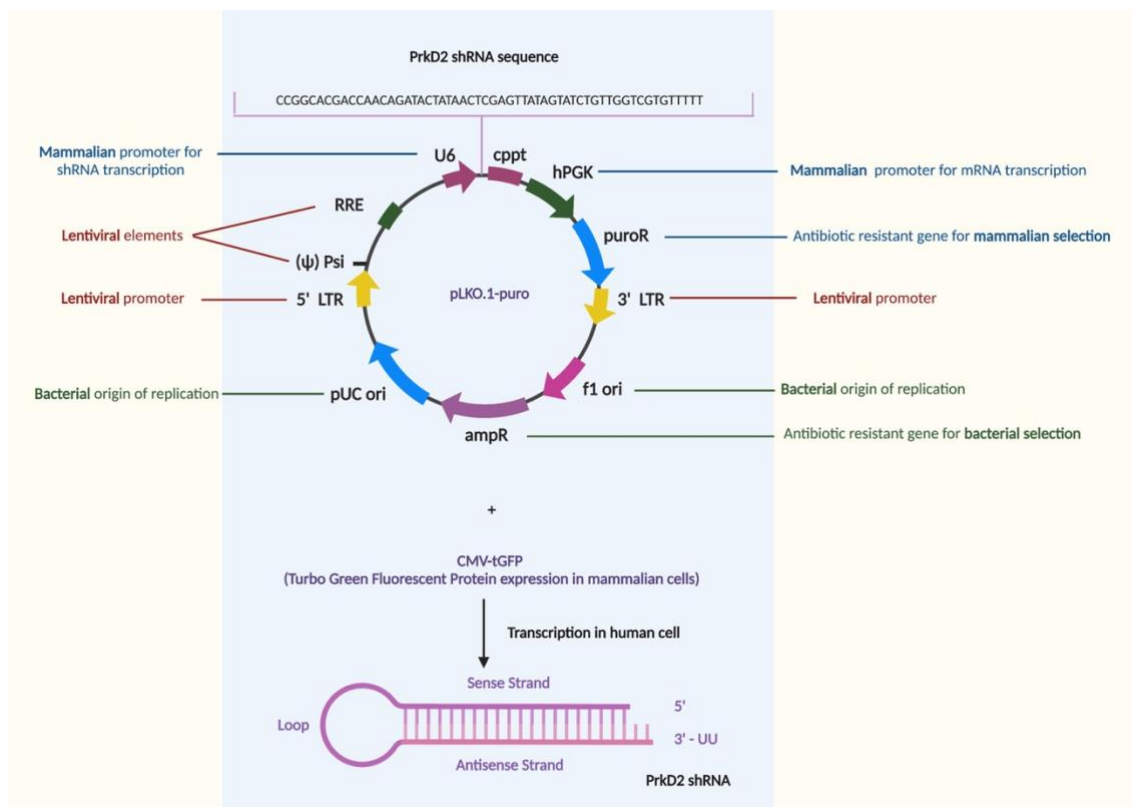
## 2.5 Intracellular protein stains

**Table 2.7. Intracellular stains**

| <b>Intracellular stain</b>                           | <b>Supplier</b> | <b>Dilution factor/<br/>working concentration</b> |
|--|-----------------|---|
| 4',6-Diamidino-2-phenylindole dihydrochloride (DAPI) | Sigma Aldrich   | 1: 5000   |
| LysoTracker® Deep Red                                | Invitrogen      | 50nM  |
| Alexa Fluor™ 488 Phalloidin                          | Invitrogen      | 1: 100  |

## 2.6 Plasmid DNA

Plasmid DNA for protein kinase D 2 (PrkD2) was purified from the MISSION puromycin-resistant lentiviral plasmid (pLKO.1-puro) vector (Sigma Aldrich). It contains a verified mammalian PrkD2 shRNA insert with a CMV-Turbo GFP promoter as an indicator of successful transfection in mammalian cells. The non-target shRNA vector was inserted with an short hairpin RNA (shRNA) that does not target any known genes from any species as a mock transfection control.



| Abbreviation | Description  |
|--------------|--|
| U6           | U6 Promoter (RNA polymerase III promoter for shRNA transcription)  |
| Cppt         | Central polypurine tract for transcription termination             |
| hPGK         | Human phosphoglycerate kinase eukaryotic promoter                  |
| puroR        | Puromycin resistance gene for mammalian selection                  |
| 3' LTR       | 3' self inactivating long terminal repeat (part of viral promoter) |
| f1 ori       | f1 origin of replication for bacterial cell                        |
| ampR         | Ampicillin resistance gene for bacterial selection                 |
| pUC ori      | pUC origin of replication for bacterial cell                       |
| 5' LTR       | 5' long terminal repeat  |
| Psi          | RNA packaging signal for viral cell                                |
| RRE          | Rev response element of viral cell                                 |

**Figure 2.1. MISSION PrkD2 shRNA pLKO.1-puro lentiviral plasmid vector containing a verified mammalian PrkD2 shRNA sequence insert.** Turbo GFP is additionally inserted as a CMV promoter within the vector. The sequence of the PrkD2 shRNA is CCGGCACGACCAACAGATACTATAACTCGAGTTATAGTATCTGTTGGTCTGTTTT (Sigma Aldrich). The abbreviations in the figure are listed with descriptions in the table. (Image created with BioRender.com based on the specification information provided by Sigma Aldrich).

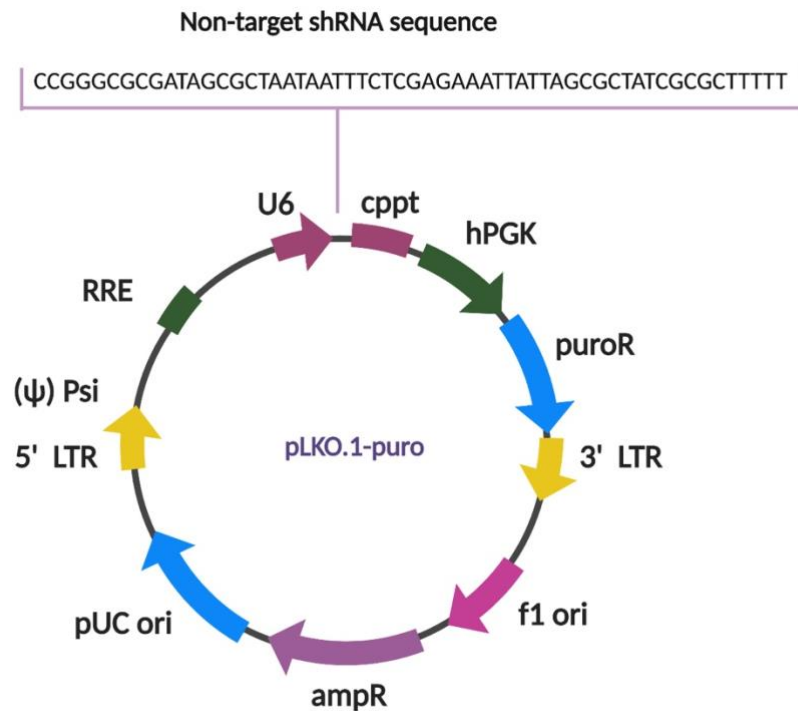


**Figure 2.2. MISSION Non-target pLKO.1-puro lentiviral plasmid vector containing a non-target shRNA sequence insert.** The plasmid contains an shRNA insert that does not target any known genes from any species. The sequence of the non-target shRNA is CCGGGCGCGATAGCGCTAATAATTTCTCGAGAAATTATTAGCGCTATCGCGCTTTTT (Sigma Aldrich). (Image created with BioRender.com based on the specification information provided by Sigma Aldrich)

Plasmid DNA for the pEGFP arrestin 2 (Arr2) and arrestin 3 (Arr3) was produced from a HindIII/ApaI-digested pEGFP-N1 plasmid vector (Clontech) ligated with a mammalian Arr2/Arr3 ORF insert as validated by E.Kelly (Bristol) (Matharu et al., 2001). Arrestin 2 mutant, characterised as the valine (Val) to aspartic acid (Asp) mutant of arrestin 2 (Arrestin 2-V53D) (Ferguson et al., 1996), was also cloned in a pEGFP-N1 plasmid vector. To ensure the transfection procedure was done properly, pEGFP.C2 plasmid (Clontech) was used as mock transfection control.

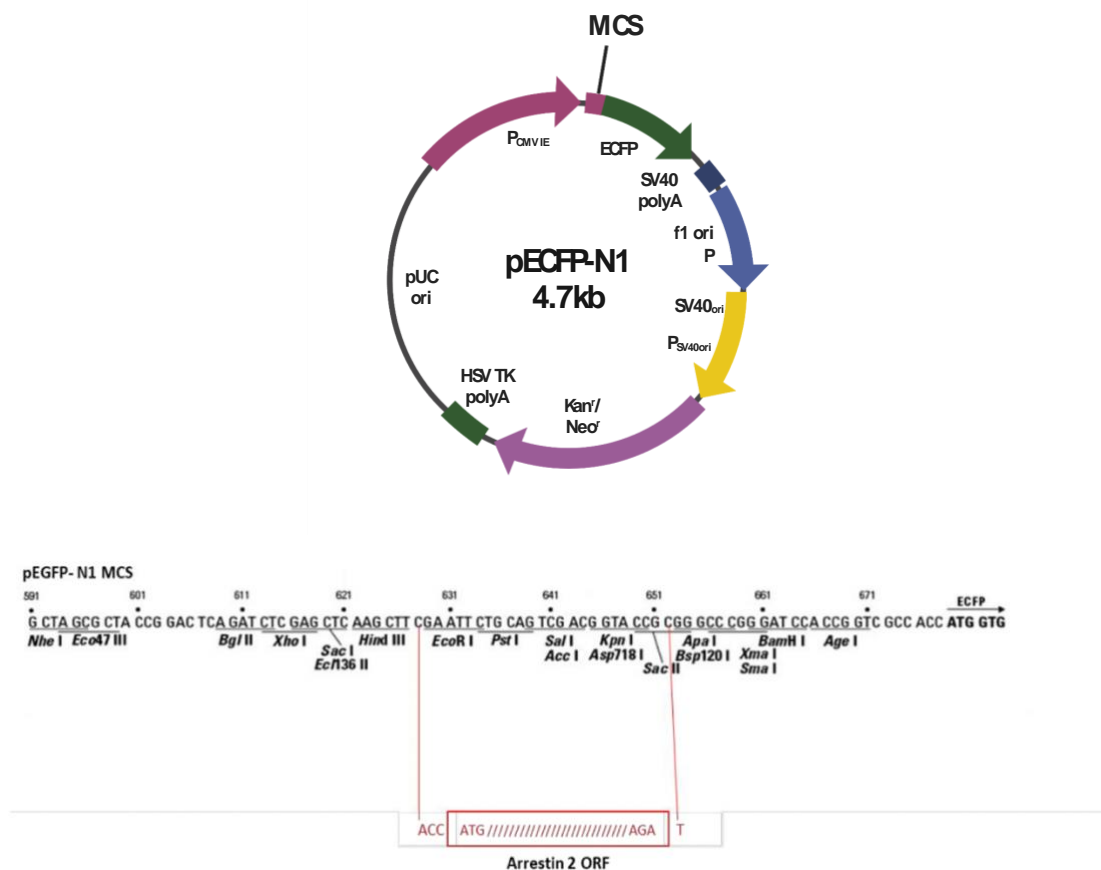


**Figure 2.3. Mammalian HindIII/ApaI digested pEGFP-N1 plasmid vector containing PCR-amplified arrestin 2 (Clontech)** (Image created with BioRender.com based on the specification information provided by Clontech).

### 2.7.1 Plasmid transformation into bacterial culture

To prepare LB agar plate, 40 g LB agar powder (Fisher Scientific) was added into 1 L sterile Millipore filtered distilled water and autoclaved at 121°C. The LB agar solution was then cooled down to 55°C. 50 ng/mL ampicillin was added onto the LB agar solution and the solution was immediately poured into 10 mL Petri plates to avoid being solidified. The plates were left at room temperature for 30 minutes to allow solidify and dry, wrapped with parafilm and stored at 4°C upside down for later use.

Chemically competent *E. coli DH5a<sup>f1</sup>* (Invitrogen) were transformed with the required plasmid DNA. 50 µL *E. coli DH5a<sup>f1</sup>* was thawed on ice for 20 – 30 minutes, in the meantime, prepared agar plates were warmed to 37°C. 10 µL plasmid DNA was tipped to the *E. coli* and gently mixed. The mixture was then

incubated on ice for 20 – 30 minutes, followed by incubating in a pre-set 42°C water bath for 30 – 60 seconds to allow transformation to occur through heat shocking. The mixture was returned to ice for 2 minutes before being plated onto a pre-warmed LB agar plate containing ampicillin. The plate was incubated upside down at 37°C overnight. To prepare liquid LB broth for inoculating the transformed bacterial strain, 20 g LB broth powder (Fisher Scientific) was dissolved in 1 L sterile Millipore filtered distilled water and autoclaved at 121°C. The liquid LB was cooled down to room temperature and 50 ng/mL ampicillin was added to liquid LB and stored at 4°C for later use. After overnight incubation, viable colonies were selected using a sterile pipette tip and tipped into the prepared LB broth containing antibiotic and gently swirled. The bacterial broth was incubated at 37°C overnight with sterile aluminium foil loosely covered in a shaking incubator. The cultured bacterial broth was frozen in 50% glycerol stock at -80°C for future use or used for plasmid amplification.

### **2.7.2 Amplification of plasmid DNA from bacterial broth**

The plasmid DNA was purified from bacterial broth following QIAGEN® Plasmid Midi kit (Qiagen) protocol. The transformed *DH5A<sup>f1</sup>* strain was grown overnight as described above and the bacterial broth was centrifuged at 3500 rpm for 5 minutes. The supernatant was removed and 4 mL P1 resuspension buffer containing RNAase was added to resuspend the cell pellet. 4 mL P2 lysis buffer was then added to the suspension, gently agitated, and left at room temperature for no longer than 3 minutes. 4 mL P3 neutralising buffer was added to the suspension to precipitate protein and vigorously agitated to mix. The mixed suspension was centrifuged at 4000 rpm for 15 minutes at 5-8°C. The supernatant was filtered through an activated Qiagen column. When the supernatant was emptied, the column was flushed with 10 mL QC wash buffer. 5 mL QF eluting buffer was then added to the column to elute the purified plasmid DNA. 3.5 mL isopropanol was added to the eluent and centrifuged at 4000 rpm at 4°C for 1 hour to precipitate DNA. The supernatant was removed, and the pellet was washed in 70% ethanol and left to dry. 500 µL Millipore filtered water was added to dissolve the pellet and purified plasmid DNA concentration was determined by Nanodrop spectrometer system (ThermoFisher Scientific).

### **2.7.3 Chemical transfection of plasmid DNA**

MCF-7 cells were seeded in 6-well/24-well plate at  $1 \times 10^5$  cells/mL in 3 mL/500  $\mu$ L of appropriate DMEM complete and incubated overnight at 37°C, 5% CO<sub>2</sub> until the optimal confluency of 70 – 90% was reached. In the preparation of plasmid DNA and transfection reagent, plasmid DNA was diluted in serum-free DMEM to the working concentration of 2  $\mu$ g /100  $\mu$ L. 5  $\mu$ L TurboFect was then mixed with the diluted plasmid DNA. The mixture was left for 20 minutes at room temperature to allow ionic interaction of DNA and prevent from DNA degradation. In the 6-well/24-well plate, cell solution was removed and replaced with 1 mL/250  $\mu$ L serum-free DMEM. The plasmid DNA/TurboFect mixture was added into each well containing cells and incubated for 20 minutes at 37°C, 5% CO<sub>2</sub>. 1 mL/750  $\mu$ L DMEM complete was then added into each well and left to incubate at 37°C, 5% CO<sub>2</sub>. Transfected cells were experimented on the following day.

For cells transfected with puromycin-resistant plasmid DNA, cells were detached with PBS/EDTA and gently scraped. Cell suspension was seeded to a 96-well plate containing DMEM complete and incubated for another 24 hours at 37°C, 5% CO<sub>2</sub> to allow cell attachment. Medium was replaced by DMEM complete containing puromycin (1  $\mu$ g / mL) to select successfully transfected cells. The optimal concentration of puromycin for cell selection was determined by MTS assay at 48-time point using a concentration range from 1 – 10  $\mu$ g/mL. Cells were incubated at 37°C, 5% CO<sub>2</sub> until a puromycin-resistant clone has developed. Medium was renewed if necessary.

### **2.7.4 Electroporation transfection of plasmid DNA**

Jurkat cells were harvested to obtain  $3 \times 10^6$  cells per tube and centrifuged. Cells were resuspended in 250  $\mu$ L HEPES buffered electroporation solution (HEPES 20 mM, NaCl 137 mM, KCl 5mM, Dextrose 6 mM, Na<sub>2</sub>HPO<sub>4</sub> 0.7 mM, pH 7.5). 5  $\mu$ L t-RNA (Sigma Aldrich) and 2  $\mu$ g plasmid DNA together with cells suspended in electroporation solution was added to 0.2 cm transfection cuvette (Sigma Aldrich). Cells were electroporated using AMAXA Nucleofector 2b (Lonza) at a relevant setting (Jurkat cells: X-005). 500  $\mu$ L serum-free RPMI was topped up in the cuvette and electroporated cells were incubated at room temperature for 10 minutes. All contents in the cuvette were transferred to a T-25 flask (Corning)

containing RPMI complete. Cells were incubated at 37°C, 5% CO<sub>2</sub> for 48 hours before assessment of transfection and experimentation.

## **2.8 Calcium (Ca<sup>2+</sup>) flux**

Cells were harvested as described above. All cells were re-suspended in calcium flux buffer (137mM NaCl, 5mM KCl, 2mM MgCl<sub>2</sub>, 1.5mM CaCl<sub>2</sub>, 1.5mM CaCl<sub>2</sub>, 10mM HEPES pH 7.4, 25mM D-glucose). Cells were centrifuged and washed twice in calcium flux buffer, then resuspended in 1 mL of calcium flux buffer. Each cell sample was treated with inhibitor at working concentration and loaded with 2 µM of Fura-2 AM (Invitrogen). All cell samples were incubated at 37°C in a humidified atmosphere and 5% CO<sub>2</sub> for 30 minutes.

Following incubation, cells were then centrifuged and washed with 1mL of Ca<sup>2+</sup> flux buffer twice. 100 µL of cell sample was loaded to each well of a black, opaque reader microplate (Thermo Fisher Scientific, UK). Calcium mobilisation was monitored for 80 seconds with injection of chemokines at working concentrations at 20 seconds into each well using BMG Labtech Fluorostar Optima plate reader (BMG Labtech, Germany). Fluorescence was sequentially measured at 37°C stimulated by 340nm and 380nm light and detected at a fixed emission wavelength of 510 nm. Data were analysed and represented as the ratio of the fluorescence reading at 340 nm/380 nm in BMG Optima Software. The change in fluorescence was calculated from the difference in 340 nm/380 nm ratio between pre-stimulation value and peak value in post-stimulation.

## **2.9 Migration assays**

### **2.9.1 ChemoTX chemotaxis assay**

ChemoTX 5 µm pore plates (Neuroprobe Inc, USA) were used in chemotaxis assays for suspension cells. Before experimentation, plate wells to be used were blocked with 30 µL blocking buffer (1% BSA in serum-free simple medium) at room temperature for at least 30 minutes.

Relevant chemokine ligands were diluted to 1 nM in working buffer (0.1% BSA in serum-free RPMI). Suspension cells were harvested and resuspended in serum-free RPMI. Cells were centrifuged and medium was replaced by working buffer to give an appropriate cell density (Jurkat: 25 x 10<sup>4</sup> cells per well; THP-1: 50 x

$10^4$  cells per well). Inhibitor treatments were added to prepared cell suspension, followed by 30 minutes incubation at 37°C, 5% CO<sub>2</sub>. All conditions were done in duplicate.

In the plate, the blocking buffer was removed and replaced with 31  $\mu$ L of diluted chemokine solution (working buffer for unstimulated controls). The plate top membrane was attached and 20  $\mu$ L of cell suspension was added on top of the membrane within the corresponding well outlier. The plate was covered and incubated in a humidified chamber for 4 hours before analysis. Cells from each bottom well were counted using a haemocytometer.



**Figure 2.4 ChemoTX 5  $\mu$ m pore plate (Neuroprobe Inc, USA).** The plate consists of a 96-well plate where diluted chemokine ligands/vehicle controls were added, a membrane cover where cell suspension were added to allow cells to migrate towards the bottom chemokine-containing wells and a cover (Image source: [https://www.neuroprobe.com/product/chemo\\_tx/](https://www.neuroprobe.com/product/chemo_tx/)).

### 2.9.2 ORIS™ Cell migration assay

The ORIS™ plate (Platypus Technologies) was left at room temperature for 1 hour to equilibrate the plate temperature before experimentation. MDA-MB-231 cells at 95% confluency were harvested and resuspended in DMEM complete at  $2.5 \times 10^4$  cells per well. 100  $\mu$ L of cell suspension was seeded into the outer region of each well surrounding the stopper (Figure 2.5) inside a 96-well ORIS™ plate (Platypus Technologies) and incubated for 24 hours at 37°C, 5% CO<sub>2</sub>.

Following 24-hour incubation, the stopper was removed from each well, in which a central cell-free detection zone was created. The diluted chemokine ligands were added, followed by another 24-hour incubation. Complete medium was removed and cells were washed and resuspended in PBS with addition of 0.5  $\mu\text{g}/\text{mL}$  of calcein AM (Cayman Chemical Company). Cells were then incubated for 45 minutes at 37°C, 5% CO<sub>2</sub>. Cells were washed and resuspended in PBS. Cells at the detection zone were imaged to determine cell migration occurring in post-stimulation of chemokines.

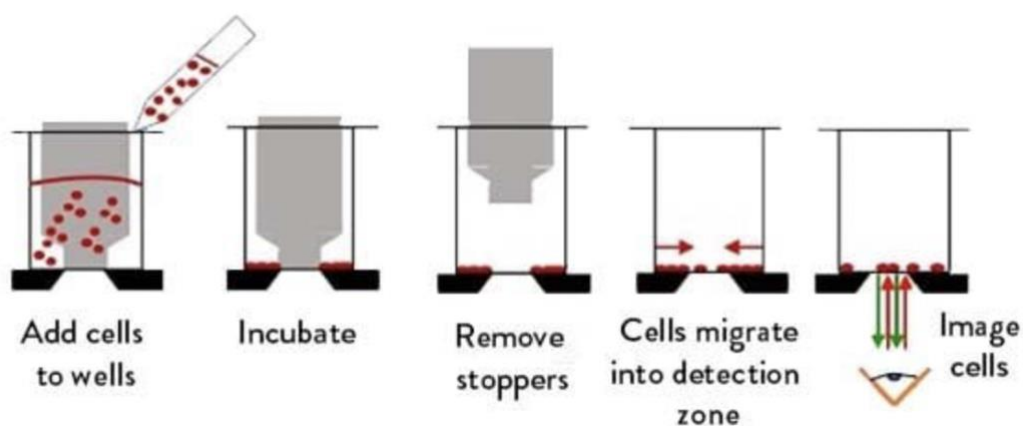


**Figure 2.5** Illustration of the steps from cell seeding, creating a cell-free detection zone to cell imaging for the detection of cell migration in a 96-well ORIS™ plate (Image source: <https://www.amsbio.com/oris-cell-migration-assays/>).

## 2.10 Imaging techniques

### 2.10.1 Intracellular protein staining

Adherent cells at 95% confluency were harvested and sparsely seeded into a 12-well plate with glass cover slips pre-washed with 70% alcohol and PBS. Cells were incubated in complete medium for 24 hours at 37°C, 5% CO<sub>2</sub> to allow cell attachment.

For phalloidin F-actin staining, cells were treated with relevant inhibitors at working concentrations for 30 minutes, followed by stimulation of chemokine ligands at working concentrations for another 30 minutes at 37°C, 5% CO<sub>2</sub>. Cells were gently washed in PBS twice and fixed with 4% formaldehyde solution at room temperature for 10 minutes. Cells were then gently washed in PBS twice

and permeabilised with 0.1% Triton X-100 (FisherBioTech) solution at room temperature for 5 minutes. Cells were washed in PBS twice and Alexa Fluor™ 488 Phalloidin (Invitrogen) was added to cells in PBS at 1: 100 dilution. The plate was incubated in dark at 4°C for 30 minutes. After incubation, cells were gently washed twice with PBS and the glass cover slips containing stained cells were mounted with DPX mountant (ThermoFisher Scientific) for imaging. Images were acquired using an inverted Leica DMII fluorescence microscope with a relevant filter setting compatible with the fluorophore used.

For caveolin-1/ dynamin-2 staining, cells were fixed and permeabilised as above after inhibitor/chemokine treatments. Cells were then incubated in desired primary antibodies at working dilutions at 4°C for 1 hour. Cells were washed twice with cold PBS, followed by incubation in secondary antibody at working dilutions at 4°C in dark for 1 hour. Cells were then washed twice with cold PBS. For background control, cells were incubated with secondary antibody matched to the host species and class of the primary antibody. Cells were mounted and imaged as above.

For staining of lysosomes and other acidic organelles, LysoTracker®, which is a weakly basic fluorophore freely permeant to cell membranes, was used. No cell fixation and permeabilisation was required. Adherent cells were treated with inhibitors and chemokines in a 12-well plate as above, followed by adding LysoTracker® (50nM) in serum-free medium. Cells were incubated at 37°C, 5% CO<sub>2</sub> for 30 minutes. The medium was replaced with fresh serum-free simple medium for imaging analysis. It should be noted that this process is performed in live cells. Samples are analysed immediately after staining to minimise lysosome alkalinisation caused by LysoTracker®.

### **2.10.2 Cell surface receptor staining**

For adherent cells, cells at 95% confluency were harvested and seeded into a 12-well plate with glass cover slips pre-washed with 70% alcohol and PBS. Cells were sparsely seeded into each well containing appropriate complete medium and incubated overnight at 37°C, 5% CO<sub>2</sub> to allow cell attachment. At 95% confluence, cells were gently washed with cold PBS twice. Cells were incubated in desired primary antibodies at working dilutions at 4°C for 1 hour. Cells were

washed twice with cold PBS, followed by incubation in secondary antibody, matched to the host species and class of the primary antibody, at working dilutions at 4°C in dark for 1 hour. Cells were then washed twice with cold PBS. For background control, cells were incubated with secondary antibody matched to the host species and class of the primary antibody. Cells were fixed with 4% formaldehyde solution at room temperature for 10 minutes. DAPI was added for cell nuclei staining at 4°C in dark for 5-10 minutes. The glass cover slips containing stained cells were mounted with DPX mountant (ThermoFisher Scientific) for imaging. Images were acquired using an inverted Leica DMII fluorescence microscope with a relevant filter setting compatible with the fluorophore used.

For suspension cells, cells were harvested and resuspended at  $1 \times 10^6$  cells/mL in cold PBS in 1.5 mL tubes. In-between inhibitor/chemokine treatments and PBS washes, cells were centrifuged, and the cell pellet was resuspended in cold PBS. The procedure was followed as adherent cells. Cell mounting was achieved by pipetting 20  $\mu$ L of cell suspension in PBS to a drop of DPX mountant on a glass slide and carefully covering with a glass cover slip. The prepared glass slides were dried at 4°C in dark overnight. Images were acquired using an inverted Leica DMII fluorescence microscope with a relevant filter setting compatible with the fluorophore used.

### **2.10.3 Image acquisition**

Cells were imaged using inverted Leica wide-field fluorescence microscope fitted with 10, 40 or 63X objectives combining with a 0.5X lens, a colour CCD camera and an array of fluorescence filter cubes. Images were captured and edited using the Leica Imaging Suite Software. All micrographs of cells in this thesis were taken in 5X, 20X or 31.5X magnification. All immunofluorescence images were validated by samples in the absence of primary antibody to test for non-specific binding of secondary antibody.

### **2.10.4 Analysis of cell area and cell circularity**

The average area and circularity of a single cell was quantified using Image J software. The outlier of each single cell was manually drawn based on phalloidin-stained F-actin and selected as a region of interest (ROI). Cell area and circularity

of the ROI were calculated by Image J software, where the formula for circularity is  $4\pi(\text{area}/\text{perimeter}^2)$ . A value of 1.0 in circularity indicates a perfect circle. Identical microscopic settings (image size, 2592 x 1944 pixel and 414.72 x 311.04  $\mu\text{m}$ ) were applied. At least 10 cells were analysed per experiment. Data was expressed as the mean from at least 3 independent F-actin staining experiments.

### **2.11 Internalisation assay and flow cytometry analysis**

Cells were harvested and resuspended in serum-free medium at a density of  $5 \times 10^6$  cells/mL in 1.5 mL tubes. Inhibitors at working concentrations were added to cell suspension and incubated at 37°C, 5% CO<sub>2</sub> for 30 minutes. For blocking of clathrin-dependent endocytic pathway using Pitstop 2, cells were incubated with Pitstop 2 for 5 minutes at 37°C, 5% CO<sub>2</sub> instead to avoid non-specific effects of the inhibitor according to the supplier's manual (Abcam). Cells were then washed with PBS and resuspended in serum-free simple medium followed by stimulation with chemokines at working concentrations at 37°C, 5% CO<sub>2</sub> for another 30 minutes. Cells were washed with cold 0.5% BSA/PBS twice. Cells were incubated in desired primary antibodies at working dilutions at 4°C for 1 hour. Cells were washed twice with cold 0.5% BSA/PBS, followed by incubation in secondary antibody, matched to the host species and class of the primary antibody, at working dilutions at 4°C in dark for 1 hour. Cells were then washed twice with cold 0.5% BSA/PBS and resuspended in cold 0.5% BSA/PBS for analysis. For background control, cells were incubated with secondary antibody matched to the host species and class of the primary antibody. Cells were fixed with 4% formaldehyde solution at room temperature for 10 minutes before staining with secondary antibody if flow cytometry analysis was not done on the same day.

For suspension cells, cells were harvested and re-suspended at  $1 \times 10^6$  cells/mL in cold PBS in 1.5 mL tubes. The procedure above was followed. Mean fluorescence intensity from cell samples were acquired and cells were gated to exclude dead cells and debris using CytoFLEX Flow Cytometer (Beckman Couter). 20,000 events from each sample were recorded at 10-20  $\mu\text{L}/\text{min}$  flow. Data was analysed using CytExpert version 2.4 (Beckman Coulter).

## **2.12 Cell viability tests**

### **2.12.1 CellTitre 96<sup>®</sup> Aqueous One Solution Cell Proliferation Assay**

CellTitre 96<sup>®</sup> Aqueous Non-Radioactive Cell Proliferation Assay (Promega) was followed to perform cytotoxicity assays using 3-(4,5-dimethylthiazol-2-yl)-5-(3-carboxymethoxyphenyl)-2-(4-sulfophenyl)-2H-tetrazolium (MTS). Suspension cells were harvested and resuspended in complete medium at  $5 \times 10^5$  cells/mL. Adherent cells were resuspended at  $1 \times 10^5$  cells/mL. 100  $\mu$ L of cell suspension was seeded into each well of a transparent 96-well plate and 1  $\mu$ L inhibitor at testing concentrations was added. Each inhibitor concentration was performed in duplicate. The plate was incubated for 72 hours at 37°C, 5% CO<sub>2</sub>. After 72 hours, 10  $\mu$ L MTS was added to each well and incubated in dark at 37°C, 5% CO<sub>2</sub> for 1 hour. The plate was then read at 490 nm in FLUOstar<sup>®</sup> OPTIMA fluorometer (BMG Labtech). The assay is colourmetric based on the principle of cellular metabolism. The MTS compound is bio-reduced by NAD(P)H dehydrogenase in viable cells into a coloured formazan product, which is quantified by measuring absorbance at 490 nm. The absorbance readings are directly proportional to cell viability (Berridge and Tan, 1993).

### **2.12.2 Trypan blue staining**

Cells were harvested and seeded into a 48-well plate. Cell was incubated in relevant complete medium with inhibitors at testing concentrations at 37°C with 5% CO<sub>2</sub> for 72 hours. After 72 hours incubation, cells were washed with PBS and replaced with serum-free simple medium. Trypan blue 0.4% filtered solution (Gibco) was added to each well in 1:1 dilution and incubated for 2-3 minutes at room temperature. The solution was removed and replaced by PBS. Cells were imaged using bright field microscopy. Cells stained in blue indicate dead cells.

# Chapter 3: Characterisation of chemokine-induced responses in different cancer cell lines

---

## 3.1 Introduction

Chemokine signalling has been of interest for decades in GPCR research for cancer, autoimmune and infectious diseases. In general, various aspects in chemokine signalling have been covered by previous literature, including structural features of receptor/ligand, receptor/ligand interactions and conformation, receptor internalisation and recycling, G protein-dependent signalling, G protein-independent signalling. In the past decade, more efforts have been made to understand the complexity underlying chemokine signalling in depth, such as biased signalling, redundancy system of chemokine, chemokine dimerisation, chemokine receptor dimerisation, homologous and heterologous receptor desensitisation and signalling modulating roles of atypical receptors (Drouillard et al., 2023). Yet, with an increasing number of studies investigating on these aspects together, some conflicting evidence has arisen from different literature. For example, a study working on breast cancer cells reported that  $\beta$ -arrestin 1 is a negative regulator of cancer metastasis (Son et al., 2019), on the other hand, another study found that CXCL12/ACKR3/ $\beta$ -arrestin 1 biased signalling promotes metastasis in colorectal cancer (Si et al., 2022). Another example of contrary findings is related to receptor internalisation pathway. One study demonstrated that CCR5 internalisation is mainly through clathrin-dependent pathway (Signoret et al., 2005), while another study argued that CCR5 internalise predominately through caveolae-dependent pathway instead (Venkatesan et al., 2003). This can be explained by two main reasons: a variety of cellular systems and different experimental approaches used between studies. Thus, it is not unusual to expect of some of the findings to contradict one another. In addition, accumulating studies have reported that chemokine signalling is context-dependent that involves various factors in combination to influence cellular functions and responses (Heuninck et al., 2019). Therefore, we set out to characterise the chemokine receptor expression profile across different cancer

cell lines commonly used in cancer research. By determining which chemokine receptors are abundantly expressed in individual cancer cell line, we then investigated how cells respond to the cognate chemokine ligands in different aspects, including intracellular calcium mobilisation, actin cytoskeletal rearrangement, chemotaxis and receptor internalisation.

## **3.2 Chapter aims**

**Hypothesis:** We hypothesised that different cancer cell types express different levels of chemokine receptors and respond differently through context-dependent chemokine signalling.

**Aims:** The aim of this chapter is to characterise endogenous quantities and localisation of chemokine receptor and intracellular responses in different cancer cell lines elicited by cognate chemokine ligands. There is emerging evidence demonstrating that the complexity of biased signalling in the field of GPCR potentially contributes to a variety of responses in different cell lines (Mills et al., 2018).

## **3.3 Results**

### **3.3.1. Localisation and quantification of endogenously expressed chemokine receptor in cancer cells**

Using immunofluorescence staining for microscopic visualisation and quantitative flow cytometry analysis, we examined the cell surface expression levels of chemokine receptors, CXCR1, CXCR2, CXCR3, CXCR4, ACKR3 and CCR5, on different cancer cell lines, MCF-7, MDA-MB-231, Jurkat and THP-1.

CXCR1 (also known as IL-8RA) is a highly selective receptor with high binding affinity to CXCL8 but low affinities to other chemokine ligands, including CXCL6 and CXCL7 (Lee et al., 1992). On the other hand, CXCR2 (also known as IL-8RB) is more promiscuous and can be activated by multiple ELR<sup>+</sup> CXC chemokines, including CXCL1-3 and CXCL8 (Addison et al., 2000). Yet, CXCL8 is the most potent ligand for CXCR2 (Addison et al., 2000). CXCL8 is known to be an autocrine growth factor discovered in a variety of cancer types, such as

pancreatic (Miyamoto et al., 1998), melanoma (Schadendorf et al., 1993) and colon cancer (Brew et al., 2000). Hence, CXCL8/CXCR1 and CXCL8/CXCR2 signalling has been of interest in the study of cancer development and metastasis.

CXCR3 is primarily expressed in CD4<sup>+</sup> and CD8<sup>+</sup> T-cells and associated with three cognate chemokine ligands: CXCL9, CXCL10 and CXCL11 (Korniejewska et al., 2011). To date, there are three isoforms of CXCR3 identified: CXCR3-A, which binds CXCL9, CXCL10 and CXCL11, CXCR3-B, which binds CXCL4, CXCL9, CXCL10 and CXCL11, and CXCR3-alt, which binds CXCL11 only (Korniejewska et al., 2011). The major three chemokine ligands, CXCL9, CXCL10 and CXCL11, have their distinct roles in regulating cancer immunity. Among these three ligands, CXCL11 was found to be the most potent CXCR3 agonist, involved in receptor internalisation, chemotaxis and intracellular Ca<sup>2+</sup> release (Cole et al., 1998). CXCL10 and CXCL11 was shown to promote the polarisation of Th1 cells via activation of different pathways (Zohar et al., 2014; Karin et al., 2016). This implies that CXCL10 and CXCL11 favour active tolerance over effector reactivity by predominantly regulating CD4<sup>+</sup> T-cells, as a result of restraint of autoimmunity (Zohar et al., 2014; Karin et al., 2016). On the other hand, CXCL9 is involved in effector reactivity by interacting with CD8<sup>+</sup> T-cells. CXCL9, usually produced by dendritic cells, interacts with CXCR3 expressed on CD8<sup>+</sup> T-cells that enhances the efficacy of anti PD-1 immune checkpoint therapy (Chow et al., 2019).

CXCR4 is the most studied chemokine receptor in the study of cancer. CXCL12 is an exclusive chemokine ligand for CXCR4 (Oberlin et al., 1996). An atypical receptor, ACKR3, is recently found to be activated through the shared ligand CXCL12 with CXCR4, playing a synergistic role in CXCL12/CXCR4 signalling (Santagata et al., 2021). ACKR3 was found to function to control the CXCL12 gradients for chemotaxis towards target site by sequestration of CXCL12 from non-target site (Graham et al., 2012). Also, ACKR3 forms heterodimer with CXCR4 to activate downstream signalling through  $\beta$ -arrestin, inducing cell migration (Hattermann and Mentlein, 2013). Relating to cancer, CXCR4 has been shown to be overexpressed in more than 23 different types of cancer (Balkwill,

2004). The CXCL12/CXCR4 signalling axis is involved in cell proliferation, cell migration, angiogenesis and cancer invasion (Balkwill, 2004).

CCR5 is gaining attention as CCR5 overexpression has been found in a number of cancer types as a consequence of oncogenic transformation (Velasco-Velázquez et al., 2012; Aldinucci et al., 2020). Unlike CXCR4, CCR5 is a promiscuous receptor that binds CCL3, CCL4, CCL5 and CCL8 with high binding affinities (Aldinucci et al., 2020). Through G protein-dependent signalling, CCR5 is involved in the activation of downstream signalling cascades, including PI3K/Akt, MAPK/ERK, NF $\kappa$ B and JAK/STAT3, contributing to cytoskeletal rearrangement and chemotaxis (Aldinucci et al., 2020). CCR5 was also found to promote cancer in the interaction with CD34 expressed in hematopoietic cells (Kulmann-Leal et al., 2020).

MCF-7 cells are adherent, non-invasive ER- and PR-positive breast ductal carcinoma cells. Previous studies reported that CCR5 (Zhang et al., 2009) and CXCR4 (Müller et al., 2001) were detected by using quantitative RT-PCR analyses. Particularly CCR5 was found to be overexpressed, contributing to cancer proliferation (Zhang et al., 2009; Murooka et al., 2009; Gao et al., 2016) and invasion (Zhang et al., 2009) induced by CCL5. Another study reported that protein expression level of CXCR1 in MCF-7 cells is undetectable by western blotting analysis (Jiang et al., 2013). Consistent with the previous findings, our results also showed that more CXCR4 and CCR5 receptors were observed on the cell surface for MCF-7 cells (**Figures 3.1 and 3.2**). The relative cell surface receptor quantities of CXCR4 and CCR5 were 11.3 and 35.4 respectively (**Table 3.1**).

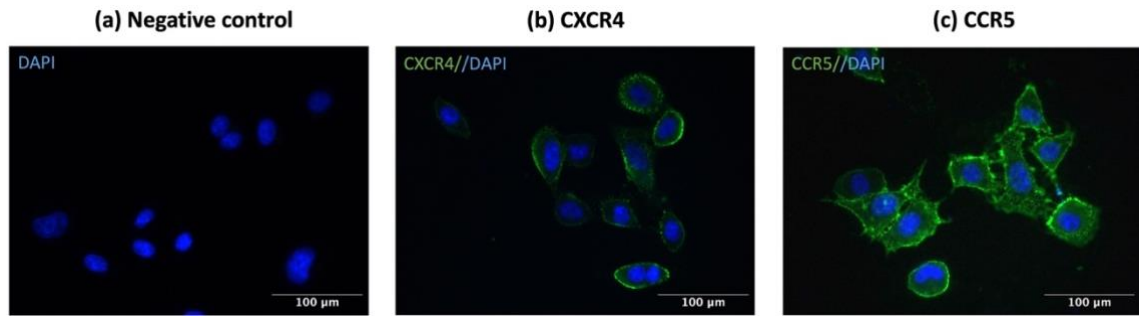


**Figure 3.1. CXCR4 and CCR5 receptors are abundantly localised on the cell surface of MCF-7 cells.** Immunofluorescence staining of cell surface chemokine receptors in MCF-7 cells. (a) negative background control with secondary antibody added only and stained with DAPI (1:1000) (blue) for the visualisation of cell nuclei; (b) mouse monoclonal antibody (mAb) against CXCR4 (1:500); (c) rat mAb against CCR5 (1:100) followed by secondary staining with secondary Alexa 488 antibody according to the host species and class of the primary antibody (1:500) (green) and DAPI (1:1000) (blue) for cell nuclei. Cells were fixed with 4% formaldehyde solution before images were acquired. Representative images from at least 3 independent experiments were acquired with a Leica DMII Fluorescence microscope using 31.5X magnification.

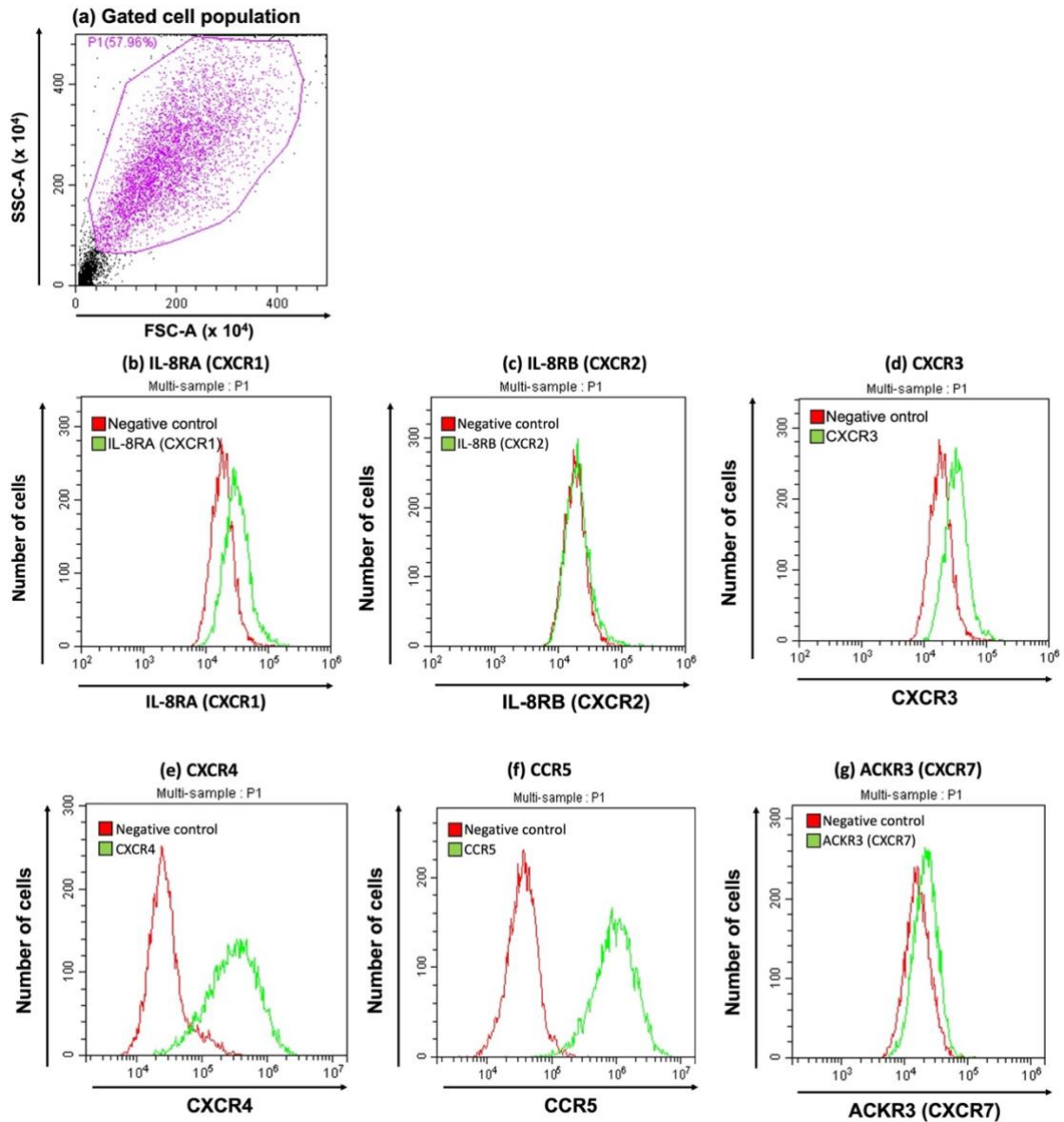


**Figure 3.2. Flow cytometry of MCF-7 showing the relative quantities of chemokine receptor localised on the cell surface.** (a) Representative scatter plot (forward scatter (FSC) vs. side scatter (SSC)) showing the gated cell population of MCF-7 cells. (b) CXCR1 (IL-8A), (c) CXCR2 (IL-8B), (d)CXCR3, (e) CXCR4, (f) CCR5 and (g) ACKR3 (CXCR7). Cells were stained with primary antibody specific to corresponding receptor at working dilution (IL-8RA: 1:50; IL-8RB: 1:50, CXCR3: 1:200, CXCR4 (4G10): 1:200; CCR5: 1:100; ACKR3: 1:50) followed by secondary antibody, matched to the host species and class of the primary antibody (1:200) (acquired in the FITC channel). Representative histograms from at least 3 independent experiments show the comparison of negative control (only secondary antibody added) (in red) and stained receptor (in green) in respect to fluorescence intensity among the gated population of each cell sample.

Fluorescence intensity of 20,000 events from each sample were quantified in flow cytometry and cell population was gated to exclude dead cells and debris before analysis. Representative scatter plot and histograms were generated using CytExpert (Beckman Coulter).

MDA-MB-231 cells are invasive, triple-negative breast cancer cells. High level of CXCR4 expression was previously detected in MDA-MB-231 cells by Western blot and RT-qPCR (Sun et al., 2014). CCR7 was also reported to express in MDA-MB-231 cells, and its cognate ligand, CCL21, is involved in intracellular filamentous actin (F-actin) polymerisation (Müller et al., 2001). CXCL12/CXCR4 and CCL5/CCR5 axes have been known to play an important role in cell migration and invasion in MDA-MB-231 cells ( Sun et al., 2014; Gao et al., 2016) . To further characterise the expression of chemokine receptors in MDA-MB-231, we attempted to visualise the total expression of a range of chemokine receptors using immunofluorescence staining of permeabilised MDA-MB-231 cells. Our results illustrated that CXCR1 and CXCR2 are abundantly expressed, and CXCR3, CXCR4 and CCR5 are also detectable in MDA-MB-231 cells (**Figure 3.3**). These receptors seem to localise intracellularly in MDA-MB-231 cells.

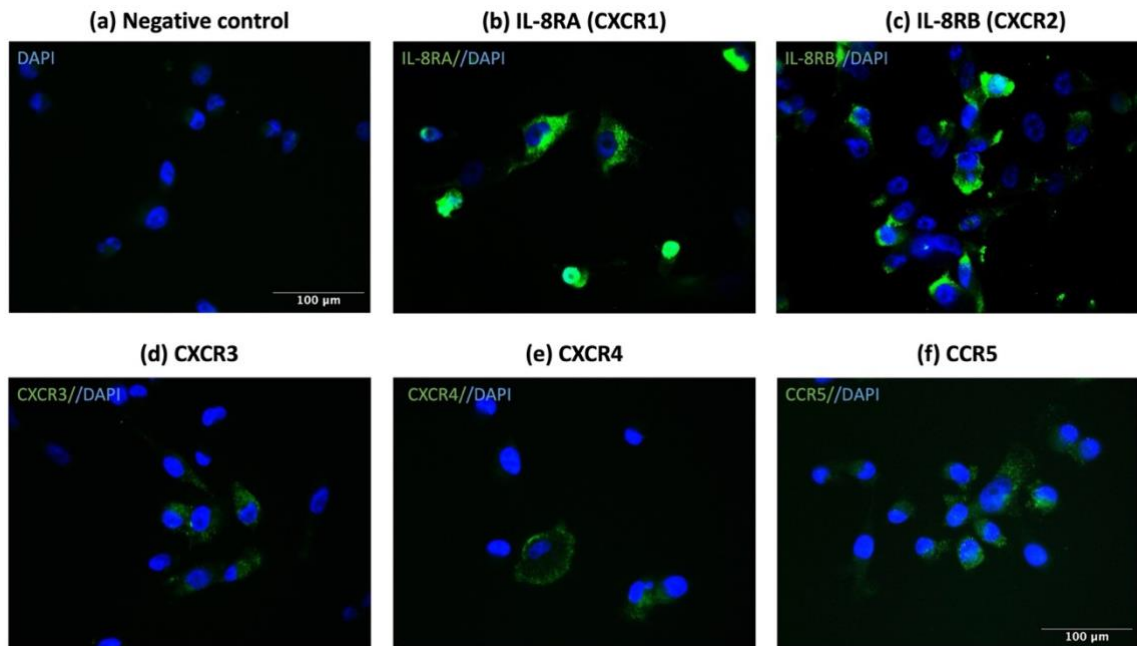


**Figure 3.3. MDA-MB-231 cells express IL-8RA and IL-8RB more abundantly compared to other chemokine receptors.**

Immunofluorescence staining of total expression of chemokine receptors including cell surface and intracellular expression in MDA-MB-231 cells. Cells were permeabilised with 0.1% Triton X-100 before cell fixation with 4% formaldehyde solution prior to immunofluorescence staining. (a) negative background control with secondary antibody added only and stained with DAPI (1:1000) (blue) for the visualisation of cell nuclei; (b) mouse mAb against IL-8RA (CXCR1) (1:50); (c) mouse mAb against IL-8-RB (CXCR2) (1:50); (d) mouse mAb CXCR3 (1:200); (e) mouse mAb against CXCR4 (1:500); (f) rat mAb against CCR5 (1:100) followed by secondary staining with secondary Alexa 488 antibody according to the host species and class of the primary antibody (1:500) (green) and DAPI (1:1000) (blue) for cell nuclei. Representative images from at least 3 independent experiments were acquired with a Leica DMII Fluorescence microscope using 31.5X magnification.

Jurkat cells are suspension, lymphoblast cell line from T cell leukaemia. It was previously reported that CXCR4 is overexpressed in Jurkat cells from flow cytometry quantitative analysis (Gao et al., 2005). From functionality studies, in response to CXCL12, Jurkat cells were found to exhibit potent chemotaxis (Gao et al., 2005; Mills et al., 2016). A multifunctional tumour suppressor, PTEN, negatively regulate CXCR4-mediated chemotaxis (Gao et al., 2005). Jurkat cells

have been an ideal cell model in the study of chemotaxis (Sonmez et al., 2020). As shown in immunofluorescence staining and flow cytometry analysis, exceptionally high cell surface localisation of cell surface CXCR4 was observed in Jurkat cells, whereas the cell surface localisation of CXCR1, CXCR2, CXCR3, ACKR3 and CCR5 was relatively low (**Figures 3.4 and 3.5**). The relative quantity of cell surface CXCR4 in Jurkat cells is 162.7 (**Table 3.1**).

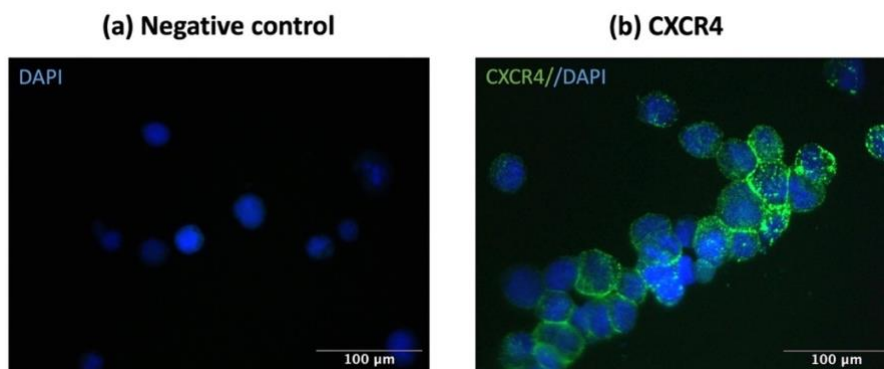


**Figure 3.4. CXCR4 receptors are abundantly localised on the cell surface of Jurkat cells.** Immunofluorescence staining of cell surface chemokine receptors in Jurkat cells. (a) negative background control with secondary antibody added only and stained with DAPI (1:1000) (blue) for the visualisation of cell nuclei; (b) mAb against CXCR4 antibody (1:500) followed by secondary staining with anti-mouse Alexa 488 antibody (1:500) (green) and DAPI (1:1000) (blue) for cell nuclei. Cells were then fixed with 4% formaldehyde solution before images were acquired. Representative images from at least 3 independent experiments were acquired with a Leica DMII Fluorescence microscope using 31.5X magnification.

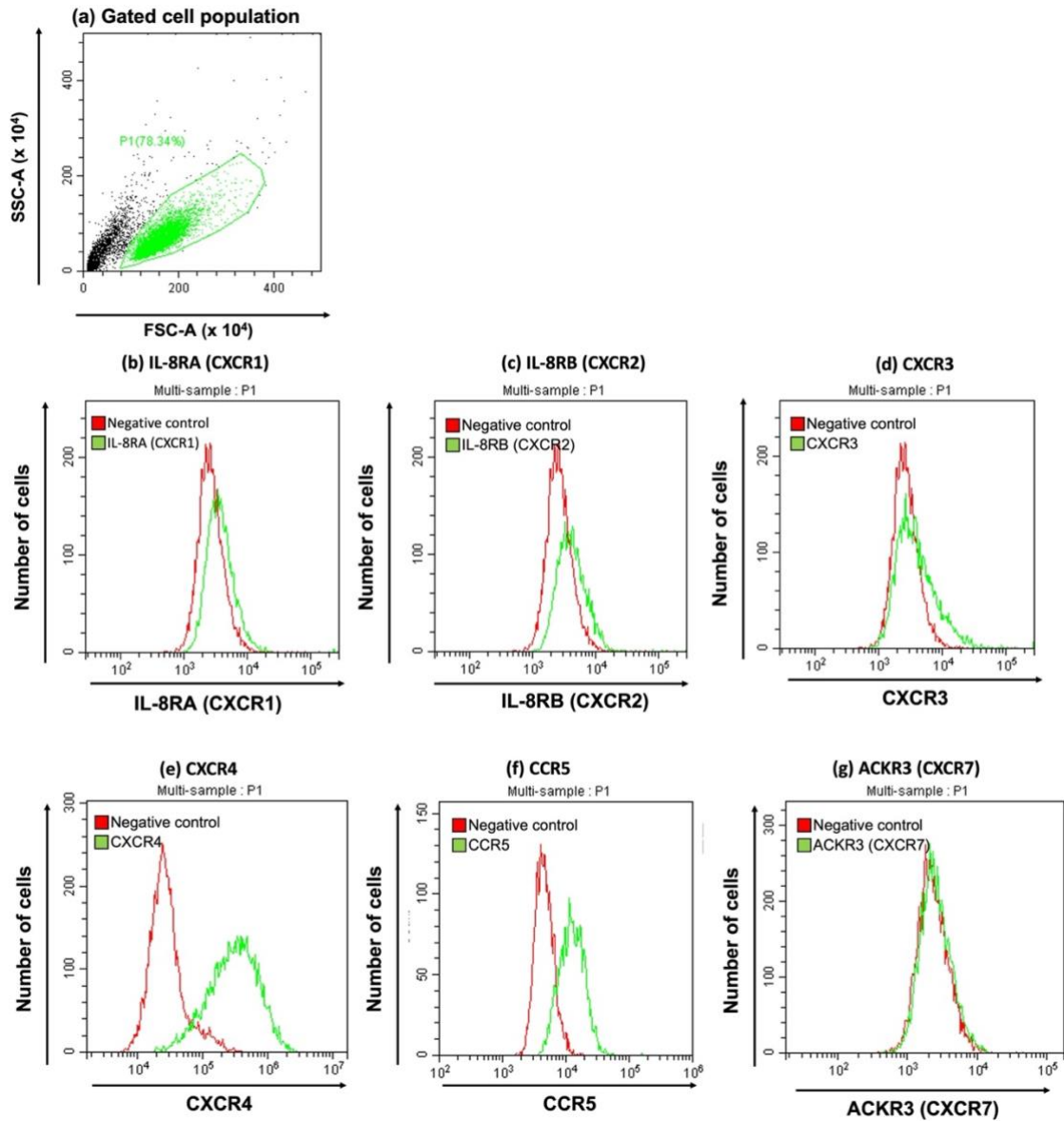


**Figure 3.5. Flow cytometry of Jurkat showing the relative quantities of chemokine receptor localised on the cell surface.** (a) Representative scatter plot (forward scatter (FSC) vs. side scatter (SSC)) showing the gated cell population of Jurkat cells. (b) CXCR1 (IL-8A), (c) CXCR2 (IL-8B), (d)CXCR3, (e) CXCR4, (f) CCR5 and (g) ACKR3 (CXCR7). Cells were stained with primary antibody specific to corresponding receptor at working dilution (IL-8RA: 1:50; IL-8RB: 1:50, CXCR3: 1:200, CXCR4 (4G10): 1:200; CCR5: 1:100; ACKR3: 1:50) followed by secondary antibody, matched to the host species and class of the primary antibody (1:200) (acquired in the FITC channel). Representative histograms from at least 3 independent experiments show the comparison of negative control (only secondary antibody added) (in red) and stained receptor (in green) in respect to fluorescence intensity among the gated population of each cell sample.

Fluorescence intensity of 20,000 events from each sample were quantified in flow cytometry and cell population was gated to exclude dead cells and debris before analysis. Representative scatter plot and histograms were generated using CytExpert (Beckman Coulter).

THP-1 cells are suspension, monocytic leukaemia cell line. A study from our group previously showed that THP-1 cells abundantly express CXCR2 and CXCR3 from immunofluorescence staining, exhibiting chemotactic responses towards CXCL8 and CXCL10 (Alassaf and Mueller, 2020). Another study demonstrated that CCL3 and CXCL12 also induce chemotaxis in THP-1 cells (Jacques et al., 2015). Our results confirmed CXCR2, CXCR3 and CCR5 are overexpressed (**Figures 3.6 and 3.7, Table 3.1**). The relative quantities of cell surface CXCR4 was also detectable but relatively low (3.81) (**Figure 3.7 and Table 3.1**).

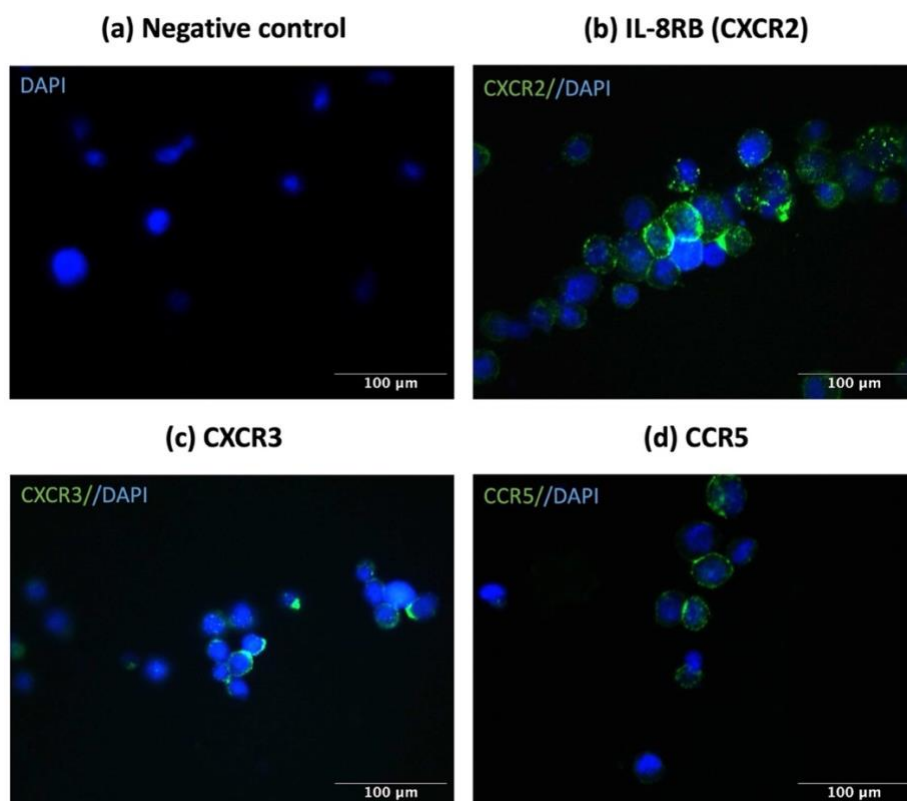


**Figure 3.6. IL-8RB receptors are abundantly localised on the cell surface of THP-1 cells.** Immunofluorescence staining of cell surface chemokine receptors in THP-1 cells. (a) negative background control with secondary antibody added only and stained with DAPI (1:1000) (blue) for the visualisation of cell nuclei. (b) mouse mAb against CXCR2 (IL-8RB)

(1:50) (c) mouse mAb CXCR3 (1:200) (d) rat mAb against CCR5 (1:100) followed by secondary staining with secondary Alexa 488 antibody according to the host species and class of the primary antibody (1:500) (green) and DAPI (1:1000) (blue) for cell nuclei. Cells were then fixed with 4% formaldehyde solution before images were acquired. Representative images from at least 3 independent experiments were acquired with a Leica DMII Fluorescence microscope using 31.5X magnification.

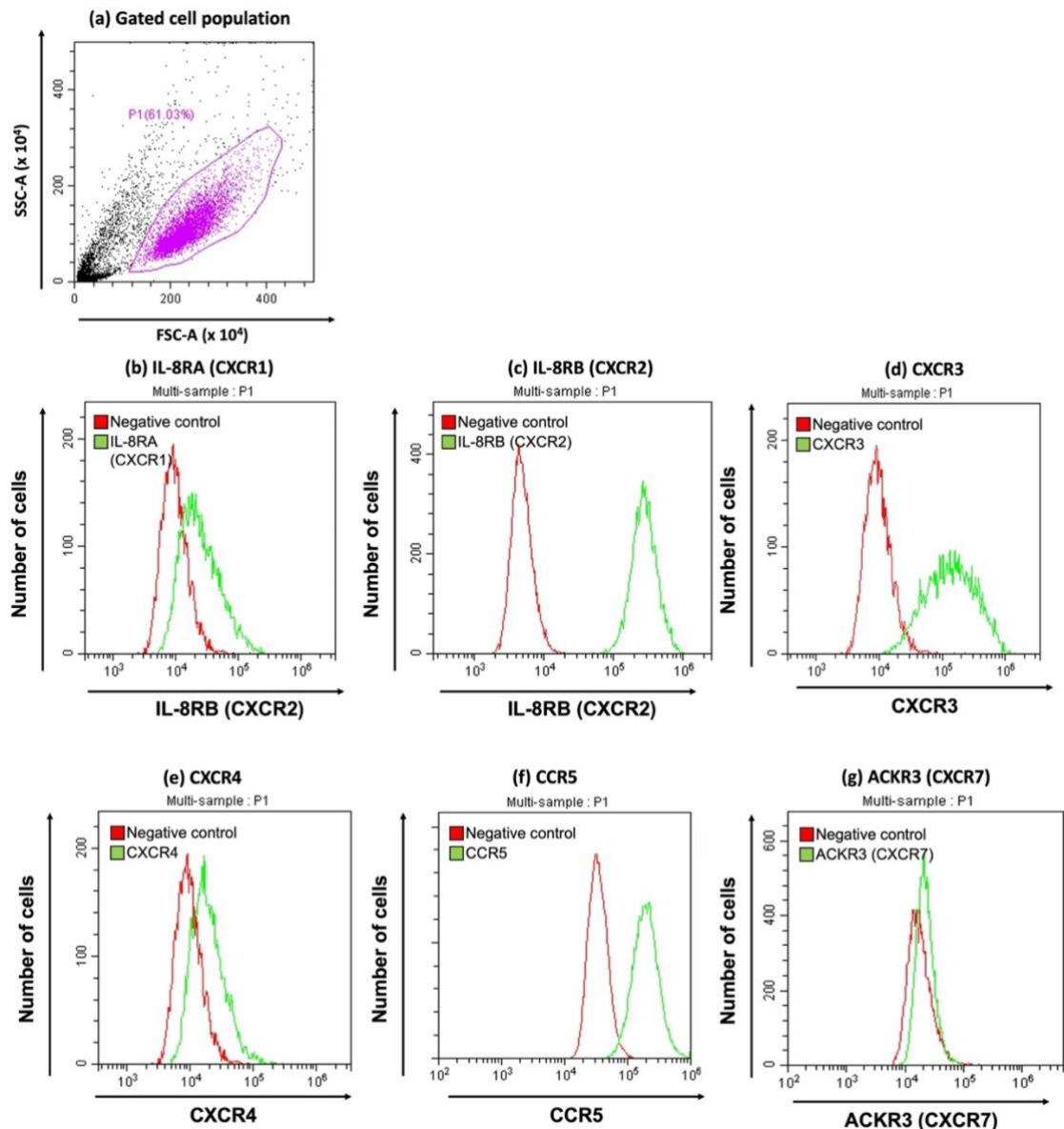


**Figure 3.7. Flow cytometry of THP-1 showing the relative quantities of chemokine receptor localised on the cell surface.** (a) Representative scatter plot (forward scatter (FSC) vs. side scatter (SSC)) showing the gated cell population of THP-1 cells. (b) CXCR1 (IL-8A), (c) CXCR2 (IL-8B), (d)CXCR3, (e) CXCR4, (f) CCR5 and (g) ACKR3 (CXCR7). Cells were stained with primary antibody specific to corresponding receptor at working

dilution (IL-8RA: 1:50; IL-8RB: 1:50, CXCR3: 1:200, CXCR4 (4G10): 1:200; CCR5: 1:100; ACKR3: 1:50) followed by secondary antibody, matched to the host species and class of the primary antibody (1:200) (acquired in the FITC channel). Representative histograms from at least 3 independent experiments show the comparison of negative control (only secondary antibody added) (in red) and stained receptor (in green) in respect to fluorescence intensity among the gated population of each cell sample. Fluorescence intensity of 20,000 events from each sample were quantified in flow cytometry and cell population was gated to exclude dead cells and debris before analysis. Representative scatter plot and histograms were generated using CytExpert (Beckman Coulter) (Data for CCR5 and ACKR4 acquired by Hamshaw I.)

**Table 3.1. Comparison of relative quantities of chemokine receptors localised on the cell surface among different cell lines.** Data represent means  $\pm$  SEM from at least 3 independent analyses.

| Cell line | Relative quantities of cell surface chemokine receptors*<br>( $\pm$ SEM) (n=3) |                       |                       |                        |                       |                       |
|-----------|--|-----------------------|-----------------------|------------------------|-----------------------|-----------------------|
|           | IL-8RA<br>(CXCR1)  | IL-8RB<br>(CXCR2)     | CXCR3                 | CXCR4                  | ACKR3<br>(CXCR7)      | CCR5                  |
| MCF-7     | 1.53<br>( $\pm$ 0.16)  | 1.33<br>( $\pm$ 0.08) | 1.47<br>( $\pm$ 0.20) | 11.3<br>( $\pm$ 0.32)  | 1.31<br>( $\pm$ 0.02) | 35.4<br>( $\pm$ 0.73) |
| Jurkat    | 1.38<br>( $\pm$ 0.06)  | 1.34<br>( $\pm$ 0.14) | 1.69<br>( $\pm$ 0.19) | 162.7<br>( $\pm$ 2.78) | 1.07<br>( $\pm$ 0.03) | 3.97<br>( $\pm$ 0.02) |
| THP-1     | 2.79<br>( $\pm$ 0.07)  | 39.1<br>( $\pm$ 2.40) | 16.1<br>( $\pm$ 1.52) | 3.81<br>( $\pm$ 0.24)  | 1.30<br>( $\pm$ 0.16) | 7.54<br>( $\pm$ 0.89) |

\*Relative quantities of cell surface chemokine receptors was based on median channel of fluorescence and calculated from median channel of fluorescence (stained cells) / median channel of fluorescence (negative control)], where negative control was stained with secondary antibody matched to the host species and class of the primary antibody only. Median channel of fluorescence was acquired from CytExpert (Beckman Coulter).

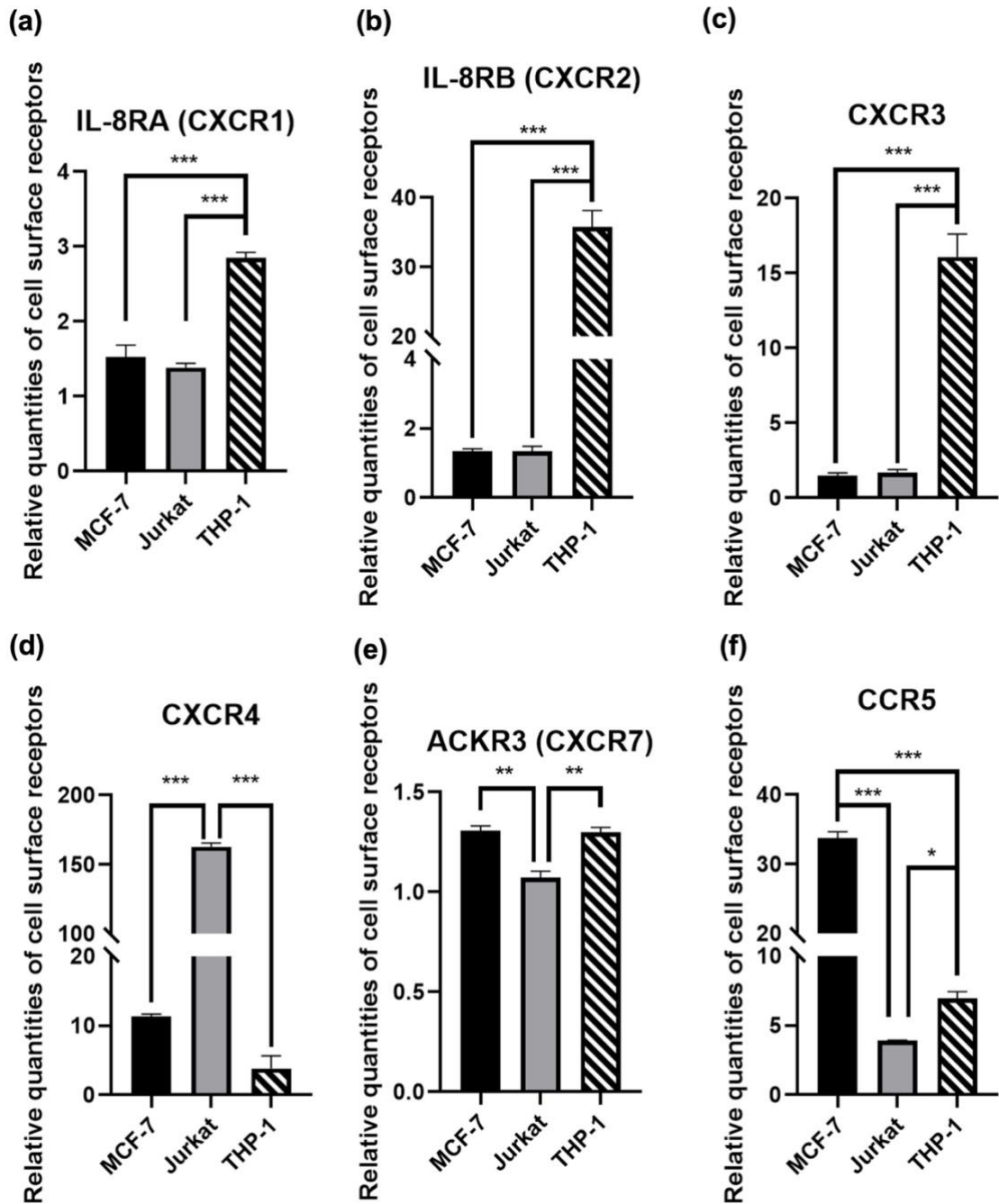


**Figure 3.8. Comparisons of relative quantities of chemokine receptors localised on the cell surface among different cancer cell lines.** Relative quantities of cell surface receptors: (a) IL-8RA, (b) IL-8RB, (c) CXCR3, (d) CXCR4, (e) ACKR3, (f) CCR5 on MCF-7, Jurkat and THP-1 cells. Relative quantities of cell surface chemokine receptors were based on median channel of fluorescence and calculated from median channel of fluorescence (stained cells) / median channel of fluorescence (negative control)], where negative control was stained with secondary antibody matched to the host species and class of the primary antibody only. Median channel of fluorescence was acquired from CytExpert (Beckman Coulter).

Data shown represent the mean  $\pm$  SEM of at least 3 independent experiments. One-way ANOVA with a Tukey's multiple comparisons test as post-hoc test, \* =  $p \leq 0.05$ ; \*\* =  $p \leq 0.01$ , \*\*\* =  $p \leq 0.001$ .

In the comparisons of the relative quantities of cell surface chemokine receptors among the three cancer cell lines: MCF-7, Jurkat and THP-1 cells, some chemokine receptors were found to localise more abundantly on the cell surface of a specific cell line than others. Particularly for CXCR4, CCR5 and IL-8RB, a significant amount of cell surface receptors was seen on Jurkat, MCF-7 and THP-1 cells respectively (**Table 3.1** and **Figure 3.8**). High levels of localisation of chemokine receptors on the cell surface might potentially contribute to significant cellular responses in the stimulation of the associated chemokine ligands accordingly. Chemokine-induced cellular responses will be investigated in more details in the next sections.

### **3.3.2 Measurement of intracellular calcium ( $\text{Ca}^{2+}$ ) mobilisation in response to chemokine stimulation in MCF-7 and THP-1 cells**

In order to determine the change in intracellular  $\text{Ca}^{2+}$  level, Fura-2-acetoxymethyl ester (Fura-2 AM) was used as a fluorescent indicator for  $\text{Ca}^{2+}$ . Fura-2 AM, which is a derivative of Fura-2, is membrane-permeable. Once Fura-2 AM passes the plasma membrane and localise in the cytosol, the acetoxymethyl group attached to Fura-2 AM is removed by the cellular esterases to become an active Fura-2, which binds  $\text{Ca}^{2+}$ . The maximum excitation wavelengths between  $\text{Ca}^{2+}$ -bound and unbound Fura-2 ( $\text{Ca}^{2+}$ -bound: 335 nm; unbound: 363 nm). In both forms, the maximum emission wavelength is the same (510 nm). The typical benchmark on excitation wavelengths in  $\text{Ca}^{2+}$  mobilisation assay is 340 nm for  $\text{Ca}^{2+}$ -bound and 380 nm for unbound Fura-2 (Martínez et al., 2017). A ratio of the fluorescence readings at 340 nm/ 380 nm is proportionally correlated to the amount of intracellular  $\text{Ca}^{2+}$  release (Martínez et al., 2017). In our study, the data is expressed as a change in fluorescence ratio (340nm/380nm), where the basal fluorescence before addition of chemokine is subtracted from peak fluorescence after addition of chemokine.

Cells were incubated with Fura-2 AM at 37°C for 30 minutes and relative intracellular Ca<sup>2+</sup> release level before and after addition of CCL3 200nM or CXCL12 20 nM was measured. The concentrations of CCL3 and CXCL12 used in our assay was determined by the titration experiments previously conducted by members of our group (Keil, PhD dissertation, 2019; Goh, PhD dissertation, 2018). In the quantification of chemokine-induced Ca<sup>2+</sup> flux, increase in intracellular Ca<sup>2+</sup> is an indication of activation of signalling pathways that involves intracellular calcium release following chemokine stimulation. As described previously (**Figure 1.10**), following receptor activation, G<sub>q/11</sub> subunits activate PLCβ<sub>2</sub> that hydrolyses PIP<sub>2</sub> into IP<sub>3</sub> and DAG. In turn, IP<sub>3</sub> triggers mobilisation of Ca<sup>2+</sup> from intracellular stores (Rosenbaum et al., 2009). **Figures 3.9 and 3.10** demonstrate that calcium signalling is detected in MCF-7 and THP-1 cells in response to both CCL3 and CXCL12 stimulation. In both cell lines, change in intracellular Ca<sup>2+</sup> levels following CCL3 stimulation is more significant in comparison of CXCL12 stimulation (**figures 3.9 and 3.10**). Moreover, for THP-1 cells, there was a spike increase in intracellular Ca<sup>2+</sup> level following CCL3 stimulation and then decline progressively. The changes in intracellular Ca<sup>2+</sup> level appeared to be different in CXCL12-stimulated THP-1 cells and MCF-7 cells stimulated with CCL3 and CXCL12. Prolonged intracellular Ca<sup>2+</sup> release was observed over time within 60 s after chemokine stimulation. Attempts have been done to determine CXCL12-induced intracellular Ca<sup>2+</sup> mobilisation in Jurkat cells, however, Ca<sup>2+</sup> responses were unable to be detected. Our group previously increase the concentration of CXCL12 to 25 nM for detectable Ca<sup>2+</sup> responses in Jurkat cells (Hamshaw, PhD dissertation, 2020). Since 20 nM has been used as the assay concentration of CXCL12 in this study, we did not decide to change the concentration only for Jurkat cells for consistency.

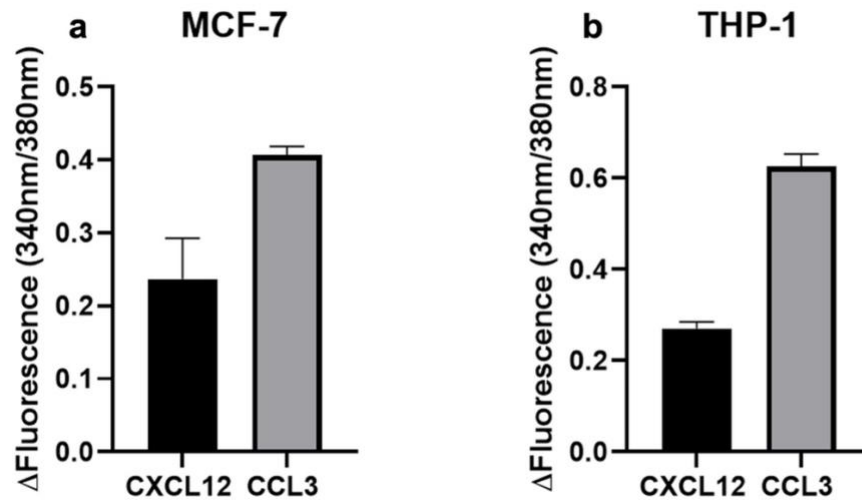


**Figure 3.9. More increase in intracellular  $\text{Ca}^{2+}$  release was observed in CCL3 stimulation compared to CXCL12 stimulation in MCF-7 and THP-1 cells.** (a) MCF-7 (b) THP-1 cells were stimulated with CXCL12 (20 nM) or CCL3 (200 nM). Data is expressed as changes in fluorescence ratio (340 nm/380nm) between peak fluorescence after stimulation with chemokine and basal fluorescence before stimulation with chemokine. Data represent mean  $\pm$  SEM from at least 3 independent experiments.

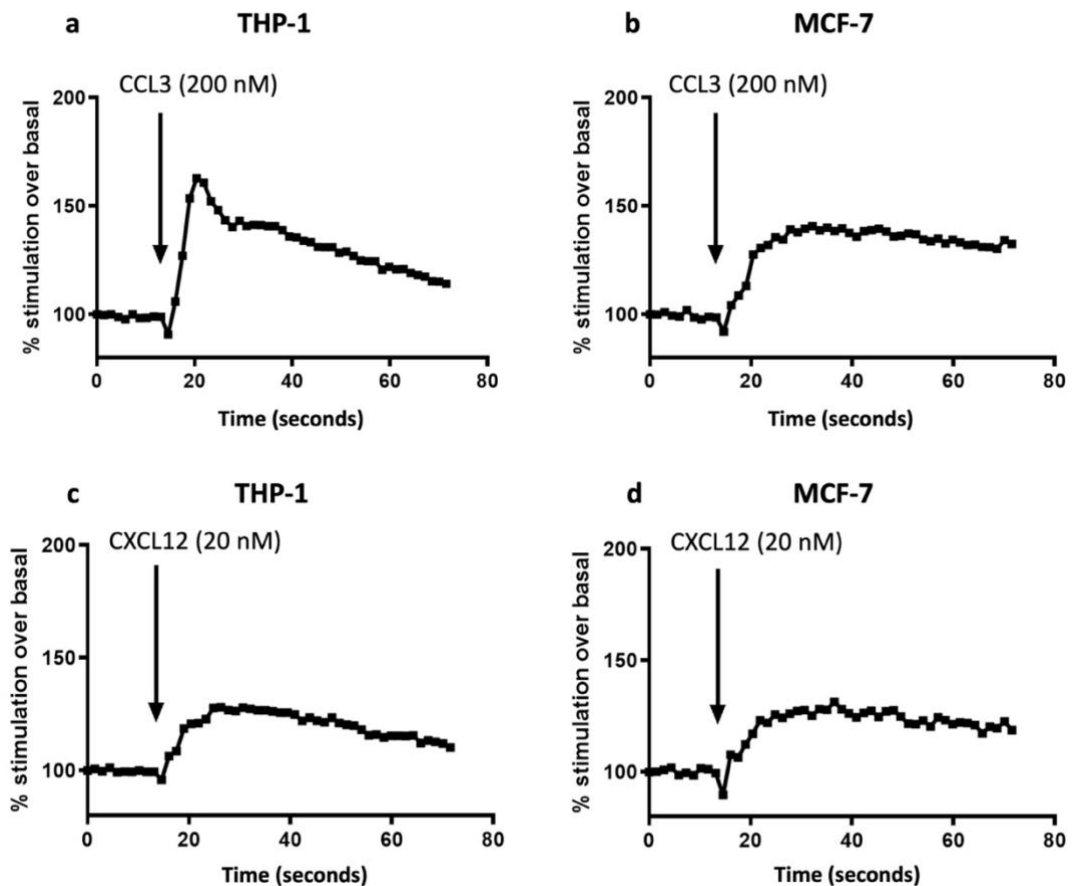


**Figure 3.10. Representative traces of real-time change in intracellular  $\text{Ca}^{2+}$  level in response to CCL3 or CXCL12 stimulation.** (a) THP-1 and (b) MCF-7 were stimulated with CCL3 (200 nM) at 15 s after the measurement started. (c) THP-1 and (d) MCF-7 were stimulated with CXCL12 (20 nM) at 15 s after the measurement started. Data are a representative trace of at least 3 independent experiments.

It is noteworthy that the calcium buffer used in our study contains  $\text{Ca}^{2+}$ , unlike the commercially available pre-made calcium buffer which is  $\text{Ca}^{2+}$ -free. This might raise concerns that presence of  $\text{Ca}^{2+}$  from the buffer would interfere with the readout and quantification of  $\text{Ca}^{2+}$  level. To reassure the possibility of generating inaccurate results, change in intracellular  $\text{Ca}^{2+}$  level change relative to basal condition was measured in our study. By taking the difference of the readings between stimulated and basal conditions, the add-on effects from extracellular  $\text{Ca}^{2+}$  will be cancelled out. Another concern could be the possibility that extracellular  $\text{Ca}^{2+}$  could influx through the transient receptor potential (TRP) channel on cells. Therefore, intracellular  $\text{Ca}^{2+}$  change observed might not solely be dependent of chemokine stimulation (Oquadid-Ahidouch et al., 2013). Our

group has previously attempted to conduct the same assay with Ca<sup>2+</sup>-free buffer using the cell lines in this study. It has been confirmed that the external effects from Ca<sup>2+</sup> in the calcium buffer is minimal (personal communication with Prof Anja Mueller).

### **3.3.3 Actin cytoskeletal rearrangement in response to chemokine stimulation**

Cell motility is a pivotal process in cancer metastasis. Cancer cells possessing increased metastasis potential are more mobile than cancer cells with low metastasis potential (Nicolson, 1993). Previous morphological studies revealed a significant increase in F-actin content with polarised movement of F-actin towards the periphery of the cells in migrating cancer cells following the stimulation of chemokines (Youngs et al., 1997; Verschueren et al., 1994). This implies that the structure of actin network correlates to the extent of cancer malignancy. In general, a high level of actin polymerisation is a prerequisite for lamellipodia formation and critical determinant for cancer cell infiltration into tissue (Friedl and Alexander, 2011). Therefore, visualisation of actin cytoskeletal rearrangement is one of the indicators of cell migration.

In order to visualise actin filaments (F-actin), F-actin binding phalloidin stain was used in our study. Phalloidin is a fluorophore (Alexa 488)-tagged cyclic peptide that binds and stabilise F-actin, allowing for the visualisation of the products of F-actin formation intracellularly (Faulstich et al., 1988). The binding affinity of phalloidin is comparable in a variety of cell lines without species-to-species variety commonly seen in anti-actin antibodies. Also, phalloidin produces very little non-specific binding, making phalloidin an ideal reagent for F-actin visualisation and quantification (Faulstich et al., 1988).

In the examination of chemokine-induced actin cytoskeletal rearrangement, a variety of chemokines, including CCL3, CCL4, CCL5, CCL23, CXCL8 (IL-8), CXCL9 and CXCL12 were investigated. As shown in **Table 1.1**, CXCL12 is the only ligand for CXCR4, whereas CCL3, CCL4 and CCL5 are associated ligands for CCR5. Both CXCR4 and CCR5 signalling are correlated to cancer metastasis as described in Section 1.6. CXCL8 (IL-8) is associated with CXCR1 (IL-8RA) and CXCR2 (IL-8RB). Accumulating evidence has supported that IL-8 signalling

axis correlates with immunosuppressive myeloid-rich tumour microenvironment, which reduces clinical benefits of anti-PD-1 immunotherapy (Schalper et al., 2020; Yuen et al., 2020). In the contrary, another chemokine signalling axis, CXCL9-CXCR3 has been revealed to have an anti-tumour role of CXCL9-CXCR3 axis in reinvigoration of CD8<sup>+</sup> T cell response in tumour microenvironment, which is beneficial for anti-PD-1 immunotherapy (Humblin and Kamphorst, 2019). Apart from their interactions with tumour-associated immune cells, it might be worthwhile to investigate the effects of IL-8-IL-8RA/IL-8RB and CXCL9-CXCR3 on cancer cells, which potentially either promote or suppress cancer cell migration. For CCL23, it is known to be a ligand for CCR1 and involved in cancer metastasis (Votta et al., 2000) and angiogenesis (Hwang et al., 2005). Although CCR1 expression was not investigated in our study, recent studies reported CCR1 is overexpressed in breast cancer cells contributing to cancer metastasis (Huang et al., 2022). Also, there are several ligands for CCR1 in common with CCR5, such as CCL3 and CCL5 (**Table 1.1**).

To examine the effects of chemokine stimulation on actin cytoskeletal change, cells were initially stimulated with chemokine ligands (100 nM CCL3, 50 nM CCL4, 50 nM CCL5, 50 nM CCL23, 50 nM CXCL8, 50 nM CXCL9 and 50 nM CXCL12) respectively for 30 minutes at 37°C, 5% CO<sub>2</sub>. Cells were then washed, fixed and permeabilised before staining with phalloidin. For basal condition, cells were treated in the same way without the addition of chemokine.

For MCF-7 cells, in comparison of basal condition, there is a significant formation of lamellipodia and filopodia at the leading edges of cells and an increase in stress fibre formation when incubated with CCL3 or CXCL12 (**Figure 3.11**). Cells appeared to be more spreading than that in the absence of chemokine stimulation (**Figure 3.11**).

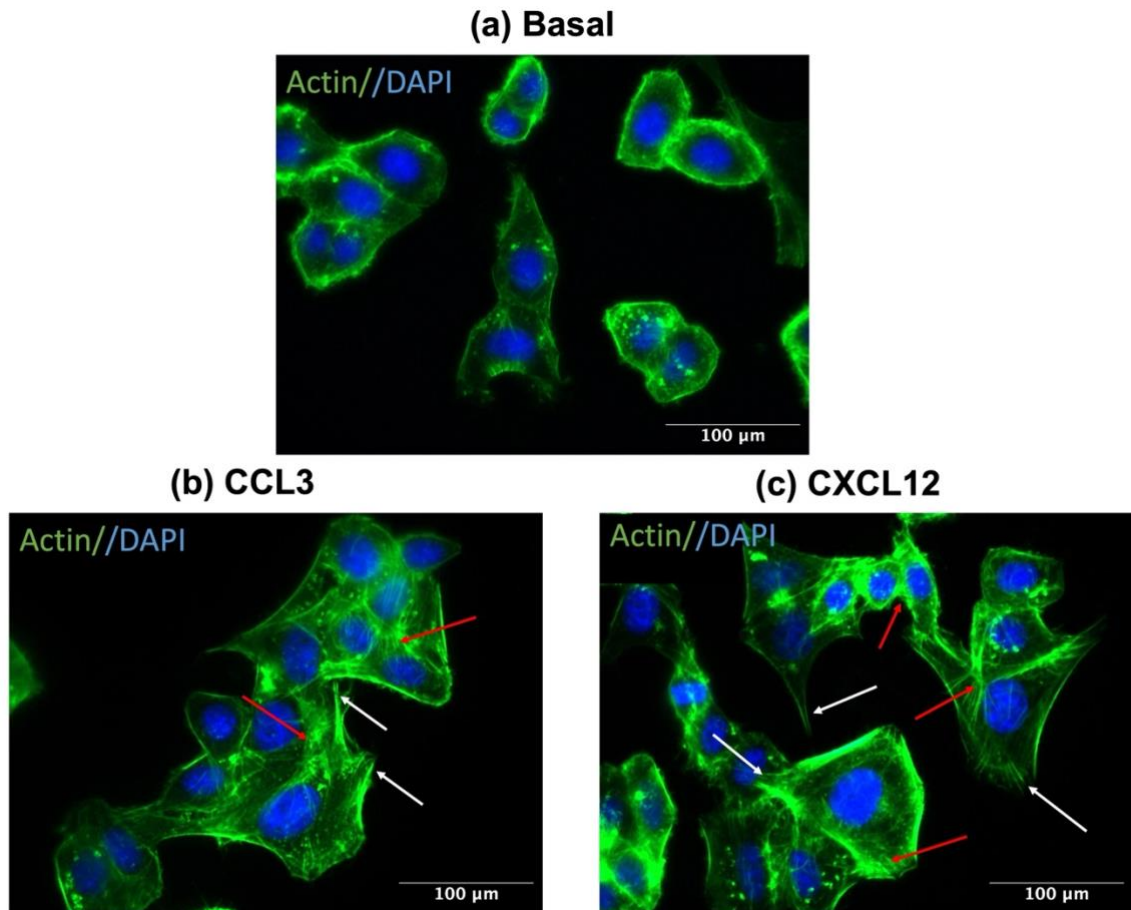


**Figure 3.11. Increase in the formation of filopodia and lamellipodia at the leading edge and formation of stress fibres at the contractile tail was observed in MCF-7 cells stimulated with CCL3 or CXCL12.** Arrows (in white) represent filopodia and lamellipodia formation; arrows (in red) represent stress fibre formation. Cells were either (a) unstimulated as basal control or stimulated with (b) CCL3 (100 nM) or (c) CXCL12 (50nM) for 30 minutes. Following chemokine stimulation, cells were fixed, permeabilised and stained with Alexa Fluor™ 488 Phalloidin (1:100) (in green) for F-actin cytoskeleton and DAPI (1:1000) (in blue) for cell nuclei. Representative images from at least 3 independent experiments were acquired with a Leica DMII Fluorescence microscope using 31.5X magnification.

For cells stimulated with other chemokines (CCL4, CCL5, CCL23, CXCL8 and CXCL9), F-actin generally accumulates at the periphery of the cells as compared to cells without chemokine stimulation. There was no significant formation of filopodia, lamellipodia and stress fibre (**Figure 3.12**). Elongated cell morphology was observed in some individual cells (**Figure 3.12**).

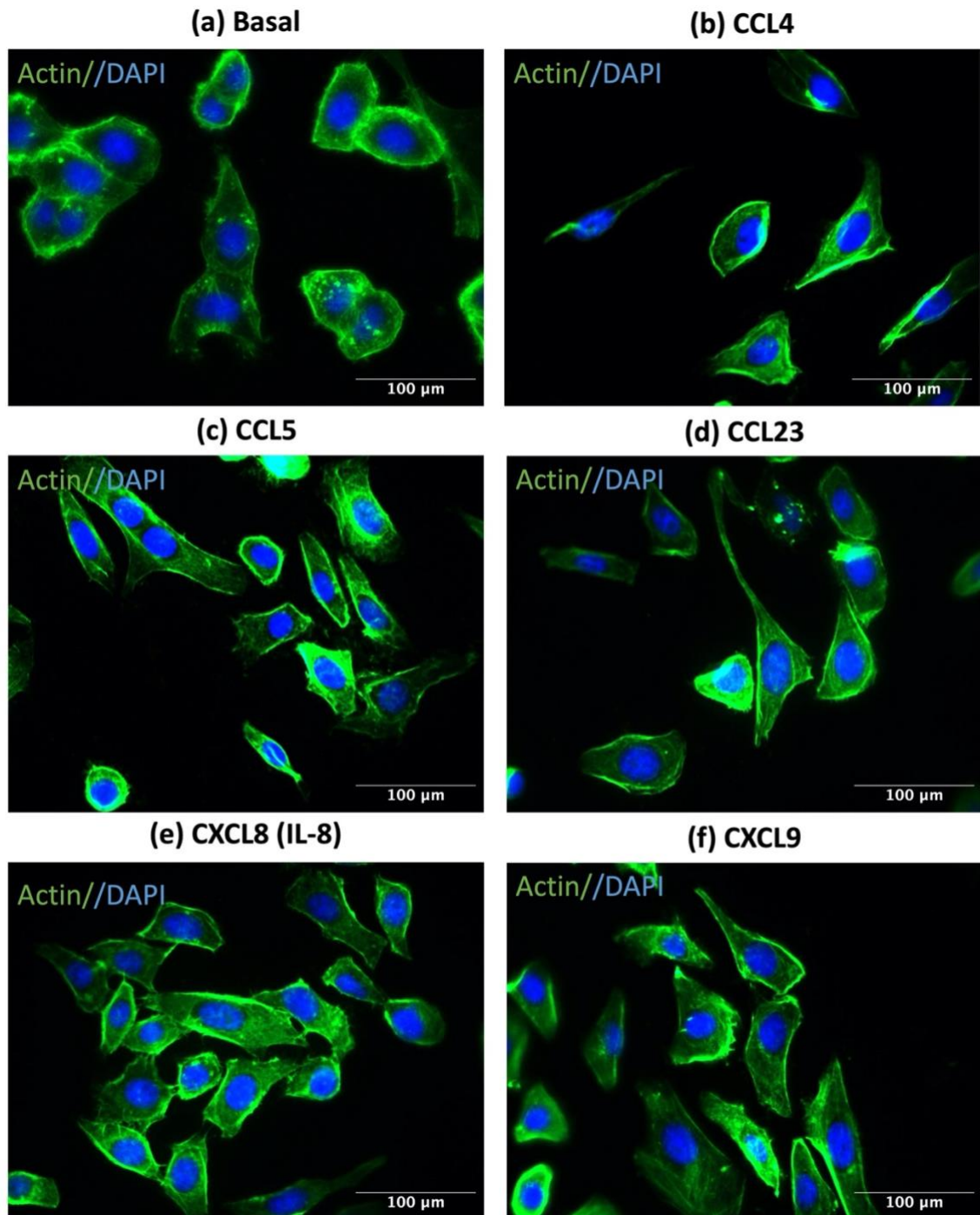


**Figure 3.12. No significant change in actin rearrangement was observed in MCF-7 cells stimulated with CCL4, CCL5, CCL23, IL-8 and CXCL9 respectively, but some individual cells appeared to be more elongated morphology.** Cells were either (a) unstimulated as basal control or stimulated with (b) CCL4 (50 nM), (c) CCL5 (50nM), (d) CCL23 (50 nM), (e) IL-8 (50 nM) or (f) CXCL9 (50 nM) for 30 minutes. Following chemokine stimulation, cells were then fixed, permeabilised and stained with Alexa Fluor™ 488 Phalloidin (in green) for F-actin cytoskeleton and DAPI (1:1000) (in blue) for cell nuclei. Representative images from at least 3 independent

experiments were acquired with a Leica DMII Fluorescence microscope using 31.5X magnification.

From the quantification analysis based on phalloidin-stained F-actin using ImageJ, a significant increase in cell area and a significant reduction in circularity were observed in MCF-7 cells stimulated with CCL3 or CXCL12 compared to basal condition (**Figure 3.13**). As cell circularity is expressed in a range of values 0.0 to 1.0, where 1.0 indicates a perfect circle, the values reflect that MCF-7 cells stimulated with CCL3 or CXCL12 appeared to be less circular. Interestingly, in the stimulation of CCL23, although there was no significant change in cell area, the circularity was significantly reduced compared to unstimulated basal control.

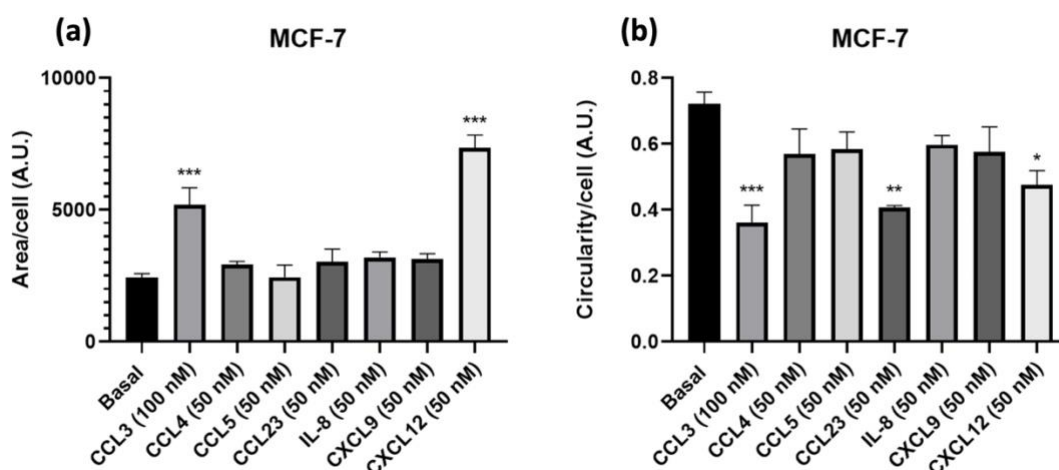


**Figure 3.13. CCL3 and CXCL12 stimulation induces a significant increase in cell area and significant reduction in cell circularity, while CCL23 induces a significant reduction in cell circularity but no significant difference in cell area in MCF-7 cells.** (a) Cell area per a single cell under stimulation of all chemokine ligands (CCL3, CCL4, CCL5, CCL23, CXCL8, CXCL9 and (b) cell circularity under stimulation of all chemokines ligands as above. At least 10 cells were analysed per experiment. Identical microscopic settings (image size, 2592 x 1944 pixel and 414.72 x 311.04  $\mu\text{m}$ ) were applied. Data shown represent the mean  $\pm$  SEM of three independent experiments. (One-way ANOVA with a Dunnett's multiple comparisons test as post-hoc test, \*\* =  $p \leq 0.01$ , \*\*\* =  $p \leq 0.001$ )

For MDA-MB-231 cells, distinct pseudopodia formation at the leading edge was seen in cells in all tested conditions with chemokine stimulation (**Figure 3.14**).

Unlike in MCF-7 cells, no lamellipodia extensions were seen in MDA-MB-231 cells. Instead, membrane blebbing and amoeboid-like morphology was seen for MDA-MB-231 cells (**Figure 3.14**). An observable increase in F-actin formation was observed in chemokine-stimulated cells compared to basal condition.

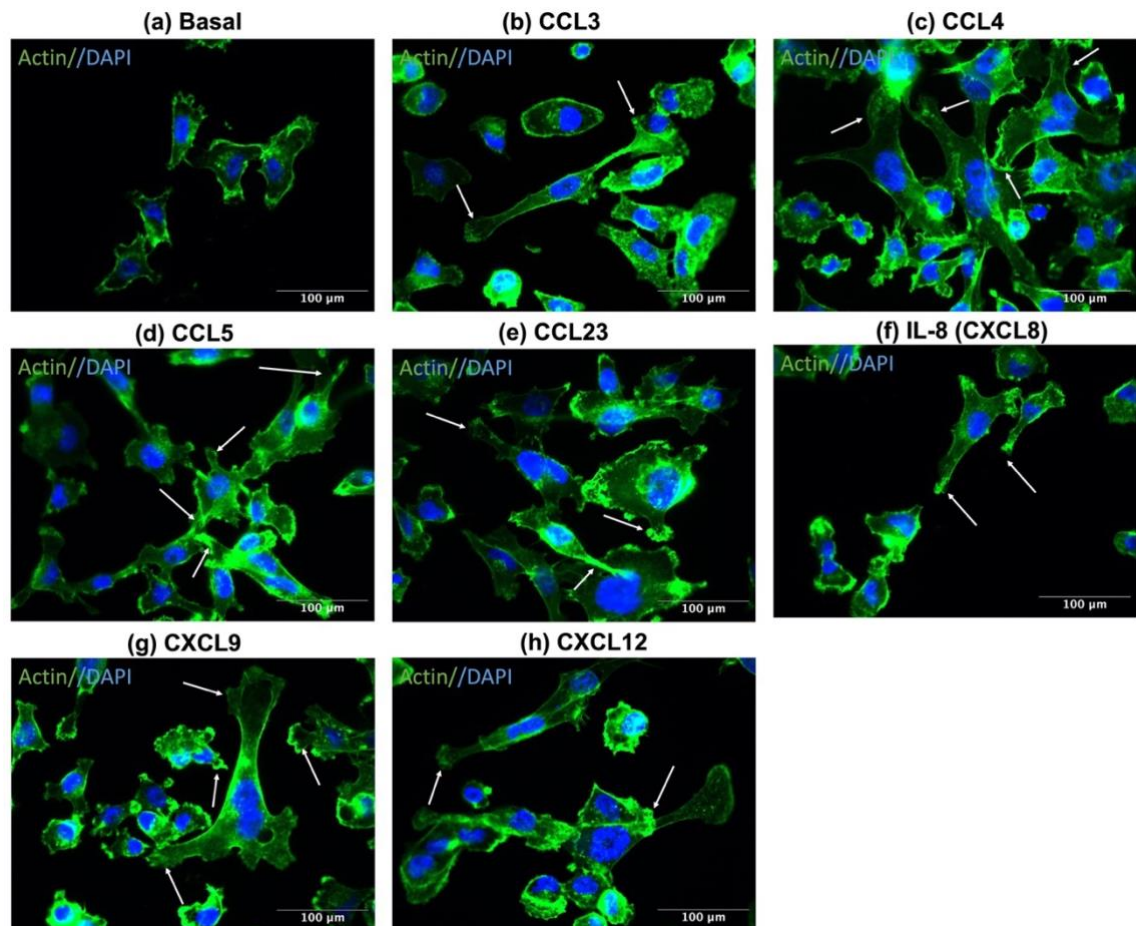


**Figure 3.14. Distinct formation of pseudopodia with membrane blebbing and amoeboid-like cell morphology was observed in MDA-MB-231 cells stimulated with all chemokine ligands tested.** Cells were either (a) unstimulated as basal control or stimulated with (b) CCL3 (100 nM), (c) CCL4 (50 nM), (d) CCL5 (50 nM), (e) CCL23 (50 nM), (f) CXCL8 (50 nM), (g) CXCL9 (50 nM) or (h) CXCL12 (50 nM) for 30 minutes. Following chemokine stimulation, cells were then fixed, permeabilised and stained with Alexa Fluor™ 488 Phalloidin (in green) for F-actin cytoskeleton and DAPI (1:1000) (in blue) for cell nuclei. Arrows (in white) represent pseudopodia. Representative images from at least 3 independent experiments were acquired with a Leica DMII Fluorescence microscope using 31.5X magnification.

From actin quantification, particularly for CCL3, CCL4, CXCL9 and CXCL12 stimulation, cell area was significantly increased compared to unstimulated basal control. In terms of circularity, cells stimulated with CCL3, CCL4, CCL5, CCL23 or CXCL9 was significantly reduced, indicating of more elongated morphology (**Figure 3.15**). Although the change in circularity was not significant in cells stimulated with IL-8 or CXCL12, the morphology appeared to be amoeboid-like but less elongated (**Figures 3.14 and 3.15**).

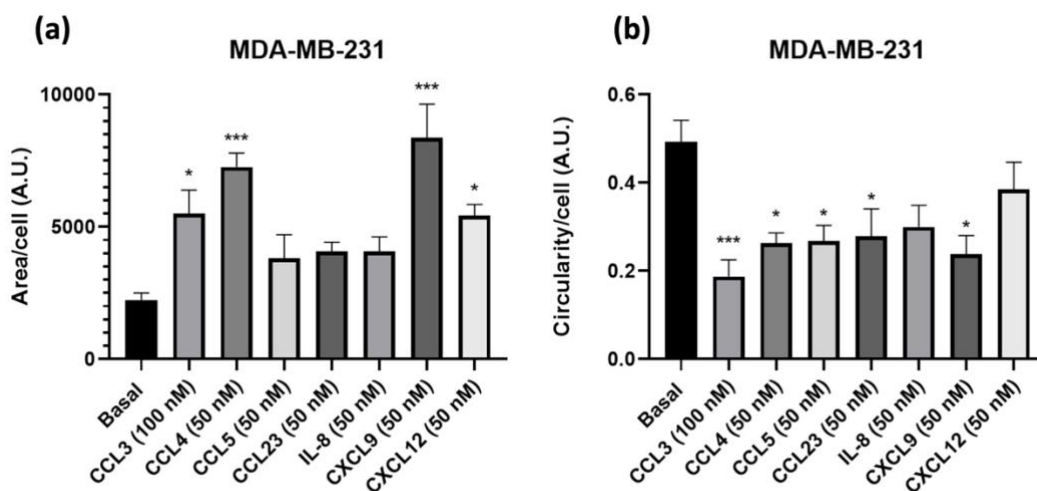


**Figure 3.15. Stimulation of CCL3, CCL4, CXCL9 and CXCL12 induces a significant increase in cell area, while cell circularity is significantly reduced following the stimulation of CCL3, CCL4, CCL5, CCL23 and CXCL9 in MDA-MB-231 cells.** (a) Cell area per a single cell under stimulation of all chemokine ligands (CCL3, CCL4, CCL5, CCL23, CXCL8, CXCL9 and (b) cell circularity under stimulation of all chemokines ligands as above. At least 10 cells were analysed per experiment. Identical microscopic settings (image size, 2592 x 1944 pixel and 414.72 x 311.04  $\mu\text{m}$ ) were applied. Data shown represent the mean  $\pm$  SEM of three independent experiments. (One-way ANOVA with a Dunnett's multiple comparisons test as post-hoc test, \* =  $p \leq 0.05$ , \*\*\* =  $p \leq 0.001$ )

### 3.3.4 Chemotaxis in response to chemokine stimulation

Chemotaxis assay is generally used to evaluate the cellular responses to soluble chemoattractant molecules by characterising directed cell motion along chemoattractant gradients (Justus et al., 2014).

A commercially available ChemoTX plate (Neuroprobe Inc, USA) was used in our chemotaxis assay. It relies upon the ability of cells to migrate through a porous membrane into the bottom compartment containing chemokine CXCL12 (1nM). Cell migration is monitored and assessed by visually counting the cell number present in the bottom compartment after 4 hours incubation. The principle is similar to the Boyden chamber commonly used for large adherent cells (Justus et al., 2014). For suspension cells (Jurkat and THP-1 cells) in this study, ChemoTX plate with a smaller pore sized (5  $\mu\text{m}$ ) membrane is more suitable (de Wit et al., 2016).

Although the Boyden chamber is commonly used in the study of chemotaxis for adherent cells, data generated from the cell lines investigated in our study was not reproducible using the Boyden chamber. Therefore, another commercially available plate, 96-well ORIS cell migration plate (Platypus Technologies) was used in this study. A cell-free detection zone was generated at the centre of a well by a designated stopper before the addition of chemokine. After incubation with chemokine for 24 hours, cells within the detection zone were imaged and counted as migrating cells. It is noteworthy that this method assesses random migration without the generation of chemokine gradient, similar to a wound healing assay. In a wound healing assay, the wound where cells migrate towards is manually generated and hence the measurement is subjective. The design of ORIS cell migration plate could minimise these man-made errors and inconsistency from the wound healing assay.

**Figure 3.16** shows that both cell lines, Jurkat and THP-1, migrate towards CXCL12 in comparison to basal condition in the absence of CXCL12. The cell densities for Jurkat and THP-1 employed in our chemotaxis assay are  $25 \times 10^4$  cells per well and  $50 \times 10^4$  cells per well respectively. These were determined from the assay optimisation experiments by our group previously (Goh, PhD dissertation, 2018). Between the two cell lines, the CXCL12-induced chemotactic response of Jurkat cells is more significant than THP-1 cells. This can be explained by the fact that CXCR4 is not abundantly expressed in THP-1 cells while Jurkat cells overexpress CXCR4 as shown in **Table 3.1**. As shown in **Table 3.1**, expression of cell surface CCR5 is more abundant in THP-1 cells. As

demonstrated by Moyano Cardaba et al., 2012, more significant chemotactic response to CCL3 was observed for THP-1 cells (approximately  $70 \times 10^4$  cells/ml of migrating cells) in the same experimental setting. For Jurkat cells, other chemokine ligands (CCL1, CCL2, CCL3, CCL5, CCL8, CCL23 and CXCL11 1nM) were investigated in chemotaxis assay previously by our group, however, no chemotactic response was observed (Goh, PhD dissertation, 2018). The observations imply that the chemotactic responses to chemokine ligands depend on the cell surface expression of chemokine receptors and whether the downstream cellular processes elicited leads to chemotaxis.

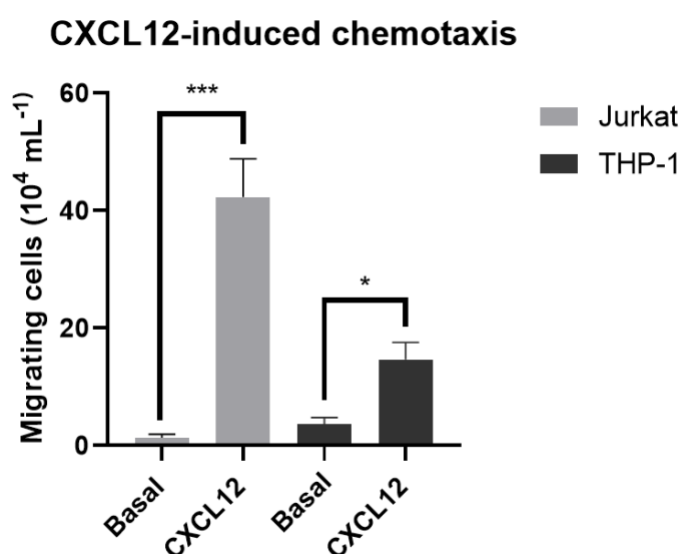


**Figure 3.16. Jurkat migrate towards CXCL12 more significantly than THP-1 in the chemotaxis assay.** Jurkat and THP-1 cells were seeded onto the membrane above the bottom compartment containing CXCL12 (1 nM) or serum-free media only (for basal controls) in the ChemoTx plate. The plate was incubated at 37°C for 4 hours. Data is expressed as the number of cells in the bottom compartment after 4-hour incubation. Data shown represent the mean  $\pm$  SEM of 3 independent experiments. Unpaired t-test, \* =  $p \leq 0.05$  and \*\*\* =  $p \leq 0.001$ .

For MDA-MB-231 cells, in the cell migration assay using 96-well ORIS™ cell migration plate (Platypus Technologies), there is no significant change in the number of migrating cells present within the migrating zone after incubation with CXCL12 as shown in **Figure 3.17**.

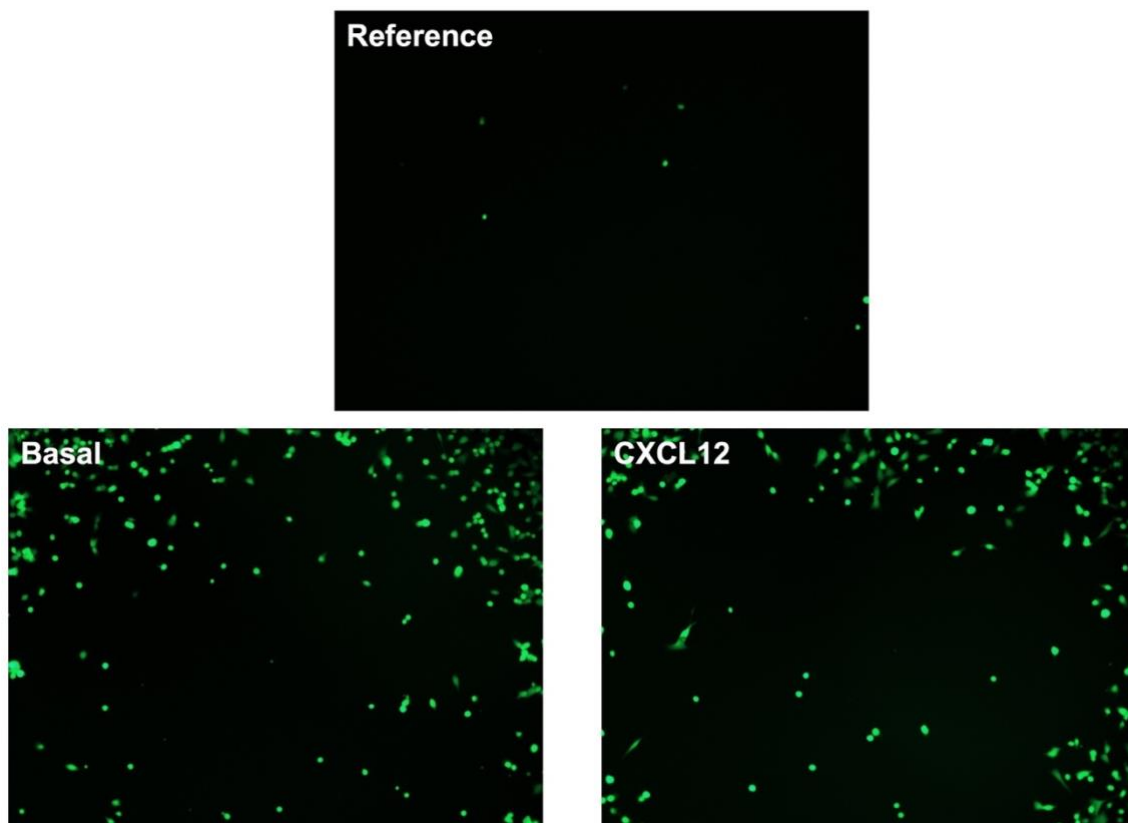


**Figure 3.17. No significant cell migration towards the detection zone following incubation with CXCL12 was observed for MDA-MB-231 cells.** Cell migration assay was conducted using 96-well ORIS™ cell migration plate (Platypus Technologies). MDA-MB-231 cells migrate into the detection zone after incubation with CXCL12 (1 nM) or in the absence of CXCL12 (basal) for 24 hours. In the reference well, the insert stopper was not removed until the image was acquired. Cells were stained and incubated with calcein AM (green) for 45 minutes and visualised. Representative images from 3 independent experiments were acquired with a Leica DMII Fluorescence microscope using 5X magnification.

### 3.3.5 Receptor internalisation in response to chemokine stimulation

The binding of chemokine ligands to their cognate chemokine receptors induce rapid desensitisation and internalisation into early endosomes, followed by sorting into late endosomes for either degradation or recycling pathway (Ferguson, 2001; Nichols and Lippincott-Schwartz, 2001) (**Figure 1.20**). The tight regulation of chemokine receptor translocation between the cell surface and intracellular compartments contributes to sensitisation of the receptors to chemokine ligands and affects the duration and magnitude of chemokine

signalling, which may alter the functionality of cells. The extent of chemokine receptor internalisation has been known to be determined by several factors, including cell types, ligand types and the phosphorylation status of the C-terminus of the receptor.

In this section, we particularly explore CCL3-induced CCR5 internalisation in breast cancer MCF-7 cells and CXCL12-induced CXCR4 internalisation in MCF-7 cells and leukaemic Jurkat cells. As Jurkat cells express relatively low level of CCR5 on cell surface (shown in **Table 3.1**), investigation of CCL3-induced CCR5 internalisation was not conducted in our study. Cells were stimulated with CCL3 (100 nM) or CXCL12 (50 nM) in serum-free medium and incubated for 30 minutes at 37°C, 5% CO<sub>2</sub> to allow receptor internalisation to take place. Cells were then washed and stained using anti-CCR5 or anti-CXCR4 antibodies at 4°C. Prolonged incubation at 37°C will induce receptor recycling. Since our study aim focuses on the process of receptor internalisation only, cell staining process was conducted at 4°C after incubation with chemokine at 37°C for 30 minutes (Mueller and Strange, 2004). Receptor internalisation was assessed by two methods: fluorescence microscopic visualisation and flow cytometry analysis for receptor expression quantification.

It is noteworthy that our study used anti-CXCR4 antibody (4G10), which is against the N-terminus amino acids of human CXCR4 according to the product information provided by the supplier (Santa Cruz Biotechnology). Another anti-CXCR4 antibody, anti-CXCR4 (12G5), is also commercially available. It was found to bind a site in the second extracellular loop 2 (ECL2) of CXCR4, which is the same site where CXCL12 binds (Carnec et al., 2005; Yang et al., 2003). It is not ideal for receptor internalisation assay due to its competitive binding feature with CXCL12. The effect of CXCL12 on CXCR4 internalisation will be hindered by anti-CXCR4 (12G5). Instead, it has been more commonly used in antibody competition assays for testing CXCR4 antagonising compounds. On the other hand, anti-CXCR4 (4G10) binds to a different site from CXCL12, and hence will not affect the binding of CXCL12 to CXCR4.

**Figures 3.18 and 3.19** illustrates that a significant reduction in CXCR4 expression from the cell surface was observed on MCF-7 and Jurkat cells in the

CXCL12-stimulated samples compared to basal samples. Next, we attempted to quantify how much reduction in CXCR4 expression as an indicative of CXCR4 internalisation using flow cytometry analysis. As shown in **Figure 3.19 and Table 3.2**, the cell surface expression level of CXCR4 was significantly decreased by 26.1% and 49.6% in MCF-7 and Jurkat cells respectively, following the stimulation of CXCL12 for 30 minutes. The results indicate that CXCR4 internalisation took place in Jurkat and MCF-7 cells after CXCL12 stimulation. The effect of CXCL12-induced CXCR4 internalisation was more significant in Jurkat cells than MCF-7 cells.

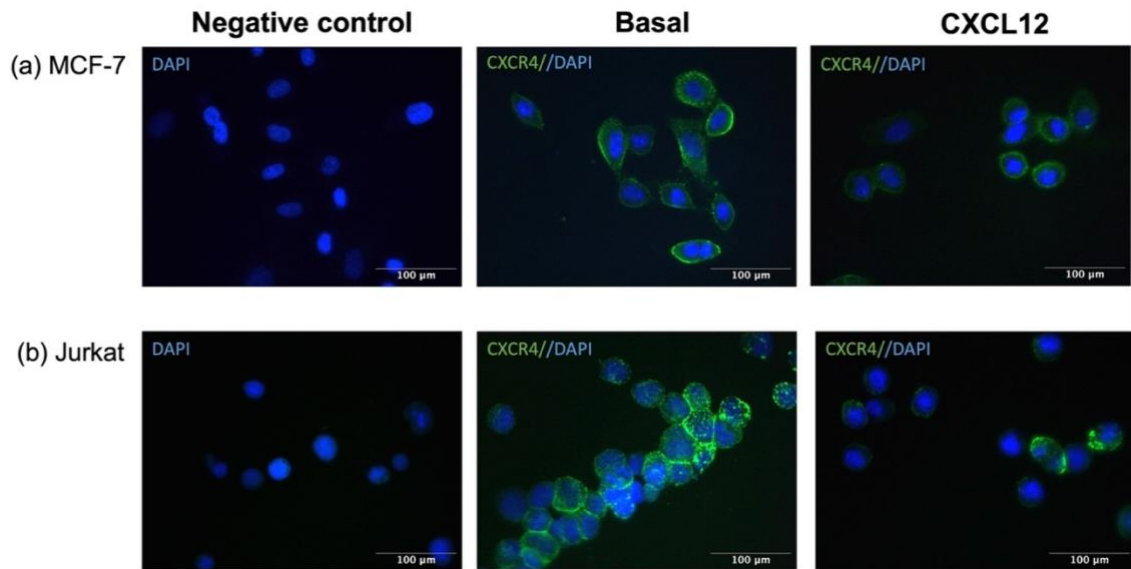


**Figure 3.18. Reduced cell surface expression of CXCR4 was observed following the stimulation with CXCL12 in MCF-7 and Jurkat cells compared to unstimulated basal controls.** (a) MCF-7 or (b) Jurkat cells were either unstimulated as a basal control or stimulated with CXCL12 (50 nM) for 30 minutes at 37°C to allow receptor to internalise. Cells were either stained with secondary anti-mouse Alexa 488 antibody (1:500) only as negative control or stained with mouse mAb against CXCR4 (1:500) followed by secondary staining with anti-mouse Alexa 488 antibody (1:500) (green) and DAPI (1:1000) (blue) for cell nuclei. Cells were then fixed with 4% formaldehyde solution before images were acquired. Representative images from at least 3 independent experiments were acquired with a Leica DMII Fluorescence microscope using 20X magnification.

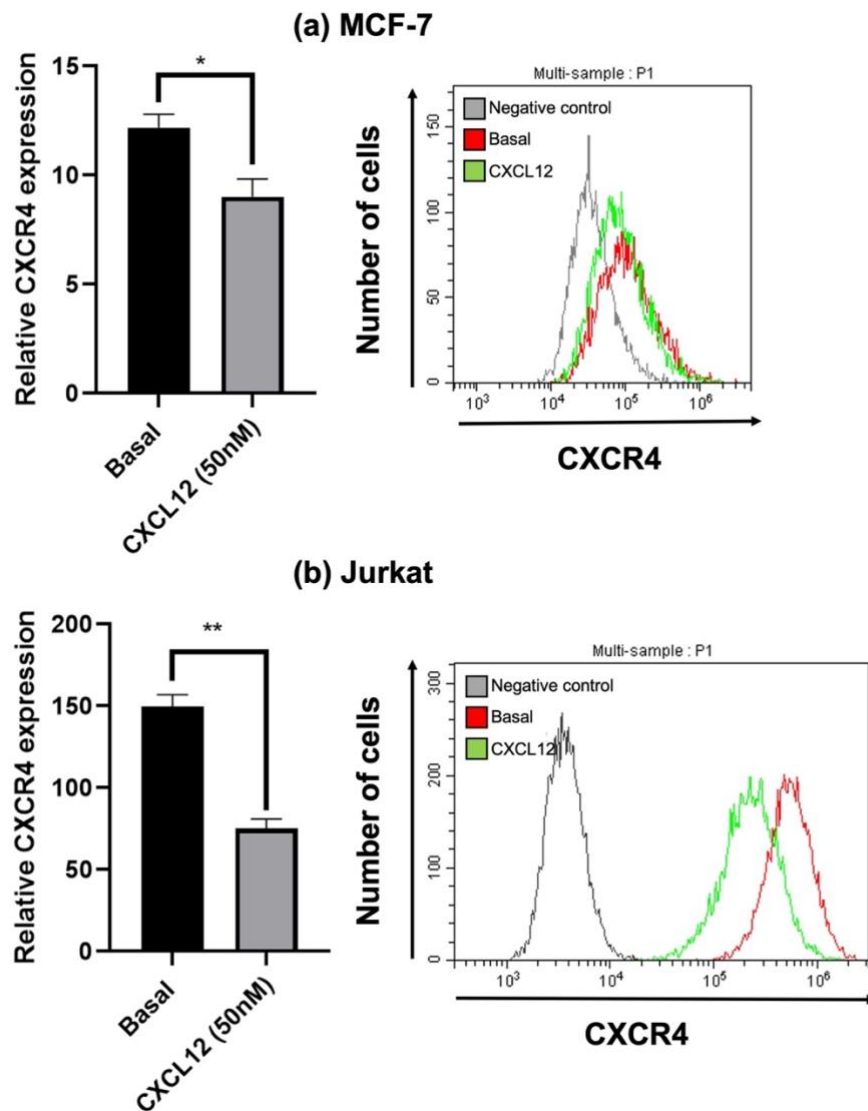


**Figure 3.19. A significant reduction in relative CXCR4 expression on cell surface following CXCL12 stimulation was observed in both MCF-7 and Jurkat cells.** (a) MCF-7 (b) Jurkat cells were either unstimulated as basal control or stimulated with CXCL12 (50 nM) for 30 minutes. Fluorescence intensity of 20,000 events from each sample were quantified in flow cytometry and cell population was gated to exclude dead cells and debris for each cell line before analysis. Representative histograms from at least 3 independent experiments show the comparison of unstained negative control (in grey), basal control without chemokine stimulation (in red) and CXCL12-stimulated cells (in green). Relative CXCR4 receptor expression was calculated from median channel of fluorescence (stained cells) / median channel of fluorescence (negative control)], where negative control was stained with secondary antibody. Median channel of fluorescence was based on the median of the fluorescence intensities in a

gated population of cells from each sample and acquired by the CytExpert software (Beckman Coulter). Data shown represent the mean  $\pm$  SEM of at least 3 independent experiments. Unpaired t-test, \* =  $p \leq 0.05$ , \*\* =  $p \leq 0.01$ .

With respect to CCR5 internalisation, CCR5 expression was reduced from cell surface in the CCL3-stimulated MCF-7 cells as shown in **Figure 3.20**. To confirm this, using flow cytometry analysis, it was found that the cell surface expression level of CCR5 was significantly decreased by 27.3% in MCF-7 cells, indicating that CCL3-induced CCR5 internalisation occurred (**Figure 3.21 and Table 3.2**). Ideally, it might be better to make a multiple comparison across basal, CCL3-stimulated and CXCL12-stimulated sample. However, since different antibodies were used for two different chemokine receptors with different basal expression levels and binding affinities, comparisons should be done independently. For Jurkat cells, due to lower expression level of cell surface CCR5, CCR5 receptor internalisation was undetectable from our attempts.

It should be noted that the receptor expression levels shown in this section represent receptor expression on cell surface only, in order to avoid confusion by internalised receptors in our analysis. Additional cell permeabilisation step was not conducted for visualising intracellular expression of the receptors.

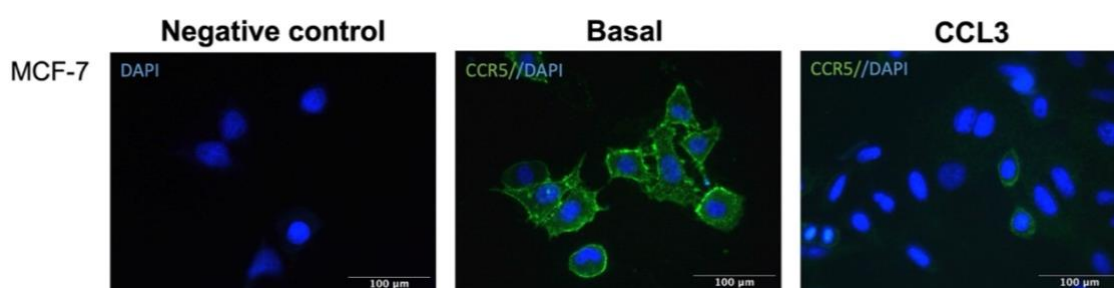


**Figure 3.20. Cell surface CCR5 expression was reduced following CCL3 stimulation in MCF-7 cells.**

MCF-7 cells were either unstimulated as a basal control or stimulated with CCL3 (100 nM) for 30 minutes at 37°C to allow receptor to internalise. Cells were either stained with secondary anti-rat Alexa 488 antibody (1:500) only as negative control or stained with rat mAb against CCR5 (1:100) followed by secondary staining with anti-rat Alexa 488 antibody (1:500) (green) and DAPI (1:1000) (blue) for cell nuclei. Cells were then fixed with 4% formaldehyde solution before images were

acquired. Representative images from at least 3 independent experiments were acquired with a Leica DMII Fluorescence microscope using 20X magnification.

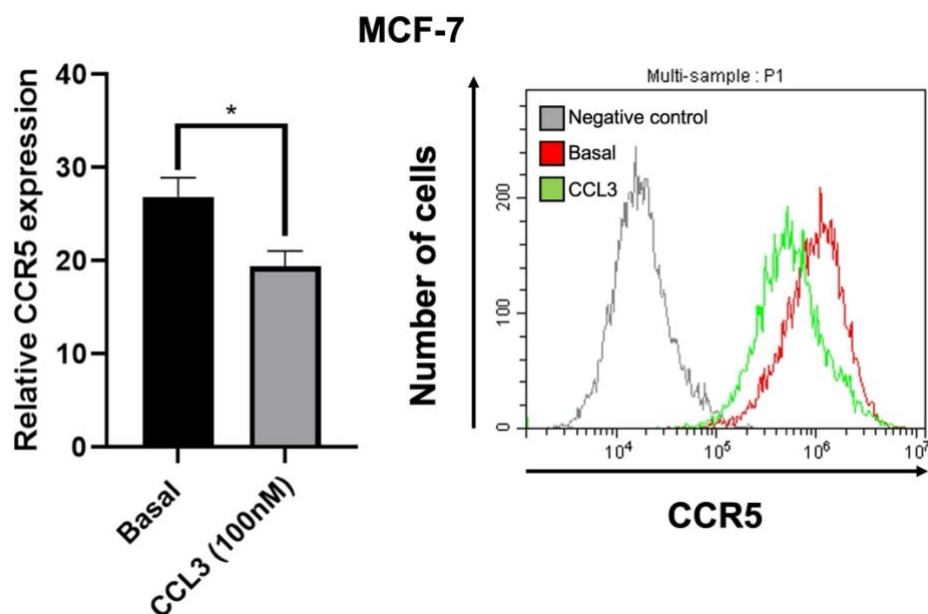


**Figure 3.21. A significant reduction in relative CCR5 expression on cell surface following CCL3 stimulation was observed in MCF-7 cells.** MCF-7 cells were either unstimulated as basal control or stimulated with CCL3 (100 nM) for 30 minutes. Fluorescence intensity of 20,000 events from each sample were quantified in flow cytometry and cell population was gated to exclude dead cells and debris for each cell line before analysis. Bar chart shows the comparison of relative CCR5 expression between basal control without chemokine stimulation ( in black) and CCL3-stimulated cells (in grey) based on data from at least 3 independent experiments. Representative histograms from at least 3 independent experiments show the comparison of unstained negative control (in grey), basal control without chemokine stimulation (in red) and CCL3-stimulated cells (in green). Relative CCR5 receptor expression was calculated from median channel of fluorescence (stained cells) / median channel of fluorescence (negative control)], where negative control was stained with secondary antibody. Median channel of fluorescence was based on the median of the fluorescence intensities in a gated population of cells from each sample and acquired by the CytExpert software (Beckman Coulter). Data shown

represent the mean  $\pm$  SEM of at least 3 independent experiments. Unpaired t-test, \* =  $p \leq 0.05$ .

**Table 3.2. Percentage of receptor expression on cell surface following chemokine stimulation in MCF-7 and Jurkat cells**

| Cell line | Chemokine         | Percentage of receptor expression on cell surface following chemokine stimulation for 30 minutes (%)*<br>Mean $\pm$ SEM |
|-----------|-------------------|---|
| MCF-7     | CCL3<br>(100 nM)  | 72.7 $\pm$ 3.8  |
|           | CXCL12<br>(50 nM) | 73.9 $\pm$ 4.8  |
| Jurkat    | CXCL12<br>(50 nM) | 50.4 $\pm$ 3.4  |

Data shown represent the mean  $\pm$  SEM of at least 3 independent experiments.

\*Percentage of receptor expression on cell surface following chemokine stimulation

= [median channel of fluorescence (chemokine-stimulated) - median channel of fluorescence (negative control)] / [median channel of fluorescence (without chemokine stimulation) - median channel of fluorescence (negative control)] (%) , where negative control was stained with secondary antibody matched to the host species and class of the primary antibody only.

### 3.4 Discussion

We examined the chemokine expression profile and chemokine-mediated cellular responses in a selection of cancer cell lines which endogenously express chemokine receptors. From our immunofluorescence staining and quantitative flow cytometry analysis, the cancer cell lines used in our study were confirmed to display distinct cell surface chemokine receptor expression profiles. Some chemokine receptors were found to be more abundantly expressed than others. Based on our preliminary findings, we could further investigate signalling events related to the overexpressed receptors for these cell lines. This could save time to avoid experimenting with chemokine ligands associated with the receptor with very low expression in cells. Previous literature determined receptor expression using other methods, such as RT-qPCR and western blotting. There are

differences in quantitative measurements among these methods due to different analytical principles involved. RT-qPCR measures gene expression at mRNA level, whereas western blotting measures protein expression. These methods are particularly useful for gene set enrichment analysis to investigate association of specific gene or protein with diseases. In our study, our research focus on the mechanisms of signalling pathways at cellular level, looking at how cell surface receptor is activated and transduces downstream signalling in cells. Thus, flow cytometry, which is an antibody-based analysis, would be ideal to identify receptors or proteins expressed on cell surface or intracellularly.

Calcium ions ( $\text{Ca}^{2+}$ ) plays a crucial role in chemokine-induced signalling, transducing downstream signalling implicated in the regulation of a variety of physiological and pathological processes (Rosenbaum et al., 2009). Measurement of change in intracellular  $\text{Ca}^{2+}$  level is an ideal indicator of chemokine receptor activation. Therefore,  $\text{Ca}^{2+}$  assay is one of the common functional assays for GPCR downstream signalling studies.

As MCF-7 and THP-1 cells have been shown to express CCR5 and CXCR4, both cell lines are hypothesised to respond to CCL3 and CXCL12. It was found that CCL3 stimulation induces more intracellular  $\text{Ca}^{2+}$  release in both cell lines compared to CXCL12 stimulation. The observation can be explained by the expression levels of chemokine receptors. More CCR5 receptors are present on cell surface of both MCF-7 and THP-1 cells as shown above (**Table 3.1**). Another explanation is that CCL3-CCR5 signalling might be more likely to activate towards the pathways that involve  $\text{Ca}^{2+}$  mobilisation via  $\text{G}_{q/11}$ . Yet,  $\text{Ca}^{2+}$  assay alone does not provide sufficient evidence to determine the exact mechanisms in the activation of chemokine signalling. Other downstream signalling pathways are possible via alternative second messengers as shown in **Figures 1.9 and 1.10**. Other downstream signalling proteins, such as Rac GEFs (Coso et al., 1995), Rho GEFs (Mikelis et al., 2013), PI3K (Welch et al., 2002) and  $\beta$ -arrestins (Sun et al., 2002), are also involved in signalling transduction, contributing to a wide range of cellular responses. Other functional assays, such as GTP $\gamma$ S binding assay (Harrison and Traynor, 2003), cAMP assay (Wang et al., 2004) and fluorescence-based analysis of GEF function (Blaise et al., 2021), can be done to investigate the activation of G-protein dependent pathways, while

luminescence-based  $\beta$ -arrestin recruitment assay (Pedersen et al., 2021) can be conducted for determining the possible roles of G-protein independent pathways.

In the aspect of intracellular structures, actin rearrangement is prerequisite for the generation of a protrusive leading edge and contractile tail in cell migration (Nourshargh and Alon, 2014). Our study demonstrated that CXCL12 and CCL3 are involved in actin rearrangement in MCF-7 cells by mediating the formation of lamellipodia and filopodia at the leading edge and stress fibre formation at the contractile tail. Based on the morphology of MCF-7 cells stimulated with CXCL12 and CCL3, cells appeared to be more spindle-like and spreading, which are the common features of mesenchymal-type protrusion and actin-driven migration. According to the mechanisms underlying actin-driven migration, Rac, which is activated by the adaptor NEDD9 and the exchange factor DOCK3, is the major mediator in actin polymerisation through WAVE2, leading to mesenchymal protrusion (Sanz-Moreno, 2012). For MDA-MB-231 cells, in response to the stimulation of chemokine ligands, membrane blebbing in the absence of lamellipodia extension was observed in general. This implies that MDA-MB-231 cells tend to adopt amoeboid-type protrusion and bleb-driven migration, which is different from MCF-7 cells. In bleb-driven migration, cells appear as spherical expansions of the membrane driven by cytoplasmic-flow propelled protrusions under hydrostatic pressure. There are three phases involved: bleb initiation, bleb expansion driving forward movement and bleb contraction driving retraction (Lorentzen et al., 2011; Wolf et al., 2003). In the mechanistic aspect, Rho-mediated activation of ROCK leads to increase in myosin contractility that facilitates bleb formation (Bergert et al., 2012). In parallel, Rac GTPase protein, ARH-GAP22, is activated, which in turn inhibit Rac-induced actin polymerisation and mesenchymal-type protrusion formation (Sanz-Moreno et al., 2008). A number of studies demonstrate that cancer cells interconvert their modes of protrusion during migration in different types of environment (Sanz-Moreno and Marshall, 2010). The balanced regulation of actin protrusion and myosin contractility is the determinant of the plasticity in the modes of cancer cell migration (Sanz-Moreno et al., 2008; Bergert et al., 2012).

Although our results showed that MCF-7 and MDA-MB-231 cells preferentially adopted one mode of migration than the other, the possibility of their capability to

switch between the two modes could not be ruled out. The experimental setting in our study was limited to a constant growth environment. Cells were grown on a 2D culture plate in serum-free growth medium at 37°C, 5% CO<sub>2</sub>. This could not represent the complex architecture of tissue and tumour microenvironment in cancer where other types of cells, such as immune cells and stromal cells, are present.

In terms of the effects of chemokine stimulation on cell migration, our results demonstrated that particularly CCL3 and CXCL12 induces mesenchymal migration in MCF-7 cells more significantly than other chemokine ligands in the study. This can be implicated by several factors: (1) Low expression level of the receptor on cell surface might diminish downstream signalling activation and transduction, (2) the NEDD9/DOCK3/Rac/WAVE2 pathway might not be involved in some of the chemokine signalling axes, (3) the concentration of chemokine ligands used might not be optimal for the effect. With respect to amoeboid migration in MDA-MB-231 in response to chemokine stimulation, our results showed that similar effects were seen across the chemokine ligands tested. Our observations are consistent with a previous study on CXCL12 and CCL21 (Müller et al., 2001). Distinct pseudopodia formation and transient increase in intracellular F-actin were observed following the stimulation with CXCL12 or CCL21 in MDA-MB-231 cells (Müller et al., 2001). In the mechanistic aspect, another literature demonstrated that the formation of pseudopodia in MDA-MB-231 cells do not require Arp2/3 complex, which is responsible for filopodia formation (Poincloux et al., 2011). This might imply that the Rho/ROCK pathway is predominant in pseudopodia formation in MDA-MB-231 cells. Also, the activation of Rho/ROCK pathway in myosin contractility is more generalised with multiple chemokines involved. Yet, further investigations should be done to confirm the involvement of chemokine signalling in Rho/ROCK pathway. Also, since MDA-MB-231 is an invasive breast cancer cell line with higher migratory potential, the sensitivity of chemokine receptors might be higher than MCF-7 cells. Even low levels of chemokine receptor expression could sensitise the ligand activation, thereby elicit significant cellular responses.

Apart from the determination of cell migration modes by visualising intracellular actin rearrangement, we also examined the chemotactic responses of cells in the

stimulation with chemokine ligands. In the generation of chemokine gradients, cells migrate towards soluble chemoattractant molecules in a directed direction, known as chemotaxis (Justus et al., 2014).

In relation to CXCL12-induced chemotaxis, our result suggested that Jurkat and THP-1 cells migrate towards CXCL12 but more migration was observed in Jurkat cells. It implies that chemotactic responses can vary between cell types even in the stimulation of the same chemokine ligand as alternative pathway that does not involve chemotaxis might preferentially be activated in some cell types. For MDA-MB-231 cells, no significant increase in migratory response was observed in the stimulation with CXCL12. Yet, our observations were contradicted to previous publication. The study showed that a significant increase in cell migration was observed in MDA-MB-231 cells stably transfected with CXCL12, compared to wild-type MDA-MB-231 cells in Matrigel invasion assay (Sun et al., 2014). This implies that CXCL12 induces cell invasion in MDA-MB-231 cells. There may be several explanations for these controversial observations. Firstly, the study was to evaluate the endogenous effect of CXCL12 transfection on cell invasion by using genetically modified cells where CXCL12 was overexpressed. Also, the addition of Matrigel was to simulate cell invasion through the extracellular matrix (ECM). The assay employed by the study measures the capability of cells to invade through ECM. Our study assessed the effect of CXCL12 stimulation exogenously on cell migration instead. There might be environmental factors that could affect the observations. Secondly, in our experimental setup, chemokine was added directly to the well once the insert stopper was removed. In this circumstance, chemokine diffuse throughout the well without the generation of chemokine gradient. Thus, cells could migrate in random directions and some migrating cells might not be detected within the detection zone. By taking end-point analysis, it might not accurately represent the whole process of cell migration in response to chemokine stimulation. Thirdly, the incubation time with chemokine might not long enough to detect the difference in the number of migrating cells. Some cell types might migrate at a slower migrating rate.

Also, it should be noted that the method using the 96-well ORIS cell migration plate (Platypus Technologies) is based on the assessment of random migration,

which is different from ChemoTx plate (Neuroprobe Inc, USA). Thus, the observations might not represent the effect of CXCL12 concentration gradient on directed migration. Also, attempts have been done with another breast cancer cell line, MCF-7 using the ORIS cell migration plate, however, no migration was observed within the assay incubation time (24 hours) (Hamshaw, PhD dissertation, 2020).

There are several factors that influence the migrating ability of cells, such as cell types and cell density. In some cell types, their migratory behaviours correlate to different phases of cell cycle. Recent findings have revealed the spatiotemporal interactions between the cyclin-dependent kinase inhibitors, p21<sup>Cip1</sup> and p27<sup>Kip1</sup>, and Rho GTPases signals, corresponding to cytoskeletal remodelling in cell migration (Lan et al., 2021). In this case, timing of passage and cell synchronisation in a specific phase of cell cycle are critical to ensure cell homogeneity for the investigation of cell migration. Also, cells might adopt different migration modes, integrin-dependent and integrin-independent migration, that result in varied rate of migration (Huttenlocher and Horwitz, 2011). Thus, incubation time might need to be prolonged to allow cells to migrate. Moreover, cell density could affect the migrating ability. Some cells might prefer individual migration, and hence lower seeding density might favour migration (Alassaf, PhD dissertation, 2020; Hamshaw, PhD dissertation, 2020). On the other hand, cells that prefer multicellular migration might require higher seeding density that allows more cell-cell interactions to trigger migration through paracrine signalling (Friedl and Alexander, 2011).

Although CCL3-induced chemotaxis was not investigated in this study, our group has previously demonstrated that THP-1 cells significantly migrate towards CCL3, whereas no chemotactic response was observed for Jurkat cells (Goh, PhD dissertation, 2018). This can be explained by the expression level of CCL3-associated receptor, CCR5, on cell surface as shown in **Figure 3.6**. Higher expression of chemokine receptors on cell surface could increase sensitivity to chemokine gradient that guides directed migration of cells.

Furthermore, it should be noted that our results might not accurately reflect the pathophysiological conditions in cancer due to limitations in our chemotaxis

assay. Cell movement in the chemotaxis plate used in our assay is basically one-dimensional from the top compartment to bottom compartment, lacking spatial and temporal parameters in the measurement of cell migration. Also, the microenvironment system is unable to generate a combination of chemokine concentration gradients relevant to gradient patterns in physiological conditions. A study demonstrated that the rate of migration is affected by different concentration slope gradients. Faster directional migration was seen in shallower concentration gradient for Jurkat cells (Sonmez et al., 2020). This observation is consistent with pathophysiological condition. During inflammation, the slope gradient at the site proximal to the inflammation site is high and it gets shallower at the distant regions. The shallow chemokine gradients at the distant regions create a cue for immune cells to rapidly sensitise chemokine and move towards the inflammation site (Griffith et al., 2014).

Recent research has been improving the design of device for monitoring chemotactic responses particularly for Jurkat cells, which is a flow-free gradient chamber with a microfluidic system (Sonmez et al., 2020). The spatiotemporally controlled fluidic environment within the device is capable of generating combinational chemokine gradients with different aspect ratio that overcomes the limitations mentioned above and more accurately measure chemotactic responses. In addition, the wide gradient chamber design in the system allows real-time visualisation of migrating cells using high resolution microscopy. Time-lapse microscopy allows us to understand cellular behaviours in response to chemokine stimulation in more depth (Sonmez et al., 2020). Yet, this device was tested with Jurkat cells as a model only. Some modifications might need to be done with the design for other cell types, especially adherent cells.

The internalisation of chemokine receptor is an important process to regulate receptor sensitisation and desensitisation through recycling and degradation pathways, which in turn influence cellular responses elicited by chemokine signalling. Our results demonstrate that cell type is one of the contributory factors affecting the extent of chemokine receptor internalisation. Particularly for CXCR4 internalisation, the effect of CXCL12-mediated CXCR4 internalisation in Jurkat is more significant than that in MCF-7 cells. Similar to our study, previous work has demonstrated that rate of chemokine receptor internalisation differs across

different cell lines (Mueller and Strange, 2004). This could be affected by several factors, such as different receptor internalisation pathways preferentially adopted and abundance of endocytic machinery components. To date, there are two main pathways of internalisation revealed by previous literature: clathrin-dependent and caveolae-dependent pathways (Mueller et al., 2002). Several studies working on CCR5 internalisation demonstrated that different cell lines preferentially adopt different internalisation pathways. For example, it was shown that Chinese hamster ovary (CHO) adopt both clathrin-dependent and caveolae-dependent pathways in CCR5 internalisation (Mueller et al., 2002), whereas CCR5 internalisation in HEK293 cells is mainly dependent of caveolae (Venkatesan et al., 2003). In addition, a study reported that the rate of receptor internalisation could also be dictated by structural difference in chemokine receptors (Venkatesan et al., 2003). On the molecular basis, it was found that C-terminal cytoplasmic domain is the main determinant of the rate of receptor internalisation and the preference of internalisation pathway. In primary T-cells investigated in the study, caveolae-dependent pathway is predominant in CCR5 internalisation since the C-terminal cytoplasmic domain of CCR5 was shown to anchor in plasma membrane rafts, as a result of slower endocytic rate. Whereas CXCR4 preferentially internalise through clathrin-dependent pathway as CXCR4 is found to be excluded from rafts, thereby, CXCR4 endocytic rate is faster than that of CCR5 (Venkatesan et al., 2003). Due to a variety of observations from the previous findings, experimental approaches in the investigation of chemokine receptor internalisation are necessary to be specified to cell types, receptors and ligands.

### **3.5 Chapter conclusions**

The final conclusions to be drawn from this chapter are:

1. The expression profile of chemokine receptors on cell surface is distinct across different cancer cell lines. MCF-7 cells abundantly express CCR5 and CXCR4. Jurkat cells abundantly express CXCR4 only. THP-1 abundantly express IL-8RB, CXCR3 and CCR5. MDA-MB-231 cells abundantly express IL-8RA, IL-8RB and CXCR3.
2. Calcium signalling following chemokine stimulation might not be necessary in all cell lines. MCF-7 and THP-1 cells respond to CCL3 and

CXCL12 stimulation respectively, which in turn induce intracellular  $\text{Ca}^{2+}$  release, but not for Jurkat cells.

3. Actin cytoskeleton is rearranged differently in different cell lines in response to chemokine stimulation, as implicated by different modes of cell migration adopted. In MCF-7 cells, the formation of lamellipodia and filopodia is predominant in response to CXCL12 or CCL3 stimulation specifically, promoting mesenchymal cell migration. On the other hand, in MDA-MB-231 cells, the formation of pseudopodia induced by more generalised chemokine stimulation is predominant, leading to amoeboid cell migration.
4. Chemotactic responses are dependent of cell types. CXCL12 stimulation predominantly mediates a signalling pathway contributing to chemotaxis in Jurkat cells, but less significant in THP-1 cells. This has proven that Jurkat cells are considered as an ideal cell model in the study of chemotaxis.
5. Cell type is a key contributory factor affecting the extent of chemokine receptor internalisation potentially due to different receptor internalisation pathways involved or the expression of endocytic machinery compartments. These will be further investigated in Chapter 4

**Table 3.3. Summary of characterisation of chemokine receptor expression and cellular responses in different cancer cell lines**

| Cell line  | Cancer type                                   | Chemokine receptor expression profile and chemokine-induced cellular responses |   |   |                                       |  |
|------------|---|--|---|---|---------------------------------------|--|
|            |   | Overexpressed chemokine receptor   | Calcium response  | Actin cytoskeletal rearrangement  | Chemotaxis                            | Receptor internalisation   |
| MCF-7      | ER <sup>+</sup> PR <sup>+</sup> breast cancer | CXCR4, CCR5  | <b>Yes</b> <ul style="list-style-type: none"> <li>In response to <b>CCL3</b> and <b>CXCL12</b></li> </ul> | In response to <b>CCL3</b> and <b>CXCL12</b> <ul style="list-style-type: none"> <li>Increased formation of filopodia and lamellipodia at the leading edge</li> <li>Increased formation of stress fibre at the contractile tail</li> </ul> | Inconclusive due to assay limitations | <b>Yes</b> <ul style="list-style-type: none"> <li>CXCR4 internalisation (In response to CXCL12) (<math>p \leq 0.05</math>)</li> <li>CCR5 internalisation (In response to CCL3) (<math>p \leq 0.05</math>)</li> </ul> |
| MDA-MB-231 | Triple negative breast cancer                 | IL-8RA, IL-8RB, CXCR3  | Not investigated †  | In response to <b>CCL3, 4, 5 and 23, IL-8. CXCL9 and 12</b> <ul style="list-style-type: none"> <li>Formation of pseudopodia with membrane blebbing</li> </ul>   | Inconclusive due to assay limitations | Not investigated†  |

| Cell line | Cancer type         | Chemokine receptor expression profile and chemokine-induced cellular responses |   |                                  |  |  |
|-----------|---------------------|--|---|----------------------------------|--|--|
|           |                     | Overexpressed chemokine receptor   | Calcium response  | Actin cytoskeletal rearrangement | Chemotaxis   | Receptor internalisation   |
| Jurkat    | T-cell leukaemia    | CXCR4  | <b>Detectable*</b> <ul style="list-style-type: none"> <li>In response to <b>CXCL12</b></li> </ul>         | Not investigated <sup>†</sup>    | <b>Yes</b> <ul style="list-style-type: none"> <li>In response to <b>CXCL12</b> stimulation (<math>p \leq 0.001</math>)</li> </ul>  | <b>Yes</b> <ul style="list-style-type: none"> <li>CXCR4 internalisation (In response to CXCL12) (<math>p \leq 0.001</math>)</li> </ul> |
| THP-1     | Monocytic leukaemia | IL-8RB, CXCR3, CCR5  | <b>Yes</b> <ul style="list-style-type: none"> <li>In response to <b>CCL3</b> and <b>CXCL12</b></li> </ul> | Not investigated <sup>†</sup>    | <b>Yes</b> <ul style="list-style-type: none"> <li>In response to <b>CCL3</b> (Moyano Cardaba et al., 2012) and <b>CXCL12</b> stimulation (<math>p \leq 0.05</math>)</li> </ul> | Not investigated <sup>†</sup>  |

\*Concentration of CXCL12 was increased to 25 nM for a detectable response (Hamshaw, PhD dissertation, 2021).

†Notes:

For MDA-MB-231 cells, Ca<sup>2+</sup> response and receptor internalisation were not investigated as inconsistent responses were observed from attempts by members of our group due to the nature of the cell line or technical issues in cell culturing (personal communication).

For Jurkat cells, actin cytoskeletal rearrangement was not investigated as F-actin expression is difficult to be clearly visualised due to small cell size.

For THP-1 cells, actin cytoskeletal rearrangement was not investigated due to small cell size. Also, cell surface receptor expression was found to be varied at different time points of cell differentiation during cell culture, leading to inconsistent cellular responses observed. Due to difficulty to manipulate and time limits, receptor internalisation was not investigated, only chemotaxis assay was conducted.

# Chapter 4: Investigations into the mechanisms underlying chemokine-induced receptor internalisation

---

## 4.1 Introduction

The dynamics of receptors through internalisation, recycling and degradation determines the sensitivity of the receptor to ligand stimulation in modulation of cellular responses (Neel et al., 2005). GPCRs can be internalised through two distinct receptor endocytic pathways dependent on either clathrin or caveolae with some receptors favouring one pathway over the other (Signoret et al., 2005), while some may utilise both (Mueller et al., 2002). There are three main factors that determine which endocytic pathway is utilised by receptors: cell type, ligand and the rate of receptor internalisation. (**Table 4.1**).

For the specificity of different cell types, the expression levels and availability of endocytic machinery components, such as clathrin, caveolae and other adaptor proteins might vary in different cell types. Using CCL5-induced CCR5 internalisation as an example, it was found that CCR5 receptors expressed on CHO cells preferably utilise clathrin-dependent pathway (Signoret et al., 2005), whereas caveolae-dependent pathway is predominant in CCR5 receptor internalisation in primary T-cells and HEK293 cells (Venkatesan et al., 2003). In addition, CCR5 is internalised at a faster rate in CHO cells than in primary T-cells and HEK293 cells (Signoret et al., 2005; Venkatesan et al., 2003). These variations among different cell lines may be due to the proximity of caveolae to the domain of the receptor, the ratio of adaptor proteins involved or the abundance of the critical proteins in receptor endocytosis.

Kraft et al., 2001 determined that there was a 70% reduction in cell surface CCR5 when stimulated with CCL5 for 30 mins while in a second study by Mueller et al., 2002 there was 50% of CCR5 receptors remaining after stimulation with CCL3 for 60 minutes. These studies suggest that different chemokine ligands can

mediate variable percentage of reduction in receptor expression and also that receptor internalisation occurs at different rates, summarised in **Table 4.1**.

Although there has been a substantial amount of evidence showing the mechanisms of receptor internalisation across different chemokine receptors, the findings between literature are sometimes conflicting. The discrepancies may be attributed to different cell types as experimental models, chemokine receptors exogenously or endogenously expressed in cell lines, ligand concentration, duration of stimulation and detection methods. Therefore, we set out to examine the pathways of receptor internalisation in a more consistent approach that can be comparable between different cell lines. We then further determined the involvement of the key adaptor proteins, dynamin and  $\beta$ -arrestins, in the regulation of chemokine-induced receptor internalisation.

**Table 4.1. Summary of the extent of receptor internalisation from studies investigating CCR5 and CXCR4 internalisation in different cell lines** (Adapted from Neel et al., 2005)

| <b>Chemokine receptors</b> | <b>Receptor expression</b> | <b>Cell lines</b> | <b>Ligands (concentration)</b> | <b>Ligand stimulation duration</b> | <b>Detection methods</b> | <b>Percentage of receptors internalised</b> | <b>Reference</b>            |
|----------------------------|----------------------------|-------------------|--------------------------------|------------------------------------|--------------------------|---|-----------------------------|
| CCR5                       | Exogenous                  | CHO               | CCL3 (50 nM)                   | 60 min                             | FACS                     | 49.20%                                      | (Mueller et al., 2002)      |
|                            | Exogenous                  | HeLa RC49         | CCL3 (50 nM)                   | 60 min                             | FACS                     | 41.40%                                      |                             |
|                            | Endogenous                 | THP-1             | CCL3 (50 nM)                   | 60 min                             | FACS                     | 34.30%                                      | (Mueller and Strange, 2004) |
|                            | Exogenous                  | HEK293            | CCL5 (200 nM)                  | 30 min                             | FACS                     | t <sub>1/2</sub> = 60 mins                  | (Venkatesan et al., 2003)   |
|                            | Exogenous                  | CHO               | CCL5 (125 nM)                  | 30 min                             | Radioligand binding      | 70%   | (Kraft et al., 2001)        |

| <b>Chemokine receptors</b> | <b>Receptor expression</b> | <b>Cell lines</b> | <b>Ligands (concentration)</b> | <b>Ligand stimulation duration</b> | <b>Detection methods</b> | <b>Percentage of receptors internalised</b> | <b>Reference</b>          |
|----------------------------|----------------------------|-------------------|--------------------------------|------------------------------------|--------------------------|---|---------------------------|
| CCR5                       | Exogenous                  | RBL-2H3           | CCL5 (50 nM)                   | 30 min                             | FACS                     | 70%   | (Signoret et al., 2005)   |
| CXCR4                      | Exogenous                  | RBL-2H3           | CXCL12 (100 nM)                | 30 min                             | Radioligand binding      | 52%   | (Haribabu et al., 1997)   |
|                            | Endogenous                 | PBL               | CXCL12 (20 nM)                 | 10 min                             | FACS                     | 90%   | (Venkatesan et al., 2003) |
|                            | Exogenous                  | HeLA-CD4          | CXCL12 (20 nM)                 | 30 min                             | FACS                     | 80%   |                           |

## 4.2 Chapter aims

**Hypothesis:** We hypothesised that the pathways of receptor internalisation vary depending on chemokine ligands used and cell types in which the chemokine receptor is expressed. These two main factors could potentially determine the likelihood of either of clathrin-dependent or caveolae-dependent endocytic pathway utilised.

**Aims:** The aim of this chapter is to examine which pathway is preferentially utilised in chemokine-induced receptor internalisation using two different cancer cell lines, and the involvement of the two key adaptor proteins, dynamin and  $\beta$ -arrestins.

## 4.3 Results

**4.3.1 Caveolin-1 (Cav-1) is expressed intracellularly in MCF-7 cells. Following CCL3 or CXCL12 stimulation, Cav-1 translocate towards the leading edge of MCF-7 cells but no significant change in Cav-1 expression is observed in MCF-7 cells.**

As mentioned in Chapter 1, caveolae (also known as lipid rafts) are known to be a key player in clathrin-independent internalisation. Caveolae are comprised of a set of proteins stabilised by cholesterol molecules in plasma membrane (Parton et al., 2020b), forming membrane invaginations for endocytosis (Ariotti et al., 2015) or serving as a scaffold for various membrane proteins to form a cell-specific signalling domain in signalling transduction (Mañes et al., 1999; Parton et al., 2020b). Following chemokine stimulation, caveolae preferentially localise at the leading edge of migrating cells. This mediates receptor and signalling protein redistribution to the leading edge which is essential for front-rear polarity, as a result of chemotaxis (Mañes et al., 1999). Hence, we attempted to determine the change in caveolae expression and localisation following CCL3 and CXCL12 stimulation in MCF-7 and Jurkat cells using a polyclonal antibody specific to caveolin-1 (Cav-1) by immunofluorescence staining.

Cav-1 is one of the structural proteins within the caveolae domain (Anderson, 1998), commonly used as a marker for the identification of caveolae. It should be

noted that a polyclonal antibody was used in our study. The advantage of using polyclonal antibody is that the sensitivity is higher for detecting proteins in lower quantity, however, there are some potential risks, such as batch-to-batch variability during production and higher chance of cross-reactivity due to a recognition of multiple epitopes. In our study, we performed all experiments using the same batch of the antibody, which should eliminate the chance of batch-to-batch variability affecting our result consistency. Also, the antibody used in our study was from a recognised supplier (Santa Cruz Biotechnology), and is claimed to be purified which should minimise the risk of cross reactivity.

In **Figure 4.1**, Cav-1 proteins scatter across the edges of MCF-7 cells in the absence of chemokine stimulation under basal conditions. After CXCL12 stimulation for 30 minutes, Cav-1 proteins were observed to translocate towards the leading edge of MCF-7 cells. Yet, the effects seem to be less significant in CCL3-stimulated cells.

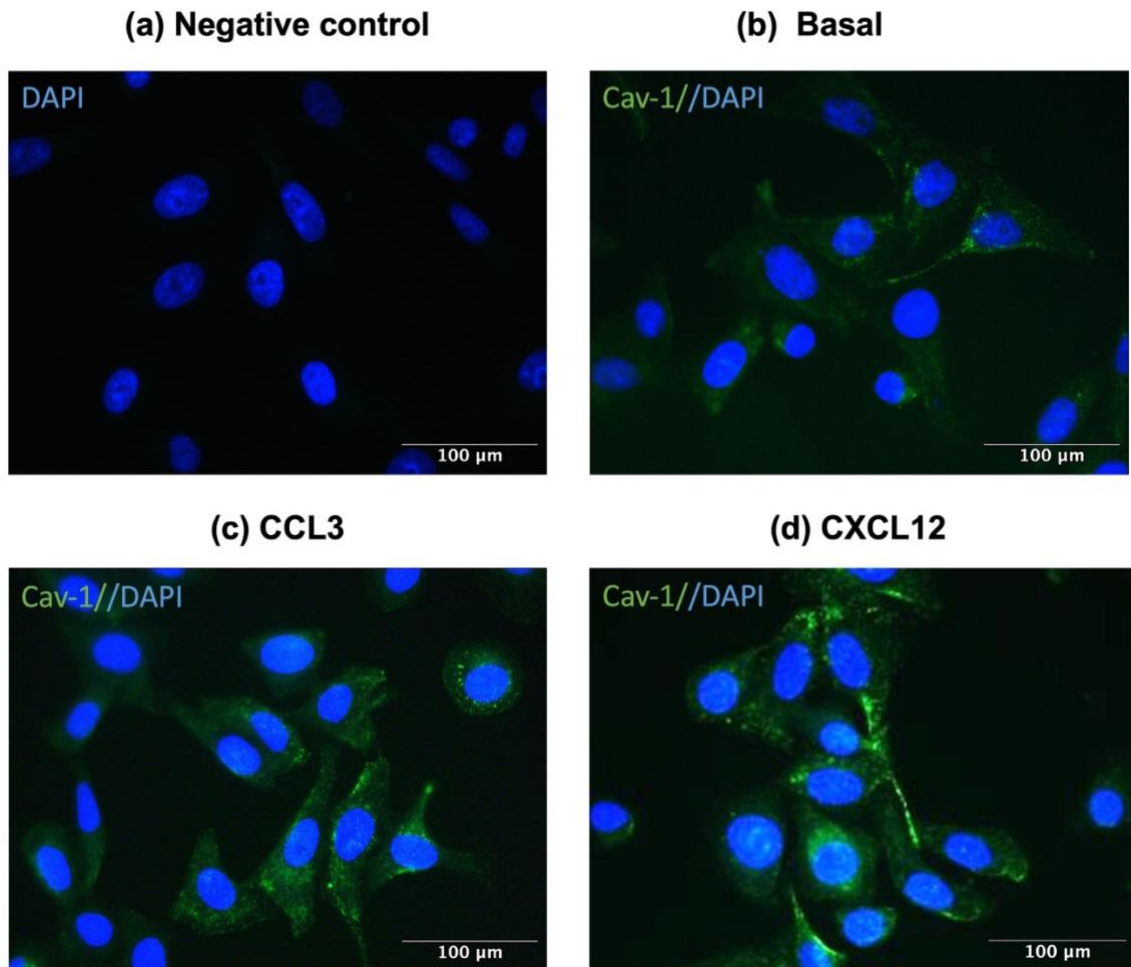


**Figure 4.1. Translocation of caveolin-1 (Cav-1) towards the leading edge of the cells following CCL3 or CXCL12 stimulation in MCF-7 cells. Immunofluorescence staining of intracellular Cav-1 in MCF-7 cells.** (a) negative background control with secondary antibody added only and stained with DAPI (1:1000) (blue) for the visualisation of cell nuclei. Cells were either unstimulated as (b) basal control or stimulated with (c) CCL3 (100 nM) or (d) CXCL12 (50 nM) for 30 minutes. Cells were then fixed, permeabilised and stained with rabbit polyclonal Cav-1 antibody (1:500), followed by secondary staining with anti-rabbit FITC antibody (1:500) (green) and DAPI (1:1000) (blue) for cell nuclei. Representative images from at least 3 independent experiments were acquired with a Leica DMII Fluorescence microscope using 31.5X magnification.

From quantitative flow cytometry analysis, MCF-7 cells express Cav-1 at detectable level (**Figure 4.2**). To determine the effects of chemokine stimulation on the expression of Cav-1, cells were stimulated with 50 nM CXCL12 or 100 nM CCL3 for 30 minutes prior to antibody staining for flow cytometry analysis. Our

results showed a trend of increased expression of Cav-1 particularly after CXCL12 stimulation in MCF-7 cells, but not statistically significant (**Figure 4.2**).

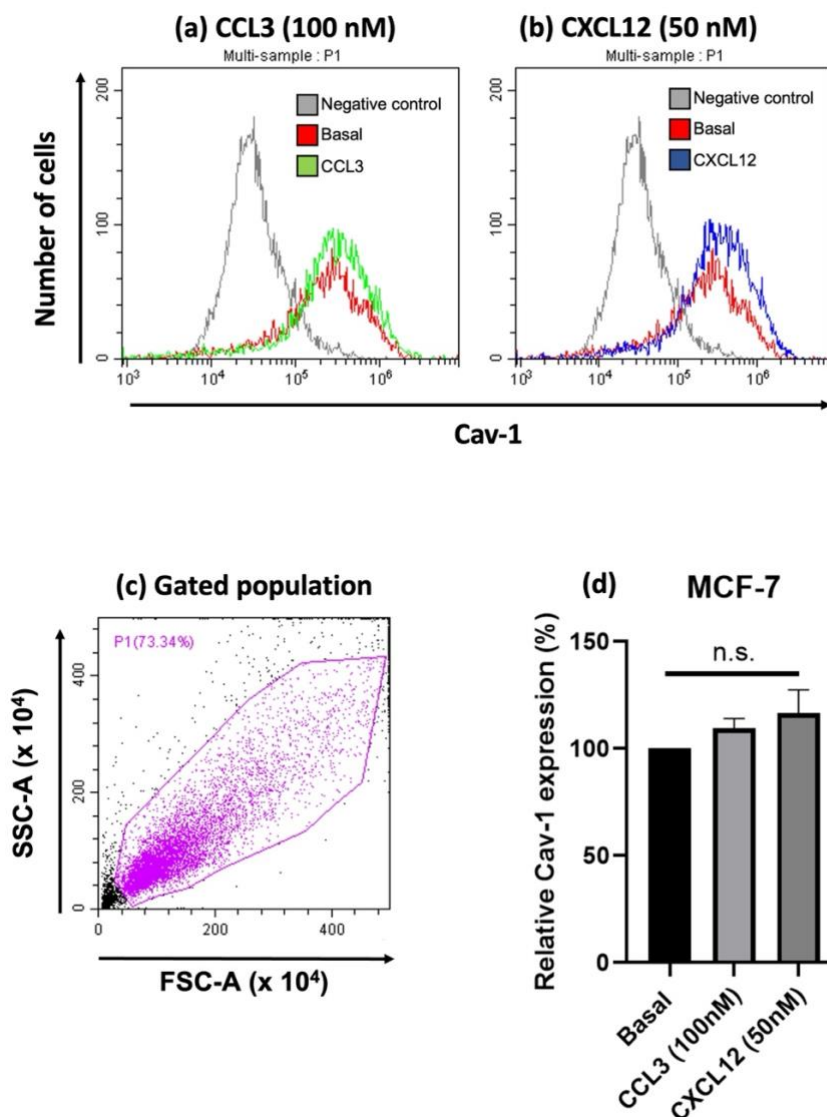


**Figure 4.2.** There was a trend of increased Cav-1 expression following CCL3 or CXCL12 stimulation in MCF-7 cells, but it was not significant. MCF-7 cells were either unstimulated as basal control or stimulated with either CCL3 (100 nM) or CXCL12 (50 nM) for 30 minutes, followed by permeabilization and fixing for intracellular Cav-1 staining. Cells were stained with rabbit polyclonal Cav-1 antibody (1:200) followed by secondary staining of anti-rabbit FITC antibody (1:200). Only secondary anti-rabbit FITC antibody (1:200) was added in negative control. Fluorescence intensity of 20,000 events from each sample were quantified in flow cytometry and cell population was gated to exclude dead cells and debris before analysis. (a, b) Representative histograms showing the comparison

of unstained negative control (in grey), basal control without chemokine stimulation (in red) and CCL3-stimulated cells (in green) or CXCL12-stimulated cells (in blue) in respect to fluorescence intensity among the gated population (P1) of each cell sample. (c) Representative scatter plot (forward scatter (FSC) vs. side scatter (SSC)) indicates the gated cell population (indicated as P1) in the analysis. (d) Bar chart showing relative expression of Cav-1 in MCF-7 cells following CCL3 (coloured in light grey) or CXCL12 stimulation (coloured in dark grey) compared to basal control (coloured in black) without chemokine stimulation. Relative Cav-1 expression was calculated from (chemokine-stimulated – negative control) / (basal control – negative control) (%), where negative control was stained with secondary antibody. Fluorescence values are based on median channel of fluorescence in a gated population (P1) of cells from each sample and acquired by the CytExpert software (Beckman Coulter). Data shown represent the mean  $\pm$  SEM of at least 3 independent experiments. One-way ANOVA with a Dunnett's multiple comparisons test as post-hoc test, n.s. = not significant.

#### **4.3.2 Cav-1 express intracellularly in Jurkat cells. CXCL12 stimulation does not induce a significant change in Cav-1 expression in Jurkat cells.**

As the cell size of Jurkat cells is small, it was challenging to visualise the distribution of Cav-1 intracellularly due to the limitations of the fluorescence microscope in our lab. Therefore, immunofluorescence imaging was not conducted with Jurkat cells.

From quantitative flow cytometry analysis, Jurkat cells express Cav-1 at detectable levels (**Figure 4.3**). In the stimulation with CXCL12 (50 nM), similar to MCF-7 cells, there was a trend of increased expression of Cav-1 but not significant (**Figure 4.3**). As cells were permeabilised before Cav-1 staining, cell surface and intracellular Cav-1 are inclusive in our quantitative analysis of Cav-1 expression. The overall expression level shown in our results cannot reflect any translocation of Cav-1.

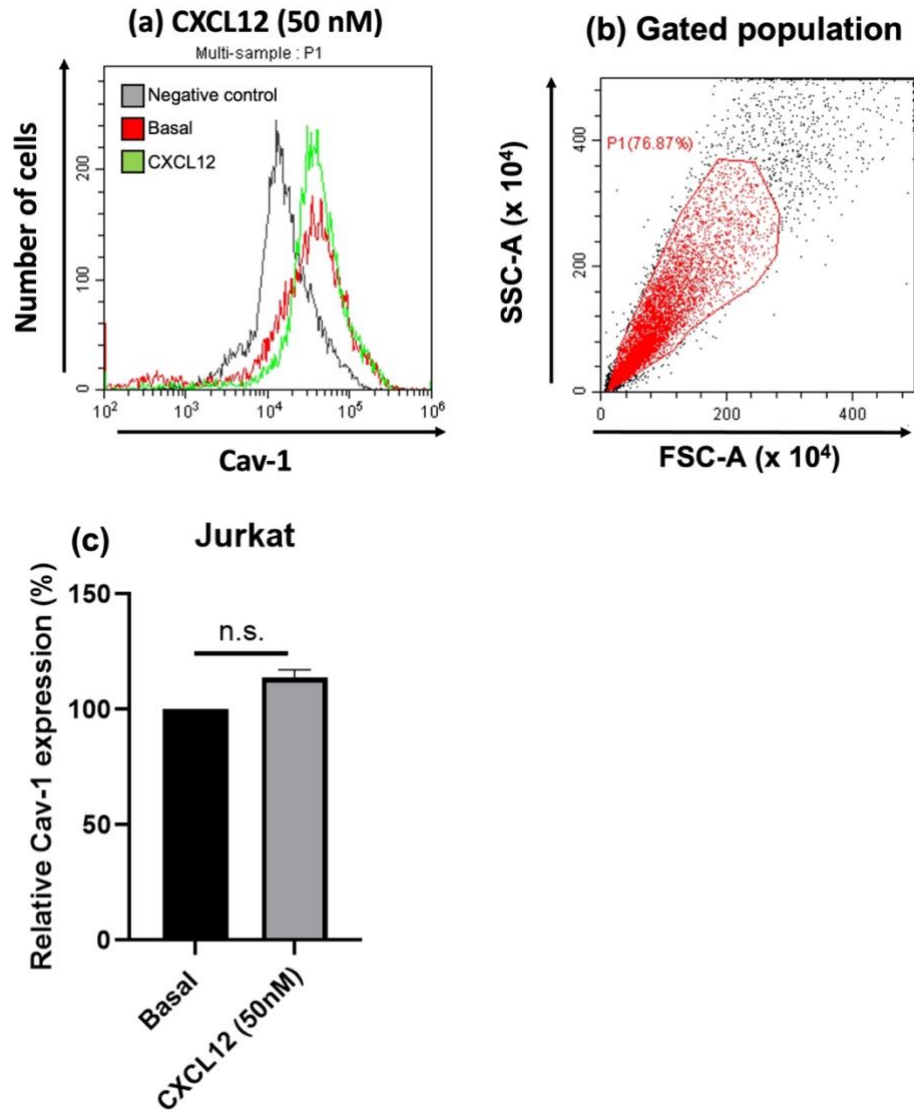


**Figure 4.3. A trend of increased Cav-1 expression following CXCL12 stimulation was observed in Jurkat cells, but it was not significant.** Jurkat cells were either unstimulated as basal control or stimulated with CXCL12 (50 nM) for 30 minutes, followed by fixing and permeabilization for intracellular Cav-1 staining. Cells were stained with rabbit polyclonal Cav-1 antibody (1:200) followed by secondary staining of anti-rabbit FITC antibody (1:200). Only secondary anti-rabbit FITC antibody (1:200) was added in negative control. Fluorescence intensity of 20,000 events from each sample were quantified in flow cytometry and cell population was gated to exclude dead cells and debris before analysis. (a) Representative histograms show the comparison of unstained negative control (in grey), basal control without chemokine stimulation (in red) and CXCL12-stimulated cells (in green) in respect to fluorescence intensity among the gated population (P1) of each cell sample. (b) Representative scatter plot (FSC vs. SSC) indicates the

gated cell population (indicated as P1) in the analysis. (c) Bar chart showing relative expression of Cav-1 in Jurkat cells following CXCL12 stimulation (coloured in grey) compared to basal control without chemokine stimulation (coloured in black). Relative Cav-1 expression was calculated from (chemokine-stimulated – negative control) / (basal control – negative control) (%), where negative control was stained with secondary antibody. Fluorescence values are based on median channel of fluorescence in a gated population (P1) of cells from each sample and acquired by the CytExpert software (Beckman Coulter). Data shown represent the mean  $\pm$  SEM of at least 3 independent experiments. Unpaired t-test, n.s. = not significant.

#### **4.3.3 Protein synthesis inhibitor, cycloheximide, has no effect on Cav-1 expression following chemokine stimulation in MCF-7 and Jurkat cells.**

To determine whether the trend of increased Cav-1 expression observed in both MCF-7 and Jurkat cells is caused by chemokine-induced protein synthesis, a protein synthesis inhibitor, cycloheximide, was used in our study. Cycloheximide is a commonly used inhibitor that blocks protein synthesis by interfering the elongation step in translation (Schneider-Poetsch et al., 2010). A previous study from our group used 10  $\mu$ g/mL of cycloheximide to inhibit protein synthesis in the investigation of receptor recycling in CHO.CCR5 cells (Mueller et al., 2002). From the MTS cytotoxicity test, cycloheximide was shown to have some toxicity in MCF-7 and Jurkat cells in a concentration range from 0.5  $\mu$ g/mL to 10  $\mu$ g/mL after 24 hours incubation. However, the toxicity effect was not significant overall (**Figure A1**). Also, the incubator time with the inhibitor in our experimental assay was 30 minutes only. Thus, the toxicity of cycloheximide at 10  $\mu$ g/mL should be minimal. Our results demonstrated that reduction in Cav-1 expression after the treatment of cycloheximide was not significant in MCF-7 and Jurkat cells in the stimulation with chemokine (**Figures 4.4 and 4.5**).

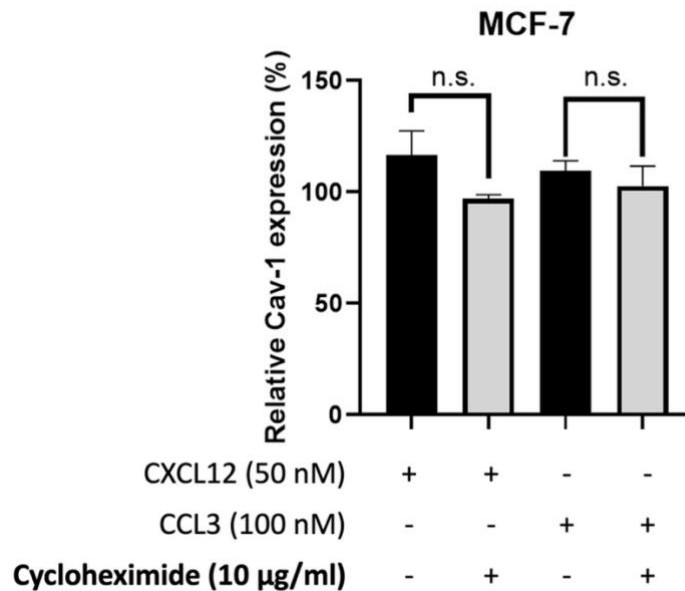


**Figure 4.4. Cycloheximide has no effect on Cav-1 expression change in MCF-7 cells stimulated with CCL3 or CXCL12.** Cells were pre-treated with cycloheximide (10 µg/ml) for 30 minutes and stimulated with either CXCL12 (50 nM) or CCL3 (100 nM) for another 30 minutes, followed by fixing and permeabilization for intracellular Cav-1 staining. Fluorescence intensity of 20,000 events were quantified in flow cytometry and cell population was gated to exclude dead cells and debris for each cell line before analysis. Graph showing relative expression of Cav-1 in MCF-7 cells pre-treated with cycloheximide and stimulated with either CCL3 or CXCL12 compared to control without inhibitor treatment. Relative Cav-1 expression was calculated from (chemokine-stimulated – negative control) / (basal control – negative control) (%), where negative control was stained with secondary antibody. Fluorescence values are based on median channel of fluorescence in a gated population of cells from each sample and acquired by the CytExpert software (Beckman Coulter). Data shown represent the mean ± SEM of at least 3 independent experiments. One-way ANOVA with Sidak’s multiple comparisons test as post-hoc test, n.s. = not significant.

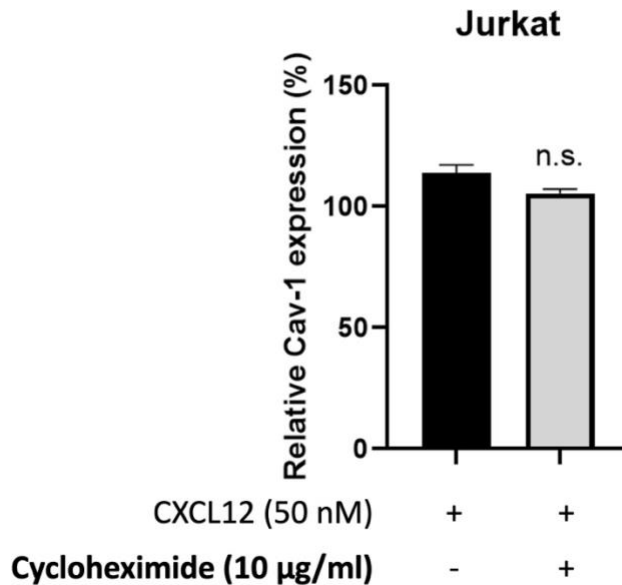


**Figure 4.5. Cycloheximide has no effect on Cav-1 expression change in Jurkat cells stimulated with CXCL12.** Cells were pre-treated with cycloheximide (10 µg/ml) for 30 minutes and stimulated with CXCL12 (50 nM) for another 30 minutes, followed by fixing and permeabilization for intracellular Cav-1 staining. Fluorescence intensity of 20,000 events from each sample were quantified in flow cytometry and cell population was gated to exclude dead cells and debris for each cell line before analysis. Graph showing relative expression of Cav-1 in Jurkat cells pre-treated with cycloheximide and stimulated with CXCL12 compared to control without inhibitor treatment. Relative Cav-1 expression was calculated from (chemokine-stimulated – negative control) / (basal control – negative control) (%), where negative control was stained with secondary antibody. Fluorescence values are based on median channel of fluorescence in a gated population of cells from each sample and acquired by the CytExpert software (Beckman Coulter). Data shown represent the mean ± SEM of at least 3 independent experiments. Unpaired t-test, n.s. = not significant.

#### **4.3.4. Caveolae-blocking agents, filipin and nystatin, disrupt intracellular localisation of Cav-1 in MCF-7 cells.**

To further investigate the roles of caveolae in chemokine-induced receptor internalisation, we used two cholesterol-depleting agents, filipin and nystatin, to

examine the effects on chemokine-induced receptor internalisation in MCF-7 and Jurkat cells.

Filipin and nystatin possess different modes of action to membrane cholesterol. Filipin binds 3- $\beta$ -hydroxysterols in a 1:1 stoichiometry, consequently forming large aggregates aligning at the centre of the lipid bilayer (De Kruijff and Demel, 1974), whereas nystatin forms sterol-dependent ion channels in the plasma membrane (Bolard, 1986).

To test the targeting effects of filipin and nystatin in MCF-7 cells as a preliminary experiment, immunofluorescence staining of Cav-1 was conducted in inhibitor-treated cells in comparison with cells without inhibitor treatment. Previous study from Cardaba et al., 2008 showed filipin and nystatin interferes with caveolae localisation in CHO.CCR5 cells at 5  $\mu$ g/mL and 50  $\mu$ g/mL respectively. Our results from MTS cytotoxicity test confirmed that there was no toxicity in MCF-7 and Jurkat cells from 5  $\mu$ g/mL filipin and 50  $\mu$ g/mL nystatin (**Figure A2**). **Figure 4.6** illustrates that both inhibitors disrupt intracellular localisation of Cav-1, and an observable reduction in Cav-1 expression on plasma membrane is observed compared to control without inhibitor treatment. Our observations were similar to the previous study (Cardaba et al., 2008). This has confirmed that filipin and nystatin have a profound effect on disrupting caveolae localisation for investigation of caveolae-dependent cellular events.

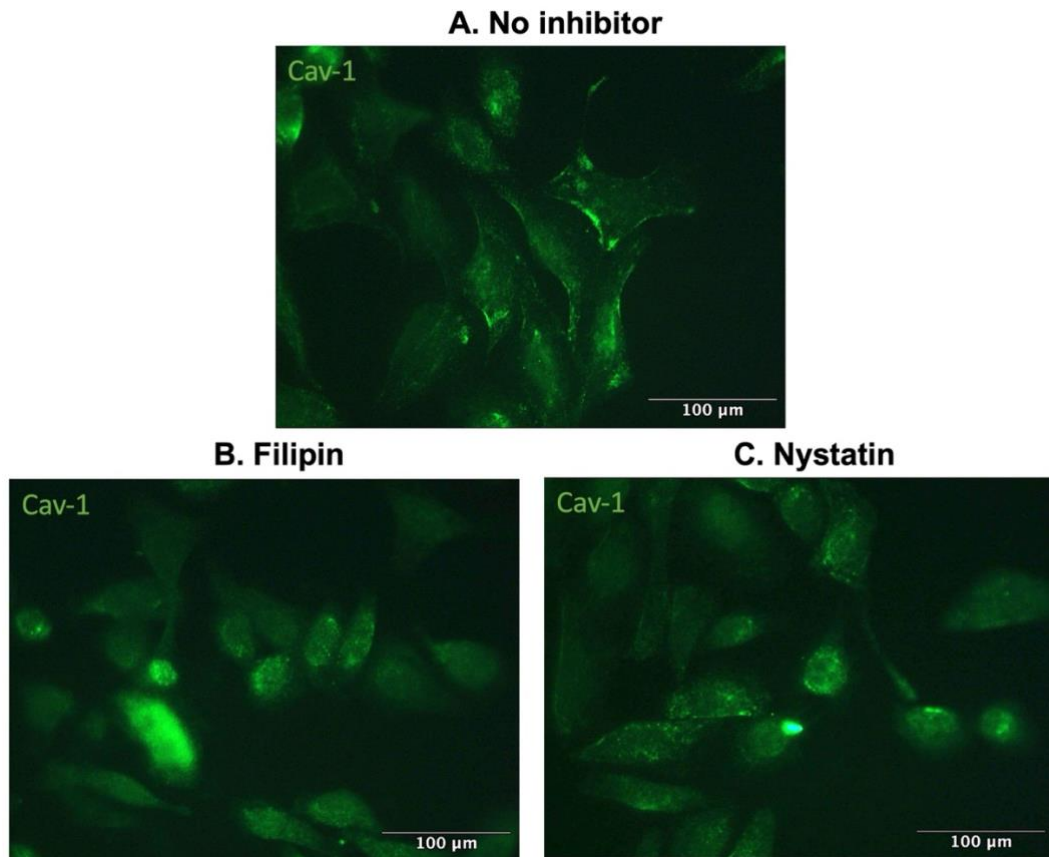


**Figure 4.6. Caveolae-blocking agents, filipin and nystatin, reduce Cav-1 localised on the plasma membrane in MCF-7 cells.** Cells were either left (a) without inhibitor treatment or treated with (b) filipin (5 µg/ml), (c) nystatin (50 µg/ml) for 30 minutes. Cells were then fixed, permeabilised and stained with rabbit polyclonal Cav-1 antibody (1:500), followed by secondary staining with anti-rabbit FITC antibody (1:500) (green). Representative images from at least 3 independent experiments were acquired under Leica DMII Fluorescence microscope using 31.5X magnification.

**4.3.5 Caveolae-blocking agents significantly block CXCL12-induced CXCR4 internalisation in Jurkat cells but mediate no significant effect on CCL3-induced CCR5 internalisation in MCF-7 cells.**

Next, we examined the effects of cholesterol-depleting agents on chemokine-induced receptor internalisation. Cells were pre-treated with filipin or nystatin for 30 minutes, followed by stimulation with CCL3 or CXCL12 for another 30 minutes and incubated at 37°C to allow receptor internalisation to take place. Staining of CCR5-specific or CXCR4-specific antibody was conducted for flow cytometry

analysis. The staining process was done at 4°C to prevent receptor recycling that might affect our results.

For Jurkat cells, **Figure 4.7** demonstrates that CXCL12-induced CXCR4 internalisation was significantly reduced in Jurkat cells treated with nystatin or filipin (**Table 4.2**). This implies that caveolae might potentially be involved in CXCR4 internalisation following CXCL12 stimulation in Jurkat cells.

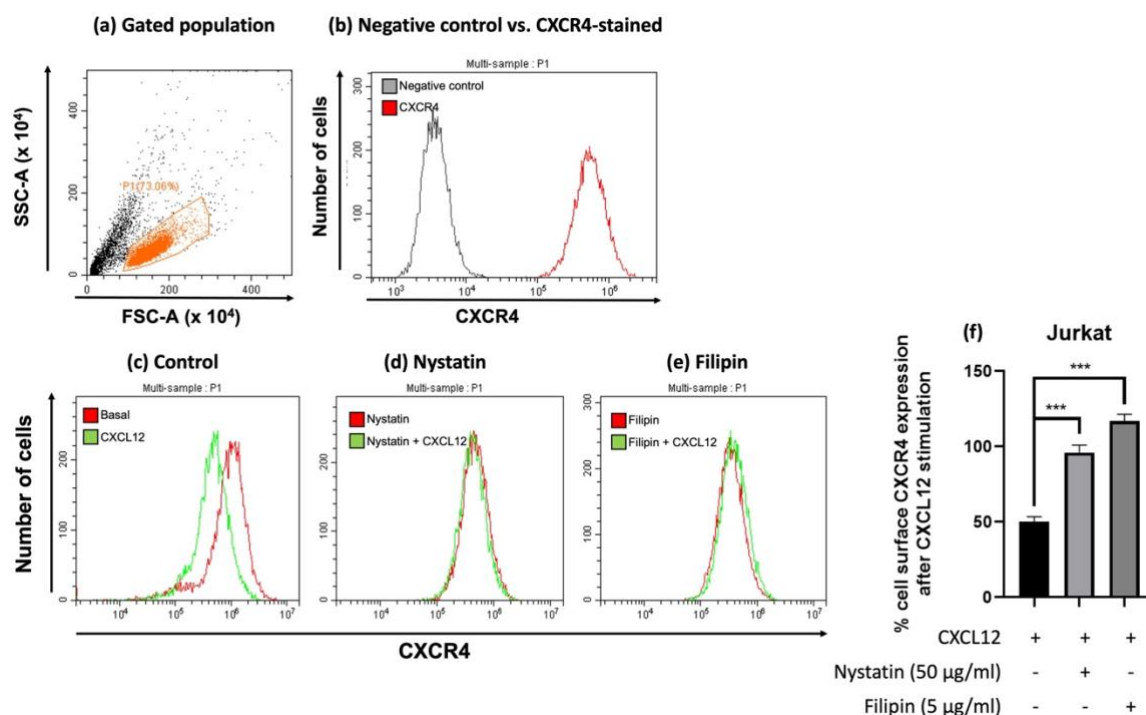


**Figure 4.7. Caveolae-blocking agents significantly block CXCL12-induced CXCR4 internalisation in Jurkat cells.** Cells were pre-treated with filipin (5 µg/ml) or nystatin (50 µg/ml) or without inhibitor treatment for 30 minutes, followed by stimulation with CXCL12 (50 nM) at 37 °C for another 30 minutes to allow CXCR4 internalisation to take place. Cells were stained with mouse monoclonal CXCR4 antibody (4G10) (1:200) followed by secondary staining of anti-mouse Alexa 488 antibody (1:200). Only secondary anti-mouse Alexa 488 antibody (1:200) was added in negative control. Fluorescence intensity of 20,000 events from each sample were quantified in flow cytometry and cell population was gated to exclude dead cells and debris before analysis. (a) Representative scatter plot (FSC vs. SSC) indicates the gated cell population (indicated as P1) in the analysis. (b) Representative histogram showing unstained cells as negative control

(in grey) and CXCR4-stained cells (in red). (c, d, e) Representative histograms showing the comparison of cells in the absence of chemokine stimulation (in red) and chemokine-stimulated cells (in green) under different conditions: (c) without inhibitor treatment, in the treatment of (d) nystatin and (e) filipin in respect to fluorescence intensity among the gated population (P1) of each cell sample. (f) Bar chart showing percentage of cell surface CXCR4 expression following CXCL12 stimulation in Jurkat cells treated with either nystatin (coloured in light grey) or filipin (coloured in dark grey) compared to control without inhibitor treatment (coloured in black). Percentage of cell surface CXCR4 expression following CXCL12 stimulation was calculated from (CXCL12-stimulated – negative control) / (unstimulated control – negative control) (%), where negative control was stained with secondary antibody. Fluorescence values are based on median channel of fluorescence in a gated population (P1) of cells from each sample and acquired by the CytExpert software (Beckman Coulter). Data shown represent the mean  $\pm$  SEM of at least 3 independent experiments. One-way ANOVA with a Dunnett's multiple comparisons test as post-hoc test, \*\*\* =  $p \leq 0.001$ .

For MCF-7 cells, as seen in **Figure 4.8**, compared to control without inhibitor treatment, there was a trend of reduced CCL3-induced CCR5 internalisation in MCF-7 cells treated with filipin or nystatin. However, the difference in percentage of CCR5 remaining on cell surface in filipin-treated or nystatin-treated MCF-7 cells was not significant compared to MCF-7 cells without inhibitor treatment (**Figure 4.8 and Table 4.2**).

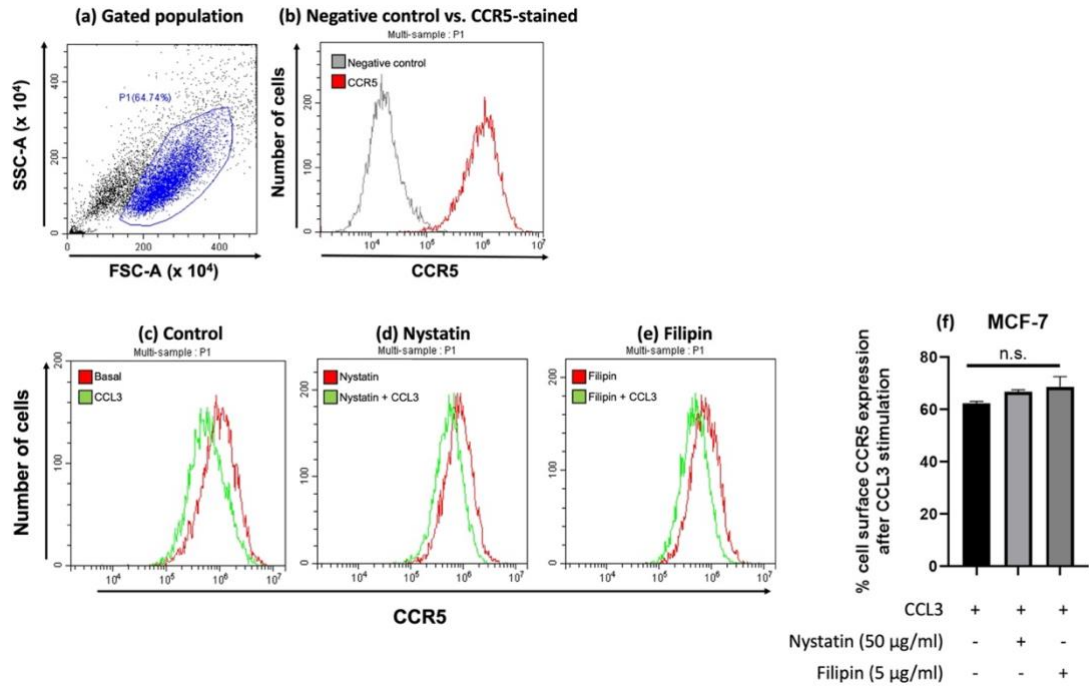


**Figure 4.8. A trend of reduced CCL3-induced CCR5 internalisation in MCF-7 cells after the treatment of caveolae-blocking agents was observed, but it was not significant.** Cells were pre-treated with filipin (5 µg/ml) or nystatin (50 µg/ml) or without inhibitor treatment for 30 minutes, followed by stimulation with CCL3 (100 nM) at 37 °C for another 30 minutes to allow CCR5 internalisation to take place. Cells were stained with rat CCR5 (HEK/1/85a/7a) antibody (1:100) followed by secondary staining of anti-rat Alexa 488 antibody (1:200). Only secondary anti-rat Alexa 488 antibody (1:200) was added in negative control. Fluorescence intensity of 20,000 events from each sample were quantified in flow cytometry and cell population was gated to exclude dead cells and debris before analysis. (a) Representative scatter plot (FSC vs. SSC) indicates the gated cell population (indicated as P1) in the analysis. (b) Representative histogram showing unstained cells as negative control (in grey) and CCR5-stained cells (in red). (c, d, e) Representative histograms showing the comparison of cells in the absence of chemokine stimulation (in red) and chemokine-stimulated cells (in green) under different conditions: (c) without inhibitor treatment, in the treatment of (d) nystatin and (e) filipin in respect to fluorescence intensity among the gated population (P1) of each cell sample. (f) Bar chart showing percentage of cell surface CCR5 expression following CCL3 stimulation in MCF-7 cells treated with either nystatin (coloured in light grey) or filipin (coloured in dark grey) compared to control (coloured in

black) without inhibitor treatment. Percentage of cell surface CCR5 expression following CCL3 stimulation was calculated from (CCL3-stimulated – negative control) / (unstimulated control – negative control) (%), where negative control was stained with secondary antibody. Fluorescence values are based on median channel of fluorescence in a gated population (P1) of cells from each sample and acquired by the CytExpert software (Beckman Coulter). Data shown represent the mean  $\pm$  SEM of at least 3 independent experiments. One-way ANOVA with a Dunnett's multiple comparisons test as post-hoc test, n.s. = not significant.

#### **4.3.6 Caveolae-blocking agents induces increased CXCR4 internalisation in MCF-7 cells potentially due to non-specific effects.**

Interestingly, percentage of CXCR4 remaining on cell surface following CXCL12 stimulation was significantly lower in MCF-7 cells treated with nystatin or filipin compared to control without inhibitor treatment (**Figures 4.9 and Table 4.2**). This indicates that filipin and nystatin induce increased CXCR4 internalisation in MCF-7 cells. The observation might be caused by non-specific effects of the cholesterol-depleting agents (Bolard, 1986). Disruption of cholesterol and membrane integrity might potentially alter receptor conformation and ligand binding. As shown earlier, CXCL12 induces Cav-1 translocation towards the leading edge, potentially causing an accumulation of CXCR4 at the front of the cells near the plasma membrane. Together with the effects of the cholesterol-depleting agents, CXCR4 receptors are more prone to translocate from the plasma membrane to the cytosol following CXCL12 stimulation. Hence, more CXCR4 receptors internalised was observed. As a result, non-specific effects of cholesterol-depleting agents potentially cause confusions by the synergistic effect promoting CXCR4 internalisation with the effect of CXCL12 stimulation.

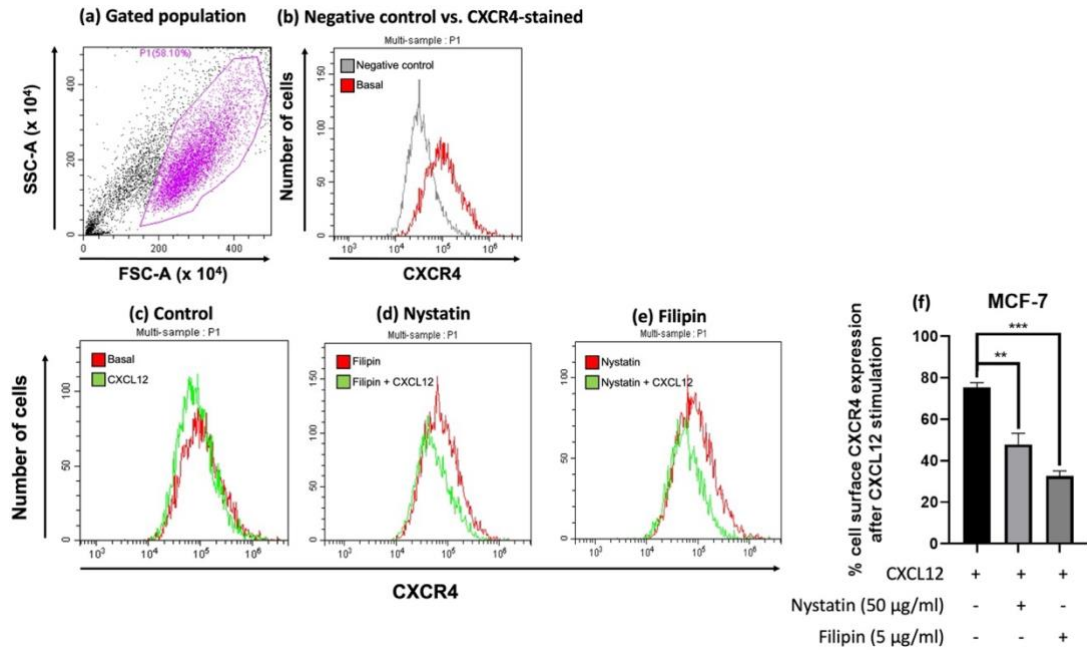


**Figure 4.9. Increased CXCL12-induced CXCR4 internalisation in MCF-7 cells treated with caveolae-blocking agents was observed.** Cells were pre-treated with filipin (5  $\mu\text{g/ml}$ ) or nystatin (50  $\mu\text{g/ml}$ ) or without inhibitor treatment for 30 minutes, followed by stimulation with CXCL12 (50 nM) at 37  $^{\circ}\text{C}$  for another 30 minutes to allow CXCR4 internalisation to take place. Cells were stained with mouse monoclonal CXCR4 antibody (4G10) (1:200) followed by secondary staining of anti-mouse Alexa 488 antibody (1:200). Only secondary anti-mouse Alexa 488 antibody (1:200) was added in negative control. Fluorescence intensity of 20,000 events from each sample were quantified in flow cytometry and cell population was gated to exclude dead cells and debris before analysis. (a) Representative scatter plot (FSC vs. SSC) indicates the gated cell population (indicated as P1) in the analysis. (b) Representative histogram showing unstained cells as negative control (in grey) and CXCR4-stained cells (in red). (c, d, e) Representative histograms showing the comparison of cells in the absence of chemokine stimulation (in red) and chemokine-stimulated cells (in green) under different conditions: (c) without inhibitor treatment, in the treatment of (d) nystatin and (e) filipin in respect to fluorescence intensity among the gated population (P1) of each cell sample. (f) Bar chart showing percentage of cell surface CXCR4 expression following CXCL12 stimulation in MCF-7 cells treated with either nystatin (coloured in light grey) or filipin (coloured in dark grey) compared to control (coloured in black) without inhibitor treatment. Percentage of cell surface CXCR4 expression following CXCL12 stimulation

was calculated from (CXCL12-stimulated – negative control) / (unstimulated control – negative control) (%), where negative control was stained with secondary antibody. Fluorescence values are based on median channel of fluorescence in a gated population (P1) of cells from each sample and acquired by the CytExpert software (Beckman Coulter). Data shown represent the mean  $\pm$  SEM of at least 3 independent experiments. One-way ANOVA with a Dunnett's multiple comparisons test as post-hoc test, \*\* =  $p \leq 0.01$ ; \*\*\* =  $p \leq 0.001$ .

#### **4.3.7 Negative control for clathrin inhibitor, Pitstop 2, causes non-specific effects on CXCR4 receptor endocytosis with significant increase in CXCR4 internalisation following CXCL12 stimulation seen in MCF-7, but not significant in Jurkat cells.**

Chemokine receptors can also internalise independent of caveolae via clathrin-mediated endocytosis, which regulates the cell surface expression levels of plasma membrane proteins through endocytic uptake (Brodsky et al., 2001). Assembly of clathrin-coated pits (CCPs) is initiated by receptor phosphorylation following activation by ligands. The process of receptor phosphorylation facilitates the recruitment of adaptor proteins, including  $\beta$ -arrestins and AP-2 (Hüttenrauch et al., 2002; Heilker et al., 1996). The CCPs have been proposed to serve as a scaffold for stabilising the adaptor proteins and recruiting other accessory factors that regulate endocytosis (Gaidarov et al., 1999). Through clathrin polymerisation together with the action of dynamin, CCPs are subsequently invaginated, leading to endocytosis (Liu et al., 2010). To summarise, clathrin is prerequisite for receptor internalisation in this endocytic pathway.

In order to address the roles of clathrin in chemokine-induced receptor internalisation, we employed a clathrin inhibitor, Pitstop 2, which is known to block the interactions between the N-terminal domain of clathrin heavy chain and one of the associated accessory proteins, amphiphysin (**Figure 4.10**) (von Kleist et al., 2011). Pitstop 2 was shown to inhibit endocytosis of transferrin receptor, which is a cargo protein in clathrin-dependent endocytosis (von Kleist et al., 2011), but not for shiga toxin, which is endocytosed independently of clathrin

(Römer et al., 2010). Hence, Pitstop 2 could serve as an inhibitor targeting clathrin-dependent receptor internalisation in our study.

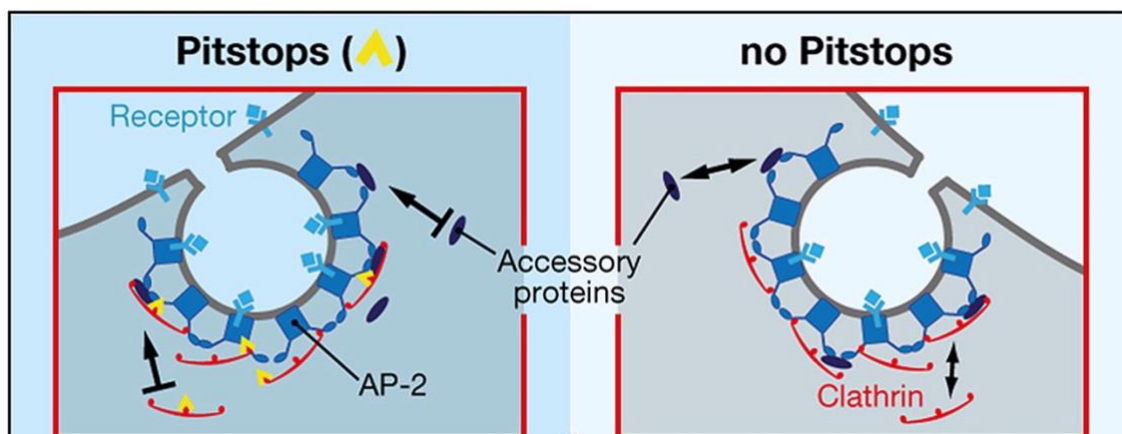


**Figure 4.10. Mode of action of clathrin inhibitor, Pitstop 2.** Schematic diagram showing the interactions of Pitstop 2 with clathrin and the accessory proteins to block the assembly of clathrin-coated pit (CCP). (Image taken from von Kleist et al., 2011)

In our study, we used Pitstop 2 together with the negative control for Pitstop 2 (Pitstop 2 neg) as a reference for non-specific effects and possible interference with fluorescence readings from Pitstop 2 (Abcam). According to the information from the supplier (Abcam), Pitstop 2 is a selective, cell membrane permeable clathrin inhibitor that selectively inhibit clathrin-mediated endocytosis (von Kleist et al., 2011). Pitstop 2 neg has a highly related chemical structure as Pitstop 2 but is unable to associate with the clathrin terminal domain, which does not interfere with receptor-mediated endocytosis (Abcam) (**Figure 4.11**). As the supplier (Abcam) suggested, 30  $\mu\text{M}$  Pitstop 2 was used for complete inhibition of clathrin-mediated endocytosis. It has been confirmed that 30  $\mu\text{M}$  Pitstop 2 has no toxicity in MCF-7 and Jurkat cells (**Figure A3**). Cells were incubated with Pitstop 2 or Pitstop 2 neg for 5 minutes to minimise the non-specific effects, according to the supplier's instruction (Abcam), followed by chemokine stimulation. After antibody staining, cells were fixed and washed before flow cytometry analysis.

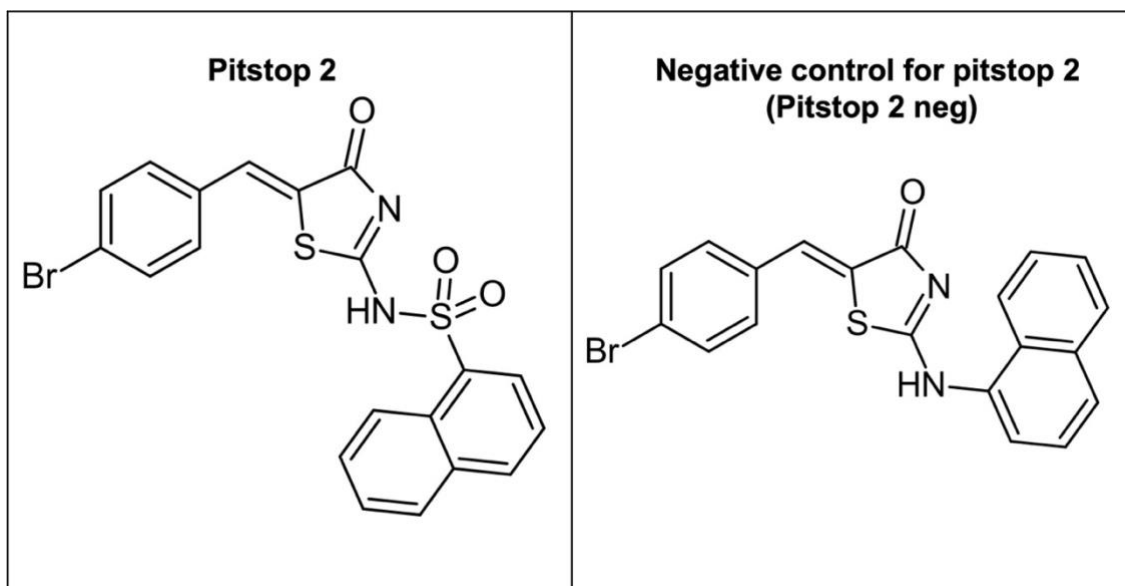


**Figure 4.11. Chemical structure of pitstop 2 and negative control for pitstop 2 (pitstop 2 neg).** Pitstop 2 neg is the same chemical class as pitstop 2 with an inhibitory property of amphiphysin binding to clathrin ( $IC_{50} > 100 \mu M$ ) but not receptor-mediated endocytosis (Abcam). (Images taken from Abcam)

For CXCL12-induced CXCR4 internalisation in MCF-7 cells, quantitative flow cytometry analysis shows that significant decrease in CXCR4 on cell surface in post-stimulation of CXCL12 was observed in the treatment of pitstop 2 neg compared to control without inhibitor treatment (**Figure 4.12 and Table 4.2**). This indicates that pitstop 2 neg induces increased receptor internalisation in MCF-7 cells. In the treatment of pitstop 2, reduced CXCR4 internalisation following CXCL12 stimulation was seen compared to pitstop 2 neg-treated cells, but no difference in the comparison with control without any inhibitor treatment was observed (**Figure 4.12 and Table 4.2**).

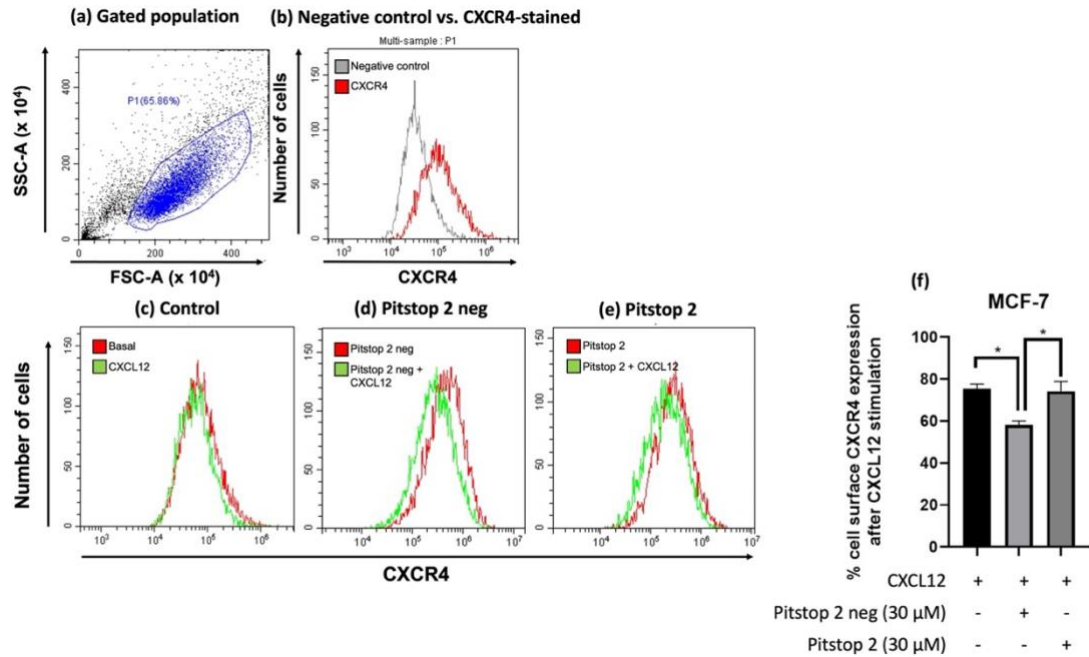


**Figure 4.12. Increased CXCR4 internalisation following CXCL12 stimulation was observed in MCF-7 cells treated with negative control for pitstop 2 (pitstop 2 neg).** Cells were treated with pitstop 2 (30 µM) or pitstop 2 neg (30 µM) or without inhibitor treatment for 5 minutes, followed by stimulation with CXCL12 (50 nM) at 37 °C for another 30 minutes to allow CXCR4 internalisation to take place. Cells were stained with mouse monoclonal CXCR4 antibody (4G10) (1:200) followed by secondary staining of anti-mouse Alexa 488 antibody (1:200). Only secondary anti-mouse Alexa 488 antibody (1:200) was added in negative control. Fluorescence intensity of 20,000 events from each sample were quantified in flow cytometry and cell population was gated to exclude dead cells and debris before analysis. (a) Representative scatter plot (FSC vs. SSC) indicates the gated cell population (indicated as P1) in the analysis. (b) Representative histogram showing unstained cells as negative control (in grey) and CXCR4-stained cells (in red). (c, d, e) Representative histograms showing the comparison of cells in the absence of chemokine stimulation (in red) and chemokine-stimulated cells (in green) under different conditions: (c) without inhibitor treatment, in the treatment of (d) pitstop 2 neg and (e) pitstop 2 in respect to fluorescence intensity among the gated population (P1) of each cell sample. (f) Bar chart showing percentage of cell surface CXCR4 expression following CXCL12 stimulation in MCF-7 cells treated with either pitstop 2 neg (coloured in light grey) or pitstop 2 (coloured in dark grey)

compared to control without inhibitor treatment (coloured in black). Percentage of cell surface CXCR4 expression following CXCL12 stimulation was calculated from  $(\text{CXCL12-stimulated} - \text{negative control}) / (\text{unstimulated control} - \text{negative control}) (\%)$ , where negative control was stained with secondary antibody. Fluorescence values are based on median channel of fluorescence in a gated population (P1) of cells from each sample and acquired by the CytExpert software (Beckman Coulter). Data shown represent the mean  $\pm$  SEM of at least 3 independent experiments. One-way ANOVA with a Dunnett's multiple comparisons test as post-hoc test, \* =  $p \leq 0.05$ .

In Jurkat cells, similar to MCF-7 cells, there was a trend in increased CXCR4 internalisation following CXCL12 stimulation in the treatment of pitstop 2 neg compared to control without inhibitor treatment. CXCR4 internalisation was reduced by the treatment of pitstop 2. Yet, the difference in the percentage of CXCR4 expression on cell surface among the experimental interventions was not significant from statistical tests (**Figure 4.13 and Table 4.2**). Combining our observations in MCF-7 and Jurkat cells, pitstop 2 might potentially interfere with the observations of CXCR4 internalisation due to non-specific effects. Therefore, there is a need to include pitstop 2 neg as a reference control particularly in the study of CXCR4 internalisation, in order to eliminate the non-specific effects that might affect the accuracy of analysis caused by the inhibitor.

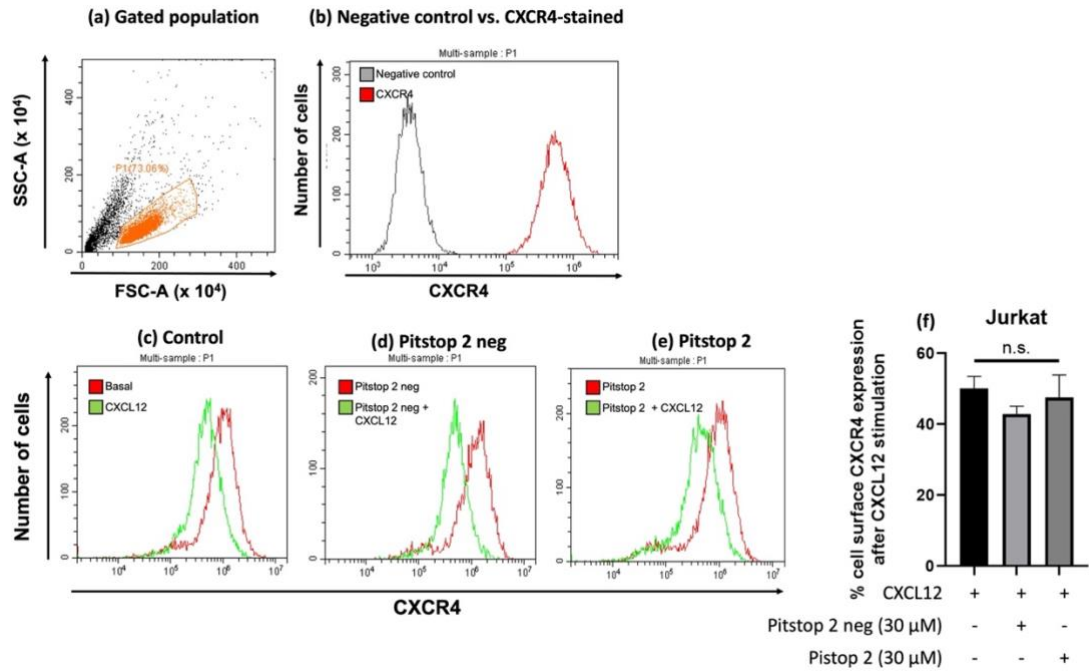


**Figure 4.13. A trend of increased CXCR4 internalisation following CXCL12 stimulation was observed in Jurkat cells treated with negative control for pitstop 2 (pitstop 2 neg).** Cells were treated with pitstop 2 (30 μM) or pitstop 2 neg (30 μM) or without inhibitor treatment for 5 minutes, followed by stimulation with CXCL12 (50 nM) at 37 °C for another 30 minutes to allow CXCR4 internalisation to take place. Cells were stained with mouse CXCR4 antibody (1:200) followed by secondary staining of anti-mouse Alexa 488 antibody (1:200). Only secondary anti-mouse Alexa 488 antibody (1:200) was added in negative control. Fluorescence intensity of 20,000 events from each sample were quantified in flow cytometry and cell population was gated to exclude dead cells and debris before analysis. (a) Representative scatter plot (FSC vs. SSC) indicates the gated cell population (indicated as P1) in the analysis. (b) Representative histogram showing unstained cells as negative control (in grey) and CXCR4-stained cells (in red). (c, d, e) Representative histograms showing the comparison of cells in the absence of chemokine stimulation (in red) and chemokine-stimulated cells (in green) under different conditions: (c) without inhibitor treatment, in the treatment of (d) pitstop 2 neg and (e) pitstop 2 in respect to fluorescence intensity among the gated population (P1) of each cell sample. (f) Bar chart showing percentage of cell surface CXCR4 expression following CXCL12 stimulation in Jurkat cells treated with either pitstop 2 neg (coloured in light grey) or pitstop 2 (coloured in dark grey) compared to

control without inhibitor treatment (colour in black). Percentage of cell surface CXCR4 expression following CXCL12 stimulation was calculated from (CXCL12-stimulated – negative control) / (unstimulated control – negative control) (%), where negative control was stained with secondary antibody. Fluorescence values are based on median channel of fluorescence in a gated population (P1) of cells from each sample and acquired by the CytExpert software (Beckman Coulter). Data shown represent the mean  $\pm$  SEM of at least 3 independent experiments. One-way ANOVA with a Dunnett's multiple comparisons test as post-hoc test, n.s. = not significant.

#### **4.3.8. Pitstop 2 has no inhibitory effect on CCL3-induced CCR5 internalisation in MCF-7 cells.**

For CCL3-induced CCR5 internalisation in MCF-7 cells, there was no significant difference in cell surface CCR5 expression following CCL3 stimulation in the treatment of pitstop 2 or pitstop 2 neg compared to control without inhibitor treatment (**Figure 4.14 and Table 4.2**). This implies that CCL3-induced CCR5 internalisation is not affected by the non-specific effects of pitstop 2 and potentially might not be dependent of clathrin.

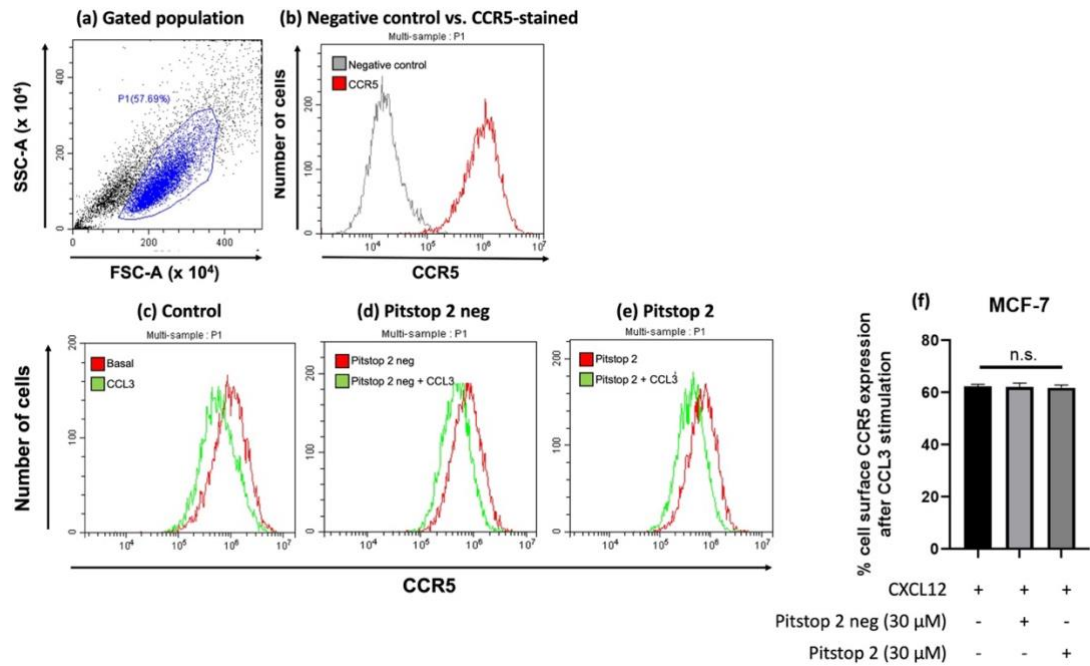


**Figure 4.14. No significant change in the level of CCL3-induced CCR5 internalisation by the treatment of pitstop 2 or pitstop 2 neg was observed in MCF-7 cells.** Cells were treated with pitstop 2 (30  $\mu$ M) or pitstop 2 neg (30  $\mu$ M) as control for 5 minutes, followed by stimulation with CCL3 (100 nM) at 37  $^{\circ}$ C for another 30 minutes to allow CCR5 internalisation to take place. Cells were stained with rat CCR5 antibody (1:100) followed by secondary staining of anti-rat Alexa 488 antibody (1:200). Only secondary anti-rat Alexa 488 antibody (1:200) was added in negative control. Fluorescence intensity of 20,000 events from each sample were quantified in flow cytometry and cell population was gated to exclude dead cells and debris before analysis. (a) Representative scatter plot (FSC vs. SSC) indicates the gated cell population (indicated as P1) in the analysis. (b) Representative histogram showing unstained cells as negative control (in grey) and CCR5-stained cells (in red). (c, d, e) Representative histograms showing the comparison of cells in the absence of chemokine stimulation (in red) and chemokine-stimulated cells (in green) under different conditions: (c) without inhibitor treatment, in the treatment of (d) pitstop 2 neg and (e) pitstop 2 in respect to fluorescence intensity among the gated population (P1) of each cell sample. (f) Bar chart showing percentage of cell surface CCR5 expression following CCL3 stimulation in MCF-7 cells treated with either pitstop 2 neg (coloured in light grey) or pitstop 2 (coloured in dark grey) compared to control without inhibitor

treatment (coloured in black). Percentage of cell surface CCR5 expression following CCL3 stimulation was calculated from  $(\text{CCL3-stimulated} - \text{negative control}) / (\text{unstimulated control} - \text{negative control}) (\%)$ , where negative control was stained with secondary antibody. Fluorescence values are based on median channel of fluorescence in a gated population (P1) of cells from each sample and acquired by the CytExpert software (Beckman Coulter). Data shown represent the mean  $\pm$  SEM of at least 3 independent experiments. One-way ANOVA with a Dunnett's multiple comparisons test as post-hoc test, n.s. = not significant.

**Table 4.2. Effect of caveolae-depleting agents and clathrin inhibitor on chemokine-induced receptor internalisation**

| Cell line | Chemokine      | Percentage of receptor expression on cell surface following chemokine stimulation for 30 minutes (%) $\pm$ SEM |                             |                           |   |                           |
|-----------|----------------|--|-----------------------------|---------------------------|---|---------------------------|
|           |                | Control <sup>†</sup>   | Inhibitor <sup>‡</sup>      |                           |   |                           |
|           |                |  | Caveolae-depleting agents   |                           | Clathrin inhibitor                                |                           |
|           |                |  | Nystatin<br>(50 $\mu$ g/mL) | Filipin<br>(5 $\mu$ g/mL) | Negative control<br>for pitstop 2<br>(30 $\mu$ M) | pitstop 2<br>(30 $\mu$ M) |
| MCF-7     | CCL3 (100 nM)  | 65.8 $\pm$ 3.1   | 67.7 $\pm$ 0.9              | 68.7 $\pm$ 3.8            | 62.1 $\pm$ 1.5                                    | 61.8 $\pm$ 1.1            |
|           | CXCL12 (50 nM) | 75.4 $\pm$ 2.2   | 47.9 $\pm$ 5.3              | 32.6 $\pm$ 2.5            | 58.2 $\pm$ 1.9                                    | 74.2 $\pm$ 4.7            |
| Jurkat    | CXCL12 (50 nM) | 50.1 $\pm$ 3.4   | 96.1 $\pm$ 4.8              | 116.9 $\pm$ 4.6           | 42.8 $\pm$ 2.3                                    | 47.6 $\pm$ 6.3            |

\*Percentage of receptor expression on cell surface following chemokine stimulation = [median channel of fluorescence (chemokine-stimulated) - median channel of fluorescence (negative control)] / [median channel of fluorescence (without chemokine stimulation) - median channel of fluorescence (negative control)] (%), where negative control was stained with secondary antibody matched to the host species and class of the primary antibody only.

<sup>†</sup> Relative to control without chemokine stimulation nor inhibitor treatment

<sup>‡</sup> Relative to inhibitor-treated control without chemokine stimulation

#### **4.3.9. Dynamin-2 (Dyn-2) translocate towards the cytosol with increased expression level following CCL3 or CXCL12 stimulation in MCF-7 cells**

Dynamin-2 (Dyn-2) GTPase is a critical adaptor protein for membrane detachment of caveolae and clathrin-coated pits triggering receptor endocytosis (Nichols and Lippincott-Schwartz, 2001; Liu et al., 2010). As Dyn-2 play a common role in both caveolae-dependent and clathrin-dependent endocytic pathways, similar observations in terms of Dyn-2 translocation would be expected in both pathways.

Although no definite conclusion on the CCR5 and CXCR4 endocytic pathways in MCF-7 could be drawn from our results in previous sections, both CCR5 and CXCR4 receptors have been shown to internalise following the stimulation of CCL3 and CXCL12 respectively (**Figures 3.17-3.20, Table 3.2**) shown in Chapter 3. Hence, we hypothesised that Dyn-2 is involved in internalisation of both receptors in MCF-7 cells regardless of which endocytic pathways adopted. Using immunofluorescence staining with antibody specific to Dyn-2, we visualised the localisation of Dyn-2 in MCF-7 cells following CCL3 or CXCL12 stimulation associated with CCR5 and CXCR4 internalisation respectively.

In **Figure 4.15**, the expression of Dyn-2 is dispersed within the periphery of the cells under basal conditions. Accumulation of Dyn-2 expression towards the cytosol within the cells was observed following the stimulation of CCL3 and CXCL12 respectively and the effects were more significant in CXCL12-stimulated cells. This implies that Dyn-2 plays a role in CCL3-induced CCR5 internalisation and CXCL12-induced CXCR4 internalisation. The observations of Dyn-2 translocation intracellularly are consistent with the evidence proposed previously by Nichols and Lippincott-Schwartz, 2001, showing that Dyn-2 is recruited to the intracellular side of the plasma membrane and aids the dissociation of receptor-associated membrane invaginations during receptor endocytosis.

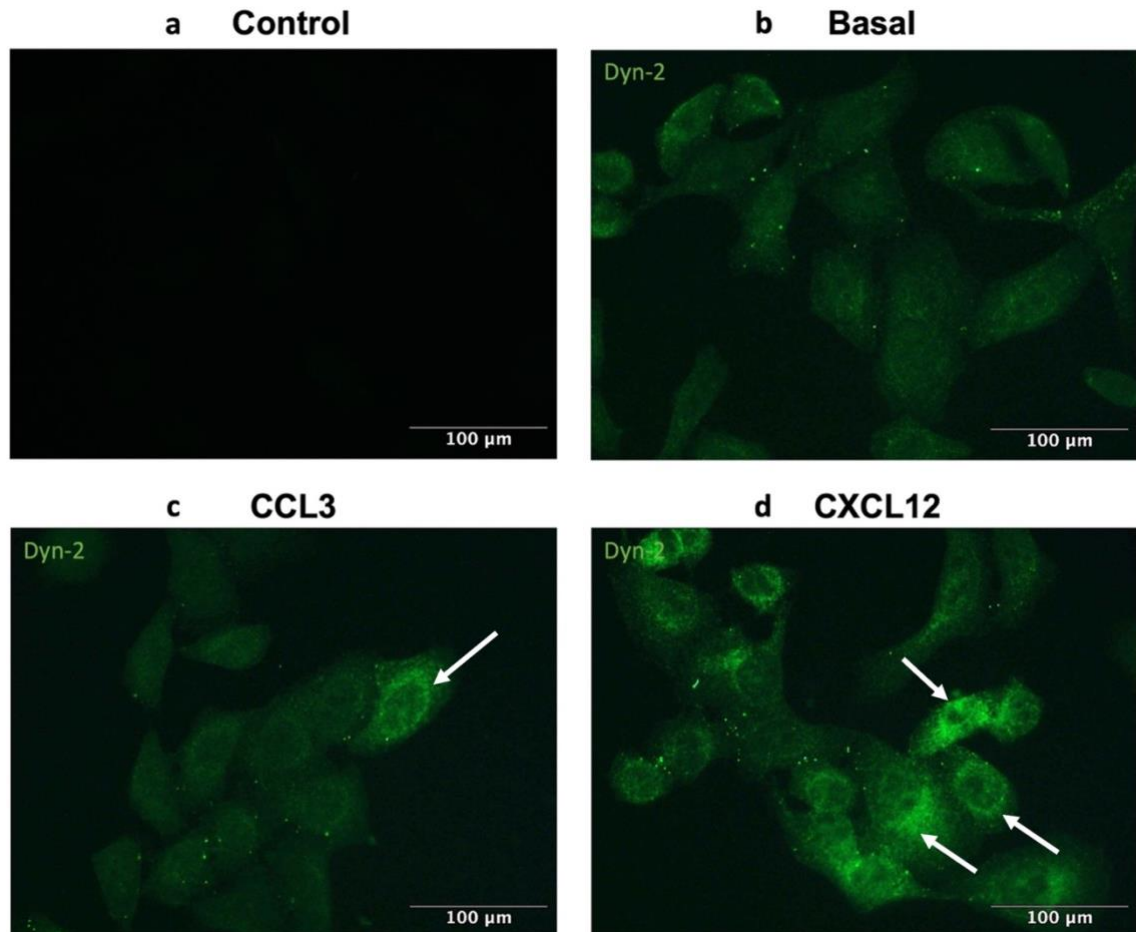


**Figure 4.15. Effects of chemokine stimulation on dynamin-2 (Dyn-2) expression in MCF-7 cells.** MCF-7 cells were stimulated with (c) CCL3 (100 nM) and (d) CXCL12 (50 nM) for 30 minutes or (b) absence of chemokine as a basal control for 30 minutes. (a) Cells only treated with secondary antibody as a background control. Cells were then fixed, permeabilised and stained with mouse Dyn-2 antibody (1:500), followed by secondary staining with anti-mouse Alexa 488 antibody (1:500) (green). Representative images from at least 3 independent experiments were acquired with a Leica DMII Fluorescence microscope using 31.5X magnification.

**4.3.10. Arrestin-2 (Arr-2) constructs translocate out of the nucleus in response to CCL3 stimulation, whereas arrestin-3 constructs translocate towards the nucleus in response to CXCL12 stimulation in MCF-7 cells.**

$\beta$ -arrestins have been known to play an important role not only in receptor desensitisation through clathrin-mediated endocytic pathway, but also transduction of G protein-independent pathway. Two major isoforms of  $\beta$ -arrestins,  $\beta$ -arrestin 1 (also known as arrestin-2) and  $\beta$ -arrestin 2 (also known as arrestin-3) have been discovered to have differences in functionality and localisation within cells despite a high degree of similarity in homology (Ferguson, 2001; Kang et al., 2015).

In receptor endocytosis, both isoforms of  $\beta$ -arrestins have been shown to interact with the adaptor proteins, AP-2 and clathrin in clathrin-coated pits and target activated GPCRs for clathrin-mediated endocytosis (Brodsky et al., 2001).

In G protein-independent chemokine signalling, accumulating evidence of biased signalling have been shown to be  $\beta$ -arrestins isoform-specific. For example, CCL2 activates CCR8 through biased signalling towards arrestin-3 over arrestin-2 (Berchiche et al., 2011). Also, isoform-specific  $\beta$ -arrestins have been revealed to be regulated by differential GRKs, resulting in different signalling outcomes. For example, GRK2 interacts with arrestin-3 to negatively modulate  $\text{Ca}^{2+}$  mobilisation and ERK1/2 activation, whereas GRK3 recruits arrestin-2 to positively regulate ERK1/2 (Busillo et al., 2010).

In respect to differential distribution of  $\beta$ -arrestins, arrestin-2 is constitutively expressed throughout the cells, including the cytoplasm and nucleus, whereas arrestin-3 is only found in the cytoplasm (Ferguson, 2001). Despite the exclusive cytoplasmic expression of arrestin-3, it was proposed to undergo constitutive nucleocytoplasmic shuttling that redirect GPCR-activated JNK3 from the nucleus to cytoplasm for transcription regulation (Scott et al., 2002).

Previous studies using HeLa cells and HEK-293 cells as experimental models demonstrated that arrestin-2 constructs were evenly distributed throughout the cytoplasm and nucleus, whereas arrestin-3 constructs expressed in the

cytoplasm exclusively (Ferguson, 2001; Scott et al., 2002). To investigate whether the localisation of  $\beta$ -arrestins is dependent of cell types, we overexpressed MCF-7 cells with plasmid DNA for EGFP-tagged arrestin-2 (Arr-2), arrestin-3 (Arr-3) and arrestin-2 mutant (Arr Mut) (Arrestin 2-V53D) respectively. Arr Mut is the mutant form of arrestin-2 with a point mutation of residues valine (Val) to aspartic acid (Asp) introduced. The plasmid DNA was produced from a HindIII/ApaI-digested pEGFP-N1 plasmid vector ligated with a validated mammalian Arr2/Arr3/ArrMut ORF insert.

In MCF-7 cells, Arr-2 constructs appeared to be distributed throughout the cells under basal conditions (**Figure 4.16**). In the stimulation of CCL3, a visible movement of Arr-2 out of the nucleus with defined spots accumulating on the plasma membrane was observed. On the other hand, no observable change in Arr-2 localisation was seen in the stimulation of CXCL12 (**Figure 4.16**).

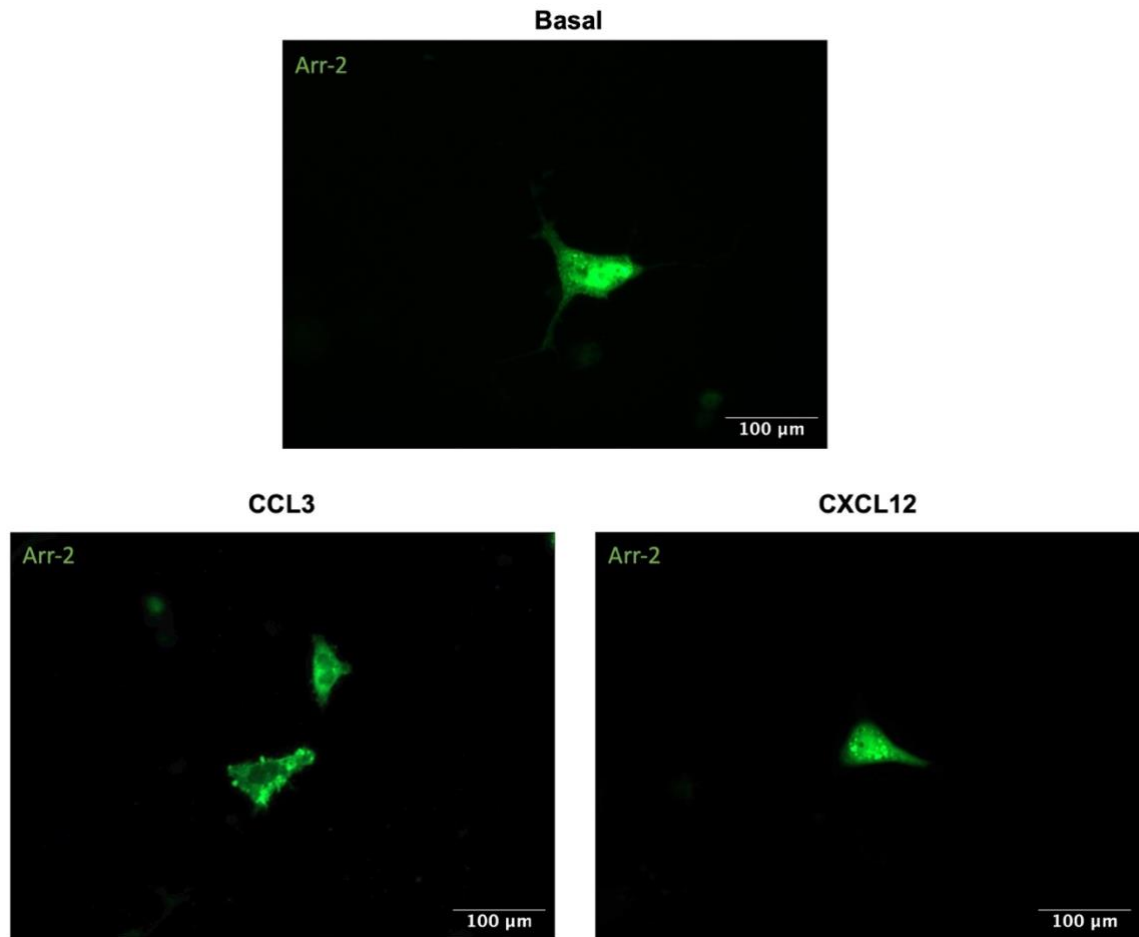


**Figure 4.16. Arrestin 2 (Arr-2) constructs translocate out of the nucleus and accumulate on the plasma membrane in CCL3-stimulated MCF-7 cells, whereas no observable change was observed following CXCL12 stimulation.** Micrographs of MCF-7 monolayers chemically transfected for 24 hours using 2  $\mu$ g plasmids DNA coding for pArr2.EGFP (green) and then stimulated with CCL3 (100 nM) or CXCL12 (50 nM) for 30 minutes. Cells were fixed with 4% paraformaldehyde before image acquisition. Representative images from at least 3 independent experiments were acquired with a Leica DMII Fluorescence microscope using 20X magnification.

**Figure 4.17** illustrates that Arr-3 constructs were present within the cytoplasm, excluded from the nucleus under basal conditions. No observable change in Arr-3 localisation was seen in the stimulation of CCL3. However, in the stimulation of CXCL12, Arr-3 appeared to accumulate towards the nucleus (**Figure 4.17**).

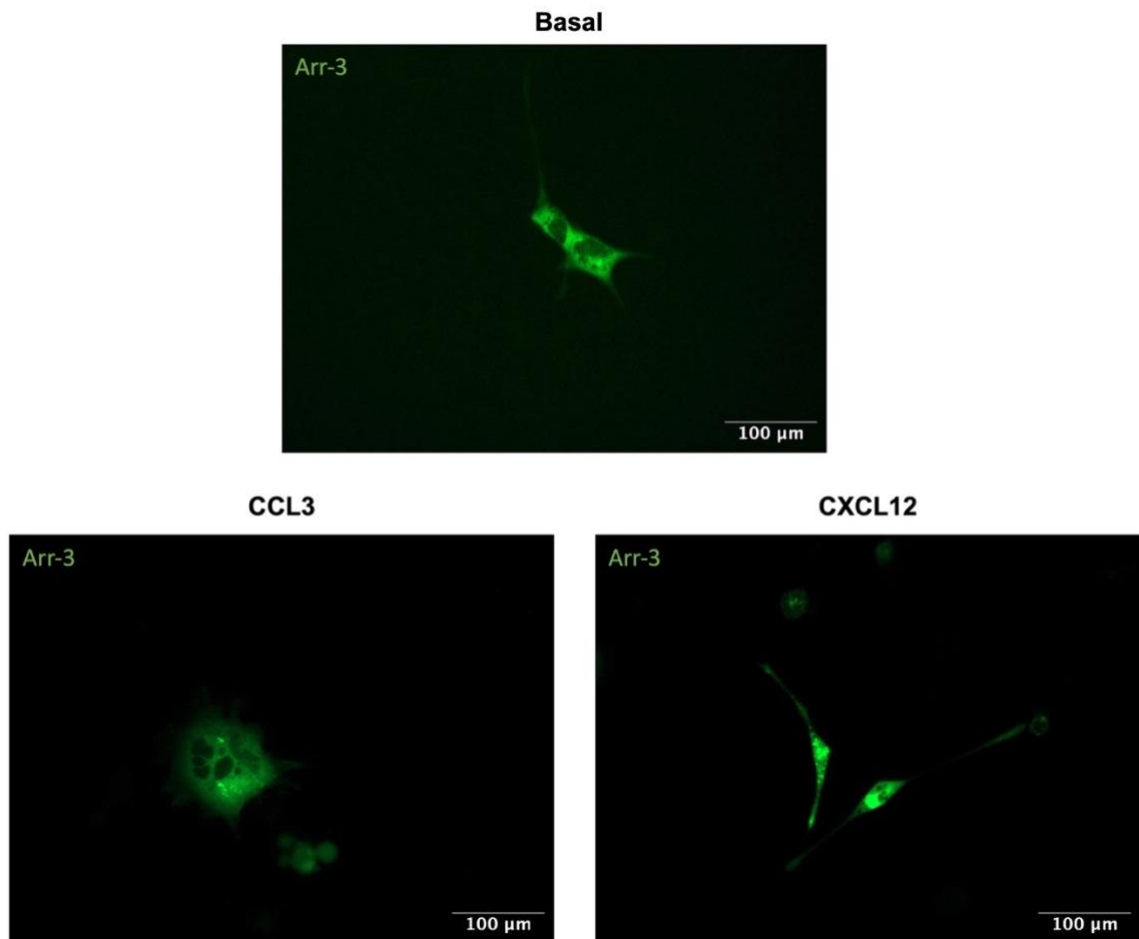


**Figure 4.17. Arrestin 3 (Arr-3) constructs translocate towards the nucleus following CXCL12 stimulation in MCF-7 cells, but no observable change was observed in CCL3 stimulation.** Micrographs of MCF-7 monolayers chemically transfected for 24 hours using 2  $\mu$ g plasmids DNA coding for pArr3.EGFP (green) and then stimulated with CCL3 (100 nM) or CXCL12 (50 nM) for 30 minutes. Cells were fixed with 4% paraformaldehyde before image acquisition. Representative images from at least 3 independent experiments were acquired with a Leica DMII Fluorescence microscope using 20X magnification.

In **Figure 4.18**, Arr Mut constructs distribute throughout the cells and more expression seemed to accumulate within the nucleus under basal conditions. There was no observable redistribution of Arr Mut seen in MCF-7 cells in response to CCL3 and CXCL12 stimulation respectively. The expression of Arr Mut remained to be high particularly within the nucleus (**Figure 4.18**). Together with the observations above (**Figure 4.16**), this implies that point mutation of the

key residues of Arr-2 blocks translocation of Arr-2 in response to CCL3 stimulation.

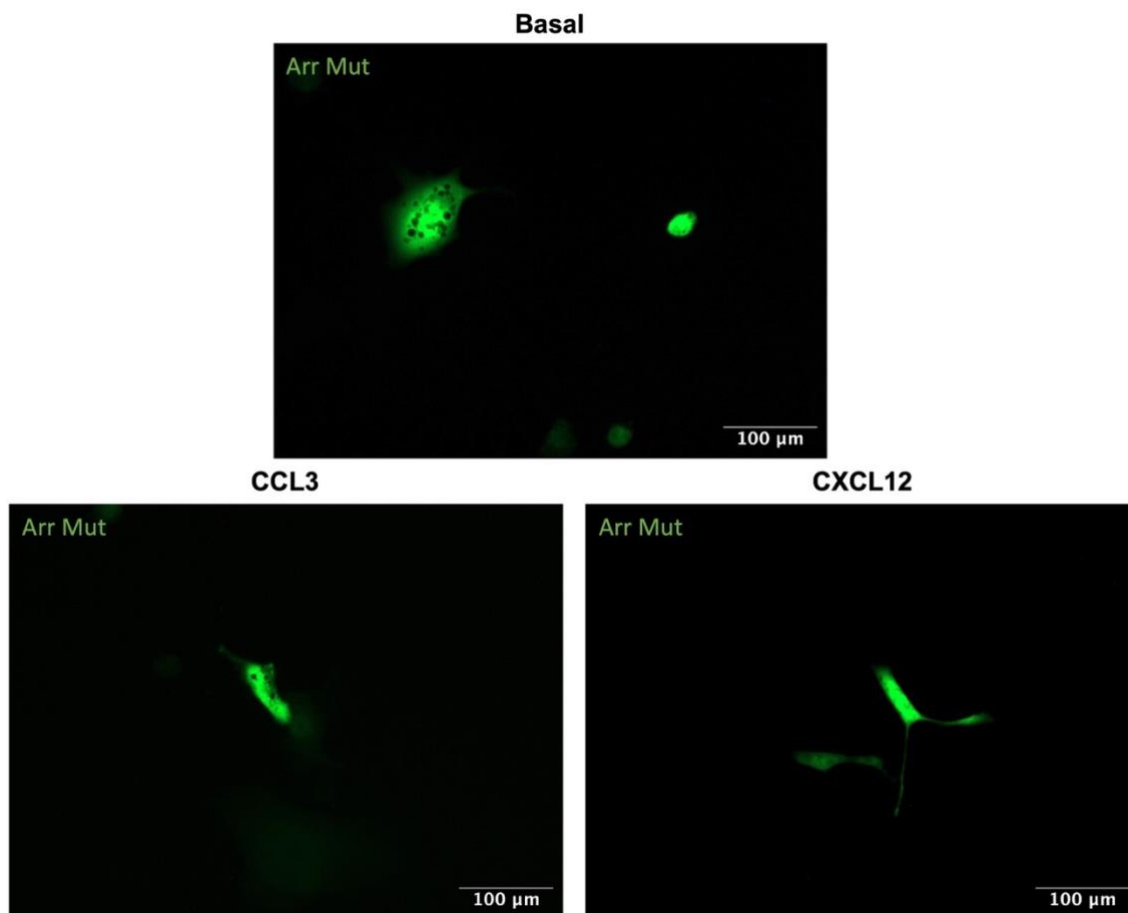


**Figure 4.18. Mutant for Arr-2 (Arr Mut) constructs mainly accumulate within the nucleus and no observable change in localisation in the stimulation of CCL3 or CXCL12.** Micrographs of MCF-7 monolayers chemically transfected for 24 hours using 2 μg plasmids DNA coding for pArrMut.EGFP (green) and then stimulated with CCL3 (100 nM) or CXCL12 (50 nM) for 30 minutes. Cells were fixed with 4% paraformaldehyde before image acquisition. Representative images from at least 3 independent experiments were acquired with a Leica DMII Fluorescence microscope using 20X magnification.

#### **4.3.11. Dynamin inhibitors, Dynasore and Dyngo-4a, have no effect on CCL3-induced Arr-2 translocation but abolish CXCL12-induced Arr-3 translocation in MCF-7 cells.**

In the process of clathrin-dependent receptor endocytosis,  $\beta$ -arrestins and clathrin are recruited to the phosphorylated receptor to form clathrin-coated pit

(CCP) associated with the receptor, followed by dissociation of the CCP from the membrane by the action of dynamin (Robinson, 2015). Hence, we hypothesised that blocking the action of dynamin would thereby inhibit receptor endocytosis as reflected by the localisation of  $\beta$ -arrestins involved.

In our study, we used two dynamin inhibitors, Dynasore and Dyngo-4a, to examine the effects of dynamin on  $\beta$ -arrestins translocation in chemokine-induced receptor endocytosis. Although both chemical structures are similar that target dynamin (**Figure 4.19**), Dyngo-4a is more potent and its mode of action is more specific (**Table 2.3**). Dyngo-4a is an allosteric inhibitor targeting the G domain of dynamin and its inhibitory effect is selective to dynamin 1 (McCluskey et al., 2013). Dynasore is a non-competitive inhibitor that is non-selective to any isoforms of dynamin (Macia et al., 2006). Our group has previously used both Dynasore and Dyngo-4a at the assay concentration of 80  $\mu$ M to determine the function of dynamin in chemokine-induced cell migration in THP-1 and Jurkat cells (Jacques et al., 2015). We have tested that 80  $\mu$ M Dynasore and Dyngo-4a has no cytotoxicity in MCF-7 cells in 7 hours incubation time (**Figure A4**), which is within the incubation required in our assay.

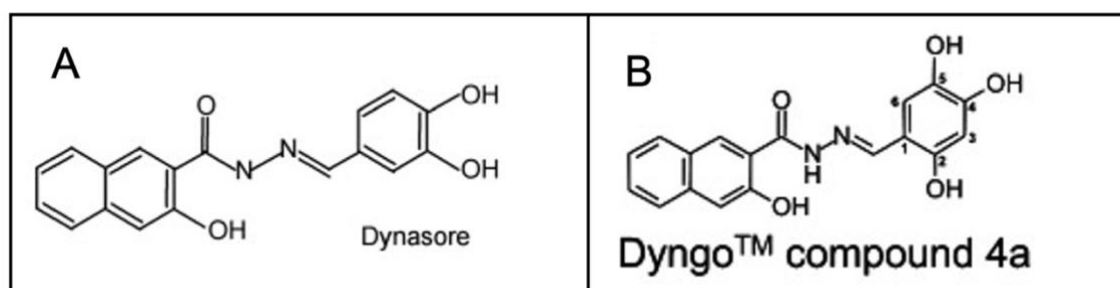


**Figure 4.19. Chemical structures of dynamin inhibitors, Dynasore and Dyngo 4a, used in our study.** A: Dynasore; B: Dyngo 4a, which has been proven to be more potent with reduced cytotoxicity, non-specific binding and detergent binding, and selective to dynamin 1 specifically, conferred by changes in the position and number of hydroxyl substituents (McCluskey et al., 2013) (Images taken from Macia et al., 2006; McCluskey et al., 2013).

In **Figure 4.20**, under basal conditions, there was no observable change in the distribution of Arr-2 in MCF-7 cells treated with Dyngo-4a, whereas Arr-2 seems to distribute less evenly with a cluster in the cytoplasm in the treatment of

Dynasore. As shown above, following CCL3 stimulation, Arr-2 was observed to translocate towards the plasma membrane (**Figure 4.16**). Similar effects with clusters of Arr-2 accumulating within the plasma membrane were observed in the pre-treatment of Dyngo-4a or Dynasore in the stimulation of CCL3. This implies that dynamin inhibitors do not block Arr-2 translocation towards the plasma membrane. In the stimulation of CXCL12, no observable change in Arr-2 distribution was seen in MCF-7 cells treated with both dynamin inhibitors, in comparison with the control in the absence of chemokine stimulation.

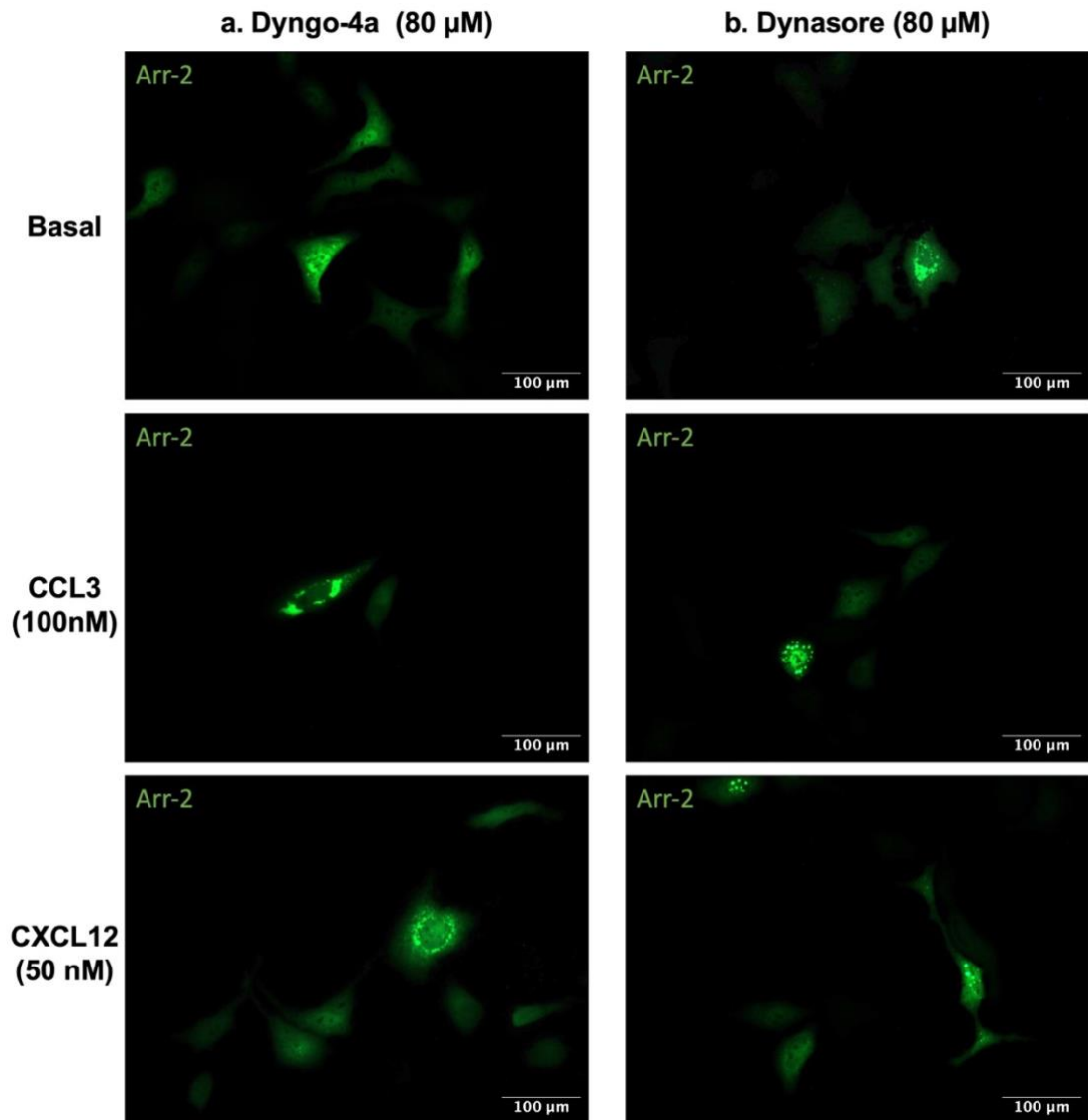


**Figure 4.20. Dynamin inhibitors, Dyngo-4a and Dynasore, had no effect on Arr-2 distribution in MCF-7 cells, particularly no inhibition was seen on CCL3-induced Arr-2 translocation.** Micrographs of MCF-7 monolayers chemically transfected for 24 hours using 2  $\mu$ g plasmids DNA coding for pArr2.EGFP (green). Transfected cells were pre-treated with (a) Dyngo-4a (80  $\mu$ M) or (b) Dynasore (80  $\mu$ M) for 30 minutes, followed by stimulation of CCL3 (100 nM) and CXCL12 (50 nM) respectively for 30 minutes or absence of chemokine as a basal control for 30 minutes. Cells were then fixed and imaged. Representative images from at least 3 independent experiments were acquired with a Leica DMII Fluorescence microscope using 20X magnification.

Under basal conditions, Arr-3 constructs were expressed evenly within the cytoplasm, except the nucleus in MCF-7 cells pre-treated with Dyngo-4a (**Figure**

**4.21**). The observation is the same as seen in cells without inhibitor treatment. However, in Dynasore-treated cells, Arr-3 was also found in the nucleus with a few bright spots seen near the nucleus. Following CCL3 stimulation, compared to the basal control, no obvious difference in Arr-3 distribution was observed in cells treated with both dynamin inhibitors (**Figure 4.21**). Comparing **Figure 4.20** with **Figure 4.17**, dynamin inhibitors abolished translocation of Arr-3 constructs towards the nucleus mediated by CXCL12. This implies that dynamin inhibitors potentially block Arr-3 translocation to the nucleus mediated by CXCL12.

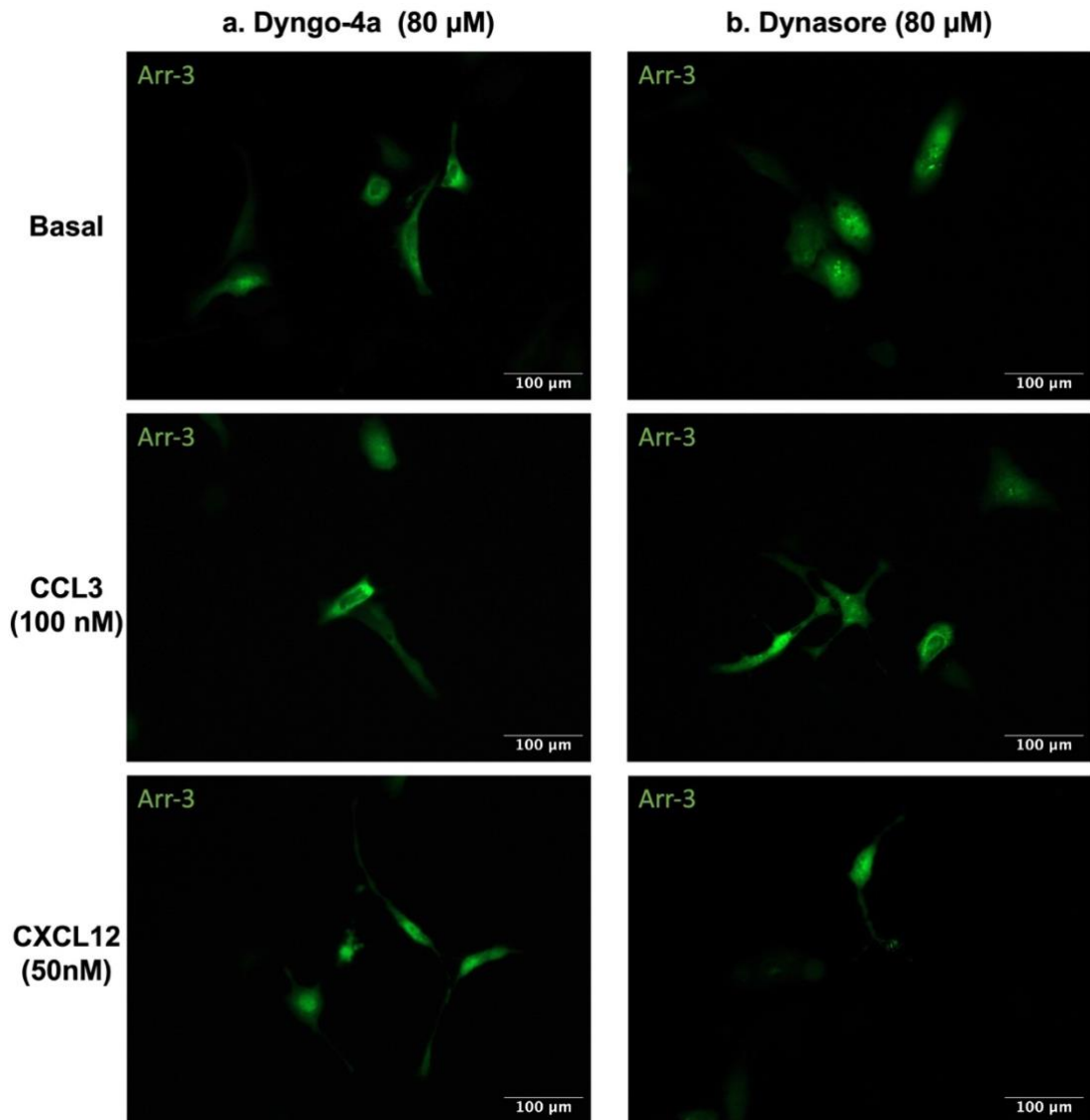


**Figure 4.21. CXCL12-induced Arr-3 translocation was abolished by the treatment of Dyngo-4a or Dynasore in MCF-7 cells, while no effect was observed under basal condition and in the stimulation of CCL3.** Micrographs of MCF-7 monolayers chemically transfected for 24 hours using 2  $\mu$ g plasmids DNA coding for pArr3.EGFP (green). Transfected cells were pre-treated with (a) Dyngo-4a (80  $\mu$ M) or (b) Dynasore (80  $\mu$ M) for 30 minutes, followed by stimulation of CCL3 (100 nM) and CXCL12 (50 nM) respectively for 30 minutes or absence of chemokine as a basal control for 30 minutes. Cells were then fixed and imaged. Representative images from at least 3 independent experiments were acquired with a Leica DMII Fluorescence microscope using 20X magnification.

In Arr Mut-transfected MCF-7 cells, after the treatment of both dynamin inhibitors, no observable difference in localisation of Arr-Mut constructs was seen between

basal control and chemokine-stimulated cell samples (**Figure 4.22**). As shown in **Figure 4.18**, Arr Mut-transfected cells failed to respond to CCL3 and CXCL12 stimulation. Therefore, it is expected that dynamin inhibitor treatment would not affect the distribution of Arr Mut following chemokine stimulation.

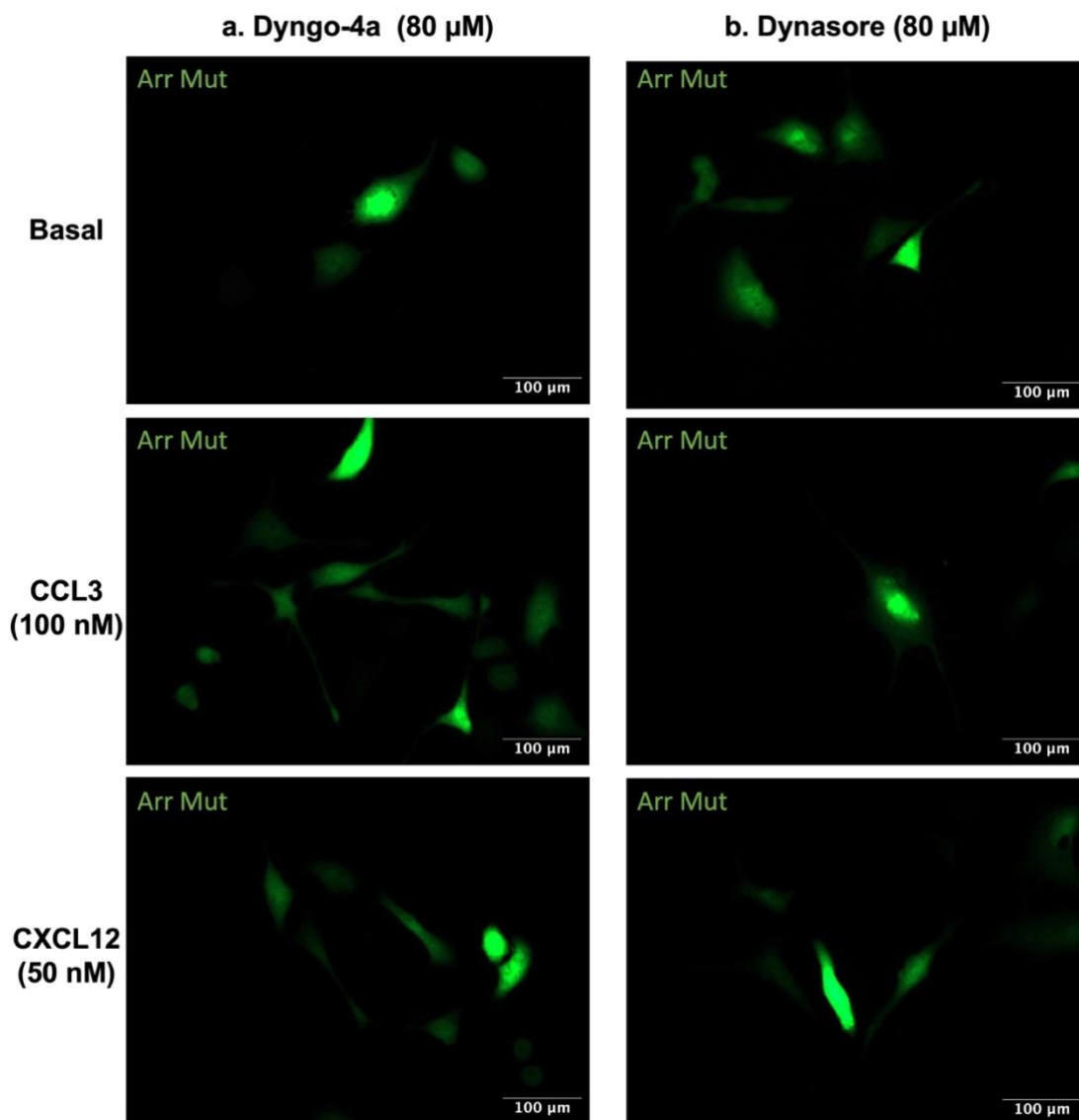


**Figure 4.22. Dyngo-4a or Dynasore had no effect on the distribution of Arr Mut under basal conditions and in the stimulation of CCL3 or CXCL12.** Micrographs of MCF-7 monolayers chemically transfected for 24 hours using 2  $\mu$ g plasmids DNA coding for the mutant form of pArr2.EGFP (green). Transfected cells were pre-treated with (a) Dyngo-4a (80  $\mu$ M) or (b) Dynasore (80  $\mu$ M) for 30 minutes, followed by stimulation of CCL3 (100 nM) and CXCL12 (50 nM) respectively for 30 minutes or absence of chemokine as a basal control for 30 minutes. Cells were then fixed and imaged. Representative images from at least 3 independent experiments were

acquired with a Leica DMII Fluorescence microscope using 20X magnification.

#### **4.4 Discussion**

Through flow cytometry analysis, breast cancer MCF-7 and leukaemic Jurkat cells were confirmed to express Cav-1 at detectable levels. In terms of localisation of Cav-1 within cells, immunofluorescence staining illustrates that majority of Cav-1 proteins scatter along the periphery of MCF-7 cells under basal conditions. Upon CXCL12 stimulation, Cav-1 proteins were observed to translocate towards the leading edge of cells. However, Cav-1 protein remains scattered along the edge of the cells following CCL3 stimulation. Our observations are consistent with a previous study demonstrating that membrane rafts translocate towards the cell leading edge induced by IGF-I in the same cell line, MCF-7. It was proposed that acquisition of cell polarity in migrating cells is determined by localisation of membrane rafts at the front (Mañes et al., 1999). This implies that membrane rafts are potentially involved in cell migration serving as a scaffold to redistribute receptors or signalling proteins at the leading edge within cells, leading to chemotaxis. Future work can be done to investigate whether membrane rafts are involved in CXCL12-induced chemotaxis in MCF-7 cells to confirm the hypothesis.

In relation to change in Cav-1 expression levels within the cells, stimulation with CCL3 or CXCL12 does not lead to a significant change in Cav-1 expression levels in both cell lines, however, a trend of increased expression of Cav-1 was observed following CXCL12 stimulation. This was implicated by increased brightness from the cell leading edge due to accumulation of fluorescence-tagged Cav-1. From our experiments using a protein synthesis inhibitor, cycloheximide, it was confirmed that this trend in increased Cav-1 expression is not caused by chemokine-induced protein synthesis.

With respect to the functional roles of caveolae in chemokine-induced receptor internalisation, our results showed that Cav-1 may play a role in CXCL12-induced CXCR4 internalisation in Jurkat cells. For MCF-7 cells, there was a trend of reduced CCL3-induced CCR5 internalisation by the two cholesterol-depleting agents, filipin and nystatin, however, the inhibitory effects were not significant. Whether caveolae are involved in CXCR4 internalisation in MCF-7 cells is

inconclusive due to non-specific effects of the cholesterol-depleting agents observed. As mentioned previously, the effects of membrane cholesterol disruption by the cholesterol-depleting agents potentially alter receptor conformation and ligand binding, and consequently receptor internalisation could be affected (Bolard, 1986). Thus, caution should be taken before the conclusion is drawn. Further investigations need to be conducted to confirm our findings on the involvement of caveolae in chemokine-induced receptor internalisation, for example, using RNA interference to knock down endogenous Cav-1 (Ge and Pachter, 2004).

On the other hand, in the investigation of clathrin-dependent receptor internalisation pathway, pitstop 2 was used to inhibit clathrin-dependent receptor endocytosis. Our findings revealed that clathrin is not involved in CCL3-induced CCR5 internalisation in MCF-7 cells. However, pitstop 2 was found to potentially interfere with CXCR4 internalisation with a trend of increased CXCR4 internalisation observed in both Jurkat and MCF-7 cells treated with the negative control for pitstop 2 (pitstop 2 neg) provided by the supplier (Abcam). Hence, whether CXCR4 internalisation is dependent of clathrin in MCF-7 and Jurkat cells is inconclusive from our results. Our observations imply that pitstop 2 may not be an ideal inhibitor targeting clathrin-dependent receptor endocytosis specifically for CXCR4.

Aside from pitstop 2, there are other options of inhibitors commonly used for blocking clathrin-dependent endocytosis in different modes of action. Monensin dissipates a proton gradient during endocytosis (Dickson et al., 1982), hyperosmotic sucrose prevents from interactions between clathrin and adaptor proteins (Hansen et al., 1993), hydrophobic amines affect clathrin (Wang et al., 1993) and clathrin-coated vesicles and cell-permeable Dynasore inhibits dynamin GTPases activity in the formation of clathrin-coated pits (Nankoe and Sever, 2006). Yet, these inhibitor treatments are not specific to clathrin-dependent pathway as the inhibitors do not selectively target proteins involved in the pathway. Apart from using clathrin inhibitors, recent studies employed small interfering RNA (siRNA) interference of key components of proteins critical for clathrin-dependent endocytosis, such as clathrin heavy chain, subunits of the AP2 and dynamin 2 (Motley et al., 2003) (Loerke et al., 2009). However, these

methods might not apply to every cell line as the success rate of transfection is low in some cell lines. Also, the whole process takes time and potentially lead to indirect effects that affect our result interpretation.

To briefly summarise, our results showed that CXCL12-induced CXCR4 internalisation in Jurkat cells is caveolae-dependent, whereas CCL3-induced CCR5 internalisation in MCF-7 cells is not dependent of clathrin (**Table 4.3**). Whether CCR5 is internalised via caveolae-dependent pathway needs to be confirmed by other approaches as mentioned above. Also, further investigations on CXCR4 internalisation in MCF-7 cells should be done due to non-specific effects of the inhibitors used in our study.

Particularly, CCR5 internalisation has extensively investigated by previous studies. Studies from our group using the same experimental approach revealed that CCL3-induced CCR5 internalisation in Chinese Hamster Ovary (CHO) cells transfected with pcDNA3 encoding CCR5 (CHO.CCR5) is caveolae-dependent (Mueller et al., 2002; Cardaba et al., 2008). Another study demonstrated that caveolae is involved in CCR5 internalisation following CCL5 stimulation for HeLa cells transfected with CCR5 (Venkatesan et al., 2003). Yet, a controversial finding from another literature showed that CCL5-induced CCR5 internalisation is clathrin-dependent instead (Signoret et al., 2005). However, different cell lines and experimental approaches were used in that study.

The controversial findings imply that several factors might affect the effects of caveolae or clathrin observed in receptor internalisation, including cell types, ligand types and concentrations, experimental approaches and receptor expression in cells. First, different cell types might utilise caveolae for chemokine receptor internalisation in different ways. It is noteworthy that the dependency of caveolae for ligand binding and signalling does not reflect the necessity of caveolae in chemokine receptor internalisation for some cell types. For example, in MCF-7 cells, caveolae might be necessary for CXCL12-induced chemotaxis but less significant in CXCL12-induced CXCR4 internalisation (Mañes et al., 1999). Secondly, different ligands used might generate different results on receptor internalisation. For example, in the investigation of CCR5 internalisation in CHO cells, Mueller et al., 2002 used CCL3 while Kraft et al., 2001 used CCL5

for stimulation. Although both ligands can activate CCR5 due to the feature of redundancy in chemokine signalling, different receptor endocytic pathways might be elicited by different ligands possibly because of biased signalling. In addition, different concentrations of the ligands used might exert different effects on signalling proteins involved in receptor internalisation. A study using 50 nM CCL5 proposed that  $\beta$ -arrestins are dispensable for CCR5 internalisation (Kraft et al., 2001), whereas another study using 200 nM CCL5 reported that CCR5 is internalised in caveolae-dependent pathway (Venkatesan et al., 2003). Another critical factor affecting the experimental results is the diversity of experimental approaches across studies. In the receptor internalisation assay, the duration of inhibitor treatment or ligand stimulation vary across different studies. The incubation time might not be optimal for receptor internalisation. Also, the detection methods utilised might influence the results. Some studies utilised radiolabelling to measure the uptake of the radiolabelled chemokine (Kraft et al., 2001), whereas studies using fluorescence-based antibodies specific to chemokine receptor measure reduction of fluorescence-tagged cell surface chemokine receptors as an indicator of receptor internalisation (Mueller et al., 2002). Furthermore, some cell lines exogenously expressing chemokine receptors are commonly used in the investigation of chemokine receptor trafficking. Yet, transfection of receptors may bypass normal regulation of expression levels, leading to artefacts of overexpressed receptors (Bernhem et al., 2018). These experimental models might not accurately represent the same receptor naturally expressed in other cell lines. This could account for controversial findings relating to cell surface receptor expression.

In the involvement of adaptor proteins in receptor endocytosis, dynamin plays a critical role in detachment of membrane invaginations in both clathrin-mediated and caveolae-dependent receptor endocytosis (Nichols and Lippincott-Schwartz, 2001; Liu et al., 2010). Dynamin constitutes multiple domains, including a GTPase domain at the N terminus, a middle domain (MD), a pleckstrin homology (PH) domain, a GTPase effector domain (GED) and a prolinerich domain at the C terminus important for the interaction with other proteins containing SH3 domains (Faelber et al., 2011) (**Figure 4.27**). To date, there are three isoforms of dynamin: dynamin 1 (Dyn-1), which is brain-specific (Ferguson et al., 2007), dynamin 2 (Dyn-2), which is ubiquitously expressed in all cell types (Cook et al.,

1994) (Durieux et al., 2010), and dynamin 3 (Dyn-3) important for postsynaptic endocytosis (Lu et al., 2007). Particularly for Dyn-2, mutations are commonly found in the MD, PH and GED domains linked to the development of human diseases (Durieux et al., 2010).

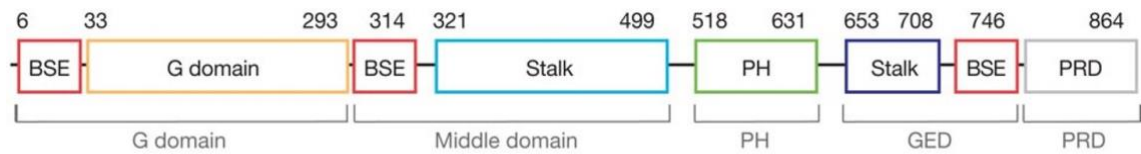


**Figure 4.23. Structure of dynamin.** Schematic diagram illustrating the multidomain structure of dynamin, constituting a GTPase domain, a middle domain, a pleckstrin homology (PH) domain, a GTPase effector domain (GED) and a prolinerich domain (PRD). BSE: bundle signalling element. (Image taken from Faelber et al., 2011)

By investigating the effects on dynamin GTPases in the process of chemokine-induced receptor internalisation, our findings revealed that Dyn-2 translocate from the periphery of the cells to the intracellular side of plasma membrane following CCL3 or CXCL12 stimulation. More significant change in localisation of Dyn-2 was seen in CXCL12 stimulation. This implies that more Dyn-2 is recruited to the membrane invaginations to aid the membrane detachment for receptor endocytosis during CXCL12-induced CXCR4 internalisation. In addition, previous literature reported that Dyn-2 is not the only adaptor protein involved in caveolae detachment. Other proteins, for example EHD2, are also found to localise at the neck of caveolae invaginations to pinch off the caveolae pit in the process of endocytosis (Morén et al., 2012). This could elucidate the relative less significant effect on Dyn-2 translocation seen in the stimulation of CCL3 that potentially mediate caveolae-dependent receptor internalisation. Yet, further investigation is needed to confirm the underlying mechanism. Furthermore, previous work done by our group showed that dynamin is involved in CCL3-induced chemotaxis but not in CXCL12-induced chemotaxis (Jacques et al., 2015). It is also noteworthy that the effect of dynamin on chemotaxis is independent of active receptor internalisation (Jacques et al., 2015). This further suggests that dynamin exhibits specific functionality for different chemokine receptor through specific signalling pathways.

Apart from dynamin,  $\beta$ -arrestins are well-known to be involved specifically in the formation of clathrin-coated pit (CCP) in receptor endocytosis. The three isoforms of  $\beta$ -arrestins have been reported to exhibit differences in functionality and localisation in cells (Ferguson, 2001; Kang et al., 2015). By overexpressing isoform-specific  $\beta$ -arrestin constructs in MCF-7 cells, our results have confirmed that arrestin-2 (also known as  $\beta$ -arrestin 1) distribute throughout the cells including the nucleus, whereas arrestin-3 (also known as  $\beta$ -arrestin 2) express in the cytoplasm only. Our observations in MCF-7 cells were consistent with other studies using other cell lines. This has proven that the distribution of  $\beta$ -arrestins is similar in different cell types under basal conditions.

With respect to the effect of chemokine stimulation on  $\beta$ -arrestin translocation, our finding demonstrated that different isoforms of  $\beta$ -arrestins have different responses to different chemokine ligands in MCF-7 cells. Following CCL3 stimulation, Arr-2 was observed to translocate to the plasma membrane, whereas no change in localisation was seen for Arr-3. Together with our findings showing that CCL3-induced CCR5 internalisation is not clathrin-dependent, this implies that the recruitment of Arr-2 to phosphorylated CCR5 possibly leading to G protein-independent signalling following CCL3 stimulation, instead of clathrin-dependent receptor internalisation. On the other hand, Arr-3 was observed to translocate towards the nucleus, but no translocation of Arr-2 was observed following CXCL12 stimulation. This implies that Arr-3 potentially is internalised together with CXCR4 through clathrin-dependent receptor internalisation pathway following CXCL12 stimulation. Also, the translocation of Arr-3 is associated with dynamin, which was confirmed by the intervention of dynamin inhibitor treatment that abolished the change in localisation of Arr-3 in MCF-7 cells. Again detailed studies should be conducted to confirm whether CXCL12-induced CXCR4 is clathrin-dependent. Also, our finding confirmed that point mutation introduced in Arr-2 construct disrupts the distribution of Arr-2 under basal condition and completely blocks CCL3-mediated Arr-2 translocation in MCF-7 cells. Further investigations are required to confirm the exact roles of Arr-2 and Arr-3 in response to CCL3 and CXCL12 stimulation respectively.

In our study, we used dynamin inhibitors to confirm the involvement of different isoforms of  $\beta$ -arrestins on clathrin-dependent receptor endocytosis. The advantage of using small molecule dynamin inhibitors over dynamin knockdown using siRNA is that the blocking effect is rapid and reversible. Small molecule inhibitors are useful tools to observe immediate cellular responses and dynamics of intracellular proteins upon the addition of stimulants. Yet, small molecule inhibitors are subject to potential limitations, such as cytotoxicity, non-specific effects and poor cell permeability. Although we have eliminated the cytotoxic effects of the inhibitors (**Figure A4**), some non-specific effects from Dynasore in our experiments were observed. A slight change in Arr-2 and Arr-3 distribution was seen under basal conditions in Dynasore-treated cells, which might not be beneficial for long-term exposure studies. In many studies, detergents are routinely used to minimise the non-specific effects of dynamin inhibitors. Inhibitors prone to the formation of aggregates, like Dynasore, might potentially adsorb onto the surface of other proteins or incorporate other proteins within them, leading to promiscuous inhibition other than target proteins (Ryan et al., 2003). However, caution should be taken when using Dynasore. A study reported that Dynasore binds stoichiometrically to detergents, leading to a significant reduction in potency. Yet, the improved design of Dyngo-4a has been proven to effectively minimise detergent binding. Thus, it is suggested to use Dyngo-4a in the study of dynamin in receptor endocytosis if addition of detergent is required in the experimental setting for minimising non-specific effects.

Our findings provide a brief insight into cell-specific and ligand-specific roles of clathrin and caveolae in chemokine-induced receptor internalisation, as well as isoform-specific functions of  $\beta$ -arrestins and dynamin. However, further experiments on visualising receptor uptake and trafficking needs to be conducted to confirm our findings and understand the underlying mechanisms in more depth. Human transferrin receptor (hTf-R) is a commonly used marker for the clathrin-mediated endocytosis (Signoret et al., 2005). By overexpressing the hTf-R in cells, the uptake of fluorescent transferrin can be visualised. If the internalisation of ligand-activated fluorescent-labelled receptor and uptake of fluorescent transferrin is observed simultaneously, it indicates that receptor internalisation is dependent of clathrin (Signoret et al., 2005).

In the past, most studies investigating caveolae-dependent endocytosis used cholera toxin and simian virus 40 as standard cargos (Tagawa et al., 2005). However, these cargos are not specifically internalised by caveolae. Unlike clathrin-mediated endocytosis, there is no caveolae-specific marker or cargo identified so far (Parton et al., 2020a). Thus, it has been challenging to monitor the process of caveolae-dependent endocytosis. Another common approach is overexpression of caveolar proteins, such as caveolin and cavin (Liu and Pilch, 2016; McMahon et al., 2019). Yet, the trafficking of the overexpressed caveolar protein observed could not generally be dictated by caveolae endocytosis. The mobilisation of the overexpressed proteins could also indicate translocation of intracellular caveolin and cavin, which are not associated with caveolae (Pol et al., 2020). In addition, a recent study has been conducted to assay caveolae dynamics by comparing caveolin overexpressed cells with genome-edited caveolin cell lines (Shvets et al., 2015). It was found that caveolin overexpression is more likely to result in accumulation of caveolin in late endosomes, whereas most caveolin proteins localised at the plasma membrane were observed in genome-edited caveolae cell lines (Shvets et al., 2015). Due to the artifacts from the approach of caveolae overexpression, the mechanisms proposed by those studies should be evaluated and re-visited with care.

In the advances of imaging techniques, emerging studies use dual colour total internal reflection fluorescence microscopy (TIR-FM) to visualise the spatial and temporal organisation of multiple components in clathrin-dependent receptor endocytosis (Taylor et al., 2011). A cohort of endocytic proteins recruited at different stages of the scission event can also be quantified using cluster analysis of protein recruitment signatures. Same for the investigation on clathrin-dependent endocytic pathway, TIR-FM is also commonly used to visualise caveolae trafficking (Senju and Suetsugu, 2020). However, since the resolution of TIR-FM is limited to 200 nm of the plasma membrane, deeper caveolar events might not be visualised (Matthaeus and Taraska, 2021). The resolution issues have been resolved by the latest imaging techniques. Electron microscopy, electron tomography (Popescu et al., 2006; Hubert et al., 2020) and even some super resolution imaging techniques, such as Stochastic Optical Reconstruction microscopy (STORM), Structured-illumination Microscopy (SIM) and Stimulated Emission Depletion (STED) microscopy (Platonova et al., 2015; Yeow et al.,

2017; Khater et al., 2018), have been utilised to visualise caveolar vesicles in three-dimensional arrangement. Specifically with the application of STED and SIM microscopy, single caveolae can be tracked throughout single live cell, which is useful in the study of intracellular trafficking (Khater et al., 2018). Ultimately, previous unsolved questions, including how the mechanisms underlying caveolae scission and trafficking pathways through ER and mitochondria can be elucidated by the application of the advanced imaging techniques in the near future.

#### **4.5 Chapter conclusions**

The final conclusions to be drawn from this chapter are:

1. CXCL12 stimulation induces translocation of caveolin-1 (Cav-1) towards the leading edge of MCF-7 cells, but not significantly affects the expression level of Cav-1.
2. CXCL12-induced CXCR4 internalisation is caveolae-dependent in Jurkat cells.
3. CCL3-induced CCR5 internalisation in MCF-7 cells is not dependent of clathrin.
4. Pitstop 2, a clathrin inhibitor, is found to have non-specific effects that specifically interfere CXCR4 internalisation.
5. Dynamin plays a significant role in CXCL12-induced CXCR4 internalisation, but less significant in CCL3-induced CCR5 internalisation in MCF-7 cells. Other adaptor proteins might be involved in CCL3-induced CCR5 endocytosis in MCF-7 cells.
6. In MCF-7 cells, under basal conditions, arrestin-2 (also known as  $\beta$ -arrestin 1) is distributed throughout the cells, including the nucleus, whereas arrestin-3 (also known as  $\beta$ -arrestin 2) is expressed exclusively in the cytoplasm.
7. Arr-2 constructs translocate from the nucleus to the plasma membrane specifically in response to CCL3 stimulation in MCF-7 cells
8. Arr-3 constructs translocate towards the nucleus dependent of dynamin following CXCL12 stimulation in MCF-7 cells.

It should be noted that the mechanisms underlying CCL3-induced CCR5 internalisation and CXCL12-induced CXCR4 internalisation in MCF-7 cells are inconclusive from our findings due to the limitations of our methodology. Further investigations should be conducted as described in the discussion section.

**Table 4.3. Summary of the experimental approaches used and extent of receptor internalisation in MCF-7 and Jurkat cells**

| <b>Chemokine receptors</b> | <b>Endogenous / Exogenous expression</b> | <b>Cell lines</b> | <b>Ligands (concentration)</b> | <b>Ligand stimulation duration</b> | <b>Detection methods</b> | <b>Percentage of receptors internalised*</b> |
|----------------------------|--|-------------------|--------------------------------|------------------------------------|--------------------------|--|
| CCR5                       | Endogenous                               | MCF-7             | CCL3 (100 nM)                  | 30 mins                            | FACS                     | 34.2%  |
| CXCR4                      | Endogenous                               | MCF-7             | CXCL12 (50nM)                  | 30 mins                            | FACS                     | 24.6%  |
|                            | Endogenous                               | Jurkat            | CXCL12 (50nM)                  | 30 mins                            | FACS                     | 49.9%  |

\*Percentage of receptors internalised (%) = 100 – percentage of receptor expression on cell surface following chemokine stimulation (see **Table 4.2**).

**Table 4.4. Summary of the involvement of intracellular proteins in receptor internalisation in MCF-7 and Jurkat cells**

| <b>Chemokine receptor internalisation</b> | <b>Cell lines</b> | <b>Caveolae-dependent?</b>   | <b>Clathrin-dependent?</b>             | <b>Involvement of dynamin?</b>             | <b>Involvement of <math>\beta</math>-arrestin isoforms</b>                  | <b><math>\beta</math>-arrestin translocation associated with dynamin?</b> |
|---|-------------------|--|--|--|---|---|
| <b>CCR5 internalisation</b>               | MCF-7             | Inconclusive<br>(Trend of inhibition by caveolae-depleting agents) | No                                     | Yes  | Arr-2<br>(Potentially involved in G protein-independent signalling)*        | No  |
| <b>CXCR4 internalisation</b>              | MCF-7             | Inconclusive<br>(Non-specific effects)                             | Inconclusive<br>(Non-specific effects) | Yes<br>(More significant in translocation) | Arr-3<br>(Potentially involved in clathrin-dependent receptor endocytosis)* | Yes   |
|   | Jurkat            | Yes  | Inconclusive<br>(Non-specific effects) | Not investigated                           | Not investigated**  | Not investigated**  |

\* Further investigations are necessary to confirm the potential roles of  $\beta$ -arrestins stated.

\*\* Attempts on electroporation transfection of  $\beta$ -arrestins have been conducted in Jurkat cells but it was not successful.

# Chapter 5: The roles of protein kinase D (PrKD) in regulating chemokine-induced cellular responses

---

## 5.1 Introduction

Protein kinase D (PrKD) is a family of conserved serine/threonine kinases and a part of the  $\text{Ca}^{2+}$ /calmodulin superfamily (Rozengurt et al., 2005). In canonical signalling pathway, a variety of stimuli, such as growth factors, hormones and phorbol esters, are involved in PrKD activation through diacylglycerol (DAG) and classical or novel protein kinase C (cPKC or nPKC) (Rozengurt et al., 2005; Wang, 2006). Based on the sequence homology of PrKD, there are three isoforms that have been discovered: PrKD1, PrKD2 and PrKD3 (Manning et al., 2002; X. Zhang et al., 2021). The three isoforms are localised in the cytoplasm basally, however, they translocate to various subcellular locations upon activation, such as nucleus, mitochondria and cytoplasm. In terms of functionality, it is well documented that PrKD takes a major part in regulating a variety of biological processes that contribute to cancer development and progression. The cellular processes involved by PrKD include cell proliferation, cell survival, epithelial-to-mesenchymal transition (EMT), cell migration and invasion and angiogenesis (Fu and Rubin, 2011). Accumulating evidence has revealed that PrKD functions in an isoform-specific manner, acting as a positive or negative regulator in cancer (Roy et al., 2017).

For example, in breast cancer cells, PrKD3 is known to be associated with the invasiveness of breast cancer (Borges et al., 2015). Mechanistically, the oestrogen receptor (ER) binds directly to the PrKD3 gene promoter and subsequently inhibit PrKD3 expression. Hence, PrKD3 is highly upregulated in ER-negative breast cancer, contributing to increased cell proliferation, migration, and invasion (Borges et al., 2015). Furthermore, PrKD2 is also found to positively regulate cell proliferation and migration in cancer (X. Zhang et al., 2021). In triple-negative breast cancer (TNBC), both PrKD2 and PrKD3 are preferentially expressed (Liu et al., 2019). In brief, PrKD1 generally functions as tumour

suppressor by negatively regulating tumour-promoting proteins, such as SNAIL (Zheng et al., 2014), SSH1L (Niwa et al., 2002) and cortactin (Eiseler et al., 2007), and positively regulating tumour-suppressing proteins, such as PAK4 (Spratley et al., 2011), RIN1 (Ziegler et al., 2011) and E-cadherin (Du et al., 2009; Jaggi et al., 2005). On the other hand, as positive regulators in cancer, PrKD2 and PrKD3 are involved in the activation of tumour-promoting pathways, including NF- $\kappa$ B activation (Zou et al., 2012), PAK/LIMK signalling (Döppler et al., 2014) and MMP activation (Wille et al., 2014).

Many cellular studies have investigated the interactions of PrKD with target substrates contributing to a variety of biological processes in cancer and uncovered some isoform-specific roles of PrKD in different cancer types (Roy et al., 2017). Yet, precise molecular cues that direct PrKD to regulate downstream substrates are not sufficiently studied. Therefore, we set out to investigate the involvement of PrKD in chemokine signalling using small molecule inhibitors targeting PrKD and unveil the potential roles of PrKD in chemokine-induced cellular responses, including calcium mobilisation, chemotaxis, actin cytoskeletal rearrangement and receptor internalisation. We also attempted to knock down PrKD2 specifically using transfection of plasmid DNA containing a PrKD2 shRNA insert for future studies on isoform-specific roles of PrKD.

## 5.2 Chapter aims

**Hypothesis:** We hypothesised that PrKD is activated through DAG or directly activated by PKC following chemokine stimulation, and subsequently mediates a diversity of cellular responses that could promote or suppress cancer cell migration.

**Aims:** The aim of this chapter is to examine the roles of PrKD in chemokine-stimulated cellular responses in cancer cell lines, including Ca<sup>2+</sup> mobilisation, chemotaxis, actin cytoskeletal rearrangement and receptor internalisation.

## 5.3 Results

### 5.3.1 Protein kinase D (PrKD) inhibitors reduce intracellular Ca<sup>2+</sup> release induced by CCL3 and CXCL12 in MCF-7 cells, while PrKD inhibitors reduce intracellular Ca<sup>2+</sup> release mediated by CCL3 but not CXCL12 in THP-1 cells.

Intracellular Ca<sup>2+</sup> is a key signalling transducer in downstream signalling as a part of chemokine signalling pathway via activated phospholipase C (PLC). Evidence showed that PLC activation leads to protein kinase C (PKC) activation (McLaughlin et al., 2002). As PrKD is activated by PKC, PrKD also acts as a downstream effector in the PLC-dependent pathway. Although no evidence shows that PKC and PrKD have a direct effect on intracellular Ca<sup>2+</sup> release, PrKD could potentially be involved in regulating intracellular Ca<sup>2+</sup> mobilisation as a positive or negative feedback loop to amplify or diminish Ca<sup>2+</sup> response activated by DAG.

To determine the roles of PrKD in chemokine signalling involving Ca<sup>2+</sup> release, we examined the effects of the PrKD inhibitors, CID755673 and CID2011756, on chemokine induced intracellular Ca<sup>2+</sup> release using Ca<sup>2+</sup> flux assay. CID2011756 is the analogue of CID755673. Both inhibitors act on all three isoforms of PrKD.

According to our results from the cytotoxicity test using MTS assay, CID755673 exhibit a trend of cytotoxicity in MCF-7 cells (**Figure A5**). As our group previously used 10 µM CID755673 to study the effects of PrKD on cellular responses in Jurkat and THP-1 cells (Mills, PhD dissertation, 2018), our results from MTS assay have confirmed that no cytotoxicity was observed in Jurkat and THP-1 cells at 10 µM (**Figure A6**). Another PrKD inhibitor, CID2011756, demonstrates some extent of cytotoxicity in both MCF-7 and MDA-MB-231 cells, while no cytotoxicity was seen in Jurkat and THP-1 cells (**Figure A7**). Using Trypan blue exclusion method as a validation for the MTS assay, an observable reduction in cell viability was seen in MCF-7 and MDA-MB-231 cells treated with CID2011756 in a concentration range from 5 µM to 20 µM following 72 hours incubation (**Figures A8 and A9**). Although there was still a small proportion of dead cells indicated by the trypan blue dye in cells treated with 2.5 µM CID2011756 (**Figures A8 and A9**), the cytotoxicity effect should be minimal in 30 minutes incubation time for

most of our experimental assays. Using 1  $\mu\text{M}$  CID2011756 might not be sufficient to inhibit PrKD as the IC<sub>50</sub> values targeting the three PrKD isoforms are between 0.6  $\mu\text{M}$  and 3.2  $\mu\text{M}$  (**Table 2.3**). By considering the balance of cytotoxicity and potency of CID755673 and CID2011756, we decided to use 2.5  $\mu\text{M}$  for MCF-7 and MDA-MB-231 cells and 10  $\mu\text{M}$  for Jurkat and THP-1 cells as assay concentration of both PrKD inhibitors.

Cells were pre-treated with CID755673 or CID2011756 for 30 minutes, followed by incubation with Fura-2 AM for another 30 minutes. Change in intracellular Ca<sup>2+</sup> level before and after CCL3 (200 nM) or CXCL12 (20 nM) stimulation was measured in real time. The principles behind Ca<sup>2+</sup> flux assay used in our study has been detailed in **Section 3.3.2**.

Our results showed that both PrKD inhibitors significantly reduce intracellular Ca<sup>2+</sup> release in the stimulation of CCL3 in THP-1 cells, whereas less significant reduction was observed in MCF-7 cells (**Figure 5.1**). Particularly for the observed effects of CID2011756 in MCF-7 cells, although the change in intracellular Ca<sup>2+</sup> level in post-CCL3 stimulation is lower in comparison to control without inhibitor treatment, but is not statistically significant, as seen from the representative trace of intracellular Ca<sup>2+</sup> release level (**Figure 5.1**). It should be noted that the concentration used in MCF-7 cells was 2.5  $\mu\text{M}$ , which is lower than the IC<sub>50</sub> for PrKD1 inhibition (3.2  $\mu\text{M}$ ) from the literature, due to the cytotoxicity of CID2011756 in MCF-7 cells (**Figures A7 and A8**). The assay concentration might not be high enough to particularly inhibit PrKD1 in MCF-7 cells. This might explain insignificant effects of CID2011756 on Ca<sup>2+</sup> response in MCF-7 cells observed in our study. Thus, PrKD, particularly PrKD1, is potentially involved in CCL3-induced intracellular Ca<sup>2+</sup> release. Yet, further investigations are necessary to confirm the exact roles of PrKD in regulating intracellular level of Ca<sup>2+</sup>.

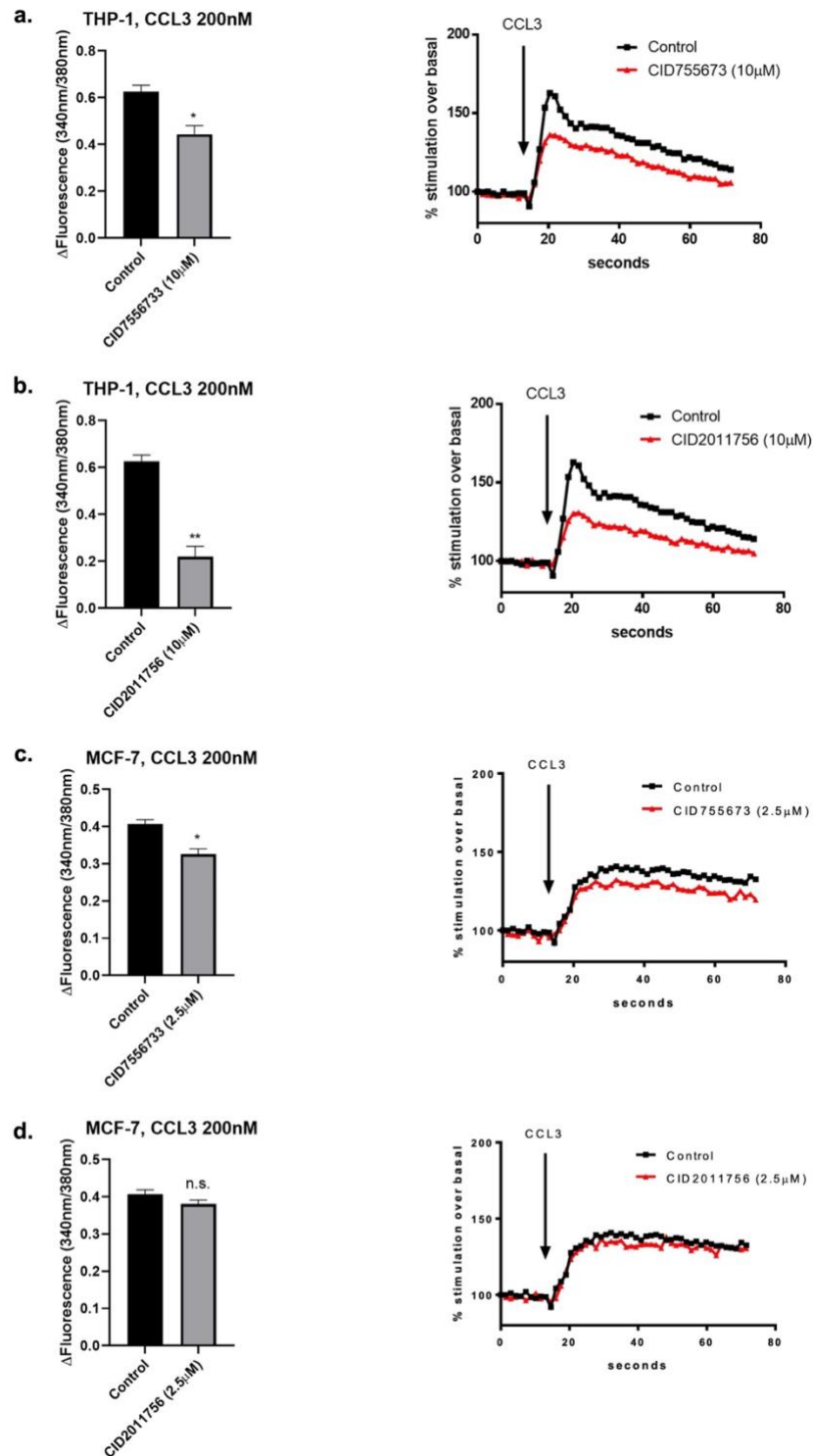


**Figure 5.1. CCL3-induced  $\text{Ca}^{2+}$  response was reduced when treated with PrKD inhibitors in both THP-1 and MCF-7 cells.** (a, b) THP-1 and (c, d) MCF-7 cells were pre-treated with PrKD inhibitors (CID755673 and CID2011756) respectively and stimulated with CCL3 (200 nM). (Left) Bar charts showing data expressed as change in fluorescence ratio (340 nm/380nm) between peak fluorescence after CCL3 and basal fluorescence before CCL3 stimulation. (Right) Representative traces of real-time

intracellular  $\text{Ca}^{2+}$  release level in the response to CCL3 stimulation. Data represent mean  $\pm$  SEM from at least 3 independent experiments. Unpaired t-test as post-hoc test, \* =  $p \leq 0.05$ , \*\* =  $p \leq 0.01$ .

In respect to CXCL12-induced intracellular  $\text{Ca}^{2+}$  mobilisation, a trend of increased intracellular  $\text{Ca}^{2+}$  release was observed in THP-1 cells pre-treated with both PrKD inhibitors, but the effect was not significant, as shown in **Figure 5.2**. On the other hand, in MCF-7 cells, a reduction in intracellular  $\text{Ca}^{2+}$  release was seen in the treatment of both PrKD inhibitors (**Figure 5.2**). Same as the phenomenon seen in CCL3-induced  $\text{Ca}^{2+}$  responses, less significant effects were observed in CID2011756-treated MCF-7 cells (**Figure 5.2**) due to relatively low concentration of the inhibitor used.

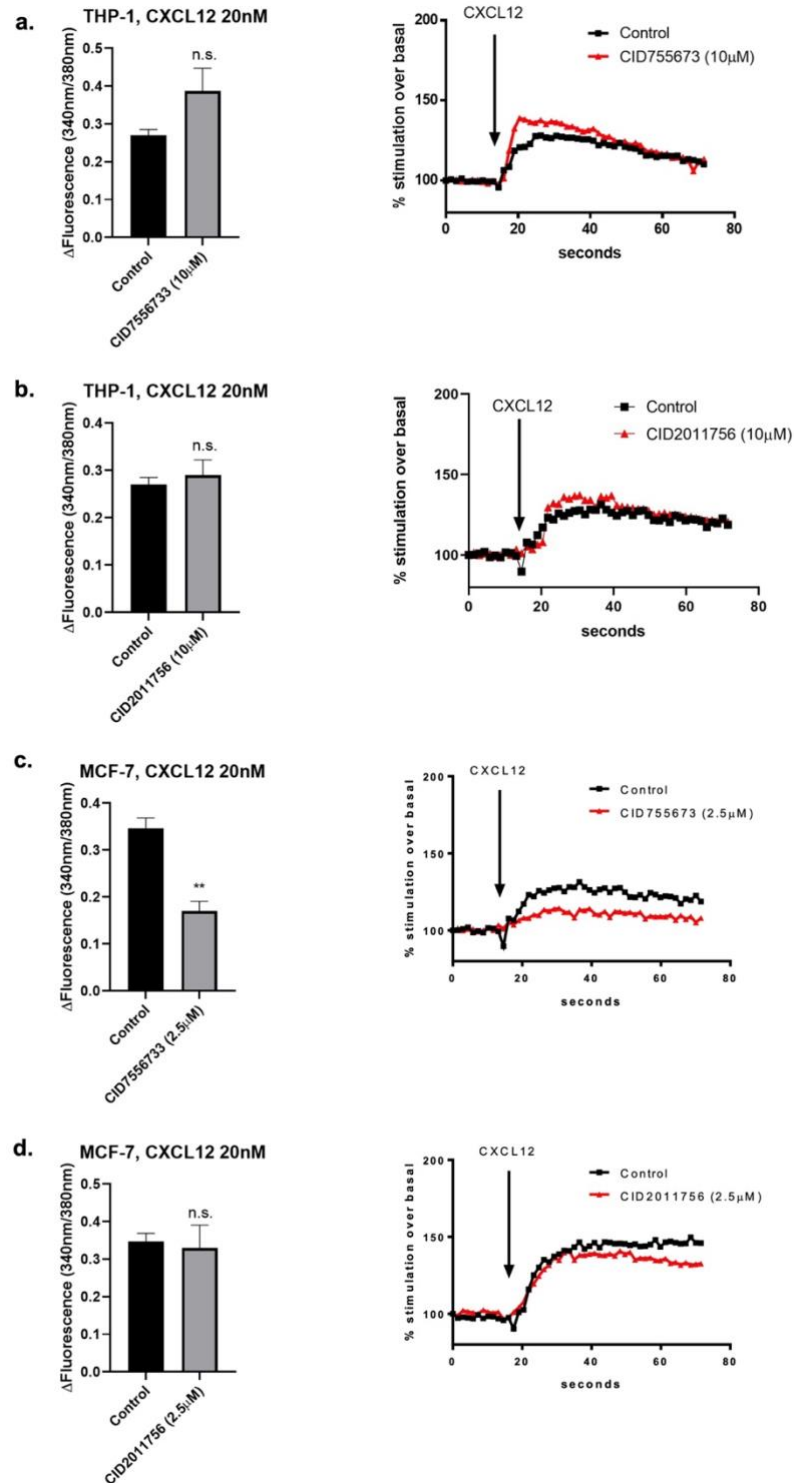


**Figure 5.2. CXCL12-induced  $\text{Ca}^{2+}$  response was reduced by the treatment of PrKD inhibitors in MCF-7 cells, but an opposing effect was seen in THP-1 cells.** (a, b) THP-1 and (c, d) MCF-7 cells were pre-treated with PrKD inhibitors (CID755673 and CID2011756) respectively and stimulated with CXCL12 (20 nM). (Left) Bar charts showing data expressed as change in fluorescence ratio (340 nm/380nm) between peak fluorescence after CXCL12 and basal fluorescence before CXCL12

stimulation. (Right) Representative traces of real-time intracellular  $\text{Ca}^{2+}$  release level in the response to CXCL12 stimulation from at least three independent experiments. Data represent mean  $\pm$  SEM from at least 3 independent experiments (bar charts). Unpaired t-test as post-hoc test, \*\* =  $p \leq 0.01$ , n.s. = not significant.

### **5.3.2 PrKD inhibitors significantly block chemotaxis driven by CXCL12 stimulation in both Jurkat and THP-1 cells.**

In the link of PrKD in cell migration, as reviewed previously in **Section 1.4.5**, several substrates of PrKD are involved in cell migration, such as SSH1L, cortactin, PAK4 and RIN1. Some of these substrates promote cell migration, while some suppress cell migration. Through phosphorylation by PrKD, target substrates can either be activated to mediate downstream signalling or inactivated by binding to 14-3-3 proteins for degradation. Hence, PrKD has been thought to regulate cell migration in an isoform-specific manner by interacting with cell migration promoters or suppressors. Whether PrKD has a role in chemokine signalling contributing to chemotaxis is yet to be elucidated.

In our study, the involvement of PrKD in CXCL12-induced chemotaxis in two leukemic cancer cell lines, Jurkat and THP-1 cells, was examined based on our chemotaxis assay using ChemoTx plate as described in **Section 3.3.4**. Cells were pre-treated with the PrKD inhibitors, CID755673 and CID2011756 respectively, for 30 minutes before being seeded onto the porous membrane of the ChemoTx plate, where the bottom compartment contains CXCL12. The plate was incubated at 37°C for 4 hours to allow chemotaxis to take place.

**Figure 5.3** illustrates that the number of migrating cells towards CXCL12 is significantly reduced in Jurkat and THP-1 cells pre-treated with CID755673 or CID2011756, compared to untreated controls. For THP-1 cells, trace amounts of cells ( $< 100,000 \text{ cells mL}^{-1}$ ) were observed to migrate towards the bottom compartment in the absence of CXCL12 in basal controls with or without treatment of the inhibitors. This could be explained by the small cell size of THP-1. As we used the same set of ChemoTx plate with the same pore sized ( $5 \mu\text{m}$ ) membrane for both cell lines, THP-1 cells with smaller cell size might possibly fall

through the pores due to mechanical movements during the experiment, leading to false positive effects. However, the false positive effects cause minimal impact without overriding the difference seen in chemokine-stimulated samples.

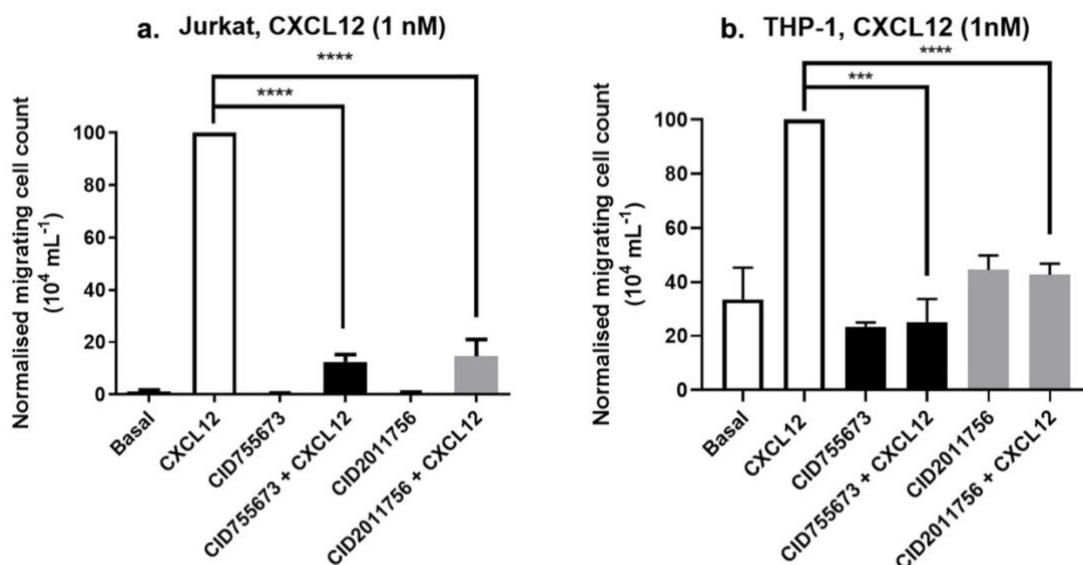


**Figure 5.3. A significant reduction in the number of cells migrating towards CXCL12 was observed in Jurkat and THP-1 cells treated with PrKD inhibitors, CID755673 and CID2011756, in the chemotaxis assay.** (a) Jurkat and (b) THP-1 cells were pre-treated with CID755673 (10  $\mu\text{M}$ ) or CID2011756 (10  $\mu\text{M}$ ) respectively or without treatment of inhibitor as untreated control. Cells were seeded onto the membrane above the bottom compartment containing CXCL12 (1 nM) or serum-free media only (for basal controls) in the ChemoTx plate. The plate was incubated at 37°C for 4 hours. Data is expressed as the number of cells in the bottom compartment after 4-hour incubation. Data shown represent the mean  $\pm$  SEM of 3 independent experiments. (One-way ANOVA with a Dunnett's multiple comparisons test as post-hoc test, \*\* =  $p \leq 0.01$ , \*\*\* =  $p \leq 0.001$ )

### **5.3.3 Protein kinase D (PrKD) inhibitors cause elongated morphology with increased cell surface area in MCF-7 cells alone in the absence of chemokine stimulation.**

As a role of negative regulator in cell migration, PrKD has been shown to interact with multiple substrates that regulate actin cytoskeletal rearrangement. To date, two major mechanisms involving PrKD in actin cytoskeletal remodelling have been proposed: (1) PrKD has been found to be co-localised with the cortical actin network to stabilise proteins involved in the formation of lamellipodia and filopodia selectively at the leading edge of migrating cells tail (Eiseler et al., 2007). (2) PrKD directly phosphorylate SSH1L, leading to inactivation of the signalling network of cofilin. Consequently, both mechanisms inhibit actin nucleation and actin polymerisation, leading to a reduction in migratory potential of cells (Borges et al., 2015; Peterburs et al., 2009).

Our study investigated the effects of PrKD inhibition on chemokine-induced actin cytoskeletal rearrangement in MCF-7 cells.

In **Figure 5.4**, compared to the control without inhibitor treatment, MCF-7 cells pre-treated with CID755673 or CID2011756 appeared to be elongated even without CCL3 or CXCL12 stimulation. The cell morphology of PrKD inhibitor-treated MCF-7 cells is similar to cells stimulated with CCL3 or CXCL12, which is more spreading. With respect to actin cytoskeleton structures, increased formation of lamellipodia and filopodia at the leading edge and more stress fibres at the tail were observed in the treatment of PrKD inhibitors, same as cells in the stimulation of CCL3 or CXCL12 (**Figure 5.4**). Owing to the effect of PrKD inhibitors on actin cytoskeletal rearrangement, there was no observable difference between cells treated with PrKD inhibitors alone and cells treated with PrKD inhibitors followed by CCL3 or CXCL12 stimulation (**Figure 5.4**). The observations are supported by the quantification analysis based on phalloidin-stained F-actin showing that a significant increase in cell area but a significant decrease in circularity was seen in MCF-7 cells treated with PrKD inhibitor in the absence of chemokine stimulation (**Figure 5.5**). This implies that inhibition of PrKD induces more spreading in cell morphology with increased formation of lamellipodia, filopodia and stress fibre in MCF-7 cells. These features potentially

favour cell migration potential. Yet, the exact roles of PrKD in chemokine-induced actin cytoskeletal change remains to be elusive due to potential synergistic effects.

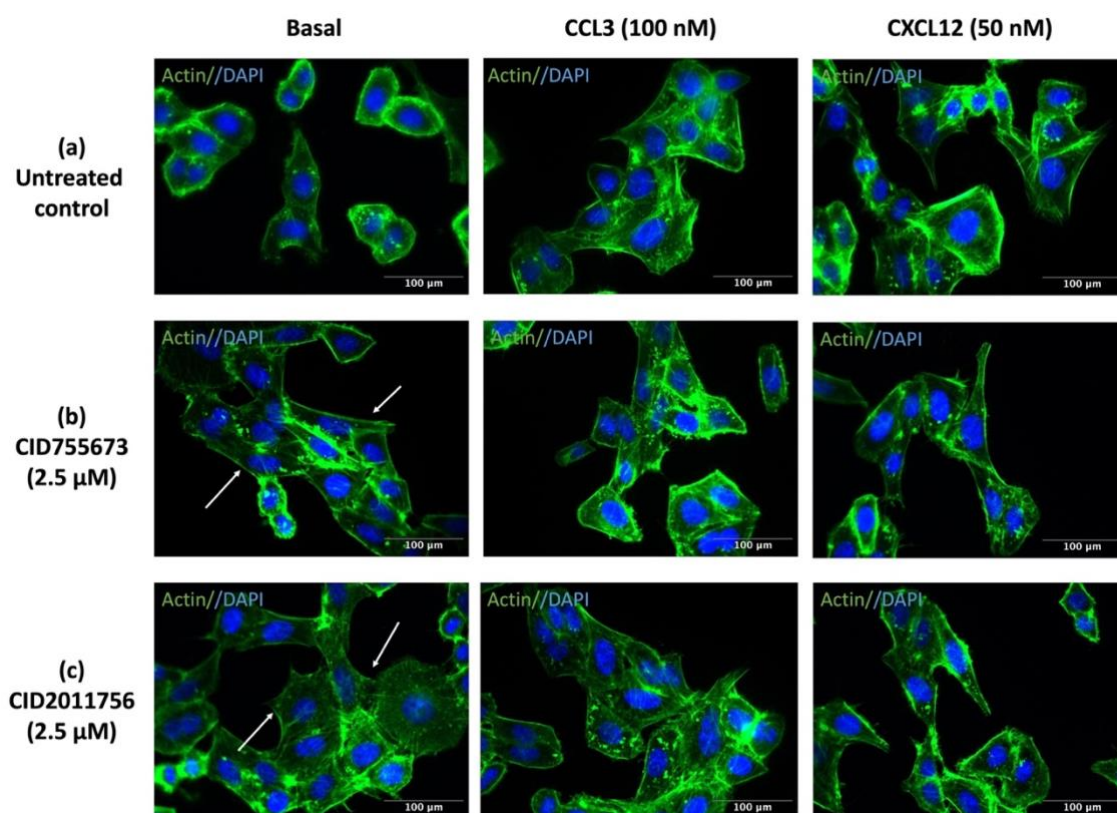
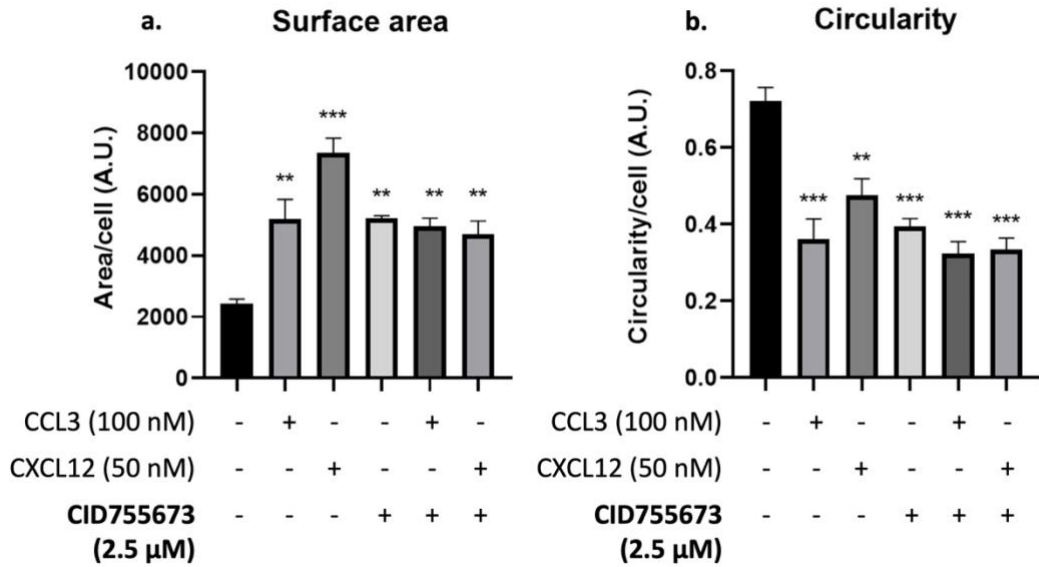


**Figure 5.4. MCF-7 cells appear to be more elongated and spreading in the treatment of PrKD inhibitor, CID755673 or CID2011756, in the absence of chemokine stimulation.** Cells were either (a) stimulated with CCL3 (100 nM) or CXCL12 (50 nM) for 30 minutes without inhibitor treatment, or pre-treated with PrKD inhibitors, (b) CID755673 (2.5  $\mu$ M) or (c) CID2011756 (2.5  $\mu$ M) for 30 minutes prior to chemokine stimulation for another 30 minutes. Cells were then fixed, permeabilised and stained with Alexa Fluor™ 488 Phalloidin (green) for F-actin cytoskeleton and DAPI (1:1000) (blue) for cell nuclei. Elongated cells treated with CID755673 or CID2011756 in the absence of chemokine stimulation were annotated by white arrows. Representative images from at least 3 independent experiments were acquired with a Leica DMII Fluorescence microscope using 31.5X magnification.

### CID755673



### CID2011756

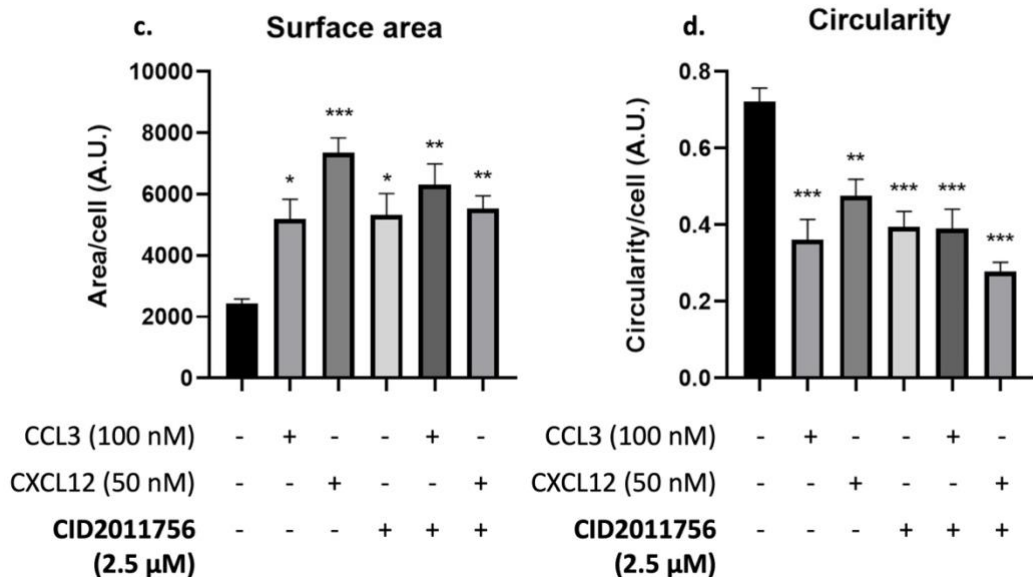


**Figure 5.5. PrKD inhibitors, CID755673 and CID2011756, induce a significant increase in cell surface area and a significant reduction in cell circularity, similar to the effects of CCL3 and CXCL12 stimulation in MCF-7 cells.** (a, b) Cell surface area and cell circularity per a single cell treated with 2.5 μM CID755673 followed by stimulation of 100 nM CCL3 or 50 nM CXCL12. (c, d) Cell area and cell circularity per a single cell treated with 2.5 μM CID2011756 followed by stimulation of 100 nM CCL3 or 50 nM CXCL12. At least 10 cells were analysed per experiment. Identical microscopic settings (image size, 2592 x 1944 pixel and 414.72 x 311.04

µm) were applied. Data shown represent the mean ± SEM of 3 independent experiments. Data were compared in relation to cells without inhibitor treatment or chemokine stimulation (One-way ANOVA with a Dunnett's multiple comparisons test as post-hoc test, \*\* =  $p \leq 0.01$ , \*\*\* =  $p \leq 0.001$ ).

#### **5.3.4 ROCK inhibitor, Y27632, disrupts the organisation of actin cytoskeleton, while Arp2/3 inhibitor, CK666, prevents the formation of lamellipodia and filopodia in MCF-7 cells stimulated with CCL3 or CXCL12.**

To further investigate whether PrKD also interact with other critical proteins involved in actin cytoskeleton rearrangement, we conducted a preliminary experiment to examine the effects of inhibition of Rho kinase (ROCK) and Arp2/3 complex on actin cytoskeleton rearrangement in the stimulation of CCL3 or CXCL12 only. ROCK is responsible for the formation of stress fibres at the contractile tail of migrating cells (Narumiya et al., 2009), whereas Arp2/3 complex is important for actin polymerisation in the formation of lamellipodia and filopodia at the leading edge of migrating cells (Mattila and Lappalainen, 2008). We used two small molecule inhibitors, Y27632 and CK666, to target ROCK and Arp2/3 complex respectively.

Y27632 is a pan-ROCK inhibitor that inhibits the two isoforms of ROCK (ROCK1 and ROCK2) (Shi et al., 2013) (**Figure 5.6**). Previous literature reported that Y27632 at 10 µM alters cell shape and disrupt the stability of stress fibres with increased cellular permeability (Rao et al., 2001; Shi et al., 2013). CK666 is an inhibitor targeting the Arp2/3 complex (**Figure 5.6**). A structural basis study has proposed that CK666 binds to the interface of Arp2 and Arp3 to stabilise the inactive conformation, which prevent F-actin and actin monomers from binding to the Arp2/3 complex. As a result, polymerisation of actin by Arp2/3 is inhibited (Hetrick et al., 2013).

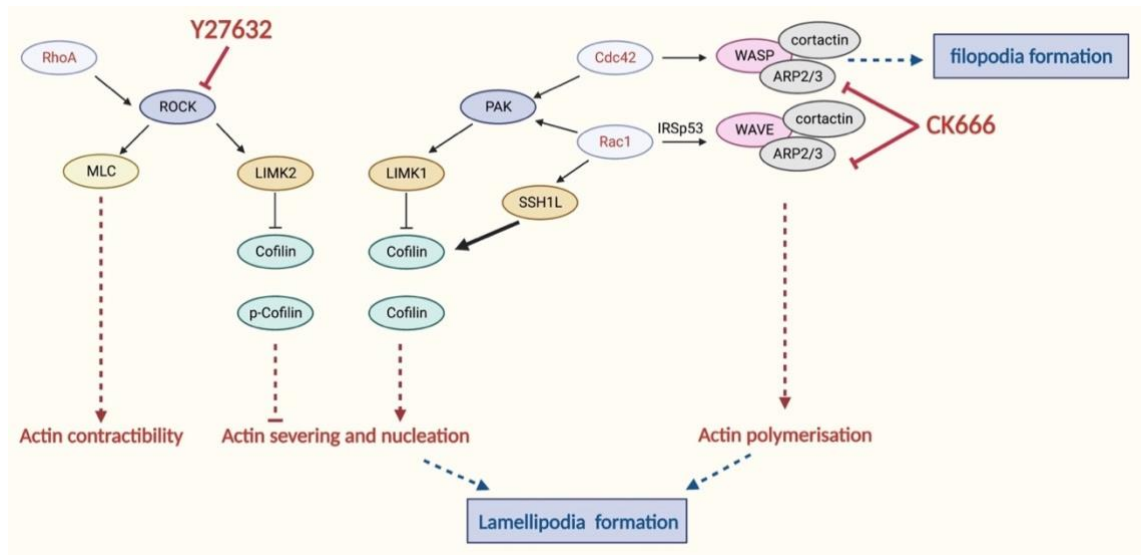


**Figure 5.6. Signalling mechanisms in the regulation of actin cytoskeleton network.** Two inhibitors were indicated at the positions where the targets of inhibition are located in the schematic diagram above (in red). Y27632 is an inhibitor targeting ROCK leading to stress fibre instability (Shi et al., 2013), while CK666 is an inhibitor targeting Arp2/3 leading to inhibition of actin polymerisation (Hetrick et al., 2013) (Image created with BioRender.com).

As previous study from our group investigating CCR5 internalisation and recycling using Y27632 at 20  $\mu$ M (Mueller and Strange, 2004), we confirmed that 20  $\mu$ M Y27632 does not cause any cytotoxicity in MCF-7 cells (**Figure A10**). For CK666, 10  $\mu$ M was used to block Arp2/3 in the investigation of F-actin remodelling by our group (Keil, PhD dissertation, 2019) and the  $IC_{50}$  of CK666 is 4  $\mu$ M for targeting Arp2/3 as stated by Nolen et al., 2009. As shown in **Figure A11**, 10  $\mu$ M CK666 causes no cytotoxicity in MCF-7 cells. Hence, our study used Y27632 at 20  $\mu$ M for targeting ROCK and CK666 at 10  $\mu$ M for targeting Arp2/3 to determine the roles of ROCK and Arp2/3 in actin cytoskeletal remodelling and its association with PrKD.

When treated with Y27632, in the absence of chemokine stimulation under basal condition, F-actin appeared to be ruffling at the tail of the cells, mostly accumulating at the periphery of MCF-7 cells (**Figure 5.7**). In CCL3 or CXCL12-stimulated MCF-7 cells, ruffling and clusters of the stress fibre at the contractile tail was seen although cells still appear to be elongated by the effect of

chemokine stimulation (**Figure 5.7**). This implies that inhibition of ROCK by Y27632 disrupts the organisation of actin cytoskeletal network, contributing to change in cell morphology. In the stimulation of CCL3 or CXCL12, ROCK inhibition only affects the formation of stress fibres at the contractile tail but not impact the formation of lamellipodia and filopodia at the leading edge. In the comparison between chemokine-stimulated cells with Y27632 treatment and without inhibitor treatment, there was a significant reduction in cell surface area but the change in circularity was not significant (**Figure 5.8**).

When treated with CK666, cell morphology was observed to be less spreading in unstimulated cells compared to that without inhibitor treatment (**Figure 5.7**). Also, F-actin was found to translocate and accumulate towards the periphery of the cells (**Figure 5.7**). In both CCL3 and CXCL12-stimulated cells, less elongated cell morphology was observed, and the formation of lamellipodia and filopodia was less distinctive compared to cells without inhibitor treatment (**Figure 5.7**). In the comparison between chemokine-stimulated cells with CK666 treatment and without inhibitor treatment, significant reduction in cell surface area and increase in circularity was seen (**Figure 5.8**). This implies that inhibition of Arp2/3 by CK666 inhibits actin severing and nucleation, leading to accumulation of F-actin at the periphery of the cells. CK666 also blocks actin polymerisation mediated by CCL3 or CXCL12, resulting in reduced formation of lamellipodia and filopodia at the leading edge.

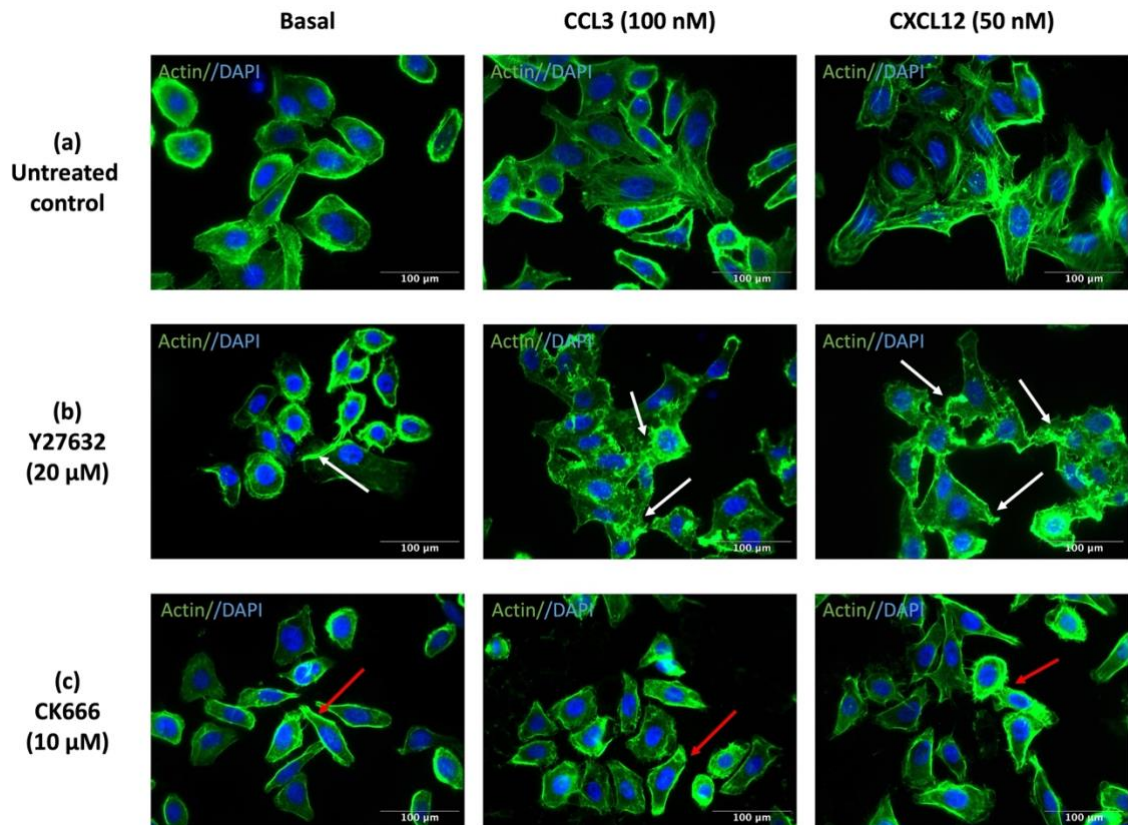
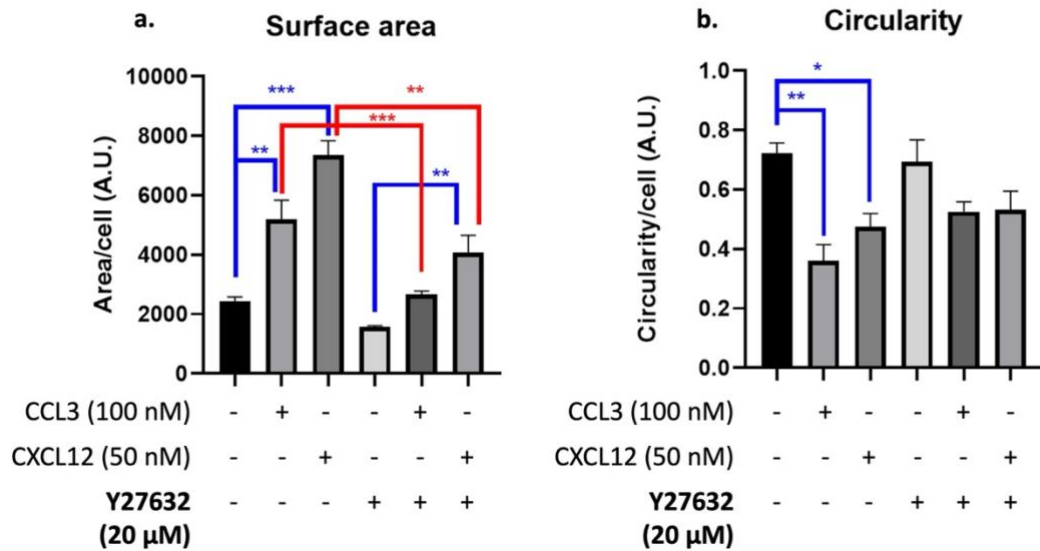


**Figure 5.7. ROCK inhibitor, Y27632, induces ruffling and clustering of F-actin, while Arp2/3 inhibitor, CK666, abolishes the elongated morphology seen in both CCL3-stimulated and CXCL12-stimulated MCF-7 cells.** Cells were pre-treated with Y27632 (20  $\mu$ M) or CK666 (10  $\mu$ M) respectively, for 30 minutes and stimulated with CXCL12 (50 nM) for another 30 minutes or absence of chemokine as a basal control. Cells were then fixed, permeabilised and stained with Alexa Fluor™ 488 Phalloidin (green) for F-actin cytoskeleton and DAPI (1:1000) (blue) for cell nuclei. Membrane ruffling of cells treated with Y27632 was annotated by white arrows. Clustering of F-actin in cells treated with CK666 was annotated by red arrows. Representative images from at least 3 independent experiments were acquired with a Leica DMII Fluorescence microscope using 31.5X magnification.

## Y27632



## CK666

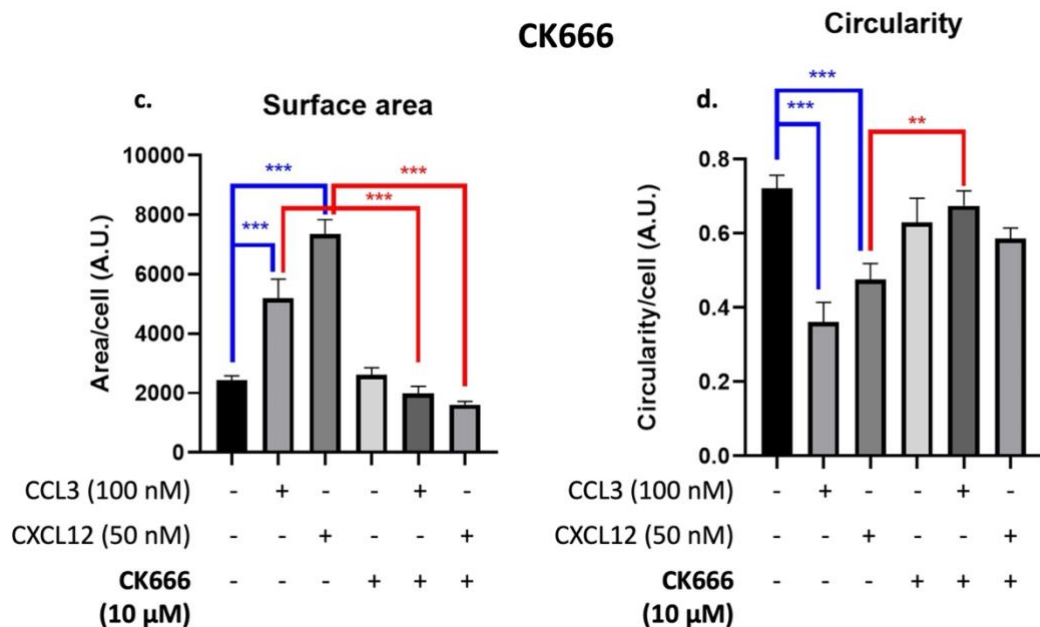


**Figure 5.8. The effects of increased cell surface area and decreased circularity mediated by chemokine stimulation are abolished by the treatment of ROCK inhibitor, Y27632, and Arp2/3 inhibitor, CK666 in MCF-7 cells.** (a, b) Cell surface area and cell circularity per a single cell treated with 20 μM Y27632 followed by stimulation of 100 nM CCL3 or 50 nM CXCL12. (c, d) Cell area and cell circularity per a single cell treated with 10 μM CK666 followed by stimulation of 100 nM CCL3 or 50 nM CXCL12. At least 10 cells were analysed per experiment. Identical microscopic settings (image size, 2592 x 1944 pixel and 414.72 x 311.04 μm) were applied. Data shown represent the mean ± SEM of 3 independent experiments. Data are compared between with and without chemokine

stimulation (in blue) and between with and without inhibitor treatment (in red) (One-way ANOVA with a Dunnett's multiple comparisons test as post-hoc test, \* =  $p \leq 0.05$ , \*\* =  $p \leq 0.01$ , \*\*\* =  $p \leq 0.001$ ).

### **5.3.5. Disruption of F-actin arrangement and elongated cell morphology with increased cell surface is resulted by the combined treatment of Y27632 and PrKD inhibitor.**

Disruption of the arrangement of F-actin was observed in the treatment of Y27632 from our preliminary experiments. In addition to the effects of ROCK inhibition, we examined any changes in F-actin arrangement implicated by PrKD inhibition at the same time. This could deduce whether PrKD is an upstream or downstream protein corresponding to ROCK in the signalling pathway regulating actin cytoskeletal rearrangement.

Cells were pre-treated with Y27632 and one of the PrKD inhibitor, CID755673 or CID2011756, at the same time for 30 minutes, followed by CCL3 or CXCL12 stimulation for another 30 minutes or in the absence of chemokine stimulation as basal controls. To eliminate the possibility of cytotoxicity in the combined use of both inhibitors, it was confirmed that a combination of 20  $\mu\text{M}$  Y27632 and 2.5  $\mu\text{M}$  PrKD inhibitor causes no cytotoxicity in MCF-7 cells (**Figure A12**).

In combined treatment of Y27632 and PrKD inhibitor, MCF-7 cells without chemokine stimulation appeared to have increased cell surface area compared to those treated with Y27632 alone, however, distinctive ruffling and clusters of F-actin was observed (**Figure 5.9**). There was no observable difference between basal and CCL3 or CXCL12 stimulation in MCF-7 cells treated with Y27632 and PrKD inhibitor. Elongated and spreading cell morphology with disordered F-actin was observed in all conditions. As shown in the quantitative analysis of F-actin, there was a significant increase in cell area and significant reduction in cell circularity in cells treated with Y27532 and PrKD inhibitor even in the absence of CCL3 or CXCL12 stimulation (**Figure 5.10**). Together with our findings described in Section 5.3.3 and 5.3.4, PrKD inhibition induces more spreading in cell morphology and ROCK inhibition disrupts F-actin arrangement. Both effects were observed when a combination of inhibitors targeting both proteins was used.

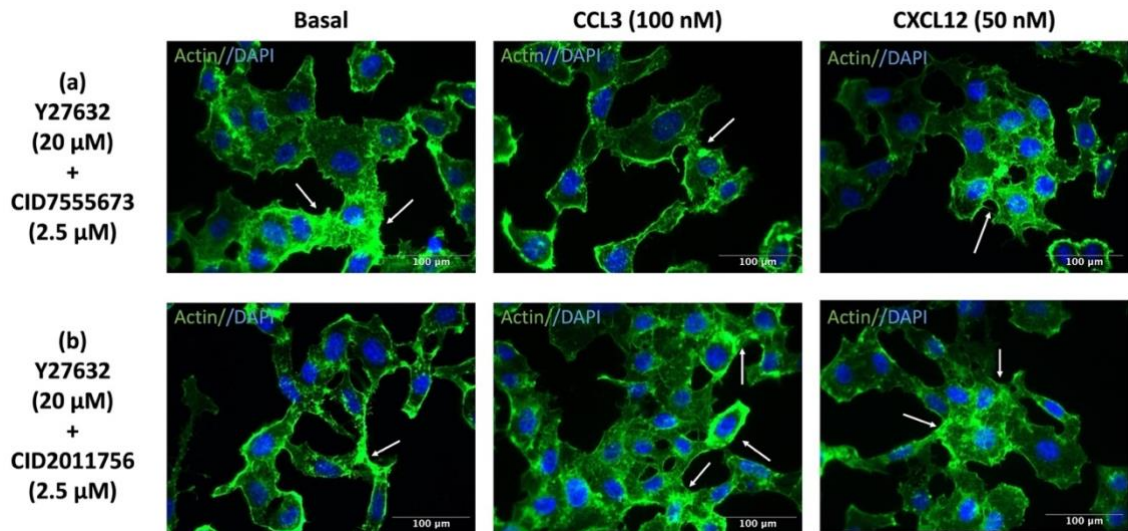
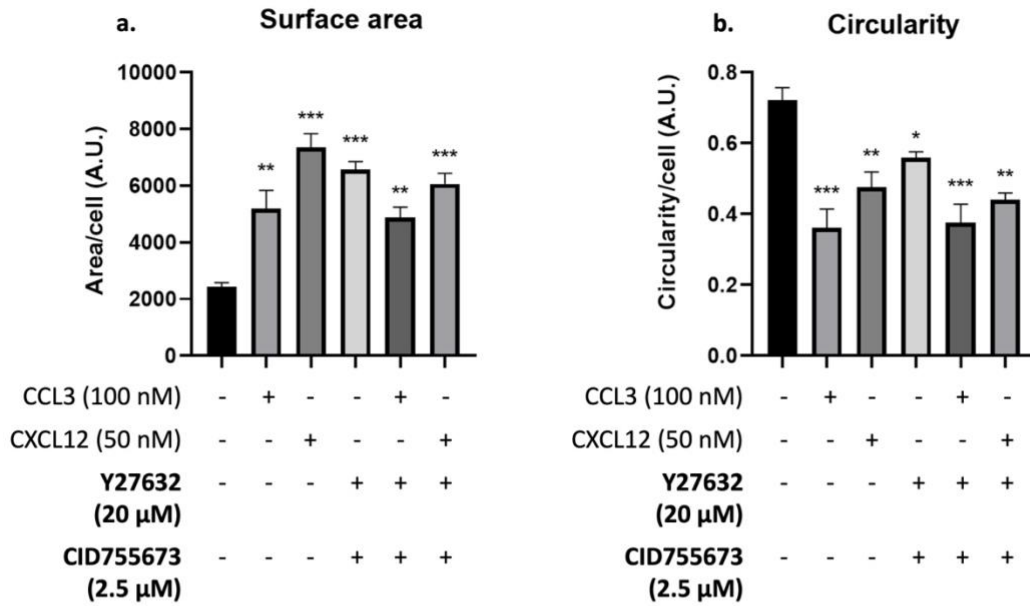


**Figure 5.9. Ruffling and clustering of F-actin is still seen in MCF-7 cells treated with Y27632 in addition of PrKD inhibitor.** Cells were pre-treated with Y27632 and PrKD inhibitor, CID755673 or CID2011756, at the same time for 30 minutes and stimulated with CXCL12 (50 nM) for another 30 minutes or absence of chemokine as a basal control. Cells were then fixed, permeabilised and stained with Alexa Fluor™ 488 Phalloidin (green) for F-actin cytoskeleton and DAPI (1:1000) (blue) for cell nuclei. Membrane ruffling of cells induced by the inhibitor treatment was annotated by white arrows. Representative images from at least 3 independent experiments were acquired with a Leica DMII Fluorescence microscope using 31.5X magnification.

### Y27632 + CID755673



### Y27632 + CID2011756

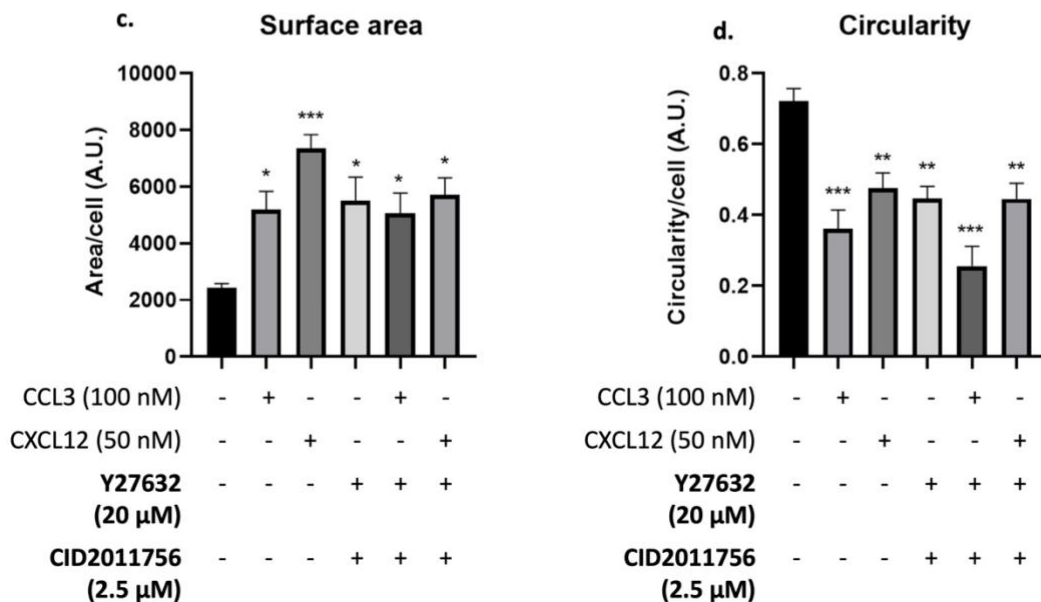


**Figure 5.10. Combined treatment of Y27632 and PrKD inhibitor, CID755673 or CID2011756, induces increase in cell area and reduction in cell circularity with or without CCL3 or CXCL12 stimulation in MCF-7 cells.** (a, b) Cell surface area and cell circularity per a single cell treated with 20 μM Y27632 and 2.5 μM CID755673 followed by stimulation of 100 nM CCL3 or 50 nM CXCL12. (c, d) Cell surface area and cell circularity per a single cell treated with 20 μM Y27632 and 2.5 μM CID2011756 followed by stimulation of 100 nM CCL3 or 50 nM CXCL12. At least 10 cells were analysed per experiment. Identical microscopic settings (image size, 2592

x 1944 pixel and 414.72 x 311.04  $\mu\text{m}$ ) were applied. Data shown represent the mean  $\pm$  SEM of 3 independent experiments. Data were compared in relation to cells without inhibitor treatment or chemokine stimulation (One-way ANOVA with a Dunnett's multiple comparisons test as post-hoc test, \* =  $p \leq 0.05$ , \*\* =  $p \leq 0.01$ , \*\*\* =  $p \leq 0.001$ ).

### **5.3.6. CK666 overrides the basal effect of PrKD inhibitor as a result of inhibition of actin polymerisation observed in MCF-7 cells.**

From our preliminary experiments, reduced cell surface area and accumulation of F-actin at the periphery of MCF-7 cells were observed in the treatment of CK666. Same as Section 5.3.5, we pre-treated the cells with the combination of CK666 and PrKD inhibitor at the same time, in order to observe the effects on actin cytoskeletal rearrangement by Arp2/3 inhibition and PrKD inhibition. It was confirmed that combined treatment of 10  $\mu\text{M}$  CK666 and PrKD inhibitor (2.5  $\mu\text{M}$  CID755673 or CID2011756) has no toxicity in MCF-7 cells from the MTS cytotoxicity tests (**Figure A12**). Under basal condition with the combined treatment of CK666 and PrKD inhibitor, the appearance of cell morphology and F-actin localisation are similar to those treated with CK666 alone (**Figures 5.7 and 5.11**). This implies that the effect of increased cell surface area by PrKD inhibitor is overridden by the effects of CK666 in the absence of chemokine stimulation. Interestingly, in the stimulation of CCL3 or CXCL12, cells in the combined inhibitor treatment appeared to be more elongated, compared to CK666 treatment alone (**Figures 5.7 and 5.11**). From the quantification analysis of F-actin, by comparing between chemokine-stimulated cells with combined inhibitor treatment and without inhibitor treatment, cell surface area was significantly reduced by the combined inhibitor treatment, while circularity was not affected (**Figure 5.12**). This dictates that the elongated cell morphology induced by chemokine stimulation was not affected by the combined inhibitor treatment. The above observation confirmed that PrKD inhibition does not induce change in actin arrangement in chemokine-stimulated cells. The elongated morphology of chemokine-stimulated cells is dependent of chemokine stimulation, but not PrKD inhibition.

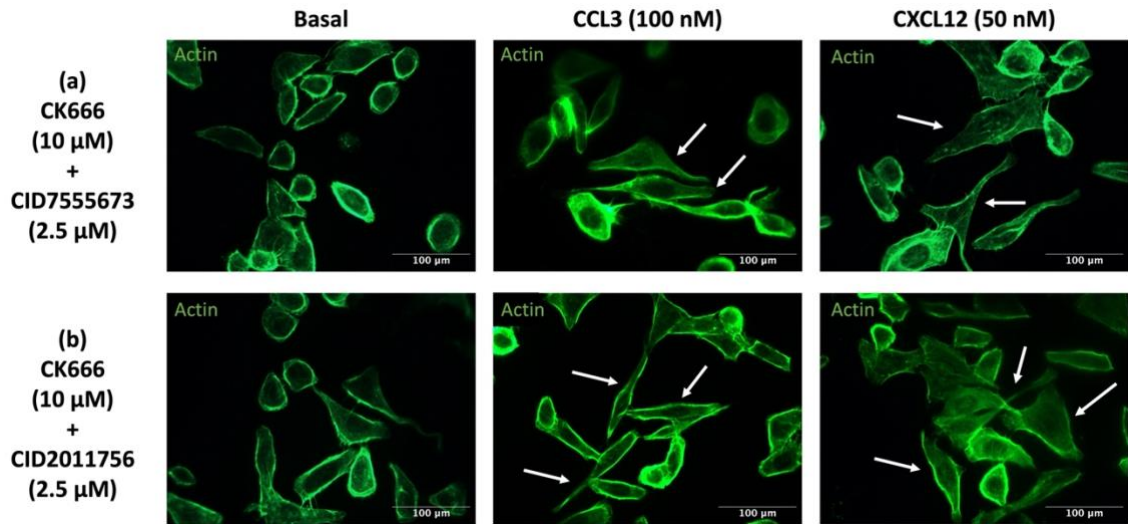


**Figure 5.11. A combination of Arp2/3 inhibitor, CK666, and PrKD inhibitor, CID755673 or CID2011756, induces elongated morphology but no observable change in cell surface area following chemokine stimulation in MCF-7 cells.** Cells were pre-treated with CK666 and PrKD inhibitor at the same time for 30 minutes and stimulated with CXCL12 (50 nM) for another 30 minutes or absence of chemokine as a basal control. Cells were then fixed, permeabilised and stained with Alexa Fluor™ 488 Phalloidin (green) for F-actin cytoskeleton. Elongated cells induced by the inhibitor treatment were annotated by white arrows. Representative images from at least 3 independent experiments were acquired with a Leica DMII Fluorescence microscope using 31.5X magnification.

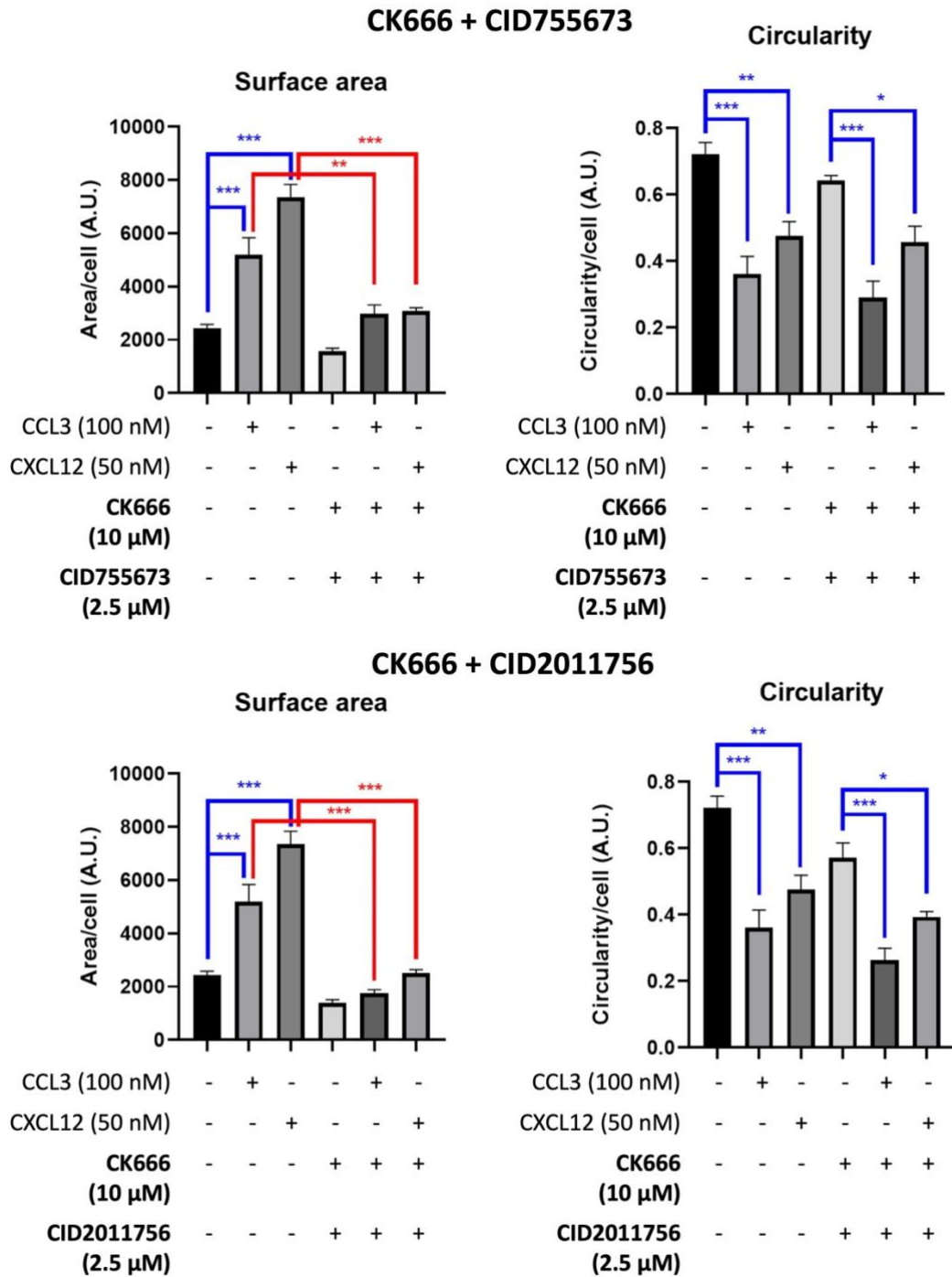


**Figure 5.12. Combined treatment of CK666 and PrKD inhibitor, CID755673 or CID2011756, induces reduction in cell circularity but no change in cell surface area with or without chemokine stimulation in MCF-7 cells.** (a, b) Cell surface area and cell circularity per a single cell treated with 20 μM Y27632 and 2.5 μM CID755673 followed by stimulation of 100 nM CCL3 or 50 nM CXCL12. (c, d) Cell surface area and cell circularity per a single cell treated with 20 μM Y27632 and 2.5 μM CID2011756 followed by stimulation of 100 nM CCL3 or 50 nM CXCL12. At least 10 cells were analysed per experiment. Identical microscopic settings

(image size, 2592 x 1944 pixel and 414.72 x 311.04  $\mu\text{m}$ ) were applied. Data shown represent the mean  $\pm$  SEM of 3 independent experiments. Data are compared between with and without chemokine stimulation (in blue) and between with and without inhibitor treatment (in red) (One-way ANOVA with a Dunnett's multiple comparisons test as post-hoc test, \* =  $p \leq 0.05$ , \*\* =  $p \leq 0.01$ , \*\*\* =  $p \leq 0.001$ ).

### **5.3.7 PrKD inhibitors, CID755673 and CID2011756, have no blocking effect on chemokine receptor internalisation following CCL3 or CXCL12 stimulation in MCF-7 and Jurkat cells.**

As described in Section 1.5.1, receptor phosphorylation by the intracellular kinases, including protein kinase C (PKC), following chemokine stimulation is crucial particularly for clathrin-dependent receptor internalisation (Borroni et al., 2010). As PrKD belongs to the family of serine/threonine kinases as PKC (Rozenfurt et al., 2005), it is hypothesised that PrKD is potentially involved in phosphorylation of chemokine receptor, in turn facilitating receptor internalisation following chemokine stimulation. Previous studies have revealed the role of PrKD1 on phosphorylation of glutamate-gated ion channels, such as N-methyl-D-aspartate receptor (NMDAR) and AMPA type glutamate receptors (AMPA), in the regulation of receptor internalisation, contributing to neuronal plasticity (Fang et al., 2015; Morales et al., 2020). The roles of PrKD in GPCR receptor internalisation are yet to be investigated.

In our study, we investigated the effects of PrKD on chemokine receptor internalisation, focusing on CCL3-induced CCR5 internalisation in MCF-7 cells, and CXCL12-induced CXCR4 internalisation in MCF-7 and Jurkat cells using the two PrKD inhibitors, CID755673 and CID2011756.

In our flow cytometry analysis, reduction of cell surface CCR5 expression following CCL3 stimulation still occurred in the treatment of CID755673 or CID2011756 in MCF-7 cells, and there was no significant difference in the change in cell surface CCR5 expression observed compared to control without inhibitor treatment (**Figure 5.13** and **Table 5.1**). This implies that PrKD inhibition does not affect CCR5 internalisation in the stimulation of CCL3. The same phenomenon

was observed in CXCL12-induced CXCR4 internalisation (**Figure 5.14** and **Table 5.1**).

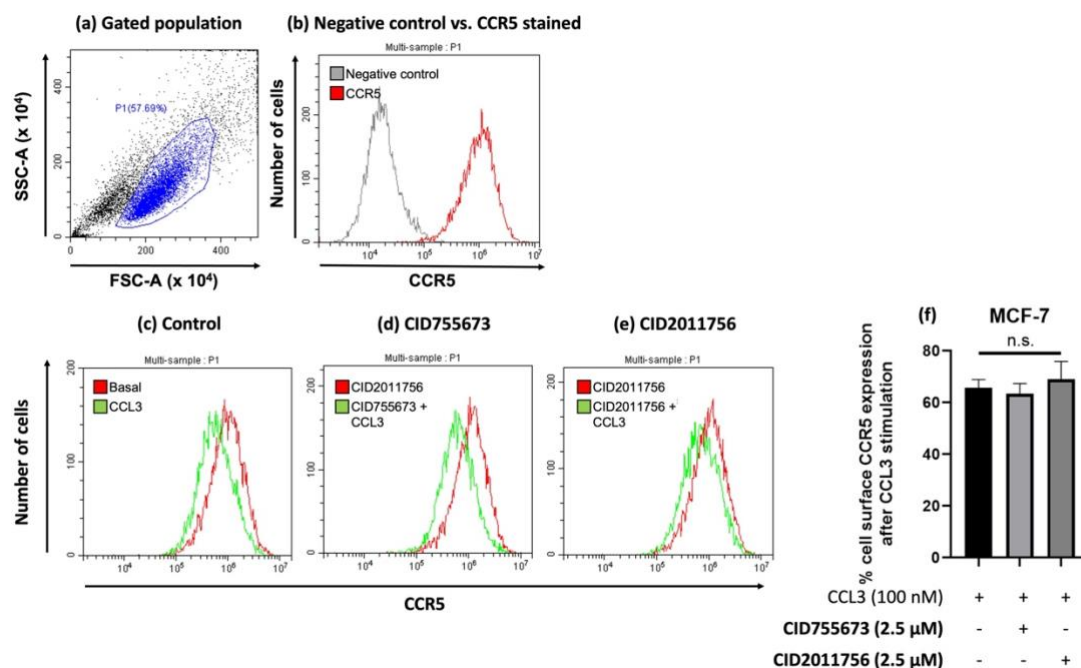


**Figure 5.13. PrKD inhibitors had no significant effect on CCL3-induced CCR5 internalisation in MCF-7 cells.** Cells were pre-treated with CID755673 (2.5 μM) or CID2011756 (2.5 μM) or without inhibitor treatment for 30 minutes, followed by stimulation with CCL3 (100 nM) at 37 °C for another 30 minutes to allow CCR5 internalisation to take place. Cells were stained with rat CCR5 antibody (1:100) followed by secondary staining of anti-rat Alexa 488 antibody (1:200). Only secondary anti-rat Alexa 488 antibody (1:200) was added in negative control. Fluorescence intensity of 20,000 events from each sample were quantified in flow cytometry and cell population was gated to exclude dead cells and debris before analysis. (a) Representative scatter plot (FSC vs. SSC) indicates the gated cell population (indicated as P1) in the analysis. (b) Representative histogram showing unstained cells as negative control (in grey) and CCR5-stained cells (in red). (c, d, e) Representative histograms showing the comparison of cells in the absence of chemokine stimulation (in red) and chemokine-stimulated cells (in green) under different conditions: (c) without inhibitor treatment, in the treatment of (d) CID755673 and (e) CID2011756 in respect to fluorescence intensity among the gated population (P1) of each cell sample. (f) Bar chart showing percentage of cell surface CCR5 expression

following CCL3 stimulation in MCF-7 cells treated with either CID755673 (light grey) or CID2011756 (dark grey) compared to control without inhibitor treatment (black). Percentage of cell surface CCR5 expression following CCL3 stimulation was calculated from  $(\text{CCL3-stimulated} - \text{negative control}) / (\text{unstimulated control} - \text{negative control}) (\%)$ , where negative control was stained with secondary antibody. Fluorescence values are based on median channel of fluorescence in a gated population (P1) of cells from each sample and acquired by the CytExpert software (Beckman Coulter). Data shown represent the mean  $\pm$  SEM of at least 3 independent experiments. One-way ANOVA with a Dunnett's multiple comparisons test as post-hoc test, n.s. = not significant.

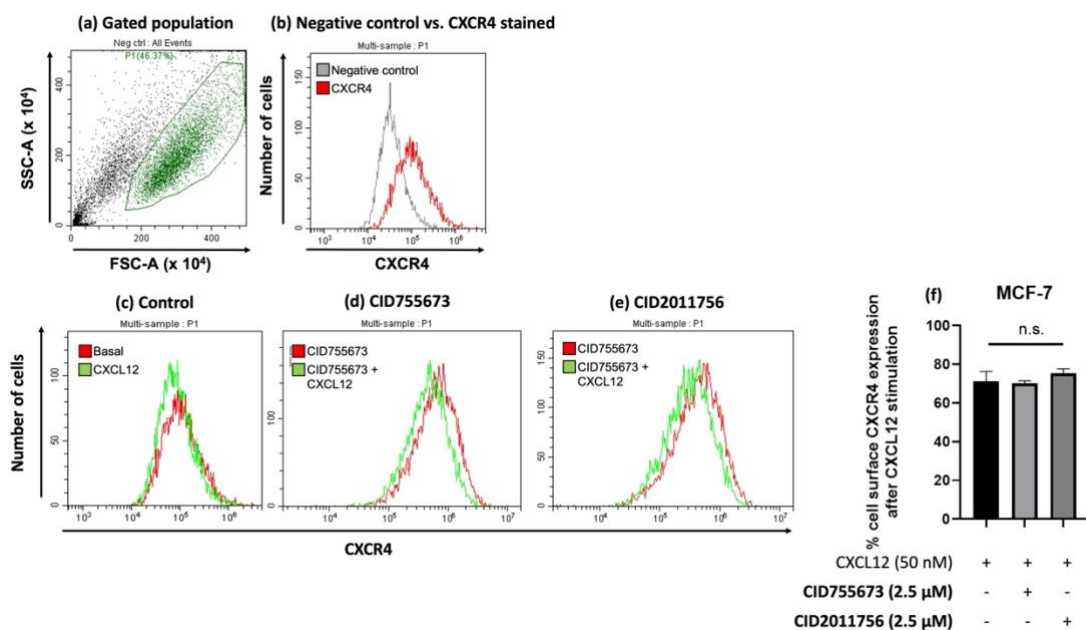


**Figure 5.14. PrKD inhibitors had no significant effect on CXCL12-induced CXCR4 internalisation in MCF-7 cells.** Cells were pre-treated with CID755673 (2.5  $\mu\text{M}$ ) or CID2011756 (2.5  $\mu\text{M}$ ) or without inhibitor treatment for 30 minutes, followed by stimulation with CXCL12 (50 nM) at 37  $^{\circ}\text{C}$  for another 30 minutes to allow CXCR4 internalisation to take place. Cells were stained with mouse CXCR4 antibody (1:200) followed by secondary staining of anti-mouse Alexa 488 antibody (1:200). Only secondary anti-mouse Alexa 488 antibody (1:200) was added in negative control. Fluorescence intensity of 20,000 events from each sample were quantified in flow cytometry and cell population was gated to exclude dead cells and debris before analysis. (a) Representative scatter plot (FSC vs.

SSC) indicates the gated cell population (indicated as P1) in the analysis. (b) Representative histogram showing unstained cells as negative control (in grey) and CXCR4-stained cells (in red). (c, d, e) Representative histograms showing the comparison of cells in the absence of chemokine stimulation (in red) and chemokine-stimulated cells (in green) under different conditions: (c) without inhibitor treatment, in the treatment of (d) CID755673 and (e) CID2011756 in respect to fluorescence intensity among the gated population (P1) of each cell sample. (f) Bar chart showing percentage of cell surface CXCR4 expression following CXCL12 stimulation in MCF-7 cells treated with either CID755673 (coloured in light grey) or CID2011756 (coloured in dark grey) compared to control without inhibitor treatment (coloured in black). Percentage of cell surface CXCR4 expression following CXCL12 stimulation was calculated from  $(\text{CXCL12-stimulated} - \text{negative control}) / (\text{unstimulated control} - \text{negative control}) (\%)$ , where negative control was stained with secondary antibody. Fluorescence values are based on median channel of fluorescence in a gated population (P1) of cells from each sample and acquired by the CytExpert software (Beckman Coulter). Data shown represent the mean  $\pm$  SEM of at least 3 independent experiments. One-way ANOVA with a Dunnett's multiple comparisons test as post-hoc test, n.s. = not significant.

For Jurkat cells, the extent of reduction in cell surface CXCR4 expression following CXCL12 stimulation in cells treated with CID755673 or CID2011756 has no significant difference from control without inhibitor treatment (**Figure 5.15** and **Table 5.1**). This implies that PrKD inhibition has no effect on CXCL12-induced CXCR4 internalisation in Jurkat cells, as seen in MCF-7 cells.

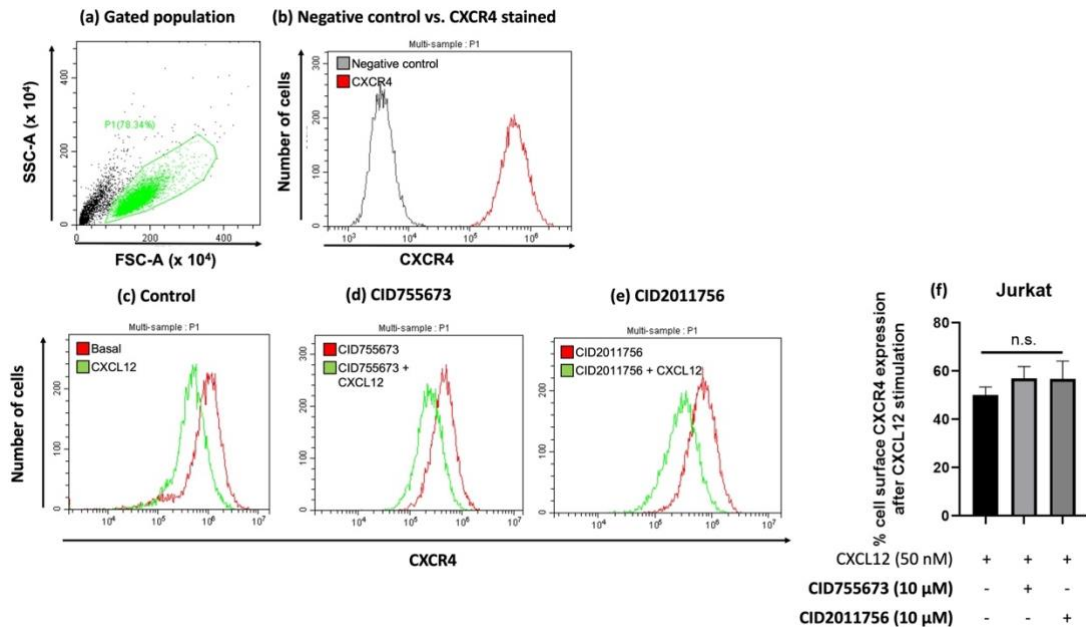


**Figure 5.15. PrKD inhibitors had no significant effect on CXCL12-induced CXCR4 internalisation in Jurkat cells.** Cells were pre-treated with CID755673 (10  $\mu$ M) or CID2011756 (10  $\mu$ M) or without inhibitor treatment for 30 minutes, followed by stimulation with CXCL12 (50 nM) at 37  $^{\circ}$ C for another 30 minutes to allow CXCR4 internalisation to take place. Cells were stained with mouse CXCR4 antibody (1:200) followed by secondary staining of anti-mouse Alexa 488 antibody (1:200). Only secondary anti-mouse Alexa 488 antibody (1:200) was added in negative control. Fluorescence intensity of 20,000 events from each sample were quantified in flow cytometry and cell population was gated to exclude dead cells and debris before analysis. (a) Representative scatter plot (FSC vs. SSC) indicates the gated cell population (indicated as P1) in the analysis. (b) Representative histogram showing unstained cells as negative control (in grey) and CXCR4-stained cells (in red). (c, d, e) Representative histograms showing the comparison of cells in the absence of chemokine stimulation (in red) and chemokine-stimulated cells (in green) under different conditions: (c) without inhibitor treatment, in the treatment of (d) CID755673 and (e) CID2011756 in respect to fluorescence intensity among the gated population (P1) of each cell sample. (f) Bar chart showing percentage of cell surface CXCR4 expression following CXCL12 stimulation in Jurkat cells treated with either CID755673 (coloured in light grey) or CID2011756 (coloured in dark grey) compared to control without inhibitor treatment (coloured in black). Percentage of cell surface CXCR4 expression

following CXCL12 stimulation was calculated from  $(\text{CXCL12-stimulated} - \text{negative control}) / (\text{unstimulated control} - \text{negative control}) (\%)$ , where negative control was stained with secondary antibody. Fluorescence values are based on median channel of fluorescence in a gated population (P1) of cells from each sample and acquired by the CytExpert software (Beckman Coulter). Data shown represent the mean  $\pm$  SEM of at least 3 independent experiments. One-way ANOVA with a Dunnett's multiple comparisons test as post-hoc test, n.s. = not significant.

**Table 5.1. Effect of PrKD inhibitors, CID755673 and CID0211756, on chemokine-induced receptor internalisation**

| Cell line | Chemokine      | Percentage of receptor expression on cell surface following chemokine stimulation for 30 minutes (%)* ± SEM |   |  |
|-----------|----------------|---|---|--|
|           |                | Control †   | Inhibitor ‡                                   |  |
|           |                |   | CID755673<br>(MCF-7: 2.5 µM<br>Jurkat: 10 µM) | CID2011756<br>(MCF-7: 2.5 µM<br>Jurkat: 10 µM) |
| MCF-7     | CCL3 (100 nM)  | 65.8 ± 3.1  | 63.5 ± 3.9                                    | 69.0 ± 3.8                                     |
|           | CXCL12 (50 nM) | 75.4 ± 2.2  | 68.2 ± 1.1                                    | 75.4 ± 2.2                                     |
| Jurkat    | CXCL12 (50 nM) | 50.1 ± 3.4  | 60.9 ± 5.8                                    | 56.7 ± 4.4                                     |

\*Percentage of receptor expression on cell surface following chemokine stimulation = [median channel of fluorescence (chemokine-stimulated) - median channel of fluorescence (negative control)] / [median channel of fluorescence (without chemokine stimulation) - median channel of fluorescence (negative control)] (%), where negative control was stained with secondary antibody matched to the host species and class of the primary antibody only.

† Relative to control without chemokine stimulation nor inhibitor treatment

‡ Relative to inhibitor-treated control without chemokine stimulation

### 5.3.8 PrKD2 knockout has no effect on the change in endosomal sorting following CXCL12 stimulation.

Owing to the limitations of PrKD inhibitors in the study of the isoform-specific roles of PrKD, we attempted to knock down PrKD2 using chemical transfection of plasmid DNA containing an PrKD2 shRNA insert (see Section 2.6 for more details). PrKD2 previously reported to act as a positive regulator in cell migration (Döppler et al., 2014; X. Zhang et al., 2021). Unlike PrKD3, PrKD2 is basally inactive that requires activation by extracellular stimuli (Döppler et al., 2014). Hence, PrKD2 would be an ideal candidate in the investigation of the involvement of PrKD in chemokine-stimulated responses.

In this study, using chemical transfection in MCF-7 cells, we generated three varieties of genetic modified cells: (1) PrKD2 knockout (PrKD2 KO) cells with a plasmid DNA containing a mammalian PrKD2 shRNA insert and a GFP promoter, (2) non-target control cells with plasmid DNA containing a non-target shRNA insert, and (3) non-transfected control cells to indicate the success of transfection (Figure 5.16).

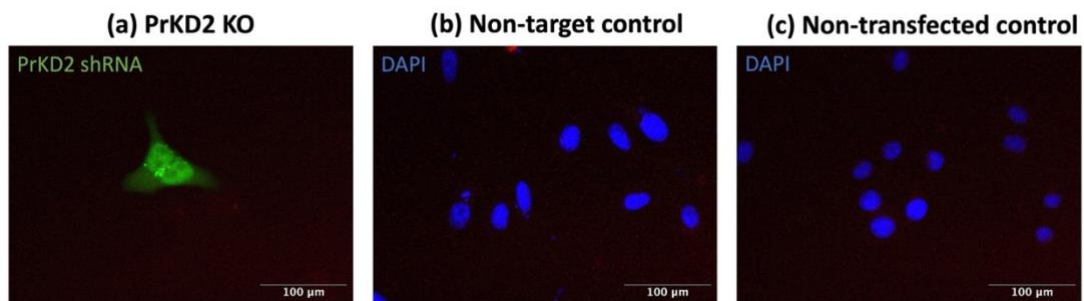


**Figure 5.16. Chemically transfected MCF-7 cells for PrKD2 knockout (PrKD2 KO) experiments.** (a) PrKD KO cells (green) chemically transfected with 2 µg of plasmid DNA encoding an insert of PrKD2 shRNA and a GFP promoter. (b) Non-target control cells chemically transfected with 2 µg of plasmid DNA encoding an insert of shRNA that does not target any known genes. (c) Non-transfected control cells as an indicator whether the transfection process is successful. Cells were stained with DAPI (1:1000) (blue) for cell nuclei in non-target control and non-transfected control samples. Cells were fixed with 4% formaldehyde solution before image acquisition. Representative images from at least 3 independent experiments

were acquired with a Leica DMII Fluorescence microscope using 20X magnification.

Although we showed that PrKD inhibition has no effect on CCL3-induced CCR5 internalisation and CXCL12-induced CXCR4 internalisation using pan-PrKD inhibitors in the section above, the outcome might be different using an approach targeting PrKD2 known as a positive regulator of cell migration. As we found that clathrin is not involved in CCL3-induced CCR5 internalisation in MCF-7 in Chapter 4, we focused on CXCL12-induced CXCR4 internalisation only in this study.

As the yield of successfully transfected cells was insufficient for the quantification of cell surface receptor expression using flow cytometry analysis, we performed live cell staining to assess lysosome acidification in the process of CXCL12-induced CXCR4 internalisation instead. Previous literature proposed that membrane proteins are transported to early sorting endosomes following internalisation (Miaczynska and Zerial, 2002). The early sorting endosomes are then matured into late endosomes responsible for sorting into either degradation or recycling pathway (Ferguson, 2001). Acidification of endosomes regulated by the action of a vacuolar ATPase (V-ATPase) is the main determinant in transport and sorting of membrane proteins. Hence, the change in acidity of endosomes is an indicative of the sorting process after internalisation (Maxfield, 2014).

We used LysoTracker Deep Red to assess lysosome acidification in our study. LysoTracker dye is a fluorescent acidotropic probe for labelling acidic organelles in live cells (Barral et al., 2022). In the mode of action, LysoTracker enters cells via simple diffusion due to its hydrophobic chemical properties. As the chemical structure of LysoTracker consists of aromatic rings with a positively charged nitrogen at acidic pH, LysoTracker becomes protonated inside the lysosomes and other acidic organelles and is sequestered in the acidic compartments (Zhitomirsky et al., 2018). The acidity inside organelles determines accumulation of LysoTracker, indicated by fluorescence intensity from LysoTracker (Zhitomirsky et al., 2018).

Live cell staining using LysoTracker was performed in PrKD2 KO, non-target control and non-transfected control. In CXCL12-stimulated samples, cells were stimulated with CXCL12 and incubated at 37°C, 5% CO<sub>2</sub> for 30 minutes. LysoTracker dye was added and samples were incubated at 37°C, 5% CO<sub>2</sub> for another 30 minutes.

In both non-target and non-transfected control samples, there is an observable reduction in endosomal acidification after CXCL12 stimulation (**Figure 5.17**). The reduced endosomal acidity in CXCL12-stimulated cells indicates that sorting of the receptor occurs following CXCL12-mediated internalisation. Similar observations were seen in PrKD2 KO cells (**Figure 5.17**). This implies that endosomal sorting of internalised receptor after CXCL12-induced CXCR4 internalisation is not affected by PrKD2 knockdown.

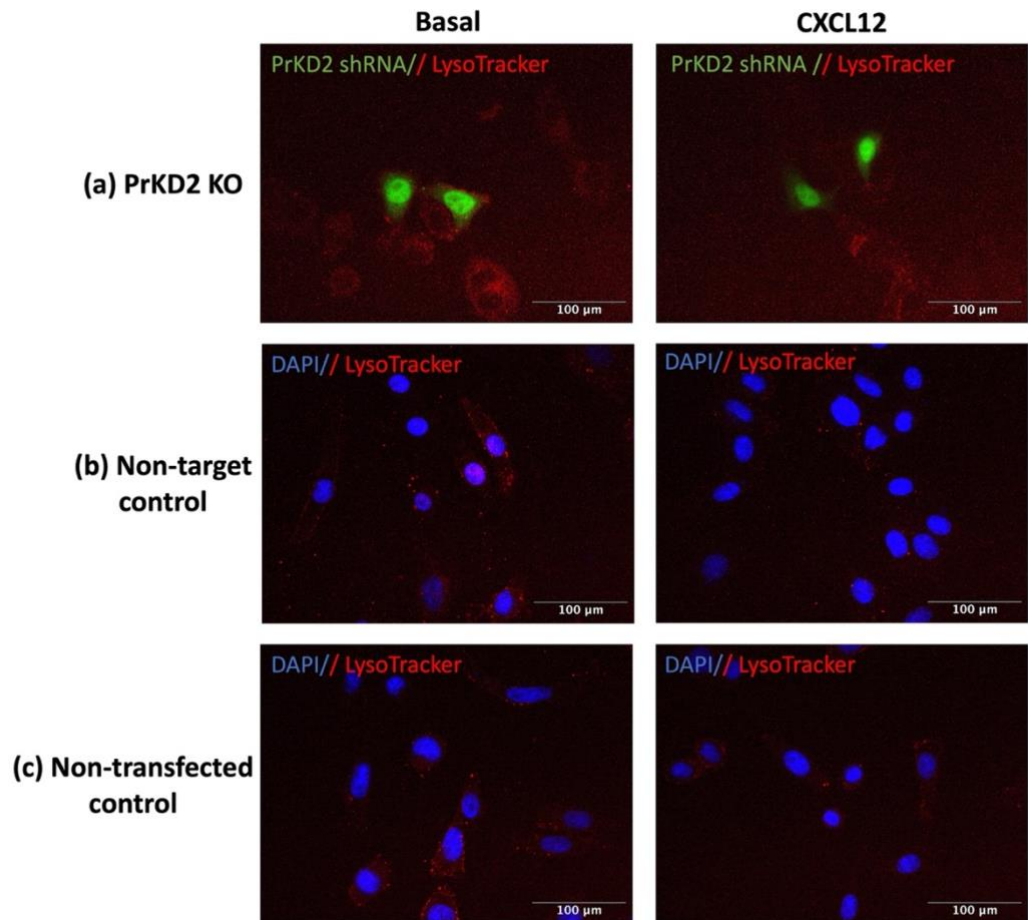


**Figure 5.17. Reduction in endosomal acidity following CXCL12 stimulation is not affected by PrKD2 knockdown in MCF-7 cells.** (a) PrKD KO cells (green) chemically transfected with 2  $\mu$ g of plasmid DNA encoding an insert of PrKD2 shRNA and a GFP promoter. (b) Non-target control cells chemically transfected with 2  $\mu$ g of plasmid DNA encoding an insert of shRNA that does not target any known genes. (c) Non-transfected control cells as an indicator whether the transfection process is successful. Cells were stimulated with CXCL12 (50nM) and incubated at 37°C, 5% CO<sub>2</sub> for 30 minutes or only incubated in medium without serum as basal control. LysoTracker dye (50nM) was added, and samples were incubated at 37°C, 5% CO<sub>2</sub> for another 30 minutes. Cells were stained with DAPI (1:1000) (blue) for cell nuclei in non-target control and non-transfected control samples. Representative images from at least 3 independent experiments were acquired with a Leica DMII Fluorescence microscope using 20X magnification.

## 5.4 Discussion

In order to investigate the roles of PrKD in chemokine signalling, we examine different chemokine-induced cellular responses using two different pan-PrKD small molecule inhibitors, CID755673 and CID2011756, which target all three isoforms of PrKD. In general, small molecule inhibitors are cell permeable that enter the cell along a concentration gradient and exert inhibitory effects to intracellular target proteins. As mentioned previously, PrKD is localised in various intracellular compartments, such as nucleus, mitochondria, trans-golgi network and cytoplasm (Fu and Rubin, 2011). In contrast to monoclonal antibodies that normally target cell surface proteins only, small molecule inhibitors would be ideal for biochemical study on PrKD signalling (Lv et al., 2021).

CID755673 is a potent non-ATP competitive inhibitor selective to PrKD (Sharlow et al., 2008). According to the IC<sub>50</sub> values from the literature, CID755673 demonstrates selective PrKD inhibition in the low nM range, compared to other protein kinases including PKC, CAK, PLK1, CAMKIIa and AKT (Sharlow et al., 2008) (**Table 5.2**). Regarding its effect on cellular activity, CID755673 has been shown to inhibit cell proliferation and migration in prostate cancer cells (Sharlow et al., 2008). Another PrKD inhibitor, CID2011756, is an analogue designed based on the chemical structure of CID755673 (**Figure 5.18**). The difference is that CID2011756 inhibits PrKD in an ATP-competitive fashion and it is cell permeable at EC<sub>50</sub> of 10 µM for PrKD1 inhibition (Sharlow et al., 2011) (**Table 5.2**). In respect to the mode of action, both inhibitors were demonstrated to inhibit the activation of PrKD1 by suppressing PrKD1 autophosphorylation at Ser<sup>916</sup> using LNCaP cells as experimental model (Sharlow et al., 2011).

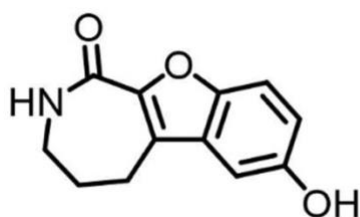
**Table 5.2. IC<sub>50</sub> values of protein kinase D inhibitor, (a) CID755673 and (b) CID2011756, for different protein kinase targets (adapted from Tocris)**

**a. CID755673**

| Protein kinases | IC <sub>50</sub> (μM) |
|-----------------|-----------------------|
| PrKD1           | 0.182                 |
| PrKD2           | 0.280                 |
| PrKD3           | 0.227                 |
| PKC             | > 10                  |
| CAK             | 15.3                  |
| PLK1            | 20.3                  |
| CAMKIIa         | 40.5                  |
| AKT             | > 50                  |

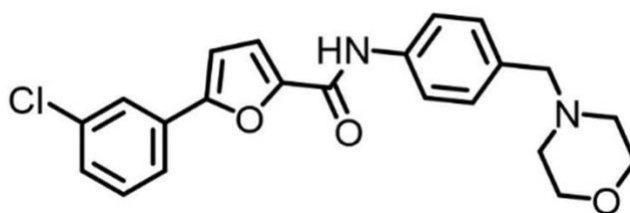
**b. CID2011756**

| Protein kinases | IC <sub>50</sub> (μM) |
|-----------------|-----------------------|
| PrKD1           | 3.2                   |
| PrKD2           | 0.6                   |
| PrKD3           | 0.7                   |



**CID755673**

IC<sub>50</sub> PKD1 = 182 nM  
 IC<sub>50</sub> PKD2 = 280 nM  
 IC<sub>50</sub> PKD3 = 227 nM



**CID 2011756**

IC<sub>50</sub> PKD1 = 3.2 μM  
 IC<sub>50</sub> PKD2 = 0.6 μM  
 IC<sub>50</sub> PKD3 = 0.7 μM

**Figure 5.18. Chemical structure and biochemical activity of PrKD inhibitors used in our study.** (Left) structure of CID755673 with the IC<sub>50</sub> values for the three PrKD isoforms; (right) structure of CID2011756 with the IC<sub>50</sub> values for the three PrKD isoforms. (Images taken from Gilles et al., 2021)

As CID755673 is non-ATP competitive inhibitor, it might potentially bind to the allosteric sites of protein kinases, instead of the active conformation of protein kinases in the ATP pocket. Theoretically, since the binding site of ATP

competitive inhibitors is the highly conserved ATP pocket of protein kinases, the selectivity of the target against other kinases would be relatively low. On the other hand, non-ATP competitive inhibitors targeting outside the ATP pockets are more selective with fewer off-target effects, compared to ATP competitive inhibitors (Bhullar et al., 2018). Despite high binding specificity of CID755673, its *in vitro* activity was found to be relatively low. Efforts have been made in the optimisation of allosteric PrKD inhibitors that demonstrate higher potency in cellular activity while retaining high binding specificity (Lavalle et al., 2010) (George et al., 2011). Yet, to date, the design of isoform-specific PrKD inhibitors remains to be elusive (Gilles et al., 2021). Particularly in the study of the roles of PrKD in cancer, accumulating evidence has revealed the opposing effects of the three PrKD isoforms in different cancer types (X. Zhang et al., 2021). Given that novel PrKD modulator selectively inhibiting specific isoforms of PrKD, it could potentially block the function of tumour-promoting isoform while remain tumour-inhibiting isoform functioning.

In respect to the effects of PrKD inhibitors on chemokine-induced intracellular  $Ca^{2+}$  release, our findings showed that CCL3-induced  $Ca^{2+}$  release is reduced by PrKD inhibitors in both THP-1 and MCF-7 cells, while reduction in CXCL12-induced  $Ca^{2+}$  release by PrKD inhibitors is only seen in MCF-7 cells. As shown in Chapter 3, relatively low level of cell surface CXCR4 is expressed in THP-1 compared to MCF-7 cells. This is one of the possibilities to elucidate less significant response to CXCL12 stimulation in THP-1 cells. A slight increase in CXCL12-induced intracellular  $Ca^{2+}$  release by PrKD inhibitor in THP-1 cells might be caused by non-specific effects of the inhibitors. Overall, the results imply that PrKD might be involved in regulating intracellular  $Ca^{2+}$  release for downstream signalling mediated by CCL3 for both MCF-7 and THP-1 cells and CXCL12 for MCF-7 cells only. However, this could need to be investigated further before a conclusion could be drawn due to potential false positive results caused by non-specific effects of the inhibitors.

A study from our group previously reported that several specific PKC inhibitors, rottlerin and Go6976, deplete intracellular  $Ca^{2+}$  store stores independent of receptor activation, leading to false positive results due to non-specific effects (Moyano Cardaba et al., 2012). It was revealed that PKC activation is not crucial

for CCL3-induced intracellular  $\text{Ca}^{2+}$  release although the PKC inhibitors exhibit inhibitory effects on  $\text{Ca}^{2+}$  release (Moyano Cardaba et al., 2012). Same for PrKD inhibition, preliminary experiments are necessary to examine whether  $\text{Ca}^{2+}$  responses are independent of chemokine stimulation. This can be determined by treatment with thapsigargin following treatment of PrKD inhibitors, instead of addition of chemokine ligands. Thapsigargin is a type of ER stress-inducing agent, which irreversibly inhibits the sarco/endoplasmic reticulum  $\text{Ca}^{2+}$ -ATPase (SERCA) (Yoshino et al., 2017). Previous literature has reported that thapsigargin induces  $\text{Ca}^{2+}$  release from the intracellular  $\text{Ca}^{2+}$  stores (Buckley and Whorton, 1997). Considering that no change in intracellular  $\text{Ca}^{2+}$  release is observed in the preliminary experiment described above, it can eliminate the possibility of chemokine-independent  $\text{Ca}^{2+}$  responses.

In the aspect of cell migration, multiple lines of evidence have indicated that PrKD is involved in regulating cell migration through interactions with downstream substrates that are either promoters or suppressors in cell migration (Roy et al., 2017). In the process of tumorigenesis, malignant cells enhance motility by downregulating the expression of PrKD1 and upregulating the expression of PrKD2 and PrKD3 (LaValle et al., 2012; Roy et al., 2017; Storz, 2018). PrKD1 has been proposed to function as a negative regulator in cell motility to maintain epithelial phenotype through multiple mechanisms including various substrates, such as PAK4 (Döppler et al., 2014), SSH1L (Peterburs et al., 2009), Snail (Zou et al., 2012), E-cadherin (Jaggi et al., 2005) and  $\beta$ -catenin (Du et al., 2009). In contrast, PrKD2 and 3 acts in an opposite manner that positively regulate cell migration. A study on invasive prostate cancer showed that PrKD2 and PrKD3 phosphorylate IKK $\beta$ , which is responsible for nuclear activation of NF- $\kappa$ B and deactivation of HDAC1 (Zou et al., 2012). In respect to actin cytoskeletal rearrangement, PrKD3 was demonstrated to phosphorylate G-protein-coupled receptor kinase-interacting protein 1 (GIT1), which is critical in the regulation of cell spreading by interacting with F-actin network (Huck et al., 2012). In addition, PrKD3 was found to be constitutively active in invasive breast cancer cells. The basal activity of PrKD3 is sufficient to mediate PAK/LIMK signalling independent of SSH1L contributing to over-activation of the cofilin activity cycle and consequently promoting cell migration (Döppler et al., 2014).

From our results in the chemotaxis assay, both PrKD inhibitors significantly block chemotaxis towards CXCL12 in both Jurkat and THP-1 cells. This implies that PrKD might be involved in CXCL12-induced chemotaxis. More specifically, PrKD can be either a positive or negative regulator in cell migration, dependent of the isoforms. As the PrKD inhibitors we used are not isoform specific, our finding showed the generalised effects of all of three PrKD isoforms in chemotaxis driven by CXCL12. More targeted investigations, for example using transfection of isoform-specific PrKD siRNA, are required for understanding the isoform-specific mechanisms of PrKD in CXCL12-induced chemotaxis.

In addition, within the actin branching system, PrKD was revealed to selectively co-localise with F-actin at the leading edge of migrating cells, instead of with stress fibre at the tail (Eiseler et al., 2007). Particularly, PrKD was found to stabilise the proteins essential for filopodia formation, ARP3 and cortactin (Bowden et al., 1999; Eiseler et al., 2007). PrKD potentially prevent the phosphorylation of cortactin by serine/threonine kinases that promote N-WASP activation and enhance binding capacity to F-actin (Eiseler et al., 2007). This implies that PrKD acts as a negative regulator in cell migration by stabilising the cortical actin network (Eiseler et al., 2007).

In immunofluorescence staining of F-actin, we observed that both PrKD inhibitors induce change in actin cytoskeletal rearrangement and increased cell surface area that favours cell migration in non-invasive MCF-7 and invasive MDA-MB-231 breast cancer cells. Our findings are consistent with a study on PrKD knockout-breast cancer cells using siRNA transfection, demonstrating that knockdown of PrKD reduces cofilin phosphorylation, inducing more spreading in cell morphology that promotes chemotactic migration (Peterburs et al., 2009). Similar findings were observed by another study using another PrKD inhibitor, CRT0066101 (Borges et al., 2015). Mechanistically, in the activation of cofilin, inactive form of phosphorylated cofilin is dephosphorylated by chronophin and the members of Slingshot (SSH) family, Slingshot 1 like (SSH1L), Slingshot 2 like (SSH2L) and Slingshot 3 like (SSH3L) (Niwa et al., 2002; Ohta et al., 2003). Particularly, SSH1L is activated by Rac1 within F-actin-rich structures at the leading edge of migrating cells (Nagata-Ohashi et al., 2004). PrKD has been found to inactivate the activity of SSH1L by direct phosphorylation of Ser937 and

978, leading to interaction with 14-3-3 proteins (Peterburs et al., 2009). Consequently, cofilin remains to be inactive in phosphorylated form. Together with the above findings, it implies that PrKD is a critical regulator of the signalling network of cofilin via direct phosphorylation of SSH1L, acting as a negative promoter of cell migration through regulating actin rearrangement (**Figure 5.19**) (Borges et al., 2015; Peterburs et al., 2009).

Yet, it is noteworthy that migration might not correlate to SSH1L-dependent actin rearrangement in some cell lines. A study reported that SSH1L depletion increased cofilin phosphorylation, leading to significant reduction in migration in invasive MDA-MB-231 cells. However, migration of MCF-7 cells was not affected by SSH1L depletion, indicating that non-invasive MCF-7 cells with low migratory potential is not dependent of SSH1L (Peterburs et al., 2009). Alternatively, evidence from previous studies supported that activation of the complex of N-WASP and Arp2/3 through Rac1 and Cdc42 proteins is predominant in cell migration in MCF-7 cells, which is independent of SSH1L (Mills et al., 2018; Y. Zhang et al., 2019). Rac1 or Cdc42 induce the Arp2/3 complex, which mediates actin nucleation in the formation of filopodia at the leading edge (Narumiya et al., 2009).

Furthermore, we also investigated potential interactions of PrKD with two other critical proteins, ROCK and Arp2/3, in the regulation of actin rearrangement. Each of the PrKD inhibitors, CID755673 or CID2011756, was used in combination with a ROCK inhibitor, Y27632, and an Arp2/3 inhibitor, CK666 respectively, in order to examine any changes in effect by ROCK inhibition or Arp2/3 inhibition in addition to PrKD inhibition.

For co-inhibition of ROCK and PrKD, our findings imply that PrKD and ROCK mediates downstream signalling in separate pathways as the effects by PrKD inhibition were not affected by ROCK inhibition. PrKD potentially might not be involved in RhoA/ROCK/MLC pathway responsible for actin contractibility at the contractile tail of migrating cells. As proposed by previous literature, PrKD preferentially regulates cofilin phosphorylation through phosphorylation of PAK (Döppler et al., 2014) and SSH1L (Peterburs et al., 2009), in order to prevent the formation of lamellipodia at the leading edge of migrating cells (**Figure 5.19**).

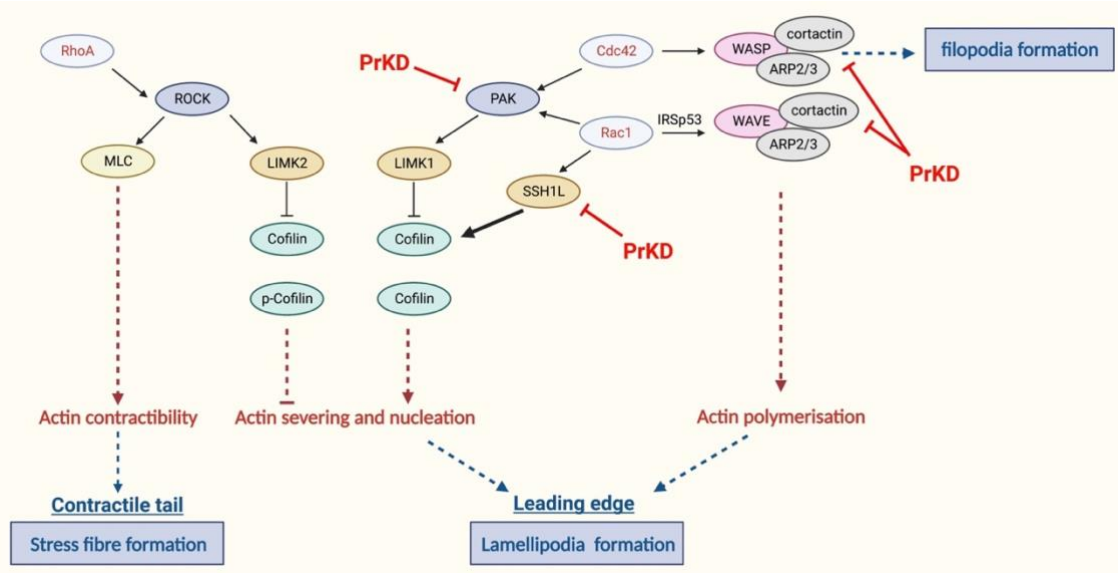


**Figure 5.19. Signalling mechanisms in the regulation of cytoskeleton dynamics in migrating cells.** Schematic diagram showing the interactions of PrKD (annotated in red) with actin-regulating proteins, including PAK (Döppler et al., 2014), SSH1L (Peterburs et al., 2009) and cortactin (Eiseler et al., 2007), proposed by previous literature. This illustrates that PrKD is preferentially involved in the pathways contributing to the formation of lamellipodia and filopodia formation at the leading edge of migrating cells, over regulation of actin contractibility at the contractile tail (Image created with BioRender.com).

With respect to co-inhibition of Arp2/3 and PrKD, we observed that the effects of PrKD causing more spreading morphology are overridden by the effects of CK666 under basal conditions in the absence of chemokine stimulation. In the chemokine-stimulated samples, the observation of elongated morphology is dependent of CCL3 or CXCL12 stimulation, but independent on PrKD inhibition. A study previously demonstrated that PrKD inactivates cortactin through phosphorylation and consequently reduce lamellipodia formation (**Figure 5.20**) (Eiseler et al., 2010). Cortactin has been known to interact with the WASP2-Arp2/3 complex responsible for filopodia and lamellipodia formation (Carrier et al., 2000). Taken together, PrKD is potentially an upstream regulator that prevents the formation and activation of WASP2/cortactin/Arp2/3 complex, leading to inhibition of lamellipodia and filopodia formation. Inhibition of PrKD allows activated cortactin to activate Arp2/3, promoting lamellipodia and filopodia formation through the WASP2/Arp2/3 complex. Together with Arp2/3 inhibition,

the formation of lamellipodia and filopodia is blocked which explains less elongated morphology observed. On the other hand, co-inhibition of Arp2/3 and PrKD in chemokine-stimulated cells are less prone to be affected by the inhibition of Arp2/3 as chemokine activation by chemokine stimulation could mediate an alternative pathway, which is cofilin activation through PAK/LIMK (Edwards et al., 1999). This pathway is also involved in the formation of lamellipodia at the leading edge of migrating cells, which replenish the inhibitory effect by CK666 (**Figure 5.20**).

(a) No inhibitor treatment

(b) PrKD inhibitor

(c) PrKD inhibitor + CK666

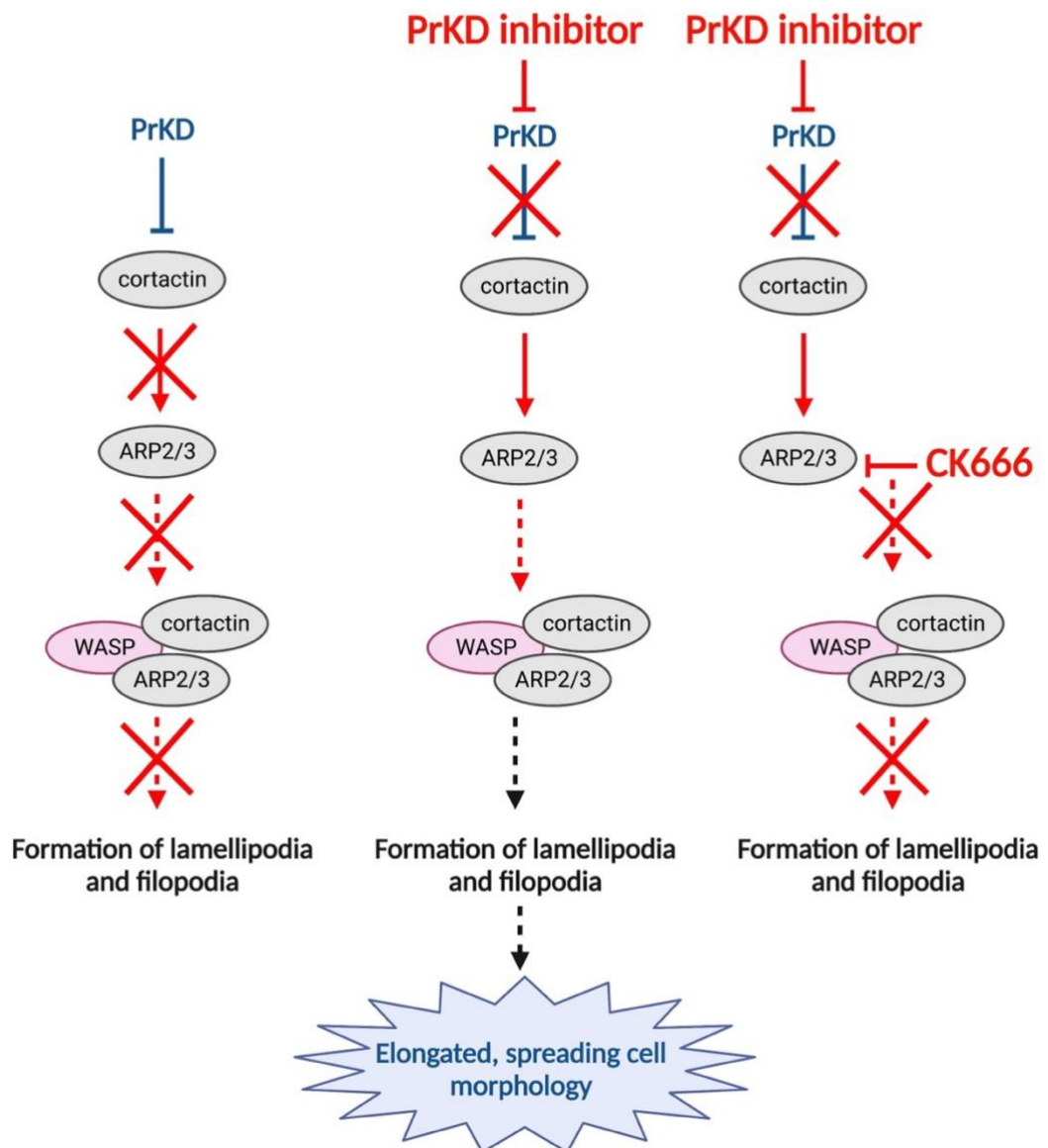


**Figure 5.20. Signalling pathway of cortactin/WASP/Arp2/3 in the regulation of actin cytoskeletal rearrangement.** Schematic diagram showing the potential outcomes from the cortactin/WASP/Arp2/3 pathway in three conditions under the intervention of PrKD: (a) no inhibitor treatment; (b) in the treatment of PrKD inhibitor; (c) in the combined treatment of PrKD inhibitor and CK666, based on our findings together with evidence from previous literature (Carlier et al., 2000; Edwards et al., 1999; Eiseler et al., 2010) (Image created with BioRender.com).

In the aspect of the involvement of PrKD in the pathways of receptor internalisation, there is a lack of research investigating the roles of PrKD specific

to chemokine signalling despite a number of studies reporting that PrKD is a key player in internalisation of ion channels plasticity (Fang et al., 2015; Morales et al., 2020). We hypothesised that PrKD potentially either interacts with other intracellular kinases or directly facilitate chemokine-induced receptor through phosphorylation. From our findings, no blocking effect on CCL3-induced CCR5 internalisation and CXCL12-induced CXCR4 internalisation was observed in MCF-7 and Jurkat cells with PrKD inhibition. This implies that PrKD is not the only protein kinase that regulates chemokine receptor internalisation or might not be involved in chemokine-induced receptor internalisation in MCF-7 and Jurkat cells. As proposed by previous literature, other kinases, such as GRKs and PKC, are also involved in facilitating chemokine receptor internalisation through receptor phosphorylation in clathrin-dependent pathway (Borroni et al., 2010). Receptor phosphorylation by intracellular kinases is not necessary in the activation of caveolae pathway independent of clathrin (Parton and Howes, 2010). This might reflect that inhibition of PrKD does not affect CXCR4 internalisation in Jurkat cells possibly due to clathrin-independent receptor internalisation pathway adapted. In addition, it should be noted that pan-PrKD inhibitors, which inhibit all three isoforms of PrKD, were used in our study. Thus, the effects seen were generalised, not isoform specific. As the three isoforms of PrKD could mediate opposing effects on cellular responses, our results might not represent an accurate role of each PrKD isoform. Instead, PrKD has been shown to be involved in regulating receptor recycling by interacting with Rab5, leading to recycling of  $\alpha v \beta 3$  integrin to the leading edge of migrating cells that promotes cell migration (Christoforides et al., 2012). As receptor recycling or degradation is a continuous process following internalisation, the isoform-specific roles of PrKD in chemokine receptor recycling and degradation would be a potential aspect in the study of chemokine-induced cell migration once a more targeted experimental methodology has been established.

Furthermore, we attempted to knock down PrKD2 using plasmid DNA containing an insert of PrKD2 shRNA in the development of a more targeted experimental approach for the study of isoform-specific roles of PrKD. Although the yield of successfully transfected cells was insufficient for cellular response experiments and quantification of receptor expression, we performed live cell staining using LysoTrack to assess the change in endosomal acidification following CXCL12

stimulation in transfected MCF-7 cells. Our observations suggested that PrKD2 might not be involved in endosomal sorting of internalised receptor following CXCL12 stimulation in MCF-7 cells. However, the finding is provisional and inconclusive as troubleshooting should be done to optimise the methodology for higher yield of transfected cells.

## 5.5 Chapter conclusions

The final conclusions to be drawn from this chapter are:

1. In MCF-7 cells, PrKD is involved in intracellular Ca<sup>2+</sup> mobilisation induced by CCL3 or CXCL12. In THP-1 cells, PrKD is only involved in CCL3-induced intracellular Ca<sup>2+</sup> mobilisation.
2. PrKD plays a role in CXCL12-stimulated chemotaxis in Jurkat and THP-1 cells.
3. In MCF-7 cells, PrKD inhibition induces increase in cell surface area and elongated cell morphology in the absence of chemokine stimulation, potentially associated with Arp2/3 but not ROCK.
4. PrKD preferentially regulate actin nucleation and polymerisation at the leading edge, other than actin contractibility at the contractile tail of migrating cells. In general, PrKD acts as negative regulator in actin cytoskeletal rearrangement involved in cell migration.
5. PrKD is not directly involved in CCL3-induced CCR5 internalisation in MCF-7 cells or CXCL12-induced CXCR4 internalisation in MCF-7 and Jurkat cells.

**Table 5.3. Summary of the involvement of protein kinase D (PrKD) in cellular responses in different cancer cell lines**

| <b>Cellular response</b>                          | <b>Cell line</b> | <b>Chemokine stimulation</b> | <b>PrKD involved? †</b>  |
|---|------------------|------------------------------|--|
| <b>Intracellular Ca<sup>2+</sup> mobilisation</b> | MCF-7            | CCL3                         | Yes  |
|   |                  | CXCL12                       | Yes  |
|   | THP-1            | CCL3                         | Yes  |
|   |                  | CXCL12                       | No   |
| <b>Chemotaxis</b>                                 | Jurkat           | CXCL12                       | Yes  |
|   | THP-1            | CXCL12                       | Yes  |
| <b>Actin cytoskeletal change</b>                  | MCF-7            | No stimulation (Basal)       | Yes* (Possibly acting as a negative regulator in actin cytoskeletal change involved in cell migration) |
|   |                  | CCL3                         | Inconclusive (due to synergistic effect of the PrKD inhibitors**)                                      |
|   |                  | CXCL12                       | Inconclusive (due to synergistic effect of the PrKD inhibitors**)                                      |

|                                 |        |        |                       |
|---------------------------------|--------|--------|-----------------------|
| <b>Receptor internalisation</b> | MCF-7  | CCL3   | Not directly involved |
|                                 |        | CXCL12 | Not directly involved |
|                                 | Jurkat | CXCL12 | Not directly involved |
| <b>Endosomal sorting</b>        | MCF-7  | CXCL12 | No (PrKD2) †          |

†Notes: PrKD represents all isoforms of PrKD, including PrKD1, PrKD2 and PrKD3, as PrKD inhibitors used in our study target all isoforms. Except for the study of endosomal sorting, the findings represent PrKD2 only by using shRNA transfection approach to knock out PrKD2.

\*Possible hypothesis from our findings together with evidence from previous literature:

- PrKD potentially is an upstream negative regulator of cortactin as the role of PrKD in regulating actin cytoskeletal change is associated with Arp2/3.
- Inhibition of PrKD could recover the activation of cortactin, which in turn forms a complex with WASP/Arp2/3, leading to the formation of lamellipodia and filopodia at the leading edge of migrating cells. As a result, cells appear to be more spreading and prone to promoting cell migration under the inhibition of PrKD.

\*\*Synergistic effect of PrKD inhibitors was observed as elongated cell morphology with increased cell surface area was observed in the treatment of PrKD inhibitor alone without chemokine stimulation. Similar observations were seen cells treated with PrKD inhibitor and stimulated with chemokines.

# Chapter 6: Final discussion and thesis conclusion

---

In this thesis, we explored the involvement of chemokine signalling in the aspects of receptor internalisation and downstream pathways contributing to cancer cell migration, mainly focusing on CCL3-CCR5 and CXCL12-CXCR4 signalling axes. Our aim is to characterise common cancer cell lines potentially useful for preliminary research and drug target screening in the field of chemokine and understand the specific roles of downstream effectors for the design of targeted cancer drugs. Overall, the conclusions are as follows:

1. Different cancer cell lines display distinct endogenous expression profile of chemokine receptors, which is one of the main determinants in the choice of cell line as an experimental model in the study of chemokine signalling. Based on the abundance of endogenously expressing chemokine receptors, breast cancer MCF-7 cells are ideal as a model system for the investigation of CXCL12-CXCR4 and CCL3-CCR5 signalling. Another cell line, leukaemic Jurkat cells, are also good for investigating CXCL12-CXCR4 signalling.
2. Cellular responses mediated by chemokine stimulation are specific to cell types and chemokine ligands. Some chemokine-induced responses might be more significant in some cell types than others due to two main factors: (1) expression level of chemokine receptor involved; (2) which signalling pathway is predominately activated in the cells.
3. The endocytic pathway, either clathrin-dependent or caveolae-dependent, utilised by chemokine receptors is specific to different cell types and chemokine ligands following chemokine stimulation. CXCL12-induced CXCR4 internalisation is caveolae-dependent in Jurkat cells, whereas CCL3-induced CCR5 internalisation is not dependent of clathrin in MCF-7 cells.
4. Caveolin-1 (Cav-1) is expressed in MCF-7 and Jurkat cells intracellularly. CXCL12 stimulation mediates translocation of Cav-1 proteins towards the leading edge of the cells. Previous studies revealed that caveolae are also

involved in chemotaxis apart from receptor internalisation. Movement of Cav-1 proteins might not necessarily reflect their involvement in receptor internalisation.

5. Dynamin-2 (Dyn-2) is involved in CCL3-induced CCR5 internalisation and CXCL12-induced CXCR4 internalisation in MCF-7 cells. Previous studies showed that Dyn-2 play a role in both clathrin-dependent and caveolae-dependent pathways. The pathways of receptor internalisation might not be deduced by the involvement of Dyn-2.
6. Arrestin-2 (Arr-2) might be involved in G-protein independent pathway in the stimulation of CCL3, whereas arrestin-3 (Arr-3) might be involved in CXCR4 internalisation dependent of dynamin following CXCL12 stimulation in MCF-7 cells. Arr-2 constructs translocate from the nucleus to the plasma membrane independently of dynamin following CCL3 stimulation, while Arr-3 constructs translocate towards the nucleus dependently of dynamin following CXCL12 stimulation.
7. Protein kinase D (PrKD) is involved in Ca<sup>2+</sup> signalling mediated by CCL3 and CXCL12 stimulation in MCF-7 and THP-1 cells. Inhibition of PrKD reduces intracellular Ca<sup>2+</sup> change following CXCL12 stimulation in MCF-7 cells and CCL3 stimulation in MCF-7 and THP-1 cells.
8. PrKD activation is essential for CXCL12-induced chemotaxis in Jurkat and THP-1 cells. PrKD inhibition blocks migration of Jurkat and THP-1 cells along CXCL12 concentration gradient.
9. Basally expressed PrKD acts as a negative regulator in actin cytoskeletal rearrangement in MCF-7 cells. PrKD inhibition causes increased cell surface area and elongated morphology in MCF-7 cells in the absence of chemokine stimulation.
10. PrKD does not directly regulate chemokine-induced receptor internalisation in MCF-7 and Jurkat cells. PrKD inhibition does not affect CCL3-induced CCR5 internalisation in MCF-7 cells and CXCL12-induced CXCR4 internalisation in both MCF-7 and Jurkat cells.

The aim of the thesis is to investigate chemokine-induced signalling pathways specific to individual cell type using cancer cell lines endogenously expressing chemokine receptors. Genetically modified cell lines by transfection of receptor of interest were avoided in our study as transfection of receptor might bypass

normal regulation of expression levels in the cell system. Physiological irrelevant cellular responses may result from the artefacts of overexpressed receptors. As discussed in the introduction, chemokine signalling is highly context-dependent and the complexity of biased signalling might contribute to different responses in different cancer cell types. Determination of biased signalling specific to cancer type is a novel approach to design targeted cancer therapy, in order to eliminate undesirable side effects by activating certain pathways but not others in specific type of cancer.

Prior to investigation of mechanisms underlying chemokine signalling pathways involved, we characterised the cell surface expression profile of chemokine receptor in a selection of commonly used cancer cell lines. Unlike cell lines exogenously expressing receptor of interest, endogenous expression level of chemokine receptors could vary across different patient-derived cancer cell lines representing different cancer types. It is not ideal to investigate further with cell lines expressing relatively low level of the receptor of interest as the cellular responses will be less likely to be reproducible. Our findings identified that breast cancer MCF-7 cells are a good study model for CCR5 and CXCR4 signalling, and leukaemic Jurkat cells are another useful model for CXCR4 signalling (**conclusion 1**). Both cell lines generally generate reproducible responses in most functional assays with very few variations from different phases of cell cycle in cell culture. For leukaemic THP-1 and invasive breast cancer MDA-MB-231 cells, our study found inconsistent responses in some functional assays due to batch-to-batch variations and experimentation at different phases of cell cycle.

As part of functional studies for chemokine signalling, we determined intracellular  $\text{Ca}^{2+}$  signalling in the stimulation of CCL3 and CXCL12 using  $\text{Ca}^{2+}$  mobilisation assay. As  $G_q$ -coupled signalling specifically leads to  $\text{Ca}^{2+}$ -involved signalling, our findings imply that CCL3-CCR5 signalling preferentially activates  $G_q$ -coupled signalling in MCF-7 and THP-1 cells. We also observed that Jurkat and MDA-MB-231 cells are less likely to generate intracellular  $\text{Ca}^{2+}$  release in response to chemokine stimulation, implying that alternative pathways independent of  $\text{Ca}^{2+}$  signalling might be involved (**conclusion 2**). Apart from  $\text{Ca}^{2+}$  mobilisation assay, other functional assays can be done to determine the involvement of G-protein

dependent and G-protein independent signalling pathways in the stimulation of chemokine.

In the activation of chemokine receptor coupled to  $G_{\alpha s}$ , intracellular cAMP level is increased by the action of adenylyl cyclases (ACs). On the other hand, activation of chemokine receptor coupled to  $G_{\alpha i}$  negatively regulate the conversion of ATP to cAMP by ACs, and reduction in cAMP level is resulted (Wang et al., 2004). cAMP regulates the activity of cAMP-dependent protein kinase A (PKA), contributing to various downstream cellular processes (Wang et al., 2004). Hence, cAMP is a good indicator in the study of chemokine signalling associated with  $G_{\alpha s}$  and  $G_{\alpha i}$  proteins. cAMP assay is to measure the cellular levels of cAMP which are dependent on the activity of ACs regulated by chemokine receptor coupled to  $G_{\alpha s}$  or  $G_{\alpha i}$  protein (Wang et al., 2004). Particularly in the investigation of  $G_{\alpha i}$  coupled receptors, an additional step to pre-stimulate ACs with forskolin is required to inhibit the response from the stimulation of chemokine ligands by the measurement of reversal effects of chemokine ligands on cAMP levels (Wang et al., 2004). cAMP assays are generally based on the use of antibodies that specifically recognise intracellular cAMP and exogenous labelled cAMP conjugate by detection of labelled cAMP using fluorescence or luciferase-based detection technology (Zhang and Xie, 2012). The latest detection methods using homogenous time-resolved fluorescence (HTRF) and bead-based proximity chemiluminescence have improved the sensitivities useful for cells expressing low levels of receptors (Zhang and Xie, 2012).

For  $G_{\alpha q}$  protein-dependent signalling, apart from  $Ca^{2+}$ ,  $IP_3/IP_1$  is key signalling transducer. Following stimulation of chemokine receptor coupled to  $G_{\alpha q}$  protein, phospholipase C (PLC) is activated and in turn hydrolyses phosphatidylinositol bisphosphate ( $PIP_2$ ) to form inositol 1,4,5-triphosphate ( $IP_3$ ) and DAG.  $IP_3$  activates the  $IP_3$ -gated ion channels on the endoplasmic reticulum (ER) resulting in an efflux of  $Ca^{2+}$  from the ER to the cytoplasm as a result of increase in intracellular  $Ca^{2+}$ . In the meantime,  $IP_3$  is hydrolysed to  $IP_2$  and then to  $IP_1$ , eventually to inositol rapidly after activation of  $IP_3$ -gated ion channel (Stephens et al., 1994). In the detection of  $IP_1$ , the latest homogenous TRF assay is based on the measurement of reduction in energy transfer between the acceptor  $IP_1$  and a europium-conjugated  $IP_1$  antibody since the accumulation of cellular  $IP_1$  from

the enzymatic reactions of IP<sub>3</sub> replaces the acceptor IP<sub>1</sub> in binding the IP<sub>1</sub> antibody (Zhang and Xie, 2012). This can be used as supportive evidence from Ca<sup>2+</sup> mobilisation assay.

In addition, more generalised GTPγS binding assay can also be used to determine G<sub>αq</sub> and G<sub>αs</sub> protein-dependent signalling (Harrison and Traynor, 2003). Following dissociation of Gα from the Gαβγ heterotrimer, the G protein heterotrimer is reformed by the conversion of Gα-GTP back to Gα-GDP by the GTPase activity. The GTPγS assay measures the guanine nucleotide exchange of G proteins by determining the binding of the non-hydrolyzable analog [<sup>35</sup>S]GTPγS to Gα subunits (Harrison and Traynor, 2003).

For G<sub>βγ</sub> protein-dependent signalling, G<sub>βγ</sub> mediates Raf GTPase to induce the activation of MAPK/ERK cascade (Gutkind, 1998). Phosphorylated ERK1/2 (p-ERK1/2) can be measured by western blot analysis traditionally (Garbison et al., 2004). Using bead-based proximity chemiluminescence, immuno-sandwich capture of endogenous p-ERK1/2 in cell lysates can be detected by the close proximity of donor and acceptor beads without the requirement of wash steps (Garbison et al., 2004).

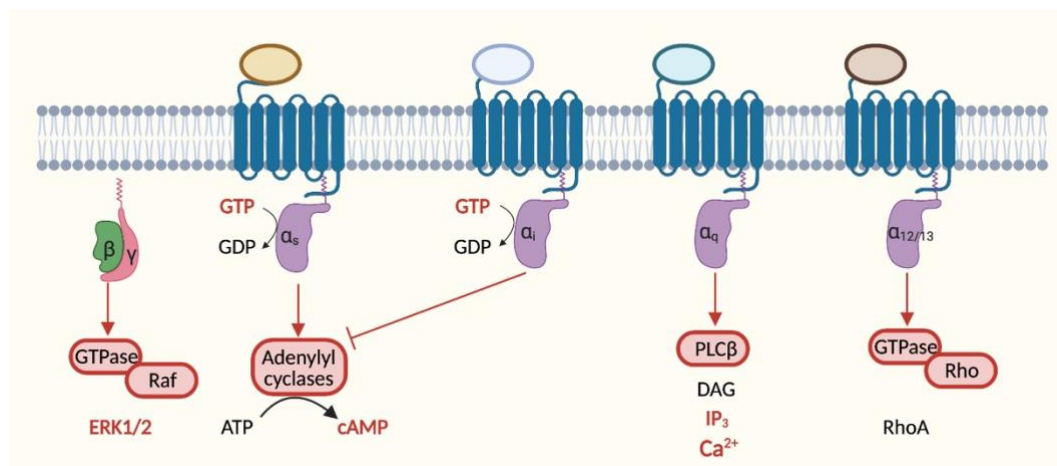


**Figure 6.1. Key downstream signalling transducers involved in the stimulation of G<sub>αs</sub>, G<sub>αi</sub>, G<sub>αq</sub> and G<sub>βγ</sub> proteins.** G<sub>αs</sub> activates ACs and converts ATP to cAMP. G<sub>αi</sub> negatively regulate ACs to reduce the production of cAMP. G<sub>αq</sub> activates PLC and in turn hydrolyses PIP<sub>2</sub> to form IP<sub>3</sub> and DAG. IP<sub>3</sub> activates the IP<sub>3</sub> receptor on the endoplasmic reticulum (ER) resulting in an efflux of Ca<sup>2+</sup> from the ER to the cytoplasm and an

elevation of intracellular  $\text{Ca}^{2+}$ .  $\text{G}_{\beta\gamma}$  mediates Raf GTPase to induce the activation of MAPK/ERK cascade. All downstream signalling transducers for functional assays are highlighted in red. (Image created with BioRender.com)

Alternatively, bioluminescence resonance energy transfer (BRET) is a popular technology used recently to study proximity within cells (Pfleger and Eidne, 2005). This technology can also be applied to study the investigation of ligand-receptor and protein-protein interactions in chemokine signalling. The basis of BRET relies on dipole-dipole non-radiative energy transfer from a luciferase energy donor to an acceptor fluorophore when a luciferase substrate is oxidised (Pfleger and Eidne, 2005). Two proteins of interest are attached to luciferase donor and acceptor fluorophore respectively. Energy transfer occurs only when the donor and acceptor are within close proximity (<10 nm), which could monitor protein-protein proximity in a highly specific manner (Pfleger and Eidne, 2005).

The most recent improved version of BRET is known as NanoBRET with increase assay sensitivity to enable monitoring protein-protein interactions (PPIs) at lower level as commonly seen in physiological relevant cell lines (Mo et al., 2016). The components used in NanoBRET assays include luciferase reporter, Nluc, as the energy donor with its associated substrate, furimazine, and a GFP variant as the energy acceptor (Hall et al., 2012). In addition to the advantage of increased luminescence, small sized Nluc is also beneficial to enhance access to targets that are difficultly reached and prevent from steric hindrance that might alter intrinsic interactions of proteins of interests, compared to conventional version (Hall et al., 2012).

Another extended version of NanoBRET, called NanoLuc Binary Technology (NanoBiT), has been emerged in the past years and is extensively used to study  $\beta$ -arrestin recruitment to chemokine receptors and GPCR interactions with G proteins (Laschet et al., 2019; Storme et al., 2018; Dixon et al., 2016). This improved version resolves the issues of steric hindrance due to large fragment size and alterations to PPIs by intrinsic affinity of complementary fragments from previous versions, which could overcome the limitations in the investigation of weak PPIs (Dixon et al., 2016). NanoBiT is a Nluc-derived split luciferase reporter

system, which comprises an 18 kDa Nluc fragment (LgBiT) and a 1.3 kDa fragment (SmBiT) (Dixon et al., 2016). LgBiT exhibits high stability with improved expression levels at physiological levels, while SmBiT exhibits low intrinsic affinity ( $KD = 190 \mu M$ ) with the complementary fragment to prevent from interfering with PPIs (Dixon et al., 2016).

NanoBiT complementation assay has been used to monitor GPCR interactions with full length G proteins ( $G_{\alpha i}$ ,  $G_{\alpha o}$ ,  $G_{\alpha s}$ ,  $G_{\alpha q}$ ,  $G_{\alpha 11}$ ,  $G_{\alpha 12}$ , and  $G_{\alpha 13}$ ) (Laschet et al., 2019). It would also be useful to monitor the proximity of isoform-specific G protein and chemokine receptor following chemokine stimulation. It should be noted that this assay monitors the proximity of receptor-G protein, not measuring functionality of G proteins in downstream signalling. Therefore, conducting NanoBiT complementary assay in parallel to the functional assays described above is necessary in mechanistic study of chemokine signalling.

For the study of  $\beta$ -arrestin recruitment, a previous study demonstrates to use an optimized system of the  $A_3$  receptor C-terminally-tagged with LgBiT and arrestin-3 (Arr-3) N-terminally-tagged with SmBiT, revealing that phosphorylation of intracellular sites is not necessary for Arr-3 recruitment to the  $A_3$  receptor (Storme et al., 2018). From our study, Arr-2, but not Arr-3, was found to translocate to the plasma membrane following CCL3 stimulation in MCF-7 cells, potentially leading to G-protein independent signalling (**conclusion 6**). By utilising NanoBiT technology, we could confirm our findings in live cells and would be able to monitor the process of  $\beta$ -arrestin recruitment in real time.

An attempt has been done by another group using CRISPR-Cas9 to perform a BRET assay. This allows the observation of the recruitment of exogenous Arr-3 to genome-edited CXCR4 fused to Nluc as well as trafficking and internalization of CXCR4 (White et al., 2017). Our findings also demonstrated that transfected Arr-3 constructs translocate towards the nucleus following CXCL12 stimulation, implying that Arr-3 is potentially involved in CXCL12-induced CXCR4 internalisation (**conclusion 6**). With the combination of CRISPR/Cas9 genome engineering and BRET technologies, we could visualise the whole process of CXCR4 internalisation through Arr-3 recruitment. In addition, we also revealed that dynamin is associated with Arr-3 recruitment in CXCR4 internalisation

(**conclusions 5 and 6**). The technique might be useful to monitor the proximity of the interactions of dynamin-Arr-3 and dynamin-CXCR4 in the combination of the application of NanoBiT.

It is noteworthy that HEK293T cells were generally used in most studies applying the advanced technology above (Laschet et al., 2019; White et al., 2017), but no attempts were done in more physiological relevant patient-derived cancer cell lines. There might be potential issues in genome editing of these cell lines for the application of BRET technique. Therefore, assay optimisation is required prior to conducting the assays described above. If it works for cancer cell lines in our study, we could expand the use of CRISPR-Cas9 and BRET to investigate the isoform-specific roles of PrKD in chemokine signalling and receptor internalisation to confirm our findings using pan-PrKD inhibitors (**conclusions 7, 8, 10**). Also, NanoBiT can be applied to monitor potential proximity of the interaction of PrKD and cortactin in the regulation of actin cytoskeletal rearrangement to confirm our hypothesis implicated by our findings (**conclusion 9**)

In the aspect of chemokine-induced chemotaxis, we showed that CXCL12 stimulation mediates chemotaxis in Jurkat and THP-1 cells and more migration was observed in Jurkat cells (**conclusion 2**). Not all cell lines could be applied to the chemotaxis assays in our study due to limitations as stated in Chapter 2. Also, the assays are not physiological relevant. Therefore, we did not progress further using chemotaxis assays.

The chemotaxis assay employed in our study is based on two-compartment design where cells are seeded on the upper compartment and control buffer or chemoattractant are added in the bottom compartment. The cells migrate towards the bottom compartment within the concentration gradient. Quantitative data generated in our assay is based on count of cells that have migrated to the bottom chemoattractant compartment in a fixed incubation time. However, the change in concentration gradient over time is unknown with this end-point analysis.

A recent study designed a chamber for the study of chemotaxis, providing stable chemoattractant concentration gradients for at least 24 hours especially for slow

migrating cells and gradients of different steepness with defined directions. Most importantly, the chamber allows direct visualisation of cell migration using time-lapse microscopy (Muinonen-Martin et al., 2010). Apart from quantification of migrating cells, real time visualisation is necessary for distinguishing directional chemotaxis from random chemokinesis, providing more detailed information on cell behaviour. The chamber is a revised version of commercially available bridge chambers. It comprises of a viewing bridge, chemoattractant well, buffer/control well and cover slip support. The small gap between the bridge and the cover slip where cells are seeded are small but large enough to allow diffusion of the chemoattractant. The main features differing from the conventional chamber is the differing widths of the two bridges with different gradient steepnesses and the unidirectional directions of two chemotactic gradients across each bridge (Muinonen-Martin et al., 2010). Also, the cover slip is compatible for an inverted time-lapse microscopy (0.16–0.18 mm) (Muinonen-Martin et al., 2010). Using time-lapse microscopy, multi-steps of the motility cycle, such as lamellipodia protrusion and detachment of the rear of the cells, can be observed within the cover slip. This device will provide more detailed information to support our findings on visualisation of actin cytoskeletal change using phalloidin F-actin stain if it works in the cancer cell lines in our study. In addition, our study showed PrKD inhibition causes increased cell surface area and elongated morphology in MCF-7 cells (**conclusion 9**). We could then investigate further the effects of PrKD on actin cytoskeletal rearrangement in the regulation of cell migration using this chemotaxis device.

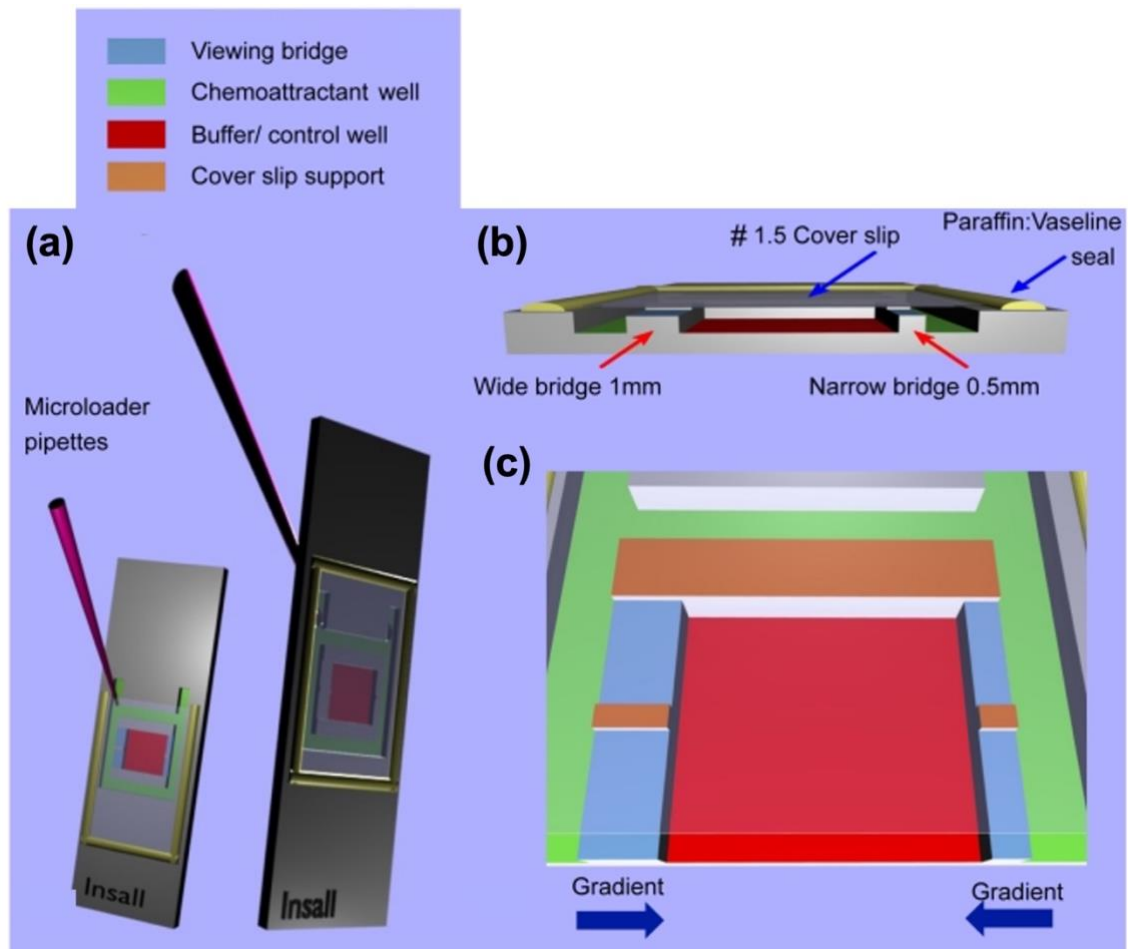


**Figure 6.2. Revised version of bridge chemotaxis chamber (Insall).**

Schematic diagram showing the components and layout of Insall chemotaxis chamber. (a) Chamber with front or reverse side chemoattractant loading with no requirement for metal clips. After loading of chemoattractant, cover slips are sealed in place with a 1:1 mix of vaseline: paraffin, producing a tight seal that reduces the risk of evaporation during experiments over several hours. (b) Cross section of the Insall chamber highlighting a feature of thin (0.16–0.18 mm) cover slips that permit visualisation under high NA oil immersion microscopy. Wide bridge and narrow bridge provide different gradient steepnesses. (c) Schematic diagram demonstrating unidirectional flow of the two chemotactic gradients, across each bridge (Image taken from Muinonen-Martin et al., 2010).

With respect to potential translation of our research into clinical uses, therapeutic nanomedicines are emerging in anti-cancer target therapy nowadays. Investigation of chemokine receptor endocytic pathways would be useful to understand how the nanomedicines are uptaken by cancer cells and reach their

intracellular targets especially for the design and engineering of chemokine receptor-specific drugs. As demonstrated by our findings together with evidence supported by previous studies, receptor internalisation pathways are not the same for all cancer cell types (**conclusion 3**) (Neel et al., 2005). Therefore, determining the mechanism of receptor endocytosis using specific cancer cell lines would facilitate the understanding of the uptake of the chemokine receptor-targeted nanoparticles into target cell types to improve the efficiency of drug delivery and therapeutic activity. Although our findings provided some insights into the roles of critical proteins in receptor internalisation, including clathrin, caveolae, dynamin and  $\beta$ -arrestins (**conclusions 3-6**), there are still some points that are inconclusive without a defined mechanism due to poor specificity of inhibitors used in the study. For example, clathrin inhibitor, pitstop 2, was found to have non-specific effect for CXCR4 internalisation. Caveolae-depleting agents, nystatin and filipin, might cause changes in membrane fluidity that might interfere with the endocytic mechanisms investigated (Bolard, 1986). Thus, alternative approaches other than using inhibitors should be considered to verify our findings. Knockout of the proteins of interest or expression of dominant-negative inhibitors could be an option to overcome the off-target effects of the inhibitors. For instance, caveolin-1 or cavin1 knockout can be done for caveolae-dependent pathway (Gilleron et al., 2013; Pelkmans et al., 2001), while clathrin knockout cells can be used for clathrin-dependent pathway (Gilleron et al., 2013; Liu et al., 1998). However, caution should be taken when the endocytic pathways may share protein components. For example, dynamin-2 is involved in both clathrin-dependent and caveolae-dependent pathways (Nichols and Lippincott-Schwartz, 2001; Liu et al., 2010). Therefore, validation step is crucial to avoid interfering between pathways.

In addition, internalisation is only the first step and the trafficking of endocytosed nanoparticles in the cytosol to the intracellular target should also be considered in design of therapeutic nanoparticles. Different endosomal compartments with different mechanisms were found to be involved in different endocytic pathways (Eyster et al., 2009). This could influence the fate of therapeutic nanoparticles. Hence, investigation of specific endosomal compartments involved in receptor trafficking is also necessary in the next stage.

## References

---

- Addison, C.L., Daniel, T.O., Burdick, M.D., Liu, H., Ehlert, J.E., Xue, Y.Y., Buechi, L., Walz, A., Richmond, A., Strieter, R.M., 2000. The CXC chemokine receptor 2, CXCR2, is the putative receptor for ELR+ CXC chemokine-induced angiogenic activity. *J Immunol* 165, 5269–5277. <https://doi.org/10.4049/jimmunol.165.9.5269>
- Ahr, B., Denizot, M., Robert-Hebmann, V., Brelot, A., Biard-Piechaczyk, M., 2005. Identification of the Cytoplasmic Domains of CXCR4 Involved in Jak2 and STAT3 Phosphorylation \*. *Journal of Biological Chemistry* 280, 6692–6700. <https://doi.org/10.1074/jbc.M408481200>
- Aicart-Ramos, C., He, S.D.Q., Land, M., Rubin, C.S., 2016. A Novel Conserved Domain Mediates Dimerization of Protein Kinase D (PKD) Isoforms: DIMERIZATION IS ESSENTIAL FOR PKD-DEPENDENT REGULATION OF SECRETION AND INNATE IMMUNITY\*. *Journal of Biological Chemistry* 291, 23516–23531. <https://doi.org/10.1074/jbc.M116.735399>
- Akashi, T., Koizumi, K., Tsuneyama, K., Saiki, I., Takano, Y., Fuse, H., 2008. Chemokine receptor CXCR4 expression and prognosis in patients with metastatic prostate cancer. *Cancer Science* 99, 539–542. <https://doi.org/10.1111/j.1349-7006.2007.00712.x>
- Alassaf, E., Mueller, A., 2020. The role of PKC in CXCL8 and CXCL10 directed prostate, breast and leukemic cancer cell migration. *European Journal of Pharmacology* 886, 173453. <https://doi.org/10.1016/j.ejphar.2020.173453>
- Aldinucci, D., Borghese, C., Casagrande, N., 2020. The CCL5/CCR5 Axis in Cancer Progression. *Cancers (Basel)* 12, 1765. <https://doi.org/10.3390/cancers12071765>
- Ali J. Ryan, Norman M. Gray, Peter N. Lowe, and, Chung\*, C., 2003. Effect of Detergent on “Promiscuous” Inhibitors [WWW Document]. ACS Publications. <https://doi.org/10.1021/jm0340896>
- Allen, S.J., Crown, S.E., Handel, T.M., 2007. Chemokine: receptor structure, interactions, and antagonism. *Annu Rev Immunol* 25, 787–820. <https://doi.org/10.1146/annurev.immunol.24.021605.090529>
- Alsaab, H.O., Sau, S., Alzhrani, R., Tatiparti, K., Bhise, K., Kashaw, S.K., Iyer, A.K., 2017. PD-1 and PD-L1 Checkpoint Signaling Inhibition for Cancer Immunotherapy: Mechanism, Combinations, and Clinical Outcome. *Front Pharmacol* 8, 561. <https://doi.org/10.3389/fphar.2017.00561>
- Ambriz-Peña, X., García-Zepeda, E.A., Meza, I., Soldevila, G., 2014. Jak3 Enables Chemokine-Dependent Actin Cytoskeleton Reorganization by Regulating Cofilin and Rac/Rhoa GTPases Activation. *PLOS ONE* 9, e88014. <https://doi.org/10.1371/journal.pone.0088014>
- Anderson, R.G.W., 1998. The Caveolae Membrane System. *Annual Review of Biochemistry* 67, 199–225. <https://doi.org/10.1146/annurev.biochem.67.1.199>
- Ariotti, N., Rae, J., Leneva, N., Ferguson, C., Loo, D., Okano, S., Hill, M.M., Walser, P., Collins, B.M., Parton, R.G., 2015. Molecular Characterization of Caveolin-induced Membrane Curvature. *J Biol Chem* 290, 24875–24890. <https://doi.org/10.1074/jbc.M115.644336>
- Bagnato, A., Rosanò, L., 2019. New Routes in GPCR/ $\beta$ -Arrestin-Driven Signaling in Cancer Progression and Metastasis. *Front Pharmacol* 10, 114. <https://doi.org/10.3389/fphar.2019.00114>

- Balkwill, F., 2004. Cancer and the chemokine network. *Nat Rev Cancer* 4, 540–550. <https://doi.org/10.1038/nrc1388>
- Ballesteros, J.A., Weinstein, H., 1995. [19] Integrated methods for the construction of three-dimensional models and computational probing of structure-function relations in G protein-coupled receptors, in: Sealfon, S.C. (Ed.), *Methods in Neurosciences, Receptor Molecular Biology*. Academic Press, pp. 366–428. [https://doi.org/10.1016/S1043-9471\(05\)80049-7](https://doi.org/10.1016/S1043-9471(05)80049-7)
- Baltoumas, F.A., Theodoropoulou, M.C., Hamodrakas, S.J., 2016. Molecular dynamics simulations and structure-based network analysis reveal structural and functional aspects of G-protein coupled receptor dimer interactions. *J Comput Aided Mol Des* 30, 489–512. <https://doi.org/10.1007/s10822-016-9919-y>
- Bannert, N., Craig, S., Farzan, M., Sogah, D., Santo, N.V., Choe, H., Sodroski, J., 2001. Sialylated O-glycans and sulfated tyrosines in the NH<sub>2</sub>-terminal domain of CC chemokine receptor 5 contribute to high affinity binding of chemokines. *J Exp Med* 194, 1661–1673. <https://doi.org/10.1084/jem.194.11.1661>
- Barlic, J., Khandaker, M.H., Mahon, E., Andrews, J., DeVries, M.E., Mitchell, G.B., Rahimpour, R., Tan, C.M., Ferguson, S.S.G., Kelvin, D.J., 1999.  $\beta$ -Arrestins Regulate Interleukin-8-induced CXCR1 Internalization\*. *Journal of Biological Chemistry* 274, 16287–16294. <https://doi.org/10.1074/jbc.274.23.16287>
- Barmania, F., Pepper, M., 2013. C-C chemokine receptor type five (CCR5): An emerging target for the control of HIV infection. *Applied & Translational Genomics* 2. <https://doi.org/10.1016/j.atg.2013.05.004>
- Barral, D.C., Staiano, L., Guimas Almeida, C., Cutler, D.F., Eden, E.R., Futter, C.E., Galione, A., Marques, A.R.A., Medina, D.L., Napolitano, G., Settembre, C., Vieira, O.V., Aerts, J.M.F.G., Atakpa-Adaji, P., Bruno, G., Capuozzo, A., De Leonibus, E., Di Malta, C., Escrevente, C., Esposito, A., Grumati, P., Hall, M.J., Teodoro, R.O., Lopes, S.S., Luzio, J.P., Monfregola, J., Montefusco, S., Platt, F.M., Polishchuck, R., De Risi, M., Sambri, I., Soldati, C., Seabra, M.C., 2022. Current methods to analyze lysosome morphology, positioning, motility and function. *Traffic* 23, 238–269. <https://doi.org/10.1111/tra.12839>
- Bashkirov, P.V., Akimov, S.A., Evseev, A.I., Schmid, S.L., Zimmerberg, J., Frolov, V.A., 2008. A partnership between dynamin and lipids defines dynamics and intermediates of membrane fission. *Cell* 135, 1276–1286. <https://doi.org/10.1016/j.cell.2008.11.028>
- Bates, D., Eastman, A., 2017. Microtubule destabilising agents: far more than just antimetabolic anticancer drugs. *Br J Clin Pharmacol* 83, 255–268. <https://doi.org/10.1111/bcp.13126>
- Berchiche, Y.A., Gravel, S., Pelletier, M.-E., St-Onge, G., Heveker, N., 2011. Different Effects of the Different Natural CC Chemokine Receptor 2b Ligands on  $\beta$ -Arrestin Recruitment, Gai Signaling, and Receptor Internalization. *Mol Pharmacol* 79, 488–498. <https://doi.org/10.1124/mol.110.068486>
- Bergert, M., Chandradoss, S.D., Desai, R.A., Paluch, E., 2012. Cell mechanics control rapid transitions between blebs and lamellipodia during migration. *Proc Natl Acad Sci U S A* 109, 14434–14439. <https://doi.org/10.1073/pnas.1207968109>

- Bernhart, E., Damm, S., Wintersperger, A., DeVaney, T., Zimmer, A., Raynham, T., Ireson, C., Sattler, W., 2013. Protein kinase D2 regulates migration and invasion of U87MG glioblastoma cells in vitro. *Exp Cell Res* 319, 2037–2048. <https://doi.org/10.1016/j.yexcr.2013.03.029>
- Bernhem, K., Blom, H., Brismar, H., 2018. Quantification of endogenous and exogenous protein expressions of Na,K-ATPase with super-resolution PALM/STORM imaging. *PLoS One* 13, e0195825. <https://doi.org/10.1371/journal.pone.0195825>
- Bernstein, B.W., Bamburg, J.R., 2010. ADF/cofilin: a functional node in cell biology. *Trends Cell Biol* 20, 187–195. <https://doi.org/10.1016/j.tcb.2010.01.001>
- Berridge, M.V., Tan, A.S., 1993. Characterization of the Cellular Reduction of 3-(4,5-dimethylthiazol-2-yl)-2,5-diphenyltetrazolium bromide (MTT): Subcellular Localization, Substrate Dependence, and Involvement of Mitochondrial Electron Transport in MTT Reduction. *Archives of Biochemistry and Biophysics* 303, 474–482. <https://doi.org/10.1006/abbi.1993.1311>
- Bhullar, K.S., Lagarón, N.O., McGowan, E.M., Parmar, I., Jha, A., Hubbard, B.P., Rupasinghe, H.P.V., 2018. Kinase-targeted cancer therapies: progress, challenges and future directions. *Molecular Cancer* 17, 48. <https://doi.org/10.1186/s12943-018-0804-2>
- Bian, J., Lei, J., Yin, X., Wang, P., Wu, Y., Yang, X., Wang, L., Zhang, S., Liu, H., Fu, M.L.X., 2019. Limited AT1 Receptor Internalization Is a Novel Mechanism Underlying Sustained Vasoconstriction Induced by AT1 Receptor Autoantibody From Preeclampsia. *Journal of the American Heart Association* 8, e011179. <https://doi.org/10.1161/JAHA.118.011179>
- Blaise, A.M., Corcoran, E.E., Wattenberg, E.S., Zhang, Y.-L., Cottrell, J.R., Koleske, A.J., 2021. In vitro fluorescence assay to measure GDP/GTP exchange of guanine nucleotide exchange factors of Rho family GTPases. *Biol Methods Protoc* 7, bpab024. <https://doi.org/10.1093/biomethods/bpab024>
- Blanpain, C., Doranz, B.J., Vakili, J., Rucker, J., Govaerts, C., Baik, S.S., Lorthioir, O., Migeotte, I., Libert, F., Baleux, F., Vassart, G., Doms, R.W., Parmentier, M., 1999a. Multiple charged and aromatic residues in CCR5 amino-terminal domain are involved in high affinity binding of both chemokines and HIV-1 Env protein. *J Biol Chem* 274, 34719–34727. <https://doi.org/10.1074/jbc.274.49.34719>
- Blanpain, C., Lee, B., Vakili, J., Doranz, B.J., Govaerts, C., Migeotte, I., Sharron, M., Dupriez, V., Vassart, G., Doms, R.W., Parmentier, M., 1999b. Extracellular cysteines of CCR5 are required for chemokine binding, but dispensable for HIV-1 coreceptor activity. *J Biol Chem* 274, 18902–18908. <https://doi.org/10.1074/jbc.274.27.18902>
- Blanpain, C., Wittamer, V., Vanderwinden, J.M., Boom, A., Renneboog, B., Lee, B., Le Poul, E., El Asmar, L., Govaerts, C., Vassart, G., Doms, R.W., Parmentier, M., 2001. Palmitoylation of CCR5 is critical for receptor trafficking and efficient activation of intracellular signaling pathways. *J Biol Chem* 276, 23795–23804. <https://doi.org/10.1074/jbc.M100583200>
- Bluemel, C., Hahner, S., Heinze, B., Fassnacht, M., Kroiss, M., Bley, T.A., Wester, H.-J., Kropf, S., Lapa, C., Schirbel, A., Buck, A.K., Herrmann, K., 2017. Investigating the Chemokine Receptor 4 as Potential Theranostic Target in Adrenocortical Cancer Patients. *Clinical Nuclear Medicine* 42, e29. <https://doi.org/10.1097/RLU.0000000000001435>

- Bolard, J., 1986. How do the polyene macrolide antibiotics affect the cellular membrane properties? *Biochim Biophys Acta* 864, 257–304. [https://doi.org/10.1016/0304-4157\(86\)90002-x](https://doi.org/10.1016/0304-4157(86)90002-x)
- Bonecchi, R., Locati, M., Galliera, E., Vulcano, M., Sironi, M., Fra, A.M., Gobbi, M., Vecchi, A., Sozzani, S., Haribabu, B., Van Damme, J., Mantovani, A., 2004. Differential Recognition and Scavenging of Native and Truncated Macrophage-Derived Chemokine (Macrophage-Derived Chemokine/CC Chemokine Ligand 22) by the D6 Decoy Receptor1. *The Journal of Immunology* 172, 4972–4976. <https://doi.org/10.4049/jimmunol.172.8.4972>
- Borges, S., Döppler, H., Perez, E.A., Andorfer, C.A., Sun, Z., Anastasiadis, P.Z., Thompson, E., Geiger, X.J., Storz, P., 2013. Pharmacologic reversion of epigenetic silencing of the PRKD1 promoter blocks breast tumor cell invasion and metastasis. *Breast Cancer Res* 15, R66. <https://doi.org/10.1186/bcr3460>
- Borges, S., Perez, E.A., Thompson, E.A., Radisky, D.C., Geiger, X.J., Storz, P., 2015. Effective Targeting of Estrogen Receptor Negative Breast Cancers with the Protein Kinase D inhibitor CRT0066101. *Mol Cancer Ther* 14, 1306–1316. <https://doi.org/10.1158/1535-7163.MCT-14-0945>
- Borroni, E.M., Mantovani, A., Locati, M., Bonecchi, R., 2010. Chemokine receptors intracellular trafficking. *Pharmacology & Therapeutics* 127, 1–8. <https://doi.org/10.1016/j.pharmthera.2010.04.006>
- Bossard, C., Bresson, D., Polishchuk, R.S., Malhotra, V., 2007. Dimeric PKD regulates membrane fission to form transport carriers at the TGN. *J Cell Biol* 179, 1123–1131. <https://doi.org/10.1083/jcb.200703166>
- Bowden, E.T., Barth, M., Thomas, D., Glazer, R.I., Mueller, S.C., 1999. An invasion-related complex of cortactin, paxillin and PKCmu associates with invadopodia at sites of extracellular matrix degradation. *Oncogene* 18, 4440–4449. <https://doi.org/10.1038/sj.onc.1202827>
- Brabletz, T., Jung, A., Reu, S., Porzner, M., Hlubek, F., Kunz-Schughart, L.A., Knuechel, R., Kirchner, T., 2001. Variable beta-catenin expression in colorectal cancers indicates tumor progression driven by the tumor environment. *Proc Natl Acad Sci U S A* 98, 10356–10361. <https://doi.org/10.1073/pnas.171610498>
- Bravo-Cordero, J.J., Magalhaes, M.A.O., Eddy, R.J., Hodgson, L., Condeelis, J., 2013. Functions of cofilin in cell locomotion and invasion. *Nat Rev Mol Cell Biol* 14, 10.1038/nrm3609. <https://doi.org/10.1038/nrm3609>
- Bravo-Sagua, R., Parra, V., Ortiz-Sandoval, C., Navarro-Marquez, M., Rodríguez, A.E., Diaz-Valdivia, N., Sanhueza, C., Lopez-Crisosto, C., Tahbaz, N., Rothermel, B.A., Hill, J.A., Cifuentes, M., Simmen, T., Quest, A.F.G., Lavandero, S., 2019. Caveolin-1 impairs PKA-DRP1-mediated remodelling of ER-mitochondria communication during the early phase of ER stress. *Cell Death Differ* 26, 1195–1212. <https://doi.org/10.1038/s41418-018-0197-1>
- Brew, R., Erikson, J.S., West, D.C., Kinsella, A.R., Slavin, J., Christmas, S.E., 2000. Interleukin-8 as an autocrine growth factor for human colon carcinoma cells in vitro. *Cytokine* 12, 78–85. <https://doi.org/10.1006/cyto.1999.0518>
- Brodsky, F.M., Chen, C.-Y., Knuehl, C., Towler, M.C., Wakeham, D.E., 2001. Biological Basket Weaving: Formation and Function of Clathrin-Coated Vesicles. *Annual Review of Cell and Developmental Biology* 17, 517–568. <https://doi.org/10.1146/annurev.cellbio.17.1.517>

- Bucci, C., Parton, R.G., Mather, I.H., Stunnenberg, H., Simons, K., Hoflack, B., Zerial, M., 1992. The small GTPase rab5 functions as a regulatory factor in the early endocytic pathway. *Cell* 70, 715–728. [https://doi.org/10.1016/0092-8674\(92\)90306-w](https://doi.org/10.1016/0092-8674(92)90306-w)
- Buckley, B.J., Whorton, A.R., 1997. Tunicamycin increases intracellular calcium levels in bovine aortic endothelial cells. *American Journal of Physiology-Cell Physiology* 273, C1298–C1305. <https://doi.org/10.1152/ajpcell.1997.273.4.C1298>
- Burg, J.S., Ingram, J.R., Venkatakrishnan, A.J., Jude, K.M., Dukkipati, A., Feinberg, E.N., Angelini, A., Waghray, D., Dror, R.O., Ploegh, H.L., Garcia, K.C., 2015. Structural basis for chemokine recognition and activation of a viral G protein–coupled receptor. *Science* 347, 1113–1117. <https://doi.org/10.1126/science.aaa5026>
- Busillo, J.M., Armando, S., Sengupta, R., Meucci, O., Bouvier, M., Benovic, J.L., 2010. Site-specific phosphorylation of CXCR4 is dynamically regulated by multiple kinases and results in differential modulation of CXCR4 signaling. *J Biol Chem* 285, 7805–7817. <https://doi.org/10.1074/jbc.M109.091173>
- Cai, X., Wang, D., Zhang, R., Chen, Y., Chen, J., 2023. The transmembrane domains of GPCR dimers as targets for drug development. *Drug Discovery Today* 28, 103419. <https://doi.org/10.1016/j.drudis.2022.103419>
- Cardaba, C.M., Kerr, J.S., Mueller, A., 2008. CCR5 internalisation and signalling have different dependence on membrane lipid raft integrity. *Cellular Signalling* 20, 1687–1694. <https://doi.org/10.1016/j.cellsig.2008.05.014>
- Carlier, M.F., Nioche, P., Broutin-L’Hermite, I., Boujemaa, R., Le Clainche, C., Egile, C., Garbay, C., Ducruix, A., Sansonetti, P., Pantaloni, D., 2000. GRB2 links signaling to actin assembly by enhancing interaction of neural Wiskott-Aldrich syndrome protein (N-WASp) with actin-related protein (ARP2/3) complex. *J Biol Chem* 275, 21946–21952. <https://doi.org/10.1074/jbc.M000687200>
- Carnec, X., Quan, L., Olson, W.C., Hazan, U., Dragic, T., 2005. Anti-CXCR4 Monoclonal Antibodies Recognizing Overlapping Epitopes Differ Significantly in Their Ability To Inhibit Entry of Human Immunodeficiency Virus Type 1. *J Virol* 79, 1930–1933. <https://doi.org/10.1128/JVI.79.3.1930-1933.2005>
- Caspar, B., Cocchiara, P., Melet, A., Van Emelen, K., Van der Aa, A., Milligan, G., Herbeuval, J.-P., 2022. CXCR4 as a novel target in immunology: moving away from typical antagonists. *Future Drug Discovery* 4, FDD77. <https://doi.org/10.4155/fdd-2022-0007>
- Cepeda, M.A., Evered, C.L., Pelling, J.J.H., Damjanovski, S., 2017. Inhibition of MT1-MMP proteolytic function and ERK1/2 signalling influences cell migration and invasion through changes in MMP-2 and MMP-9 levels. *J Cell Commun Signal* 11, 167–179. <https://doi.org/10.1007/s12079-016-0373-3>
- Chen, H., Zhang, S., Zhang, X., Liu, H., 2022. QR code model: a new possibility for GPCR phosphorylation recognition. *Cell Communication and Signaling* 20, 23. <https://doi.org/10.1186/s12964-022-00832-4>
- Chen, H.-W., Du, C.-W., Wei, X.-L., Khoo, U.-S., Zhang, G.-J., 2013. Cytoplasmic CXCR4 High-Expression Exhibits Distinct Poor Clinicopathological Characteristics and Predicts Poor Prognosis in Triple-Negative Breast Cancer. *Current Molecular Medicine* 13, 410–416. <https://doi.org/10.2174/156652413805076803>

- Chen, J., Deng, F., Li, J., Wang, Q.J., 2008. Selective binding of phorbol esters and diacylglycerol by individual C1 domains of the PKD family. *Biochem J* 411, 333–342. <https://doi.org/10.1042/BJ20071334>
- Cheng, J.P.X., Nichols, B.J., 2016. Caveolae: One Function or Many? *Trends in Cell Biology* 26, 177–189. <https://doi.org/10.1016/j.tcb.2015.10.010>
- Cheng, Z.-J., Zhao, J., Sun, Y., Hu, W., Wu, Y.-L., Cen, B., Wu, G.-X., Pei, G., 2000.  $\beta$ -Arrestin Differentially Regulates the Chemokine Receptor CXCR4-mediated Signaling and Receptor Internalization, and This Implicates Multiple Interaction Sites between  $\beta$ -Arrestin and CXCR4\*. *Journal of Biological Chemistry* 275, 2479–2485. <https://doi.org/10.1074/jbc.275.4.2479>
- Chew, A.L., Tan, W.Y., Khoo, B.Y., 2013. Potential combinatorial effects of recombinant atypical chemokine receptors in breast cancer cell invasion: A research perspective. *Biomedical Reports* 1, 185. <https://doi.org/10.3892/br.2013.57>
- Chow, M.T., Ozga, A.J., Servis, R.L., Frederick, D.T., Lo, J.A., Fisher, D.E., Freeman, G.J., Boland, G.M., Luster, A.D., 2019. Intratumoral Activity of the CXCR3 Chemokine System Is Required for the Efficacy of Anti-PD-1 Therapy. *Immunity* 50, 1498-1512.e5. <https://doi.org/10.1016/j.immuni.2019.04.010>
- Christoforides, C., Rainero, E., Brown, K.K., Norman, J.C., Toker, A., 2012. PKD controls  $\alpha\beta 3$  integrin recycling and tumor cell invasive migration through its substrate Rabaptin-5. *Dev Cell* 23, 560–572. <https://doi.org/10.1016/j.devcel.2012.08.008>
- Chrzanowska-Wodnicka, M., Burridge, K., 1996. Rho-stimulated contractility drives the formation of stress fibers and focal adhesions. *J Cell Biol* 133, 1403–1415. <https://doi.org/10.1083/jcb.133.6.1403>
- Ciraolo, E., Iezzi, M., Marone, R., Marengo, S., Curcio, C., Costa, C., Azzolino, O., Gonella, C., Rubinetto, C., Wu, H., Dastrù, W., Martin, E.L., Silengo, L., Altruda, F., Turco, E., Lanzetti, L., Musiani, P., Rùckle, T., Rommel, C., Backer, J.M., Forni, G., Wymann, M.P., Hirsch, E., 2008. Phosphoinositide 3-Kinase p110 $\beta$  activity: Key Role in Metabolism and Mammary Gland Cancer but not Development. *Sci Signal* 1, ra3. <https://doi.org/10.1126/scisignal.1161577>
- Clore, G.M., Gronenborn, A.M., 1995. Three-dimensional structures of alpha and beta chemokines. *FASEB J* 9, 57–62. <https://doi.org/10.1096/fasebj.9.1.7821760>
- Coggins, N.L., Trakimas, D., Chang, S.L., Ehrlich, A., Ray, P., Luker, K.E., Linderman, J.J., Luker, G.D., 2014. CXCR7 Controls Competition for Recruitment of  $\beta$ -Arrestin 2 in Cells Expressing Both CXCR4 and CXCR7. *PLOS ONE* 9, e98328. <https://doi.org/10.1371/journal.pone.0098328>
- Cole, K.E., Strick, C.A., Paradis, T.J., Ogborne, K.T., Loetscher, M., Gladue, R.P., Lin, W., Boyd, J.G., Moser, B., Wood, D.E., Sahagan, B.G., Neote, K., 1998. Interferon-inducible T Cell Alpha Chemoattractant (I-TAC): A Novel Non-ELR CXC Chemokine with Potent Activity on Activated T Cells through Selective High Affinity Binding to CXCR3. *Journal of Experimental Medicine* 187, 2009–2021. <https://doi.org/10.1084/jem.187.12.2009>
- Connell, B.J., Sadir, R., Baleux, F., Laguri, C., Kleman, J.-P., Luo, L., Arenzana-Seisdedos, F., Lortat-Jacob, H., 2016. Heparan sulfate differentially controls CXCL12 $\alpha$ - and CXCL12 $\gamma$ -mediated cell migration through differential presentation to their receptor CXCR4. *Science Signaling* 9, ra107–ra107. <https://doi.org/10.1126/scisignal.aaf1839>

- Cook, T.A., Urrutia, R., McNiven, M.A., 1994. Identification of dynamin 2, an isoform ubiquitously expressed in rat tissues. *Proceedings of the National Academy of Sciences* 91, 644–648. <https://doi.org/10.1073/pnas.91.2.644>
- Coso, O.A., Chiariello, M., Yu, J.-C., Teramoto, H., Crespo, P., Xu, N., Miki, T., Silvio Gutkind, J., 1995. The small GTP-binding proteins Rac1 and Cdc42 regulate the activity of the JNK/SAPK signaling pathway. *Cell* 81, 1137–1146. [https://doi.org/10.1016/S0092-8674\(05\)80018-2](https://doi.org/10.1016/S0092-8674(05)80018-2)
- D'Agostino, G., Cecchinato, V., Ugucioni, M., 2018. Chemokine Heterocomplexes and Cancer: A Novel Chapter to Be Written in Tumor Immunity. *Front Immunol* 9, 2185. <https://doi.org/10.3389/fimmu.2018.02185>
- Dale, D.C., Firkin, F.C., Bolyard, A.A., Tang, W., Jiang, H., MacLeod, R., Cadavid, D., Hu, Y., 2021. Mavorixafor, an Oral CXCR4 Antagonist, for Treatment of Patients with WHIM Syndrome: Results from the Long-Term Extension of the Open-Label Phase 2 Study. *Blood* 138, 1121. <https://doi.org/10.1182/blood-2021-145759>
- D'Alterio, C., Nasti, G., Polimeno, M., Ottaiano, A., Conson, M., Circelli, L., Botti, Giovanni, Scognamiglio, G., Santagata, S., De Divitiis, C., Nappi, A., Napolitano, M., Tatangelo, F., Pacelli, R., Izzo, F., Vuttariello, E., Botti, Gerardo, Scala, S., 2016. CXCR4–CXCL12–CXCR7, TLR2–TLR4, and PD-1/PD-L1 in colorectal cancer liver metastases from neoadjuvant-treated patients. *Oncol Immunology* 5, e1254313. <https://doi.org/10.1080/2162402X.2016.1254313>
- Dasgupta, P., Rizwani, W., Pillai, S., Davis, R., Banerjee, S., Hug, K., Lloyd, M., Coppola, D., Haura, E., Chellappan, S.P., 2011. ARRB1-Mediated Regulation of E2F Target Genes in Nicotine-Induced Growth of Lung Tumors. *J Natl Cancer Inst* 103, 317–333. <https://doi.org/10.1093/jnci/djq541>
- De Clercq, E., 2019. Mozobil® (Plerixafor, AMD3100), 10 years after its approval by the US Food and Drug Administration. *Antivir Chem Chemother* 27, 2040206619829382. <https://doi.org/10.1177/2040206619829382>
- De Clercq, E., 2005. Potential clinical applications of the CXCR4 antagonist bicyclam AMD3100. *Mini Rev Med Chem* 5, 805–824. <https://doi.org/10.2174/1389557054867075>
- De Kruijff, B., Demel, R.A., 1974. Polyene antibiotic-sterol interactions in membranes of *Acholeplasma laidlawii* cells and lecithin liposomes. III. Molecular structure of the polyene antibiotic-cholesterol complexes. *Biochimica et Biophysica Acta (BBA) - Biomembranes* 339, 57–70. [https://doi.org/10.1016/0005-2736\(74\)90332-0](https://doi.org/10.1016/0005-2736(74)90332-0)
- de Munnik, S.M., Smit, M.J., Leurs, R., Vischer, H.F., 2015. Modulation of cellular signaling by herpesvirus-encoded G protein-coupled receptors. *Front Pharmacol* 6, 40. <https://doi.org/10.3389/fphar.2015.00040>
- de Wit, R.H., de Munnik, S.M., Leurs, R., Vischer, H.F., Smit, M.J., 2016. Chapter Twenty-One - Molecular Pharmacology of Chemokine Receptors, in: Handel, T.M. (Ed.), *Methods in Enzymology, Chemokines*. Academic Press, pp. 457–515. <https://doi.org/10.1016/bs.mie.2015.12.002>
- Décaillot, F.M., Kazmi, M.A., Lin, Y., Ray-Saha, S., Sakmar, T.P., Sachdev, P., 2011a. CXCR7/CXCR4 Heterodimer Constitutively Recruits  $\beta$ -Arrestin to Enhance Cell Migration \*. *Journal of Biological Chemistry* 286, 32188–32197. <https://doi.org/10.1074/jbc.M111.277038>
- Décaillot, F.M., Kazmi, M.A., Lin, Y., Ray-Saha, S., Sakmar, T.P., Sachdev, P., 2011b. CXCR7/CXCR4 heterodimer constitutively recruits beta-arrestin to

- enhance cell migration. *J Biol Chem* 286, 32188–32197. <https://doi.org/10.1074/jbc.M111.277038>
- Dequiedt, F., Van Lint, J., Lecomte, E., Van Duppen, V., Seufferlein, T., Vandenneede, J.R., Wattiez, R., Kettmann, R., 2005. Phosphorylation of histone deacetylase 7 by protein kinase D mediates T cell receptor-induced Nur77 expression and apoptosis. *J Exp Med* 201, 793–804. <https://doi.org/10.1084/jem.20042034>
- Derivery, E., Gautreau, A., 2010. Generation of branched actin networks: assembly and regulation of the N-WASP and WAVE molecular machines. *Bioessays* 32, 119–131. <https://doi.org/10.1002/bies.200900123>
- DesMarais, V., Ghosh, M., Eddy, R., Condeelis, J., 2005. Cofilin takes the lead. *Journal of Cell Science* 118, 19–26. <https://doi.org/10.1242/jcs.01631>
- Dickson, R.B., Willingham and, M.C., Pastan, I.H., 1982. RECEPTOR-MEDIATED ENDOCYTOSIS OF  $\alpha$ 2-MACROGLOBULIN: INHIBITION BY IONOPHORES AND STIMULATION BY  $\text{Na}^+$  AND  $\text{HCO}_3^-$ . *Annals of the New York Academy of Sciences* 401, 38–49. <https://doi.org/10.1111/j.1749-6632.1982.tb25705.x>
- Dixon, A.S., Schwinn, M.K., Hall, M.P., Zimmerman, K., Otto, P., Lubben, T.H., Butler, B.L., Binkowski, B.F., Machleidt, T., Kirkland, T.A., Wood, M.G., Eggers, C.T., Encell, L.P., Wood, K.V., 2016. NanoLuc Complementation Reporter Optimized for Accurate Measurement of Protein Interactions in Cells. *ACS Chem. Biol.* 11, 400–408. <https://doi.org/10.1021/acscchembio.5b00753>
- Dohlman, H.G., Caron, M.G., DeBlasi, A., Frielle, T., Lefkowitz, R.J., 1990. Role of extracellular disulfide-bonded cysteines in the ligand binding function of the beta 2-adrenergic receptor. *Biochemistry* 29, 2335–2342. <https://doi.org/10.1021/bi00461a018>
- Döppler, H., Bastea, L.I., Borges, S., Spratley, S.J., Pearce, S.E., Storz, P., 2014. Protein Kinase D Isoforms Differentially Modulate Cofilin-Driven Directed Cell Migration. *PLOS ONE* 9, e98090. <https://doi.org/10.1371/journal.pone.0098090>
- Dragic, T., Trkola, A., Lin, S.W., Nagashima, K.A., Kajumo, F., Zhao, L., Olson, W.C., Wu, L., Mackay, C.R., Allaway, G.P., Sakmar, T.P., Moore, J.P., Maddon, P.J., 1998. Amino-terminal substitutions in the CCR5 coreceptor impair gp120 binding and human immunodeficiency virus type 1 entry. *J Virol* 72, 279–285. <https://doi.org/10.1128/JVI.72.1.279-285.1998>
- Drouillard, D., Craig, B.T., Dwinell, M.B., 2023. Physiology of chemokines in the cancer microenvironment. *American Journal of Physiology-Cell Physiology* 324, C167–C182. <https://doi.org/10.1152/ajpcell.00151.2022>
- Drury, L.J., Ziarek, J.J., Gravel, S., Veldkamp, C.T., Takekoshi, T., Hwang, S.T., Heveker, N., Volkman, B.F., Dwinell, M.B., 2011. Monomeric and dimeric CXCL12 inhibit metastasis through distinct CXCR4 interactions and signaling pathways. *Proc Natl Acad Sci U S A* 108, 17655–17660. <https://doi.org/10.1073/pnas.1101133108>
- Du, C., Jaggi, M., Zhang, C., Balaji, K.C., 2009. Protein kinase D1-mediated phosphorylation and subcellular localization of beta-catenin. *Cancer Res* 69, 1117–1124. <https://doi.org/10.1158/0008-5472.CAN-07-6270>
- Du, C., Zhang, C., Hassan, S., Biswas, M.H.U., Balaji, K.C., 2010. Protein kinase D1 suppresses epithelial-to-mesenchymal transition through phosphorylation of snail. *Cancer Res* 70, 7810–7819. <https://doi.org/10.1158/0008-5472.CAN-09-4481>

- Durieux, A.-C., Prudhon, B., Guichenev, P., Bitoun, M., 2010. Dynamin 2 and human diseases. *J Mol Med* 88, 339–350. <https://doi.org/10.1007/s00109-009-0587-4>
- Dyer, D.P., Salanga, C.L., Volkman, B.F., Kawamura, T., Handel, T.M., 2016. The dependence of chemokine–glycosaminoglycan interactions on chemokine oligomerization. *Glycobiology* 26, 312–326. <https://doi.org/10.1093/glycob/cwv100>
- Edwards, D.C., Sanders, L.C., Bokoch, G.M., Gill, G.N., 1999. Activation of LIM-kinase by Pak1 couples Rac/Cdc42 GTPase signalling to actin cytoskeletal dynamics. *Nat Cell Biol* 1, 253–259. <https://doi.org/10.1038/12963>
- Ehrlich, M., Boll, W., Van Oijen, A., Hariharan, R., Chandran, K., Nibert, M.L., Kirchhausen, T., 2004. Endocytosis by random initiation and stabilization of clathrin-coated pits. *Cell* 118, 591–605. <https://doi.org/10.1016/j.cell.2004.08.017>
- Eichel, K., Jullié, D., Barsi-Rhyne, B., Latorraca, N.R., Masureel, M., Sibarita, J.-B., Dror, R.O., von Zastrow, M., 2018. Catalytic activation of  $\beta$ -arrestin by GPCRs. *Nature* 557, 381–386. <https://doi.org/10.1038/s41586-018-0079-1>
- Eichel, K., Jullié, D., von Zastrow, M., 2016.  $\beta$ -Arrestin drives MAP kinase signalling from clathrin-coated structures after GPCR dissociation. *Nat Cell Biol* 18, 303–310. <https://doi.org/10.1038/ncb3307>
- Eiseler, T., Döppler, H., Yan, I.K., Goodison, S., Storz, P., 2009. Protein kinase D1 regulates matrix metalloproteinase expression and inhibits breast cancer cell invasion. *Breast Cancer Res* 11, R13. <https://doi.org/10.1186/bcr2232>
- Eiseler, T., Hausser, A., De Kimpe, L., Van Lint, J., Pfizenmaier, K., 2010. Protein Kinase D Controls Actin Polymerization and Cell Motility through Phosphorylation of Cortactin. *J Biol Chem* 285, 18672–18683. <https://doi.org/10.1074/jbc.M109.093880>
- Eiseler, T., Schmid, M.A., Topbas, F., Pfizenmaier, K., Hausser, A., 2007. PKD is recruited to sites of actin remodelling at the leading edge and negatively regulates cell migration. *FEBS Letters* 581, 4279–4287. <https://doi.org/10.1016/j.febslet.2007.07.079>
- El-Asmar, L., Springael, J.-Y., Ballet, S., Andrieu, E.U., Vassart, G., Parmentier, M., 2005. Evidence for negative binding cooperativity within CCR5-CCR2b heterodimers. *Mol Pharmacol* 67, 460–469. <https://doi.org/10.1124/mol.104.003624>
- Ellyard, J.I., Simson, L., Bezos, A., Johnston, K., Freeman, C., Parish, C.R., 2007. Eotaxin Selectively Binds Heparin: AN INTERACTION THAT PROTECTS EOTAXIN FROM PROTEOLYSIS AND POTENTIATES CHEMOTACTIC ACTIVITY IN VIVO. *Journal of Biological Chemistry* 282, 15238–15247. <https://doi.org/10.1074/jbc.M608046200>
- Elsner, D.J., Siess, K.M., Gossenreiter, T., Hartl, M., Leonard, T.A., 2019. A ubiquitin-like domain controls protein kinase D dimerization and activation by trans-autophosphorylation. *J Biol Chem* 294, 14422–14441. <https://doi.org/10.1074/jbc.RA119.008713>
- Ene-Obong, A., Clear, A.J., Watt, J., Wang, J., Fatah, R., Riches, J.C., Marshall, J.F., Chin-Aleong, J., Chelala, C., Gribben, J.G., Ramsay, A.G., Kocher, H.M., 2013. Activated Pancreatic Stellate Cells Sequester CD8+ T Cells to Reduce Their Infiltration of the Juxtatumoral Compartment of Pancreatic

- Ductal Adenocarcinoma. *Gastroenterology* 145, 1121–1132. <https://doi.org/10.1053/j.gastro.2013.07.025>
- Eyster, C.A., Higginson, J.D., Huebner, R., Porat-Shliom, N., Weigert, R., Wu, W.W., Shen, R.-F., Donaldson, J.G., 2009. Discovery of New Cargo Proteins that Enter Cells through Clathrin-Independent Endocytosis. *Traffic* 10, 590–599. <https://doi.org/10.1111/j.1600-0854.2009.00894.x>
- Faelber, K., Posor, Y., Gao, S., Held, M., Roske, Y., Schulze, D., Haucke, V., Noé, F., Daumke, O., 2011. Crystal structure of nucleotide-free dynamin. *Nature* 477, 556–560. <https://doi.org/10.1038/nature10369>
- Fan, G.-H., Lapierre, L.A., Goldenring, J.R., Richmond, A., 2003. Differential regulation of CXCR2 trafficking by Rab GTPases. *Blood* 101, 2115–2124. <https://doi.org/10.1182/blood-2002-07-1965>
- Fang, X.-Q., Qiao, H., Groveman, B.R., Feng, S., Pflueger, M., Xin, W.-K., Ali, M.K., Lin, S.-X., Xu, J., Duclot, F., Kabbaj, M., Wang, W., Ding, X.-S., Santiago-Sim, T., Jiang, X.-H., Salter, M.W., Yu, X.-M., 2015. Regulated internalization of NMDA receptors drives PKD1-mediated suppression of the activity of residual cell-surface NMDA receptors. *Molecular Brain* 8, 75. <https://doi.org/10.1186/s13041-015-0167-1>
- Farber, J.M., 1990. A macrophage mRNA selectively induced by gamma-interferon encodes a member of the platelet factor 4 family of cytokines. *Proc Natl Acad Sci U S A* 87, 5238–5242. <https://doi.org/10.1073/pnas.87.14.5238>
- Farzan, M., Mirzabekov, T., Kolchinsky, P., Wyatt, R., Cayabyab, M., Gerard, N.P., Gerard, C., Sodroski, J., Choe, H., 1999. Tyrosine sulfation of the amino terminus of CCR5 facilitates HIV-1 entry. *Cell* 96, 667–676. [https://doi.org/10.1016/s0092-8674\(00\)80577-2](https://doi.org/10.1016/s0092-8674(00)80577-2)
- Faulstich, H., Zobeley, S., Rinnerthaler, G., Small, J.V., 1988. Fluorescent phallotoxins as probes for filamentous actin. *J Muscle Res Cell Motil* 9, 370–383. <https://doi.org/10.1007/BF01774064>
- Ferguson, S.M., Brasnjo, G., Hayashi, M., Wölfel, M., Collesi, C., Giovedi, S., Raimondi, A., Gong, L.-W., Ariel, P., Paradise, S., O'Toole, E., Flavell, R., Cremona, O., Miesenböck, G., Ryan, T.A., De Camilli, P., 2007. A Selective Activity-Dependent Requirement for Dynamin 1 in Synaptic Vesicle Endocytosis. *Science* 316, 570–574. <https://doi.org/10.1126/science.1140621>
- Ferguson, S.M., Raimondi, A., Paradise, S., Shen, H., Mesaki, K., Ferguson, A., Destaing, O., Ko, G., Takasaki, J., Cremona, O., O'Toole, E., De Camilli, P., 2009. Coordinated actions of actin and BAR proteins upstream of dynamin at endocytic clathrin-coated pits. *Dev Cell* 17, 811–822. <https://doi.org/10.1016/j.devcel.2009.11.005>
- Ferguson, S.S., 2001. Evolving concepts in G protein-coupled receptor endocytosis: the role in receptor desensitization and signaling. *Pharmacol Rev* 53, 1–24.
- Ferguson, S.S.G., Downey, W.E., Colapietro, A.-M., Barak, L.S., Ménard, L., Caron, M.G., 1996. Role of  $\beta$ -Arrestin in Mediating Agonist-Promoted G Protein-Coupled Receptor Internalization. *Science* 271, 363–366. <https://doi.org/10.1126/science.271.5247.363>
- Fong, A.M., Premont, R.T., Richardson, R.M., Yu, Y.-R.A., Lefkowitz, R.J., Patel, D.D., 2002. Defective lymphocyte chemotaxis in beta-arrestin2- and GRK6-deficient mice. *Proc Natl Acad Sci U S A* 99, 7478–7483. <https://doi.org/10.1073/pnas.112198299>

- Foster, C.R., Satomi, S., Kato, Y., Patel, H.H., 2020. The caveolar-mitochondrial interface: regulation of cellular metabolism in physiology and pathophysiology. *Biochemical Society Transactions* 48, 165–177. <https://doi.org/10.1042/BST20190388>
- Fraile-Ramos, A., Kohout, T.A., Waldhoer, M., Marsh, M., 2003. Endocytosis of the viral chemokine receptor US28 does not require beta-arrestins but is dependent on the clathrin-mediated pathway. *Traffic* 4, 243–253. <https://doi.org/10.1034/j.1600-0854.2003.00079.x>
- Friedl, P., Alexander, S., 2011. Cancer Invasion and the Microenvironment: Plasticity and Reciprocity. *Cell* 147, 992–1009. <https://doi.org/10.1016/j.cell.2011.11.016>
- Friedl, P., Borgmann, S., Bröcker, E.B., 2001. Amoeboid leukocyte crawling through extracellular matrix: lessons from the Dictyostelium paradigm of cell movement. *J Leukoc Biol* 70, 491–509.
- Fu, Y., Rubin, C.S., 2011. Protein kinase D: coupling extracellular stimuli to the regulation of cell physiology. *EMBO Rep* 12, 785–796. <https://doi.org/10.1038/embor.2011.139>
- Fumagalli, A., Zarca, A., Neves, M., Caspar, B., Hill, S.J., Mayor, F., Smit, M.J., Marin, P., 2019. CXCR4/ACKR3 Phosphorylation and Recruitment of Interacting Proteins: Key Mechanisms Regulating Their Functional Status. *Mol Pharmacol* 96, 794–808. <https://doi.org/10.1124/mol.118.115360>
- Futahashi, Y., Komano, J., Urano, E., Aoki, T., Hamatake, M., Miyauchi, K., Yoshida, T., Koyanagi, Y., Matsuda, Z., Yamamoto, N., 2007. Separate elements are required for ligand-dependent and -independent internalization of metastatic potentiator CXCR4. *Cancer Science* 98, 373–379. <https://doi.org/10.1111/j.1349-7006.2007.00388.x>
- Gaidarov, I., Santini, F., Warren, R.A., Keen, J.H., 1999. Spatial control of coated-pit dynamics in living cells. *Nat Cell Biol* 1, 1–7. <https://doi.org/10.1038/8971>
- Gambin, Y., Ariotti, N., McMahon, K.-A., Bastiani, M., Sierrecki, E., Kovtun, O., Polinkovsky, M.E., Magenau, A., Jung, W., Okano, S., Zhou, Y., Leneva, N., Mureev, S., Johnston, W., Gaus, K., Hancock, J.F., Collins, B.M., Alexandrov, K., Parton, R.G., 2014. Single-molecule analysis reveals self assembly and nanoscale segregation of two distinct cavin subcomplexes on caveolae. *eLife* 3, e01434. <https://doi.org/10.7554/eLife.01434>
- Gao, D., Rahbar, R., Fish, E.N., 2016. CCL5 activation of CCR5 regulates cell metabolism to enhance proliferation of breast cancer cells. *Open Biol* 6, 160122. <https://doi.org/10.1098/rsob.160122>
- Gao, H., Sun, Y., Wu, Y., Luan, B., Wang, Y., Qu, B., Pei, G., 2004. Identification of beta-arrestin2 as a G protein-coupled receptor-stimulated regulator of NF-kappaB pathways. *Mol Cell* 14, 303–317. [https://doi.org/10.1016/s1097-2765\(04\)00216-3](https://doi.org/10.1016/s1097-2765(04)00216-3)
- Gao, P., Wange, R.L., Zhang, N., Oppenheim, J.J., Howard, O.M.Z., 2005. Negative regulation of CXCR4-mediated chemotaxis by the lipid phosphatase activity of tumor suppressor PTEN. *Blood* 106, 2619–2626. <https://doi.org/10.1182/blood-2004-08-3362>
- Garbison, K.E., Heinz, B.A., Lajiness, M.E., 2004. Phospho-ERK Assays, in: Weidner, J.R., Sittampalam, G.S., Markossian, S., Grossman, A., Brimacombe, K., Arkin, M., Auld, D., Austin, C., Baell, J., Chung, T.D.Y., Coussens, N.P., Dahlin, J.L., Devanarayan, V., Foley, T.L., Glicksman, M., Gorshkov, K., Haas, J.V., Hall, M.D., Hoare, S., Inglese, J., Iversen, P.W., Kales, S.C., Lal-Nag, M., Li, Z., McGee, J., McManus, O., Riss, T.,

- Saradjian, P., Sittampalam, G.S., Tarselli, M., Trask, O.J., Wang, Y., Weidner, J.R., Wildey, M.J., Wilson, K., Xia, M., Xu, X. (Eds.), *Assay Guidance Manual*. Eli Lilly & Company and the National Center for Advancing Translational Sciences, Bethesda (MD).
- García Lopez, M.A., Aguado Martínez, A., Lamaze, C., Martínez-A, C., Fischer, T., 2009. Inhibition of dynamin prevents CCL2-mediated endocytosis of CCR2 and activation of ERK1/2. *Cell Signal* 21, 1748–1757. <https://doi.org/10.1016/j.cellsig.2009.07.010>
- García-Cuesta, E.M., Santiago, C.A., Vallejo-Díaz, J., Juarranz, Y., Rodríguez-Frade, J.M., Mellado, M., 2019. The Role of the CXCL12/CXCR4/ACKR3 Axis in Autoimmune Diseases. *Frontiers in Endocrinology* 10.
- García-Perez, J., Rueda, P., Alcami, J., Rognan, D., Arenzana-Seisdedos, F., Lagane, B., Kellenberger, E., 2011a. Allosteric model of maraviroc binding to CC chemokine receptor 5 (CCR5). *J Biol Chem* 286, 33409–33421. <https://doi.org/10.1074/jbc.M111.279596>
- García-Perez, J., Rueda, P., Staropoli, I., Kellenberger, E., Alcami, J., Arenzana-Seisdedos, F., Lagane, B., 2011b. New insights into the mechanisms whereby low molecular weight CCR5 ligands inhibit HIV-1 infection. *J Biol Chem* 286, 4978–4990. <https://doi.org/10.1074/jbc.M110.168955>
- Ge, S., Pachter, J.S., 2004. Caveolin-1 Knockdown by Small Interfering RNA Suppresses Responses to the Chemokine Monocyte Chemoattractant Protein-1 by Human Astrocytes\*. *Journal of Biological Chemistry* 279, 6688–6695. <https://doi.org/10.1074/jbc.M311769200>
- George, K.M., Frantz, M.-C., Bravo-Altamirano, K., LaValle, C.R., Tandon, M., Leimgruber, S., Sharlow, E.R., Lazo, J.S., Wang, Q.J., Wipf, P., 2011. Design, Synthesis, and Biological Evaluation of PKD Inhibitors. *Pharmaceutics* 3, 186–228. <https://doi.org/10.3390/pharmaceutics3020186>
- Gérard, A., Mertens, A.E.E., van der Kammen, R.A., Collard, J.G., 2007. The Par polarity complex regulates Rap1- and chemokine-induced T cell polarization. *J Cell Biol* 176, 863–875. <https://doi.org/10.1083/jcb.200608161>
- Gilleron, J., Querbes, W., Zeigerer, A., Borodovsky, A., Marsico, G., Schubert, U., Manygoats, K., Seifert, S., Andree, C., Stöter, M., Epstein-Barash, H., Zhang, L., Koteliansky, V., Fitzgerald, K., Fava, E., Bickle, M., Kalaidzidis, Y., Akinc, A., Maier, M., Zerial, M., 2013. Image-based analysis of lipid nanoparticle-mediated siRNA delivery, intracellular trafficking and endosomal escape. *Nat Biotechnol* 31, 638–646. <https://doi.org/10.1038/nbt.2612>
- Gilles, P., Voets, L., Van Lint, J., De Borggraeve, W.M., 2021. Developments in the Discovery and Design of Protein Kinase D Inhibitors. *ChemMedChem* 16, 2158–2171. <https://doi.org/10.1002/cmcd.202100110>
- Gok Yavuz, B., Gunaydin, G., Gedik, M.E., Kosemehmetoglu, K., Karakoc, D., Ozgur, F., Guc, D., 2019. Cancer associated fibroblasts sculpt tumour microenvironment by recruiting monocytes and inducing immunosuppressive PD-1+ TAMs. *Sci Rep* 9, 3172. <https://doi.org/10.1038/s41598-019-39553-z>
- Gomariz, R.P., Gutiérrez-Cañas, I., Arranz, A., Carrión, M., Juarranz, Y., Leceta, J., Martínez, C., 2010. Peptides targeting Toll-like receptor signalling pathways for novel immune therapeutics. *Curr Pharm Des* 16, 1063–1080. <https://doi.org/10.2174/138161210790963841>

- González-Martín, A., Mira, E., Mañes, S., 2012. CCR5 in cancer immunotherapy: More than an “attractive” receptor for T cells. *Oncolmmunology* 1, 106–108. <https://doi.org/10.4161/onci.1.1.17995>
- Goodman, O.B., Krupnick, J.G., Santini, F., Gurevich, V.V., Penn, R.B., Gagnon, A.W., Keen, J.H., Benovic, J.L., 1996.  $\beta$ -Arrestin acts as a clathrin adaptor in endocytosis of the  $\beta$ 2-adrenergic receptor. *Nature* 383, 447–450. <https://doi.org/10.1038/383447a0>
- Govaerts, C., Blanpain, C., Deupi, X., Ballet, S., Ballesteros, J.A., Wodak, S.J., Vassart, G., Pardo, L., Parmentier, M., 2001. The TXP motif in the second transmembrane helix of CCR5. A structural determinant of chemokine-induced activation. *J Biol Chem* 276, 13217–13225. <https://doi.org/10.1074/jbc.M011670200>
- Gowhari Shabgah, A., Jadidi-Niaragh, F., Mohammadi, H., Ebrahimzadeh, F., Oveisee, M., Jahanara, A., Gholizadeh Navashenaq, J., 2022. The Role of Atypical Chemokine Receptor D6 (ACKR2) in Physiological and Pathological Conditions; Friend, Foe, or Both? *Frontiers in Immunology* 13.
- Graham, G.J., Locati, M., Mantovani, A., Rot, A., Thelen, M., 2012. The biochemistry and biology of the atypical chemokine receptors. *Immunology Letters, Chemokines from complexity to bedside* 145, 30–38. <https://doi.org/10.1016/j.imlet.2012.04.004>
- Griffith, J.W., Sokol, C.L., Luster, A.D., 2014. Chemokines and Chemokine Receptors: Positioning Cells for Host Defense and Immunity. *Annual Review of Immunology* 32, 659–702. <https://doi.org/10.1146/annurev-immunol-032713-120145>
- Griner, E.M., Kazanietz, M.G., 2007. Protein kinase C and other diacylglycerol effectors in cancer. *Nat Rev Cancer* 7, 281–294. <https://doi.org/10.1038/nrc2110>
- Guan, E., Wang, J., Norcross, M.A., 2001. Identification of Human Macrophage Inflammatory Proteins 1 $\alpha$  and 1 $\beta$  as a Native Secreted Heterodimer \*. *Journal of Biological Chemistry* 276, 12404–12409. <https://doi.org/10.1074/jbc.M006327200>
- Gupton, S.L., Gertler, F.B., 2007. Filopodia: the fingers that do the walking. *Sci STKE* 2007, re5. <https://doi.org/10.1126/stke.4002007re5>
- Gurevich, V.V., Hanson, S.M., Song, X., Vishnivetskiy, S.A., Gurevich, E.V., 2011. The functional cycle of visual arrestins in photoreceptor cells. *Prog Retin Eye Res* 30, 405–430. <https://doi.org/10.1016/j.preteyeres.2011.07.002>
- Gutkind, J.S., 1998. The pathways connecting G protein-coupled receptors to the nucleus through divergent mitogen-activated protein kinase cascades. *J Biol Chem* 273, 1839–1842. <https://doi.org/10.1074/jbc.273.4.1839>
- Haider, R.S., Matthees, E.S.F., Drube, J., Reichel, M., Zabel, U., Inoue, A., Cheigné, A., Krasel, C., Deupi, X., Hoffmann, C., 2022.  $\beta$ -arrestin1 and 2 exhibit distinct phosphorylation-dependent conformations when coupling to the same GPCR in living cells. *Nat Commun* 13, 5638. <https://doi.org/10.1038/s41467-022-33307-8>
- Halama, N., Zoernig, I., Berthel, A., Kahlert, C., Klupp, F., Suarez-Carmona, M., Suetterlin, T., Brand, K., Krauss, J., Lasitschka, F., Lerchl, T., Luckner-Minden, C., Ulrich, A., Koch, M., Weitz, J., Schneider, M., Buechler, M.W., Zitvogel, L., Herrmann, T., Benner, A., Kunz, C., Luecke, S., Springfield, C., Grabe, N., Falk, C.S., Jaeger, D., 2016. Tumoral Immune Cell Exploitation in Colorectal Cancer Metastases Can Be Targeted Effectively

- by Anti-CCR5 Therapy in Cancer Patients. *Cancer Cell* 29, 587–601. <https://doi.org/10.1016/j.ccell.2016.03.005>
- Hall, A., 1992. Ras-related GTPases and the cytoskeleton. *Mol Biol Cell* 3, 475–479. <https://doi.org/10.1091/mbc.3.5.475>
- Hall, M.P., Unch, J., Binkowski, B.F., Valley, M.P., Butler, B.L., Wood, M.G., Otto, P., Zimmerman, K., Vidugiris, G., Machleidt, T., Robers, M.B., Benink, H.A., Eggers, C.T., Slater, M.R., Meisenheimer, P.L., Klaubert, D.H., Fan, F., Encell, L.P., Wood, K.V., 2012. Engineered Luciferase Reporter from a Deep Sea Shrimp Utilizing a Novel Imidazopyrazinone Substrate. *ACS Chem. Biol.* 7, 1848–1857. <https://doi.org/10.1021/cb3002478>
- Hanahan, D., Weinberg, R.A., 2011. Hallmarks of Cancer: The Next Generation. *Cell* 144, 646–674. <https://doi.org/10.1016/j.cell.2011.02.013>
- Handel, T.M., Johnson, Z., Crown, S.E., Lau, E.K., Proudfoot, A.E., 2005. Regulation of protein function by glycosaminoglycans--as exemplified by chemokines. *Annu Rev Biochem* 74, 385–410. <https://doi.org/10.1146/annurev.biochem.72.121801.161747>
- Hansen, C.G., Howard, G., Nichols, B.J., 2011. Pacsin 2 is recruited to caveolae and functions in caveolar biogenesis. *Journal of Cell Science* 124, 2777–2785. <https://doi.org/10.1242/jcs.084319>
- Hansen, S.H., Sandvig, K., van Deurs, B., 1993. Clathrin and HA2 adaptors: effects of potassium depletion, hypertonic medium, and cytosol acidification. *Journal of Cell Biology* 121, 61–72. <https://doi.org/10.1083/jcb.121.1.61>
- Hanyaloglu, A.C., Zastrow, M. von, 2008. Regulation of GPCRs by Endocytic Membrane Trafficking and Its Potential Implications. *Annual Review of Pharmacology and Toxicology* 48, 537–568. <https://doi.org/10.1146/annurev.pharmtox.48.113006.094830>
- Haribabu, B., Richardson, R.M., Fisher, I., Sozzani, S., Peiper, S.C., Horuk, R., Ali, H., Snyderman, R., 1997. Regulation of Human Chemokine Receptors CXCR4: ROLE OF PHOSPHORYLATION IN DESENSITIZATION AND INTERNALIZATION\*. *Journal of Biological Chemistry* 272, 28726–28731. <https://doi.org/10.1074/jbc.272.45.28726>
- Harrison, C., Traynor, J.R., 2003. The [35S]GTPγS binding assay: approaches and applications in pharmacology. *Life Sciences* 74, 489–508. <https://doi.org/10.1016/j.lfs.2003.07.005>
- Hattermann, K., Mentlein, R., 2013. An Infernal Trio: The chemokine CXCL12 and its receptors CXCR4 and CXCR7 in tumor biology. *Annals of Anatomy - Anatomischer Anzeiger* 195, 103–110. <https://doi.org/10.1016/j.aanat.2012.10.013>
- Hauser, M.A., Legler, D.F., 2016. Common and biased signaling pathways of the chemokine receptor CCR7 elicited by its ligands CCL19 and CCL21 in leukocytes. *J Leukoc Biol* 99, 869–882. <https://doi.org/10.1189/jlb.2MR0815-380R>
- Hawila, E., Razon, H., Wildbaum, G., Blattner, C., Sapir, Y., Shaked, Y., Umansky, V., Karin, N., 2017. CCR5 Directs the Mobilization of CD11b+Gr1+Ly6Clow Polymorphonuclear Myeloid Cells from the Bone Marrow to the Blood to Support Tumor Development. *Cell Reports* 21, 2212–2222. <https://doi.org/10.1016/j.celrep.2017.10.104>
- Hayer, A., Stoeber, M., Bissig, C., Helenius, A., 2010. Biogenesis of caveolae: stepwise assembly of large caveolin and cavin complexes. *Traffic* 11, 361–382. <https://doi.org/10.1111/j.1600-0854.2009.01023.x>

- Hébert, C.A., Vitangcol, R.V., Baker, J.B., 1991. Scanning mutagenesis of interleukin-8 identifies a cluster of residues required for receptor binding. *J Biol Chem* 266, 18989–18994.
- Heilker, R., Manning-Krieg, U., Zuber, J.F., Spiess, M., 1996. In vitro binding of clathrin adaptors to sorting signals correlates with endocytosis and basolateral sorting. *The EMBO Journal* 15, 2893–2899. <https://doi.org/10.1002/j.1460-2075.1996.tb00650.x>
- Hemmings, B.A., Restuccia, D.F., 2012. PI3K-PKB/Akt pathway. *Cold Spring Harb Perspect Biol* 4, a011189. <https://doi.org/10.1101/cshperspect.a011189>
- Hernanz-Falcón, P., Rodríguez-Frade, J.M., Serrano, A., Juan, D., del Sol, A., Soriano, S.F., Roncal, F., Gómez, L., Valencia, A., Martínez-A, C., Mellado, M., 2004. Identification of amino acid residues crucial for chemokine receptor dimerization. *Nat Immunol* 5, 216–223. <https://doi.org/10.1038/ni1027>
- Hetrick, B., Han, M.S., Helgeson, L.A., Nolen, B.J., 2013. Small molecules CK-666 and CK-869 inhibit Arp2/3 complex by blocking an activating conformational change. *Chem Biol* 20, 701–712. <https://doi.org/10.1016/j.chembiol.2013.03.019>
- Heuninck, J., Viciano, C.P., İşbilir, A., Caspar, B., Capoferri, D., Bridson, S.J., Durroux, T., Hill, S.J., Lohse, M.J., Milligan, G., Pin, J.-P., Hoffmann, C., 2019. Context-Dependent Signaling of CXC Chemokine Receptor 4 and Atypical Chemokine Receptor 3. *Mol Pharmacol* 96, 778–793. <https://doi.org/10.1124/mol.118.115477>
- Hjortø, G.M., Larsen, O., Steen, A., Daugvilaite, V., Berg, C., Fares, S., Hansen, M., Ali, S., Rosenkilde, M.M., 2016. Differential CCR7 Targeting in Dendritic Cells by Three Naturally Occurring CC-Chemokines. *Front Immunol* 7, 568. <https://doi.org/10.3389/fimmu.2016.00568>
- Hoogewerf, A.J., Kuschert, G.S., Proudfoot, A.E., Borlat, F., Clark-Lewis, I., Power, C.A., Wells, T.N., 1997. Glycosaminoglycans mediate cell surface oligomerization of chemokines. *Biochemistry* 36, 13570–13578. <https://doi.org/10.1021/bi971125s>
- Howe, A.K., 2011. Cross-talk between calcium and protein kinase A in the regulation of cell migration. *Curr Opin Cell Biol* 23, 554–561. <https://doi.org/10.1016/j.ceb.2011.05.006>
- Huang, C.-C., Lam, S.N., Acharya, P., Tang, M., Xiang, S.-H., Hussan, S.S.-U., Stanfield, R.L., Robinson, J., Sodroski, J., Wilson, I.A., Wyatt, R., Bewley, C.A., Kwong, P.D., 2007. Structures of the CCR5 N terminus and of a tyrosine-sulfated antibody with HIV-1 gp120 and CD4. *Science* 317, 1930–1934. <https://doi.org/10.1126/science.1145373>
- Huang, K.-S., Wang, Y.-T., Byadgi, O., Huang, T.-Y., Tai, M.-H., Shaw, J.-F., Yang, C.-H., 2022. Screening of Specific and Common Pathways in Breast Cancer Cell Lines MCF-7 and MDA-MB-231 Treated with Chlorophyllides Composites. *Molecules* 27, 3950. <https://doi.org/10.3390/molecules27123950>
- Huang, T.Y., DerMardirossian, C., Bokoch, G.M., 2006. Cofilin phosphatases and regulation of actin dynamics. *Curr Opin Cell Biol* 18, 26–31. <https://doi.org/10.1016/j.ceb.2005.11.005>
- Hubbard, K.B., Hepler, J.R., 2006. Cell signalling diversity of the Gqα family of heterotrimeric G proteins. *Cellular Signalling* 18, 135–150. <https://doi.org/10.1016/j.cellsig.2005.08.004>

- Hubert, M., Larsson, E., Vegesna, N.V.G., Ahnlund, M., Johansson, A.I., Moodie, L.W., Lundmark, R., 2020. Lipid accumulation controls the balance between surface connection and scission of caveolae. *Elife* 9, e55038. <https://doi.org/10.7554/eLife.55038>
- Huck, B., Kemkemer, R., Franz-Wachtel, M., Macek, B., Hausser, A., Olayioye, M.A., 2012. GIT1 phosphorylation on serine 46 by PKD3 regulates paxillin trafficking and cellular protrusive activity. *J Biol Chem* 287, 34604–34613. <https://doi.org/10.1074/jbc.M112.374652>
- Humblin, E., Kamphorst, A.O., 2019. CXCR3-CXCL9: It's All in the Tumor. *Immunity* 50, 1347–1349. <https://doi.org/10.1016/j.immuni.2019.05.013>
- Hunyady, L., Baukal, A.J., Gáborik, Z., Olivares-Reyes, J.A., Bor, M., Szaszák, M., Lodge, R., Catt, K.J., Balla, T., 2002. Differential PI 3-kinase dependence of early and late phases of recycling of the internalized AT1 angiotensin receptor. *Journal of Cell Biology* 157, 1211–1222. <https://doi.org/10.1083/jcb.200111013>
- Huttenlocher, A., Horwitz, A.R., 2011. Integrins in Cell Migration. *Cold Spring Harb Perspect Biol* 3, a005074. <https://doi.org/10.1101/cshperspect.a005074>
- Hüttenrauch, F., Nitzki, A., Lin, F.-T., Höning, S., Oppermann, M., 2002.  $\beta$ -Arrestin Binding to CC Chemokine Receptor 5 Requires Multiple C-terminal Receptor Phosphorylation Sites and Involves a Conserved Asp-Arg-Tyr Sequence Motif\*. *Journal of Biological Chemistry* 277, 30769–30777. <https://doi.org/10.1074/jbc.M204033200>
- Hwang, J., Son, K.-N., Kim, C.W., Ko, J., Na, D.S., Kwon, B.S., Gho, Y.S., Kim, J., 2005. Human CC chemokine CCL23, a ligand for CCR1, induces endothelial cell migration and promotes angiogenesis. *Cytokine* 30, 254–263. <https://doi.org/10.1016/j.cyto.2005.01.018>
- Iglesias, T., Rozengurt, E., 1999. Protein kinase D activation by deletion of its cysteine-rich motifs. *FEBS Lett* 454, 53–56. [https://doi.org/10.1016/s0014-5793\(99\)00772-3](https://doi.org/10.1016/s0014-5793(99)00772-3)
- Iglesias, T., Waldron, R.T., Rozengurt, E., 1998. Identification of in vivo phosphorylation sites required for protein kinase D activation. *J Biol Chem* 273, 27662–27667. <https://doi.org/10.1074/jbc.273.42.27662>
- Işbilir, A., Möller, J., Arimont, M., Bobkov, V., Perpiñá-Viciano, C., Hoffmann, C., Inoue, A., Heukers, R., de Graaf, C., Smit, M.J., Annibale, P., Lohse, M.J., 2020. Advanced fluorescence microscopy reveals disruption of dynamic CXCR4 dimerization by subpocket-specific inverse agonists. *Proceedings of the National Academy of Sciences* 117, 29144–29154. <https://doi.org/10.1073/pnas.2013319117>
- Ishiguro, K., Cao, Z., Ilasca, M.L., Ando, T., Xavier, R., 2004. Wave2 activates serum response element via its VCA region and functions downstream of Rac. *Exp Cell Res* 301, 331–337. <https://doi.org/10.1016/j.yexcr.2004.09.003>
- Jacques, R.O., Mills, S.C., Cazonatto Zerwes, P., Fagade, F.O., Green, J.E., Downham, S., Sexton, D.W., Mueller, A., 2015. Dynamin function is important for chemokine receptor-induced cell migration. *Cell Biochemistry and Function* 33, 407–414. <https://doi.org/10.1002/cbf.3131>
- Jaggi, M., Rao, P.S., Smith, D.J., Wheelock, M.J., Johnson, K.R., Hemstreet, G.P., Balaji, K.C., 2005. E-cadherin phosphorylation by protein kinase D1/protein kinase C $\mu$  is associated with altered cellular aggregation and motility in prostate cancer. *Cancer Res* 65, 483–492.

- Jansma, A.L., Kirkpatrick, J.P., Hsu, A.R., Handel, T.M., Nietlispach, D., 2010. NMR analysis of the structure, dynamics, and unique oligomerization properties of the chemokine CCL27. *J Biol Chem* 285, 14424–14437. <https://doi.org/10.1074/jbc.M109.091108>
- Jean-Charles, P.-Y., Freedman, N.J., Shenoy, S. K., 2016. Chapter Nine - Cellular Roles of Beta-Arrestins as Substrates and Adaptors of Ubiquitination and Deubiquitination, in: Shenoy, Sudha K. (Ed.), *Progress in Molecular Biology and Translational Science, Ubiquitination and Transmembrane Signaling*. Academic Press, pp. 339–369. <https://doi.org/10.1016/bs.pmbts.2016.04.003>
- Jiang, Q.-F., Wu, T.-T., Yang, J.-Y., Dong, C.-R., Wang, N., Liu, X.-H., Liu, Z.-M., 2013. 17 $\beta$ -Estradiol promotes the invasion and migration of nuclear estrogen receptor-negative breast cancer cells through cross-talk between GPER1 and CXCR1. *The Journal of Steroid Biochemistry and Molecular Biology* 138, 314–324. <https://doi.org/10.1016/j.jsbmb.2013.07.011>
- Johnson, Z., Proudfoot, A.E., Handel, T.M., 2005. Interaction of chemokines and glycosaminoglycans: A new twist in the regulation of chemokine function with opportunities for therapeutic intervention. *Cytokine & Growth Factor Reviews*, Chemokines 16, 625–636. <https://doi.org/10.1016/j.cytogfr.2005.04.006>
- Jordens, I., Fernandez-Borja, M., Marsman, M., Dusseljee, S., Janssen, L., Calafat, J., Janssen, H., Wubbolts, R., Neefjes, J., 2001. The Rab7 effector protein RILP controls lysosomal transport by inducing the recruitment of dynein-dynactin motors. *Curr Biol* 11, 1680–1685. [https://doi.org/10.1016/s0960-9822\(01\)00531-0](https://doi.org/10.1016/s0960-9822(01)00531-0)
- Joseph, P.R.B., Sawant, K.V., Isley, A., Pedroza, M., Garofalo, R.P., Richardson, R.M., Rajarathnam, K., 2013. Dynamic conformational switching in the chemokine ligand is essential for G-protein-coupled receptor activation. *Biochem J* 456, 241–251. <https://doi.org/10.1042/BJ20130148>
- Justus, C.R., Leffler, N., Ruiz-Echevarria, M., Yang, L.V., 2014. In vitro Cell Migration and Invasion Assays. *J Vis Exp* 51046. <https://doi.org/10.3791/51046>
- Kang, Y., Zhou, X.E., Gao, X., He, Y., Liu, W., Ishchenko, A., Barty, A., White, T.A., Yefanov, O., Han, G.W., Xu, Q., de Waal, P.W., Ke, J., Tan, M.H.E., Zhang, C., Moeller, A., West, G.M., Pascal, B.D., Van Eps, N., Caro, L.N., Vishnivetskiy, S.A., Lee, R.J., Suino-Powell, K.M., Gu, X., Pal, K., Ma, J., Zhi, X., Boutet, S., Williams, G.J., Messerschmidt, M., Gati, C., Zatsepin, N.A., Wang, D., James, D., Basu, S., Roy-Chowdhury, S., Conrad, C.E., Coe, J., Liu, H., Lisova, S., Kupitz, C., Grotjohann, I., Fromme, R., Jiang, Y., Tan, M., Yang, H., Li, J., Wang, M., Zheng, Z., Li, D., Howe, N., Zhao, Y., Standfuss, J., Diederichs, K., Dong, Y., Potter, C.S., Carragher, B., Caffrey, M., Jiang, H., Chapman, H.N., Spence, J.C.H., Fromme, P., Weierstall, U., Ernst, O.P., Katritch, V., Gurevich, V.V., Griffin, P.R., Hubbell, W.L., Stevens, R.C., Cherezov, V., Melcher, K., Xu, H.E., 2015. Crystal structure of rhodopsin bound to arrestin by femtosecond X-ray laser. *Nature* 523, 561–567. <https://doi.org/10.1038/nature14656>
- Karin, N., Wildbaum, G., Thelen, M., 2016. Biased signaling pathways via CXCR3 control the development and function of CD4<sup>+</sup> T cell subsets. *Journal of Leukocyte Biology* 99, 857–862. <https://doi.org/10.1189/jlb.2MR0915-441R>

- Katritch, V., Cherezov, V., Stevens, R.C., 2013. Structure-function of the G protein-coupled receptor superfamily. *Annu Rev Pharmacol Toxicol* 53, 531–556. <https://doi.org/10.1146/annurev-pharmtox-032112-135923>
- Khater, I.M., Meng, F., Wong, T.H., Nabi, I.R., Hamarneh, G., 2018. Super Resolution Network Analysis Defines the Molecular Architecture of Caveolae and Caveolin-1 Scaffolds. *Sci Rep* 8, 9009. <https://doi.org/10.1038/s41598-018-27216-4>
- Kiermaier, E., Moussion, C., Veldkamp, C.T., Gerardy-Schahn, R., de Vries, I., Williams, L.G., Chaffee, G.R., Phillips, A.J., Freiburger, F., Imre, R., Taleski, D., Payne, R.J., Braun, A., Förster, R., Mechtler, K., Mühlhoff, M., Volkman, B.F., Sixt, M., 2016. Polysialylation controls dendritic cell trafficking by regulating chemokine recognition. *Science* 351, 186–190. <https://doi.org/10.1126/science.aad0512>
- Kim, J., Ahn, S., Ren, X.-R., Whalen, E.J., Reiter, E., Wei, H., Lefkowitz, R.J., 2005. Functional antagonism of different G protein-coupled receptor kinases for  $\beta$ -arrestin-mediated angiotensin II receptor signaling. *Proceedings of the National Academy of Sciences* 102, 1442–1447. <https://doi.org/10.1073/pnas.0409532102>
- Kleist, A.B., Getschman, A.E., Ziarek, J.J., Nevins, A.M., Gauthier, P.-A., Chevigné, A., Szpakowska, M., Volkman, B.F., 2016. New paradigms in chemokine receptor signal transduction: Moving beyond the two-site model. *Biochem Pharmacol* 114, 53–68. <https://doi.org/10.1016/j.bcp.2016.04.007>
- Kligys, K., Claiborne, J.N., DeBiase, P.J., Hopkinson, S.B., Wu, Y., Mizuno, K., Jones, J.C.R., 2007. The slingshot family of phosphatases mediates Rac1 regulation of cofilin phosphorylation, laminin-332 organization, and motility behavior of keratinocytes. *J Biol Chem* 282, 32520–32528. <https://doi.org/10.1074/jbc.M707041200>
- Korniejewska, A., McKnight, A.J., Johnson, Z., Watson, M.L., Ward, S.G., 2011. Expression and agonist responsiveness of CXCR3 variants in human T lymphocytes. *Immunology* 132, 503–515. <https://doi.org/10.1111/j.1365-2567.2010.03384.x>
- Kraft, K., Olbrich, H., Majoul, I., Mack, M., Proudfoot, A., Oppermann, M., 2001. Characterization of Sequence Determinants within the Carboxyl-terminal Domain of Chemokine Receptor CCR5 That Regulate Signaling and Receptor Internalization\*. *Journal of Biological Chemistry* 276, 34408–34418. <https://doi.org/10.1074/jbc.M102782200>
- Kulmann-Leal, B., Ellwanger, J.H., Chies, J.A.B., 2020. A functional interaction between the CCR5 and CD34 molecules expressed in hematopoietic cells can support (or even promote) the development of cancer. *Hematol Transfus Cell Ther* 42, 70–76. <https://doi.org/10.1016/j.htct.2019.10.001>
- Kunkel, M.T., Garcia, E.L., Kajimoto, T., Hall, R.A., Newton, A.C., 2009. The protein scaffold NHERF-1 controls the amplitude and duration of localized protein kinase D activity. *J Biol Chem* 284, 24653–24661. <https://doi.org/10.1074/jbc.M109.024547>
- Kuscher, K., Danelon, G., Paoletti, S., Stefano, L., Schiraldi, M., Petkovic, V., Locati, M., Gerber, B.O., Uguccioni, M., 2009. Synergy-inducing chemokines enhance CCR2 ligand activities on monocytes. *Eur J Immunol* 39, 1118–1128. <https://doi.org/10.1002/eji.200838906>
- Lai, W.Y., Mueller, A., 2021. Latest update on chemokine receptors as therapeutic targets. *Biochemical Society Transactions* 49, 1385–1395. <https://doi.org/10.1042/BST20201114>

- Lan, T., Yu, M., Chen, W., Yin, J., Chang, H.-T., Tang, S., Zhao, Y., Svoronos, S., Wong, S.W.K., Tseng, Y., 2021. Decomposition of cell activities revealing the role of the cell cycle in driving biofunctional heterogeneity. *Sci Rep* 11, 23431. <https://doi.org/10.1038/s41598-021-02926-4>
- Laplante, M., Sabatini, D.M., 2012. mTOR Signaling. *Cold Spring Harb Perspect Biol* 4, a011593. <https://doi.org/10.1101/cshperspect.a011593>
- Laporte, S.A., Oakley, R.H., Zhang, J., Holt, J.A., Ferguson, S.S.G., Caron, M.G., Barak, L.S., 1999. The  $\beta$ 2-adrenergic receptor/ $\beta$ arrestin complex recruits the clathrin adaptor AP-2 during endocytosis. *Proc Natl Acad Sci U S A* 96, 3712–3717.
- Laschet, C., Dupuis, N., Hanson, J., 2019. A dynamic and screening-compatible nanoluciferase-based complementation assay enables profiling of individual GPCR–G protein interactions. *Journal of Biological Chemistry* 294, 4079–4090. <https://doi.org/10.1074/jbc.RA118.006231>
- Latorraca, N.R., Masureel, M., Hollingsworth, S.A., Heydenreich, F.M., Suomivuori, C.-M., Brinton, C., Townshend, R.J.L., Bouvier, M., Kobilka, B.K., Dror, R.O., 2020. How GPCR phosphorylation patterns orchestrate arrestin-mediated signaling. *Cell* 183, 1813–1825.e18. <https://doi.org/10.1016/j.cell.2020.11.014>
- Latorraca, N.R., Wang, J.K., Bauer, B., Townshend, R.J.L., Hollingsworth, S.A., Olivieri, J.E., Xu, H.E., Sommer, M.E., Dror, R.O., 2018. Molecular mechanism of GPCR-mediated arrestin activation. *Nature* 557, 452–456. <https://doi.org/10.1038/s41586-018-0077-3>
- Lavalle, C.R., Bravo-Altamirano, K., Giridhar, K.V., Chen, J., Sharlow, E., Lazo, J.S., Wipf, P., Wang, Q.J., 2010. Novel protein kinase D inhibitors cause potent arrest in prostate cancer cell growth and motility. *BMC Chem Biol* 10, 5. <https://doi.org/10.1186/1472-6769-10-5>
- LaValle, C.R., Zhang, L., Xu, S., Eiseman, J.L., Wang, Q.J., 2012. Inducible silencing of protein kinase D3 inhibits secretion of tumor-promoting factors in prostate cancer. *Mol Cancer Ther* 11, 1389–1399. <https://doi.org/10.1158/1535-7163.MCT-11-0887>
- Le, Y., Zhou, Y., Iribarren, P., Wang, J., 2004. Chemokines and chemokine receptors: their manifold roles in homeostasis and disease. *Cell Mol Immunol* 1, 95–104.
- Lee, D.-W., Wu, X., Eisenberg, E., Greene, L.E., 2006. Recruitment dynamics of GAK and auxilin to clathrin-coated pits during endocytosis. *J Cell Sci* 119, 3502–3512. <https://doi.org/10.1242/jcs.03092>
- Lee, J., Horuk, R., Rice, G.C., Bennett, G.L., Camerato, T., Wood, W.I., 1992. Characterization of two high affinity human interleukin-8 receptors. *J Biol Chem* 267, 16283–16287.
- Liles, W.C., Broxmeyer, H.E., Rodger, E., Wood, B., Hübel, K., Cooper, S., Hangoc, G., Bridger, G.J., Henson, G.W., Calandra, G., Dale, D.C., 2003. Mobilization of hematopoietic progenitor cells in healthy volunteers by AMD3100, a CXCR4 antagonist. *Blood* 102, 2728–2730. <https://doi.org/10.1182/blood-2003-02-0663>
- Lima-Fernandes, E., Enslin, H., Camand, E., Kotelevets, L., Boularan, C., Achour, L., Benmerah, A., Gibson, L.C.D., Baillie, G.S., Pitcher, J.A., Chastre, E., Etienne-Manneville, S., Marullo, S., Scott, M.G.H., 2011. Distinct functional outputs of PTEN signalling are controlled by dynamic association with  $\beta$ -arrestins. *EMBO J* 30, 2557–2568. <https://doi.org/10.1038/emboj.2011.178>

- Lin, T., Zeng, L., Liu, Y., DeFea, K., Schwartz, M.A., Chien, S., Shyy, J.Y.-J., 2003. Rho-ROCK-LIMK-cofilin pathway regulates shear stress activation of sterol regulatory element binding proteins. *Circ Res* 92, 1296–1304. <https://doi.org/10.1161/01.RES.0000078780.65824.8B>
- Liu, H., Zhang, Q., Li, K., Gong, Z., Liu, Z., Xu, Y., Swaney, M.H., Xiao, K., Chen, Y., 2016. Prognostic significance of USP33 in advanced colorectal cancer patients: new insights into  $\beta$ -arrestin-dependent ERK signaling. *Oncotarget* 7, 81223–81240. <https://doi.org/10.18632/oncotarget.13219>
- Liu, J., Sun, Y., Oster, G.F., Drubin, D.G., 2010. Mechanochemical crosstalk during endocytic vesicle formation. *Curr Opin Cell Biol* 22, 36–43. <https://doi.org/10.1016/j.ceb.2009.11.009>
- Liu, L., Pilch, P.F., 2016. PTRF/Cavin-1 promotes efficient ribosomal RNA transcription in response to metabolic challenges. *Elife* 5, e17508. <https://doi.org/10.7554/eLife.17508>
- Liu, S.-H., Marks, M.S., Brodsky, F.M., 1998. A Dominant-negative Clathrin Mutant Differentially Affects Trafficking of Molecules with Distinct Sorting Motifs in the Class II Major Histocompatibility Complex (MHC) Pathway. *Journal of Cell Biology* 140, 1023–1037. <https://doi.org/10.1083/jcb.140.5.1023>
- Liu, Y., Wang, Y., Yu, S., Zhou, Y., Ma, X., Su, Q., An, L., Wang, F., Shi, A., Zhang, J., Chen, L., 2019. The Role and Mechanism of CRT0066101 as an Effective Drug for Treatment of Triple-Negative Breast Cancer | *Cell Physiol Biochem. Cellular Physiology & Biochemistry* 52, 382–396.
- Loerke, D., Mettlen, M., Yarar, D., Jaqaman, K., Jaqaman, H., Danuser, G., Schmid, S.L., 2009. Cargo and dynamin regulate clathrin-coated pit maturation. *PLoS Biol* 7, e57. <https://doi.org/10.1371/journal.pbio.1000057>
- Lorentzen, A., Bamber, J., Sadok, A., Elson-Schwab, I., Marshall, C.J., 2011. An ezrin-rich, rigid uropod-like structure directs movement of amoeboid blebbing cells. *Journal of Cell Science* 124, 1256–1267. <https://doi.org/10.1242/jcs.074849>
- Lu, J., Helton, T.D., Blanpied, T.A., Rácz, B., Newpher, T.M., Weinberg, R.J., Ehlers, M.D., 2007. Postsynaptic Positioning of Endocytic Zones and AMPA Receptor Cycling by Physical Coupling of Dynamin-3 to Homer. *Neuron* 55, 874–889. <https://doi.org/10.1016/j.neuron.2007.06.041>
- Luo, J., Busillo, J.M., Stumm, R., Benovic, J.L., 2017. G Protein-Coupled Receptor Kinase 3 and Protein Kinase C Phosphorylate the Distal C-Terminal Tail of the Chemokine Receptor CXCR4 and Mediate Recruitment of  $\beta$ -Arrestin. *Mol Pharmacol* 91, 554–566. <https://doi.org/10.1124/mol.116.106468>
- Luttrell, L.M., Roudabush, F.L., Choy, E.W., Miller, W.E., Field, M.E., Pierce, K.L., Lefkowitz, R.J., 2001. Activation and targeting of extracellular signal-regulated kinases by beta-arrestin scaffolds. *Proc Natl Acad Sci U S A* 98, 2449–2454. <https://doi.org/10.1073/pnas.041604898>
- Lutz, S., Shankaranarayanan, A., Coco, C., Ridilla, M., Nance, M.R., Vettel, C., Baltus, D., Evelyn, C.R., Neubig, R.R., Wieland, T., Tesmer, J.J.G., 2007. Structure of Galphaq-p63RhoGEF-RhoA complex reveals a pathway for the activation of RhoA by GPCRs. *Science* 318, 1923–1927. <https://doi.org/10.1126/science.1147554>
- Lv, D., Chen, H., Feng, Y., Cui, B., Kang, Y., Zhang, P., Luo, M., Chen, J., 2021. Small-Molecule Inhibitor Targeting Protein Kinase D: A Potential

- Therapeutic Strategy. *Front Oncol* 11, 680221. <https://doi.org/10.3389/fonc.2021.680221>
- Lv, Y., Zhao, Y., Wang, X., Chen, N., Mao, F., Teng, Y., Wang, T., Peng, L., Zhang, J., Cheng, P., Liu, Y., Kong, H., Chen, W., Hao, C., Han, B., Ma, Q., Zou, Q., Chen, J., Zhuang, Y., 2019. Increased intratumoral mast cells foster immune suppression and gastric cancer progression through TNF- $\alpha$ -PD-L1 pathway. *J Immunother Cancer* 7, 54. <https://doi.org/10.1186/s40425-019-0530-3>
- Macia, E., Ehrlich, M., Massol, R., Boucrot, E., Brunner, C., Kirchhausen, T., 2006. Dynasore, a Cell-Permeable Inhibitor of Dynamin. *Developmental Cell* 10, 839–850. <https://doi.org/10.1016/j.devcel.2006.04.002>
- Madsen, C.D., Sahai, E., 2010. Cancer dissemination--lessons from leukocytes. *Dev Cell* 19, 13–26. <https://doi.org/10.1016/j.devcel.2010.06.013>
- Maekawa, M., Ishizaki, T., Boku, S., Watanabe, N., Fujita, A., Iwamatsu, A., Obinata, T., Ohashi, K., Mizuno, K., Narumiya, S., 1999. Signaling from Rho to the actin cytoskeleton through protein kinases ROCK and LIM-kinase. *Science* 285, 895–898. <https://doi.org/10.1126/science.285.5429.895>
- Mañes, S., del Real, G., Lacalle, R.A., Lucas, P., Gómez-Moutón, C., Sánchez-Palomino, S., Delgado, R., Alcamí, J., Mira, E., Martínez-A, C., 2000. Membrane raft microdomains mediate lateral assemblies required for HIV-1 infection. *EMBO Rep* 1, 190–196. <https://doi.org/10.1093/embo-reports/kvd025>
- Mañes, S., Mira, E., Gómez-Moutón, C., Ana Lacalle, R., Keller, P., Pablo Labrador, J., Martínez-A, C., 1999. Membrane raft microdomains mediate front–rear polarity in migrating cells. *The EMBO Journal* 18, 6211–6220. <https://doi.org/10.1093/emboj/18.22.6211>
- Manning, G., Whyte, D.B., Martinez, R., Hunter, T., Sudarsanam, S., 2002. The protein kinase complement of the human genome. *Science* 298, 1912–1934. <https://doi.org/10.1126/science.1075762>
- Marchese, A., Benovic, J.L., 2001. Agonist-promoted Ubiquitination of the G Protein-coupled Receptor CXCR4 Mediates Lysosomal Sorting\*. *Journal of Biological Chemistry* 276, 45509–45512. <https://doi.org/10.1074/jbc.C100527200>
- Mariani, M., Lang, R., Binda, E., Panina-Bordignon, P., D'Ambrosio, D., 2004. Dominance of CCL22 over CCL17 in induction of chemokine receptor CCR4 desensitization and internalization on human Th2 cells. *European Journal of Immunology* 34, 231–240. <https://doi.org/10.1002/eji.200324429>
- Marshall, F.H., 2016. Visualizing GPCR “Megaplexes” Which Enable Sustained Intracellular Signaling. *Trends Biochem Sci* 41, 985–986. <https://doi.org/10.1016/j.tibs.2016.10.006>
- Martínez, M., Martínez, N.A., Silva, W.I., 2017. Measurement of the Intracellular Calcium Concentration with Fura-2 AM Using a Fluorescence Plate Reader. *Bio Protoc* 7, e2411. <https://doi.org/10.21769/BioProtoc.2411>
- Martínez-Muñoz, L., Rodríguez-Frade, J.M., Barroso, R., Sorzano, C.Ó.S., Torreño-Pina, J.A., Santiago, C.A., Manzo, C., Lucas, P., García-Cuesta, E.M., Gutierrez, E., Barrio, L., Vargas, J., Cascio, G., Carrasco, Y.R., Sánchez-Madrid, F., García-Parajo, M.F., Mellado, M., 2018. Separating Actin-Dependent Chemokine Receptor Nanoclustering from Dimerization Indicates a Role for Clustering in CXCR4 Signaling and Function.

- Martins, E., Brodier, H., Rossitto-Borlat, I., Ilgaz, I., Villard, M., Hartley, O., 2020. Arrestin Recruitment to C-C Chemokine Receptor 5: Potent C-C Chemokine Ligand 5 Analogs Reveal Differences in Dependence on Receptor Phosphorylation and Isoform-Specific Recruitment Bias. *Mol Pharmacol* 98, 599–611. <https://doi.org/10.1124/molpharm.120.000036>
- Matharu, A.-L., Mundell, S.J., Benovic, J.L., Kelly, E., 2001. Rapid Agonist-induced Desensitization and Internalization of the A2B Adenosine Receptor Is Mediated by a Serine Residue Close to the COOH Terminus\*. *Journal of Biological Chemistry* 276, 30199–30207. <https://doi.org/10.1074/jbc.M010650200>
- Matthaeus, C., Taraska, J.W., 2021. Energy and Dynamics of Caveolae Trafficking. *Frontiers in Cell and Developmental Biology* 8.
- Mattila, P.K., Lappalainen, P., 2008. Filopodia: molecular architecture and cellular functions. *Nat Rev Mol Cell Biol* 9, 446–454. <https://doi.org/10.1038/nrm2406>
- Maxfield, F.R., 2014. Role of Endosomes and Lysosomes in Human Disease. *Cold Spring Harb Perspect Biol* 6, a016931. <https://doi.org/10.1101/cshperspect.a016931>
- Mayo, K.H., Roongta, V., Ilyina, E., Milius, R., Barker, S., Quinlan, C., La Rosa, G., Daly, T.J., 1995. NMR solution structure of the 32-kDa platelet factor 4 ELR-motif N-terminal chimera: a symmetric tetramer. *Biochemistry* 34, 11399–11409. <https://doi.org/10.1021/bi00036a012>
- McCluskey, A., Daniel, J.A., Hadzic, G., Chau, N., Clayton, E.L., Mariana, A., Whiting, A., Gorgani, N.N., Lloyd, J., Quan, A., Moshkanbaryans, L., Krishnan, S., Perera, S., Chircop, M., von Kleist, L., McGeachie, A.B., Howes, M.T., Parton, R.G., Campbell, M., Sakoff, J.A., Wang, X., Sun, J., Robertson, M.J., Deane, F.M., Nguyen, T.H., Meunier, F.A., Cousin, M.A., Robinson, P.J., 2013. Building a Better Dynasore: The Dyngo Compounds Potently Inhibit Dynamin and Endocytosis. *Traffic* 14, 1272–1289. <https://doi.org/10.1111/tra.12119>
- McDonald, P.H., Chow, C.-W., Miller, W.E., Laporte, S.A., Field, M.E., Lin, F.-T., Davis, R.J., Lefkowitz, R.J., 2000.  $\beta$ -Arrestin 2: A Receptor-Regulated MAPK Scaffold for the Activation of JNK3. *Science* 290, 1574–1577. <https://doi.org/10.1126/science.290.5496.1574>
- McGovern, K.W., DeFea, K.A., 2014. Molecular mechanisms underlying beta-arrestin-dependent chemotaxis and actin-cytoskeletal reorganization. *Handb Exp Pharmacol* 219, 341–359. [https://doi.org/10.1007/978-3-642-41199-1\\_17](https://doi.org/10.1007/978-3-642-41199-1_17)
- McLaughlin, S., Wang, J., Gambhir, A., Murray, D., 2002. PIP(2) and proteins: interactions, organization, and information flow. *Annu Rev Biophys Biomol Struct* 31, 151–175. <https://doi.org/10.1146/annurev.biophys.31.082901.134259>
- McMahon, K.-A., Wu, Y., Gambin, Y., Sieracki, E., Tillu, V.A., Hall, T., Martel, N., Okano, S., Moradi, S.V., Ruelcke, J.E., Ferguson, C., Yap, A.S., Alexandrov, K., Hill, M.M., Parton, R.G., 2019. Identification of intracellular cavin target proteins reveals cavin-PP1 $\alpha$  interactions regulate apoptosis. *Nat Commun* 10, 3279. <https://doi.org/10.1038/s41467-019-11111-1>
- Meiser, A., Mueller, A., Wise, E.L., McDonagh, E.M., Petit, S.J., Saran, N., Clark, P.C., Williams, T.J., Pease, J.E., 2008. The chemokine receptor CXCR3

- is degraded following internalization and is replenished at the cell surface by de novo synthesis of receptor. *Journal of Immunology* 180, 6713–6724. <https://doi.org/10.4049/jimmunol.180.10.6713>
- Merzoug-Larabi, M., Spasojevic, C., Eymard, M., Hugonin, C., Auclair, C., Karam, M., 2017. Protein kinase C inhibitor Gö6976 but not Gö6983 induces the reversion of E- to N-cadherin switch and metastatic phenotype in melanoma: identification of the role of protein kinase D1. *BMC Cancer* 17, 12. <https://doi.org/10.1186/s12885-016-3007-5>
- Miaczynska, M., Zerial, M., 2002. Mosaic Organization of the Endocytic Pathway. *Experimental Cell Research* 272, 8–14. <https://doi.org/10.1006/excr.2001.5401>
- Mikelis, C.M., Palmby, T.R., Simaan, M., Li, W., Szabo, R., Lyons, R., Martin, D., Yagi, H., Fukuhara, S., Chikumi, H., Galisteo, R., Mukoyama, Y.-S., Bugge, T.H., Gutkind, J.S., 2013. PDZ-RhoGEF and LARG are essential for embryonic development and provide a link between thrombin and LPA receptors and Rho activation. *J Biol Chem* 288, 12232–12243. <https://doi.org/10.1074/jbc.M112.428599>
- Miki, H., Suetsugu, S., Takenawa, T., 1998. WAVE, a novel WASP-family protein involved in actin reorganization induced by Rac. *EMBO J* 17, 6932–6941. <https://doi.org/10.1093/emboj/17.23.6932>
- Miki, H., Yamaguchi, H., Suetsugu, S., Takenawa, T., 2000. IRSp53 is an essential intermediate between Rac and WAVE in the regulation of membrane ruffling. *Nature* 408, 732–735. <https://doi.org/10.1038/35047107>
- Miller, M.C., Mayo, K.H., 2017. Chemokines from a Structural Perspective. *Int J Mol Sci* 18, 2088. <https://doi.org/10.3390/ijms18102088>
- Mills, S.C., Goh, P.H., Kudatsih, J., Ncube, S., Gurung, R., Maxwell, W., Mueller, A., 2016. Cell migration towards CXCL12 in leukemic cells compared to breast cancer cells. *Cellular Signalling* 28, 316–324. <https://doi.org/10.1016/j.cellsig.2016.01.006>
- Mills, S.C., Howell, L., Beekman, A., Stokes, L., Mueller, A., 2018. Rac1 plays a role in CXCL12 but not CCL3-induced chemotaxis and Rac1 GEF inhibitor NSC23766 has off target effects on CXCR4. *Cellular Signalling* 42, 88–96. <https://doi.org/10.1016/j.cellsig.2017.10.006>
- Miyamoto, M., Shimizu, Y., Okada, K., Kashii, Y., Higuchi, K., Watanabe, A., 1998. Effect of interleukin-8 on production of tumor-associated substances and autocrine growth of human liver and pancreatic cancer cells. *Cancer Immunol Immunother* 47, 47–57. <https://doi.org/10.1007/s002620050503>
- Mo, X.-L., Luo, Y., Ivanov, A.A., Su, R., Havel, J.J., Li, Z., Khuri, F.R., Du, Y., Fu, H., 2016. Enabling systematic interrogation of protein–protein interactions in live cells with a versatile ultra-high-throughput biosensor platform. *Journal of Molecular Cell Biology* 8, 271–281. <https://doi.org/10.1093/jmcb/mjv064>
- Mollica Poeta, V., Massara, M., Capucetti, A., Bonecchi, R., 2019. Chemokines and Chemokine Receptors: New Targets for Cancer Immunotherapy. *Frontiers in Immunology* 10.
- Mona, C.E., Besserer-Offroy, É., Cabana, J., Leduc, R., Lavigne, P., Heveker, N., Marsault, É., Escher, E., 2016. Design, synthesis, and biological evaluation of CXCR4 ligands. *Org. Biomol. Chem.* 14, 10298–10311. <https://doi.org/10.1039/C6OB01484D>
- Morales, C.O.O., Ignácz, A., Bencsik, N., Rátkai, A.E., Lieb, W.S., Eisler, S.A., Szűcs, A., Schlett, K., Hausser, A., 2020. Protein Kinase D promotes

- activity-dependent AMPA receptor endocytosis in hippocampal neurons. <https://doi.org/10.1101/2020.04.09.033514>
- Morén, B., Shah, C., Howes, M.T., Schieber, N.L., McMahon, H.T., Parton, R.G., Daumke, O., Lundmark, R., 2012. EHD2 regulates caveolar dynamics via ATP-driven targeting and oligomerization. *Mol Biol Cell* 23, 1316–1329. <https://doi.org/10.1091/mbc.E11-09-0787>
- Mortezaei, K., 2020. CXCL12/CXCR4 axis in the microenvironment of solid tumors: A critical mediator of metastasis. *Life Sciences* 249, 117534. <https://doi.org/10.1016/j.lfs.2020.117534>
- Motley, A., Bright, N.A., Seaman, M.N.J., Robinson, M.S., 2003. Clathrin-mediated endocytosis in AP-2-depleted cells. *J Cell Biol* 162, 909–918. <https://doi.org/10.1083/jcb.200305145>
- Moyano Cardaba, C., Jacques, R.O., Barrett, J.E., Hassell, K.M., Kavanagh, A., Remington, F.C., Tse, T., Mueller, A., 2012. CCL3 induced migration occurs independently of intracellular calcium release. *Biochemical and Biophysical Research Communications* 418, 17–21. <https://doi.org/10.1016/j.bbrc.2011.12.081>
- Moyer, R.A., Wendt, M.K., Johanesen, P.A., Turner, J.R., Dwinell, M.B., 2007. Rho activation regulates CXCL12 chemokine stimulated actin rearrangement and restitution in model intestinal epithelia. *Lab Invest* 87, 807–817. <https://doi.org/10.1038/labinvest.3700595>
- Mueller, A., Kelly, E., Strange, P.G., 2002. Pathways for internalization and recycling of the chemokine receptor CCR5. *Blood* 99, 785–791. <https://doi.org/10.1182/blood.V99.3.785>
- Mueller, Anja, Strange, P.G., 2004. CCL3, acting via the chemokine receptor CCR5, leads to independent activation of Janus kinase 2 (JAK2) and Gi proteins. *FEBS Letters* 570, 126–132. <https://doi.org/10.1016/j.febslet.2004.04.100>
- Mueller, A., Strange, P.G., 2004. Mechanisms of internalization and recycling of the chemokine receptor, CCR5. *European Journal of Biochemistry* 271, 243–252. <https://doi.org/10.1046/j.1432-1033.2003.03918.x>
- Muinonen-Martin, A.J., Veltman, D.M., Kalna, G., Insall, R.H., 2010. An Improved Chamber for Direct Visualisation of Chemotaxis. *PLoS One* 5, e15309. <https://doi.org/10.1371/journal.pone.0015309>
- Müller, A., Homey, B., Soto, H., Ge, N., Catron, D., Buchanan, M.E., McClanahan, T., Murphy, E., Yuan, W., Wagner, S.N., Barrera, J.L., Mohar, A., Verástegui, E., Zlotnik, A., 2001. Involvement of chemokine receptors in breast cancer metastasis. *Nature* 410, 50–56. <https://doi.org/10.1038/35065016>
- Murooka, T.T., Rahbar, R., Fish, E.N., 2009. CCL5 promotes proliferation of MCF-7 cells through mTOR-dependent mRNA translation. *Biochemical and Biophysical Research Communications* 387, 381–386. <https://doi.org/10.1016/j.bbrc.2009.07.035>
- Murphy, P.M., Baggiolini, M., Charo, I.F., Hébert, C.A., Horuk, R., Matsushima, K., Miller, L.H., Oppenheim, J.J., Power, C.A., 2000. International Union of Pharmacology. XXII. Nomenclature for Chemokine Receptors. *Pharmacol Rev* 52, 145–176.
- Nagata-Ohashi, K., Ohta, Y., Goto, K., Chiba, S., Mori, R., Nishita, M., Ohashi, K., Kousaka, K., Iwamatsu, A., Niwa, R., Uemura, T., Mizuno, K., 2004. A pathway of neuregulin-induced activation of cofilin-phosphatase Slingshot and cofilin in lamellipodia. *J Cell Biol* 165, 465–471. <https://doi.org/10.1083/jcb.200401136>

- Nakagawa, H., Miki, H., Ito, M., Ohashi, K., Takenawa, T., Miyamoto, S., 2001. N-WASP, WAVE and Mena play different roles in the organization of actin cytoskeleton in lamellipodia. *J Cell Sci* 114, 1555–1565. <https://doi.org/10.1242/jcs.114.8.1555>
- Nankoe, S.R., Sever, S., 2006. Dynasore puts a new spin on dynamin: a surprising dual role during vesicle formation. *Trends Cell Biol* 16, 607–609. <https://doi.org/10.1016/j.tcb.2006.10.004>
- Narumiya, S., Ishizaki, T., Ufhata, M., 2000. Use and properties of ROCK-specific inhibitor Y-27632, in: Balch, W.E., Der, C.J., Hall, A. (Eds.), *Methods in Enzymology, Regulators and Effectors of Small GTPases - Part D: Rho Family*. Academic Press, pp. 273–284. [https://doi.org/10.1016/S0076-6879\(00\)25449-9](https://doi.org/10.1016/S0076-6879(00)25449-9)
- Narumiya, S., Tanji, M., Ishizaki, T., 2009. Rho signaling, ROCK and mDia1, in transformation, metastasis and invasion. *Cancer Metastasis Rev* 28, 65–76. <https://doi.org/10.1007/s10555-008-9170-7>
- Neel, N.F., Schutyser, E., Sai, J., Fan, G.-H., Richmond, A., 2005. Chemokine receptor internalization and intracellular trafficking. *Cytokine Growth Factor Rev* 16, 637–658. <https://doi.org/10.1016/j.cytogfr.2005.05.008>
- Nesmelova, I.V., Sham, Y., Gao, J., Mayo, K.H., 2008. CXC and CC chemokines form mixed heterodimers: association free energies from molecular dynamics simulations and experimental correlations. *J Biol Chem* 283, 24155–24166. <https://doi.org/10.1074/jbc.M803308200>
- Nguyen, H.T., Reyes-Alcaraz, A., Yong, H.J., Nguyen, L.P., Park, H.-K., Inoue, A., Lee, C.S., Seong, J.Y., Hwang, J.-I., 2020. CXCR7: a  $\beta$ -arrestin-biased receptor that potentiates cell migration and recruits  $\beta$ -arrestin2 exclusively through G $\beta\gamma$  subunits and GRK2. *Cell & Bioscience* 10, 134. <https://doi.org/10.1186/s13578-020-00497-x>
- Nibbs, R.J.B., Graham, G.J., 2013. Immune regulation by atypical chemokine receptors. *Nat Rev Immunol* 13, 815–829. <https://doi.org/10.1038/nri3544>
- Nichols, B.J., Lippincott-Schwartz, J., 2001. Endocytosis without clathrin coats. *Trends in Cell Biology* 11, 406–412. [https://doi.org/10.1016/S0962-8924\(01\)02107-9](https://doi.org/10.1016/S0962-8924(01)02107-9)
- Nicolson, G.L., 1993. Paracrine and autocrine growth mechanisms in tumor metastasis to specific sites with particular emphasis on brain and lung metastasis. *Cancer Metastasis Rev* 12, 325–343. <https://doi.org/10.1007/BF00665961>
- Nimnual, A.S., Taylor, L.J., Bar-Sagi, D., 2003. Redox-dependent downregulation of Rho by Rac. *Nat Cell Biol* 5, 236–241. <https://doi.org/10.1038/ncb938>
- Nishita, M., Aizawa, H., Mizuno, K., 2002. Stromal cell-derived factor 1 $\alpha$  activates LIM kinase 1 and induces cofilin phosphorylation for T-cell chemotaxis. *Mol Cell Biol* 22, 774–783. <https://doi.org/10.1128/MCB.22.3.774-783.2002>
- Niwa, R., Nagata-Ohashi, K., Takeichi, M., Mizuno, K., Uemura, T., 2002. Control of Actin Reorganization by Slingshot, a Family of Phosphatases that Dephosphorylate ADF/Cofilin. *Cell* 108, 233–246. [https://doi.org/10.1016/S0092-8674\(01\)00638-9](https://doi.org/10.1016/S0092-8674(01)00638-9)
- Nobles, K.N., Xiao, K., Ahn, S., Shukla, A.K., Lam, C.M., Rajagopal, S., Strachan, R.T., Huang, T.-Y., Bressler, E.A., Hara, M.R., Shenoy, S.K., Gygi, S.P., Lefkowitz, R.J., 2011. Distinct Phosphorylation Sites on the  $\beta$ 2-Adrenergic Receptor Establish a Barcode That Encodes Differential Functions of  $\beta$ -Arrestin. *Science Signaling* 4, ra51–ra51. <https://doi.org/10.1126/scisignal.2001707>

- Nolen, B.J., Tomasevic, N., Russell, A., Pierce, D.W., Jia, Z., McCormick, C.D., Hartman, J., Sakowicz, R., Pollard, T.D., 2009. Characterization of two classes of small molecule inhibitors of Arp2/3 complex. *Nature* 460, 1031–1034. <https://doi.org/10.1038/nature08231>
- Nourshargh, S., Alon, R., 2014. Leukocyte migration into inflamed tissues. *Immunity* 41, 694–707. <https://doi.org/10.1016/j.immuni.2014.10.008>
- Oberlin, E., Amara, A., Bachelier, F., Bessia, C., Virelizier, J.L., Arenzana-Seisdedos, F., Schwartz, O., Heard, J.M., Clark-Lewis, I., Legler, D.F., Loetscher, M., Baggiolini, M., Moser, B., 1996. The CXC chemokine SDF-1 is the ligand for LESTR/fusin and prevents infection by T-cell-line-adapted HIV-1. *Nature* 382, 833–835. <https://doi.org/10.1038/382833a0>
- Öhlund, D., Elyada, E., Tuveson, D., 2014. Fibroblast heterogeneity in the cancer wound. *Journal of Experimental Medicine* 211, 1503–1523. <https://doi.org/10.1084/jem.20140692>
- Ohta, Y., Kousaka, K., Nagata-Ohashi, K., Ohashi, K., Muramoto, A., Shima, Y., Niwa, R., Uemura, T., Mizuno, K., 2003. Differential activities, subcellular distribution and tissue expression patterns of three members of Slingshot family phosphatases that dephosphorylate cofilin. *Genes Cells* 8, 811–824. <https://doi.org/10.1046/j.1365-2443.2003.00678.x>
- Olayioye, M.A., Barisic, S., Hausser, A., 2013. Multi-level control of actin dynamics by protein kinase D. *Cell Signal* 25, 1739–1747. <https://doi.org/10.1016/j.cellsig.2013.04.010>
- Oppermann, M., 2004. Chemokine receptor CCR5: insights into structure, function, and regulation. *Cell Signal* 16, 1201–1210. <https://doi.org/10.1016/j.cellsig.2004.04.007>
- Oppermann, M., Mack, M., Proudfoot, A.E., Olbrich, H., 1999. Differential effects of CC chemokines on CC chemokine receptor 5 (CCR5) phosphorylation and identification of phosphorylation sites on the CCR5 carboxyl terminus. *J Biol Chem* 274, 8875–8885. <https://doi.org/10.1074/jbc.274.13.8875>
- Orlandi, P.A., Fishman, P.H., 1998. Filipin-dependent Inhibition of Cholera Toxin: Evidence for Toxin Internalization and Activation through Caveolae-like Domains. *J Cell Biol* 141, 905–915.
- Oser, M., Condeelis, J., 2009. The cofilin activity cycle in lamellipodia and invadopodia. *J Cell Biochem* 108, 1252–1262. <https://doi.org/10.1002/jcb.22372>
- Otero, C., Groettrup, M., Legler, D.F., 2006. Opposite Fate of Endocytosed CCR7 and Its Ligands: Recycling versus Degradation<sup>1</sup>. *The Journal of Immunology* 177, 2314–2323. <https://doi.org/10.4049/jimmunol.177.4.2314>
- Ouadid-Ahidouch, H., Dhennin-Duthille, I., Gautier, M., Sevestre, H., Ahidouch, A., 2013. TRP channels: diagnostic markers and therapeutic targets for breast cancer? *Trends in Molecular Medicine* 19, 117–124. <https://doi.org/10.1016/j.molmed.2012.11.004>
- P, P., J, H., G, L., K, P., Ma, O., A, H., 2009. Protein kinase D regulates cell migration by direct phosphorylation of the cofilin phosphatase slingshot 1 like. *Cancer research* 69. <https://doi.org/10.1158/0008-5472.CAN-09-0718>
- Pan, J., Mestas, J., Burdick, M.D., Phillips, R.J., Thomas, G.V., Reckamp, K., Belperio, J.A., Strieter, R.M., 2006. Stromal Derived Factor-1 (SDF-1/CXCL12) and CXCR4 in renal cell carcinoma metastasis. *Molecular Cancer* 5, 56. <https://doi.org/10.1186/1476-4598-5-56>

- Paoletti, S., Petkovic, V., Sebastiani, S., Danelon, M.G., Uguccioni, M., Gerber, B.O., 2005. A rich chemokine environment strongly enhances leukocyte migration and activities. *Blood* 105, 3405–3412. <https://doi.org/10.1182/blood-2004-04-1648>
- Parton, R.G., Del Pozo, M.A., Vassilopoulos, S., Nabi, I.R., Le Lay, S., Lundmark, R., Kenworthy, A.K., Camus, A., Blouin, C.M., Sessa, W.C., Lamaze, C., 2020a. Caveolae: The FAQs. *Traffic* 21, 181–185. <https://doi.org/10.1111/tra.12689>
- Parton, R.G., Howes, M.T., 2010. Revisiting caveolin trafficking: the end of the caveosome. *J Cell Biol* 191, 439–441. <https://doi.org/10.1083/jcb.201009093>
- Parton, R.G., McMahon, K.-A., Wu, Y., 2020b. Caveolae: Formation, dynamics, and function. *Curr Opin Cell Biol* 65, 8–16. <https://doi.org/10.1016/j.ceb.2020.02.001>
- Pedersen, M.H., Pham, J., Mancebo, H., Inoue, A., Asher, W.B., Javitch, J.A., 2021. A novel luminescence-based  $\beta$ -arrestin recruitment assay for unmodified receptors. *Journal of Biological Chemistry* 296. <https://doi.org/10.1016/j.jbc.2021.100503>
- Peled, A., Abraham, M., Avivi, I., Rowe, J.M., Beider, K., Wald, H., Tiomkin, L., Ribakovskiy, L., Riback, Y., Ramati, Y., Aviel, S., Galun, E., Shaw, H.L., Eizenberg, O., Hardan, I., Shimoni, A., Nagler, A., 2014. The high-affinity CXCR4 antagonist BKT140 is safe and induces a robust mobilization of human CD34+ cells in patients with multiple myeloma. *Clin Cancer Res* 20, 469–479. <https://doi.org/10.1158/1078-0432.CCR-13-1302>
- Pelkmans, L., Bürli, T., Zerial, M., Helenius, A., 2004. Caveolin-Stabilized Membrane Domains as Multifunctional Transport and Sorting Devices in Endocytic Membrane Traffic. *Cell* 118, 767–780. <https://doi.org/10.1016/j.cell.2004.09.003>
- Pelkmans, L., Kartenbeck, J., Helenius, A., 2001. Caveolar endocytosis of simian virus 40 reveals a new two-step vesicular-transport pathway to the ER. *Nat Cell Biol* 3, 473–483. <https://doi.org/10.1038/35074539>
- Peng, S.-B., Zhang, X., Paul, D., Kays, L.M., Gough, W., Stewart, J., Uhlik, M.T., Chen, Q., Hui, Y.-H., Zamek-Gliszczynski, M.J., Wijsman, J.A., Credille, K.M., Yan, L.Z., 2015. Identification of LY2510924, a novel cyclic peptide CXCR4 antagonist that exhibits antitumor activities in solid tumor and breast cancer metastatic models. *Mol Cancer Ther* 14, 480–490. <https://doi.org/10.1158/1535-7163.MCT-14-0850>
- Percherancier, Y., Planchenault, T., Valenzuela-Fernandez, A., Virelizier, J.L., Arenzana-Seisdedos, F., Bachelier, F., 2001. Palmitoylation-dependent control of degradation, life span, and membrane expression of the CCR5 receptor. *J Biol Chem* 276, 31936–31944. <https://doi.org/10.1074/jbc.M104013200>
- Pérez-Rivero, G., Cascio, G., Soriano, S.F., Sanz, Á.G., de Guinoa, J.S., Rodríguez-Frade, J.M., Gomariz, R.P., Holgado, B.L., Cabañas, C., Carrasco, Y.R., Stein, J.V., Mellado, M., 2013. Janus kinases 1 and 2 regulate chemokine-mediated integrin activation and naïve T-cell homing. *Eur J Immunol* 43, 1745–1757. <https://doi.org/10.1002/eji.201243178>
- Perlman, J.H., Wang, W., Nussenzveig, D.R., Gershengorn, M.C., 1995. A disulfide bond between conserved extracellular cysteines in the thyrotropin-releasing hormone receptor is critical for binding. *J Biol Chem* 270, 24682–24685. <https://doi.org/10.1074/jbc.270.42.24682>

- Pernas, S., Martin, M., Kaufman, P.A., Gil-Martin, M., Pardo, P.G., Lopez-Tarruella, S., Manso, L., Ciruelos, E., Perez-Fidalgo, J.A., Hernando, C., Ademuyiwa, F.O., Weilbaecher, K., Mayer, I., Pluard, T.J., Garcia, M.M., Vahdat, L., Perez-Garcia, J., Wach, A., Barker, D., Fung, S., Romagnoli, B., Cortes, J., 2018. Balixafortide plus eribulin in HER2-negative metastatic breast cancer: a phase 1, single-arm, dose-escalation trial. *The Lancet Oncology* 19, 812–824. [https://doi.org/10.1016/S1470-2045\(18\)30147-5](https://doi.org/10.1016/S1470-2045(18)30147-5)
- Pertz, O., Hodgson, L., Klemke, R.L., Hahn, K.M., 2006. Spatiotemporal dynamics of RhoA activity in migrating cells. *Nature* 440, 1069–1072. <https://doi.org/10.1038/nature04665>
- Peterburs, P., Heering, J., Link, G., Pfizenmaier, K., Olayioye, M.A., Hausser, A., 2009. Protein Kinase D Regulates Cell Migration by Direct Phosphorylation of the Cofilin Phosphatase Slingshot 1 Like. *Cancer Research* 69, 5634–5638. <https://doi.org/10.1158/0008-5472.CAN-09-0718>
- Peterson, Y.K., Luttrell, L.M., 2017. The Diverse Roles of Arrestin Scaffolds in G Protein-Coupled Receptor Signaling. *Pharmacol Rev* 69, 256–297. <https://doi.org/10.1124/pr.116.013367>
- PFLEGER, K.D.G., EIDNE, K.A., 2005. Monitoring the formation of dynamic G-protein-coupled receptor–protein complexes in living cells. *Biochemical Journal* 385, 625–637. <https://doi.org/10.1042/BJ20041361>
- Pierce, K.L., Premont, R.T., Lefkowitz, R.J., 2002. Seven-transmembrane receptors. *Nat Rev Mol Cell Biol* 3, 639–650. <https://doi.org/10.1038/nrm908>
- Platonova, E., Winterflood, C.M., Junemann, A., Albrecht, D., Faix, J., Ewers, H., 2015. Single-molecule microscopy of molecules tagged with GFP or RFP derivatives in mammalian cells using nanobody binders. *Methods* 88, 89–97. <https://doi.org/10.1016/j.ymeth.2015.06.018>
- Poincloux, R., Collin, O., Lizárraga, F., Romao, M., Debray, M., Piel, M., Chavrier, P., 2011. Contractility of the cell rear drives invasion of breast tumor cells in 3D Matrigel. *Proc Natl Acad Sci U S A* 108, 1943–1948. <https://doi.org/10.1073/pnas.1010396108>
- Pol, A., Morales-Paytuví, F., Bosch, M., Parton, R.G., 2020. Non-caveolar caveolins - duties outside the caves. *J Cell Sci* 133, jcs241562. <https://doi.org/10.1242/jcs.241562>
- Popescu, L.M., Gherghiceanu, M., Mandache, E., Cretoiu, D., 2006. Caveolae in smooth muscles: nanocontacts. *J Cell Mol Med* 10, 960–990. <https://doi.org/10.1111/j.1582-4934.2006.tb00539.x>
- Prevarskaya, N., Skryma, R., Shuba, Y., 2011. Calcium in tumour metastasis: new roles for known actors. *Nat Rev Cancer* 11, 609–618. <https://doi.org/10.1038/nrc3105>
- Proudfoot, A.E., Fritchley, S., Borlat, F., Shaw, J.P., Vilbois, F., Zwahlen, C., Trkola, A., Marchant, D., Clapham, P.R., Wells, T.N., 2001. The BBXB motif of RANTES is the principal site for heparin binding and controls receptor selectivity. *J Biol Chem* 276, 10620–10626. <https://doi.org/10.1074/jbc.M010867200>
- Proudfoot, A.E.I., Handel, T.M., Johnson, Z., Lau, E.K., LiWang, P., Clark-Lewis, I., Borlat, F., Wells, T.N.C., Kosco-Vilbois, M.H., 2003. Glycosaminoglycan binding and oligomerization are essential for the in vivo activity of certain chemokines. *Proceedings of the National Academy of Sciences* 100, 1885–1890. <https://doi.org/10.1073/pnas.0334864100>

- Proudfoot, A.E.I., Uguccioni, M., 2016. Modulation of Chemokine Responses: Synergy and Cooperativity. *Front Immunol* 7, 183. <https://doi.org/10.3389/fimmu.2016.00183>
- Qin, L., Kufareva, I., Holden, L.G., Wang, C., Zheng, Y., Zhao, C., Fenalti, G., Wu, H., Han, G.W., Cherezov, V., Abagyan, R., Stevens, R.C., Handel, T.M., 2015. Crystal structure of the chemokine receptor CXCR4 in complex with a viral chemokine. *Science* 347, 1117–1122. <https://doi.org/10.1126/science.1261064>
- Rajagopal, S., Kim, J., Ahn, S., Craig, S., Lam, C.M., Gerard, N.P., Gerard, C., Lefkowitz, R.J., 2010. Beta-arrestin- but not G protein-mediated signaling by the “decoy” receptor CXCR7. *Proc Natl Acad Sci U S A* 107, 628–632. <https://doi.org/10.1073/pnas.0912852107>
- Rajagopalan, L., Rajarathnam, K., 2006. Structural Basis of Chemokine Receptor Function—A Model for Binding Affinity and Ligand Selectivity. *Bioscience Reports* 26, 325–339. <https://doi.org/10.1007/s10540-006-9025-9>
- Raju, R., Gadakh, S., Gopal, P., George, B., Advani, J., Soman, S., Prasad, T.S.K., Girijadevi, R., 2015. Differential ligand-signaling network of CCL19/CCL21-CCR7 system. *Database* 2015, bav106. <https://doi.org/10.1093/database/bav106>
- Raman, R., Sasisekharan, V., Sasisekharan, R., 2005. Structural insights into biological roles of protein-glycosaminoglycan interactions. *Chem Biol* 12, 267–277. <https://doi.org/10.1016/j.chembiol.2004.11.020>
- Rao, P.V., Deng, P.F., Kumar, J., Epstein, D.L., 2001. Modulation of aqueous humor outflow facility by the Rho kinase-specific inhibitor Y-27632. *Invest Ophthalmol Vis Sci* 42, 1029–1037.
- Reinhardt, R., Truebestein, L., Schmidt, H.A., Leonard, T.A., 2020. It Takes Two to Tango: Activation of Protein Kinase D by Dimerization. *BioEssays* 42, 1900222. <https://doi.org/10.1002/bies.201900222>
- Rek, A., Brandner, B., Geretti, E., Kungl, A.J., 2009. A biophysical insight into the RANTES-glycosaminoglycan interaction. *Biochim Biophys Acta* 1794, 577–582. <https://doi.org/10.1016/j.bbapap.2009.01.001>
- Richard-Bildstein, S., Aissaoui, H., Pothier, J., Schäfer, G., Gnerre, C., Lindenberg, E., Lehembre, F., Pouzol, L., Guerry, P., 2020. Discovery of the Potent, Selective, Orally Available CXCR7 Antagonist ACT-1004-1239. *J Med Chem* 63, 15864–15882. <https://doi.org/10.1021/acs.jmedchem.0c01588>
- Richmond, A., Fan, G.-H., 2004. Chemokine Receptors, in: Lennarz, W.J., Lane, M.D. (Eds.), *Encyclopedia of Biological Chemistry*. Elsevier, New York, pp. 413–418. <https://doi.org/10.1016/B0-12-443710-9/00106-X>
- Ridley, A.J., Paterson, H.F., Johnston, C.L., Diekmann, D., Hall, A., 1992. The small GTP-binding protein rac regulates growth factor-induced membrane ruffling. *Cell* 70, 401–410. [https://doi.org/10.1016/0092-8674\(92\)90164-8](https://doi.org/10.1016/0092-8674(92)90164-8)
- Riento, K., Ridley, A.J., 2003. Rocks: multifunctional kinases in cell behaviour. *Nat Rev Mol Cell Biol* 4, 446–456. <https://doi.org/10.1038/nrm1128>
- Robinson, M.S., 2015. Forty Years of Clathrin-coated Vesicles. *Traffic* 16, 1210–1238. <https://doi.org/10.1111/tra.12335>
- Römer, W., Pontani, L.-L., Sorre, B., Rentero, C., Berland, L., Chambon, V., Lamaze, C., Bassereau, P., Sykes, C., Gaus, K., Johannes, L., 2010. Actin Dynamics Drive Membrane Reorganization and Scission in Clathrin-Independent Endocytosis. *Cell* 140, 540–553. <https://doi.org/10.1016/j.cell.2010.01.010>

- Rosenbaum, D.M., Rasmussen, S.G.F., Kobilka, B.K., 2009. The structure and function of G-protein-coupled receptors. *Nature* 459, 356–363. <https://doi.org/10.1038/nature08144>
- Rosenfeldt, H., Vázquez-Prado, J., Gutkind, J.S., 2004. P-REX2, a novel PI-3-kinase sensitive Rac exchange factor. *FEBS Lett* 572, 167–171. <https://doi.org/10.1016/j.febslet.2004.06.097>
- Rosenkilde, M.M., Gerlach, L.-O., Hatse, S., Skerlj, R.T., Schols, D., Bridger, G.J., Schwartz, T.W., 2007. Molecular Mechanism of Action of Monocyclam Versus Bicyclam Non-peptide Antagonists in the CXCR4 Chemokine Receptor \*. *Journal of Biological Chemistry* 282, 27354–27365. <https://doi.org/10.1074/jbc.M704739200>
- Roy, A., Ye, J., Deng, F., Wang, Q.J., 2017. Protein kinase D signaling in cancer: A friend or foe? *Biochim Biophys Acta Rev Cancer* 1868, 283–294. <https://doi.org/10.1016/j.bbcan.2017.05.008>
- Roy, I., Getschman, A.E., Volkman, B.F., Dwinell, M.B., 2017. Exploiting Agonist Biased Signaling of Chemokines to Target Cancer. *Mol Carcinog* 56, 804–813. <https://doi.org/10.1002/mc.22571>
- Rozengurt, E., Rey, O., Waldron, R.T., 2005. Protein Kinase D Signaling \*. *Journal of Biological Chemistry* 280, 13205–13208. <https://doi.org/10.1074/jbc.R500002200>
- Rybin, V.O., Guo, J., Steinberg, S.F., 2009. Protein Kinase D1 Autophosphorylation via Distinct Mechanisms at Ser744/Ser748 and Ser916. *J Biol Chem* 284, 2332–2343. <https://doi.org/10.1074/jbc.M806381200>
- Ryx, A., De Kimpe, L., Mikhalap, S., Vantus, T., Seufferlein, T., Vandenheede, J.R., Van Lint, J., 2003. Protein kinase D: a family affair. *FEBS Lett* 546, 81–86. [https://doi.org/10.1016/s0014-5793\(03\)00487-3](https://doi.org/10.1016/s0014-5793(03)00487-3)
- Samson, M., Labbe, O., Mollereau, C., Vassart, G., Parmentier, M., 1996. Molecular cloning and functional expression of a new human CC-chemokine receptor gene. *Biochemistry* 35, 3362–3367. <https://doi.org/10.1021/bi952950g>
- Santagata, S., Ieranò, C., Trotta, A.M., Capiluongo, A., Auletta, F., Guardascione, G., Scala, S., 2021. CXCR4 and CXCR7 Signaling Pathways: A Focus on the Cross-Talk Between Cancer Cells and Tumor Microenvironment. *Frontiers in Oncology* 11.
- Sanz-Moreno, V., 2012. Tumour invasion: a new twist on Rac-driven mesenchymal migration. *Curr Biol* 22, R449-451. <https://doi.org/10.1016/j.cub.2012.04.024>
- Sanz-Moreno, V., Gadea, G., Ahn, J., Paterson, H., Marra, P., Pinner, S., Sahai, E., Marshall, C.J., 2008. Rac activation and inactivation control plasticity of tumor cell movement. *Cell* 135, 510–523. <https://doi.org/10.1016/j.cell.2008.09.043>
- Sanz-Moreno, V., Marshall, C.J., 2010. The plasticity of cytoskeletal dynamics underlying neoplastic cell migration. *Curr Opin Cell Biol* 22, 690–696. <https://doi.org/10.1016/j.ceb.2010.08.020>
- Sawant, K.V., Poluri, K.M., Dutta, A.K., Sepuru, K.M., Troshkina, A., Garofalo, R.P., Rajarathnam, K., 2016. Chemokine CXCL1 mediated neutrophil recruitment: Role of glycosaminoglycan interactions. *Sci Rep* 6, 33123. <https://doi.org/10.1038/srep33123>
- Schadendorf, D., Möller, A., Algermissen, B., Worm, M., Sticherling, M., Czarnetzki, B.M., 1993. IL-8 produced by human malignant melanoma

- cells in vitro is an essential autocrine growth factor. *J Immunol* 151, 2667–2675.
- Schalper, K.A., Carleton, M., Zhou, M., Chen, T., Feng, Y., Huang, S.-P., Walsh, A.M., Baxi, V., Pandya, D., Baradet, T., Locke, D., Wu, Q., Reilly, T.P., Phillips, P., Nagineni, V., Gianino, N., Gu, J., Zhao, H., Perez-Gracia, J.L., Sanmamed, M.F., Melero, I., 2020. Elevated serum interleukin-8 is associated with enhanced intratumor neutrophils and reduced clinical benefit of immune-checkpoint inhibitors. *Nat Med* 26, 688–692. <https://doi.org/10.1038/s41591-020-0856-x>
- Schneider-Poetsch, T., Ju, J., Eyster, D.E., Dang, Y., Bhat, S., Merrick, W.C., Green, R., Shen, B., Liu, J.O., 2010. Inhibition of eukaryotic translation elongation by cycloheximide and lactimidomycin. *Nat Chem Biol* 6, 209–217. <https://doi.org/10.1038/nchembio.304>
- Schwartz, T.W., Frimurer, T.M., Holst, B., Rosenkilde, M.M., Elling, C.E., 2006. Molecular Mechanism of 7tm Receptor Activation—a Global Toggle Switch Model. *Annual Review of Pharmacology and Toxicology* 46, 481–519. <https://doi.org/10.1146/annurev.pharmtox.46.120604.141218>
- Scott, M.G.H., Rouzic, E.L., Périanin, A., Pierotti, V., Enslin, H., Benichou, S., Marullo, S., Benmerah, A., 2002. Differential Nucleocytoplasmic Shuttling of  $\beta$ -Arrestins: CHARACTERIZATION OF A LEUCINE-RICH NUCLEAR EXPORT SIGNAL IN  $\beta$ -ARRESTIN2 \*. *Journal of Biological Chemistry* 277, 37693–37701. <https://doi.org/10.1074/jbc.M207552200>
- Scott, R.W., Olson, M.F., 2007. LIM kinases: function, regulation and association with human disease. *J Mol Med (Berl)* 85, 555–568. <https://doi.org/10.1007/s00109-007-0165-6>
- Senju, Y., Suetsugu, S., 2020. Spatiotemporal Analysis of Caveolae Dynamics Using Total Internal Reflection Fluorescence Microscopy. *Methods Mol Biol* 2169, 63–70. [https://doi.org/10.1007/978-1-0716-0732-9\\_6](https://doi.org/10.1007/978-1-0716-0732-9_6)
- Seo, Y., Andaya, A., Bleiholder, C., Leary, J.A., 2013. Differentiation of CC vs CXC Chemokine Dimers with GAG Octasaccharide Binding Partners: An Ion Mobility Mass Spectrometry Approach. *J. Am. Chem. Soc.* 135, 4325–4332. <https://doi.org/10.1021/ja310915m>
- Sepuru, K.M., Nagarajan, B., Desai, U.R., Rajarathnam, K., 2016. Molecular Basis of Chemokine CXCL5-Glycosaminoglycan Interactions \*. *Journal of Biological Chemistry* 291, 20539–20550. <https://doi.org/10.1074/jbc.M116.745265>
- Sharlow, E.R., Giridhar, K.V., LaValle, C.R., Chen, J., Leimgruber, S., Barrett, R., Bravo-Altamirano, K., Wipf, P., Lazo, J.S., Wang, Q.J., 2008. Potent and selective disruption of protein kinase D functionality by a benzoxoloazepinolone. *J Biol Chem* 283, 33516–33526. <https://doi.org/10.1074/jbc.M805358200>
- Sharlow, E.R., Mustata Wilson, G., Close, D., Leimgruber, S., Tandon, M., Reed, R.B., Shun, T.Y., Wang, Q.J., Wipf, P., Lazo, J.S., 2011. Discovery of diverse small molecule chemotypes with cell-based PKD1 inhibitory activity. *PLoS One* 6, e25134. <https://doi.org/10.1371/journal.pone.0025134>
- Shaw, J.P., Johnson, Z., Borlat, F., Zwahlen, C., Kungl, A., Roulin, K., Harrenga, A., Wells, T.N.C., Proudfoot, A.E.I., 2004. The X-ray structure of RANTES: heparin-derived disaccharides allows the rational design of chemokine inhibitors. *Structure* 12, 2081–2093. <https://doi.org/10.1016/j.str.2004.08.014>

- Shi, J., McAtee, J.J., Schlueter Wirtz, S., Tharnish, P., Juodawlkis, A., Liotta, D.C., Schinazi, R.F., 1999. Synthesis and biological evaluation of 2',3'-dideoxy-2',3'-dideoxy-5-fluorocytidine (D4FC) analogues: discovery of carbocyclic nucleoside triphosphates with potent inhibitory activity against HIV-1 reverse transcriptase. *J Med Chem* 42, 859–867. <https://doi.org/10.1021/jm980510s>
- Shi, J., Wu, X., Surma, M., Vemula, S., Zhang, L., Yang, Y., Kapur, R., Wei, L., 2013. Distinct roles for ROCK1 and ROCK2 in the regulation of cell detachment. *Cell Death Dis* 4, e483–e483. <https://doi.org/10.1038/cddis.2013.10>
- Shukla, A.K., Dwivedi-Agnihotri, H., 2020. Structure and function of  $\beta$ -arrestins, their emerging role in breast cancer, and potential opportunities for therapeutic manipulation. *Adv Cancer Res* 145, 139–156. <https://doi.org/10.1016/bs.acr.2020.01.001>
- Shvets, E., Bitsikas, V., Howard, G., Hansen, C.G., Nichols, B.J., 2015. Dynamic caveolae exclude bulk membrane proteins and are required for sorting of excess glycosphingolipids. *Nat Commun* 6, 6867. <https://doi.org/10.1038/ncomms7867>
- Si, M., Song, Y., Wang, X., Wang, D., Liu, X., Qu, X., Song, Z., Yu, X., 2022. CXCL12/CXCR7/ $\beta$ -arrestin1 biased signal promotes epithelial-to-mesenchymal transition of colorectal cancer by repressing miRNAs through YAP1 nuclear translocation. *Cell & Bioscience* 12, 171. <https://doi.org/10.1186/s13578-022-00908-1>
- Signoret, N., Hewlett, L., Wavre, S., Pelchen-Matthews, A., Oppermann, M., Marsh, M., 2005. Agonist-induced Endocytosis of CC Chemokine Receptor 5 Is Clathrin Dependent. *Mol Biol Cell* 16, 902–917. <https://doi.org/10.1091/mbc.E04-08-0687>
- Signoret, N., Oldridge, J., Pelchen-Matthews, A., Klasse, P.J., Tran, T., Brass, L.F., Rosenkilde, M.M., Schwartz, T.W., Holmes, W., Dallas, W., Luther, M.A., Wells, T.N.C., Hoxie, J.A., Marsh, M., 1997. Phorbol Esters and SDF-1 Induce Rapid Endocytosis and Down Modulation of the Chemokine Receptor CXCR4. *Journal of Cell Biology* 139, 651–664. <https://doi.org/10.1083/jcb.139.3.651>
- Simsek Papur, O., Sun, A., Glatz, J.F.C., Luiken, J.J.F.P., Nabben, M., 2018. Acute and Chronic Effects of Protein Kinase-D Signaling on Cardiac Energy Metabolism. *Front Cardiovasc Med* 5, 65. <https://doi.org/10.3389/fcvm.2018.00065>
- Son, D., Kim, Y., Lim, S., Kang, H.-G., Kim, D.-H., Park, J.W., Cheong, W., Kong, H.K., Han, W., Park, W.-Y., Chun, K.-H., Park, J.H., 2019. miR-374a-5p promotes tumor progression by targeting ARRB1 in triple negative breast cancer. *Cancer Lett* 454, 224–233. <https://doi.org/10.1016/j.canlet.2019.04.006>
- Song, Q., Ji, Q., Li, Q., 2018. The role and mechanism of  $\beta$ -arrestins in cancer invasion and metastasis (Review). *International Journal of Molecular Medicine* 41, 631–639. <https://doi.org/10.3892/ijmm.2017.3288>
- Sonmez, U.M., Wood, A., Justus, K., Jiang, W., Syed-Picard, F., LeDuc, P.R., Kalinski, P., Davidson, L.A., 2020. Chemotactic Responses of Jurkat Cells in Microfluidic Flow-Free Gradient Chambers. *Micromachines (Basel)* 11, 384. <https://doi.org/10.3390/mi11040384>
- Spiering, D., Hodgson, L., 2011. Dynamics of the Rho-family small GTPases in actin regulation and motility. *Cell Adh Migr* 5, 170–180. <https://doi.org/10.4161/cam.5.2.14403>

- Spitaler, M., Emslie, E., Wood, C.D., Cantrell, D., 2006. Diacylglycerol and protein kinase D localization during T lymphocyte activation. *Immunity* 24, 535–546. <https://doi.org/10.1016/j.immuni.2006.02.013>
- Spratley, S.J., Bastea, L.I., Döppler, H., Mizuno, K., Storz, P., 2011. Protein Kinase D Regulates Cofilin Activity through p21-activated Kinase 4 \*. *Journal of Biological Chemistry* 286, 34254–34261. <https://doi.org/10.1074/jbc.M111.259424>
- Stephens, L., Smrcka, A., Cooke, F.T., Jackson, T.R., Sternweis, P.C., Hawkins, P.T., 1994. A novel phosphoinositide 3 kinase activity in myeloid-derived cells is activated by G protein beta gamma subunits. *Cell* 77, 83–93. [https://doi.org/10.1016/0092-8674\(94\)90237-2](https://doi.org/10.1016/0092-8674(94)90237-2)
- Storme, J., Cannaert, A., Van Craenenbroeck, K., Stove, C.P., 2018. Molecular dissection of the human A3 adenosine receptor coupling with  $\beta$ -arrestin2. *Biochemical Pharmacology* 148, 298–307. <https://doi.org/10.1016/j.bcp.2018.01.008>
- Storz, P., 2018. Protein kinase D1: gatekeeper of the epithelial phenotype and key regulator of cancer metastasis? *Br J Cancer* 118, 459–461. <https://doi.org/10.1038/bjc.2018.1>
- Storz, P., Toker, A., 2003. Protein kinase D mediates a stress-induced NF- $\kappa$ B activation and survival pathway. *EMBO J* 22, 109–120. <https://doi.org/10.1093/emboj/cdg009>
- Stossel, T.P., Fenteany, G., Hartwig, J.H., 2006. Cell surface actin remodeling. *Journal of Cell Science* 119, 3261–3264. <https://doi.org/10.1242/jcs.02994>
- Sun, Y., Cheng, Z., Ma, L., Pei, G., 2002. Beta-arrestin2 is critically involved in CXCR4-mediated chemotaxis, and this is mediated by its enhancement of p38 MAPK activation. *J Biol Chem* 277, 49212–49219. <https://doi.org/10.1074/jbc.M207294200>
- Sun, Y., Mao, X., Fan, C., Liu, C., Guo, A., Guan, S., Jin, Q., Li, B., Yao, F., Jin, F., 2014. CXCL12-CXCR4 axis promotes the natural selection of breast cancer cell metastasis. *Tumour Biol* 35, 7765–7773. <https://doi.org/10.1007/s13277-014-1816-1>
- Svitkina, T.M., Bulanova, E.A., Chaga, O.Y., Vignjevic, D.M., Kojima, S., Vasiliev, J.M., Borisy, G.G., 2003. Mechanism of filopodia initiation by reorganization of a dendritic network. *J Cell Biol* 160, 409–421. <https://doi.org/10.1083/jcb.200210174>
- Symons, M., Derry, J.M., Karlak, B., Jiang, S., Lemahieu, V., McCormick, F., Francke, U., Abo, A., 1996. Wiskott-Aldrich syndrome protein, a novel effector for the GTPase CDC42Hs, is implicated in actin polymerization. *Cell* 84, 723–734. [https://doi.org/10.1016/s0092-8674\(00\)81050-8](https://doi.org/10.1016/s0092-8674(00)81050-8)
- Szpakowska, M., Nevins, A.M., Meyrath, M., Rhains, D., D’huys, T., Guité-Vinet, F., Dupuis, N., Gauthier, P.-A., Counson, M., Kleist, A., St-Onge, G., Hanson, J., Schols, D., Volkman, B.F., Heveker, N., Chevigné, A., 2018. Different contributions of chemokine N-terminal features attest to a different ligand binding mode and a bias towards activation of ACKR3/CXCR7 compared with CXCR4 and CXCR3. *British Journal of Pharmacology* 175, 1419–1438. <https://doi.org/10.1111/bph.14132>
- Tagawa, A., Mezzacasa, A., Hayer, A., Longatti, A., Pelkmans, L., Helenius, A., 2005. Assembly and trafficking of caveolar domains in the cell : caveolae as stable, cargo-triggered, vesicular transporters. *Journal of Cell Biology* 170, 769–779. <https://doi.org/10.1083/jcb.200506103>
- Tan, Q., Zhu, Y., Li, Jian, Chen, Z., Han, G.W., Kufareva, I., Li, T., Ma, L., Fenalti, G., Li, Jing, Zhang, W., Xie, X., Yang, H., Jiang, H., Cherezov, V., Liu, H.,

- Stevens, R.C., Zhao, Q., Wu, B., 2013. Structure of the CCR5 chemokine receptor – HIV entry inhibitor Maraviroc complex. *Science* 341, 10.1126/science.1241475. <https://doi.org/10.1126/science.1241475>
- Tania, N., Prosk, E., Condeelis, J., Edelstein-Keshet, L., 2011. A Temporal Model of Cofilin Regulation and the Early Peak of Actin Barbed Ends in Invasive Tumor Cells. *Biophys J* 100, 1883–1892. <https://doi.org/10.1016/j.bpj.2011.02.036>
- Taussig, R., Iñiguez-Lluhi, J.A., Gilman, A.G., 1993. Inhibition of adenylyl cyclase by Gi alpha. *Science* 261, 218–221. <https://doi.org/10.1126/science.8327893>
- Taylor, M.J., Perrais, D., Merrifield, C.J., 2011. A High Precision Survey of the Molecular Dynamics of Mammalian Clathrin-Mediated Endocytosis. *PLOS Biology* 9, e1000604. <https://doi.org/10.1371/journal.pbio.1000604>
- Theme, C.-C., 2019. To Assess the Safety of Continuous IV Administration of the CXCR4 Antagonist, Plerixafor (Mozobil), and Assess Its Impact on the Immune Microenvironment in Patients With Advanced Pancreatic, High Grade Serous Ovarian and Colorectal Adenocarcinomas. (Clinical trial registration No. NCT02179970). [clinicaltrials.gov](http://clinicaltrials.gov).
- Thoma, G., Streiff, M.B., Kovarik, J., Glickman, F., Wagner, T., Beerli, C., Zerwes, H.-G., 2008. Orally Bioavailable Isothioureas Block Function of the Chemokine Receptor CXCR4 In Vitro and In Vivo. *J. Med. Chem.* 51, 7915–7920. <https://doi.org/10.1021/jm801065q>
- Thomsen, A.R.B., Plouffe, B., Cahill, T.J., Shukla, A.K., Tarrasch, J.T., Dosey, A.M., Kahsai, A.W., Strachan, R.T., Pani, B., Mahoney, J.P., Huang, L., Breton, B., Heydenreich, F.M., Sunahara, R.K., Skiniotis, G., Bouvier, M., Lefkowitz, R.J., 2016. GPCR-G Protein-β-Arrestin Super-Complex Mediates Sustained G Protein Signaling. *Cell* 166, 907–919. <https://doi.org/10.1016/j.cell.2016.07.004>
- Tobin, A.B., 2008. G-protein-coupled receptor phosphorylation: where, when and by whom. *Br J Pharmacol* 153, S167–S176. <https://doi.org/10.1038/sj.bjp.0707662>
- Tobin, A.B., Butcher, A.J., Kong, K.C., 2008. Location, location, location...site-specific GPCR phosphorylation offers a mechanism for cell-type-specific signalling. *Trends Pharmacol Sci* 29, 413–420. <https://doi.org/10.1016/j.tips.2008.05.006>
- Tripathi, A., Vana, P.G., Chavan, T.S., Brueggemann, L.I., Byron, K.L., Tarasova, N.I., Volkman, B.F., Gaponenko, V., Majetschak, M., 2015. Heteromerization of chemokine (C-X-C motif) receptor 4 with α1A/B-adrenergic receptors controls α1-adrenergic receptor function. *Proc Natl Acad Sci U S A* 112, E1659-1668. <https://doi.org/10.1073/pnas.1417564112>
- Ullrich, O., Reinsch, S., Urbé, S., Zerial, M., Parton, R.G., 1996. Rab11 regulates recycling through the pericentriolar recycling endosome. *J Cell Biol* 135, 913–924. <https://doi.org/10.1083/jcb.135.4.913>
- Uy, G.L., Rettig, M.P., Motabi, I.H., McFarland, K., Trinkaus, K.M., Hladnik, L.M., Kulkarni, S., Abboud, C.N., Cashen, A.F., Stockerl-Goldstein, K.E., Vij, R., Westervelt, P., DiPersio, J.F., 2012. A phase 1/2 study of chemosensitization with the CXCR4 antagonist plerixafor in relapsed or refractory acute myeloid leukemia. *Blood* 119, 3917–3924. <https://doi.org/10.1182/blood-2011-10-383406>
- Valenzuela-Fernández, A., Palanche, T., Amara, A., Magerus, A., Altmeyer, R., Delaunay, T., Virelizier, J.-L., Baleux, F., Galzi, J.-L., Arenzana-

- Seisededos, F., 2001. Optimal Inhibition of X4 HIV Isolates by the CXC Chemokine Stromal Cell-derived Factor 1 $\alpha$  Requires Interaction with Cell Surface Heparan Sulfate Proteoglycans \*. *Journal of Biological Chemistry* 276, 26550–26558. <https://doi.org/10.1074/jbc.M100411200>
- van der Blik, A.M., Redelmeier, T.E., Damke, H., Tisdale, E.J., Meyerowitz, E.M., Schmid, S.L., 1993. Mutations in human dynamin block an intermediate stage in coated vesicle formation. *J Cell Biol* 122, 553–563. <https://doi.org/10.1083/jcb.122.3.553>
- Velasco-Velázquez, M., Jiao, X., De La Fuente, M., Pestell, T.G., Ertel, A., Lisanti, M.P., Pestell, R.G., 2012. CCR5 antagonist blocks metastasis of basal breast cancer cells. *Cancer Res* 72, 3839–3850. <https://doi.org/10.1158/0008-5472.CAN-11-3917>
- Venkatesan, S., Rose, J.J., Lodge, R., Murphy, P.M., Foley, J.F., 2003. Distinct Mechanisms of Agonist-induced Endocytosis for Human Chemokine Receptors CCR5 and CXCR4. *Molecular Biology of the Cell* 14, 3305. <https://doi.org/10.1091/mbc.E02-11-0714>
- Verschueren, H., Van der Taelen, I., Dewit, J., De Braekeleer, J., De Baetselier, P., 1994. Metastatic competence of BW5147 T-lymphoma cell lines is correlated with in vitro invasiveness, motility and F-actin content. *Journal of Leukocyte Biology* 55, 552–556. <https://doi.org/10.1002/jlb.55.4.552>
- Vinay, D.S., Ryan, E.P., Pawelec, G., Talib, W.H., Stagg, J., Elkord, E., Lichtor, T., Decker, W.K., Whelan, R.L., Kumara, H.M.C.S., Signori, E., Honoki, K., Georgakilas, A.G., Amin, A., Helferich, W.G., Boosani, C.S., Guha, G., Ciriolo, M.R., Chen, S., Mohammed, S.I., Azmi, A.S., Keith, W.N., Bilsland, A., Bhakta, D., Halicka, D., Fujii, H., Aquilano, K., Ashraf, S.S., Nowsheen, S., Yang, X., Choi, B.K., Kwon, B.S., 2015. Immune evasion in cancer: Mechanistic basis and therapeutic strategies. *Seminars in Cancer Biology, A broad-spectrum integrative design for cancer prevention and therapy* 35, S185–S198. <https://doi.org/10.1016/j.semcancer.2015.03.004>
- von Hundelshausen, P., Agten, S.M., Eckardt, V., Blanchet, X., Schmitt, M.M., Ippel, H., Neideck, C., Bidzhekov, K., Leberzammer, J., Wichapong, K., Faussner, A., Drechsler, M., Grommes, J., van Geffen, J.P., Li, H., Ortega-Gomez, A., Megens, R.T.A., Naumann, R., Dijkgraaf, I., Nicolaes, G.A.F., Döring, Y., Soehnlein, O., Lutgens, E., Heemskerk, J.W.M., Koenen, R.R., Mayo, K.H., Hackeng, T.M., Weber, C., 2017. Chemokine interactome mapping enables tailored intervention in acute and chronic inflammation. *Science Translational Medicine* 9, eaah6650. <https://doi.org/10.1126/scitranslmed.aah6650>
- von Kleist, L., Stahlschmidt, W., Bulut, H., Gromova, K., Puchkov, D., Robertson, M.J., MacGregor, K.A., Tomilin, N., Pechstein, A., Chau, N., Chircop, M., Sakoff, J., von Kries, J.P., Saenger, W., Kräusslich, H.-G., Shupliakov, O., Robinson, P.J., McCluskey, A., Haucke, V., 2011. Role of the Clathrin Terminal Domain in Regulating Coated Pit Dynamics Revealed by Small Molecule Inhibition. *Cell* 146, 471–484. <https://doi.org/10.1016/j.cell.2011.06.025>
- Votta, B.J., White, J.R., Dodds, R.A., James, I.E., Connor, J.R., Lee-Rykaczewski, E., Eichman, C.F., Kumar, S., Lark, M.W., Gowen, M., 2000. CKbeta-8 [CCL23], a novel CC chemokine, is chemotactic for human osteoclast precursors and is expressed in bone tissues. *J Cell Physiol* 183, 196–207. [https://doi.org/10.1002/\(SICI\)1097-4652\(200005\)183:2<196::AID-JCP6>3.0.CO;2-8](https://doi.org/10.1002/(SICI)1097-4652(200005)183:2<196::AID-JCP6>3.0.CO;2-8)

- Wang, L.H., Rothberg, K.G., Anderson, R.G., 1993. Mis-assembly of clathrin lattices on endosomes reveals a regulatory switch for coated pit formation. *J Cell Biol* 123, 1107–1117. <https://doi.org/10.1083/jcb.123.5.1107>
- Wang, Q.J., 2006. PKD at the crossroads of DAG and PKC signaling. *Trends Pharmacol Sci* 27, 317–323. <https://doi.org/10.1016/j.tips.2006.04.003>
- Wang, T., Li, Z., Cvijic, M.E., Zhang, L., Sum, C.S., 2004. Measurement of cAMP for Gas- and Gai Protein-Coupled Receptors (GPCRs), in: Markossian, S., Grossman, A., Brimacombe, K., Arkin, M., Auld, D., Austin, C., Baell, J., Chung, T.D.Y., Coussens, N.P., Dahlin, J.L., Devanarayan, V., Foley, T.L., Glicksman, M., Gorshkov, K., Haas, J.V., Hall, M.D., Hoare, S., Inglese, J., Iversen, P.W., Kales, S.C., Lal-Nag, M., Li, Z., McGee, J., McManus, O., Riss, T., Saradjian, P., Sittampalam, G.S., Tarselli, M., Trask, O.J., Wang, Y., Weidner, J.R., Wildey, M.J., Wilson, K., Xia, M., Xu, X. (Eds.), *Assay Guidance Manual*. Eli Lilly & Company and the National Center for Advancing Translational Sciences, Bethesda (MD).
- Wang, X., Watson, C., Sharp, J.S., Handel, T.M., Prestegard, J.H., 2011. Oligomeric structure of the chemokine CCL5/RANTES from NMR, MS, and SAXS data. *Structure* 19, 1138–1148. <https://doi.org/10.1016/j.str.2011.06.001>
- Wasilko, D.J., Johnson, Z.L., Ammirati, M., Che, Y., Griffor, M.C., Han, S., Wu, H., 2020. Structural basis for chemokine receptor CCR6 activation by the endogenous protein ligand CCL20. *Nat Commun* 11, 3031. <https://doi.org/10.1038/s41467-020-16820-6>
- Webb, L.M., Ehrenguber, M.U., Clark-Lewis, I., Baggiolini, M., Rot, A., 1993. Binding to heparan sulfate or heparin enhances neutrophil responses to interleukin 8. *Proceedings of the National Academy of Sciences* 90, 7158–7162. <https://doi.org/10.1073/pnas.90.15.7158>
- Weill Medical College of Cornell University, 2020. To Assess the Safety of Continuous IV Administration of the CXCR4 Antagonist, Plerixafor at Potentially Active Plasma Concentrations and Assess Its Impact on the Immune Microenvironment in Patients With Advanced Pancreatic, High Grade Serous Ovarian and Colorectal Adenocarcinomas (Clinical trial registration No. NCT03277209). [clinicaltrials.gov](https://clinicaltrials.gov).
- Welch, H.C.E., Coadwell, W.J., Ellson, C.D., Ferguson, G.J., Andrews, S.R., Erdjument-Bromage, H., Tempst, P., Hawkins, P.T., Stephens, L.R., 2002. P-Rex1, a PtdIns(3,4,5)P3- and Gbetagamma-regulated guanine-nucleotide exchange factor for Rac. *Cell* 108, 809–821. [https://doi.org/10.1016/s0092-8674\(02\)00663-3](https://doi.org/10.1016/s0092-8674(02)00663-3)
- Wheatley, M., Wooten, D., Conner, M., Simms, J., Kendrick, R., Logan, R., Poyner, D., Barwell, J., 2012. Lifting the lid on GPCRs: the role of extracellular loops. *British Journal of Pharmacology* 165, 1688–1703. <https://doi.org/10.1111/j.1476-5381.2011.01629.x>
- White, C.W., Caspar, B., Vanyai, H.K., Pflieger, K.D.G., Hill, S.J., 2020. CRISPR-Mediated Protein Tagging with Nanoluciferase to Investigate Native Chemokine Receptor Function and Conformational Changes. *Cell Chemical Biology* 27, 499-510.e7. <https://doi.org/10.1016/j.chembiol.2020.01.010>
- White, C.W., Vanyai, H.K., See, H.B., Johnstone, E.K.M., Pflieger, K.D.G., 2017. Using nanoBRET and CRISPR/Cas9 to monitor proximity to a genome-edited protein in real-time. *Sci Rep* 7, 3187. <https://doi.org/10.1038/s41598-017-03486-2>

- Wille, C., Köhler, C., Armacki, M., Jamali, A., Gössele, U., Pfizenmaier, K., Seufferlein, T., Eiseler, T., 2014. Protein kinase D2 induces invasion of pancreatic cancer cells by regulating matrix metalloproteinases. *Mol Biol Cell* 25, 324–336. <https://doi.org/10.1091/mbc.E13-06-0334>
- Williams, T.M., Lisanti, M.P., 2004. The caveolin proteins. *Genome Biology* 5, 214. <https://doi.org/10.1186/gb-2004-5-3-214>
- Witt, D.P., Lander, A.D., 1994. Differential binding of chemokines to glycosaminoglycan subpopulations. *Curr Biol* 4, 394–400. [https://doi.org/10.1016/s0960-9822\(00\)00088-9](https://doi.org/10.1016/s0960-9822(00)00088-9)
- Wolf, K., Müller, R., Borgmann, S., Bröcker, E.-B., Friedl, P., 2003. Amoeboid shape change and contact guidance: T-lymphocyte crawling through fibrillar collagen is independent of matrix remodeling by MMPs and other proteases. *Blood* 102, 3262–3269. <https://doi.org/10.1182/blood-2002-12-3791>
- Wolf, K., Wu, Y.I., Liu, Y., Geiger, J., Tam, E., Overall, C., Stack, M.S., Friedl, P., 2007. Multi-step pericellular proteolysis controls the transition from individual to collective cancer cell invasion. *Nat Cell Biol* 9, 893–904. <https://doi.org/10.1038/ncb1616>
- Wood, B.M., Bossuyt, J., 2017. Emergency Spatiotemporal Shift: The Response of Protein Kinase D to Stress Signals in the Cardiovascular System. *Front Pharmacol* 8, 9. <https://doi.org/10.3389/fphar.2017.00009>
- Wu, B., Chien, E.Y.T., Mol, C.D., Fenalti, G., Liu, W., Katritch, V., Abagyan, R., Brooun, A., Wells, P., Bi, F.C., Hamel, D.J., Kuhn, P., Handel, T.M., Cherezov, V., Stevens, R.C., 2010b. Structures of the CXCR4 Chemokine GPCR with Small-Molecule and Cyclic Peptide Antagonists. *Science* 330, 1066–1071. <https://doi.org/10.1126/science.1194396>
- Yang, F., Yu, X., Liu, C., Qu, C.-X., Gong, Z., Liu, H.-D., Li, F.-H., Wang, H.-M., He, D.-F., Yi, F., Song, C., Tian, C.-L., Xiao, K.-H., Wang, J.-Y., Sun, J.-P., 2015. Phospho-selective mechanisms of arrestin conformations and functions revealed by unnatural amino acid incorporation and 19F-NMR. *Nat Commun* 6, 8202. <https://doi.org/10.1038/ncomms9202>
- Yang, H., Lan, C., Xiao, Y., Chen, Y.-H., 2003. Antibody to CD14 like CXCR4-specific antibody 12G5 could inhibit CXCR4-dependent chemotaxis and HIV Env-mediated cell fusion. *Immunol Lett* 88, 27–30. [https://doi.org/10.1016/s0165-2478\(03\)00048-8](https://doi.org/10.1016/s0165-2478(03)00048-8)
- Yang, J., Kumar, A., Vilgelm, A.E., Chen, S.-C., Ayers, G.D., Novitskiy, S.V., Joyce, S., Richmond, A., 2018. Loss of CXCR4 in Myeloid Cells Enhances Antitumor Immunity and Reduces Melanoma Growth through NK Cell and FASL Mechanisms. *Cancer Immunology Research* 6, 1186–1198. <https://doi.org/10.1158/2326-6066.CIR-18-0045>
- Yang, L., Huang, J., Ren, X., Gorska, A.E., Chytil, A., Aakre, M., Carbone, D.P., Matrisian, L.M., Richmond, A., Lin, P.C., Moses, H.L., 2008. Abrogation of TGF $\beta$  Signaling in Mammary Carcinomas Recruits Gr-1+CD11b+ Myeloid Cells that Promote Metastasis. *Cancer Cell* 13, 23–35. <https://doi.org/10.1016/j.ccr.2007.12.004>
- Yang, W., Wang, D., Richmond, A., 1999. Role of Clathrin-mediated Endocytosis in CXCR2 Sequestration, Resensitization, and Signal Transduction\*. *Journal of Biological Chemistry* 274, 11328–11333. <https://doi.org/10.1074/jbc.274.16.11328>
- Yeow, I., Howard, G., Chadwick, J., Mendoza-Topaz, C., Hansen, C.G., Nichols, B.J., Shvets, E., 2017. EHD Proteins Cooperate to Generate Caveolar

- Clusters and to Maintain Caveolae during Repeated Mechanical Stress. *Curr Biol* 27, 2951-2962.e5. <https://doi.org/10.1016/j.cub.2017.07.047>
- Yoshino, H., Kumai, Y., Kashiwakura, I., 2017. Effects of endoplasmic reticulum stress on apoptosis induction in radioresistant macrophages. *Molecular Medicine Reports* 15, 2867–2872. <https://doi.org/10.3892/mmr.2017.6298>
- Youngs, S.J., Ali, S.A., Taub, D.D., Rees, R.C., 1997. Chemokines induce migrational responses in human breast carcinoma cell lines. *Int J Cancer* 71, 257–266. [https://doi.org/10.1002/\(sici\)1097-0215\(19970410\)71:2<257::aid-ijc22>3.0.co;2-d](https://doi.org/10.1002/(sici)1097-0215(19970410)71:2<257::aid-ijc22>3.0.co;2-d)
- Yu, X., Wang, D., Wang, X., Sun, S., Zhang, Y., Wang, S., Miao, R., Xu, X., Qu, X., 2019. CXCL12/CXCR4 promotes inflammation-driven colorectal cancer progression through activation of RhoA signaling by sponging miR-133a-3p. *J Exp Clin Cancer Res* 38, 32. <https://doi.org/10.1186/s13046-018-1014-x>
- Yuan, J., Pandol, S.J., 2016. PKD signaling and pancreatitis. *J Gastroenterol* 51, 651–659. <https://doi.org/10.1007/s00535-016-1175-3>
- Yuen, K.C., Liu, L.-F., Gupta, V., Madireddi, S., Keerthivasan, S., Li, C., Rishipathak, D., Williams, P., Kadel, E.E., Koeppen, H., Chen, Y.-J., Modrusan, Z., Grogan, J.L., Banachereau, R., Leng, N., Thastrom, A., Shen, X., Hashimoto, K., Tayama, D., van der Heijden, M.S., Rosenberg, J.E., McDermott, D.F., Powles, T., Hegde, P.S., Huseni, M.A., Mariathasan, S., 2020. High systemic and tumor-associated IL-8 correlates with reduced clinical benefit of PD-L1 blockade. *Nat Med* 26, 693–698. <https://doi.org/10.1038/s41591-020-0860-1>
- Zboralski, D., Hoehlig, K., Eulberg, D., Frömmling, A., Vater, A., 2017. Increasing Tumor-Infiltrating T Cells through Inhibition of CXCL12 with NOX-A12 Synergizes with PD-1 Blockade. *Cancer Immunology Research* 5, 950–956. <https://doi.org/10.1158/2326-6066.CIR-16-0303>
- Zhang, H., Chen, K., Tan, Q., Shao, Q., Han, S., Zhang, C., Yi, C., Chu, X., Zhu, Y., Xu, Y., Zhao, Q., Wu, B., 2021. Structural basis for chemokine recognition and receptor activation of chemokine receptor CCR5. *Nat Commun* 12, 4151. <https://doi.org/10.1038/s41467-021-24438-5>
- Zhang, J., Liu, C., Mo, X., Shi, H., Li, S., 2018. Mechanisms by which CXCR4/CXCL12 cause metastatic behavior in pancreatic cancer. *Oncology Letters* 15, 1771–1776. <https://doi.org/10.3892/ol.2017.7512>
- Zhang, J., Pang, Y., Xie, T., Zhu, L., 2019. CXCR4 antagonism in combination with IDO1 inhibition weakens immune suppression and inhibits tumor growth in mouse breast cancer bone metastases. *Onco Targets Ther* 12, 4985–4992. <https://doi.org/10.2147/OTT.S200643>
- Zhang, R., Xie, X., 2012. Tools for GPCR drug discovery. *Acta Pharmacol Sin* 33, 372–384. <https://doi.org/10.1038/aps.2011.173>
- Zhang, X., Connelly, J., Chao, Y., Wang, Q.J., 2021. Multifaceted Functions of Protein Kinase D in Pathological Processes and Human Diseases. *Biomolecules* 11, 483. <https://doi.org/10.3390/biom11030483>
- Zhang, Y., Li, J., Lai, X.-N., Jiao, X.-Q., Xiong, J.-P., Xiong, L.-X., 2019. Focus on Cdc42 in Breast Cancer: New Insights, Target Therapy Development and Non-Coding RNAs. *Cells* 8, 146. <https://doi.org/10.3390/cells8020146>
- Zhang, Y., Yang, C.-Q., Gao, Y., Wang, C., Zhang, C.-L., Zhou, X.-H., 2014. Knockdown of CXCR7 inhibits proliferation and invasion of osteosarcoma cells through inhibition of the PI3K/Akt and  $\beta$ -arrestin pathways. *Oncol Rep* 32, 965–972. <https://doi.org/10.3892/or.2014.3290>

- Zhang, Y., Yao, F., Yao, X., Yi, C., Tan, C., Wei, L., Sun, S., 2009. Role of CCL5 in invasion, proliferation and proportion of CD44+/CD24- phenotype of MCF-7 cells and correlation of CCL5 and CCR5 expression with breast cancer progression. *Oncology Reports* 21, 1113–1121. [https://doi.org/10.3892/or\\_00000331](https://doi.org/10.3892/or_00000331)
- Zheng, H., Shen, M., Cha, Y.-L., Li, W., Wei, Y., Blanco, M.A., Ren, G., Zhou, T., Storz, P., Wang, H.-Y., Kang, Y., 2014. PKD1 phosphorylation-dependent degradation of SNAIL by SCF-FBXO11 regulates epithelial-mesenchymal transition and metastasis. *Cancer Cell* 26, 358–373. <https://doi.org/10.1016/j.ccr.2014.07.022>
- Zhitomirsky, B., Farber, H., Assaraf, Y.G., 2018. LysoTracker and MitoTracker Red are transport substrates of P-glycoprotein: implications for anticancer drug design evading multidrug resistance. *J Cell Mol Med* 22, 2131–2141. <https://doi.org/10.1111/jcmm.13485>
- Zhu, Y., Cheng, Y., Guo, Y., Chen, J., Chen, F., Luo, R., Li, A., 2016. Protein kinase D2 contributes to TNF- $\alpha$ -induced epithelial mesenchymal transition and invasion via the PI3K/GSK-3 $\beta$ / $\beta$ -catenin pathway in hepatocellular carcinoma. *Oncotarget* 7, 5327–5341. <https://doi.org/10.18632/oncotarget.6633>
- Zidar, D.A., Violin, J.D., Whalen, E.J., Lefkowitz, R.J., 2009. Selective engagement of G protein coupled receptor kinases (GRKs) encodes distinct functions of biased ligands. *Proc Natl Acad Sci U S A* 106, 9649–9654. <https://doi.org/10.1073/pnas.0904361106>
- Ziegler, S., Eiseler, T., Scholz, R.-P., Beck, A., Link, G., Hausser, A., 2011. A novel protein kinase D phosphorylation site in the tumor suppressor Rab interactor 1 is critical for coordination of cell migration. *Mol Biol Cell* 22, 570–580. <https://doi.org/10.1091/mbc.E10-05-0427>
- Zirafi, O., Kim, K.-A., Ständker, L., Mohr, K.B., Sauter, D., Heigle, A., Kluge, S.F., Wiercinska, E., Chudziak, D., Richter, R., Moepps, B., Gierschik, P., Vas, V., Geiger, H., Lamla, M., Weil, T., Burster, T., Zgraja, A., Daubeuf, F., Frossard, N., Hachet-Haas, M., Heunisch, F., Reichetzedler, C., Galzi, J.-L., Pérez-Castells, J., Canales-Mayordomo, A., Jiménez-Barbero, J., Giménez-Gallego, G., Schneider, M., Shorter, J., Telenti, A., Hocher, B., Forssmann, W.-G., Bonig, H., Kirchhoff, F., Münch, J., 2015. Discovery and characterization of an endogenous CXCR4 antagonist. *Cell Rep* 11, 737–747. <https://doi.org/10.1016/j.celrep.2015.03.061>
- Zlotnik, A., Yoshie, O., 2000. Chemokines: a new classification system and their role in immunity. *Immunity* 12, 121–127. [https://doi.org/10.1016/s1074-7613\(00\)80165-x](https://doi.org/10.1016/s1074-7613(00)80165-x)
- Zohar, Y., Wildbaum, G., Novak, R., Salzman, A.L., Thelen, M., Alon, R., Barsheshet, Y., Karp, C.L., Karin, N., 2014. CXCL11-dependent induction of FOXP3-negative regulatory T cells suppresses autoimmune encephalomyelitis. *J Clin Invest* 124, 2009–2022. <https://doi.org/10.1172/JCI71951>
- Zou, Z., Zeng, F., Xu, W., Wang, C., Ke, Z., Wang, Q.J., Deng, F., 2012. PKD2 and PKD3 promote prostate cancer cell invasion by modulating NF- $\kappa$ B- and HDAC1-mediated expression and activation of uPA. *J Cell Sci* 125, 4800–4811. <https://doi.org/10.1242/jcs.106542>

## Appendix 1

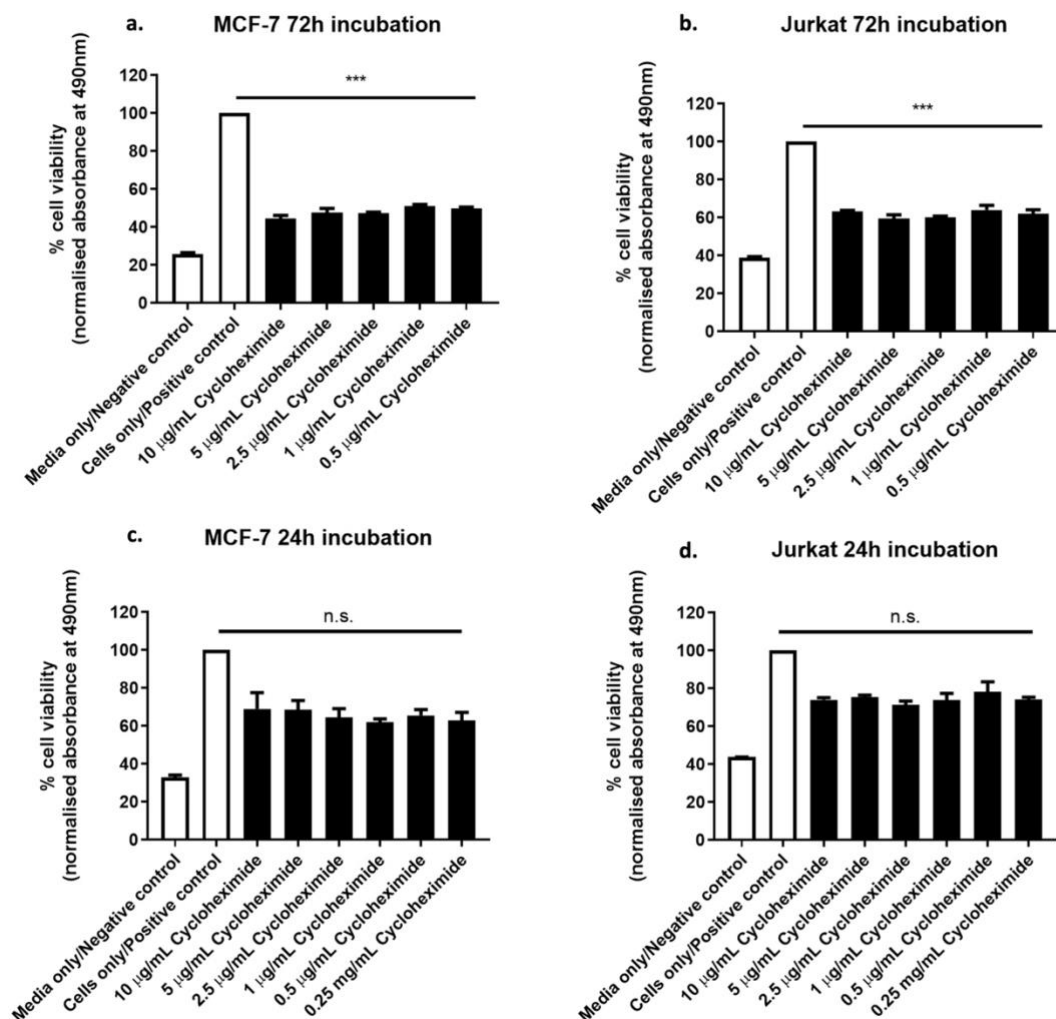


**Figure A1. Protein synthesis inhibitor, cycloheximide, is toxic in MCF-7 and Jurkat cells following 72 hours incubation while the trend of toxicity following 24 hours incubation is less significant.** (a, c) MCF-7; (b, d) Jurkat cells were incubated with cycloheximide in a range of concentrations (10 µg/mL, 5 µg/mL, 2.5 µg/mL, 1 µg/mL, 0.5 µg/mL and 0.25 µg/mL) diluted in the inhibitor vehicle (1% DMSO) for (a, b) 72 hours or (c, d) 24 hours, where negative control contains cell culture media only and positive control contains cells treated with 1% DMSO only. Percentage of cell viability was calculated relative to the absorbance reading of the positive control in the MTS assay. Data shown represent the mean  $\pm$  SEM of at least 3 independent experiments. Kruskal-Wallis test with Dunn's multiple comparisons test as post-hoc test, \*\*\* =  $p \leq 0.001$ .

## Appendix 2

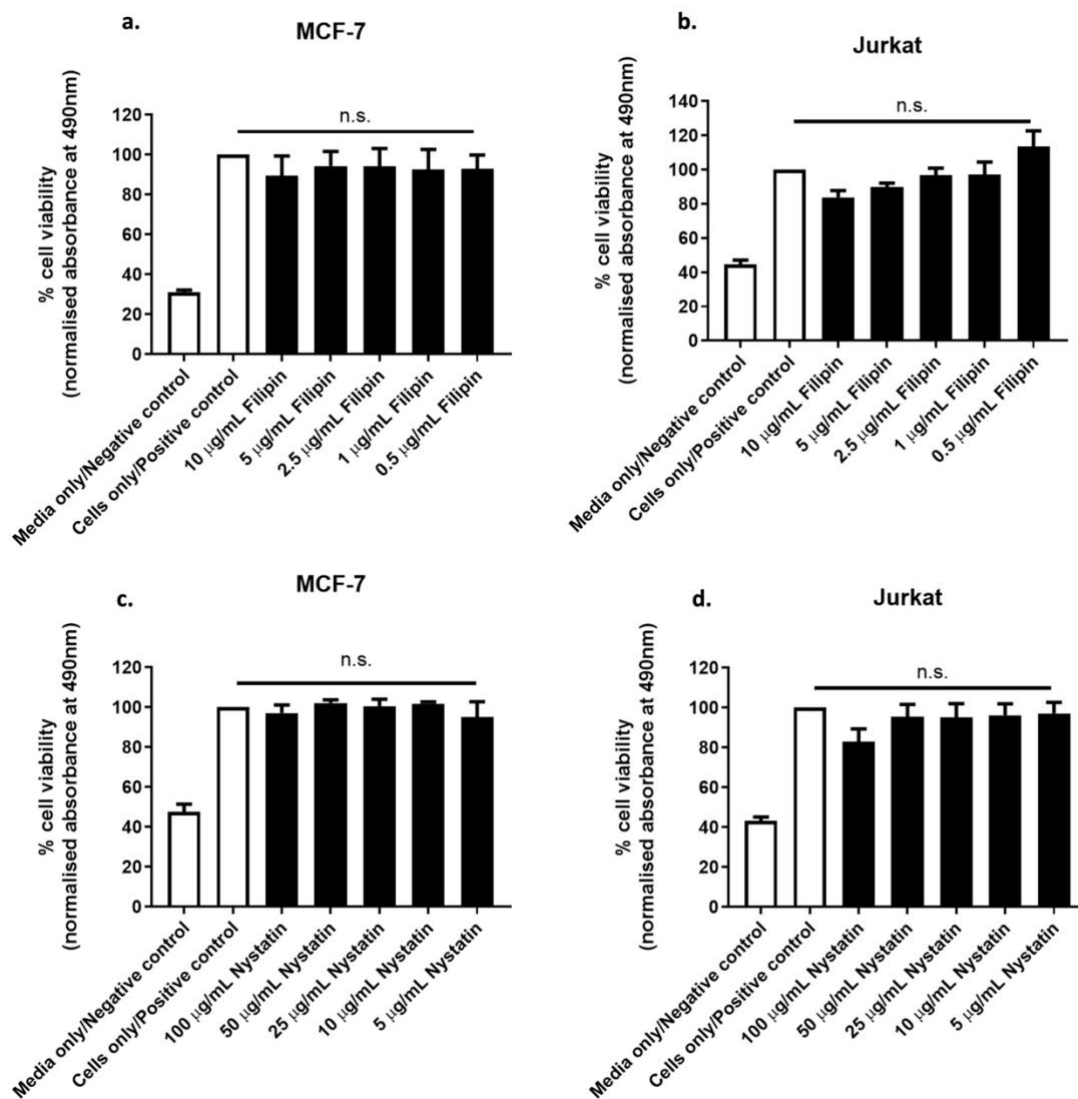


**Figure A2. Caveolae-blocking agents, filipin and nystatin, have no toxicity in MCF-7 and Jurkat cell.** (a, c) MCF-7; (b, d) Jurkat cells were incubated with (a, b) filipin (10  $\mu\text{g/mL}$ , 5  $\mu\text{g/mL}$ , 2.5  $\mu\text{g/mL}$ , 1  $\mu\text{g/mL}$  and 0.5  $\mu\text{g/mL}$ ) or (c, d) nystatin (100  $\mu\text{g/mL}$ , 50  $\mu\text{g/mL}$ , 25  $\mu\text{g/mL}$ , 10  $\mu\text{g/mL}$  and 5  $\mu\text{g/mL}$ ) diluted in the inhibitor vehicle (1% ethanol) for 72 hours, where negative control contains cell culture media only and positive control contains cells treated with 1% ethanol only. Percentage of cell viability was calculated relative to the absorbance reading of the positive control in the MTS assay. Data shown represent the mean  $\pm$  SEM of at least 3 independent experiments. Kruskal-Wallis test with Dunn's multiple comparisons test as post-hoc test, n.s. = not significant.



### Appendix 3

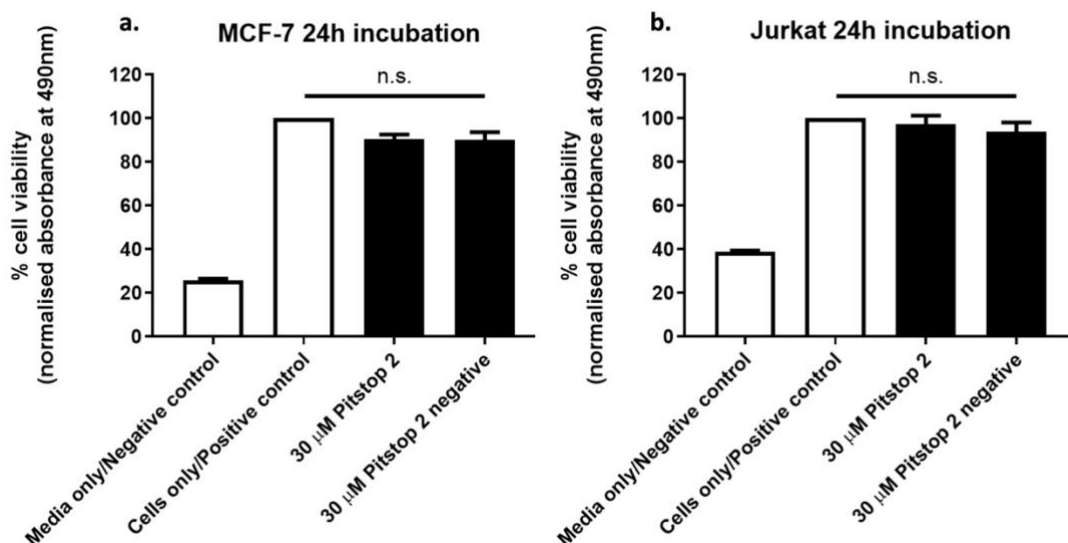


**Figure A3. Clathrin inhibitor, pitstop 2, and negative control for pitstop 2 (pitstop 2 negative) have no toxicity in MCF-7 and Jurkat cell.** (a) MCF-7; (b) Jurkat cells were incubated with 30 µM Pitstop 2 and 30 µM pitstop 2 negative diluted in the inhibitor vehicle (1% DMSO) for 24 hours, where negative control contains cell culture media only and positive control contains cells treated with 1% DMSO only. Percentage of cell viability was calculated relative to the absorbance reading of the positive control in the MTS assay. Data shown represent the mean  $\pm$  SEM of at least 3 independent experiments. Kruskal-Wallis test with Dunn's multiple comparisons test as post-hoc test, n.s. = not significant.

## Appendix 4

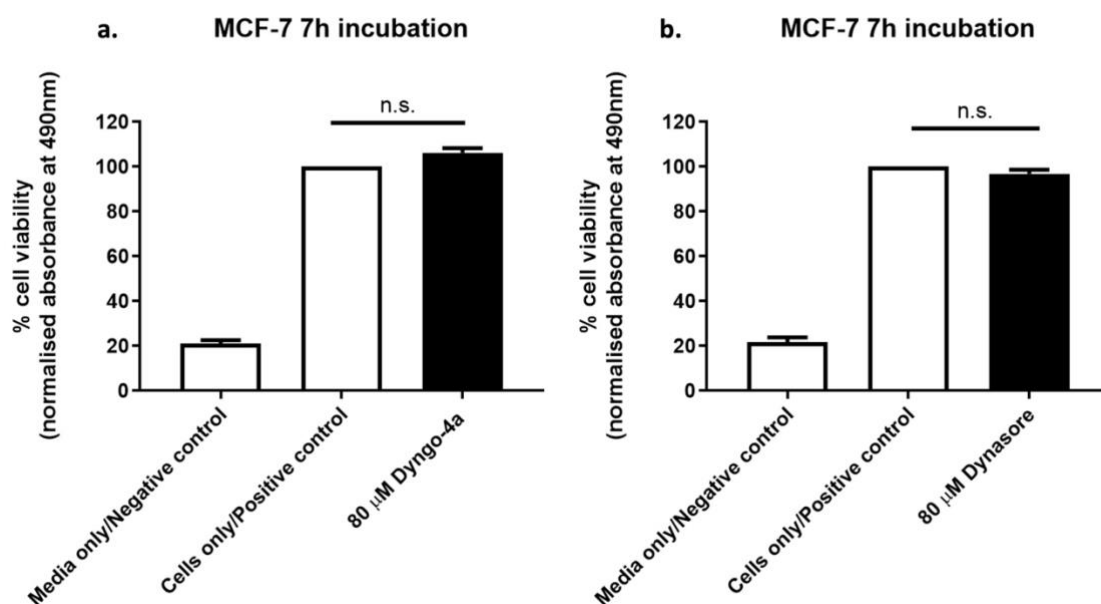


**Figure A4. Dyn-2 inhibitors, Dyngo-4a and Dynasore have no toxicity in MCF-7 and Jurkat cell.** MCF-7 cells were incubated with (a) 80  $\mu$ M Dyngo-4a or (b) 80  $\mu$ M Dynasore diluted in the inhibitor vehicle (1% DMSO) for 7 hours, where negative control contains cell culture media only and positive control contains cells treated with 1% DMSO only. Percentage of cell viability was calculated relative to the absorbance reading of the positive control in the MTS assay. Data shown represent the mean  $\pm$  SEM of at least 3 independent experiments. Kruskal-Wallis test with Dunn's multiple comparisons test as post-hoc test, n.s. = not significant. (Data for Dyngo-4a acquired by Hamshaw I.)

## Appendix 5

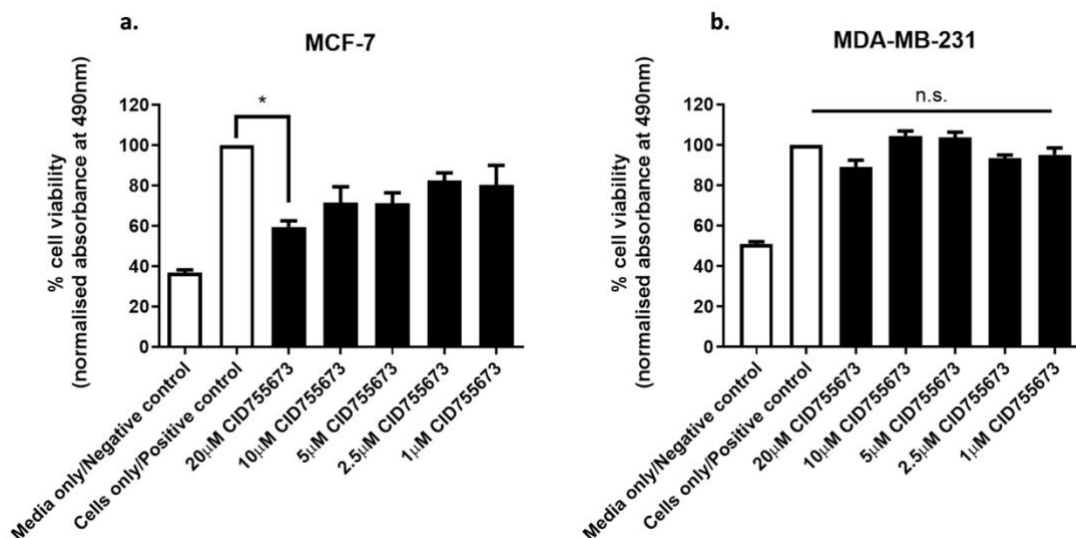


**Figure A5. PrKD inhibitor, CID755673, is toxic in MCF-7 cells at 20  $\mu$ M with a trend of toxicity at lower concentrations, while no toxicity was observed in MDA-MB-231 cells across all tested concentrations.** (a) MCF-7; (b) MDA-MB-231 cells were incubated with CID755673 in a range of concentrations (20  $\mu$ M, 10  $\mu$ M, 5  $\mu$ M, 2.5  $\mu$ M and 1  $\mu$ M) diluted in the inhibitor vehicle (1% DMSO) for 72 hours, where negative control contains cell culture media only and positive control contains cells treated with 1% DMSO only. Percentage of cell viability was calculated relative to the absorbance reading of the positive control in the MTS assay. Data shown represent the mean  $\pm$  SEM of at least 3 independent experiments. Kruskal-Wallis test with Dunn's multiple comparisons test as post-hoc test, \* =  $p \leq 0.05$ , n.s. = not significant.

## Appendix 6

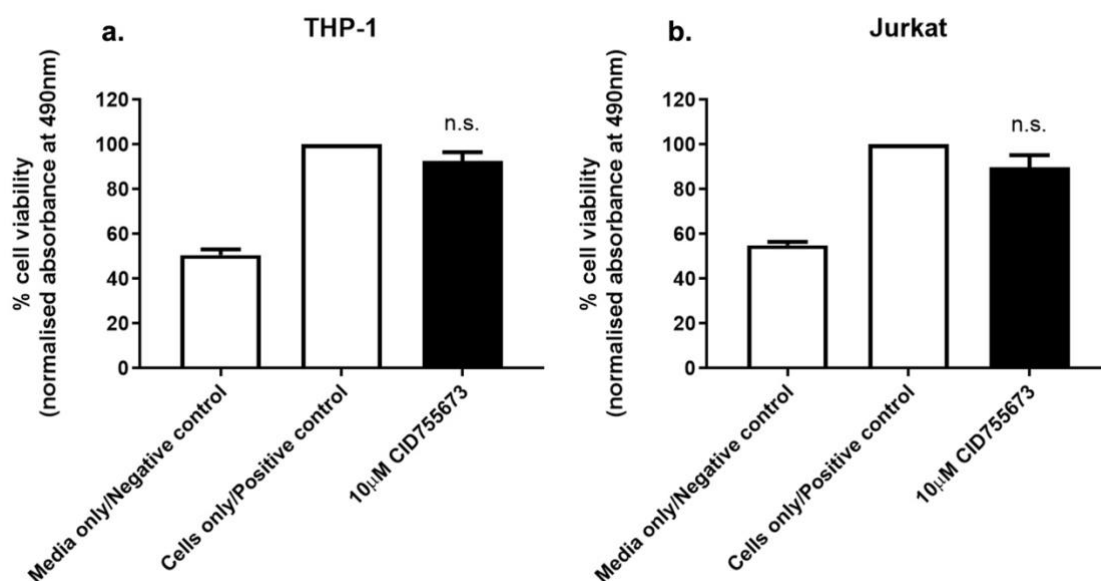


**Figure A6. PrKD inhibitor, CID755673, is not toxic at 10  $\mu$ M in THP-1 and Jurkat cells.** (a) THP-1; (b) Jurkat cells were incubated with 10  $\mu$ M CID755673 diluted in the inhibitor vehicle (1% DMSO) for 72 hours, where negative control contains cell culture media only and positive control contains cells treated with 1% DMSO only. Percentage of cell viability was calculated relative to the absorbance reading of the positive control in the MTS assay. Data shown represent the mean  $\pm$  SEM of at least 3 independent experiments. Kruskal-Wallis test with Dunn's multiple comparisons test as post-hoc test, n.s. = not significant.

## Appendix 7

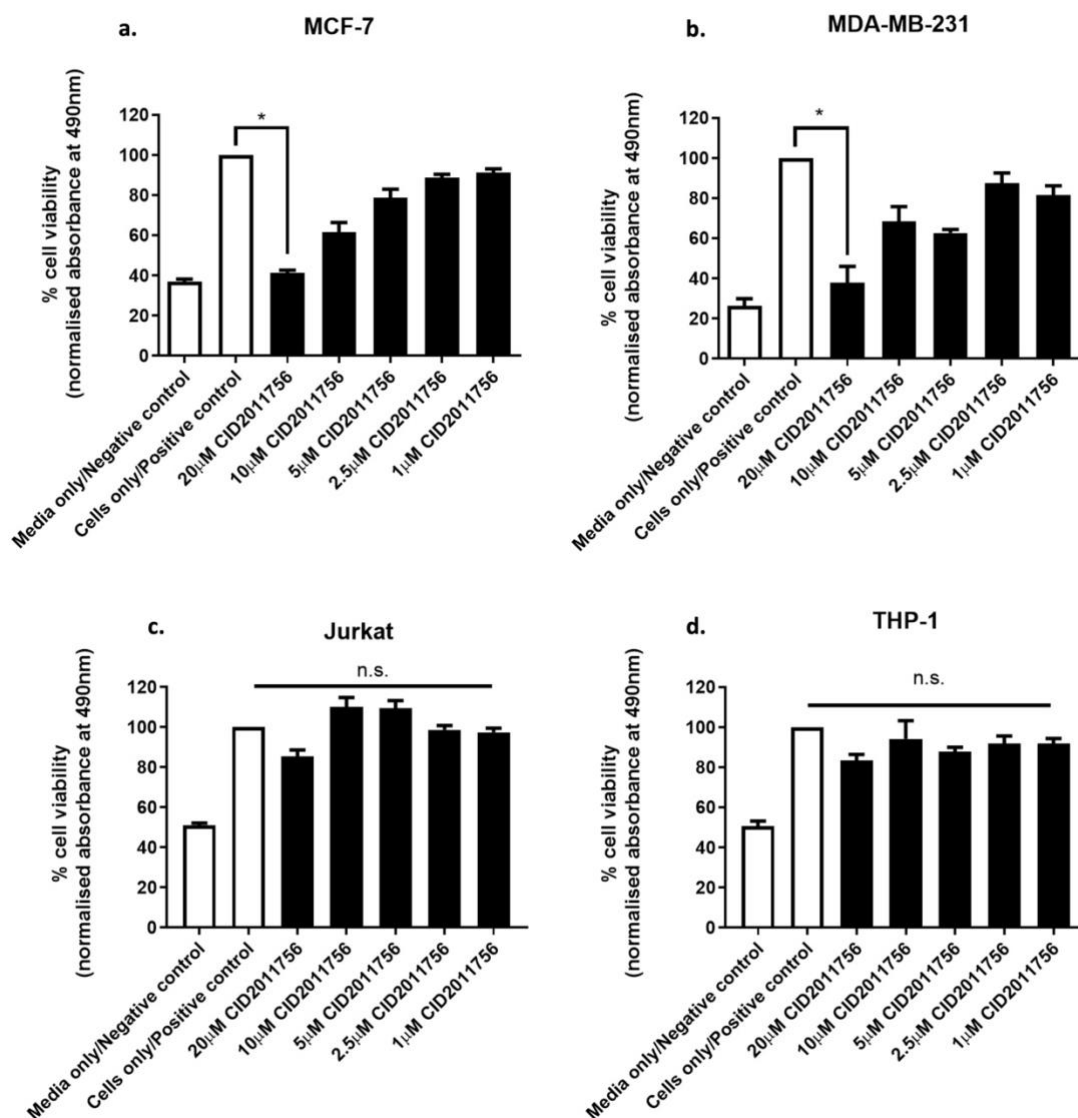


**Figure A7. PrKD inhibitor, CID2011756, is toxic in MCF-7 and MDA-MB-231 cells at 20  $\mu$ M with a trend of toxicity at lower concentrations, while no toxicity was observed in MDA-MB-231 cells across all tested concentrations.** (a) MCF-7; (b) MDA-MB-231; (c) Jurkat; (d) THP-1 cells were incubated with CID2011756 in a range of concentrations (20  $\mu$ M, 10  $\mu$ M, 5  $\mu$ M, 2.5  $\mu$ M and 1  $\mu$ M) diluted in the inhibitor vehicle (1% DMSO) for 72 hours, where negative control contains cell culture media only and positive control contains cells treated with 1% DMSO only. Percentage of cell viability was calculated relative to the absorbance reading of the positive control in the MTS assay. Data shown represent the mean  $\pm$  SEM of at least 3 independent experiments. Kruskal-Wallis test with Dunn's multiple comparisons test as post-hoc test, \* =  $p \leq 0.05$ , n.s. = not significant.

## Appendix 8

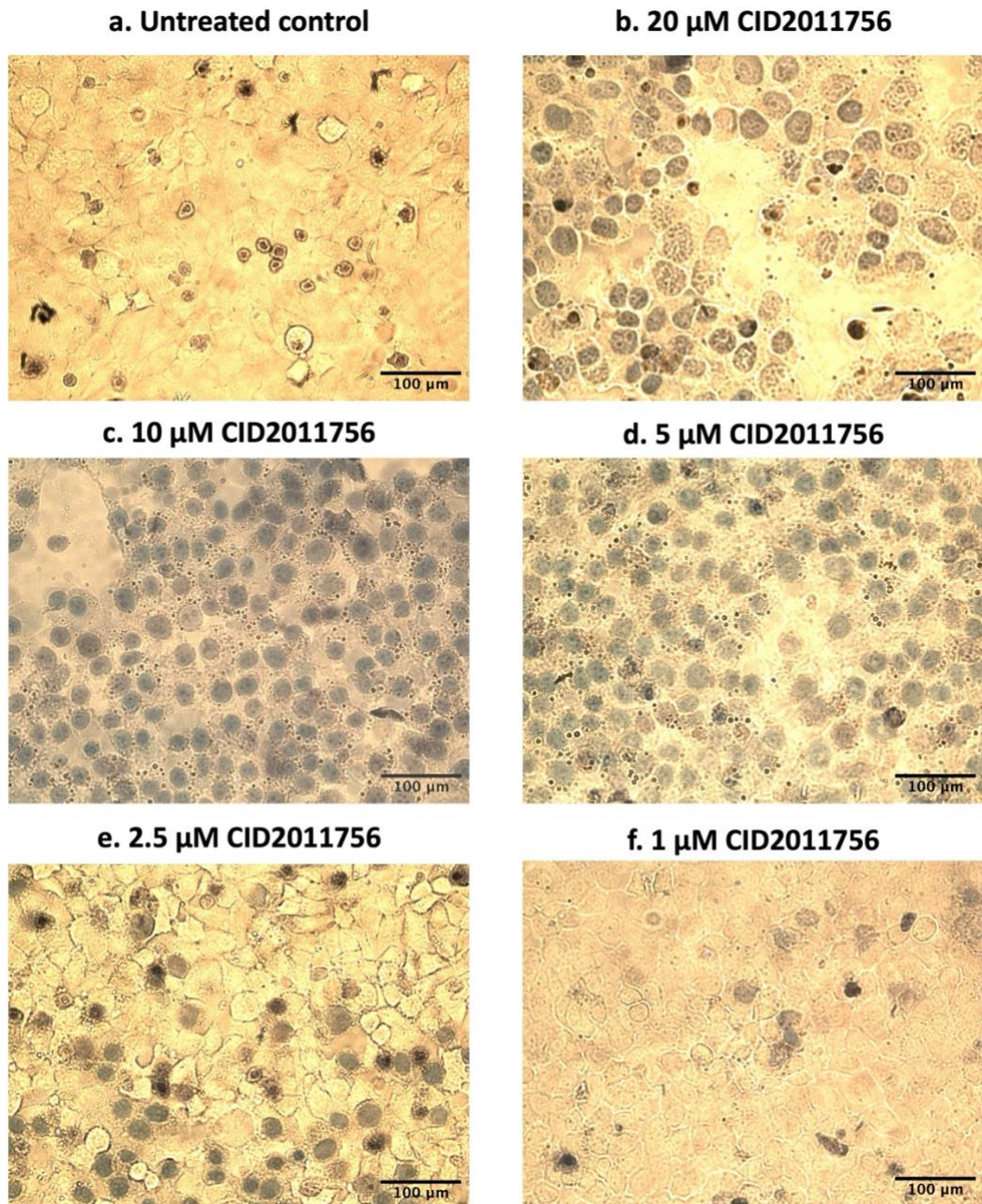


**Figure A8. PrKD inhibitor, CID2011756, is toxic in MCF-7 cells at high concentrations, while the toxicity at 1 μM is minimal.** MCF-7 cells were either left untreated as (a) control or incubated with CID2011756 at (b) 20 μM; (c) 10 μM; (d) 5 μM; (e) 2.5 μM; (f) 1 μM diluted in the inhibitor vehicle (1% DMSO) for 72 hours, where control contains cells treated with 1% DMSO only. Trypan blue 0.4% filtered solution was then added as an indicator of the presence of dead cells. Cells stained in blue indicate non-viable cells with the loss of membrane integrity. Representative images

were acquired with a Leica DMII Fluorescence microscope in brightfield setting using 20X magnification (n=1 as a validation test for the MTS assay shown in **Figure A7**).

## Appendix 9

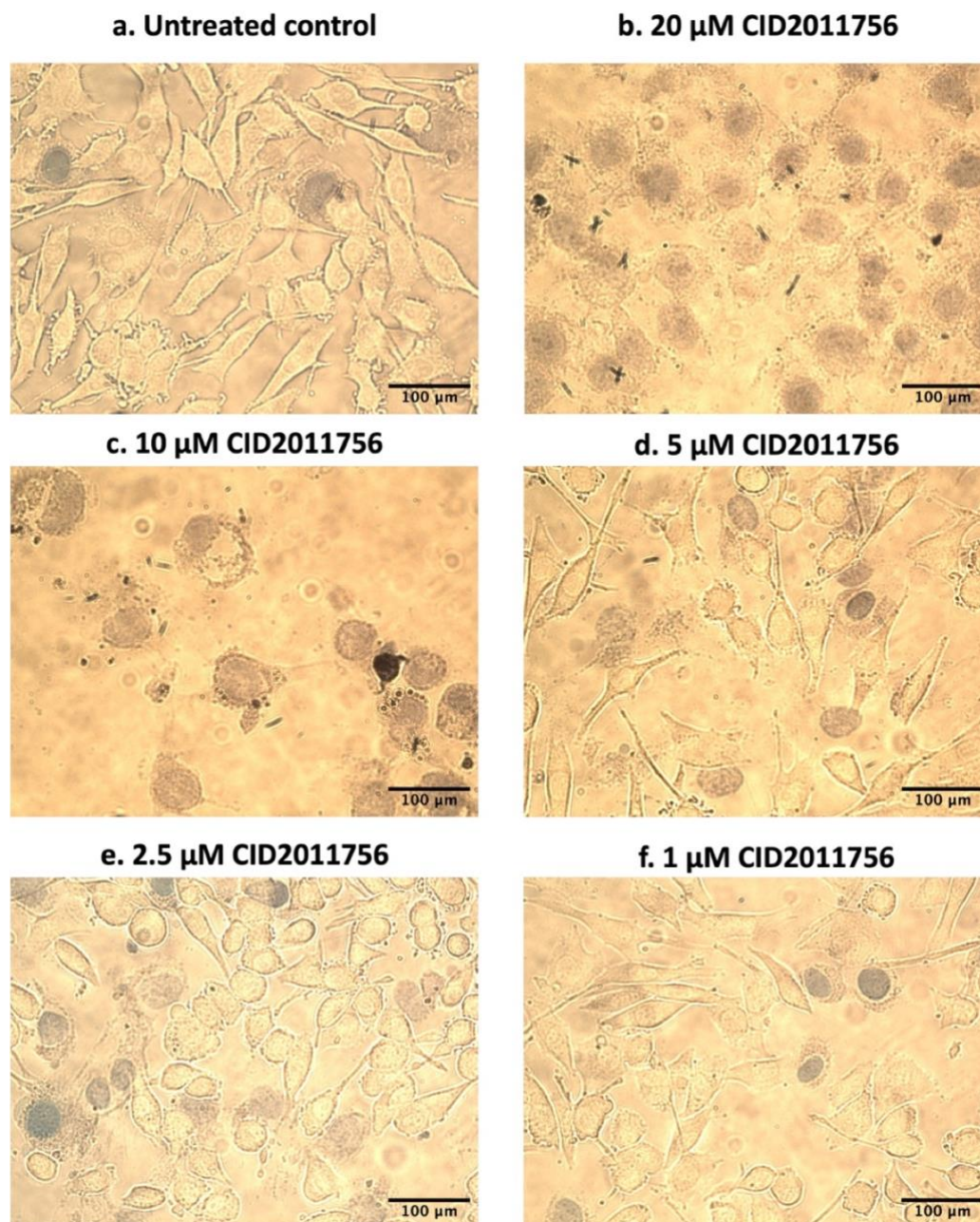


**Figure A9. PrKD inhibitor, CID2011756, is toxic in MDA-MB-231 cells at high concentrations, while the toxicity at 1 μM is minimal. MDA-MB-231 cells were either left untreated as (a) control or incubated with CID2011756 at (b) 20 μM; (c) 10 μM; (d) 5 μM; (e) 2.5 μM; (f) 1 μM diluted in the inhibitor vehicle (1% DMSO) for 72 hours, where control contains cells**

treated with 1% DMSO only. Trypan blue 0.4% filtered solution was then added as an indicator of the presence of dead cells. Cells stained in blue indicate non-viable cells with the loss of membrane integrity. Representative images were acquired with a Leica DMII Fluorescence microscope in brightfield setting using 20X magnification (n=1 as a validation test for the MTS assay shown in **Figure A7**)

## Appendix 10

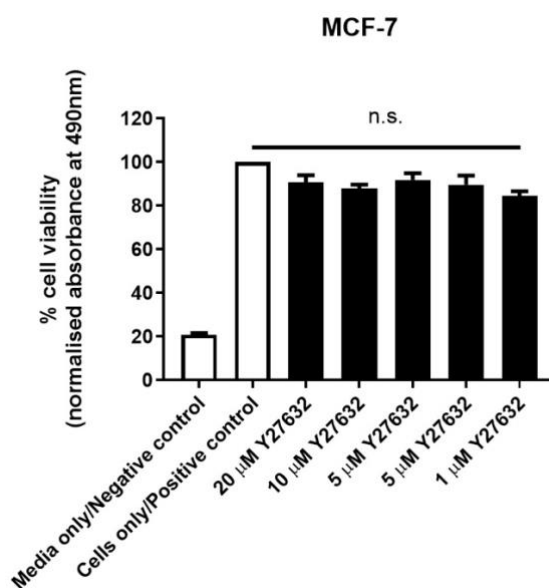


**Figure A10. ROCK inhibitor, Y27632, is not toxic in MCF-7 cells.** Cells were incubated with Y27632 in a range of concentrations (20 µM, 10 µM, 5 µM, 2.5 µM and 1 µM) diluted in the inhibitor vehicle (1% DMSO) for 72 hours, where negative control contains cell culture media only and positive control contains cells treated with 1% DMSO only. Percentage of cell viability was calculated relative to the absorbance reading of the positive control in the MTS assay. Data shown represent the mean  $\pm$  SEM of at least 3 independent experiments. Kruskal-Wallis test with Dunn's multiple comparisons test as post-hoc test, n.s. = not significant.

## Appendix 11

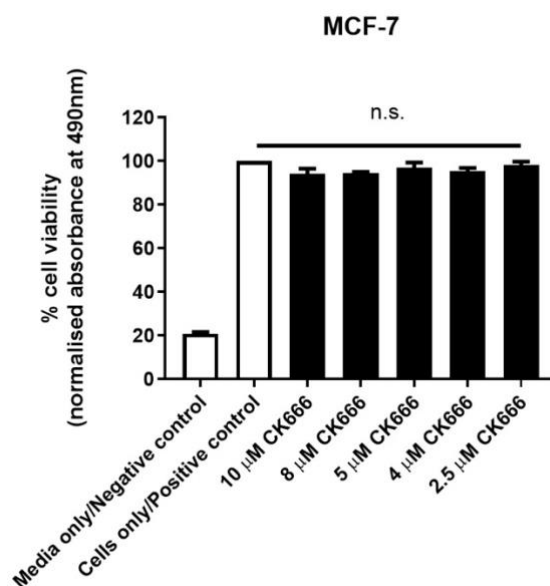


**Figure A11. Arp2/3 inhibitor, CK666, is not toxic in MCF-7 cells.** Cells were incubated with Ck666 in a range of concentrations (10  $\mu$ M, 8  $\mu$ M, 5  $\mu$ M, 4  $\mu$ M and 2.5  $\mu$ M) diluted in the inhibitor vehicle (1% DMSO) for 72 hours, where negative control contains cell culture media only and positive control contains cells treated with 1% DMSO only. Percentage of cell viability was calculated relative to the absorbance reading of the positive control in the MTS assay. Data shown represent the mean  $\pm$  SEM of at least 3 independent experiments. Kruskal-Wallis test with Dunn's multiple comparisons test as post-hoc test, n.s. = not significant.

## Appendix 12

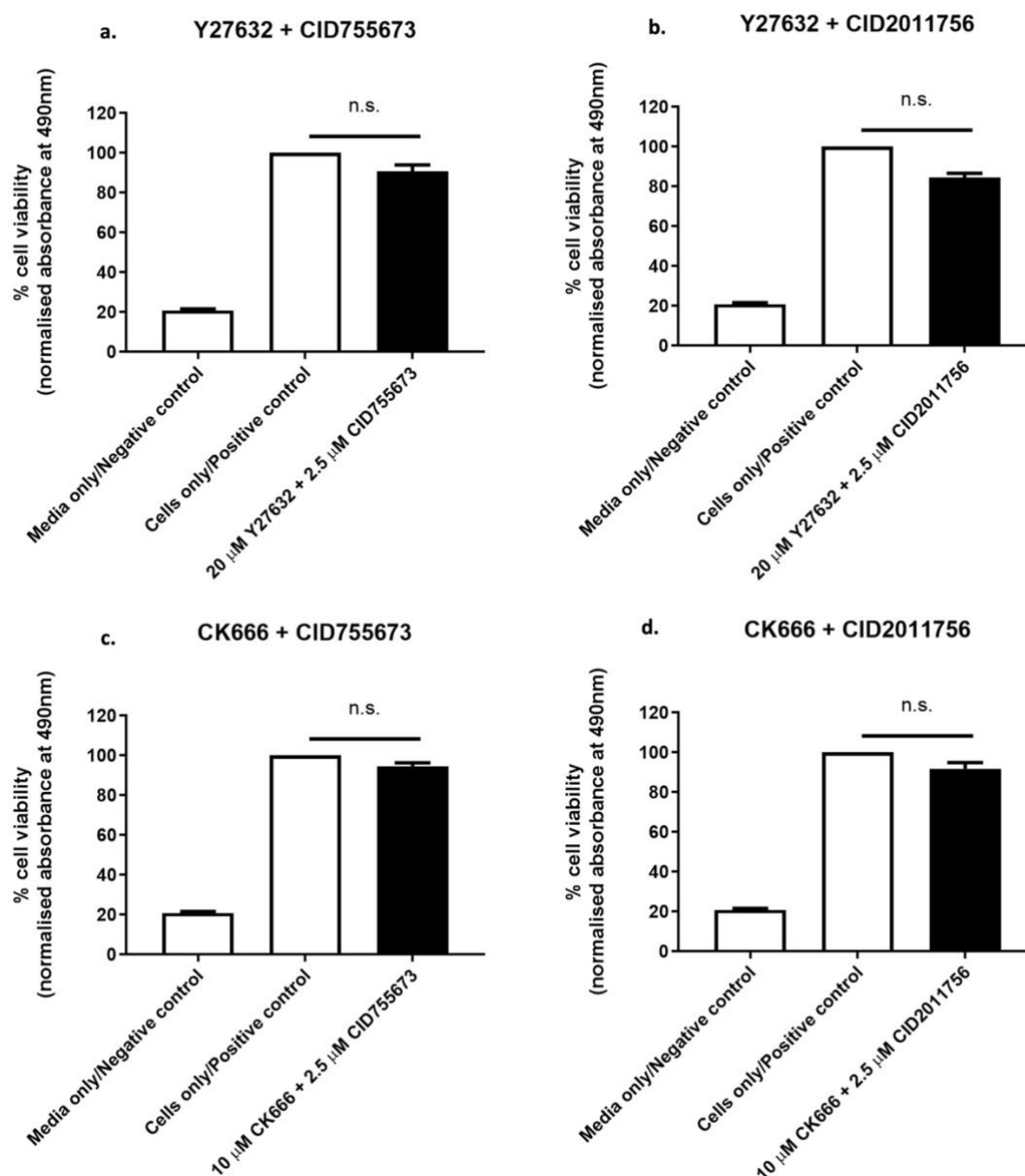


**Figure A12. Two sets of combinations of inhibitors, CK666 and PrKD inhibitor (CID755673 or CID2011756), and Y27632 and PrKD inhibitor are not toxic in MCF-7 cells.** Cells were incubated with (a) 20  $\mu\text{M}$  Y27632 and 2.5  $\mu\text{M}$  CID755673; (b) 20  $\mu\text{M}$  Y27632 and 2.5  $\mu\text{M}$  CID2011756; (c) 10  $\mu\text{M}$  CK666 and 2.5  $\mu\text{M}$  CID755673; (d) 10  $\mu\text{M}$  CK666 and 2.5  $\mu\text{M}$  CID2011756 diluted in the inhibitor vehicle (1% DMSO) for 72 hours, where negative control contains cell culture media only and positive control contains cells treated with 1% DMSO only. Percentage of cell viability was calculated relative to the absorbance reading of the positive control in the MTS assay. Data shown represent the mean  $\pm$  SEM of at least 3

independent experiments. Kruskal-Wallis test with Dunn's multiple comparisons test as post-hoc test, n.s. = not significant.